GEOLOGICAL SURVEY OF CANADA
COMMISSION GÉOLOGIQUE DU CANADA

CURRENT RESEARCH 1995-E

RECHERCHES EN COURS 1995-E

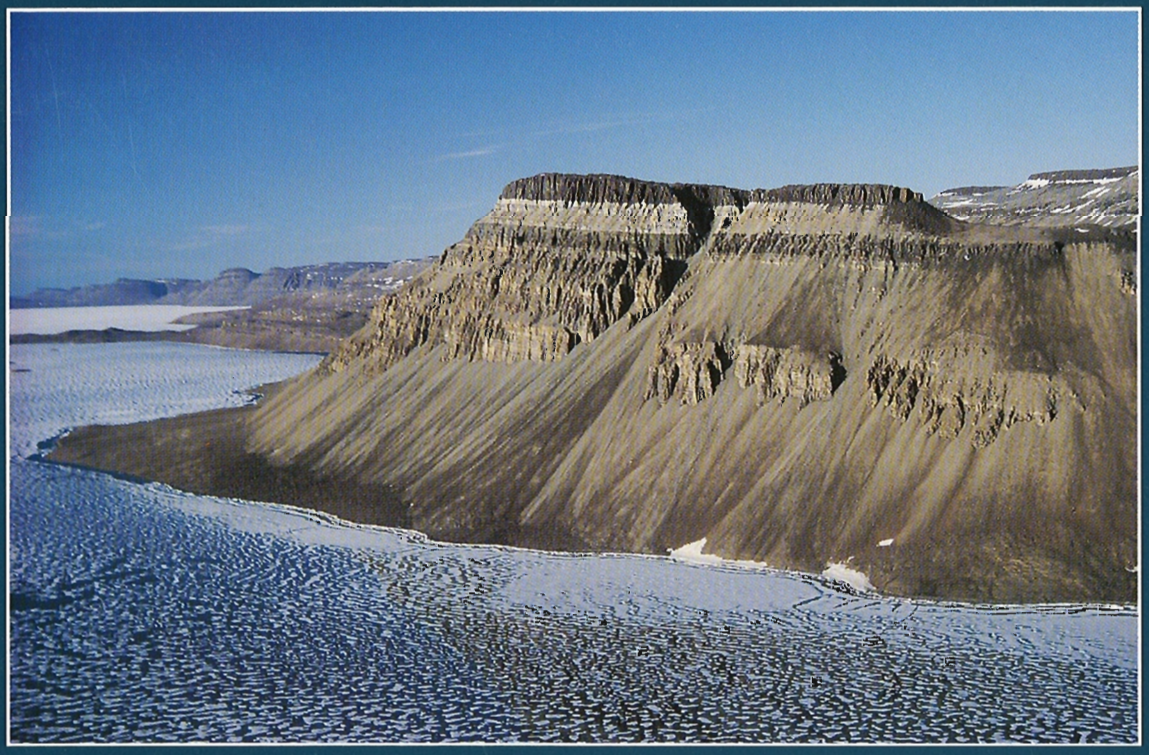

1995

Natural Resources Canada
Ressources naturelles Canada

Canada

NOTICE TO LIBRARIANS AND INDEXERS

The Geological Survey's Current Research series contains many reports comparable in scope and subject matter to those appearing in scientific journals and other serials. Most contributions to Current Research include an abstract and bibliographic citation. It is hoped that these will assist you in cataloguing and indexing these reports and that this will result in a still wider dissemination of the results of the Geological Survey's research activities.

AVIS AUX BIBLIOTHÉCAIRES ET PRÉPARATEURS D'INDEX

La série Recherches en cours de la Commission géologique contient plusieurs rapports dont la portée et la nature sont comparables à ceux qui paraissent dans les revues scientifiques et autres périodiques. La plupart des articles publiés dans Recherches en cours sont accompagnés d'un résumé et d'une bibliographie, ce qui vous permettra, on l'espère, de cataloguer et d'indexer ces rapports, d'où une meilleure diffusion des résultats de recherche de la Commission géologique.

GEOLOGICAL SURVEY OF CANADA
COMMISSION GÉOLOGIQUE DU CANADA

CURRENT RESEARCH 1995-E

RECHERCHES EN COURS 1995-E

1995

Includes/comprend:

Cordillera and Pacific Margin
Cordillère et marge du Pacifique

Interior Plains and Arctic Canada
Plaines intérieures et région arctique du Canada

Canadian Shield
Bouclier canadien

Eastern Canada and National and General Programs
Est du Canada et programmes nationaux et généraux

Available in Canada from

Geological Survey of Canada offices:

601 Booth Street
Ottawa, Canada K1A 0E8

3303-33rd Street N.W.,
Calgary, Alberta T2L 2A7

or from

Canada Communication Group - Publishing
Ottawa, Canada K1A 0S9

and through authorized bookstore agents
and other bookstores

A deposit copy of this publication is also available for reference
in public libraries across Canada

Cat. No. M44-1995/5E
ISBN 0-660-16197-4

Price subject to change without notice

Cover description

Diabase sills of the Franklin igneous suite intruding Neoproterozoic platformal carbonates of the Shaler Supergroup. Top of cliff is approximately 500 m above Wynniatt Bay (Viscount Melville Sound) on northern Victoria Island, Northwest Territories. Photo by R. Rainbird. See Park and Rainbird (this volume).

Description de la photo couverture

Filons-couches de diabase de la suite ignée de Franklin qui recoupent des roches carbonatées de plate-forme du Supergroupe de Shaler (Néoprotérozoïque). Le sommet de l'escarpement a une hauteur d'environ 500 m au-dessus des eaux de la baie Wynniatt (détroit de Viscount Melville), dans le nord de l'île Victoria, Territoires du Nord-Ouest. Photo de R. Rainbird. Voir Park et Rainbird (ce volume).

Separates

A limited number of separates of the papers that appear in this volume are available by direct request to the individual authors. When no location accompanies an author's name in the title of a paper, the Ottawa address should be used. The addresses of the Geological Survey of Canada offices follow:

601 Booth Street
OTTAWA, Ontario
K1A 0E8
(FAX: 613-996-9990)

Geological Survey of Canada (Calgary)
3303-33rd Street N.W.
CALGARY, Alberta
T2L 2A7
(FAX: 403-292-5377)

Geological Survey of Canada (Victoria)
100 West Pender Street
VANCOUVER, B.C.
V6B 1R8
(FAX: 604-666-1124)

P.O. Box 6000
9860 Saanich Road
SIDNEY, B.C.
V8L 4B2
(Fax: 604-363-6565)

Geological Survey of Canada (Atlantic)
Bedford Institute of Oceanography
P.O. Box 1006
DARTMOUTH, N.S.
B2Y 4A2
(FAX: 902-426-2256)

Geological Survey of Canada (Québec)
2700, rue Einstein
C.P. 7500
Sainte-Foy (Québec)
G1V 4C7
(FAX: 418-654-2615)

Tirés à part

On peut obtenir un nombre limité de «tirés à part» des articles qui paraissent dans cette publication en s'adressant directement à chaque auteur. Lorsque l'adresse de l'auteur ne figure pas sous le titre d'un document, on doit alors utiliser l'adresse d'Ottawa. Les adresses des différents bureaux de la Commission géologique du Canada sont les suivantes :

601, rue Booth
OTTAWA, Ontario
K1A 0E8
(facsimilé : 613-996-9990)

Commission géologique du Canada (Calgary)
3303-33rd St. N.W.,
CALGARY, Alberta
T2L 2A7
(facsimilé : 403-292-5377)

Commission géologique du Canada (Victoria)
100 West Pender Street
VANCOUVER, British Columbia
V6B 1R8
(facsimilé : 604-666-1124)

P.O. Box 6000
9860 Saanich Road
SIDNEY, British Columbia
V8L 4B2
(facsimilé : 604-363-6565)

Commission géologique du Canada (Atlantique)
Institut océanographique Bedford
P.O. Box 1006
DARTMOUTH, Nova Scotia
B2Y 4A2
(facsimilé : 902-426-2256)

Commission géologique du Canada (Québec)
2700, rue Einstein
C.P. 7500
Sainte-Foy (Québec)
G1V 4C7
(facsimilé : 418-654-2615)

CONTENTS

CORDILLERA AND PACIFIC MARGIN
CORDILLÈRE ET MARGE DU PACIFIQUE

INTERIOR PLAINS AND ARCTIC CANADA
PLAINES INTÉRIEURES ET RÉGION ARCTIQUE DU CANADA

CANADIAN SHIELD
BOUCLIER CANADIEN

EASTERN CANADA AND NATIONAL AND GENERAL PROGRAMS
EST DU CANADA ET PROGRAMMES NATIONAUX ET GÉNÉRAUX

Cordillera and Pacific Margin

Cordillère et marge du Pacifique

Stratigraphy and structure of the Clarence River area, Yukon-Alaska north slope: a USGS-GSC co-operative project

L.S. Lane, J.S. Kelley[1], and C.T. Wrucke[2]
GSC Calgary, Calgary

Lane, L.S., Kelley, J.S., and Wrucke, C.T., 1995: Stratigraphy and structure of the Clarence River area, Yukon-Alaska north slope: a USGS-GSC co-operative project; in Current Research 1995-E; Geological Survey of Canada, p. 1-9.

Abstract: Two pre-Carboniferous stratigraphic successions, consisting of a southern slope facies and a northern outer-slope to basin facies, are present in the Clarence River area. *Oldhamia*-bearing trace fossil assemblages establish that both facies are, in part, Early to Middle Cambrian in age. Turbiditic sandstone, which overlies and contains *Oldhamia*-bearing strata in the southern facies, were previously mapped as Neruokpuk schist. If that correlation is correct, the Neruokpuk schist is Cambrian in age. Two new Early Silurian graptolite localities are reported in strata correlative with the Road River Formation.

The two early Paleozoic facies were juxtaposed during Devonian orogenesis. The northern basin facies was deformed by a combination of isoclinal folding and thrust faulting, whereas the more competent southern facies was deformed by north-directed thrust faulting, which imbricated the sandstone-dominant succession. Laramide deformation involving Carboniferous and younger rocks generated transverse faults, and broad upright folds which rotated the earlier-formed structures.

Résumé : Deux successions stratigraphiques précarbonifères, composées d'un faciès de talus méridional et d'un faciès septentrional allant de talus extérieur à bassin, sont présentes dans la région de la rivière Clarence. Des associations d'ichnofossiles renfermant *Oldhamia* confirment que les deux faciès datent, en partie, du Cambrien précoce à moyen. Le grès turbiditique, qui repose sur les couches renfermant *Oldhamia* et qui contient de ces couches dans le faciès méridional, a été cartographié dans le passé comme le schiste de Neruokpuk. Si cette corrélation est exacte, le schiste de Neruokpuk est d'âge cambrien. Deux nouvelles localités de graptolites du Silurien précoce sont signalées dans des couches corrélatives de la Formation de Road River.

Les deux faciès du Paléozoïque précoce se sont juxtaposés durant l'orogenèse dévonienne. Le faciès de bassin septentrional a été déformé par une combinaison de plis isoclinaux et de failles chevauchantes tandis que le faciès méridional plus compétent a été déformé par des failles chevauchantes à direction nord qui ont imbriqué la succession surtout gréseuse. La déformation laramienne qui a touché les roches carbonifères et les roches plus récentes a créé des failles transversales et de vastes plis droits qui ont provoqué la rotation des structures plus anciennes.

[1] United States Geological Survey, 4200 University Dr., Anchorage, AK
[2] United States Geological Survey, 345 Middlefield Rd., Menlo Park, CA

INTRODUCTION

Six weeks of fieldwork in 1994 along the international boundary in northern Yukon and Alaska improved our understanding of the geological framework of an area known mostly from reconnaissance mapping (Fig. 1, 2). This work, begun in 1990, continues to resolve differences in geological interpretations across the international boundary (Lane et al., 1991). Geological Survey of Canada and U.S. Geological Survey field parties completed coordinated parallel transects that extend 1:50 000 scale mapping southward along the border to latitude 69°18¢N. This work addressed fundamental stratigraphic and structural problems in rocks of latest Proterozoic(?) and early Paleozoic age.

STRATIGRAPHY

North of a prominent syncline cored by strata of Carboniferous to Triassic age (units C_{EN}, C_L, and PTR_S, Fig. 2), the pre-Carboniferous stratigraphy consists of a succession of outer slope to basinal sedimentary deposits of possibly latest Proterozoic to Devonian(?) age, based on trace and body fossils including four *Oldhamia* localities (Lane et al., 1991; Hofmann et al., 1994), an Ordovician graptolite locality (Dutro et al., 1971), a conodont locality (Kelley et al., 1994), and two new Early Silurian graptolite sites (Table 1; Fig. 2). Basin facies strata, equivalent to the Road River Formation, and volcanic-sedimentary rocks of Cambro-Ordovician age, equivalent to the informally named Whale Mountain volcanic rocks, are components of that succession (Lane et al., 1991; Kelley et al., 1994).

At its base, this succession has limestone (unit PoL) with small amounts of sandstone, argillite, and chert. The limestone unit is considered to be Proterozoic or Cambrian in age based on its position beneath strata of Cambrian age. The depositionally overlying red and green argillite succession (unit oa) includes grey argillite, laminated chert, and subsidiary sandstone and quartzite. Its age is Early to Middle Cambrian, based on the trace fossil Oldhamia found at four localities

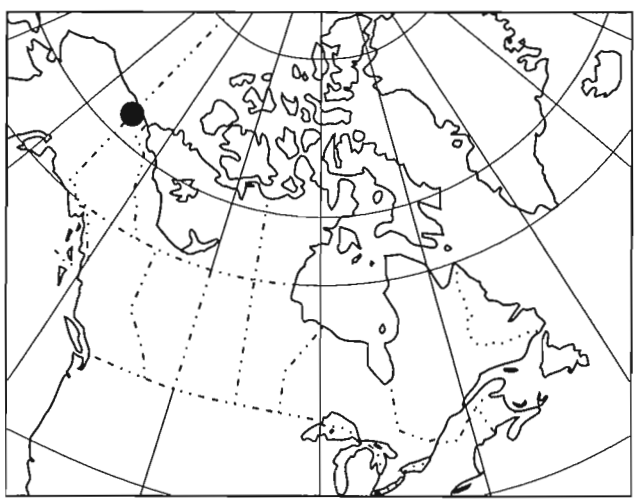

Figure 1. Location map.

(Fig. 2; Table 2; Sweet and Narbonne, 1993; Hofmann et al., 1994). During 1994, the mapping of this unit was extended 17 km westward from the international boundary (Fig. 2) and it was found to contain a lithofacies unlike that mapped in 1990. The new facies is dark grey to greyish-black argillite, one of several facies that previously were considered as separate units (Reiser et al., 1980). Our mapping shows these facies to be one unit consisting largely of fine textured argillite with a greater variety of textures than was previously reported (Lane et al., 1991; Kelley et al., 1994). An additional stratigraphic refinement is the identification of a breccia (not mapped) containing volcanic clasts in the lower part of the red and green argillite unit near the northwestern corner of the map area (Fig. 2). The *Oldhamia*-bearing, Cambrian red and green argillite unit has been correlated with the Narchilla Formation (Hyland Group) of the Selwyn Basin (Lane, 1991). The Narchilla Formation also contains a prominent component of dark blue-grey slate, in addition to pale green, maroon, and purple slate (Gordey and Anderson, 1993).

Volcaniclastic rocks (unit ϵO_{VC}) that depositionally overlie the red and green argillite unit contain: dark coloured tuffs; commonly calcareous volcanic sandstone and conglomerate; dark grey and maroon mudstone; and lesser amounts of argillite resembling those of the underlying and overlying units. Its Cambrian and Ordovician age is interpreted from its gradation into the underlying Cambrian red and green argillite, and on its gradational contact with overlying Ordovician rocks. It is correlated with the Whale Mountain volcanic rocks to the south (Lane et al., 1991) on the basis of lithological similarity of the volcanic components, the calcareous aspect of some members, and because the Whale Mountain volcanic rocks depositionally overlie fossiliferous Upper Cambrian limestone, and underlie "Cambrian and Ordovician" chert and phyllite (Reiser et al., 1980), which independently establishes an approximate age equivalence.

Ridge-forming Ordovician chert and interbedded dark grey argillite (unit Oca) overlie the volcaniclastic unit. This unit has been correlated with a graptolitic Ordovician chert and argillite unit mapped in the Firth River area about 50 km east of the border (Lane and Cecile, 1989), and in the Barn Mountains farther east (Cecile and Lane, 1991).

As a result of work in 1994, argillaceous rocks that depositionally overlie the Ordovician chert-argillite unit have been separated into a lower part of mostly light olive-grey argillite and cherty argillite (unit Sa) and an upper part of dark grey to greyish-black argillite with subordinate lithic sandstone beds, locally containing abundant feldspar and chert clasts (unit D?a). Unit Sa contains two new Early Silurian graptolite localities (F4 and F5; Fig. 2; Table 1), located 5 and 7 km east of the Yukon-Alaska border, and latest Silurian or earliest Devonian conodonts (F2; Fig. 2; Table 1; Kelley et al., 1994). The new graptolite sites occur in white weathering black carbonaceous shale, depositionally overlying the major bedded chert-argillite unit (Oca), and confirm our previous interpretation that the major chert unit in the border area is correlative with the Ordovician chert unit present farther east. The upper unit (D?a) contains locally abundant trace fossils including *Nereites*-type trails. In its western exposures in the map area, the Devonian(?) map unit appears to overlie

conformably the Silurian unit. However, locally in the eastern part of the map area, it lies directly on the Cambrian red and green argillite unit, indicating a significant unconformity at its base. This relationship is similar to that found in the Firth River area, where the unit locally lies on the Ordovician chert-argillite unit (Lane and Cecile, 1989), implying that early stages of Devonian orogenesis may have created relief and erosion prior to deposition of the Devonian(?) unit (Lane, 1991).

Additional work on structurally higher units in the northern facies has contributed to a resolution of uncertainties regarding the stratigraphic position and age of two map units. They include the volcaniclastic unit (ϵO_{VC}) that lies structurally above the greyish-black argillite (unit D?a); and the Paleozoic limestone unit (Pz_L) above the volcaniclastic-tuffaceous rocks. The Paleozoic limestone unit was included in Paleozoic map units by Lane et al. (1991) and was designated as Devonian(?) by Kelley et al. (1994). Lane et al. (1991) suggested the possibility that the volcaniclastic-tuffaceous rocks and overlying limestone were a structural repetition of the Ordovician section and included a slightly more calcareous facies than is exposed farther north, whereas Kelley et al. (1994) treated the succession as part of a generally intact Cambrian through Devonian(?) succession. We are now convinced that the volcaniclastic-tuffaceous unit is part of the structurally lower volcaniclastic unit (ϵO_{VC}) because our 1994 mapping east and west along strike support the interpretation of a regionally important thrust fault at the base of this unit. This interpretation is further strengthened by recent clarification of the Ordovician graptolite locality 17 of Reiser et al. (1980). According to W.P. Brosgé (pers. comm., 1994), locality 17 actually comprises two fossil collections; the more northerly marks the site of *Nereites* trace fossils within unit D?a, consistent with our mapping, whereas the Ordovician graptolite was collected, together with some trace fossils, about 300 m farther south, within unit ϵO_{VC} (F1; Fig. 2; Table 1; see Reiser et al., 1980). This is consistent with the site description as comprising black slate associated with volcanic rocks (Dutro et al., 1971; Lane, 1992).

In Alaska, a low-angle fault at the base of the limestone (unit Pz_L) was mapped west of Clarence River. Farther east, this structural break likely separates light olive-grey argillite, interbedded with the lower part of the limestone unit, from the Devonian(?) argillite unit. This fault is likely a regional thrust fault. Reiser et al. (1980) mapped the fault westward 40 km from the border. In the Yukon, the limestone and overlying pale green siliceous argillite (Pza) project beneath the sub-Carboniferous unconformity. However, toward the eastern limit of mapping, the succession overlying the Devonian(?) argillite unit becomes structurally complex, consisting of several repetitions of the Ordovician chert and argillite unit (Oca), the volcaniclastic unit (ϵO_{VC}), and the

Table 1. Fossil localities.

Locality no. (Map unit)	Sample no.	Fauna and Age
F1 (ϵOvc, D?a)	71ABe430D[1] 71ABe431E[1]	*Orthograptus* of the *O. quadrimucronatus* type. *Nereites; Paleodictyon?; Zoophycos?; Dictyodora* **Age:** Late Ordovician
F2 (Sa)	90AK-5A[2]	*Ozarkodina remscheidensis remscheidensis* (Zeigler) transitional to *O. pandora* Murphy, Matti and Walliser *Belodella* sp. indet. **Age:** late Late Silurian-early Early Devonian (Pridolian-earliest Pragian)
F3 (PzL)	90AK-2A[2]	limonite-replaced pelmatozoan columnals and ossicles. **Age:** post-Early Cambrian
F4 (Sa)	C-247172[3] C-247173[3]	*Cyrtograptus* sp. or *Monograptus* sp. *Cyrtograptus* sp. *Monograptus* spp. *Pseudoplegmatograptus* sp. *Retiolites* cf. *R. geinitzianus angustidens* Elles and Wood undetermined retiolitid graptolite. **Age:** Lower Silurian, most probably latest Telychian (*sakmaricus-laqueus* Zone), possibly early Wenlock
F5 (Sa)	C-247174[3]	*Cyrtograptus* sp. or *Monograptus* sp. *Monograptus* spp. *?Pseudoplegmatograptus* sp. **Age:** Lower Silurian, probably Telychian or Wenlock

[1]Dutro et al. (1971), see also Reiser et al. (1980)
[2]A. Harris (pers. comm., 1990), see Kelley et al. (1994)
[3]B.S. Norford (pers. comm., 1994)

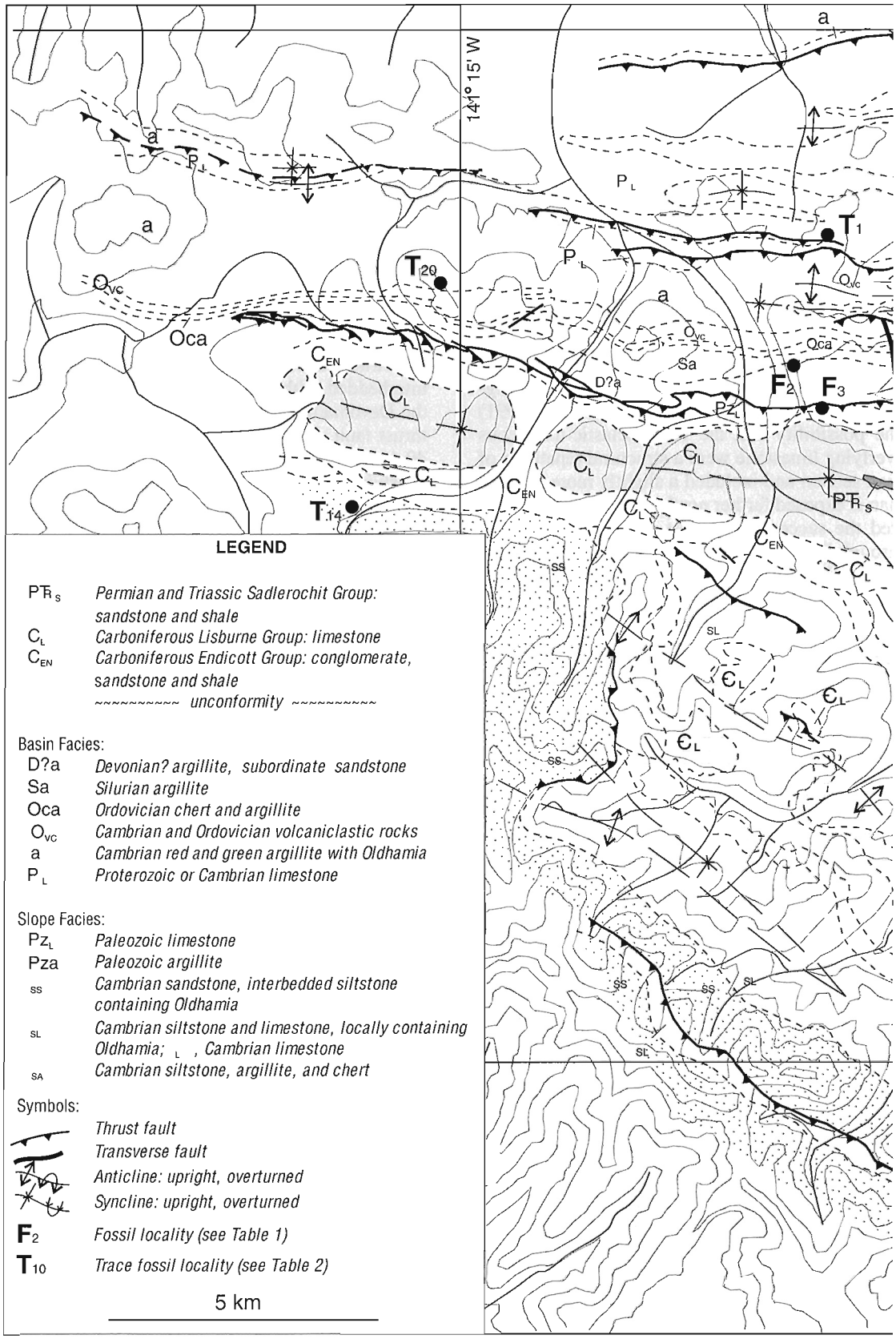

Figure 2. *Preliminary geological map of the Clarence River area.*

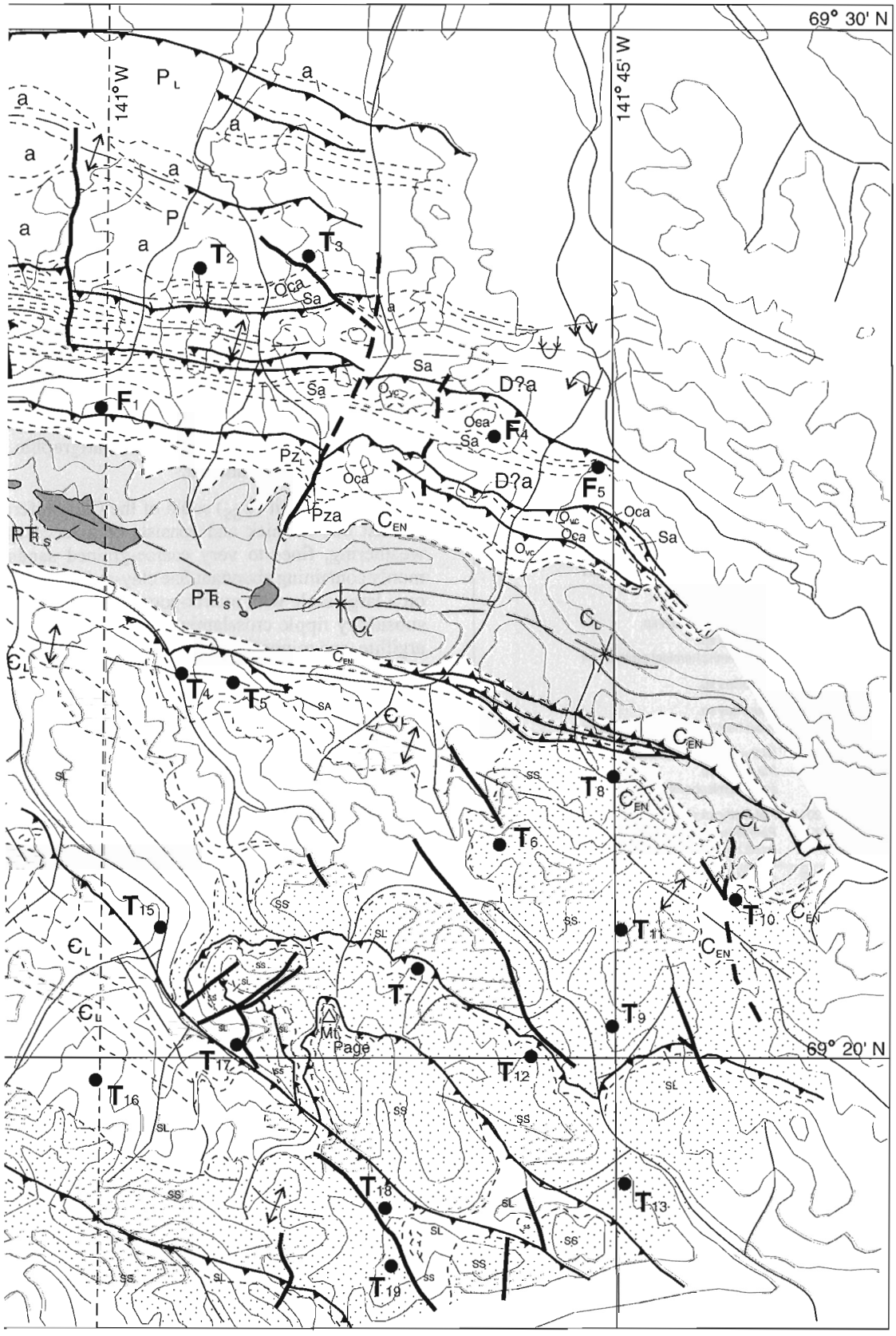
69° 30' N
141° W
141° 45' W
69° 20' N
Mt. Page
F1
F4
F5
T2
T3
T4
T5
T6
T7
T8
T9
T10
T11
T12
T13
T15
T16
T17
T18
T19
a
Sa
Oca
D?a
Pza
PZL
PL
CEN
CL
SL
SS
SA

Table 2. Trace fossil localities

Locality no. (Map Unit)	Sample no.	Fauna
T1 (Єa)	BR7*	*Oldhamia* sp. *Planolites* spp.
T2 (Єa)	BR8*	*Oldhamia antiqua*? Forbes *Oldhamia curvata* Lindholm and Casey *Oldhamia* sp. *Planolites* spp.
T3 (Єa)	BR9*	*Oldhamia curvata* Lindholm and Casey *Oldhamia flabellata* Aceñolaza and Durand *Oldhamia radiata* Forbes *Oldhamia*? *wattsi*? (Sollas) *Oldhamia* sp. *Planolites* spp. *Protopaleodictyon* sp.
T4 (Єsa)	BR12*	*Oldhamia*? *wattsi* (Sollas)
T5 (Єsa)	BR13*	*Planolites* spp. *Tuberculichnus*? sp.
T6 (Єss)	C-247177	*Planolites* sp. *Protopaleodictyon* sp. *Helminthoidichnites* sp.
T7 (ЄSL)	C-247182	*Helminthoidichnites* sp. *Planolites* sp. small hemispheroidal protrusions
T8 (Єss)	C-247186	*Planolites* sp. small hemispheroidal protrusions
T9 (Єss)	C-247187	*Planolites* sp.
T10 (Єss)	C-247189	*Helminthoidichnites* sp. *Planolites* sp. small hemispheroidal protrusions
T11 (Єss)	C-247190	*Planolites* sp.
T12 (Єss)	C-247191	*Planolites* sp. small hemispheroidal protrusions
T13 (Єss)	C-247194	*Oldhamia*? *wattsi* (Sollas) *Planolites* sp. small hemispheroidal protrusions
T14 (Єss)	C-247201 C-247202	*Helminthoidichnites* sp. *Planolites* sp. small hemispheroidal protrusions
T15 (ЄSL)	C-247203	*Helminthoidichnites* sp. *Planolites* sp.
T16 (ЄSL)	C-247206	*Oldhamia radiata* Forbes *Oldhamia*? *wattsi* (Sollas) *Planolites* sp. - fine form small hemispheroidal protrusions
	C-247207	*Oldhamia curvata* Lindholm and Casey *Oldhamia*? *wattsi* (Sollas) *Planolites* sp. small hemispheroidal protrusions *Helminthoidichnites* sp.
	C-247208	*Planolites* sp.
T17 (ЄSL)	C-247220	*Planolites* sp. - fine form small hemispheroidal protrusions
T18 (Єss)	C-247228	cf. *Oldhamia flabellata* Aceñolaza and Durand cf. *Oldhamia*? *wattsi* (Sollas) *Planolites* sp. - fine form *Planolites* sp. - coarse form
T19 (Єss)	C-247229	*Oldhamia*? sp. *Planolites* sp. *Helminthoidichnites* sp.
T20 (Єa)	94AK-18**	*Oldhamia* sp. (cf. *Oldhamia antiqua*?)

Identifications by A.W. Norris (pers. comm., 1994), except as noted.
* Hofmann et al. (1994)
** R. Gangloff (pers. comm., 1994)

Silurian argillite unit (Sa; Fig. 2). This complicated geometry is interpreted as being due to the inclusion and imbrication of these units within the regional thrust fault, which comprises a broader, more complex zone in the east than it does farther west.

South of the Carboniferous inlier, resolution of the stratigraphy was hampered by numerous transverse faults, and extensive talus cover. Detailed mapping in 1994 has established a gross two-part stratigraphic order. The lower unit (mostly $Є_{SL}$) is interbedded medium grey limestone, siltstone, and slaty argillite (including red and green argillite and siltstone), grey laminated chert, and subsidiary sandstone and quartzite. The thickness of unit $Є_{SL}$ is unknown, but greater than 700 m. A unit of sandstone argillite and limestone ($Є_{SA}$) at the base of the section was mapped separately. Also, larger limestone units within $Є_{SL}$ have been differentiated as $Є_L$. Unit Pz_L north of the Carboniferous rocks may be one of these limestone bodies (Fig. 2). Owing to structural complexity and limited exposure, details of the stratigraphic succession (within $Є_{SL}$) remain unclear.

The upper unit ($Є_{SS}$) south of the Carboniferous inlier is at least 600 m thick and consists of a succession of rusty weathering, fine- to very coarse-grained sandstone, commonly containing abundant fine clay-rich matrix, interbedded on a large scale with matrix-poor sandstone, as well as with subsidiary ripple crosslaminated light green siltstone, slaty argillite, and minor limestone and chert. This siliciclastic unit locally contains prominent red and green siltstone and argillite, and maroon and red sandstone.

Blocky weathering, matrix-poor sandstone can be mapped for short distances, depending on talus cover and the abundance of transverse faults. Some of these units contain grit beds, locally coarsening to quartz-pebble conglomerates with clast sizes up to 2 cm. The association of coarser and adjacent finer beds, predominance of relatively poorly sorted sandstone, presence of ripple crosslaminated siltstone, local presence of flute and load casts on sandstone bases, and thickness of the succession suggest deposition on a continental slope as a succession of turbidites.

Sixteen trace fossil localities have been found in units $Є_{SL}$ and $Є_{SS}$ of the turbiditic southern succession (Table 2; Fig. 2), predominantly in light green siltstone units interbedded with sandstones, and locally with limestones. Five of these localities contain trace fossils tentatively identified as *Oldhamia*, suggesting an Early Cambrian age for this succession (Sweet and Narbonne, 1993; Hofmann et al., 1994). Our studies suggest that rocks previously mapped in the border area as correlative with the Neruokpuk schist of Leffingwell (1919; see Reiser et al., 1980) may be Early Cambrian in age. The new data also strengthen the interpretation that the *Oldhamia*-bearing quartzite succession of Early Cambrian age in the Firth River area (Lane and Cecile, 1989) is stratigraphically equivalent to the slope sandstone of the border area. The new mapping largely confirms the interpretation of Lane (1991, 1992) that facies variations and structural repetitions are both significant elements of the regional geology of the border area.

Parts of the ϵ_{SS} unit have been mapped in Alaska by Reiser et al. (1980) as the Neruokpuk schist of Leffingwell (1919), the type section of which is about 150 km west of the border. Sandstone that Reiser et al. (1980) mapped as Neruokpuk in the Clarence River area is in the farthest north of three east-trending belts of sandstone that they included in the formation. The southern belt extends eastward from the type area, reaching the border about 25 km south of the area shown in Figure 2. H.N. Reiser and W.P. Brosgé (pers. comm., 1994) reported that sandstone in the northern belt, which does not extend to the "type" area, is the least similar of these sandstones to the "type" Neruokpuk. The principal contrast is that the metamorphic fabric in hand specimen of the "type" Neruokpuk is better developed than in the sandstone mapped as Neruokpuk in the Clarence River area. Both H.N. Reiser and W.P. Brosgé (pers. comm., 1994) now express reservations whether all sandstone mapped as Neruokpuk schist of Leffingwell (1919) is the same lithostratigraphic unit.

In contrast, aspects of gross lithology and petrography suggest that sandstones of the Clarence River area may correlate with the "type" Neruokpuk. Reed (1968) characterized the latter as consisting of well-bedded, turbiditic, matrix-rich sandstone interbedded with phyllite and metachert. The phyllite varies in colour from greyish-black to light grey, commonly greyish green and greyish red-purple (Reed, 1968). Also, Reed's petrographic descriptions of the sandstone, including poorly sorted subangular to angular quartz clasts, detrital feldspar and muscovite, in an abundant sericitic and chloritic matrix, are strikingly similar to the sandstone of the Clarence River area. Uncertainty over the correlation of the Clarence River sandstone with the "type" Neruokpuk cannot be resolved at present. However, if the major differences can be attributed to variations in metamorphic grade, the lithological and petrographic similarities would suggest a correlation. Detailed mapping in the "type" area of the Neruokpuk offers the best opportunity to clarify this uncertainty.

STRUCTURE

Three deformation events are distinguished in the Clarence River area on the basis of crosscutting relationships. The first event predates, and the second and third events post-date deposition of Lower Carboniferous rocks. The oldest deformation produced tight to isoclinal folds, associated with northward-directed thrust faults, locally distributed mesoscopic minor folds, a penetrative slaty cleavage in argillaceous rocks, and a spaced fracture (locally pressure solution) cleavage in matrix-rich sandstones. Map-scale folds predominate north of the syncline containing rocks of the Lisburne Group in its core. Good stratigraphic control combined with cleavage-bedding asymmetry allows identification of fold closures and thrust-related repetitions of stratigraphy. Local availability of stratigraphic facing indicators and mappable fold closures have assisted in defining the structure there.

South of the Lisburne-cored syncline, map-scale first generation folds are not documented, although mesoscopic minor folds are present in thin bedded units, and the slaty cleavage is ubiquitous in argillites. Thrust faults predominate here, presumably due to the greater competence of the thick sandstone-rich succession (unit ϵ_{SS}). This interpretation is supported by the strong dominance of southward-dipping, right-way-up strata where slaty cleavage dips more steeply southward than does bedding. At least three, and possibly four repetitions of the same stratigraphic interval appear to be present near Mount Page (Fig. 2). This conclusion is based on the interpretation of a particular red and green argillite and limestone unit as a décollement horizon responsible for the thrust-repetition of the overlying sandstone unit. The alternative interpretation that the succession is intact and the argillite-limestone unit occurs as four distinct horizons cannot be ruled out. However, four lines of evidence favour the thrust fault interpretation. First, the argillite-limestone unit commonly contains isoclinal, mesoscopic, intrafolial folds that are overturned northward and locally reclined, indicating that these units are localized high strain zones within the sandstone-dominated succession. Second, the proposed décollement horizons are lithologically the same as the uppermost unit in the siltstone-limestone succession (unit ϵ_{SL}) gradationally underlying the sandstone succession. Third, unit thicknesses appear to vary considerably over short distances, and the proposed décollement horizon appears to be locally absent. Fourth, elsewhere the red and green argillites are well known to be prominent décollement horizons (e.g. Lane and Cecile, 1989; Cecile and Lane, 1991). The interpretation that seems most consistent with the available data favours a thrust fault model where the argillite-limestone units within the sandstone succession represent repetitions of a décollement horizon slightly below the base of the sandstone succession.

The two contrasting northern and southern facies were juxtaposed by a major thrust system, prior to deposition of the unconformably overlying Lower Carboniferous rocks. That thrust system is exposed in Alaska, and emplaces the limestone unit (Pz_L) onto the Devonian(?) argillite (D?a) north of the Carboniferous inlier. Imbricate faults that cut the limestone flatten into this thrust fault. The structure becomes more complex along strike eastward, and consists of several imbrications carrying repetitions of units ϵO_{VC}, Oca and Sa. In this part of the map area, the thrust system is partially buried beneath the sub-Carboniferous unconformity, and the entire zone appears to project beneath the unconformity a short distance east of the map area.

The age of the first generation structures is constrained as pre-Carboniferous within the map area because they project at an oblique angle beneath the sub-Carboniferous unconformity. However, regional considerations indicate that they relate to the Middle Devonian Ellesmerian tectonomagmatic event in northern Yukon and Alaska (Lane et al., 1993). Among the considerations are: the well-known, pronounced, angular unconformity at the base of the Carboniferous succession; the intrusion of Devonian post-tectonic granites together with related contact metamorphic aureoles; and the ubiquity of a penetrative slaty cleavage in argillaceous rocks of Devonian and older ages, whereas cleavages in Carboniferous and younger rocks are only locally developed, and variably oriented.

A second generation of structures consists of a series of transverse faults trending predominantly northward to northwestward with generally indeterminate but steep dips. They appear prominently as lineaments on airphotos, and are locally abundant. In places, they are the dominant structural features. The magnitudes and senses of displacement are seldom definable; however, locally they are observed to truncate beds, or to produce up to 400 m of bedding separation. A few northeast-trending faults have produced dextral stratigraphic separations. Some north-trending faults have either dextral or west-side-down separations. One northeast-trending fault appears to bend into (or intersect) a north-trending fault. Several northwest-trending faults are present, and show either left- or right-lateral separations of bedding. Specific kinematic data are rare because the fault zones are rarely exposed. Despite this, some fault-striation data were collected from adjacent subsidiary shear fractures, and are currently being analyzed. Although the transverse structures have produced only a small component of the regional strain, they are significant features from a mapping perspective because, when combined with limited exposure, they are a local impediment to tracing the regional extent of map units.

The second generation structures are known to have affected the Carboniferous and Permian successions in the vicinity of the map area (Fig. 2; Reiser et al., 1980; Norris, 1981a), and must postdate the Permian. Similar structures have been mapped elsewhere in the region, and have affected rocks as young as Early Tertiary (Norris, 1981b; Cecile and Lane, 1991), suggesting that they relate to the Tertiary Brookian deformation (Lane and Dietrich, in press). Ongoing kinematic analyses may help to constrain the tectonic setting of these structures.

Third generation structures are the local expression of the regional northeastern Brooks Range deformation. The most prominent of these structures in the map area is the large syncline cored by Carboniferous and locally Permian and Triassic units. A notable element of this structure is a set of south-directed thrust faults that imbricate the southern fold limb (Fig. 2). This structure is shown to be complex, involving at least three imbrications, accounting for anomalously steep dips on the south limb of the structure. The thrusts appear to be detached in the Carboniferous Kayak shale, well known regionally as a décollement horizon (e.g. Kelley and Foland, 1987; Wallace and Hanks, 1990). North of the Lisburne-cored syncline, mesoscopic structures that may be attributable to this event are locally present. Also, a gradual northward overturning of first-generation structures may be a Brookian effect relating to the progressively increasing distance from the hinge of the syncline.

South of the Lisburne-cored syncline are two large, and several smaller, anticlinal hinges of Brookian age. The first one trends nearly parallel to the Carboniferous rocks on the south limb of the syncline approximately 1 km from the unconformity. The second Brookian anticline is a pronounced feature resembling a fault-bend fold, obliquely crossing the southern one-third of the map area. Its axial surface strikes northwestward, oblique to the trend of the Lisburne-cored structure, and dips northeastward. On its southern limb, beds dip nearly vertically, locally with pronounced overturning, though stratigraphic facing is consistently southward. On the northern limb, beds typically dip gently eastward or northeastward, reflecting the local southeastward plunge. These structures are inferred to be Brookian because both the bedding and the first-generation slaty cleavage are rotated on them. A smaller anticline-syncline pair was mapped in the southwest corner of the map area, but it does not appear to project into Canada. However, it does project northwestward beneath a fold characterized by significant disharmony between the sandstone unit and the underlying limestone and argillite succession. In contrast, the same contact in Canada appears to be relatively intact.

At least one mapped thrust fault indicates late (presumably Tertiary) displacement across the southern part of the map area (Fig. 2), although the displacement magnitude appears to be modest. Hanks (1993) inferred 46 per cent Cenozoic shortening in the pre-Carboniferous succession about 60 km west of the border. Such a large shortening has not yet been documented in the border area.

The obliquity of the southern Brookian structure to the Lisburne-cored syncline, another Brookian structure, is notable. However, elsewhere in the northeastern Brooks Range, Brookian structures have been shown to be controlled by Ellesmerian structural trends, except where they have been mechanically decoupled from the pre-Carboniferous rocks by décollement on the Kayak shale (Wallace and Hanks, 1990).

The Brookian deformation is locally accompanied by a spaced crenulation cleavage in the slaty argillites. The crenulation is typically steeply dipping to the northeast and appears to be best developed where the first generation slaty cleavage is suitably oriented with shallow dips. Also, it tends to be better developed closer to the Lisburne-cored syncline, perhaps because the most favourably oriented slaty cleavage is found on the northeast limbs of the anticlines.

The age of the northeastern Brooks Range structures is well known regionally from previous mapping and apatite fission track dating in Alaska (e.g. Grantz, 1966; Kelley and Foland, 1987; O'Sullivan et al., 1990); and from mapping and seismic stratigraphic analysis in Canada (e.g. Lane, 1988; Dietrich and Lane, 1992; Lane and Dietrich, in press). Those studies, among others, have shown that the structures in the northeastern Brooks Range developed from the latest Cretaceous through the Quaternary, with major pulses occurring in the early Eocene and in the late Miocene.

SUMMARY

Six weeks of fieldwork in the Alaska-Yukon border area in 1994 have resulted in important clarifications of both stratigraphy and structure. Facies variations and structural repetitions were found to be significant elements of the regional geology. Two new Silurian graptolite localities and sixteen new trace fossil localities help to relate the local stratigraphy to the regional stratigraphic framework (e.g. Lane and Cecile, 1989; Lane et al., 1991; Kelley et al., 1994). Parts of the sandstone-dominant slope facies present in this map area have been previously mapped as correlative with the Neruokpuk

schist of Leffingwell (1919; see Reiser et al., 1980). If that correlation is correct, our mapping suggests that the Neruokpuk may be as young as Early Cambrian (Sweet and Narbonne, 1993; Hofmann et al., 1994).

Several newly mapped thrust faults are interpreted to have repeated parts of the succession. The sandstone-dominated turbiditic slope succession in particular has been repeated at least three times within the map area, indicating that the real thickness of the succession is probably much thinner than was previously supposed. In addition, numerous transverse faults corresponding to prominent airphoto lineaments have been shown to significantly disrupt the continuity of map units.

ACKNOWLEDGMENTS

The authors wish to thank Parks Canada and the U.S. Fish and Wildlife Service for permission to work in this protected area. Polar Continental Shelf Project (PCSP) and Sunrise Helicopters provided logistical support. J. McDonald provided excellent assistance in the field. D.G. Cook, W.P. Brosgé, and J.P. Galloway critically read the manuscript.

REFERENCES

Cecile, M.P. and Lane, L.S.
1991: Geology of the Barn Uplift; Geological Survey of Canada, Open File 2342, 1 sheet, 1:50 000 scale.

Dietrich, J.R. and Lane, L.S.
1992: Geology and structural evolution of the Demarcation Subbasin and Herschel High, Beaufort-Mackenzie Basin, Arctic Canada; Bulletin of Canadian Petroleum Geology, v. 40, p. 188-197.

Dutro, J.T., Jr., Reiser, H.N., Detterman, R.L., and Brosgé, W.P.
1971: Early Paleozoic fossils in the Neruokpuk Formation, northeast Alaska; U.S. Geological Survey, Open File Report 499, 4 p.

Gordey, S.P. and Anderson, R.G.
1993: Evolution of the northern Cordilleran miogeocline, Nahanni map area (105-I), Yukon and Northwest Territories; Geological Survey of Canada, Memoir 428, 214 p.

Grantz, A.
1966: Strike-slip faults in Alaska; U.S. Geological Survey, Open File Report 267, 82 p.

Hanks, C.L.
1993: The Cenozoic structural evolution of a fold-and-thrust belt, northeastern Brooks Range, Alaska; Geological Society of America Bulletin, v. 105, p. 287-305.

Hofmann, H.J., Cecile, M.P., and Lane, L.S.
1994: New Occurrences of *Oldhamia* and other trace fossils from Arctic North America; Canadian Journal of Earth Sciences, v. 31, p. 767-782.

Kelley, J.S. and Foland, R.L.
1987: Structural style and framework geology of the Coastal Plain and adjacent Brooks Range. Chapter 20; in Petroleum Geology of the Northern Part of the Arctic National Wildlife Refuge, Northeastern Alaska, K.J. Bird and L.B. Magoon (ed.); United States Geological Survey, Bulletin 1778, p. 255-270.

Kelley, J.S., Wrucke, C.T., and Lane, L.S.
1994: Pre-Mississippian rocks in the Clarence and Malcolm rivers area, Alaska and Yukon Territory; in Proceedings of the 1992 International Conference on Arctic Margins, D.K. Thurston and K. Fujita (ed.); United States Department of the Interior, Minerals Management Service, OCS Study MMS94-0040, p. 59-64.

Lane, L.S.
1988: The Rapid Fault Array: a Foldbelt in Arctic Yukon; in Current Research, Part D; Geological Survey of Canada, Paper 88-1D, p. 95-98.
1991: The Pre-Mississippian "Neruokpuk Formation", northeastern Alaska and northwestern Yukon: review and new regional correlation; Canadian Journal of Earth Sciences, v. 28, p. 1521-1533.
1992: The pre-Mississippian "Neruokpuk Formation", northeastern Alaska and northwestern Yukon: review and new regional correlation: Reply; Canadian Journal of Earth Sciences, v. 29, p. 1808-1811.

Lane, L.S. and Cecile, M.P.
1989: Stratigraphy and structure of the Neruokpuk Formation, northern Yukon; in Current Research, Part G; Geological Survey of Canada, Paper 89-1G, p. 57-62.

Lane, L.S. and Dietrich, J.R.
in press: Tertiary structural evolution of the Beaufort sea - Mackenzie Delta region, Arctic Canada; Bulletin of Canadian Petroleum Geology, v. 43.

Lane, L.S., Kelley, J.S., and Wrucke, C.T.
1991: Preliminary report on stratigraphy and structure, northeastern Brooks Range, Alaska and Yukon: a USGS-GSC cooperative project; in Current Research, Part A; Geological Survey of Canada, Paper 91-1A, p. 111-117.

Lane, L.S., Mortensen, J.K., and Theriault, R.J.
1993: Tectonic setting, U-Pb geochronology and geochemistry of Late Devonian plutons, northern Yukon; Geological Association of Canada/Mineralogical Association of Canada, Joint Annual Meeting, Edmonton, Alberta, May 1993, Program and Abstracts, v. 18, p. A55.

Leffingwell, E. de K.
1919: The Canning River region, northern Alaska; United States Geological Survey, Professional Paper 109.

Norris, D.K.
1981a: Geology, Herschel Island and Demarcation Point, Yukon Territory; Geological Survey of Canada, Map 1514A (scale 1:250 000).
1981b: Geology, Blow River and Davidson Mountains, Yukon Territory-District of Mackenzie; Geological Survey of Canada, Map 1516A (scale 1:250 000).

O'Sullivan, P.B., Decker, J., and Bergman, S.C.
1990: Two phases of Tertiary uplift in the Umiat-Colville River region, North Slope Alaska; an apatite fission track study; Geological Association of Canada/ Mineralogical Association of Canada, Joint Annual Meeting, Vancouver, B.C., May 1990, Program with Abstracts, v. 15, p. A98.

Reed, B.L.
1968: Geology of the Lake Peters area, northeastern Brooks Range, Alaska; United States Geological Survey, Bulletin 1236, 127 p.

Reiser, H.N., Brosgé, W.P., Dutro, J.T., Jr., and Detterman, R.L.
1980: Geologic map of the Demarcation Point Quadrangle, Alaska; United States Geological Survey, Miscellaneous Investigation Series, Map I-1133 (Scale 1:250 000).

Sweet, N.L. and Narbonne, G.M.
1993: Occurrence of the Cambrian trace fossil *Oldhamia* in southern Quebec; Atlantic Geology, v. 29, p. 69-73.

Wallace, W.K. and Hanks, C.L.
1990: Structural provinces of the northeastern Brooks Range, Arctic National Wildlife Refuge, Alaska; American Association of Petroleum Geologists Bulletin, v. 74, p. 1100-1118.

Geological Survey of Canada Project 890065

Mineralogical and geochemical analyses of the Crowsnest Volcanics, southwest Alberta[1]

N.J. Bégin[2], R.E. Beiersdorfer[3], and E.D. Ghent[2]
GSC Calgary, Calgary

Bégin, N.J., Beiersdorfer, R.E., and Ghent, E.D., 1995: Mineralogical and geochemical analyses of the Crowsnest Volcanics, southwest Alberta; in Current Research 1995-E; Geological Survey of Canada, p. 11-25.

Abstract: The analcime-phyric rocks of the Crowsnest volcanics are dominated by breccias and epiclastic rocks. Igneous phenocrysts consist of sanidine feldspar, analcime, melanite-garnet, pyroxene, and titanite in a matrix with trachytic alignment of albite and sanidine laths. The Crowsnest Volcanics are altered to zeolite facies and contain veins of analcime±quartz, amygdular prehnite, and pore-filling cement of laumontite. The matrix is recrystallized to quartz, adularia, albite, and chlorite. Calcite veining and pseudomorphs over igneous minerals are also common. The veinal nature of the analcime is interpreted as a product of metamorphic alteration, as opposed to an igneous product. Physical conditions for this metamorphism are constrained by the stability of the zeolite minerals, at 1 to 3 kbar and 180 to 300°C. The potential for economic mineralization is low. Except for mafic inclusions, oxide and sulphide minerals are rare in the Crowsnest Volcanics. XRF whole rock chemistry shows that base metals content is very low.

Résumé : Les roches à phénocristaux d'analcime des volcanites de Crowsnest sont dominées par des brèches et des roches épiclastiques. Les phénocristaux ignés consistent en sanidine, analcime, mélanite, pyroxène et titanite dans une matrice caractérisée par un alignement trachytique de cristaux prismatiques d'albite et de sanidine. Les volcanites de Crowsnest ont été altérées au faciès à zéolites et continnent des veines d'analcime±quartz, de la laumontite comme ciment dans les pores et de la préhnite amygdaloïde. La matrice a été recristallisée en quartz, adulaire, albite et chlorite. Des veines et des pseudomorphes de calcite sur les minéraux ignés sont fréquents. La nature veinée de l'analcime serait plutôt le produit d'une altération métamorphique que d'une cristallisation magmatique. Cette altération métamorphique se serait produit à entre 1 et 3 kbar et entre 180 et 300 °C. Le potentiel en minéralisation économique y est faible. Les oxydes et les sulfures sont rares, exception faite des inclusions mafiques. Les analyses chimiques XRF de la roche totale montrent que la teneur en métaux de base est très faible.

[1] Contribution to Canada-Alberta Agreement on Mineral Development (1992-1995), a subsidiary agreement under the Canada-Alberta Economic and Regional Development Agreement. Project funded by the Geological Survey of Canada.
[2] Department of Geology and Geophysics, University of Calgary, Calgary, Alberta T2N 1N4
[3] Department of Geology, Youngstown State University, Ohio, USA, 44555-3612

INTRODUCTION

As part of the Canada-Alberta Mineral Development Agreement, 1992-1995, the Geological Survey of Canada (GSC) and University of Calgary (U of C) personnel are conducting detailed studies of the Crowsnest Volcanics in southwestern Alberta. The ultimate purpose of these MDA-funded studies is to assess the likelihood of significant mineralization within these rocks, in accordance with the overall goals of the Mineral Development Agreement. An important part of the assessment of potential economic mineralization is chemical and mineralogical analysis of a suite of samples collected from outcrops of the Lower Cretaceous Crowsnest Volcanic unit. We have acquired and interpreted major and minor

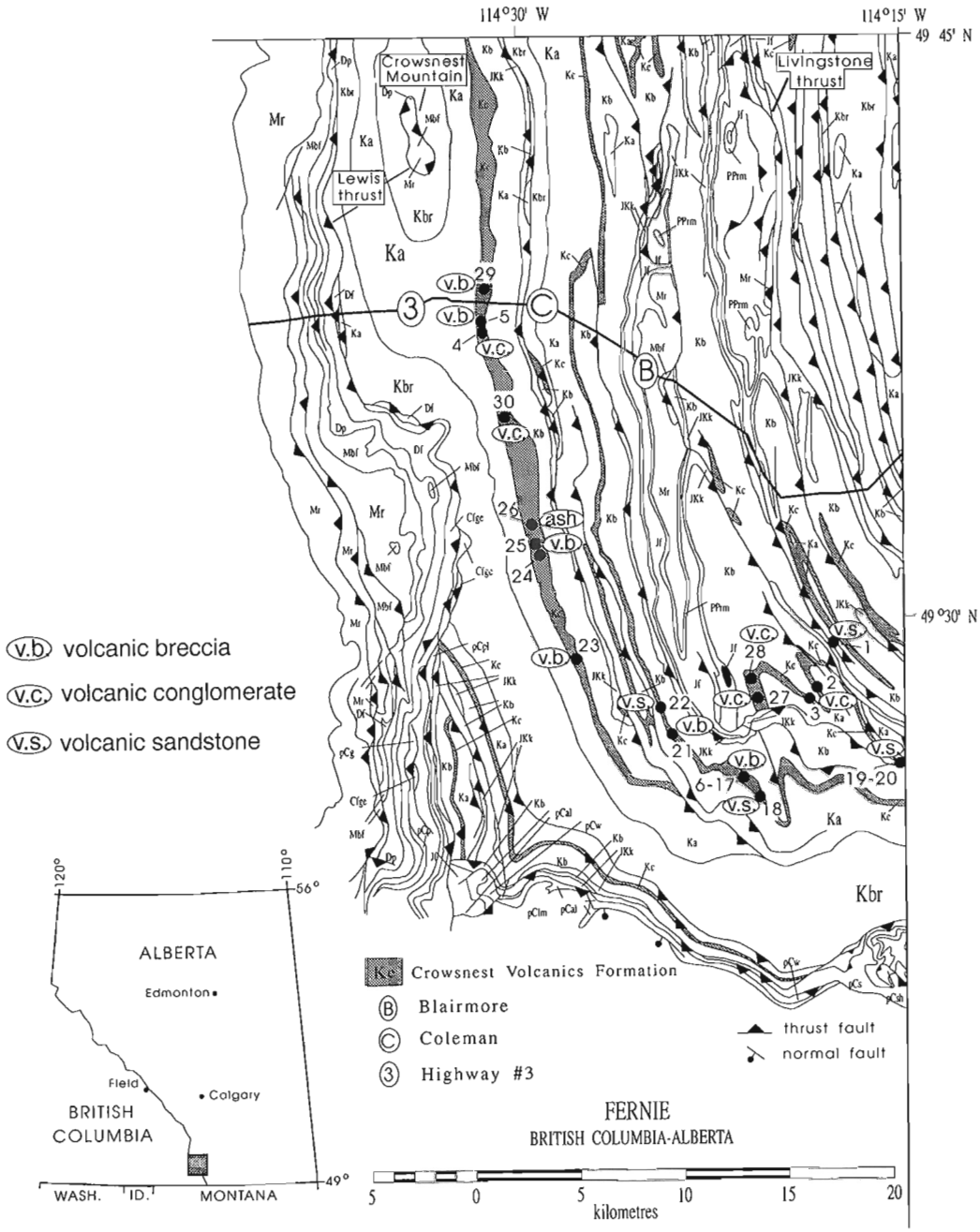

Figure 1. Geological map of the Coleman-Blairmore area, southwestern Alberta (Fernie geology compilation from Tony Peterson, pers. comm.), showing the distribution of the Crowsnest Volcanics Formation in grey. Sample locations refer to those in Table 1. Each station location includes a symbol that corresponds to the dominant rock type observed at the station.

element chemical analyses, and mineralogical compositions, from selected samples of the Crowsnest Volcanic unit. The project was initiated during the summer of 1992 by Ray Beiersdorfer, under the supervision of Tony Peterson (GSC, Ottawa), Roger Macqueen (GSC, Calgary), and Ed Ghent (U of C). Normand Bégin took over the project as principal contractor from October 1, 1993 to March 31, 1994. The results of all the work done by Bégin, Beiersdorfer and Ghent over that period are presented in this report.

Previous work

The Crowsnest Volcanics (CNV) of southwestern Alberta are best known as the type occurrence of blairmorite (analcime-phyric phonolite). The analcime-bearing volcanic rocks from the Crowsnest Pass region of Alberta were first described by Dawson (1885), Knight (1904) and MacKenzie (1914). No further work was published on the Crowsnest Volcanics until the 1960s (Norris, 1964; Pearce, 1967, 1970). The emphasis of the early work was on the volcanological and sedimentological aspects and/or the igneous petrogenesis. A long-standing debate concerning the primary or secondary origin of the analcime in the Crowsnest Volcanics has emerged over the years (MacKenzie, 1914; Pirsson, 1915; Ferguson and Edgar, 1978; Karlsson and Clayton, 1991, 1993; Pearce, 1993). Recent studies by Goble et al. (1993), Peterson and Currie (1993) and Peterson (pers. comm., 1994) suggest that analcime phenocrysts crystallize from a melt, as opposed to a conversion from primary leucite phenocrysts (e.g. Karlsson and Clayton, 1991). In this Alberta MDA-funded project, we did not intend to take part in this debate. However, an important aspect of this debate, particularly with regards to the secondary-origin hypothesis, is the character of the Crowsnest Volcanics low-temperature metamorphism. Is it compatible with crystallization of analcime-bearing alteration assemblages? Although a large emphasis has been put on the origin of the analcime over the last two decades, no detailed study has been published on the nature and extent of low-temperature metamorphism in the Crowsnest Volcanics, nor on its bearing on economic mineralization. These aspects are documented in this report.

GEOLOGICAL SETTING

The Crowsnest Volcanics rocks occur within a series of westward-dipping, north-striking, en echelon thrust sheets (Fig. 1). Crowsnest Volcanics rocks range in thickness from 0 to 400 m (Norris, 1964; Pearce, 1970). The Crowsnest Volcanics consist of volcanic breccias, agglomerates, volcanic-rich conglomerates, crystal tuffs, and tuffaceous sandstones (Norris, 1964). The Crowsnest Volcanics exhibit a high degree of lithological heterogeneity over short vertical and lateral distances. Based on fossil flora, Norris (1964) assigned the Crowsnest Volcanics to the Albian stage of the Early Cretaceous. Isotopic ages from extrusive fragments in the Crowsnest Volcanics are consistent with this assignment (Norris, 1964). The base of the Crowsnest Volcanics is a gradational contact with volcanogenic, nonmarine sandstones of the Blairmore Group (Lower Cretaceous). The top of the Crowsnest Volcanics is marked by a disconformity above which lie marine shales and siltstones of the Blackstone Formation (Upper Cretaceous). Most likely only the easternmost part of the Crowsnest Volcanics is exposed because the region to the west of the study area is covered by Paleozoic and older rocks of the Lewis thrust sheet (Fig. 1).

Depositional environment

The most abundant lithology in the Crowsnest Volcanics is a volcanic breccia which is heterolithic, poorly sorted, and lacks any internal stratification. Ricketts (1982) proposed that these breccias formed as lahars derived from the brecciation of trachytic domes and that meteoric water was responsible for their formation. Although several workers have reported flows within the Crowsnest Volcanics (e.g. Pearce, 1970), we have not observed flow-rocks in the field. Dykes within volcanic breccias and older sedimentary units occur sporadically.

Igneous petrogenesis

The igneous lithologies occurring in the Crowsnest Volcanics have been divided into three types according to the phenocrystic assemblages recognizable in the field (Peterson and Currie, 1993): 1) trachytes with sanidine+melanite; 2) analcime-phonolites with sanidine+analcime; and 3) blairmorites with analcime cumulates only. Based predominantly on the assumption that the analcime in the Crowsnest Volcanics crystallized from a magma, several workers (Pearce, 1967, 1970; Ferguson and Edgar, 1978; Peterson and Currie, 1993) have concluded that the Crowsnest Volcanics could have originated from a parental alkali basalt magma at depths greater than 20 km. According to Ferguson and Edgar (1978), the analcime phonolites and blairmorites could have formed as differentiates after the fractionation of a trachytic melt. Trace element data are completely incompatible with this interpretation (Peterson and Currie, pers. comm.) (e.g. no negative Eu anomaly) and thermobarometry and isotopic data strongly indicate the melting of mafic granulite at H_2O-saturated conditions (Peterson and Currie, pers. comm.).

PETROGRAPHY, WHOLE ROCK AND MINERAL CHEMISTRY

Sampling strategy, preparation, and analytical procedures

The goal of field sampling of the Crowsnest Volcanics was to obtain representative samples over the entire outcrop area. Each thrust slice was sampled at several places along strike. A larger number of samples was obtained from the Coleman thrust slice (Fig. 1). Of 105 hand samples collected from 29 different field locations (Fig. 1; Table 1), 62 were examined petrographically (Table 2). All of the sample preparation and analysis was performed at the Department of Geology and Geophysics, University of Calgary. During thin-section preparation, the epoxy was cured slowly (one week) at a low temperature (<50°C) to avoid any alteration of the zeolites

Table 1. A list of sample numbers, lithology, and UTM coordinates (North, East) for locations.

Station	Sample	Lithology	Quad	North	East	T.S.	XRF	Pet.	Probe	XRD ?	XRD
RBC92-1	1.1	v.c.g. sandstone	BM	5484700	695050	X					
	1.2	c.g. sandstone	BM	5484700	695050	X					
RBC92-2	2.1	crystal rich v.c.	BM	5482700	694750	X					
	2.2	kspar. rich v.c.	BM	5482700	694750	X					
	2.3	v.c.g. volc. breccia	BM	5482700	694750	X					
	2.4	garnet/kspar. rich epiclastic	BM	5482700	694750	X		X		Yes	Clay
RBC92-3	3.1	crystal rich c.g. v.c.	BM	5482250	694400	X					
	3.2	crystal rich c.g. v.c.	BM	5482250	694400	X	X	X	12-Mar	Yes	Clay
	3.3	matrix of c.g. volc. breccia	BM	5482250	694400	X					
	3.4	pink ? (kspar.)	BM	5482250	694400						
	3.5	vesicle rich rock (float)	BM	5482250	694400	X					
RBC92-4	4.1	c.g. v.c. or epi.	CN	5499950	677500	X	X	X		Yes	Clay
	4.2	c.g. v.c. w/ veins	CN	5499950	677500	X		X		Yes	Clay
	4.3	volc. breccia	CN	5499950	677500	X					
RBC92-5	5.1	volc. breccia	CN	5500500	677750	X		X	12-Mar		
	5.2	sill	CN	5500500	677750	X		X		Yes	
RBC92-6	6.1	volc. breccia	BM	5478600	691500	X					
RBC92-7	7.1	volc. breccia w/ pits	BM	5478600	691500	X					
	7.2	volc. breccia	BM	5478600	691500	X					
RBC92-8	8.1	volc. breccia w/ dike margin	BM	5478570	691500						
	8.2	volc. breccia	BM	5478570	691500	X		X			
RBC92-9	9.1	volc. breccia	BM	5478540	691500	24-Mar					
RBC92-10	10.1	ss. block in volc. breccia	BM	5478510	691500	24-Mar					
	10.2	volc. breccia	BM	5478510	691500	24-Mar					
RBC92-11	11.1	volc. breccia	BM	5478480	691500						
RBC92-12	12.1	volc. breccia	BM	5478450	691500	X		X	Yes/Lgt.	Yes	Clay
	12.2	volc. breccia w/ fibers?	BM	5478450	691500	24-Mar					
RBC92-13	13.1	volc. breccia	BM	5478420	691500	24-Mar					
RBC92-14	14.1	volc. breccia	BM	5478390	691500	24-Mar					
RBC92-15	15.1	volc. breccia (fresh)	BM	5478360	691500	24-Mar					
	15.2	volc. breccia (weathered)	BM	5478360	691500	24-Mar					
RBC92-16	16.1	volc. breccia	BM	5478330	691500	X		X		Yes	Clay
RBC92-17	17.1	garnet rich sandstone	BM	5478300	691500						
RBC92-18	18.1	volc. sandstone	BM	5477500	691950	X		X		Yes	Clay
	18.2	volc. sandstone	BM	5477500	691950	24-Mar					
RBC92-19	19.1	garnet rich volc. sandstone	BM	5480750	697150	X		X	Pol	Yes	Clay
	19.2	v.f.g. volc. sandstone	BM	5480750	697150	24-Mar					
RBC92-20	20.1	v.f.g. volc. sandstone	BM	5481000	697050						
	20.2	volc. sandstone w/ rip-ups	BM	5481000	697050	X	X	X	Yes/Lgt.	Yes	Clay
RBC92-21	21.1	analcime rich ?	BM	5480650	687700	X		X			
	21.2	volc. breccia w/o visible clasts	BM	5480650	687700						
	21.3	volc. breccia w/ visible clasts	BM	5480650	687700						
	21.4	c.g. volc. sandstone	BM	5480650	687700	X	X	X	Yes	Yes	7-Apr
	21.5	c.g. volc. sandstone	BM	5480650	687700						
	21.6	c.g. volc. sandstone	BM	5480650	687700						
	21.7	dike	BM	5480650	687700						
RBC92-21	21.8	dike	BM	5480650	687700	X	X	X	Yes	Yes	Clay
	21.9	kspar. rich volc. cong.	BM	5480650	687700	X		X	Yes	Yes	
RBC92-22	22.1	c.g. sandstone	BM	5481400	687200	X	X	X	12-Mar	Yes	7-Apr
RBC92-23	23.1	volc. breccia	BM	5483050	683250	X		X		Yes	
	23.2	volc. breccia	BM	5483050	683250						
RBC92-24	24.1	volc. breccia	CN	5489500	680550	X		X			
RBC92-25	25.1	volc. breccia	CN	5490200	680650						
	25.2	dike?	CN	5490200	680650						
	25.3	volc. breccia	CN	5490200	680650	X		X			
	25.4	volc. breccia	CN	5490200	680650						
RBC92-26	26.1	brown ash?	CN	5490550	680650	X		X			
	26.2	volc. breccia	CN	5490550	680650						
	26.3	garnet rich volc.	CN	5490550	680650						
	26.4	f.g. kspar. rich volc.	CN	5490550	680650						
	26.5	garnet rich volc.	CN	5490550	680650	X		X	12-Mar	Yes	7-Apr

Lithology abbreviations are: cc., calcite; c.g., coarse grained; v.c.g., very coarse grained; v.f.g., very fine grained; v.c., volcaniclastic rock; epi., epiclastic rock; ss., sandstone; volc., volcanic; v.s., volcanic sandstone; cong., conglomerate; foli., foliated; kspar., potassium feldspar; porph., porphyritic. Quadrant (Quad) abbreviations are: BM, Blairmore; CN, Crowsnest; FR, Fernie. Other columns are: T.S., thin section prepared; XRF, X-ray fluorescence analysis performed on whole rock powder; Pet., petrography performed; Probe, probe mount prepared; XRD, samples chosen for X-ray diffraction analysis.

Table 1. (cont.)

Station	Sample	Lithology	Quad	North	East	T.S.	XRF	Pet.	Probe	XRD ?	XRD
	26.7	kspar. rich volc. breccia	CN	5490550	680650						
RBC92-27	27.1	v.c.	BM	5482250	691850	X		X	Pol	Yes	7-Apr
RBC92-28	28.1	volc. breccia	BM	5483250	691300						
	28.2	v.c.	BM	5483250	691300	X		X		Yes	
RBC92-28	28.3	epidote?	BM	5483250	691300	X		X		Yes	Clay
RBC92-29	29.1	volc. breccia	CN	5500800	678000	X		X	Yes	Yes	7-Apr
	29.2A	volc. breccia	CN	5500800	678000						
	29.2B	volc. breccia	CN	5500800	678000						
	29.3	v.c.	CN	5500800	678000						
	29.4	v.c.	CN	5500800	678000	X	X			Yes	
	29.5A	sulfide rich v.c.	CN	5500800	678000	X	X	X	Pol	Yes	
	29.5B	black v.c.	CN	5500800	678000			X			
	29.6A	volc. breccia/v.c.	CN	5500800	678000						
	29.6B	volc. breccia/v.c.	CN	5500800	678000	X			Pol	Yes	7-Apr
	29.7	v.c.	CN	5500800	678000						
	29.8	v.c.	CN	5500800	678000						
	29.9	v.c.	CN	5500800	678000						
	29.10A	volc. breccia w/ black dike	CN	5500800	678000						
	29.10B	volc. breccia	CN	5500800	678000						
	29.11	v.c.	CN	5500800	678000						
	29.12A	grey dike	CN	5500800	678000	X	X	X	Pol	Yes	7-Apr
	29.12B	black dike	CN	5500800	678000						
	29.12C	black dike w/ cc vein	CN	5500800	678000						
	29.14	volc. breccia	CN	5500800	678000						
	29.15	volc. breccia/v.c.	CN	5500800	678000						
	29.16A	volc. breccia/v.c.	CN	5500800	678000						
	29.16B	volc. breccia/v.c.	CN	5500800	678000	X					
	29.17	volc. breccia/v.c.	CN	5500800	678000						
	29.18	volc. breccia	CN	5500800	678000						
	29.19	volc. breccia	CN	5500800	678000						
	29.20	volc. breccia	CN	5500800	678000	X		X	Yes	Yes	7-Apr
	29.21	volc. breccia	CN	5500800	678000						
	29.22A	red v.c.	CN	5500800	678000						
	29.22B	green v.c.	CN	5500800	678000						
	29.22C	red v.c.	CN	5500800	678000						
	29.22D	black ??	CN	5500800	678000						
	29.23	green volc. breccia	CN	5500800	678000	X	X	X	Yes	Yes	7-Apr
RBC92-29	29.24	Blairmore Sandstone	CN	5500800	678000	X		X		Yes	
	29.25	Blairmorite	CN	5500800	678000						
	29.26	Blairmorite (weathered)	CN	5500800	678000						
	29.27	float w/ cc. vein	CN	5500800	678000						
RBC92-30	30.1	kspar. rich v.c.	CN	5495250	679400	X		X			
	30.2	dark coloured v.c.	CN	5495250	679400						
RBC92-31	31.1	garnet/kspar. rich epiclastic	CN	5504650	678000						
RBC93-32	32.1	Volcanic Breccia	CN								
	32.2	Volcanic Breccia	CN								
	32.3	Fresh Analcite Phonolite	CN								
RBC93-33	33.1	Trachyte clast	CN								
RBC93-34	34.1	Trachyte	CN								
RBC93-35		Epiclastite	CN								
RBC93-36	36.1	Epiclastite	CN								
	36.2	Mudstone	CN								
	36.3	Epiclastite w/ charred wood	CN								
RBC93-37	37.1	Sandstone	CN								
RBC93-38	38.1	Red Siltstone	CN								
RBC93-39	39.1	Float-Felsite Dike or Hydro. Alt.	CN								
RBC93-40	40.1	Blairmore	CN								
RBC93-41	41.1	Volcanic	CN								
	41.2	Volcanic	CN								
RBC93-42	42.1	Epiclastite	FR								
	42.2	Epiclastite	FR								
	42.3	Epiclastite	FR								

present. Selected minerals in 15 samples were analyzed by electron microprobe analysis (Tables 1, 2). The mineral analyses were obtained using an ARL-SEMQ electron microprobe, equipped with nine wavelength dispersive spectrometers. Analytical conditions were 15 kV accelerating potential and 0.15 nA beam current. Spot size was 1 µm for all minerals except analcime (7 µm). Counting time was 20 seconds. Silicates were used as standards and the data were reduced using the methods of Bence and Albee (1968).

Ten samples were selected for analysis of whole-rock major and trace element composition (Tables 1, 3) using a Phillips PW1410 X-Ray Fluorescence Spectrometer (XRF) equipped with a Rhodium X-ray tube. Analytical conditions were 35 kV accelerating potential and 70 mA current. Nineteen samples were chosen for X-ray diffraction studies (XRD) (Table 1). Each sample was broken into fragments approximately 1 cm in diameter with a hammer. Further crushing was done using a hand steel and crush cylinder. The crushed sample was sieved and a <2 µm fraction was separated by centrifuge methods. Samples were glycol solvated at 60°C for

Table 2. Mineral occurrences in samples of the Crowsnest Volcanics. See Figure 1 for location. Sample numbers (No.) are according to the station location followed by the sample label (e.g. station 18, sample label 2 = sample number 18.2). Mineral abbreviations are from Kretz (1983), except for: Px, pyroxene; Adl, adularia; Am, amphibole; and Msc, miscellaneous.

		Primary phases (igneous phenocrysts)					Secondary phases (metamorphic alteration)									
No.	Rock	Kfs	Grt	Px	Ttn	Anl	Prh	Pmp	Ep	Chl	Ab	Adl	Qtz	Cal	Am	Msc
1.1	v.s.	x			x				x	x	x		x			a
1.2	v.s.	x							x	x	x		x			a,b
2.1	v.c.	x			x						x		x	x		c
2.2	v.b.	x	x		x						x	?				c
2.3[G]	v.b.	x	x							x		x	x			
2.4	epi.	x	x						x	x		x		x		c
3.1	v.c.	x	x		x		?						x	x		
3.2	v.c.	x	x		x	x			x	x	x	x	x	x		v1
3.3	v.b.	x	x	x		x							x	x		c
4.1	v.c.	x	x						x				x	x		d
4.2	v.c.	x	x	x					x		x		x	x		c
4.3	v.b.	x									x	x	x	x		c
5.1	v.b.	x	x		x				x			x	x	x		
6.1	v.b.	x	x	x	x	x			x				x			
7.1	v.b.	x	x	x					x		x			x		
7.2	v.b.	x	x	x		x						x	x			
8.2	v.b.	x	x	x		x						x				
9.1	v.b.	x	x	x		x						x				
10.1	v.b.	x	x			x					x	x				
10.2	v.b.	x	x	x		x				x			x			
12.1	v.b.	x	x			x					x		x		x	c
12.2	v.b.	x	x	x	x	x							x			
13.1	v.b.	x	x			x			x		x					
14.1	v.b.	x	x	x	x	x										
15.1	v.b.	x	x		x	x						x	x			
15.2	v.b.	x	x		x							x	x			
16.1	v.b.	x	x	x	x	x						x	x			
18.1	v.s.	x	x	x	x	x				x			x	x		
18.2	v.s.	x	x		x				x	x		x	x	x		
19.1	v.s.	x			x	x				x						e
19.2	v.s.	x			x	x				x			x			c
20.1	v.s.	x	x		x	x				x				x		
20.2	v.s.	x			x	x				x						e

at least 12 hours and heat treated at 550°C for 30 minutes. A light mineral fraction (specific gravity <2.45) was separated from the 100 to 200 mesh sieved portion using heavy liquids. A Phillips-Norelco X-Ray Diffractometer with FeKα radiation was operated at 40 kV accelerating potential and 20 mA current was used.

Petrography of igneous (primary) assemblages

Mineral assemblages of 62 samples are listed in Table 2. Igneous phenocrysts are represented by euhedral crystals of sanidine, melanite-garnet, aegirine/augite-pyroxene and analcime. Sanidine is by far the most common primary phase encountered in any rock type observed in the field (Table 2). Rocks with abundant modal analcime (>40%; Table 2) are found in either volcanic breccia or volcanic sandstone. Titanite is also common in most samples examined. Oriented sanidine laths define a trachytic texture in the matrix. Heterolithic fragments containing some of the phenocrysts described above were observed in a few samples (sample 10.2, Fig. 2a). Xenocrystic garnets and pyroxenes are present in several samples. Opaque minerals are rare and consist primarily of pyrite with some ilmenite. Average compositions of analcime phenocryst are listed in Table 4. The compositions of analcime phenocryst documented here are comparable to those reported by Ferguson and Edgar (1978) (Fig. 3).

Table 2. (cont.)

		Primary phases (igneous phenocrysts)					Secondary phases (metamorphic alteration)									
No.	Rock	Kfs	Grt	Px	Ttn	Anl	Prh	Pmp	Ep	Chl	Ab	Adl	Qtz	Cal	Am	Msc
21.1	v.b.	x	x			x				x			x	x		c,e
21.2	v.b.	x	x	x	x	?					?	x	x	x		
21.3	v.b.	x	x	x	x	x				x			x			
21.4	v.s.	x	x		x					x		x	x	x		
21.6	v.s.	x	x		x	?				x	x		x	x		
21.7	dike	x	x	x	x	x				x			x			
21.8	dike	x	x		x					x	x			x		
21.9	v.cg.	x	x		x		x		x		x		x			
22.1	v.s.	x	x	x	x		x				x	?	x	x		f
23.1	v.b.	x	x	x	x					x	x		x	x		
24.1	v.b.	x	x	x	x					x	x					c
25.1	v.b.	x	x	x	x						x		x	x		
25.2	dike	x	x		x						x	x	x	x		
25.3	v.b.	x	x	x	x							x		x		
25.4	v.b.	x	x	x					x				x	x		
26.5	ash	x	x	x		x				x		x		x		v2
27.1	v.c.	x		x	x	x				x				x		e
28.2	v.c.	x			x					x	x		x			c
28.3	v.c.	x	x		x					x		x	x			
29.1	v.b.	x	x	x		?				x	x	x		x		
29.4	v.c.	x								x			x	x	x	
29.5A	v.c.	x		x						x		x	x	x		
29.6B	v.b.	x		x	x					x		x	x	x		
29.12A	dike	x		x	x					x		x	x	x		
29.16B	v.b.	x								x		x	x	x		b,c
29.20	v.b.	x	x		x				x	x		x	x	x	x	d
29.23[G]	v.b.	x	x	x						x			x	x		
29.24	v.s.	x	x	x	x					x	x		x			
30.1	v.c.	x		x	x						x		x	x		

a, sericite/muscovite; b, biotite; c, opaque mineral (unidentified); d, rutile needles on potassium feldspar; e, lots of analcime (> 40 %); f, laumontite identified by XRD analysis; G, large euhedral Ti-garnet; mode and rim-rim transects done on sample 29.23; v1, vein of analcime and quartz together; v2, vein of analcime alone

Table 3. XRF whole rock analysis for major and trace elements.

Element	3.2	4.1	20.2	21.4	21.8	22.1	29.4-1	29.4-2	29.5A-1	29.5A-2	29.12A-1	29.12A-2	29.23	29.4-OX	29.5A-OX	29.12A-OX
SiO_2*	66.2 ± 0.098	55.1 ± 0.235	56.6 ± 0.106	61.1 ± 0.122	60.7 ± 0.124	58.1 ± 0.149	51.4 ± 0.222	51.2 ± 0.118	50.9 ± 0.123	50.8 ± 0.044	53.8 ± 0.101	53.6 ± 0.158	6.2 ± 0.105	53.9 ± 0.136	53.9 ± 0.076	55.8 ± 0.166
Al_2O_3	17.3 ± 0.041	16.8 ± 0.033	16.7 ± 0.033	18.2 ± 0.041	18.2 ± 0.062	18.6 ± 0.071	16.3 ± 0.036	16.3 ± 0.037	14.9 ± 0.150	15.0 ± 0.033	16.3 ± 0.077	16.2 ± 0.027	19.8 ± 0.035	17.1 ± 0.050	15.8 ± 0.072	16.9 ± 0.036
Fe_2O_3	2.96 ± 0.005	6.87 ± 0.061	9.15 ± 0.003	3.44 ± 0.006	3.46 ± 0.006	5.70 ± 0.010	7.42 ± 0.021	7.44 ± 0.006	6.50 ± 0.034	6.51 ± 0.021	7.01 ± 0.018	7.01 ± 0.022	2.83 ± 0.004	7.77 ± 0.043	6.83 ± 0.021	7.27 ± 0.016
MgO	0.39 ± 0.049	0.86 ± 0.032	2.08 ± 0.013	0.56 ± 0.084	0.568 ± 0.036	0.921 ± 0.021	0.689 ± 0.020	0.173 ± 0.053	0.539 ± 0.029	0.542 ± 0.029	0.560 ± 0.022	0.527 ± 0.035	0.277 ± 0.044	0.711 ± 0.029	0.583 ± 0.022	0.557 ± 0.052
Na_2O	4.93 ± 0.080	1.13 ± 0.021	6.94 ± 0.037	2.97 ± 0.016	1.71 ± 0.060	5.15 ± 0.039	0.746 ± 0.029	0.748 ± 0.025	0.460 ± 0.033	0.462 ± 0.040	0.457 ± 0.038	0.415 ± 0.035	5.05 ± 0.055	0.794 ± 0.039	0.481 ± 0.012	0.489 ± 0.025
CaO	1.15 ± 0.007	2.94 ± 0.020	1.42 ± 0.001	2.07 ± 0.016	1.10 ± 0.007	2.35 ± 0.007	4.34 ± 0.028	4.34 ± 0.013	6.01 ± 0.016	6.02 ± 0.029	2.87 ± 0.005	2.88 ± 0.016	4.08 ± 0.017	4.50 ± 0.032	6.28 ± 0.041	2.96 ± 0.018
K_2O	4.75 ± 0.013	11.1 ± 0.015	0.281 ± 0.016	8.30 ± 0.017	11.8 ± 0.035	5.82 ± 0.021	11.8 ± 0.042	12.0 ± 0.022	12.4 ± 0.004	12.4 ± 0.015	13.1 ± 0.020	13.1 ± 0.037	6.88 ± 0.014	12.4 ± 0.012	12.9 ± 0.010	13.6 ± 0.007
TiO_2	0.295 ± 0.005	0.785 ± 0.035	1.24 ± 0.003	0.416 ± 0.012	0.390 ± 0.019	0.663 ± 0.024	0.734 ± 0.052	0.772 ± 0.029	0.652 ± 0.021	0.665 ± 0.020	0.623 ± 0.022	0.637 ± 0.026	0.339 ± 0.015	0.817 ± 0.024	0.705 ± 0.005	0.679 ± 0.006
P_2O_5	0.079 ± 0.001	0.270 ± 0.003	0.256 ± 0.002	0.083 ± 0.003	0.117 ± 0.006	0.150 ± 0.003	0.227 ± 0.003	0.228 ± 0.005	0.251 ± 0.003	0.252 ± 0.005	0.299 ± 0.002	0.299 ± 0.006	0.049 ± 0.004	0.237 ± 0.003	0.267 ± 0.003	0.310 ± 0.004
MnO	0.089 ± 0.001	0.165 ± 0.005	0.233 ± 0.000	0.110 ± 0.002	0.108 ± 0.004	0.220 ± 0.010	0.197 ± 0.009	0.202 ± 0.008	0.246 ± 0.010	0.249 ± 0.008	0.151 ± 0.004	0.154 ± 0.007	0.143 ± 0.007	0.205 ± 0.008	0.252 ± 0.007	0.165 ± 0.004
SO_3	<d1	0.122 ± 0.004	0.254 ± 0.011	<d1	<d1	<d1	1.46 ± 0.013	1.41 ± 0.011	1.26 ± 0.003	1.13 ± 0.008	1.53 ± 0.007	1.56 ± 0.011	<d1	0.136 ± 0.002	0.353 ± 0.007	0.136 ± 0.002
V**	90.3 ± 2.90	392.0 ± 3.08	367.0 ± 7.85	170.0 ± 6.07	75.8 ± 2.99	180.0 ± 4.18	383.0 ± 4.65		345.0 ± 11.03		367.0 ± 7.00		59.8 ± 1.55			
Cr	47.5 ± 0.70	24.0 ± 1.31	15.3 ± 0.54	33.7 ± 1.17	24.0 ± 1.16	26.0 ± 0.59	17.4 ± 0.88		17.0 ± 0.66		13.0 ± 0.24		35.2 ± 1.18			
Ni	6.2 ± 0.92	5.0 ± 1.37	4.8 ± 1.22	5.2 ± 1.53	11.2 ± 0.19	8.1 ± 1.03	4.8 ± 0.78		5.5 ± 2.14		4.0 ± 0.96		4.1 ± 1.05			
Zn	92.6 ± 1.84	106.0 ± 1.58	120.0 ± 0.55	74.9 ± 1.93	111.0 ± 3.50	115.0 ± 0.57	127.0 ± 2.20		114.9 ± 2.07		160.3 ± 0.73		91.9 ± 1.78			
Ga	23.5 ± 1.28	26.8 ± 1.96	26.5 ± 0.57	23.1 ± 1.18	23.4 ± 0.67	22.6 ± 1.15	28.9 ± 0.66		26.0 ± 0.56		32.2 ± 1.01		24.3 ± 1.99			
Rb	153.0 ± 1.10	291.0 ± 2.00	14.4 ± 0.35	193.0 ± 2.47	272.0 ± 3.38	125.0 ± 0.24	509.0 ± 3.55		436.0 ± 3.23		419.0 ± 1.76		209.0 ± 3.50			
Sr	1186.0 ± 8.78	1413.0 ± 5.18	372.0 ± 0.92	2827.0 ± 12.0	978.0 ± 4.71	2009.0 ± 19.83	938.0 ± 8.85		950.7 ± 6.67		1280.2 ± 4.01		2680.0 ± 26.0			
Y	11.5 ± 0.85	16.3 ± 1.08	18.3 ± 0.39	15.2 ± 1.46	17.6 ± 0.18	25.5 ± 0.69	17.6 ± 3.60		10.9 ± 3.05		12.4 ± 1.01		15.6 ± 2.26			
Zr	174.0 ± 3.38	169.0 ± 2.31	217.0 ± 0.81	112.0 ± 4.74	212.0 ± 2.75	201.0 ± 5.73	181.0 ± 6.00		141.8 ± 2.76		142.5 ± 0.91		186.0 ± 9.27			
Nb	30.2 ± 0.85	93.5 ± 1.18	34.1 ± 0.61	35.3 ± 0.40	34.6 ± 1.65	34.1 ± 1.27	98.4 ± 0.94		106.0 ± 0.94		101.3 ± 1.06		42.7 ± 1.30			
Ba	1667.0 ± 31.04	4167.0 ± 61.25	339.0 ± 8.51	4000.0 ± 69.57	2428.0 ± 32.0	3086.0 ± 59.0	4584.0 ± 17.0		5670.0 ± 117.0		5011.0 ± 26.0		2166.0 ± 59.0			
La	38.9 ± 2.85	60.2 ± 0.87	49.6 ± 2.28	41.9 ± 1.91	54.1 ± 0.84	69.5 ± 1.27	74.1 ± 7.06		80.1 ± 0.76		84.6 ± 1.58		68.4 ± 4.28			
Pb	26.6 ± 1.42	47.9 ± 2.12	22.6 ± 0.85	13.4 ± 1.76	26.6 ± 3.01	21.9 ± 1.26	49.0 ± 1.49		61.3 ± 2.09		80.8 ± 2.29		20.0 ± 0.40			
Th	8.8 ± 0.58	20.8 ± 1.48	13.5 ± 0.72	6.5 ± 0.40	7.5 ± 0.13	11.5 ± 1.74	25.9 ± 3.46		23.9 ± 1.74		26.8 ± 0.17		11.0 ± 0.68			
LOI*	1.52 ± 0.028	2.48 ± 0.026	5.82 ± 0.059	1.85 ± 0.015	1.45 ± 0.035	1.76 ± 0.020	4.91 ± 0.015	4.91 ± 0.015	5.58 ± 0.017	5.58 ± 0.017	3.20 ± 0.006	3.20 ± 0.006	3.82 ± 0.029	0.0	0.0	0.0
Sum*	100.0	99.4	101.1	99.8	100.1	100.1	100.9	100.3	100.4	99.6	100.7	99.6	100.0	98.6	98.4	98.9

*=%; **=ug/g

a. Lithoclast with analcime and pyroxene phenocrysts (sample 10.2). Anl, analcime; Px, pyroxene.

b. Analcime alteration to calcite (sample 3.3). Anl, analcime; Cal, calcite.

c. Lithoclast with trachytic alignment of albite lamellae. Pyroxene phenocrysts are partially replaced by calcite (sample 21.2).

d. Abundant calcite veining cutting across the matrix and sanidine phenocrysts (sample 2.1). Kfs, sanidine phenocryst; Cal, calcite.

e. Vein of analcime and quartz (sample 3.2). Anl, analcime; Qtz, quartz.

f. Interstitial analcime between garnet phenocrysts. Analcime phenocrysts are also abundant (sample 21.1). Kfs, sanidine phenocryst; Grt, garnet; Anl, analcime.

g. Prehnite (Prh) in amygdule (sample 22.1).

h. Melanite-garnet (Grt) phenocryst with strong optical oscillatory zoning (sample 29.23).

***Figure 2.** Photomicrographs of the Crowsnest Volcanics. Scale bars are in micrometres.*

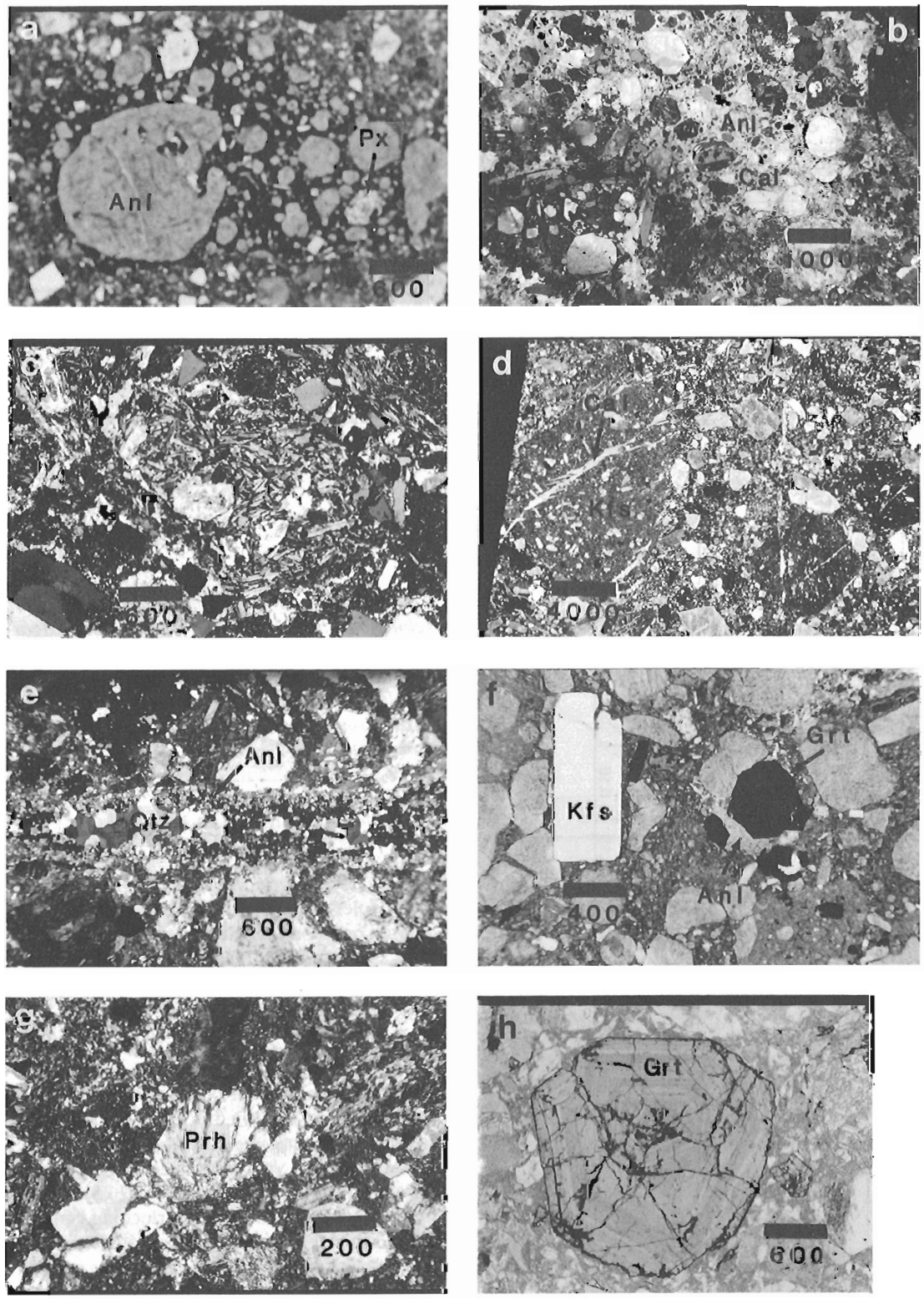
a
Anl
Px
600
b
Anl
Cal
1000
c
600
d
Cal
Kfs
1000
e
Anl
Qtz
600
f
Kfs
Grt
Anl
400
g
Prh
200
h
Grt
600

Table 4. Microprobe analyses of analcime phenocrysts (phenoxt), veinal analcime (veinal), and amygdular prehnite.

Sample	SiO_2	Al_2O_3	FeO	MnO	MgO	CaO	Na_2O	K_2O	H_2O	Total	Si	Al	Fe	Mn	Mg	Ca	Na	K
10.1 phenoxt	57.35	21.65	0.11	0.00	0.00	0.01	12.31	0.02	8.24	99.69	2.085	0.928	0.003	0.000	0.000	0.000	0.868	0.001
26.5 phenoxt	58.45	22.56	0.07	0.02	0.00	0.05	10.42	0.05	8.34	99.96	2.100	0.955	0.002	0.001	0.000	0.002	0.726	0.002
3.2 phenoxt	58.55	20.09	0.00	0.00	0.00	0.00	11.66	0.35	7.89	98.55	2.141	0.866	0.000	0.000	0.000	0.000	0.827	0.016
19.1 phenoxt	56.27	21.75	1.41	0.01	0.02	0.07	12.46	0.13	8.06	100.18	2.053	0.935	0.043	0.000	0.001	0.003	0.882	0.006
3.2 veinal	58.17	20.84	0.01	0.00	0.00	0.00	10.67	0.63	8.19	98.51	2.129	0.899	0.000	0.000	0.000	0.000	0.757	0.029
3.2 veinal	58.20	20.85	0.02	0.00	0.00	0.00	11.01	0.65	8.20	98.94	2.124	0.897	0.001	0.000	0.000	0.000	0.779	0.030
3.2 veinal	59.54	20.58	0.01	0.00	0.00	0.00	10.27	0.68	8.29	99.37	2.154	0.877	0.000	0.000	0.000	0.000	0.720	0.031
22.1 prehnite	44.56	20.30	4.13	0.09	0.02	26.19	0.10	0.00	4.28	99.67	3.105	1.667	0.217	0.005	0.002	1.956	0.013	0.000

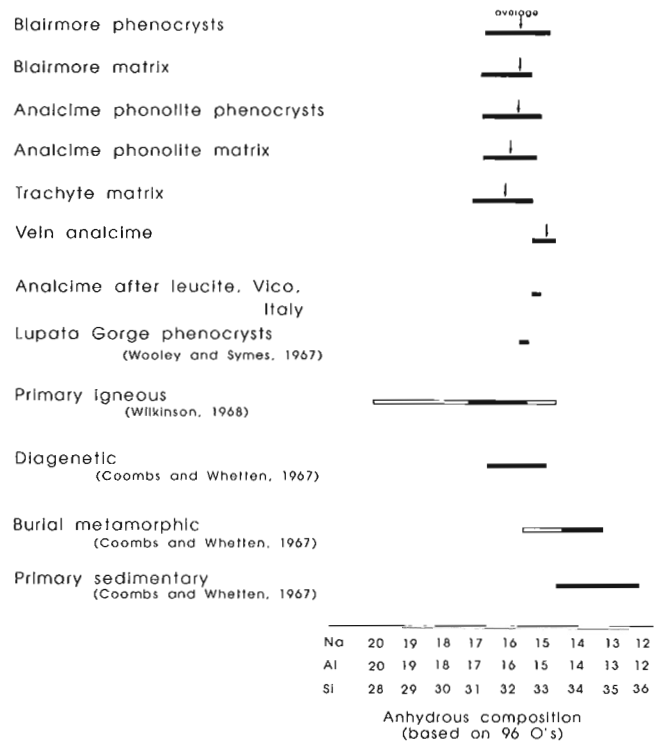

Figure 3. *Range of analcime compositions in Crowsnest suite relative to other suites (Ferguson and Edgar, 1978). The compositions of analcime phenocrysts and veinal analcime reported here are similar to those summarized by Ferguson and Edgar (1978) for the Crowsnest Volcanics. Heavy boxes indicate bulk of analyses, dashed boxes extreme compositions.*

Metamorphic alteration assemblages

Alteration assemblages are dominantly in the matrix as a mixture of fine grained chlorite, quartz, calcite, and albite. Amygdules are commonly filled by albite microlaths, calcite, chlorite or colourless clusters of radiating aggregates of adularia. Microprobe analyses of adularia are listed in Table 4. Most of the igneous phases are fresh, although some have been pseudomorphed by calcite (sample 3.3, Fig. 2b; sample 21.2, Fig. 2c). Calcite veining is also abundant in some samples (sample 2.1, Fig. 2d).

In addition to their occurrence as phenocrysts, veins of analcime were identified in two samples (3.2, 26.5). In one sample (3.2), analcime occurs as idioblastic equant isotropic crystals lining a vein with quartz in the centre (sample 3.2, Fig. 2e). Another sample (sample 26.5) contains veins composed solely of colourless interlocking xenoblastic analcime that exhibits faint birefringence. Veinal analcime in both samples cuts across phenocrysts of sanidine and garnet, as well as lithoclasts with a trachytic alignment of albite lamellae. Interstitial analcime in the groundmass between garnet phenocrysts was also observed (sample 21.1, Fig. 2f). The veinal and interstitial nature of this analcime are our reasons for interpreting it as a product of late alteration (metamorphic), as opposed

Table 5. Microprobe analyses of veinal albite (alb-vein), adularia in matrix (adl-mtrx) and in amygdules (adl-amyg).

Sample		SiO_2	Al_2O_3	CaO	Na_2O	K_2O	Total	Si	Al	Ca	Na	K
R9.1	adl-amyg	64.54	18.25	0.01	2.00	13.89	98.69	2.999	1.000	0.000	0.180	0.823
R10.1	alb-vein	68.95	19.65	0.07	11.52	0.08	100.27	2.999	1.007	0.003	0.972	0.004
R10.1	adl-mtrx	65.87	19.29	0.01	1.15	13.74	100.06	2.999	1.035	0.000	0.102	0.798
R18.2	adl-amyg	65.03	18.21	0.14	1.95	13.95	99.28	3.004	0.991	0.007	0.175	0.822
R18.2	adl-mtrx	63.78	19.04	0.17	1.09	14.47	98.55	2.972	1.046	0.008	0.098	0.860
R26.5	adl-mtrx	65.98	18.62	0.20	3.75	11.43	99.98	2.999	0.997	0.010	0.331	0.663

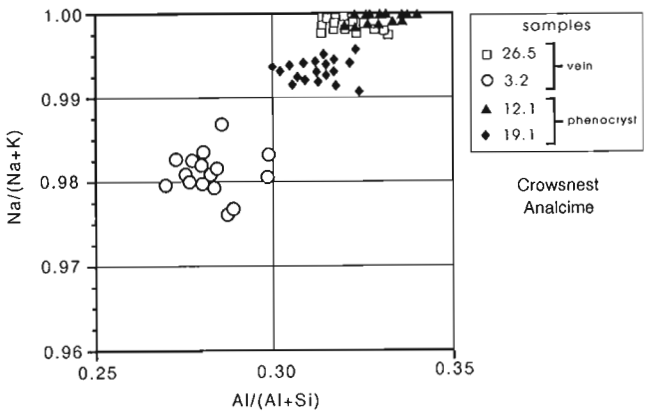

Figure 4. Plot of the distribution of Na/(Na+K) against Al/(Al+Si) in analcimes of this study.

to a product of igneous crystallization. Similar distinct generations of analcime have been described recently by Goble et al. (1993) in an analcime phonolite sill from the Proterozoic Purcell Supergroup of southwestern Alberta. Microprobe analyses of veinal analcime are listed in Table 5. The compositions of veinal analcime reported here exhibit a wider range of Na, Al and Si (Fig. 4) than the Crowsnest Volcanics vein analcime compositions of Ferguson and Edgar (1978). In addition, they overlap with those of Crowsnest Volcanics phenocrysts and matrix analcime (Fig. 4) as well as with compositions of analcime from burial metamorphic rocks (Coombs and Whetten, 1967).

Other alteration minerals identified include laumontite and prehnite. Although not observed in thin section, laumontite was identified by XRD of the low specific gravity fraction (<2.45) from a separate of sample 22.1, a prehnite-bearing sample. In the study area, laumontite had been detected previously by Miller and Ghent (1973) as a pore-filling cement in the underlying nonmarine sandstones of the Blairmore Group. Prehnite was identified in one sample (22.1) in which it occurs as colourless, radiating aggregates of bladed or columnar hypidioblastic crystals (Fig. 2g). Microprobe compositions of prehnite are listed in Table 5. Average XFe for this sample is 0.12 which is comparable to the X_{Fe} reported for other very-low temperature metamorphic (e.g., zeolite facies) terranes (Cho et al., 1986; Bevins et al., 1991).

Whole rock XRF chemistry

X-ray fluorescence for bulk and trace analyses were done for ten rock powders (Table 3). Degree of metamorphic alteration in these rocks is quite variable, with chlorite and/or calcite as a secondary phase. All the samples analyzed contain sanidine as the most abundant phenocryst. Rocks with garnet and/or analcime, in addition to sanidine phenocrysts, in general are richer in SiO_2, Al_2O_3, and Na_2O, and poorer in Fe_2O_3 and K_2O than those with only sanidine as primary igneous phase. Data from Peterson (pers. comm., 1993), for relatively unaltered Crowsnest Volcanics rocks, show different trends with analcime and garnet rocks having less SiO_2 than sanidine rocks, while phonolites have less SiO_2 than trachytes. Fourteen trace elements (V, Cr, Ni, Zn, Ga, Rb, Sr, Y, Zr, Nb, Ba, La, Pb, Th) were analyzed (Table 3). With the available data, no direct correlation can be made between a given element and the primary rock assemblage. Except for Sr and Ba values ranging from ~1000 to 5000 ppm, concentrations of most of the elements are usually very low (<200-300 ppm), especially for base metals (Zn, Pb, Ni, Cr) with values of less than 160 ppm (Table 3). Whole rock analyses of Peterson (pers. comm., 1993) give copper values of less than 100 ppm. The similarity between altered rocks (this study) and less altered rocks of the Crowsnest Volcanics Formation in trace elements suggests that metamorphic alteration was not responsible for an enrichment or a depletion in the primary distribution of minor elements.

PHYSICAL CONDITIONS OF METAMORPHIC ALTERATION

A detailed investigation of the petrology and physical conditions (pressure, temperature, fluid composition) for the alteration of the Crowsnest Volcanics is in preparation (Bégin, Ghent and Beiersdorfer, unpublished data). For this report, only the principal thermobarometric results are presented.

Although diagnostic, low-variance assemblages have not been observed in the Crowsnest Volcanics, the pressure and temperature of metamorphism can be estimated with the petrogenetic grid of Frey et al. (1991) for very low grade rocks. The presence of prehnite and laumontite in sample 22.1 constrain the burial depth of late alteration between 0.9 and 2.9 kbar, for a temperature range of 200 and 250°C. This range

of pressure estimate includes that of maximum burial depths, between 4.7 and 7.8 km, given a structural-stratigraphic reconstruction (Ghent and Miller, 1974) for rocks of the Blairmore Group, stratigraphically below the Crowsnest Volcanics rocks. More accurate pressure-temperature (P-T) estimates for the Crowsnest Volcanics metamorphic alteration is provided by the multiequilibrium program TWEEQU of Berman (1991). The veins of coexisting analcime and quartz (sample 3.2, Fig. 2d) indicate an upper temperature limit of 200°C (Fig. 5), while the presence of laumontite (sample 22.1) indicates an upper pressure limit of 3.0 kbar (10 km) for the univariant assemblage Anl+Qtz+Ab (Fig. 5). Such estimates are also in agreement with those stated above. Alteration temperatures based on chlorite thermometry (Cathelineau and Viena, 1985) give results in the scatter of estimates in the range of 150 to 300°C (Fig. 6).

ECONOMIC MINERAL POTENTIAL

As mentioned earlier, base metals (Zn, Cu, Pb, Ni, Cr) contents are minor (<200-300 ppm). Other than Ba and Sr, rare-earth values are low. Gossan zones of notable size were not observed in the field, and sulphide and oxide minerals are rare in the rocks examined in this study. Peterson and Currie (1993) have reported a significant pyrite content associated with cumulate clasts in a lithic tuff at Coleman.

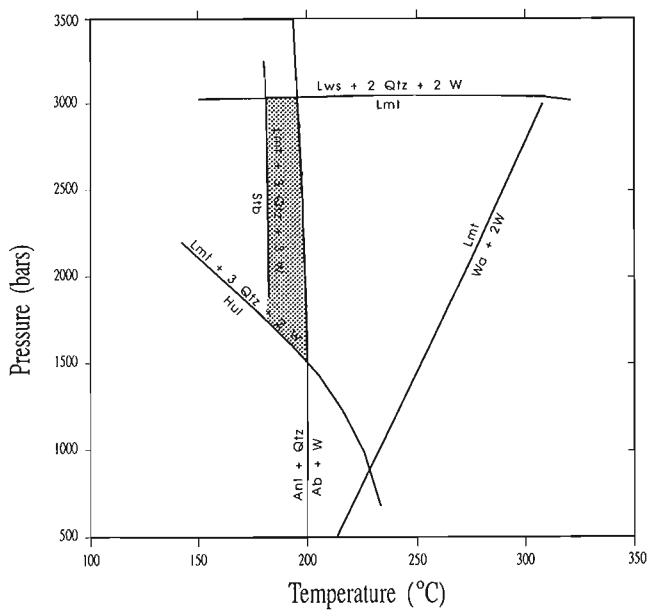

Figure 5. Petrogenetic grid for low-temperature analcime- and laumontite-bearing alteration assemblages in the Crowsnest Volcanics. The equilibrium curve of Anl+Qtz=Ab+W (water) was calculated with the program TWEEQU of Berman (1991). The position of laumontite-bearing equilibria are from de Capitani and Liou (in press). The coexistence of analcime+quartz in veins and presence of laumontite constrain the PT conditions of this low grade metamorphism between 1.5 and 3.0 kbar and Â°C (heavy line).

Any anomalous gold values could be associated with pyrite. The clearly volcaniclastic origin for the Crowsnest Volcanics and lack of flows have probably prevented the preservation of any syngenetic-related mineral ore as massive horizons. The metamorphic alteration does not appear to have remobilized and/or concentrated the primary contents of base metals and gold, as shown earlier by similarity in chemistry between altered and relatively unaltered rocks and the general lack of secondary sulphides and oxides.

Some samples examined contain up to 40 per cent modal analcime phenocrysts (Table 2). Iron contamination preventing their freshness could cause a problem for an industrial mining operation (Peterson and Currie, 1993). Analcime is sometimes altered to calcite as well (e.g. Fig. 2b). The presence of garnet as up to 10 per cent of the whole rock volume indicates that garnet might be mined for its abrasive properties. One of the best outcrops of Crowsnest Volcanics with abundant garnet is located just west of the community of Coleman, on Highway 3 (location 29, Fig. 1). Garnets in the field are fresh and usually euhedral with a size of 2 to 6 mm. Their colour is dark brown to black in the outcrops. In thin section, they are yellow and display strong optical oscillatory zoning (Fig. 2h). Microprobe analyses (Table 6) show that their chemistry is typical of a melanite garnet with 2 to 5 wt.% TiO_2, 5 to 10 wt.% Al_2O_3, 31 to 32 wt.% CaO and 16 to 22 wt.% total iron as FeO. Based on stoichiometric calculations, 25 to 30 per cent of the iron is ferric. Rim-to-rim chemical zonation is very erratic (Fig. 7) and probably reflects a primary crystallization feature.

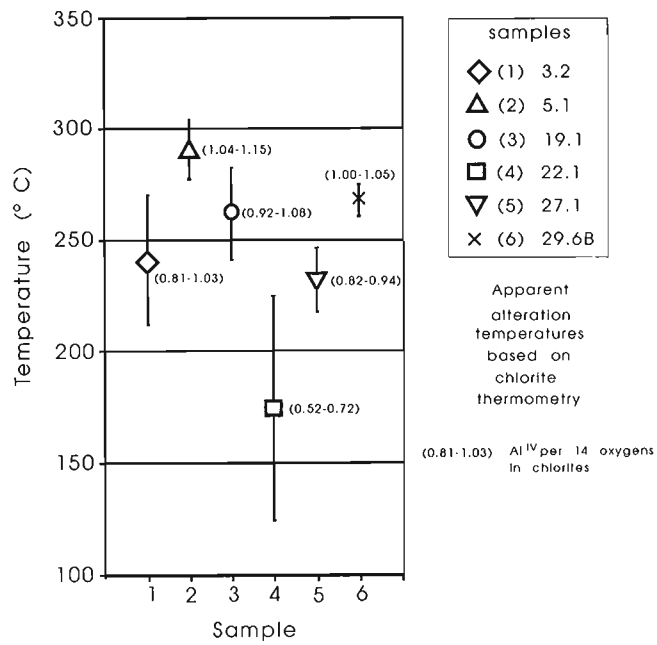

Figure 6. Alteration temperatures based on chlorite thermometry from matrix chlorite, using the calibration of Cathelineau and Viena (1985).

Table 6. Microprobe analyses of melanite-garnet (sample 29.23) for lowest (low) and highest (high) wt.% TiO_2 and Al_2O_3. Fe is total iron (Fe^{2+}+Fe^{3+}). TFA=Ti/(Ti+Al+Fe^{3+}); ATF=Al/(Al+Ti+Fe^{3+}).

Sample	SiO_2	TiO_2	Al_2O_3	FeO	MnO	MgO	CaO	Total	Si	Ti	Al	Fe	Mn	Mg	Ca	Fe^{3+}	Fe^{3+}/Fe	TFA	ATF	Ca/FeCa
29.23 high-Ti	34.94	5.27	5.95	18.56	0.86	0.30	31.63	97.51	3.018	0.342	0.606	1.341	0.063	0.039	2.928	0.337	0.251	0.267	0.472	0.745
29.23 low-Ti	36.67	2.09	7.96	18.70	1.28	0.23	31.21	98.14	3.119	0.134	0.798	1.330	0.092	0.029	2.845	0.348	0.261	0.105	0.624	0.743
29.23 high-Al	36.13	3.97	9.70	16.02	1.25	0.22	30.93	98.22	3.025	0.250	0.957	1.122	0.089	0.027	2.775	0.246	0.219	0.172	0.659	0.760
29.23 low-Al	35.31	3.34	4.85	21.62	1.02	0.28	30.98	97.40	3.098	0.220	0.502	1.586	0.076	0.037	2.912	0.431	0.272	0.191	0.435	0.716

To summarize, the economic potential for mineralization in the Crowsnest Formation appears to be low. No evidence for cogenetic carbonatites, an alternative source for certain metal ores, was found.

CONCLUSIONS

The Crowsnest Volcanics rocks are dominated by volcanic breccias, commonly epiclastics and rare pyroclastics. Igneous phases consist mainly of sanidine feldspar, melanite garnet, and analcime within a matrix with trachytic alignment of albite lamellae of sanidine laths. Aegirinite-augite pyroxene and titanite are also present. Petrological study of the Crowsnest Formation has documented alteration assemblages consistent with crystallization under zeolite-facies metamorphic conditions. Alteration assemblages are made of veinal analcime, with or without quartz, and interstitial analcime between igneous phenocrysts (garnet and analcime). The textural occurrence for such analcime is evidence for its secondary origin, rather than as a product from igneous crystallization. Other zeolite minerals are found in amygdules (e.g. prehnite) and in the matrix (e.g. laumontite). Chlorite is commonly observed as an important matrix-filling mineral. Petrogenetic considerations suggest that this low-grade metamorphism did not exceed pressures of 3 kbar at temperatures ranging from 180 to 300°C, but possibly not higher than 200°C from the coexistence of analcime and quartz in veins.

Base metals (Zn, Pb, Cu, Ni, Cr) concentrations are usually less than 200 ppm, based on XRF analyses. Sr and Ba values are significantly higher (1000-5000 ppm). Some analcime-phyric rocks may contain up to 40 per cent modal analcime, but its mining potential might be low due to contamination and secondary alteration. The melanite-garnets can reach up to 10 per cent of the whole rock volume, the best example being from a road-cut outcrop just west of Coleman, on Highway 3. Garnet could be easily mined out of the rock for its abrasive properties. The data presented in this report support a low potential for economic mineralization.

ACKNOWLEDGMENTS

This project was part of an investigation on the mineralogy, geochemistry and economic potential of the Crowsnest Volcanics, as a contribution to the Canada-Alberta Mineral Development Agreement (MDA). Funding for the period of 1992-1994 was provided by the Geological Survey of Canada and the Canada-Alberta MDA to NJB and REB, and by an NSERC research operating grant (A-4379) to EDD. Debbie Glatiotis and Pat Michael are thanked for carrying out XRD and XRF analyses, respectively, at the University of Calgary. This report benefitted from the helpful critical reviews of Roger Macqueen and Tony Peterson.

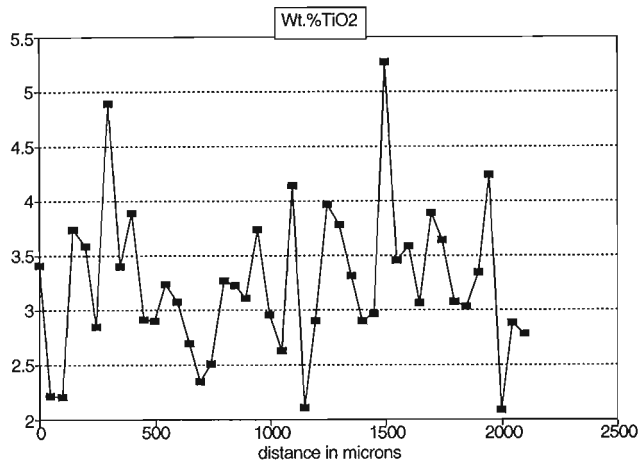

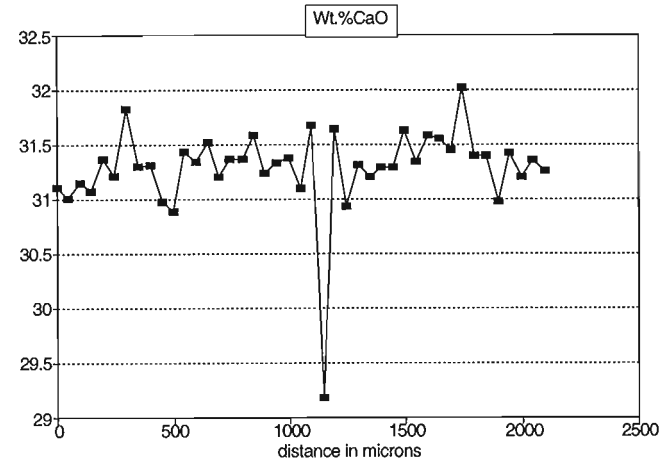

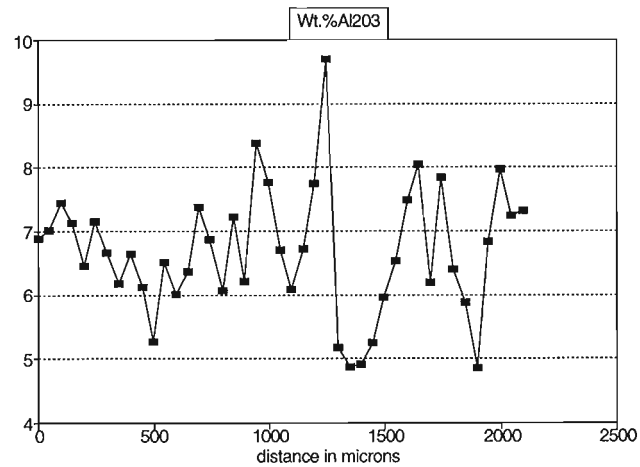

Figure 7.

Rim-to-rim chemical profiles in a garnet phenocryst (sample 29.23). The profiles display erratic zoning in %TiO_2 (a) and %Al_2O_3 (b), but relatively uniform values of %CaO (c).

REFERENCES

Bence, A.E. and Albee, A.L.
1968: Empirical correction factors for the electron microanalysis of silicates and oxides; Journal of Geology, v. 76, p. 382-403.

Berman, R.G.
1991: Thermobarometry using multiequilibrium calculations: a new technique with petrological applications; Canadian Mineralogist, v. 29, p. 833-855.

Bevins, R.E., Robinson, D., and Rowbotham, G.
1991: Compositional variations in mafic phyllosilicates from regional low-grade metabasites and application of the chlorite thermometer; Journal of Metamorphic Geology, v. 9, p. 711-721.

Cathelineau, M. and Viena, D.
1985: A chlorite solid solution geothermometer. The Los Azufres (Mexico) geothermal system; Contributions to Mineralogy and Petrology, v. 91, p. 235-244.

Cho, M., Liou, J.G., and Maruyama, S.
1986: Transition from the zeolite to prehnite-pumpellyite facies in the Karmutsen metabasites, Vancouver Island, British Columbia; Journal of Petrology, v. 27, p. 467-494.

Coombs, D.S. and Whetten, J.T.
1967: Composition of analcime from sedimentary and burial metamorphic rocks; Geological Society of America Bulletin, v. 78, p. 264-282.

Dawson, G.M.
1885: Preliminary report on the physical and geological features of that portion of the Rocky Mountains between latitudes 49° and 51°30'; Geological Survey of Canada, Annual Report, Part B, 69 p.

de Capitani, C. and Liou, J.G.
in press: Thermodynamic analyses of some Ca-zeolites and Mg-Al pumpellyite; Geochemica et Cosmochimca Acta, v. 58.

Ferguson, L.J. and Edgar, A.D.
1978: The petrogenesis and origin of the analcime in the volcanic rocks of the Crowsnest Formation, Alberta; Canadian Journal of Earth Sciences, v. 15, p. 69-77.

Frey, M., de Capitani, C., and Liou, J.G.
1991: A new petrogenetic grid for low-grade metabasites; Journal of Metamorphic Geology, v. 9, p. 497-509.

Ghent, E.D. and Miller, B.E.
1974: Zeolite and clay-carbonate assemblages in the Blairmore Group (Cretaceous) southern Alberta Foothills, Canada; Contributions to Mineralogy and Petrology, v. 44, p. 313-329.

Goble, R.J., Treves, S.B., and Ghazi, A.M.
1993: Comparison of the Rainy Ridge analcime phonolite sill and the Crowsnest volcanics, Alberta, Canada; Canadian Journal of Earth Sciences, v. 30, p. 1644-1649.

Karlsson, H.R. and Clayton, R.N.
1991: Analcime phenocrysts in igneous rocks; primary or secondary? American Mineralogist, v. 76, p. 189-199.
1993: Analcime phenocrysts in igneous rocks; primary or secondary? - Reply; American Mineralogist, v. 78, p. 230-232.

Knight, C.W.
1904: Analcite-trachyte tuffs and breccias from south-west Alberta, Canada; Canadian Record of Science, v. 9, p. 265-278.

Kretz, R.
1983: Symbols for rock-forming minerals; American Mineralogist, v. 68, p. 277-279.

Mackenzie, J.D.
1914: The Crowsnest Volcanics; Geological Survey of Canada, Museum Bulletin, no. 4, 33 p.

Miller, B.E. and Ghent, E.D.
1973: Laumontite and barian-strontian heulandite from the Blairmore Group (Cretaceous), Alberta; Canadian Mineralogist, v. 12, p. 188-192.

Norris, D.K.
1964: The Lower Cretaceous of the southeastern Canadian Cordillera; Bulletin of Canadian Petoleum Geology, v. 12, p. 512-535.

Pearce, T.H.
1967: The analcime-bearing volcanic rocks of the Crowsnest Formation; Ph.D. thesis, Queen's University, Kingston, Ontario.
1970: The analcime-bearing volcanic rocks of the Crowsnest Formation, Alberta; Canadian Journal of Earth Sciences, v. 7, p. 46-66.
1993: Analcime phenocrysts in igneous rocks: primary or secondary? - Discussion; American Mineralogist, v. 78, p. 225-229.

Peterson, T.D. and Currie, K.L.
1993: Analcime-bearing igneous rocks from the Crowsnest Formation, southwestern Alberta; in Current Research, Part B; Paper 93-1B, p. 51-56.

Pirsson, L.V.
1915: The Crowsnest Volcanics; American Journal of Science, v. 39, p. 222-223.

Ricketts, B.D.
1982: Laharic breccias from the Crowsnest Formation, southern Alberta; in Current Research, Part A; Geological Survey of Canada, Paper 82-1A, p. 83-87.

Geological Survey of Canada Project 680071

Observations of post-Wapiabi Formation to pre-Bearpaw Formation stratigraphy, Maycroft map sheet: implications for structural mapping in the southern Alberta Foothills[1]

G.S. Stockmal
GSC Calgary, Calgary

Stockmal, G.S., 1995: Observations of post-Wapiabi Formation to pre-Bearpaw Formation stratigraphy, Maycroft map sheet: implications for structural mapping in the southern Alberta Foothills; in Current Research 1995-E; Geological Survey of Canada, p. 27-36.

Abstract: The Campanian post-Wapiabi Formation to pre-Bearpaw Formation interval within the southern Alberta Foothills along and adjacent to the Oldman River (Maycroft east-half map sheet, 82G/16) has been examined with the goal of improving resolution of structures mappable at 1:50 000 scale. Observations on four measured sections and on hillside exposures typical of local Foothills terrane indicate that this interval can be consistently mapped as two units. The first unit (approximate total thickness 175 m) encompasses strata equivalent to the Milk River and Pakowki formations known from the Plains to the east. The second unit (approximate total thickness 450 m) is the Belly River Group (undivided). Structure elucidated using this two-fold subdivision significantly improves our understanding of the Foothills belt in the Maycroft map sheet.

Résumé : L'intervalle campanien postérieure à la Formation de Wapiabi et antérieur à la Formation de Bearpaw dans le sud des contreforts de l'Alberta bordant la rivière Oldman (moitié est de la carte de la région de Maycroft, 82G/6) a été examiné dans le but d'améliorer la résolution des structures cartographiables à l'échelle de 1/50 000. L'observation des quatre coupes mesurées et d'affleurements sur versant représentatifs d'un terrane local des contreforts indique que cet intervalle peut être cartographié en deux unités sans perdre de sa cohérence. La première unité (épaisseur approximative totale de 175 m) englobe des couches équivalentes aux formations de Milk River et de Pakowki reposant dans les plaines à l'est. La seconde unité (épaisseur approximative totale de 450 m) est le Groupe de Belly River (non divisé). Les renseignements sur la structure obtenus grâce à la subdivision en deux parties de la structure accroissent considérablement notre compréhension de la zone des contreforts figurée sur la carte de la région de Maycroft.

[1] Contribution to the Eastern Cordillera NATMAP Project

INTRODUCTION

Campanian strata between the Wapiabi and Bearpaw formations along and adjacent to the Oldman River, southern Alberta Foothills, were examined during the 1994 field season with the goal of improving 1:50 000 scale mapping and associated cross-section construction of Foothills structures, and to make comparisons with a subdivision of this interval recently proposed for the Crowsnest Pass area by Jerzykiewicz and Norris (1994). The Oldman River affords a number of very good to excellent exposures of portions of this stratigraphic interval, interrupted and repeated by steep, east-vergent thrusts.

Here, I discuss four measured sections which together completely span the interval. Observations made on these sections and on hillside exposures away from the Oldman River in terrain typical of the Foothills, coupled with well penetrations within the triangle zone and the Alberta syncline to the east, suggest that the post-Wapiabi, pre-Bearpaw interval can be mapped consistently as two units: (1) strata equivalent to the Milk River plus Pakowki formations known from the Plains (Chungo plus Nomad members of Stott, 1963), total thickness approximately 175 m; and (2) the Belly River Group (after Jerzykiewicz and Norris, 1994), total thickness approximately 450 m.

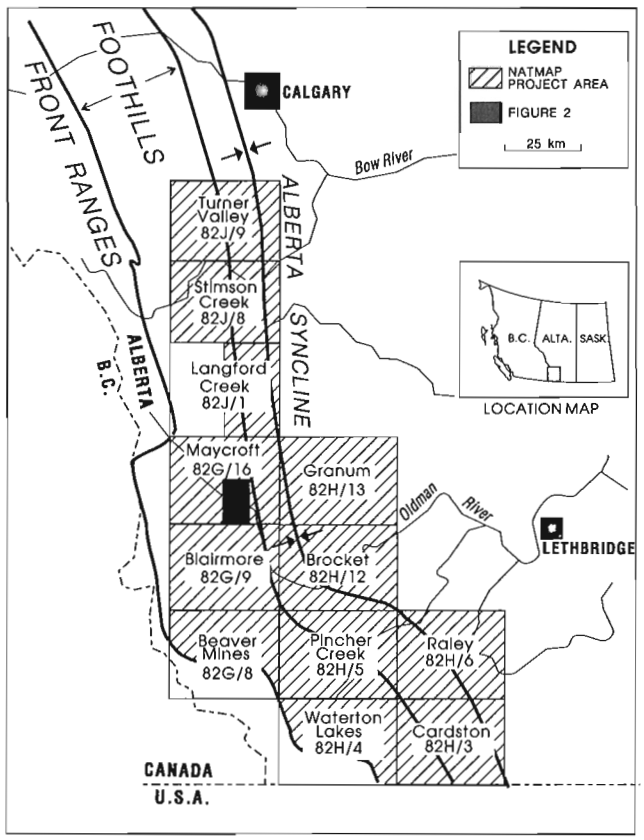

Figure 1. Location of the study area in southwestern Alberta, centred in the Southeastern Cordilleran NATMAP project area.

LOCATION AND STRUCTURAL SETTING

This study, undertaken as part of the GSC's Eastern Cordilleran NATMAP project, examines exposures in the Maycroft east-half map sheet (82G/16), located in the middle of the NATMAP project area (Fig. 1). It addresses one of the purposes of this project, which is to develop and apply mappable subdivisions of the existing stratigraphy. Figure 2, simplified from Stockmal et al. (in press), shows the locations of the four measured sections along the Oldman River in relation to the principal thrust sheets. The sections are best accessed from the unpaved road immediately north of the Oldman River, which extends west from Alberta Provincial Highway 22 (Fig. 2).

The Big Coulee Fault (Fig. 2) forms the upper detachment to the triangle zone in the Maycroft area (Stockmal and MacKay, 1994; Stockmal et al., in press), forming a structural domain boundary between dominantly west-vergent structures to the east and dominantly east-vergent structures to the west. The four measured sections are all west of the trace of the Big Coulee Fault, with the easternmost in its immediate footwall (Fig. 2). The cross-strike separation of the easternmost and westernmost sections is approximately 4 km; palinspastic restoration of a cross-section constructed along the Oldman River (Stockmal et al., in press), indicates that the cross-strike separation of these sections was initially 10 to 12 km.

PREVIOUS WORK

The Maycroft map sheet was mapped previously at 1:63 360 scale by Douglas (1950) as the Callum Creek and Gap GSC A-series maps. Douglas (1950) mapped the post-Wapiabi, pre-Bearpaw interval as a single unit, the Belly River

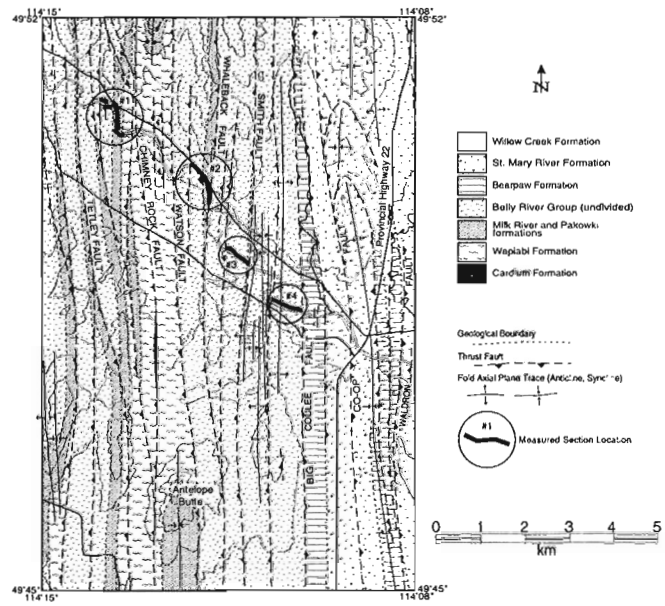

Figure 2. Geology of the southwestern quadrant of the east half of the Maycroft (82G/16) map sheet, simplified after Stockmal et al. (in press), showing the locations of the four measured sections.

Formation (Fig. 3), although he later noted (Douglas, 1951) that to the south this interval is divisible into three units, with the uppermost divisible into five zones where exposure is excellent and the section is undeformed.

Stott (1963) measured the lower portion of the westernmost section discussed here (his section 7-4, fig. 11), immediately above the Wapiabi Formation, and included the Chungo and Nomad members as basal units within the Belly River Formation. Stott (1963, p. 119) stated: "... the term [Belly River] has continued to be used where the sequence cannot be subdivided easily. It is used for those sandstones and shales lying above the dark shales of the Wapiabi formation and includes beds equivalent to the Milk River and Pakowki formations". Stott (1963) interpreted the basal contact of the Belly River Formation to lie above the Nomad Member from south of the Bow River northward, but below the Chungo Member from the Sheep River southward.

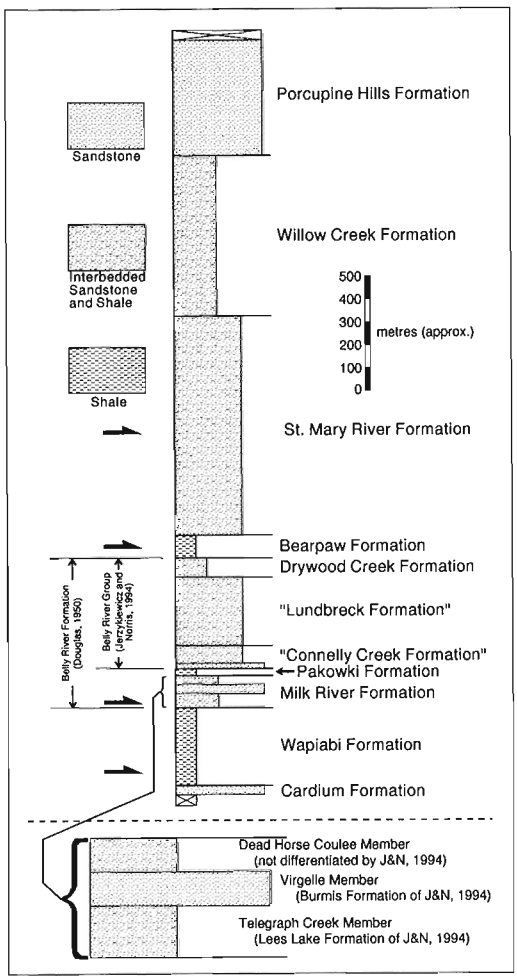

Figure 3. Generalized stratigraphic column for the east half of the Maycroft map sheet. The section between the Wapiabi and Bearpaw formations has been mapped and subdivided in a number of ways. The three members of the Milk River Formation are shown in the expanded section at the bottom of the figure.

Jerzykiewicz and Norris (1994) subdivided the post-Wapiabi, pre-Bearpaw interval into six formations. In ascending order they are: the Lees Lake, Burmis, and Pakowki formations of the Alberta Group, and the Connelly Creek, Lundbreck, and Drywood Creek formations of the Belly River Group. The Pakowki Formation is equivalent to the Nomad Member of Stott (1963), whereas the Lees Lake and Burmis formations are equivalent to the Chungo Member. The utility of this subdivision, developed in the Crowsnest Pass area to the south (Blairmore map sheet, Fig. 1), was demonstrated by Stockmal and MacKay (1994) in the Maycroft area by an increase in map scale structural detail based upon observations along the Oldman River. However, as discussed below, application of the proposed subdivisions of the Belly River Group (Fig. 3) to 1:50 000 scale mapping has proven to be difficult. This is because exposure of the shale-dominated facies, crucial to correct stratigraphic identification of the individual formations within the group, is rarely adequate in areas away from river exposures.

In the subsurface of the southern Alberta Plains, the post-Wapiabi (post-Colorado), pre-Pakowki interval is represented by the Milk River Formation (Meijer Drees and Mhyr, 1981; Jerzykiewicz and Norris, 1994). As discussed below, strata equivalent to the three members of the Milk River Formation are all represented in the Maycroft map sheet.

Douglas (1950, p. 30) estimated the total thickness of the post-Wapiabi, pre-Bearpaw interval (his Belly River Formation) in the Maycroft east-half area to be "not less than 3000 feet" (approximately 900 m). However, in the Cow Creek well (LSD 6-30-8-1W5), located within the triangle zone approximately 8 km south of the Maycroft map sheet, Jerzykiewicz and Norris (1994) noted a drilled thickness of 2100 ft. (640 m) for the same interval. This latter estimate must be considered a maximum value, due to possible tectonic thickening and tilting of the drilled succession.

MEASURED SECTIONS

Figures 4 and 5 present the four measured sections located on the Oldman River (Fig. 2). The westernmost section (#1, Fig. 4) begins at the top of the Wapiabi Formation and includes strata well up into the Lundbreck Formation. Sections #2 and #3 (Fig. 4, 5) begin within strata equivalent to the Milk River Formation and extend up into the Lundbreck Formation. Section #4 (Fig. 5) begins within the Lundbreck Formation and extends up through the Drywood Creek Formation to the Big Coulee Fault.

Immediately above the Wapiabi Formation (Section #1, -47-0 m) lie thickening- and coarsening-upward, fine- to very fine-grained sandstone interbedded with locally nodular siltstone and mudstone. These strata represent a nearshore environment, shallowing-upward, transitional to the shoreface sandstones above. They correlate sedimentologically with the Telegraph Creek Member of the Milk River Formation in the Plains (Meijer Drees and Mhyr, 1981), and with the Lees Lake Formation of Jerzykiewicz and Norris (1994).

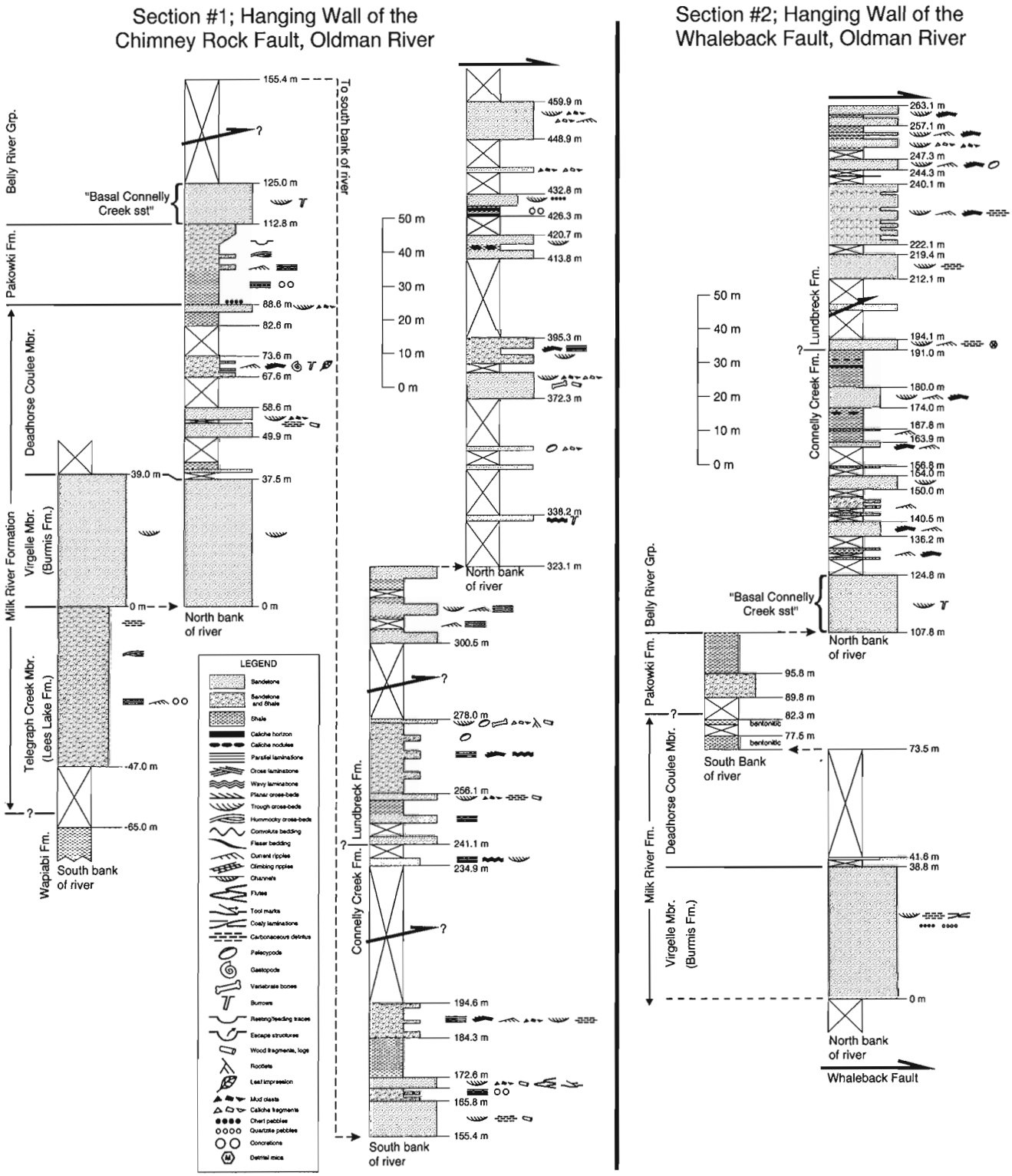

Figure 4. Measured Sections #1 and #2, in the hanging walls of the Chimney Rock and Whaleback faults, respectively.

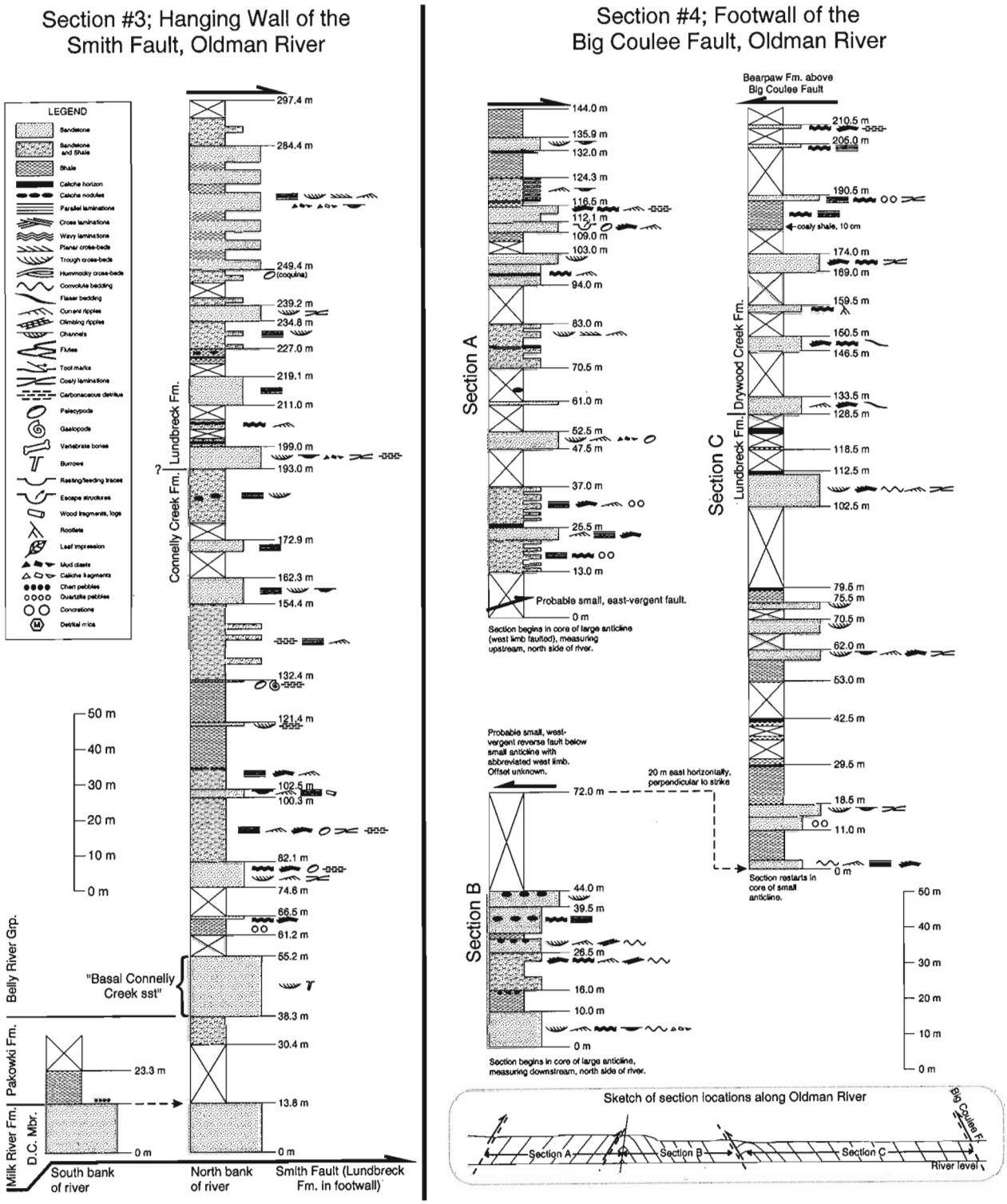

Figure 5. Measured Sections #3 and #4, in the hanging wall of the Smith Fault and the footwall of the Big Coulee Fault, respectively.

Lying abruptly above the Telegraph Creek/Lees Lake interval at Section #1 are medium grained, clean quartz arenites, massive to very thickly trough crossbedded. This interval, 37.5 to 39 m thick at Section #1 and 38.8 m thick at Section #2, correlates sedimentologically with the Virgelle Member of the Milk River Formation (Meijer Drees and Mhyr, 1981) and with the Burmis Formation of Jerzykiewicz and Norris (1994). The thick and erosionally resistant Virgelle Member is a prominent cliff and ridge former. It is approximately 40 m thick where well exposed on Antelope Butte (Fig. 6a), near the southern edge of the map sheet (Fig. 2).

Abruptly overlying the Virgelle/Burmis interval in Section #1 (37.5-88.6 m) are thinly to thickly interbedded, medium grained, massive and trough crossbedded greenish-grey sandstones, fine grained current rippled sandstones, and

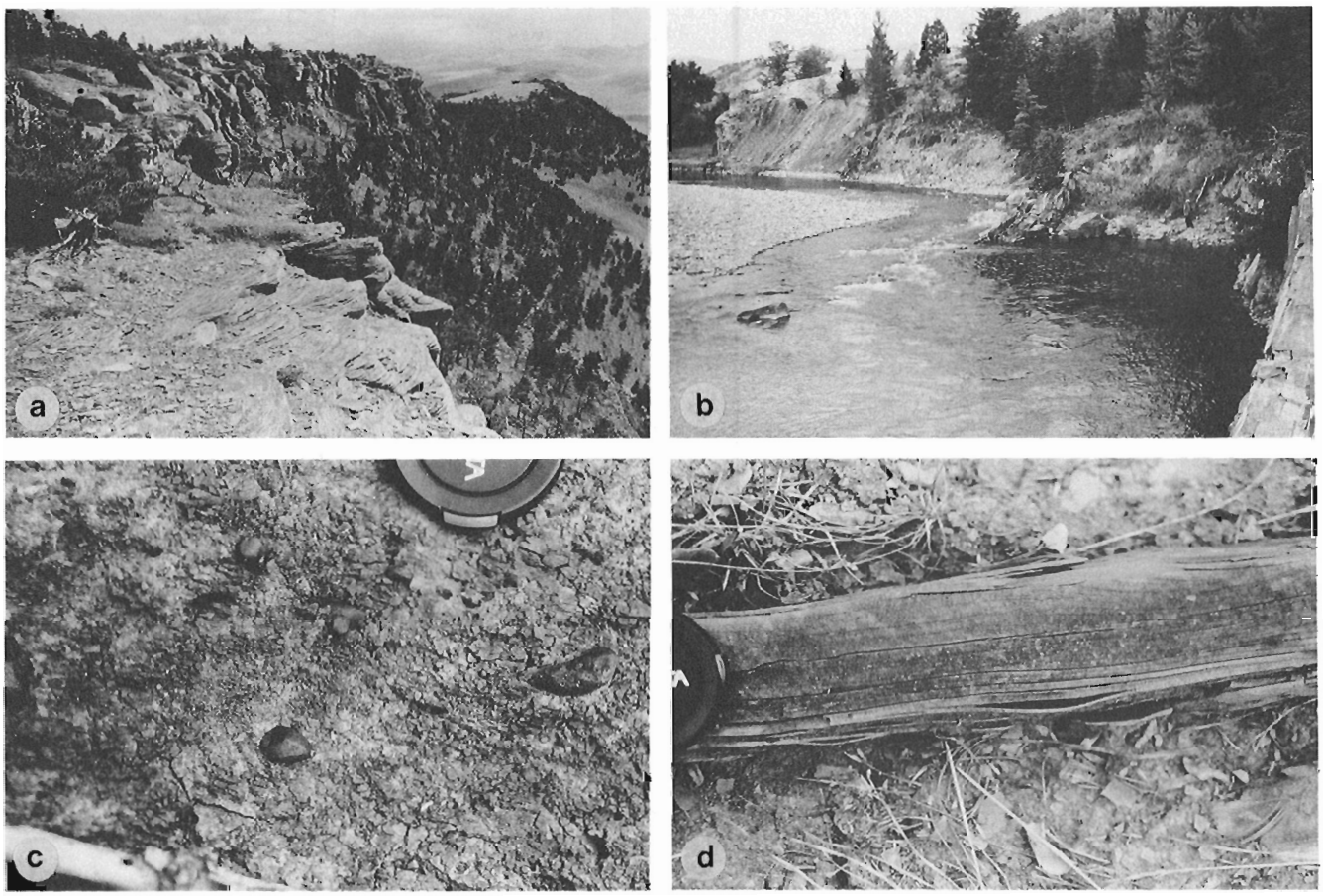

a. Spectacular exposure of the massive to trough crossbedded Virgelle Member, Milk River Formation, on Antelope Butte, southern edge of Maycroft map sheet (Fig. 2); view is to the south. The 40 m thick member here displays castellated forms, hoodoos, and cliff faces. The most northerly exposure of a dark brown weathering magnetite-bearing sandstone interval (here 10 cm thick) occurs a few hundred metres to the south. Good exposure of the underlying Telegraph Creek Member occurs along strike, approximately 1 km south. ISPG 4449-2.

b. Overview of steeply west-dipping strata of the Deadhorse Coulee Member (Milk River Formation) and the Pakowki Formation, north side of Oldman River, 36 to 117 m, Section #1. The resistant top of the Virgelle Member is visible in the foreground on the right-hand side. The Deadhorse Coulee Member spans the interval from the top of the Virgelle Member to the top of the second resistant sandstone rib from the left-hand side of the photo (above the cobble point bar). The Pakowki Formation lies in the recessive but very well-exposed interval between the top of the Deadhorse Coulee Member and the base of the left-most resistant sandstone rib. This latter sandstone rib is the "basal Connelly Creek sandstone". Person for scale. ISPG 4449-6.

c. Black chert pebbles up to 3 cm in diameter lie within marine shales of the basal Pakowki Formation at 88.8 m, Section #1. The pebbles, characteristic of the contact with the underlying Deadhorse Coulee Member in the Plains, were also observed at the same stratigraphic position in Section #3. Lens cap for scale. ISPG 4449-10.

d. Detail of a very fine to fine grained sandstone bed, Pakowki Formation, at approximately 100 m, Section #1. Gradation upward from parallel laminations to current ripples suggests a turbidite/tempestite origin. Lens cap for scale. ISPG 4449-7.

Figure 6a-d

rubbly, greenish, silty mudstones (Fig. 6b). Leaf impressions and thin-walled gastropod shells are present near 70 m. Shale samples taken in this interval for micropaleontological and palynological analyses were barren (A.R. Sweet and D.H. McNeil, pers. comm., 1995). This interval is tentatively interpreted as an overall nonmarine nearshore environment, which correlates with the Deadhorse Coulee Member of the Milk River Formation (Meijer Drees and Mhyr, 1981). An equivalent interval was not described by Jerzykiewicz and Norris (1994), although they stated (p. 377-378): "Fine-grained sediments are virtually absent in the Burmis Formation except for mudstone, siltstone, and very fine sandstone present at the top of the Burmis Formation in a 10 m thick interval below the Pakowki Formation in

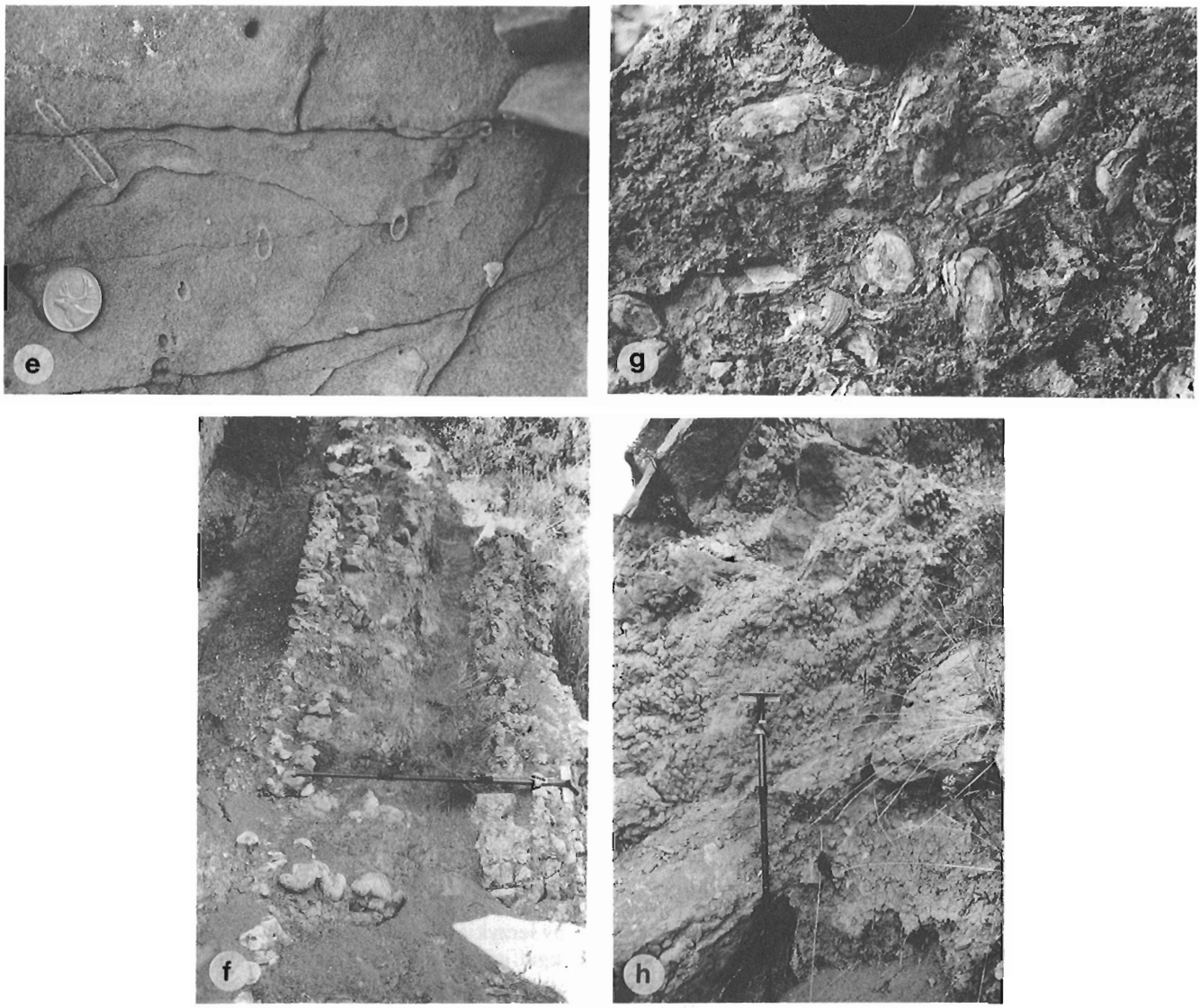

e. Probable ***Skolithos*** *ichnofacies lined burrows, oriented subvertically with respect to bedding, within the "basal Connelly Creek sandstone", at approximately 50 m, Section #3. Similar, possibly unlined burrows have been observed up to 30 cm in length. Quarter for scale. ISPG 4449-11.*

f. Well-exposed caliche hardpans and isolated nodules within a recessive shaly interval of the Lundbreck Formation, 426.3 to 429.4 m, Section #1. Pogo stick 1.5 m in length. ISPG 4449-13.

g. Pelecypod coquina, medium grained sublithic arenite matrix, Lundbreck Formation; at approximately 247.5 m, Section #3. ISPG 4449-9.

h. Hundreds of tightly packed dwelling-and-escape structures, well preserved in a multi-story succession of massive to low-angle, crossbedded and current-rippled, medium grained sublithic arenite. Redeposited shells occur as lags in overlying beds. Lundbreck Formation, approximately 110 to 112 m, Section #4. ISPG 4449-14.

Figure 6e-h

locality 4." The interval from -47 to 88.6 m, Section #1, was described by Stott (1963) as the Chungo Member of the Belly River Formation. It represents a regressive succession above the Wapiabi Formation.

Abruptly (disconformably to unconformably?) overlying the Milk River interval are dark grey shales containing 1 to 3 cm diameter black chert pebbles concentrated in the lowermost 20 cm (Fig. 6c) but occurring up to 3 m from the contact (88.6 m in Section #1 and 13.8 m in Section #3). Similar chert pebbles are known from the Plains at the base of the Pakowki Formation (Meijer Drees and Mhyr, 1981). This interval, from 88.6 to 112.8 m in Section #1 and from 13.8 to 38.3 m in Section #3, displays an overall coarsening- and thickening-upward pattern, which includes thinly bedded, fine- to very fine-grained sandstones, displaying scoured bases, parallel laminations grading upward to current-ripples (Fig. 6d), and possible hummocky cross-stratification near the top of the interval. Burrows as well as feeding and resting traces are numerous locally. Preliminary micropaleontological and palynological analyses from these intervals, and from 95.8 to 107.8 m in Section #2, indicate a marine fauna and a flora which post-dates the Milk River/Pakowki disconformity (A.R. Sweet and D.H. McNeil, pers. comm., 1995). Therefore, this interval represents the Pakowki Formation known from the Plains. Note the comparable measured thicknesses of the Pakowki Formation in Sections #1 and #3, 24.2 and 24.5 m, respectively, and of the Pakowki plus Deadhorse Coulee interval in Sections #1 and #2, 75.3 and 69.0 m, respectively.

Abruptly overlying the Pakowki interval is the Belly River Group, marked by the "basal Connelly Creek sandstone" (112.8 to 125.0 m in Section #1, 107.8 to 124.8 m in Section #2, and 38.3 to 55.2 m in Section #3), a medium- to fine-grained, massive to very thickly trough crossbedded quartz arenite nearly identical to that of the Virgelle Member. In isolated hillside exposures it is difficult to impossible to distinguish these two sandstone units. However, the Virgelle Member is at least twice as thick, and contains few to no trace fossils. The "basal Connelly Creek sandstone", however, often contains probable *Skolithos* ichnofacies trace fossils consisting of burrows, both lined (Fig. 6e) and unlined, oriented subvertical to bedding and up to 30 cm in length.

A clear, though transitional, change in grain size, sedimentology, and colour of the sandstone facies occurs in the Belly River Group between 83 and 155 m above its base, at 241.1 m in Section #1, 191.0 m in Section #2, and 193.0 m in Section #3. [Although the moderately well-exposed section in the hanging wall of the Tetley Fault (Fig. 2) was not measured in detail, the measured thickness from the base of the group to this transition is less than 100 m.] Sandstone units dominated by fine grained, dark grey, medium bedded and current-rippled multi-story strata are superseded by sandstone dominated by medium to coarse grained (occasionally conglomeratic), light to very light grey, thickly to very thickly bedded and trough crossbedded multi-story strata. Caliche hardpans and nodules associated with the shale-dominated facies, considered diagnostic of the Lundbreck Formation when abundant (Jerzykiewicz and Norris, 1994), occur throughout much of the Belly River Group exposed along the Oldman River. Although they occur in the lowermost 100 m, they do not become prominent until more than 200 m above the base of the group, stratigraphically well above the transition in the sandstone facies (e.g., at 428 m in Section #1, Fig. 6f, and approximately 50 m stratigraphically above the faulted top of Section #2). Furthermore, facies considered diagnostic of the Connelly Creek Formation, including dark grey to coaly shale and abundant redeposited probable freshwater pelecypods and dwelling-and-escape structures (cf. Jerzykiewicz and Norris, 1994), occur at a variety of levels throughout the Belly River Group (e.g. at 247.5 m in Section #3, Fig. 6g, and at 50 and 111 m in "Section A" of Section #4, Fig. 6h, approximately 240 and 180 m below the top of the Belly River Group). The location and significance of the interpreted position of the Connelly Creek/Lundbreck boundary is discussed below.

The uppermost proposed formation of the Belly River Group, the mudstone-dominated Drywood Creek Formation (Fig. 3), is extremely recessive and is only known to be exposed in the Maycroft area at one locality on the Oldman River where its measured thickness is 83 m (Section #4; the type section thickness is 55 m). This interval includes flaser to wavy bedding, coaly laminations, and coaly shale. It is considered by Jerzykiewicz and Norris (1994) to represent a unit in transition into the overlying Bearpaw Formation. At the Oldman River locality, the Bearpaw Formation is in thrust contact with the Drywood Creek Formation, along the Big Coulee Fault (the triangle zone upper detachment).

DISCUSSION

The principal issues are: (1) which of the units or packages of units described in the measured sections are mappable at 1:50 000 scale in terrane typical of the southern Alberta Foothills, away from river exposures; and (2) what names should be applied to these intervals. Mapping in concert with observations along the Oldman River (Stockmal, 1995; Stockmal et al., in press) suggests that the post-Wapiabi, pre-Bearpaw interval can be mapped confidently and consistently in the Maycroft area using a two-fold subdivision: (1) strata equivalent to the Milk River and Pakowki formations; and (2) the Belly River Group (undivided), as defined by Jerzykiewicz and Norris (1994). This two-fold subdivision significantly improves the map scale resolution of foothills structures and substantially aids in constraining displacement on individual thrusts (compare Stockmal et al., in press, with Douglas, 1950).

The term Pakowki Formation has already been extended from the Plains into the Foothills by Jerzykiewicz and Norris (1994), and should be applied to the measured intervals noted above on the basis of their sedimentological characteristics, stratigraphic position, and fauna and flora as noted above.

Stott (1963) called the post-Wapiabi, pre-Pakowki interval the Chungo Member, but because he included the Chungo in the Belly River Formation in the south and in the Wapiabi Formation in the north, use of the term as a mappable unit separate from the Belly River Group would cause confusion. As described above, this interval in the Maycroft area includes

three distinct members, each corresponding to known members of the Milk River Formation in the Plains (Meijer Drees and Mhyr, 1981). The Milk River Formation and its enclosed members have been mapped in the subsurface of southern Alberta from its outcrop type area at Writing-On-Stone Provincial Park west to the 5th Meridian (the eastern boundary of the Maycroft map sheet; Fig. 1) by A.P. Hamblin (unpublished data, 1994). Jerzykiewicz and Norris (1994) described units equivalent to the Telegraph Creek and Virgelle Members (their Lees Lake and Burmis formations), but they did not formally define a clear equivalent to the Deadhorse Coulee Member. Because all three members can be identified, I suggest that the term Milk River Formation be adopted for the post-Wapiabi, pre-Pakowki interval in the Maycroft area.

The Milk River Formation is mappable by virtue of the thick and erosionally resistant Virgelle Member (Burmis Formation). Although the Telegraph Creek Member (Lees Lake Formation) has been identified on the west flank of Antelope Butte, and it and the Deadhorse Coulee Member above the Virgelle Member are sufficiently thick (about 50 m each) that they can be depicted as separate units for the purposes of 1:50 000 scale mapping, such depiction is fully dependent upon the outcropping and the identification of the Virgelle Member. Similarly, mapping of the Pakowki Formation is dependent upon confident identification of the Virgelle Member and/or the "basal Connelly Creek sandstone". Therefore, the Milk River and Pakowki formations are considered to form a single mappable interval.

The subdivision of the Belly River Group, as proposed by Jerzykiewicz and Norris (1994), is not easily applied in the Maycroft area. First, the distinction between the Connelly Creek and Lundbreck formations as defined by Jerzykiewicz and Norris (1994) is not as clear along the Oldman River where facies associations are more complex. Second, because the diagnostic features lie dominantly within the shaly facies, mapping these distinctions in hillside exposures is difficult or impossible. If the clear but gradational change observed in the sandstone facies, as noted in the section above, is tentatively adopted as a characteristic distinguishing the Connelly Creek and Lundbreck formations, then the Connelly Creek Formation changes thickness substantially from thrust sheet to thrust sheet (e.g. 128 m thick in Section #1, 83 m thick in Section #2, 155 m thick in Section #3, and less than 100 m in the hanging wall of the Tetley Fault). Such thickness changes, coupled with differences in facies associations within the "Lundbreck Formation" between exposures on the Crowsnest and Oldman rivers, suggest that changes in both the sandstone and shale facies may be profound within the Belly River Group across and along strike, calling into question the validity of formalizing formations within it in the Oldman River area.

The utility of the Drywood Creek Formation for the purposes of structural mapping is limited by its extremely recessive nature and its stratigraphic position between the recessive Bearpaw and Lundbreck formations. Only one outcrop of the Drywood Creek Formation is known in the Maycroft area, this being on the Oldman River (Section #4).

Total thicknesses for these intervals is constrained directly by the measured sections and well observations reported by Jerzykiewicz and Norris (1994), and indirectly by the requirements of cross-section balancing. The thickness of the Milk River and Pakowki formations in Section #1 is approximately 160 to 178 m (the Wapiabi/Telegraph Creek contact is not exposed). A nominal thickness of 175 m was used in cross-section construction (Stockmal et al., in press). The drilled thickness of 640 m for the post-Wapiabi, pre-Bearpaw interval in the Cow Creek well (LSD 6-30-8-1W5; Jerzykiewicz and Norris, 1994) is a maximum thickness, as noted above. Reducing this thickness by the 175 m nominal thickness of the Milk River and Pakowki interval results in an estimated maximum thickness of about 450 m for the Belly River Group. Recognizing that modest orogenward thickening is expected in a foreland basin setting, this thickness is consistent with: the sections measured here; the number of thrust sheet repeats within the triangle zone as constrained by seismic data and balanced cross-section construction (MacKay et al., 1994; Stockmal et al., in press); the thickness estimated from seismic data across the Maycroft area tied to a well in the axis of the Alberta syncline (Lawton et al., 1994); and thicknesses of 350 to 400 m in wells of the western Plains near the 5th Meridian (A.P. Hamblin, pers. comm., 1995).

CONCLUSIONS

The post-Wapiabi, pre-Bearpaw interval in the southern Alberta Foothills in the vicinity of the Oldman River, mapped as a single interval by Douglas (1950; his "Belly River Formation"), can be mapped consistently using a two-fold subdivision which significantly improves the resolution of Foothills structures. These two units are: (1) the Milk River and Pakowki formations, equivalent to strata in the Plains; and (2) the Belly River Group (undivided), as defined by Jerzykiewicz and Norris (1994). Each of these two units can be further subdivided locally where outcrop exposures warrant, but for terrane typical of the southern Alberta Foothills and for the purposes of 1:50 000 scale structural mapping, the two-fold subdivision suggested here may be a practical limit.

Field studies in the 1995 season will be directed in part to understanding the apparent differences in mappable post-Wapiabi, pre-Bearpaw strata in the Maycroft and Crowsnest Pass areas. These mappable units will also be traced to the west into Maycroft west-half, and to the north into the Langford Creek map sheet (82J/1) and then to the Highwood and Sheep rivers in Stimson Creek (82J/8) and Turner Valley (82J/9) map sheets.

ACKNOWLEDGMENTS

I thank Tony Hamblin, Doug Cant, Art Sweet, Daniel Lebel, and Margot McMechan for discussions both in and out of the field, Art Sweet and Dave McNeil for preliminary palynological and micropaleontological analyses, and Tony Hamblin, Art Sweet, and Margot McMechan for critical reviews of the manuscript.

REFERENCES

Douglas, R.J.W.
1950: Callum Creek, Langford Creek, and Gap map-areas, Alberta; Geological Survey of Canada, Memoir 255, 124 p.
1951: Pincher Creek, Alberta; Geological Survey of Canada, Preliminary Map, Paper 51-22.

Jerzykiewicz, T. and Norris, D.K.
1994: Stratigraphy, structure and syntectonic sedimentation of the Campanian 'Belly River' clastic wedge in the southern Canadian Cordillera; Cretaceous Research, v. 15, p. 367-399.

Lawton, D.C., Stockmal, G.S., and Spratt, D.A.
1994: Seismic definition of the triangle zone east of Maycroft, Alberta; in Current Research 1994-E; Geological Survey of Canada, p. 109-116.

MacKay, P.A., Spratt, D.A., Soule, G., and Lawton, D.C.
1994: The triangle zone of southern Alberta – geometry, lateral variations and associated oil and gas fields; Field-Trip Guidebook (PR-2), Canadian Society of Exploration Geophysicists/Canadian Society of Petroleum Geologists, 1994 Joint National Convention, Calgary, Alberta, 105 p.

Meijer Drees, N.C. and Mhyr, D.W.
1981: The Upper Cretaceous Milk River and Lea Park formations in southeastern Alberta; Bulletin of Canadian Petroleum Geology, v. 29, p. 42-74.

Stockmal, G.S.
1995: Southern Alberta NATMAP mapping in Maycroft (82G/16) (Whaleback Ridge area): progress to date; in Proceedings of the Oil and Gas Forum '95 – Energy from Sediments, Calgary, Alberta, March 28-29, 1995, J.S. Bell, T.D. Bird, T.L. Hillier, and P.L. Greener (ed.); Geological Survey of Canada, Open File 3058, p. 133-135.

Stockmal, G.S. and MacKay, P.A.
1994: Triangle zone and foothills structures along and adjacent to the Oldman River, southwestern Alberta; in Current Research 1994-E; Geological Survey of Canada, p. 101-108.

Stockmal, G.S., MacKay, P.A., Lawton, D.C., and Spratt, D.A.
in press: The Oldman River triangle zone: A complex tectonic wedge delineated by new structural mapping and seismic interpretation; Bulletin of Canadian Petroleum Geology.

Stott, D.F.
1963: The Cretaceous Alberta Group and equivalent rocks, Rocky Mountain Foothills, Alberta; Geological Survey of Canada, Memoir 317, 306 p.

Geological Survey of Canada Project 930006

Multichannel and high resolution seismic reflection survey of the marine Fraser River delta, Vancouver, British Columbia: Tully PGC95001

David C. Mosher[1], Brian C. Nichols[2], and Scientific Party of PGC95001[3]

Mosher, D.C. Nichols, B.C., and Scientific Party of PGC95001, 1995: Multichannel and high resolution seismic reflection survey of the marine Fraser River delta, Vancouver, British Columbia: Tully PGC95001; in Current Research 1995-E; Geological Survey of Canada, p. 37-45.

Abstract: The internal structure of the Fraser River delta holds the key to understanding its development and stability. Survey PGC95001 mapped the southern part of the Strait of Georgia using multichannel and high resolution seismic reflection techniques. The purpose was to define better the structure of the delta, including failure features known as the Foreslope Hills and the southern Roberts Bank Failure Complex. A rectangular grid of lines spaced 500 m apart was run over each of the latter features to achieve this objective.

The multichannel data are of excellent quality and provide new information about the detailed structure and properties of the delta sediments. Brute stacks of these data have increased signal to noise ratios significantly and show good definition of structure at depth. The Huntec sparker system has proven effective on the delta for high resolution profiling. Digital collection of these data permit use of hi-fidelity, numerical post-processing techniques to enhance interpretation.

Résumé : La structure interne du delta du fleuve Fraser recèle les renseignements permettant de comprendre son évolution et sa stabilité. L'équipe de levé PGC95001 a cartographié la partie méridionale du détroit de Georgia en utilisant des techniques de sismique réflexion multicanales et haute résolution, pour affiner les structures, notamment les formes de rupture appelées collines d'avant-talus et le sud du complexe de rupture du banc Roberts. Un réseau rectangulaire de lignes espacées de 500 m a été parcouru au-dessus de chacune des formes pour atteindre ces objectifs.

Les données multicanales sont d'excellente qualité et fournissent des informations détaillées sur la structure et les propriétés des sédiments deltaïques. Les sommations brutes de ces données ont considérablement augmenté les rapports signal-bruit et donnent une bonne définition de la structure en profondeur. L'étinceleur Huntec s'est avéré efficace sur le delta pour produire des profils haute résolution. L'enregistrement numérique de ces données permet d'améliorer l'interprétation par les techniques post-traitement numériques haute fidélité.

[1] GSC Victoria, Sidney
[2] GSC Atlantic, Dartmouth
[3] Scientific Party: David Mosher, Brian Nichols, Mel Best, Harold Christian, Ralph Currie, Ivan Frydecky, Jamie Harris, Bill Hill, Gail Jewsbury, Fred Jodrey, Bill LeBlanc, David Lintern, and Bob MacDonald.

INTRODUCTION

The marine portion of the Fraser River delta, covering an area of some 1000 km^2, is adjacent to Vancouver and underlies the marine route connecting the southern mainland of British Columbia to Vancouver Island within the Strait of Georgia (Fig. 1). This region is the most earthquake-prone zone in Canada and is subject to intense societal use. A variety of geological and geotechnical issues must be considered to assess potential effects of normal delta and earthquake-induced processes on development. The internal structure of the delta is paramount in understanding the delta's development, the distribution of sediments that comprise it, and its stability. At least two regions with possible slope failure events on the delta front have been identified from earlier geophysical surveys. These are the Foreslope Hills within the lower Strait of Georgia (Tiffen et al., 1971; Hamilton and Wigen, 1987; Hart, 1993), and the Roberts Bank Failure Complex on the slope off southern Roberts Bank (Terra Surveys, 1994). GSC cruise PGC95001 surveyed the Strait of Georgia and these two areas in particular with multichannel seismic reflection techniques to define better the structure of the Fraser Delta, the Foreslope Hills, and the southern Roberts Bank Failure Complex. This paper presents preliminary results from this activity.

REGIONAL GEOLOGICAL SETTING

The Fraser River delta is a deep water river delta built out into the Strait of Georgia during the Holocene epoch (Clague et al., 1991; Luternauer et al., 1993). The subaerial and submarine extent of the delta are each over 1000 km^2. Progradation of the delta into the Strait of Georgia has resulted in a 40 km-long coastal zone and tidal flats that extend about 9 km from the dyked edge of the delta to the subtidal slope (Fig. 1). The slope break, marking the modern transition from the delta plain to the foreslope, lies in about 50 m water depth. The western delta slope is inclined 1-23° (average ~2-3°) towards the marine basin of the Strait of Georgia and terminates at about 300 m water depth, 5-10 km seaward of the edge of the tidal flats. Present-day deposition on the Fraser Delta is controlled by tidal and fluvial processes operating in a high-energy, semi-enclosed marine basin (the Strait of Georgia) (Luternauer and Finn, 1983; Luternauer et al., 1993).

Stratigraphy of the Fraser Delta has been derived from onshore and offshore seismic and drilling programs (Tiffen, 1969; Hamilton, 1991; Hart et al., 1992a, 1993; Luternauer et al., 1993; Monahan et al., 1993). Deltaic sediments have a maximum reported thickness of 213 m and overlie Late Pleistocene till and stratified glacial drift (Clague et al., 1991). The delta has prograded into the Strait of Georgia as relative sea level rose from 13 m below its present position. The general stratigraphic sequence of the delta has been studied by Monahan et al. (1993): clays, silts, and sands that constitute the bottomset facies of the delta may conformably overlie Pleistocene glaciomarine deposits. Foreset beds, dipping at about 7°, overlie the bottomset facies or unconformably overlie Pleistocene material. The foresets consist of interbedded and interlaminated sands and silts. Topset sediments thin westward from 40 m at the apex of the delta to 20 m or less at the western margin of the dyked delta plain. Topset deposits are composed of distributary channel sands, channel fill sands, and channel fill silts. Intertidal and floodplain silts and sands cap these topset beds and are over 15 m thick at the apex of the delta. They thin westward to 5 m at the western margin of the dyked delta plain.

Four seismo-stratigraphic units have been recognized in the subsurface as a result of marine seismic surveys (Tiffen, 1969; Hamilton, 1991; Hart et al., 1992b): 1) acoustic basement (thrusted Tertiary and older sedimentary rocks), 2) ice-sculpted Pleistocene stratified and unstratified sediments of till or glacial drift, 3) glaciomarine sediments deposited during retreat of the ice front (Lower Postglacial unit), and 4) prodelta and deltaic sediments deposited during the Holocene progradation of the Fraser Delta (Upper Postglacial unit). Much of the marine seismic data over the delta are obscured by the presence of shallow gas contained within the sediments (Hart and Hamilton, 1993). The presence of gas causes absorption of acoustic energy, resulting in acoustic turbidity in the seismic record. This gas is likely biogenic in origin, and likely due to the high organic carbon content of the Fraser Delta sediments and high rates of burial.

METHODS

Defining the structure of the Fraser Delta has been restricted in previous geophysical surveys by the presence of significant amounts of in situ gas. It was hoped that with a significantly energetic sound source and trace stacking, the gas could be penetrated to reveal the deeper structure of the delta. To this end, a Haliburton Geophysical 0.65 L (40 in^3) sleeve gun and Innovative Transducers ST-5 24-channel hydrophone array were employed, collecting over 1000 line-km (Fig. 1) and 30 gigabytes of multichannel seismic reflection data. In addition to the multichannel seismic data, Huntec deep tow sparker data were collected to image the near surface sediments at high resolution. These data were collected simultaneously with the multichannel data.

The gun was towed 1 m below the sea surface and 8 m behind the ship. It was fired on distance every 16 m using differential global positioning (DGPS) and computer control. Each group in the 24 channel hydrophone array comprised 3 hydrophones and were separated by 8 m. The streamer was a solid polyethylene foam, as opposed to traditional oil-filled streamers. It was towed 5 m below the sea surface at an offset of 54 m between the first group and the stern of the ship. This source-receiver configuration yielded a frequency reponse peak between 0 and 400+ Hz. One second of traveltime data at a sample interval of 0.25 ms (sample rate of 4 kHz) was recorded by a Geometrics StrataView® acquisition system. Data were written to an external SCSI hard drive, then archived to CD-ROM in SEG–2 format. Data were downloaded to an HP 715 work station while at sea, converted to SEG–Y format, merged with navigation data and collated into line segments. They were then backed up on Exabyte tape and the near-trace data were extracted. Digital data could be processed and visualized on the work station in semi-real time

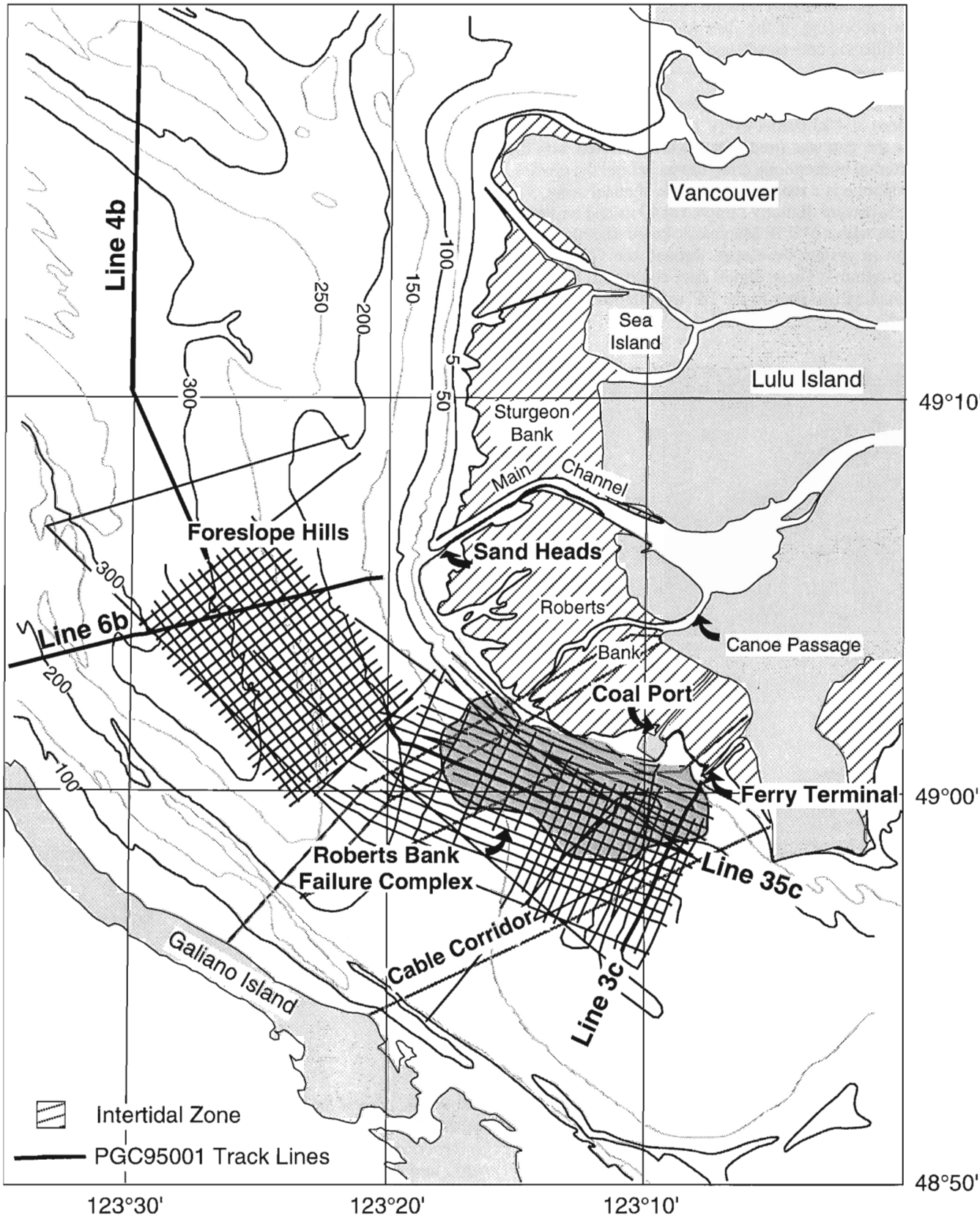

Figure 1. Location diagram showing PGC95001 cruise track where multichannel and Huntec seismic reflection data were collected. Bold track lines represent the lines shown as figures within this paper.

with GSC Digital Initiative software for data quality assessment. Post-processing of the data so far has involved only broadband filtering between 40 and 800 Hz, and six-fold brute stacking.

The sparker unit was towed between 30 and 60 m depth and was fired at 4 kJ output every 1.5 m (except for a 1 sec delay after the gun was fired). Data were collected with the Huntec external hydrophone array towed behind the towfish. This hydrophone is a ten element, single channel array, 5 m in length. Data were digitally sampled at 40 μs and written to Exabyte tape with a MUSE Macintosh-based digital acquisition system (a system developed through the GSC Digital Initiative program). These digital data could also be downloaded from Exabyte tape to the HP workstation, processed and viewed.

RESULTS OF PGC95001 SURVEY

Several regional lines were run down and across the lower Strait of Georgia to assess the regional stratigraphic and structural framework of the delta (Fig. 1-3). The main thrust of the survey, however, was to run a grid of lines with 500 m line spacing over the Foreslope Hills and the Roberts Bank Failure Complex (Fig. 1) to better understand their structure and possible genesis. The regional lines have been given the suffix "b", the southern Roberts Bank survey grid lines have been given the suffix "c", and the Foreslope Hills grid lines have been annotated with the suffix "d".

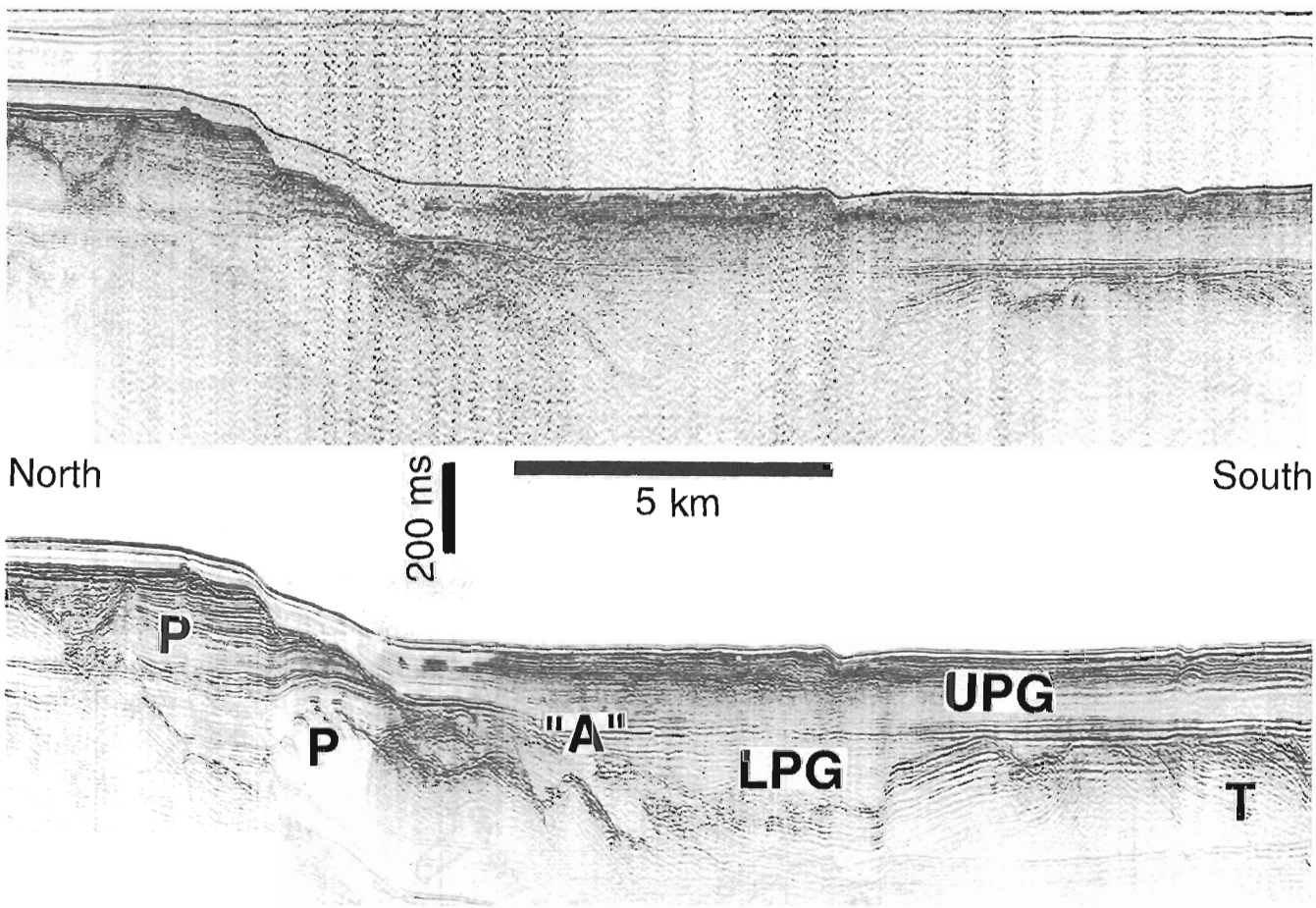

Figure 2. A regional 0.65 L (40 in^3) sleeve gun profile down the central Strait of Georgia (line 4b). The top profile is the near trace data, with a bandpass filter of 40-800 Hz. The lower profile is the multichannel stack (6 fold) of the same data with no filtering and no other processing. Each profile displays 1 second of data (two-way traveltime), and are 21.8 km long. ***T*** *is Tertiary and older bedrock,* ***P*** *is Pleistocene glacial and glacio-marine sediment,* ***LPG*** *is the Lower Postglacial unit, and* ***UPG*** *is the Upper Postglacial unit (after Hamilton, 1991). Note dipping reflectors of the Tertiary sediments, the rough, hummocky surface of the Pleistocene glacial sediments, lateral truncation of flat-lying Pleistocene glacio-marine sediments, the flat-lying and gas-laden nature of the post-glacial sediments, and the strong regional reflector separating the LPG and UPG units (reflector "A").*

Regional

Line 4b (Fig. 2) ran from Bowen Island towards the south to connect with the Foreslope Hills and Roberts Bank detailed surveys. Five lines were run west to east across the Strait of Georgia. Line 6b is one of these lines and is shown in Figure 3. Six basic seismo-stratigraphic units, which compare to those described by Hamilton (1991), can be identified from these data and can be seen in Figures 2 to 5:

1. The lowestmost unit, bedrock, is acoustic basement and reflects no coherent acoustic energy. This unit is particularly notable on the western side of the strait near Galiano Island. It is not always discernable through the thick sediment sequence.
2. The next stratigraphic unit, which is sometimes imaged into but never through, and is not present everywhere, is a unit with an unconformable surface and dipping internal reflectors. These reflectors dip at about 1°. This unit has been described in previous studies as Tertiary sedimentary strata.
3. A unit of relatively horizontal reflectors with an apparent erosional upper surface overlies the Tertiary. Reflectors of this unit appear coherent but truncate against steep erosional walls. This unit is not seen within the axis nor western side of the strait. Hamilton (1991) described this unit as Pleistocene glaciomarine sediment.
4. Another unit, not always seen in direct association with the forementioned unit of horizontal reflectors, is one with a rough hummocky surface with point reflectors and incoherent or amorphous internal reflections. This unit is seen mainly on the very outer margins of the banks and has been interpreted as Pleistocene diamict (Hamilton, 1991).
5. Unconformably overlying all previous units mentioned and present particularly in the deeper parts of the Strait of Georgia is a unit of flat-lying, semi-coherent, high amplitude reflections. This unit has previously been designated as the Lower Postglacial (LPG) unit (Hamilton, 1991). It is up to 250 ms thick. It is separated from the overlying unit by a regionally correlatable, high amplitude, low frequency reflection horizon termed reflector "A" (Fig. 2-4).

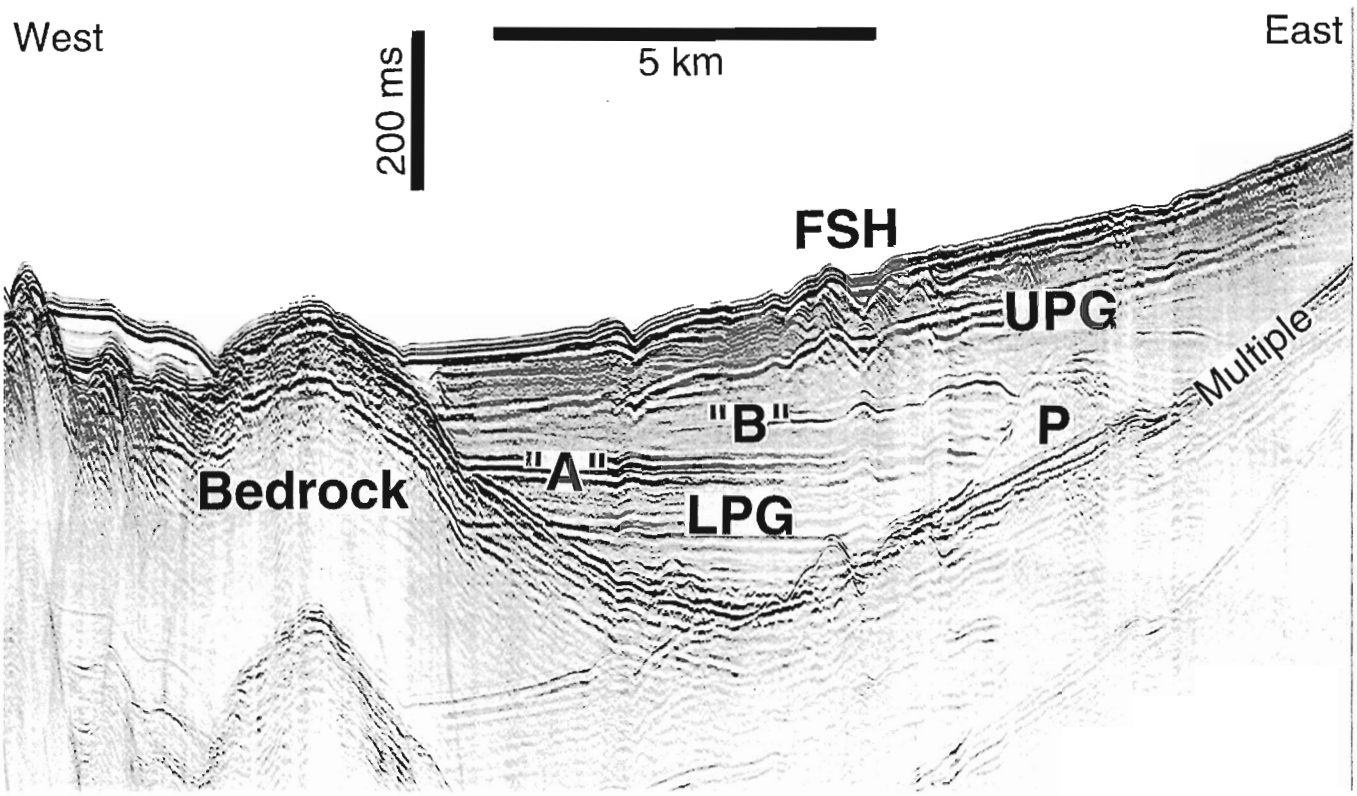

Figure 3. *A regional 0.65 L (40 in^3) sleeve gun profile of a west to east cross-section of the Strait of Georgia (Line 6b) (6-fold stack). The profile displays 1 second of data (two-way traveltime) and is 17.5 km long.* ***Bedrock*** *is Tertiary and older,* ***P*** *is Pleistocene glacial and glacio-marine sediment,* ***LPG*** *is the Lower Postglacial unit,* ***UPG*** *is the Upper Postglacial unit, and* ***FSH*** *are the Foreslope Hills. Note the bedrock highs in the west, the gradual slope away from Sand Heads (sediment source) from east to west of postglacial sediments, the Pleistocene mound in subbottom on the east side of the strait, reflector "A", and the strong single wavelet reflector underlying the Foreslope Hills (reflector "B").*

6. Overlying this regional horizon is a unit of coherent, low amplitude reflections referred to as the Upper Postglacial unit (UPG) by Hamilton (1991). In the central portion of the strait these reflections are parallel and the unit is in the order of 300 ms thick. On the delta foreslope these reflections may describe a number of clinoform shapes representing the foreset beds of the delta front and the thickness varies.

In general, seismic reflection data describe the lower Strait of Georgia as a deep basin, with an axis oriented nearly north-south, and which is U-shaped from west to east. Pleistocene sediments may rim the outer portions of this basin, but are not apparent in the central parts. Sediment from the Fraser River has provided most of the sediment fill within the basin, thinning in a distal sense from east to west. These sediments occur as the Lower Postglacial and Upper Postglacial units.

Foreslope Hills

The grid of survey lines over the Foreslope Hills has yet to be processed and described. Hart (1991) has described them in detail from 0.082 L (5 in^3) single channel reflection data. Their wavelengths are in the order of 500-700 m and they are about 20 m in height. Individual ridges can be traced up to 5 km in length. In the southeastern part of the complex, ridge crests trend nearly north, with a progressive rotation (through nearly 45°) to northeast in the northwestern part of the complex. This ridge and trough morphology covers an area about 60 km^2 in size. Sparker data show no internal structure, likely because of shallow gas. The 0.65 L (40 in^3) sleeve gun data, however, show structure within the hills (Fig. 3). They demonstrate internal reflectors which thicken on their eastern and southern sides and thin or pinch on their western and northern flanks, giving an internal structure similar in appearance to bedding within migrating sandwaves. Towards the eastern side of the Foreslope Hills the troughs are sites for ponding by apparently modern river derived sediments. These sediments are flat-lying and are thickest in troughs of the easternmost parts and thin to the west.

Seismic data show the underlying structure of the Foreslope Hills may be contained within a small basin bounded to the west by bedrock which comes to surface at Galiano Island and to the east by a ridge of Pleistocene material that lies in the subsurface under the Sand Heads area (Fig. 3). A relatively strong, single wavelet reflector underlies the Foreslope Hills. It is termed reflector "B". This strong reflector also appears folded or deformed, but apparently 180° out of phase with the ridge-trough morphology of the Foreslope Hills.

Southern Roberts Bank

A large failure complex has been identified on the foreslope of southern Roberts Bank from previous high resolution geophysical data (Terra Surveys, 1994). It is estimated to include about 10^9 m^3 of sediment. The 0.65 L (40 in^3) sleeve gun – multichannel system was used to define better the limits and size of this failure complex, especially to image the lower bounding surface (Fig. 4). It was hoped the Huntec system would highlight any internal structure (Fig. 5). The complex appears to lie on the steepest part of the foreslope; an area with an average slope of about 7° (ranging from 2 to >8°). It thins at the bottom of this steep part of the foreslope in about 150 m water depth, pinching out in a wedge-shape at its base (Fig. 5). The north-south cross lines roughly parallel the slope contours (Fig. 4). In this orientation, the complex appears to be about 50 m thick in its southern portion (Fig. 4). The surface of the complex, which forms the seafloor or very near to the seafloor, shows more relief than the foreslope elsewhere on the delta.

Due to significant gas within the sediments found below the failure complex, it was not possible to image the underlying structure. The gas does serve to highlight the reflector at

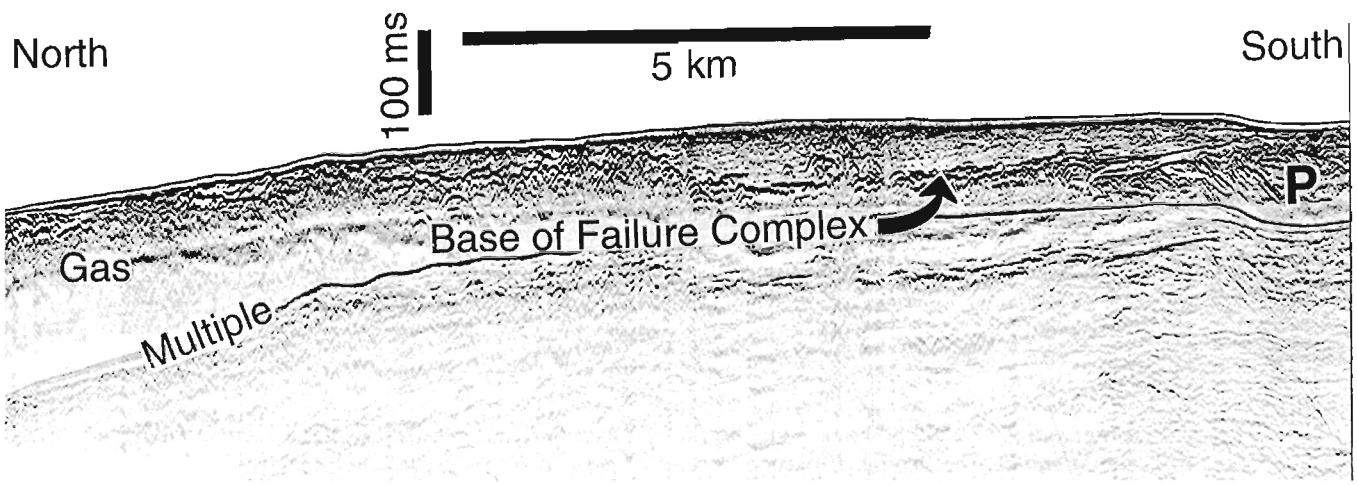

Figure 4. A 0.65 L (40 in^3) sleeve gun profile (line 35c – 6 fold stacked multichannel data) showing a cross-section (along slope) of the Roberts Bank Failure Complex. The section displays 600 ms of data in two-way travel time and is 14.5 m long. Note the strong basal reflector, which appears to be gas-brightened.

the lower boundary of the failed material (gas brightening). The structure could be imaged best in the southernmost portion of the complex, offshore of the BC Ferry Terminal, where Holocene delta sediments thin enough that significant amounts of gas have not accumulated. A Huntec sparker line in this area (Fig. 5) showed a sequence of coherent, well-defined reflections abruptly truncated by commencement of the failure complex.

DISCUSSION

Regional

The regional survey lines provide data on the general seismic stratigraphy of the Strait of Georgia. Brute stacking of multichannel data improves signal to noise ratio significantly (Fig. 2). Results agree completely with the seismic units defined by Hamilton (1991) (Acoustic Basement, Tertiary, Pleistocene, Lower Postglacial and Upper Postglacial). A detailed analysis must be performed to understand the stratigraphic relationships of the units. In general, the western side of the strait is composed of bedrock. Eroded Tertiary sedimentary rock and eroded Pleistocene sediment dominate in the middle and eastern flanks. Pleistocene glacial and glaciomarine sediment seem to rim the western side of the Georgia Basin, and a ridge of it appears to exist in the subbottom on the eastern side of the basin. These units may represent ice limits within the Strait of Georgia during the Wisconsinan, although they may have been eroded subsequently.

Holocene sediments are flat-lying for the most part and dominate the sediment column within the strait. They represent Fraser Delta outflow sediments and tend to thin slightly to the west and pinch out (onlap) onto bedrock on the western flank. The regional high amplitude reflector separating the Lower and Upper Postglacial units (reflector "A") likely marks a significant oceanographic or sedimentological change, and should be further investigated.

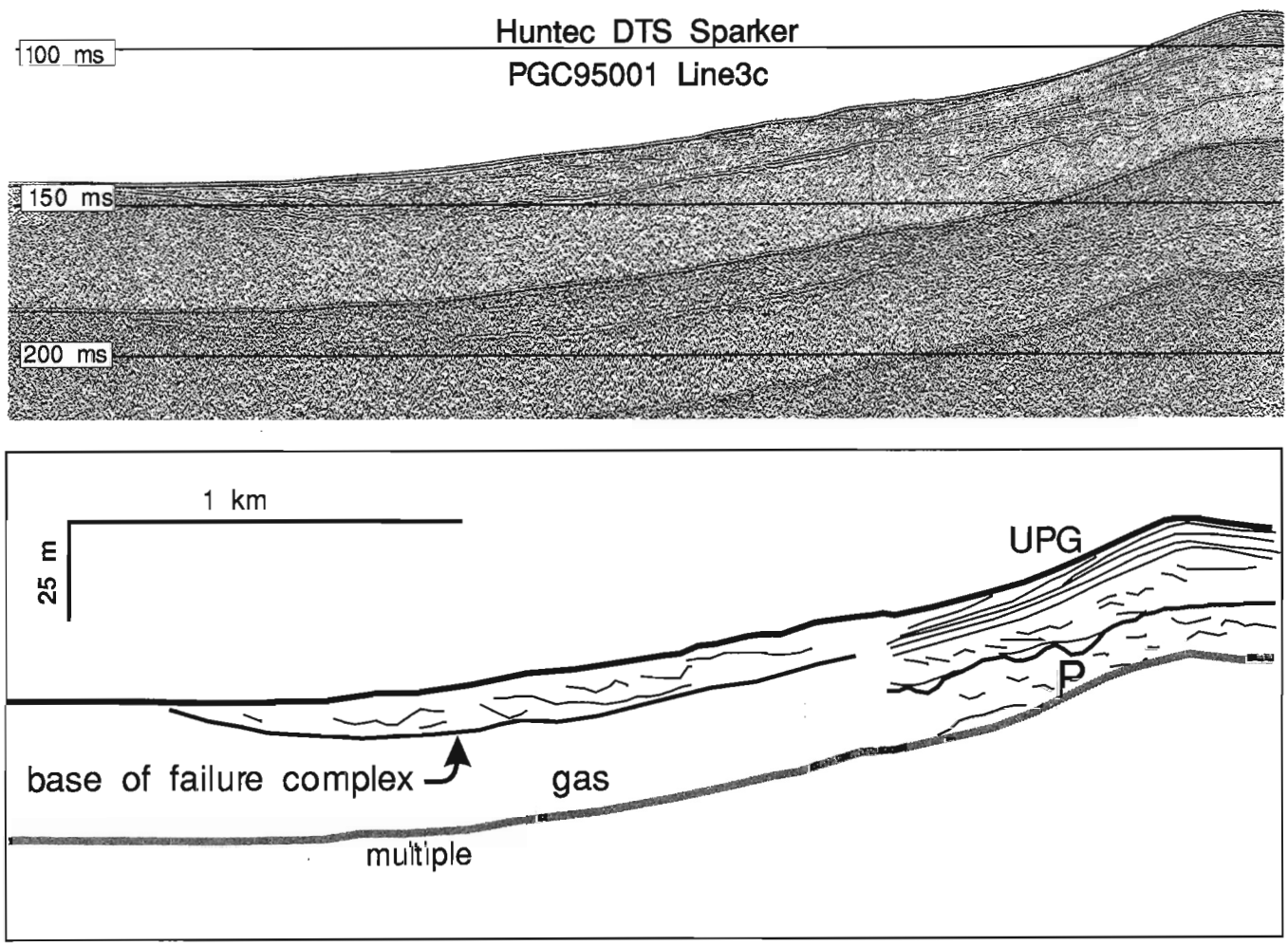

*Figure 5. A Huntec DTS sparker profile (line 3c) showing a cross-section through the southern edge of the failure complex. Note again the gas-brightened basal reflector of the complex, Pleistocene sediments (**P**) at the top of the slope, and the sequence of conformable postglacial bedded sediments (**UPG**) at the top of the slope, truncated at the commencement of the failure complex. The failure complex occurs over the steepest part of the slope off of southern Roberts Bank.*

Gas within the sediments prevents high resolution definition of the modern stratigraphy and structure of the delta. Only in the southern Roberts Banks area, however, does gas completely attenuate the acoustic signal of the large sleeve gun, impeding visualization of the deeper structure. One of the determinants of the apparent amount of interstitial gas seems to be the thickness of Holocene sediment (greater thickness means more gas and more acoustic attenuation).

Foreslope Hills

There are four theories for explaining the mechanism of formation of the Foreslope Hills. (1) Hamilton and Wigen (1987) described the Foreslope Hills as a single, large submarine slump deposit, representing material swept down slope from the delta foreslope in a catastrophic event. The "hills" are a result of rotation and significant transport of coherent blocks of material. (2) Hart (1993) argued that the Foreslope Hills do represent a single mass-failure event, but with no significant transport of sediment. He felt the complex consists of thick blocks of base-of-slope stratified muds that have undergone extension and rotation with only moderate downslope movement. (3) Hart (1993) discussed the possibility that the Foreslope Hills' ridges and troughs represent migrating sediment waves, but concluded this as unlikely. (4) Formation of the Foreslope Hills involved a creep style deformation within distal sediments resulting from deviatoric loading by the prograding delta. Mass from the prograding delta might create a load with a lateral component, causing compressional folding of the fine grained prodelta muds of the Foreslope Hills (H. Christian, pers. comm.). Being confined in a structural basin or trough may have enhanced the compressional effects. Asymmetry of the internal reflectors can be explained by vertical extension on the side of the fold proximal to the lateral force, and vertical compression of the distal side.

In all of the above explanations, the mechanism of formation can no longer be active because more recent sediments filling the troughs remain horizontal at an angular discordance with the dipping reflectors of the Foreslope Hills. In order to distinguish the mechanism of formation of the Foreslope Hills, their morphology, internal and subbottom geometry must be determined accurately. The data set now exists with this survey to address these points.

Roberts Bank Failure Complex

The Roberts Bank Failure Complex is a large, lens-shaped unit of chaotic reflectors. The unit is up to 80 m thick and tapers in the offshore direction. The area encompassed by this feature is about 40 km^2 and involves about 1 x 10^9 m^3 of sediment volume (Terra Surveys, 1994). This feature has been interpreted as consisting of one or perhaps several slope mass-failure deposits. An alternative interpretation is that this feature may represent simply a change in depositional style from other areas on the delta slope. The favoured interpretation is that it represents a failure complex. Reasons for this conclusion include the following:

1. significant degassing (allowing acoustic penetration), as expected from remobilized sediment;
2. chaotic internal reflections suggestive of remoulding;
3. rough, hummocky seafloor topography;
4. a strong, phase-reversed basal reflector, indicating a large impedance contrast with underlying sediments. The phase change and high amplitude are indicative of gas-brightening, where the sediment underlying the failure complex is gas-laden. This basal reflector appears concave upwards, and the whole complex is roughly lens-shaped;
5. a wedge-shaped toe at the downslope edge overlying gas-charged sediments with parallel reflectors, which are more characteristic of "normal" delta slope sediments;
6. burial of chaotic reflectors by apparently undisturbed recent sediments; and,
7. abrupt truncation of parallel reflectors along the landward margin of the complex (Fig 5).

Data from PGC95001 support this interpretation and will lead to better estimates of the size of the complex. Hopefully they will provide evidence to conclude the more exact mechanisms of failure that produced the feature as well.

SUMMARY AND CONCLUSIONS

Conclusions about the nature and condition of sedimentary features on the Fraser River delta, in particular sediment mass-failure features, bear significantly on the assessment of present day stability of the delta and its suitability for hosting engineering structures and associated industries. Survey PGC95001 was designed to address the overall structure of the Strait of Georgia and the genesis of several probable sediment failures. Significant results have already been extracted from some of the data. The 0.65 L (40 in^3) sleeve gun multichannel system has given excellent quality data. Techniques such as velocity analysis, wide-angle reflection analysis, and amplitude versus offset analysis will tell much about the detailed structure and properties of the delta sediments. Brute trace stacking has been shown to lend greater definition of the deeper structure within the Strait of Georgia, and more sophisticated velocity analysis and stacking should lead to even better resolution. Gridded surveys, as was done for this expedition, lend themselves to processing and visualization techniques which lead to better interpretation. Interstitial gas within offshore sediments remains a problem for defining the detailed stratigraphy and structure of the delta in some areas. The Huntec sparker system has proven effective in many areas of the delta for giving good, high resolution reflection profiling data. Digital collection of these data has permitted the use of hi-fidelity post-processing and imaging techniques as an aid to interpretation.

REFERENCES

Clague, J.J., Luternauer, J.L., Pullan, S.E., and Hunter, J.A.
1991: Postglacial deltaic sediments, southern Fraser River delta, British Columbia; Canadian Journal of Earth Sciences. v. 28, p. 1386-1393.

Hamilton, T.S.
1991: Seismic stratigraphy of unconsolidated sediments in the central Strait of Georgia: Hornby Island to Roberts Bank; Geological Survey of Canada, Open File 2350, 7 map sheets.

Hamilton, T.S. and Wigen, S.O.
1987: The Foreslope Hills of the Fraser Delta: Implications for tsunamis in Georgia Strait; International Journal of the Tsunamis Society, v. 5, p. 15-33.

Hart, B.S.
1993: Large-scale in situ rotational failure on a low-angle delta slope: The Foreslope Hills, Fraser Delta, British Columbia, Canada; Geo-Marine Letters, v. 13, p. 219-226.

Hart, B.S. and Hamilton, T.S.
1993: High-resolution acoustic mapping of shallow gas in unconsolidated sediments beneath the Strait of Georgia, British Columbia; Geo-Marine Letters, v. 13, p. 49-55.

Hart, B.S., Hamilton, T.S., Prior, D.B., and Barrie, J.V.
1993: Seisomstratigraphy and sedimentary framework of a deep water Holocene delta: the Fraser River Delta, Canada; in Geology of Deltas, M.N. Oti (ed.); A.A. Balkema Publishers.

Hart, B.S., Hamilton, T.S., Barrie, J.V., Currie, R.G., and Prior, D.B.
1992a: Marine geophysical and geological surveys of the Fraser Delta slope and adjacent Strait of Georgia: 1991 geophysical survey tracklines and 1983-1992 core locations; Geological Survey of Canada, Open File 2543, 5 map sheets.

Hart, B.S., Horel, G., Olynyk, H.W., and Frydecky, I.
1992b: An airgun seismic survey of the Fraser Delta slope; in Current Research, Part E; Geological Survey of Canada, Paper 92-1E, p. 33-39.

Luternauer, J. and Finn, W.D.L.
1983: Stability of the Fraser River Delta front; Canadian Geotechnical Journal, v. 20, p. 603-616.

Luternauer, J.L., Clague, J.J., Hunter, J.A.M., Pullan, S.E., Roberts, M.C., Woeller, D.J., Kostaschuk, R.A., Moslow, T.F., Monahan, P.A., and Hart, B.S.
1993: The Fraser River delta, British Columbia: architecture, geological dynamics and human impact; Deltas of the World, proceedings, 8th Symposium on Coastal and Ocean Management, New Orleans, Louisiana, July 19-23, 1993.

Monahan, P.A., Luternauer, J.L., and Barrie, J.V.
1993: A delta topset sheet sand and modern sedimentary processes in the Fraser River delta, British Columbia; Current Research, Part A; Geological Survey of Canada, Paper 93-1A, p. 263-272.

Terra Surveys Ltd.
1994: The Roberts Bank Failure Deposit, Fraser River Delta, British Columbia; Unpublished Contract Report to Geological Survey of Canada, Pacific Geoscience Centre, Sidney, B.C., 29 pp.

Tiffen, D.L.
1969: Continuous Seismic Reflection Profiling in the Strait of Georgia, British Columbia; Ph.D. Thesis, Department of Oceanography, University of British Columbia, Vancouver, British Columbia, 177 p.

Tiffen, D.L., Murray, J.W., Mayers, I.R., and Garrison, R.E.
1971: Structure and origin of Foreslope Hills, Fraser Delta, British Columbia; Bulletin Canadian Petroleum Geology, v. 19, p. 589-600.

Geological Survey of Canada Project 890052

Geological setting, geochronology, and thermal modelling of the Portland Canal dyke swarm, Stewart area, northwestern British Columbia[1]

Darwin Green[2], Charles J. Greig[3], and Richard M. Friedman[2]
GSC Victoria

Green, D., Greig, C.J., and Friedman, R.M., 1995: Geological setting, geochronology, and thermal modelling of the Portland Canal dyke swarm, Stewart area, northwestern British Columbia; in Current Research 1995-E; Geological Survey of Canada, p. 47-57.

Abstract: The Portland Canal dyke swarm comprises at least four lithologically distinct phases: plagioclase-quartz porphyritic rhyolite; potassium feldspar-plagioclase-quartz porphyritic dacite-rhyolite; hornblende-biotite monzonite; and aphyric basalt. The swarm, situated along the eastern margin of the Coast Belt, records ~30% extension across its 1-2 km width. Relative ages determined from field relations for the dykes and the cospatial Bitter Creek pluton, are not reflected in coeval U-Pb ages determined for the rhyolite (50.5 ± 0.3 Ma), dacite-rhyolite (50.4 ± 0.3 Ma), and pluton (50.4 ± 0.3 Ma). The ages concur with many of the region's post-kinematic intrusions. Modelling of conductive heat transfer of multiple, closely-spaced dykes from a 225 m measured section, shows that after 5 years, the host rocks between dykes attained temperatures of at least 500°C.

Résumé : L'essaim de dykes de Portland Canal comprend au moins quatre phases lithologiquement distinctes : rhyolite porphyrique à quartz-plagioclase; dacite-rhyolite porphyrique à feldspath potassique-plagioclase-quartz; monzonite à hornblende-biotite; et basalte aphyrique. L'essaim, situé le long de la bordure est du Domaine côtier, subit une extension de 30 % sur sa largeur de 1 à 2 km. Les âges relatifs déterminés à partir des relations sur le terrain des dykes et du pluton cospatial de Bitter Creek, ne correspondent pas aux âges U-Pb contemporains déterminés pour la rhyolite (50,5 ± 0,3 Ma), l'association dacite-rhyolite (50,4 ± 0,3 Ma) et le pluton (50,4 ± 0,3 Ma). Les âges coïncident avec de nombreuses intrusions post-cinématiques de la région. La modélisation du transfert de chaleur par conduction de dykes multiples faiblement espacés dans un profil mesuré de 225 m, montre qu'après cinq ans les roches hôtes entre les dykes ont atteint des températures d'au moins 500°C.

[1] Industrial Partners Project, involving the Geological Survey of Canada and LAC Minerals Ltd.

[2] Department of Geological Sciences, The University of British Columbia, 6339 Stores Road, Vancouver, British Columbia V6T 1Z4
[3] Westmin Resources, #904 - 1055 Dunsmuir Street, Vancouver, British Columbia V7X 1C4

INTRODUCTION

The Portland Canal dyke swarm (PCDS) is a striking, 1-2 km wide concentration of pale-weathering Tertiary dykes which intrude dark-weathering stratified rocks of Stikinia near the eastern margin of the Coast Belt (Fig. 1, 2). It is situated within glaciated, high relief terrain and can be visually traced for ~40 km along strike between Mount Trevor, a large nunatak in the Cambria Icefield, and Mount Bayard, on the east edge of the Frank Mackie Icefield. Maximum strike length is uncertain because dykes extend underneath ice sheets at both ends of the swarm. The swarm consists of at least four distinct intrusive phases that range in composition from basalt to rhyolite. They intrude deformed, mainly Triassic and Jurassic volcanic and clastic rocks, and are spatially, temporally, and perhaps genetically related to the Bitter Creek pluton. The Portland Canal dyke swarm records at least 30% extension across its width, and was emplaced within a subduction-related, convergent-margin setting. It is the largest of a number of Tertiary dyke swarms recognized in the region, including: the Boundary (to the west), the Berendon (to the north), and the Nelson Glaciers (to the east) (Fig. 1; Grove, 1971, 1986; Alldrick, 1993; Greig et al., 1994a,b). The swarms, together

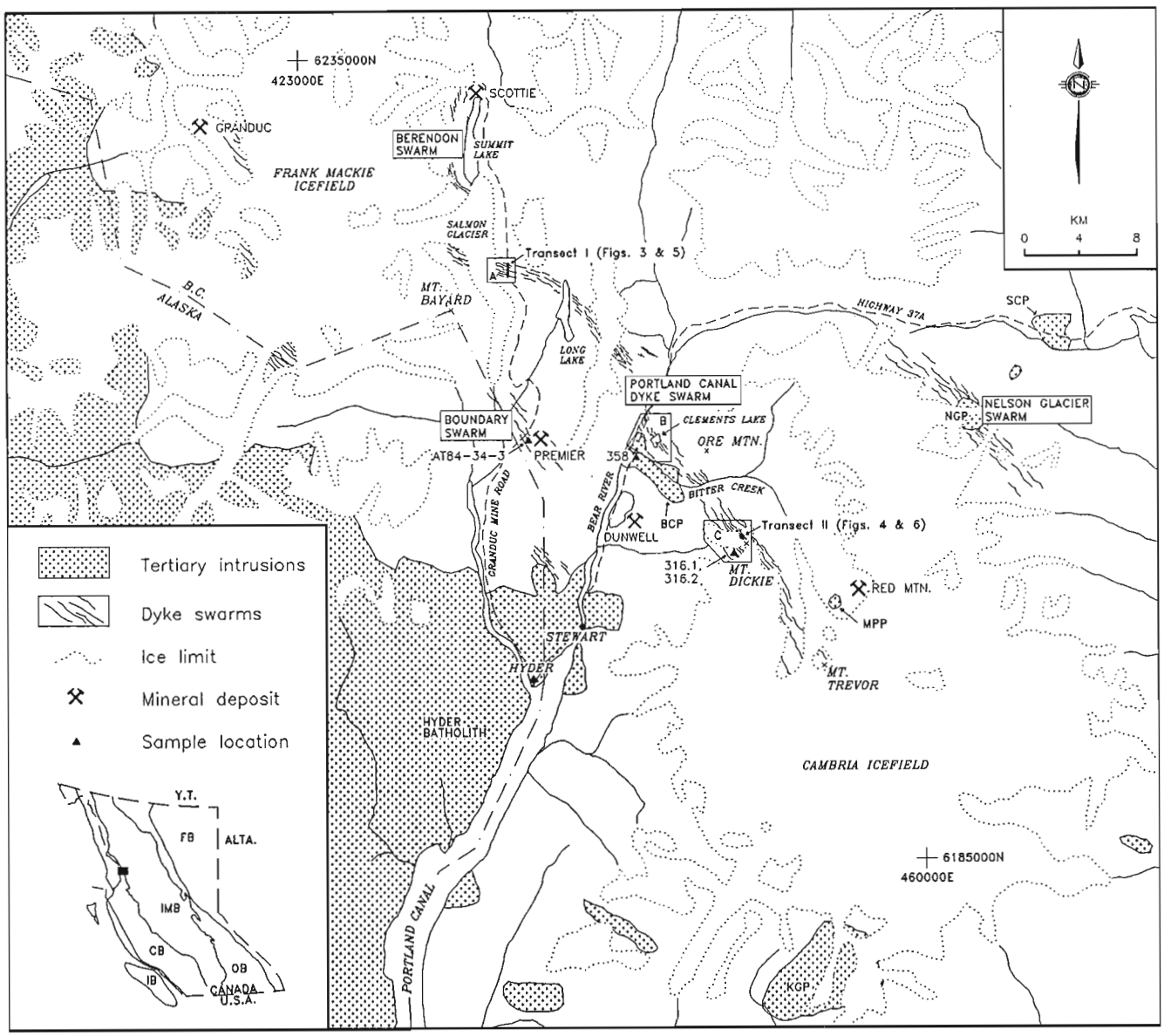

Figure 1. Distribution of Tertiary intrusive rocks in the Stewart area (modified from Grove, 1971, 1986, and Greig et al., 1994a). Boxes A, B, and C outline areas of detailed study (A = Salmon Glacier area, B = Clements Lake area, C = Mount Dickie area). BCP = Bitter Creek pluton, SCP = Strohn Creek pluton, MPP = McAdam Point pluton, NGP = Nelson Glaciers pluton, KGP = Kshwan Glacier pluton. Inset map of British Columbia shows the morphological belts of the Canadian Cordillera (FB = Foreland Belt, OB = Omineca Belt, IMB = Intermontane Belt, CB = Coast Belt, and IB = Insular Belt), and the shaded region shows the location of the Stewart area.

with nearby high level stocks and plutons, are commonly associated with Ag-Pb-Zn veins, and locally, with porphyry Mo mineralization (Carter, 1981; Grove, 1986).

This study was undertaken to characterize the Portland Canal dyke swarm, and to better understand its age, genesis, and tectonic setting. Of particular interest was its relationship to the Bitter Creek pluton, which Grove (1986) suggested was continuous with the swarm. The swarm has received no prior systematic, detailed work, although it has been described briefly in regional studies (e.g. Hanson, 1935; Grove, 1971, 1986; Alldrick, 1993; Greig et al., 1994b). Ten days of fieldwork in August 1994 were focused directly on the Portland Canal dyke swarm. The work involved detailed measurement of sections, and sample collection in the Salmon Glacier, Clements Lake, and Mount Dickie areas for U-Pb isotopic dating and petrography (Fig. 1). As well, regional reconnaissance mapping (e.g. Greig et al., 1994a,b) involved recording the pattern of dykes from vantage points, and collection of compositional and orientation data wherever traverses intersected the swarm.

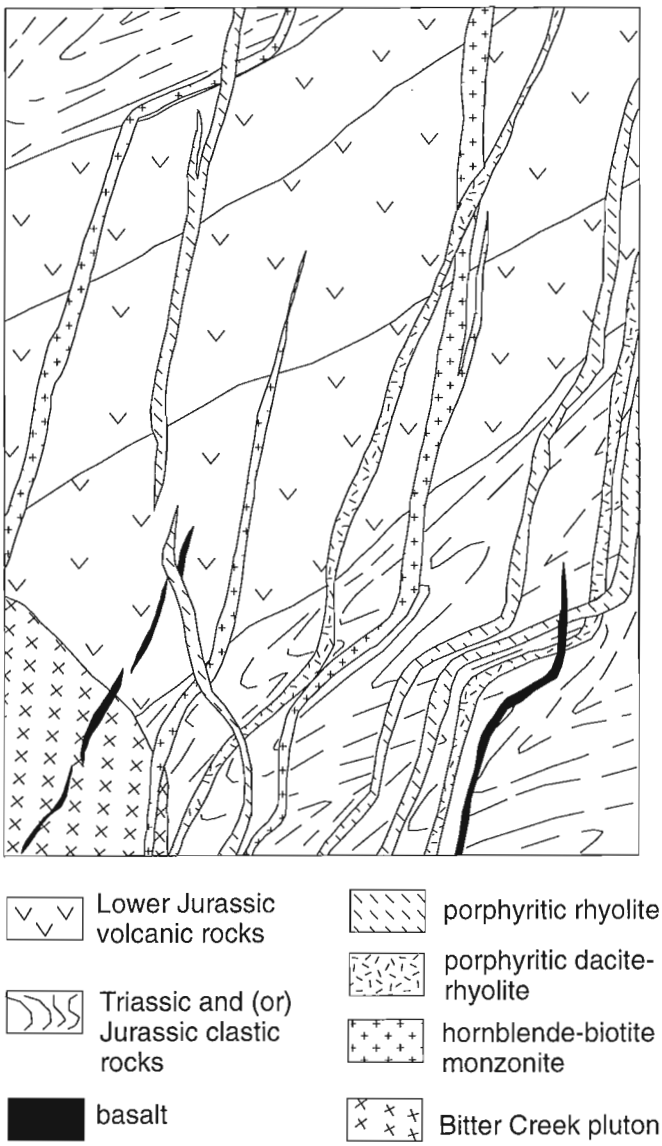

Figure 2. Schematic diagram showing crosscutting relationships of the Portland Canal dyke swarm, as well as variations in dyke orientation with host rock lithology.

GEOLOGICAL SETTING

The Portland Canal dyke swarm forms part of a regionally extensive, post-kinematic Tertiary plutonic suite, the Hyder plutonic suite (Woodsworth et al., 1991), which intrudes deformed Upper Jurassic and older volcanic and sedimentary rocks of Stikinia. The larger Tertiary intrusive bodies define the eastern margin of the Coast Belt, which in the Stewart region is represented by the elongate and composite Hyder batholith, which extends for 175 km, from the Unuk River on the northwest, to Alice Arm on the southeast (Grove, 1986). The Hyder batholith is bordered on the southwest by the Central Gneiss Complex (Grove, 1986) and, to the northeast, much smaller plutons, and dyke swarms, including the Portland Canal dyke swarm, are its equivalents. The Tertiary plutons vary in composition from quartz monzonite and monzogranite to granodiorite or quartz diorite, and are generally medium grained, unfoliated, and little altered (Grove, 1986; Greig et al., 1994b).

The mainly Triassic to Upper Jurassic host rocks to the Portland Canal dyke swarm were disrupted during latest Jurassic or Early Cretaceous to Tertiary northeasterly directed Skeena Fold Belt contraction (Evenchick, 1991). Massive, relatively competent Lower Jurassic volcanic rocks are broadly folded and faulted, and both underlying and overlying clastic rocks are more commonly tightly folded. Folds and faults predate emplacement of the dykes, disrupt stratigraphy, and are largely responsible for variations in the orientation of host rocks. Southeast of Bear River, the swarm primarily intrudes tightly folded, thin bedded, siltstone and mudstone of probable Late Triassic to earliest Jurassic age. Northwest of Bear River, the swarm is hosted primarily by resistant Lower Jurassic volcanic rocks. Near Long Lake, the Portland Canal dyke swarm intrudes Middle to Upper(?) Jurassic clastic rocks (Grove, 1986).

LOCAL GEOLOGY

The Portland Canal dyke swarm forms a 1 to 2.5 km wide, weakly arcuate to sigmoidal, northwest-trending zone which at any one locality consists of about 60 parallel dykes. Intrusions are subvertical and transect layering in massive volcanic and volcaniclastic host rocks, but in southwest-dipping clastic sequences the intrusions are commonly oriented parallel to bedding (Fig. 2). The geometries suggest that orientations are partially controlled by rheology of the host rock. No obvious variations in trends between constituent phases were observed. Post-Middle Eocene dextral strike-slip faulting has locally offset the swarm up to 1.4 km (Brown, 1987).

Dykes in the Portland Canal dyke swarm were emplaced at high crustal levels. Hornfelsing appears minimal in country rocks, because no macroscopic contact metamorphic mineral

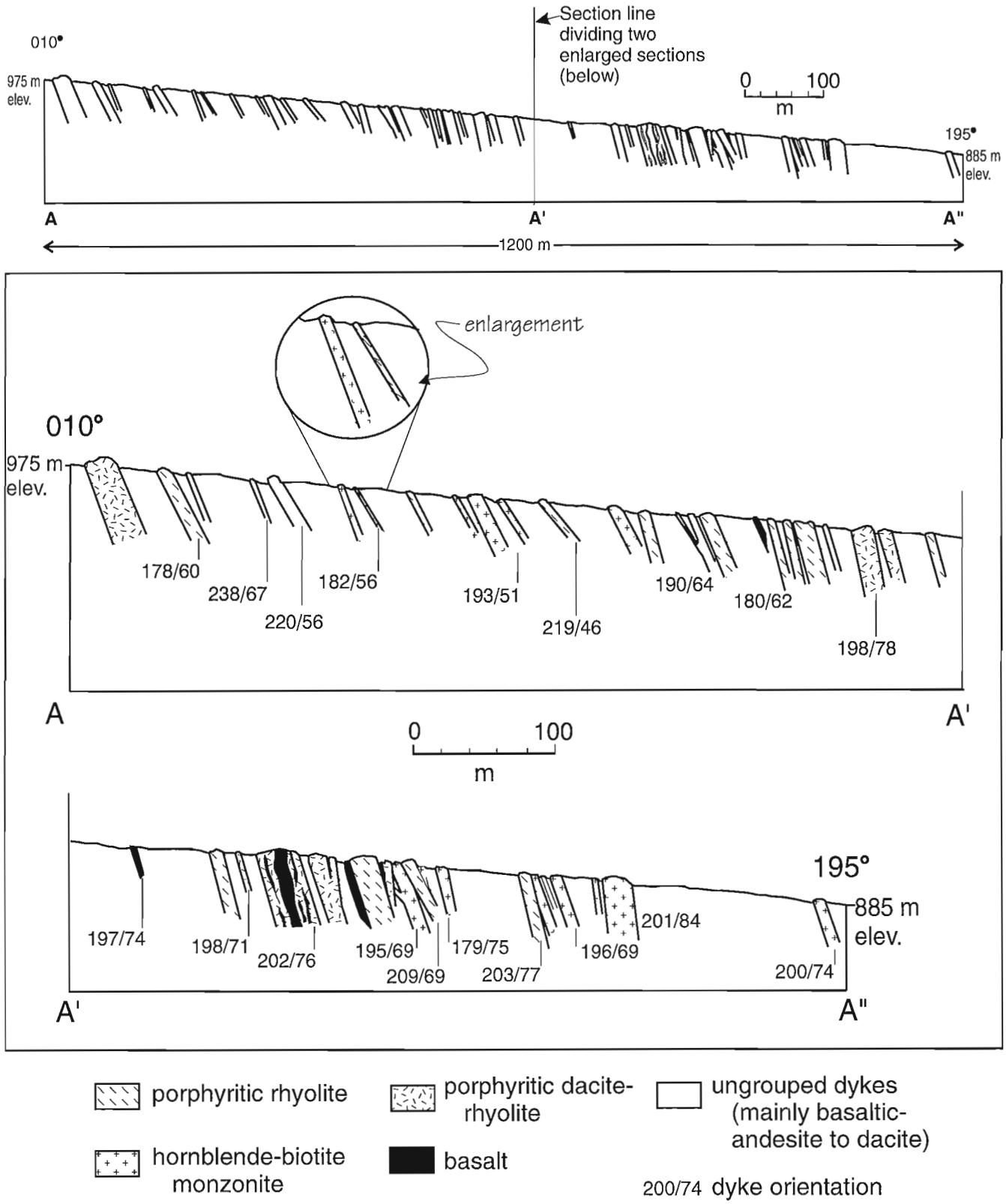

Figure 3. Cross-section through Portland Canal dyke swarm in the Salmon Glacier area; showing measured dip directions and dips and including all dykes >1 m in thickness (Transect I, Fig. 1).

assemblages were observed. However, contact metamorphic mineral assemblages comprising andalusite, cordierite, and biotite are common in the aureoles of coeval and cospatial plutons. Possible volcanic equivalents to the dykes have likely been removed by erosion.

Individual dykes and sills may be as much as 52 m thick, but most commonly range in thickness from 5 to 11 m. On the megascopic scale, contacts appear planar and individual dykes can be traced for hundreds of metres. In detail, contacts are sharp, with common centimetre-scale irregularities. A common cryptocrystalline groundmass precludes observation of chilled margins. Inclusions within dykes are generally very rare, although locally they are abundant.

COMPOSITION

Four distinct lithologies, or phases, are widespread throughout the study area and, where the swarm was mapped in detail, account for at least 90% of the cumulative dyke thickness (Fig. 3, 4). The phases, distinguished in the field on the basis of mineralogy, texture, and colour, are rhyolite, dacite-rhyolite, hornblende-biotite monzonite, and basalt. Several dykes encountered within the Portland Canal dyke swarm are clearly different lithologically from the four main phases. These include rare, recessive weathering lamprophyre dykes, which crosscut all other dykes, and feldspar-phyric basaltic-andesite to dacite dykes, some of which are altered, have variable orientations, and may be much older than the principal components of the swarm. Others are likely variations of the four main phases, which are described below in decreasing order of abundance.

Rhyolite

The buff-weathering character of rhyolite dykes (buff to pale yellow-green on fresh surfaces) enables them to be distinguished from most other phases. Flow layers, typically 1-2 cm thick, define zones up to 40 cm thick along the margins of some dykes. The layering mimics irregularities along contacts with both country rocks and other dyke phases. Rhyolite dykes are sparsely porphyritic, and contain about 4% fine- to medium-grained, euhedral quartz and plagioclase feldspar phenocrysts. The quartz phenocrysts appear to dominate in hand sample, but in thin section quartz and plagioclase phenocrysts are subequal in abundance. Determination of groundmass composition was hindered by its moderately altered, cryptocrystalline nature. However, staining and petrography indicates that the matrix is dominated by potassium feldspar and quartz. Very fine grained muscovite is subordinate, forms about 6% of the matrix, and typically occurs as interstitial fibrous mats between radial growths of quartz and potassium feldspar.

Hornblende-biotite monzonite

Monzonite dykes are light grey weathering, and light to medium grey on fresh surfaces. Most dykes are seriate, very fine- to medium-grained, and have a cryptocrystalline groundmass, which staining suggests largely comprises potassium feldspar. The phaneritic minerals comprise 24% to 62% of the rock, and consist of plagioclase feldspar (19-59%), and biotite, hornblende, and quartz (3-4%). In most dykes, mafic minerals are altered to chlorite, and feldspars are intensely saussuritized.

Dacite-rhyolite

Dykes of this phase vary from faint salmon pink to light yellow-brown to medium green in weathering colour. They are characterized by subequal amounts of medium- to coarse-grained potassium feldspar, plagioclase, and quartz phenocrysts, and trace amounts of fine grained biotite and hornblende, which make up about 20% of the rock. Quartz phenocrysts are generally rounded and embayed, and plagioclase phenocrysts commonly occur in synneusis texture. The groundmass is cryptocrystalline to microcrystalline, and is weakly

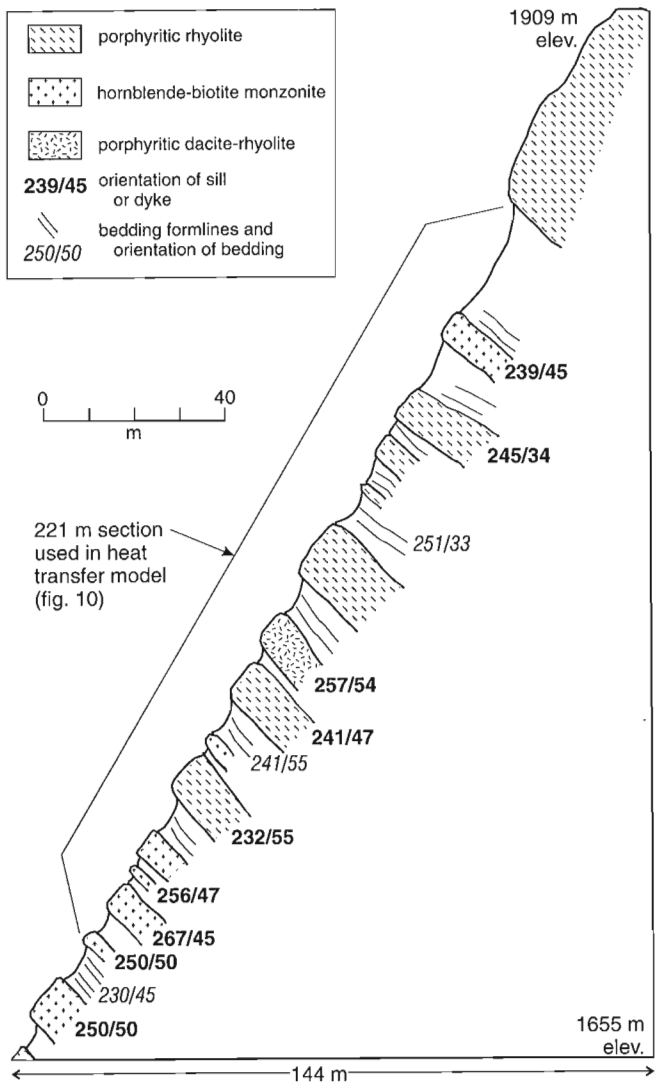

Figure 4. Cross-section through the central part of the swarm, Mount Dickie area; showing measured dip directions and dips and including all dykes >1 m in thickness (Transect II, Fig. 1).

to moderately potassic. Inclusions are generally uncommon; however, dark green, quartz and plagioclase phyric inclusions are locally abundant.

Basalt

Basalt dykes are common throughout the study area, although they are typically narrow (<1 m), discontinuous, and account for only a very small proportion of the total volume of the swarm. They are dark green to black on weathered and fresh surfaces, and are typically aphyric. Orientations of individual basalt dykes are locally irregular, but overall they maintain parallelism with the swarm.

DETAILED STUDY AREAS

Salmon Glacier area

The Salmon Glacier area is 24 km north-northwest of Stewart, and is accessed by the Granduc Mine road. Dykes are well exposed along the road on the east side of the glacier (Fig. 5), which permits detailed mapping of a strike-perpendicular section along roadcuts (Fig. 3). A total of 55 dykes were measured across a 1.2 km transect. Cumulative dyke thickness is about 400 m, indicating extension due to dyke emplacement of 30%. Rhyolite accounts for 33% of the cumulative thickness, hornblende-biotite monzonite 28%, dacite-rhyolite 26%, basalt 4%, and dykes of indeterminate or other composition 10%.

Dykes in the Salmon Glacier area dip moderately to steeply south-southwest (average dip of 65° toward 197°), with dip magnitudes shallowing slightly from south to north (Fig. 3). Host rocks consist of poorly bedded, altered, pyritic siliceous tuff and minor siltstone. Individual dykes range from less than 1 m to 34 m in thickness, although zones composed of multiple dykes attain thicknesses as great as 60 m. Locally, apophyses of the larger dykes form discontinuous dyklets, typically <1 m in thickness. The thickest dyke occurs near the centre of the swarm, is of dacite-rhyolite composition, and is cored by a 5 m basalt dyke which shows mutual crosscutting relationships. The basalt is fine grained and displays irregular lobate contacts with the host dacite-rhyolite. Locally, lobes of the basalt appear to be detached and surrounded by dacite-rhyolite. Thin (<1 m) aphanitic basalt dykes with sharp contacts are common peripheral to the fine grained central basalt and nearer the margins of the host. It is possible that the basalt dykes were emplaced soon after intrusion of the host, after its margins had solidified, but before its centre had. Heat transfer calculations discussed in a later section lend support to these interpretations.

Clements Lake area

The Clements Lake area is located along Highway 37A in Bear River Valley, 15 km north-northeast of Stewart. The Bitter Creek pluton and the Portland Canal dyke swarm occur there, and limited exposures indicate that monzonite and basalt dykes intrude the pluton. Other host rocks include mafic fragmental volcanic rocks, and black, cleaved siltstone. Pervasive fractures, slickensides, and weak to moderate sericitic and chloritic alteration occur in the dykes and in the Bitter Creek pluton, particularly in outcrops close to the centre of the valley. On the microscopic scale, a history of strain is recorded in the dykes by weakly polygonized quartz phenocrysts, and by calcite filled fractures. Deformation is assumed to be related to post-Middle Eocene brittle faulting localized along the north-northeast-trending Bear River Valley (Hanson, 1935). Sulphide mineralization, occurring within quartz and quartz-carbonate veins found along dyke walls, and locally within dykes, has high values in Au, Ag, Pb, Zn, and Cu, and has prompted sporadic small-scale mining activity since the early 1900s. Immediately south, similar vein mineralization, such as at the Dunwell Mine, occurs in the Portland Canal Fissure Zone of Hanson (1935), a fault zone which roughly parallels the valley.

Mount Dickie area

The Mount Dickie area is located ~12 km northeast of Stewart, and was accessed by helicopter. The swarm intrudes tightly folded, thin-bedded, black to dark brown, Upper

Figure 5.

Portland Canal dyke swarm in the Salmon Glacier area; view to east (see Fig. 1, 3).

Figure 6.

View south towards Mount Dickie and cliffy exposure through the central part of the swarm (see Fig. 1, 4). Intrusions parallel bedding in the black, siltstone and mudstone host rocks.

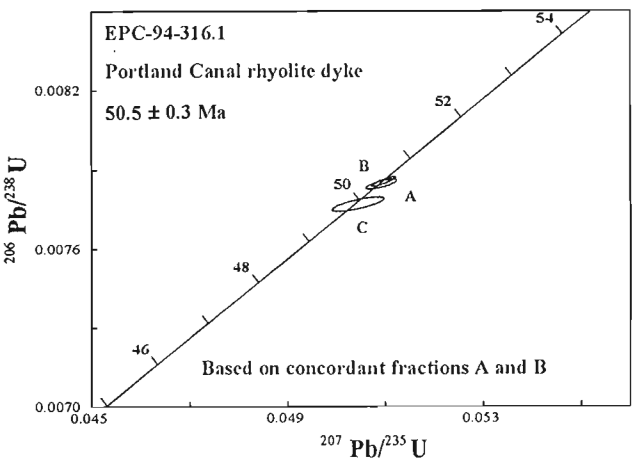

Figure 7. U-Pb concordia plot for zircon from sample EPC-94-316.1, a rhyolite dyke of the Portland Canal dyke swarm.

Triassic and (or) lowermost Jurassic siltstone and mudstone. Intrusions are dominantly bedding parallel sills, which locally transect bedding with subvertical orientations (Fig. 2). The sills, which comprise 67% rhyolite, 27% hornblende-biotite monzonite, and 6% dacite-rhyolite, are closely spaced, and are rarely more than 10 m apart (Fig. 6). Other compositions are rare, but locally, basalt dykes intrude rhyolite dykes. Sills in the central section (221 m) have a cumulative thickness of 162 m, and therefore record 58% extension (Fig. 4).

RELATIVE AGE CONTROL

The sequence of emplacement of the various dyke phases and the Bitter Creek pluton is based on crosscutting relationships; however, crosscutting relationships among dykes are uncommon and rarely observed. For example, the age of the Bitter Creek pluton relative to the dykes is constrained by a single monzonite dyke intruding the pluton near its eastern margin. The sequence is (oldest to youngest): 1) Bitter Creek pluton, 2) hornblende-biotite monzonite, 3) dacite-rhyolite, and 4) rhyolite. Basalt dyking occurred during at least two events: during or shortly after intrusion of dacite-rhyolite in the Salmon Glacier area, and following intrusion of rhyolite in the Salmon Glacier and Mount Dickie areas. Basalt and lamprophyre dykes are relatively common throughout the region, and many are Oligocene in age (Carter, 1981; Brown, 1987).

U-Pb GEOCHRONOLOGY

No previous dates for the Portland Canal dyke swarm exist. A dyke from the Boundary swarm, situated near the Premier mine, south of the Portland Canal dyke swarm, yielded a U-Pb zircon date of 54.8 ± 1.3 Ma (Sample no. AT84-34-3, Fig. 1, Alldrick et al., 1987), and a single rhyolite sill to the southeast of the Cambria Icefield yielded a U-Pb date of 53.7 ± 2 Ma (Greig et al., 1994a). There are also numerous plutons in the Cambria Icefield area which have yielded Middle Eocene K-Ar dates. The Bitter Creek pluton was dated by Alldrick (1993; 48.4 ± 3.4 Ma), the McAdam Point pluton by Schroeter et al. (1992; 45 ± 4 Ma) and the Nelson Glaciers pluton (50.5 ± 2.4 Ma), Strohn Creek pluton (51.9 ± 2.6 Ma), and Kshwan Glacier pluton (48.3 ± 1.3 Ma) by Greig et al. (1995; Fig. 1).

New U-Pb zircon analytical data are presented and interpreted herein for the Bitter Creek pluton and for the rhyolite and dacite-rhyolite phases of the Portland Canal dyke swarm (Table 1, Fig. 7, 8, 9). Mineral separation and analytical procedures were performed at the University of British Columbia Geochronology Laboratory, and procedural details may be found in Journeay and Friedman (1993).

Rhyolite dyke (EPC-94-316.1)

The plagioclase-quartz porphyritic rhyolite was collected from a dyke about 1 km southwest of Mount Dickie, where it intrudes a dacite-rhyolite dyke (sample EPC-94-316.2, see below) as well as Upper Triassic or lowermost Jurassic black clastic country rocks. The sample yielded abundant good quality, translucent to transparent, brown prismatic zircon. Data for three analyzed fractions intersect concordia between

49.9 and 50.5 Ma. The best age estimate, 50.5 ± 0.3 Ma, is based on concordant fractions A and B. Fraction C likely suffered minor Pb-loss.

Dacite-rhyolite dyke (EPC-94-316.2)

The potassium feldspar-plagioclase-quartz porphyritic dacite-rhyolite yielded good quality, transparent zircon of prismatic and tabular morphology. Four analyzed fractions define an array indicative of inheritance and possible minor Pb loss. The best age estimate, 50.4 ± 0.3 Ma, is based on concordant fraction C. Data for fraction D, which consisted of stubby prismatic grains, clearly contains minor inherited zircon. Traces of inheritance are also likely to explain the minor shifts of analyses A and B off of concordia. Fraction A also appears to have suffered minor Pb-loss.

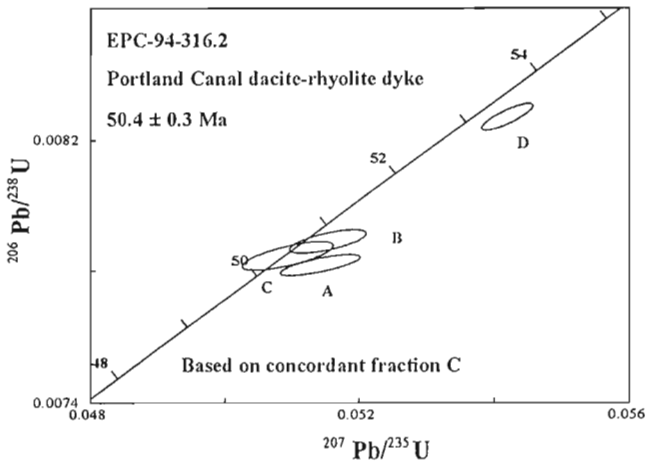

Figure 8. U-Pb concordia plot for zircon from sample EPC-94-316.2, a dacite-rhyolite dyke of the Portland Canal dyke swarm.

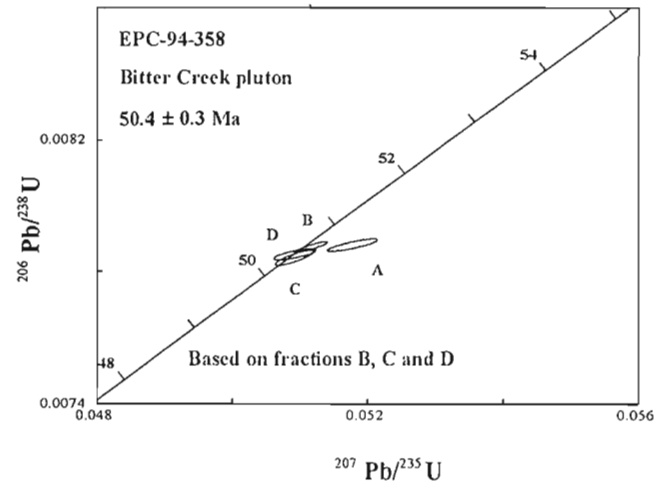

Figure 9. U-Pb concordia plot for zircon from sample EPC-94-358, of the Bitter Creek pluton.

Table 1. U-Pb Zircon Analytical Data

Fraction[1]	Wt.	U	Pb[2]	^{206}Pb[3]	Pb[4]	^{208}Pb[5]	Isotopic ratios(±1σ,%)[6]			Isotopic dates(Ma,±2σ)[6]		
	mg	ppm	ppm	^{204}Pb	pg	%	$^{206}Pb/^{238}U$	$^{207}Pb/^{235}U$	$^{207}Pb/^{206}Pb$	$^{206}Pb/^{238}U$	$^{207}Pb/^{235}U$	$^{207}Pb/^{206}Pb$
EPC-94-316.1: Portland Canal rhyolite dyke; UTM (zone 9) 448550E, 6204890N												
A,m,N20,p	0.120	2466	19.6	1239	111	11.0	0.00785±0.12	0.0509±0.31	0.04704±0.23	50.4±0.1	50.4±0.3	51.2±11.2
B,m,N20,p	0.087	4374	34.9	1928	90	11.3	0.00787±0.12	0.0510±0.24	0.04703±0.15	50.5±0.1	50.5±0.2	50.8±7.0
C,m,N20,p	0.118	4245	33.5	435	544	11.2	0.00778±0.17	0.0505±0.53	0.04708±0.42	49.9±0.2	50.0±0.5	53.3±20.0
EPC-94-316.2: Portland Canal dacite-rhyolite dyke; UTM (zone 9) 448460E, 6204850N												
A,cc,N2,p,e	0.258	547	4.3	403	176	10.9	0.00782±0.21	0.0514±0.58	0.04769±0.45	50.2±0.2	50.9±0.6	84.1±21.5
B,c,N2,p,e	0.120	661	5.3	336	123	11.2	0.00789±0.23	0.0515±0.56	0.04736±0.44	50.7±0.2	51.0±0.6	67.5±20.9
C,c,N2,p,e	0.350	788	6.3	292	486	11.0	0.00785±0.28	0.0509±0.67	0.04707±0.50	50.4±0.3	50.4±0.7	52.9±24.3
D,c,N2,p,eq	0.227	723	6.0	2103	39	10.3	0.00827±0.25	0.0542±0.35	0.04751±0.20	53.1±0.3	53.6±0.4	75.0±9.3
EPC-94-358: Bitter Creek pluton; UTM (zone 9) 443250E, 6210325N												
A,c,N2,p	0.153	817	6.4	758	77	9.4	0..00788±0.12	0.0518±0.36	0.04766±0.27	50.6±0.1	51.3±0.4	82.4±12.7
B,m,N2,p,e	0.131	1111	8.6	1864	36	8.6	0.00787±0.11	0.0512±0.24	0.04713±0.15	50.6±0.1	50.7±0.2	55.7±7.2
C,m,N2,p,eq	0.159	1427	10.9	1389	76	7.8	0.00784±0.15	0.0509±0.28	0.04709±0.17	50.4±0.1	50.4±0.3	54.0±8.4
D,m,N2,t	0.112	797	8.7	1666	25	8.7	0.00785±0.11	0.0509±0.31	0.04704±0.24	50.4±0.1	50.4±0.3	51.1±11.4

[1]All fractions are air abraded; Grain size, smallest dimension: cc= +149 μm, c= +134μm, m=-134μm+74μm, f=-74μm; Magnetic codes
Franz magnetic separator sideslope at which grains are nonmagnetic; e.g., N1=nonmagnetic at 1°; Field strength for all fractions =1.8A; Front slope for all fractions=20°; Grain character codes: e=elongate, eq=equant, p=prismatic, ti=tips; t=tabular
[2]Radiogenic Pb
[3]Measured ratio corrected for spike and Pb fractionation of 0.0043/amu ±20% (Daly collector)
[4]Total common Pb in analysis based on blank isotopic composition
[5]Radiogenic Pb
[6]Corrected for blank Pb, U and common Pb (Stacey-Kramers model Pb composition at the $^{207}Pb/^{206}Pb$ date of fraction, or age of sample)

Bitter Creek pluton (EPC-94-358)

Medium- to coarse-grained, inequigranular (coarse grained quartz), unfoliated monzogranite was collected from a quarry on the east side of Highway 37A, about 0.6 km west of the Bitter Creek bridge. It yielded high quality, transparent, colourless zircon, predominantly of elongate prismatic morphology. Data for four analyzed fractions define an array indicative of inheritance. The best estimate for the age of this rock, 50.4 ± 0.3 Ma, is based on concordant fractions B, C, and D.

Discussion

The new U-Pb ages confirm an assumed Eocene age for the Portland Canal dyke swarm and revise the age of the Bitter Creek pluton to indicate that the pluton and dykes are essentially coeval. The ages are all concordant and do not further constrain the relative timing of dyke emplacement within the Portland Canal dyke swarm. The Portland Canal dyke swarm and Bitter Creek pluton are coeval with the Nelson Glaciers pluton, which is cospatial and presumably coeval with the Nelson Glaciers swarm, but are apparently younger than the Boundary swarm.

There is a close similarity in the isotopic ages of post-kinematic intrusions in the Stewart area, which, with the exception of Oligocene mafic dykes (35-25 Ma), are between 55-45 Ma (Carter, 1981; Brown, 1987; Schroeter et al., 1992; Alldrick, 1993; Greig et al., 1994a,b, 1995). This coincides with data collected along the entire length of the Coast Plutonic Complex, and defines one of the most voluminous plutonic episodes in the Canadian Cordillera (Woodsworth et al., 1991).

THERMAL MODELLING

Modelling parameters

The effect of Portland Canal dykes on the thermal state of the country rocks was modelled using a finite difference approximation to simulate conductive heat transfer perpendicular to dyke walls (Fig. 10). The model, based on the Crank-Nicolson method (Crank, 1990), attempts to approximate the emplacement of rhyolite dykes into siltstone and mudstone across 221 m of measured section near Mount Dickie (Fig. 4, 6).

The model assumes equivalent thermal conductivity for both dyke and host rock. Boundary conditions were chosen to be constant country rock temperature (200°C) at a distance of 60 m on either side of the swarm. With distance steps of 1 m and a thermal conductivity of 10^{-6} m^2/s, time steps were fixed at intervals of 11.56 days. It was assumed that the rhyolite dykes were emplaced synchronously, following equilibration of any thermal perturbations caused by previous dyke phases. Such assumptions are supported by the uniformity of rhyolite dyke compositions in the Mount Dickie area, and the presence of sharp, well defined crosscutting relationships of rhyolite dykes with other intrusive phases.

Initial host rock temperature of 200°C was based on the geotherm and an estimated depth of about 4 km within an active magmatic arc environment, taking into account slight heating due to previous magmatic activity. The initial intrusion temperature of the rhyolite magma was estimated at 900°C (Philpotts, 1990). Latent heat of crystallization is accounted for in the model by defining an equivalent intrusion temperature in which the heat liberated from crystallization is added to the initial intrusion temperature (Delaney, 1987).

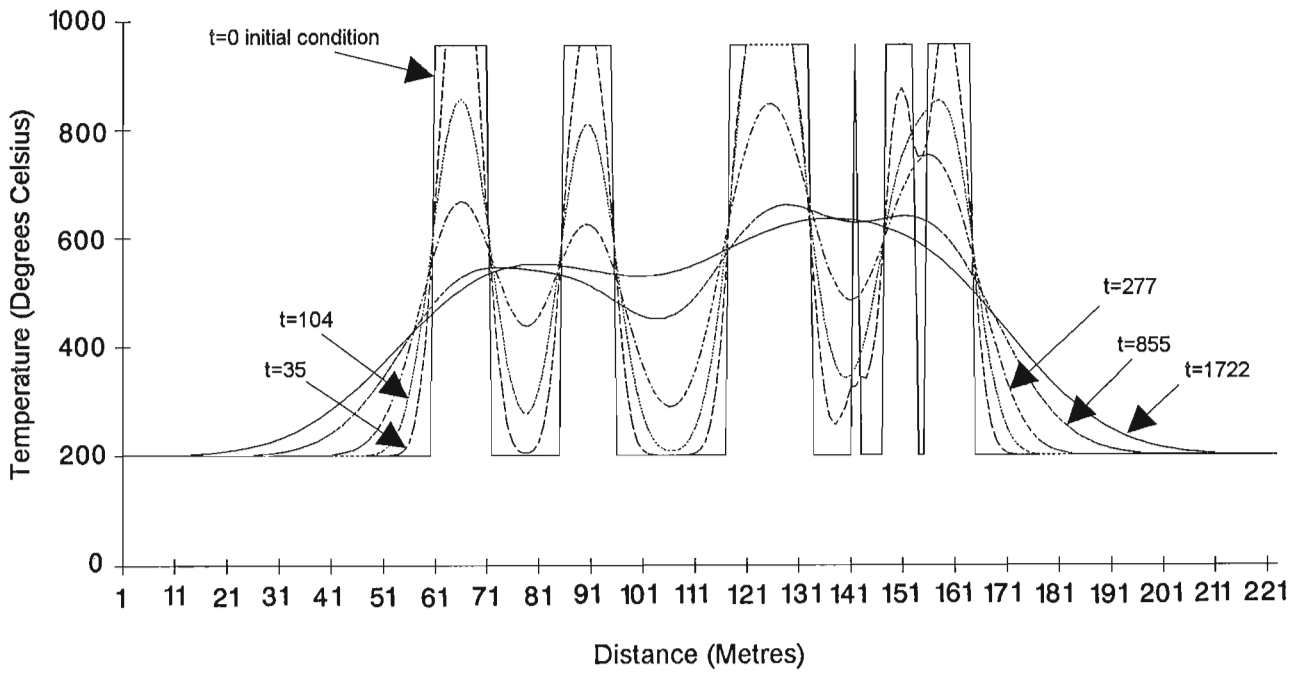

Figure 10. *Thermal profile at various time intervals (t = days), following synchronous emplacement of multiple dykes. Density and thickness of the dykes is modelled after a section measured near Mount Dickie (see Fig. 4, 6).*

For the rhyolite dykes, the latent heat of crystallization is assumed to be minimal because of their cryptocrystalline groundmass. Therefore only 55°C was added to the initial magma temperature, a somewhat arbitrarily reduced value based on the 113°C obtained from Bowers et al.'s (1990) 35 cal/g heat of crystallization for a granite. Also accounted for in the model was magma flow, and an inwardly propagating isotherm represents the solidification of melt. By tracking the solidification isotherm into the dykes, one can roughly estimate the duration for which they can remain open to flow. Dykes with widths of 9 m or greater had cores which never dropped below the solidification isotherm, and therefore the duration of magmatic flow had to be arbitrarily restricted.

Results

The modelling indicates that conduction of heat from multiple, closely spaced dykes increased the ambient temperatures of intervening host rocks by 300°C or more (Fig. 10). The elevated temperatures were maintained for an extended period; after 5 years host rocks among the dykes had reached temperatures of at least 500°C, much higher than the temperatures attained in host rocks peripheral to the swarm. Thicker dykes were more likely to remain open conduits for magmatic flow, and would therefore introduce more heat to the country rocks. The ability of thick dykes to remain open to magma flow is corroborated in the 34 m thick, basalt-cored, dacite-rhyolite dyke in the Salmon Glacier area.

From the results of the modelling, one might expect to find contact metamorphic mineral assemblages, and possibly evidence for hydrothermal circulation. No metamorphic minerals were observed during field mapping, but may have been missed because of microscopic grain sizes, or because the bulk composition or duration of heating or lack of a hydrous phase may have affected the kinetics of mineral growth. A history of hydrothermal fluid circulation may be evidenced by the occurrence of vein mineralization proximal to the swarm.

TECTONIC AND MAGMATIC IMPLICATIONS

Dykes, as a general rule, propagate in a direction perpendicular to the least compressive stress, whereby magmatic pressure fractures the host rock and forms dilations into which dykes are injected (Pollard, 1987). The process is dynamic, and dependent on both the magnitude of the magmatic pressure head, and the ability of the host rock to fracture. Any substantial volume of dyke emplacement must occur in an extensional structural regime. It is proposed here that the timing of intrusion of the Portland Canal dyke swarm's four distinct phases was largely controlled by the build up and release of crustal tension, in which magmatic pressure triggered fracture in the rock. Evidence for host rock structural control on the orientation of Portland Canal dyke swarm intrusions is apparent in their common sill-like geometry where they intrude clastic rocks, and suggests that the magnitude of least compressive stress probably did not vary greatly from that of one or both of the other principal stresses (Pollard, 1987).

An apparent trend of increasing fractionation with time is observed in the dyke swarm: from hornblende-biotite monzonite, to dacite-rhyolite, to rhyolite. It may represent the sequential draining of a continuously fractionating source, in which successive extensional events activated dyke propagation and allowed separate batches of magma to rise from their source (Sawyer, 1994). Further geochemical study is required to evaluate the genetic relationships between dykes and to support the assumptions of source magma evolution, but the geochronological data and field relations are permissive.

It is clear from the abundance of dyke swarms in the Stewart area that there was active upper crustal extension during Middle Eocene time, but its cause remains unclear. The somewhat sigmoidal trend of the Portland Canal dyke swarm suggests the possibility that extension may have occurred between bounding transcurrent faults. However, large-displacement Middle Eocene transcurrent faults have not been documented in the Stewart area, and it may be that the previously existing, northwest-trending regional structural grain, in concert with local north-northwest- to north-northeast-trending faults, may have had an influence on the siting of the Portland Canal dyke swarm. Alternatively, the extensional structural regime may be related to upwarping and extension in response to emplacement of large magmatic bodies, such as the Hyder batholith, immediately southwest of, and possibly underlying, the Portland Canal dyke swarm.

ACKNOWLEDGMENTS

Fieldwork was supported by the Geological Survey of Canada (GSC) and LAC Minerals Ltd.; we are indebted to Garfield MacVeigh and Hans Smit of LAC, and to Bob Anderson and Tom Foerster of the GSC for arranging the support. Bob Anderson is also acknowledged for a thorough review. Paul Lhotka of Westmin Resources Ltd. is thanked for allowing access to unpublished property maps of the Salmon Glacier area. The use of University of British Columbia facilities (Geochronology and Igneous Petrology labs, and Mineral Deposit Research Unit) is acknowledged, and Jim Mortensen, Kelly Russell, and John Thompson are thanked for their advice and co-operation. Thanks are also due Tanya Mauthner and Claire Floriet for field assistance, Lindsie Nicholson and Tonia Williams for drafting, and Bev Vanlier for formatting.

REFERENCES

Alldrick, D.A.
1993: Geology and metallogeny of the Stewart Mining Camp, northwestern British Columbia; British Columbia Ministry of Energy, Mines and Petroleum Resources, Bulletin 85, 105 p.

Alldrick, D.J., Brown, D.A., Harakal, J.E., Mortensen, J.K., and Armstrong, R.L.
1987: Geochronology of the Stewart mining camp (104B/1); in Geological Fieldwork 1986; British Columbia Ministry of Energy, Mines and Petroleum Resources, Paper 1987-1, p. 81-92.

Bowers, J.R., Kerrick, D.M., and Furlong, K.P.
1990: Conduction model for the thermal evolution of the Cupsuptic aureole, Maine; American Journal of Science, v. 290, p. 644-655.

Brown, D.A.
1987: Geological setting of the volcanic-hosted Silbak Premier Mine, northwestern British Columbia (104 A/4, B1); M.Sc. thesis, University of British Columbia, Vancouver, British Columbia, 216 p.

Carter, N.C.
1981: Porphyry copper and molybdenum deposits of west-central British Columbia; British Columbia Ministry of Energy, Mines and Petroleum Resources, Bulletin 64, 150 p.

Crank, J.
1990: The Mathematics of Diffusion; Oxford University Press, New York, 414 p.

Delaney, P.T.
1987: Heat transfer during emplacement and cooling of mafic dykes; in Mafic Dyke Swarms, H.C. Halls and W.F. Fahring (ed.); Geological Association of Canada, Special Paper 34, p. 31-46.

Evenchick, C.A.
1991: Geometry, evolution, and tectonic framework of the Skeena Fold Belt, north-central British Columbia; Tectonics, v. 10, p. 527-546.

Greig, C.J., Anderson, R.G., Daubeny, P.H., and Bull, K.F.
1994a: Geology of the Cambria Icefield area, northwestern British Columbia; Geological Survey of Canada, Open File 2931.

Greig, C.J., Anderson, R.G., Daubeny, P.H., Bull, K.F., and Hinderman, T.K.
1994b: Geology of the Cambria Icefield: regional setting for Red Mountain Au deposit, northwestern British Columbia; in Current Research 1994-A; Geological Survey of Canada, p. 45-46.

Greig, C.J., McNicoll, V.J., Anderson, R.G., Daubeny, P.H., Harakal, J.E., and Runkle, D.
1995: New K-Ar and U-Pb dates for the Cambria Icefield area, northwestern British Columbia; in Current Research 1995-A; Geological Survey of Canada, p. 97-104.

Grove, E.W.
1971: Geology and mineral deposits of the Stewart area, British Columbia; British Columbia Department of Mines and Petroleum Resources, Bulletin 58, 219 p.

Grove, E.W. (cont.)
1986: Geology and mineral deposits of the Unuk River-Salmon River-Anyox area; British Columbia Ministry of Energy, Mines and Petroleum Resources, Bulletin 63, 152 p.

Hanson, G.
1935: Portland Canal area, British Columbia; Geological Survey of Canada, Memoir 175, 179 p.

Journeay, J.M. and Friedman, R.M.
1993: The Coast Belt thrust system: Evidence of shortening in the Coast Belt of southwestern British Columbia; Tectonics, v. 12, p. 756-775.

Philpotts, A.R.
1990: Principles of Igneous and Metamorphic Petrology; Prentice Hall, Englewood Cliffs, New Jersey.

Pollard, D.D.
1987: Elementary fracture mechanics applied to the structural interpretation of dykes; in Mafic Dyke Swarms, H.C. Halls and W.F. Fahring (ed.); Geological Association of Canada, Special Paper 34, p. 5-24.

Sawyer, E.W.
1994: Melt segregation in the continental crust; Geology, v. 22, p. 1019-1022.

Schroeter, T., Lane, B., and Bray, A.
1992: Red Mountain (103P 086); in Exploration in B.C. 1991; British Columbia Ministry of Energy, Mines and Petroleum Resources, Paper 1992-1, p. 117-125.

Woodsworth, G.J., Anderson, R.G., and Armstrong, R.L.
1991: Plutonic Regimes; Chapter 15, in Geology of the Cordilleran Orogen in Canada, Geological Survey of Canada, Geology of Canada, no. 4, p. 491-531.

Geological Survey of Canada Project 940007

Effects of limnological variation on element distribution in lake sediments from Tatin Lake, central British Columbia – implications for the use of lake sediment data in exploration and environmental studies

P.W.B. Friske
Mineral Resources Division

Friske, P.W.B., 1995: Effects of limnological variation on element distribution in lake sediments from Tatin Lake, central British Columbia – implications for the use of lake sediment data in exploration and environmental studies; in Current Research 1995-E; Geological Survey of Canada, p. 59-67.

Abstract: Three lake sediment cores were collected from Tatin Lake to evaluate the effects of changing limnological conditions on the distribution of trace metals in lake sediments. Two cores were taken from sites where the hypolimnion was relatively oxygenated and the third from a sub-basin where distinctly anoxic conditions existed.

Sediments deposited in the relatively oxidizing environments have significant enrichments of Fe and Mn in the surface sediments due to diagenetic cycling. Vertical trends in As, Co and Ni are similar to Fe and Mn, suggesting co-migration and enrichment of these elements during diagenesis. Concentrations of Cu, Cr, Mo, Sr, V and Zn are not significantly different in the surface sediments compared to the background sediments.

Limnological variations are a significant factor in controlling the accumulation and preservation of trace metals in lake sediments. The usefulness of lake sediment data, whether for exploration or environmental purposes, could be enhanced by evaluating it in the context of limnological information.

Résumé : Trois carottes de sédiments lacustres ont été prélevées au lac Tatin afin d'évaluer les effets de l'évolution des conditions limnologiques sur la répartition des métaux présents à l'état de traces dans les sédiments lacustres. Deux de ces carottes ont été recueillies à des endroits où l'hypolimnion était relativement oxygéné et la troisième provient d'un sous-bassin où existaient des conditions nettement anoxiques.

Les sédiments superficiels dans les milieux relativement oxydants présentent des enrichissements importants en Fe et en Mn en raison d'un recyclage diagénétique. Les variations suivant la verticale des concentrations de As, de Co et de Ni sont similaires à celles observées pour le Fe et le Mn, ce qui suggère une migration et une concentration combinées de ces éléments pendant la diagenèse. Les concentrations en Cu, Cr, Mo, Sr, V et Zn des sédiments superficiels ne diffèrent pas de manière significative des fonds géochimiques sédimentaires.

Les variations limnologiques constituent un important facteur déterminant l'accumulation et la conservation de métaux à l'état de traces dans les sédiments lacustres. L'utilité des données sur les sédiments lacustres, pour l'exploration ou à des fins environnementales, pourrait être améliorée par leur évaluation dans le contexte de l'information limnologique.

INTRODUCTION

The Geological Survey of Canada (GSC) and provincial geological surveys have collected lake sediment samples from over 100 000 sites throughout Canada under the auspices of the National Geochemical Reconnaissance (NGR) program. The surveys were initially undertaken to assist mineral exploration by mapping regional geochemical patterns and anomalous element concentrations potentially related to economic mineral deposits (Friske and Hornbrook, 1991). Recently the data have been also used in environmental studies providing valuable information on the natural distribution and base line levels for upwards of 35 elements (e.g. Friske and Coker, in press; Friske et al., 1994a, b).

To better understand the processes that control element distribution in lake sediment and water, orientation and follow-up studies are being undertaken on particular aspects of lake sediment geochemistry. Information obtained from these directed studies will be used to enhance interpretative techniques for the voluminous NGR lake sediment database. In July 1993, 3 short cores were taken from Tatin Lake, in central British Columbia (Fig. 1). The primary objective was to evaluate the effects of changing limnological conditions on the distribution of trace metals in lake sediments. Tatin Lake was chosen for this detailed work because: 1) it has three distinct sub-basins that vary in their limnological characteristics; 2) the lake is essentially surrounded by one rock type, thereby removing a significant variable controlling lake sediment composition; and 3) it is relatively isolated with no known source of anthropogenic input.

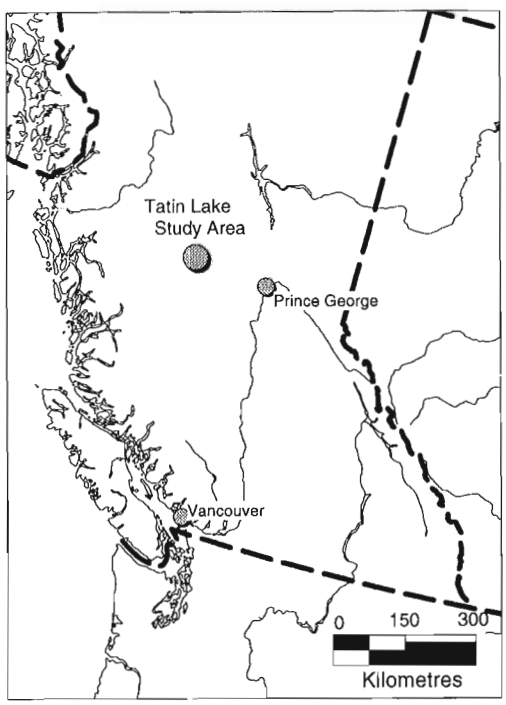

Figure 1. Location map of the Tatin Lake study area.

STUDY AREA

Tatin lake is located in the Nechako Plateau, approximately 175 km west of Prince George (Fig. 1). Access is by way of Highway 16 west from Prince George to Endako and then north along local logging roads. The local terrain is low, rolling and covered by extensive tracts of coniferous forests. The lake is elongated in an east-west direction, has a surface area of 2.3 km^2, and has three distinct basins as defined by the 15 m depth contour (Walsh, 1977). Mean depth is 9.5 m with a maximum depth of 22 m. There are several inlets and outlets.

The catchment bedrock is primarily quartz-monzonite, part of the Late Jurassic Francois Lake intrusions (Fig. 2). Volcanic rocks also occur in the region but only constitute a small portion of the total shoreline at the far western end of the lake. The granitoid rocks host the Ken Mo-Cu occurrence located just north of the lake. Molybdenite is the dominant ore mineral with trace amounts of chalcopyrite and magnetite (Lodder, 1969). The bedrock is covered by extensive glacial deposits, predominately till, related to Pleistocene ice movement that generally trended to the northeast (Tipper, 1971).

SAMPLING AND ANALYTICAL METHODS

Samples and data were collected from the central (site 9301) and eastern basins (site 9302) and a basin within a channel running between the two (site 9303). A sonar unit was used to guide the final site selection. At each station temperature and dissolved oxygen measurements were taken at 1 m intervals using a YSI Model 57 oxygen meter with cable probe.

A Van Dorn sampler was used to collect 1.5 L surface and bottom water samples that were divided into 3 aliquots. The first was used immediately to measure pH, temperature, conductivity and dissolved oxygen using a Corning M90 meter. The other two aliquots were placed in 250 mL Nalgene™ linear polyethylene bottles and stored at 4°C until analyzed. One of these was filtered using 0.45 μm filter paper and acidified with 2 mL of 8 M HNO_3 (pH <2). within 12 hours of collection. No special sample preparation was undertaken on the other split. These waters were then analyzed for a wide range of variables by a number of different techniques, summarized in Table 1.

Sediment cores were collected using a modified Kajak-Brinkhurst corer. A 1.1 m long acrylic tube (inside diameter 7.0 cm) was attached to the sampler and slowly lowered into the sediment to avoid disturbance of the upper sediment. After retrieval the core tubes were sealed and carried upright until extruded. Subsectioning was completed within 24 hours at an interval of 2 cm for the top 10 cm and then generally at 4 cm intervals to the bottom of the core. In the laboratory the samples were freeze dried and then passed through a minus 80-mesh sieve to disaggregate the sample and remove larger fragments. As with the water samples the sediments were analyzed for a wide range of variables by a number of different techniques, summarized in Table 1.

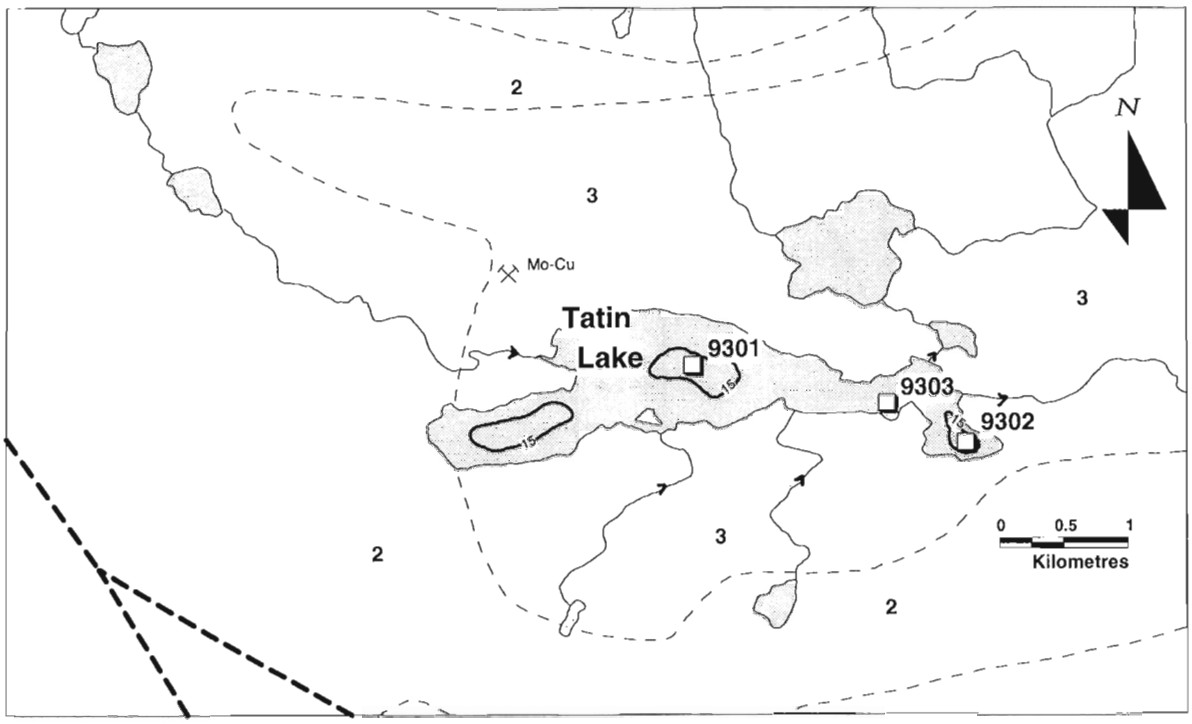

Figure 2. Sample locations, bathymetry, and bedrock geology of the Tatin Lake study area (2: volcanic unit; 3: granitoid unit).

Table 1. Variables determined and methods used for Tatin Lake lake sediment and water samples.

LAKE SEDIMENT	LAKE WATER
Al, Ti, K, Na, Mg, Ca, As, Cr, Sr *(Total digestion--ICP-ES)*	Fe, Mn, Mo, Zn, Cu *(GF-AAS)*
	Ca, Na *(AAS)*
Co, Cu, Mo, Ni, V, Zn *(Total digestion--AAS)*	SO4 *(Ion Chromatography)*
Hg *(Total--CV-AAS)*	Total Alkalinity *(titration to pH 4.5)*
LOI *(gravimetry)*	

RESULTS AND DISCUSSION

Lake water chemistry

Figure 3 and Table 2 summarize the lake water data. All 3 sites exhibit distinct thermal stratification (Fig. 3). In each case a thermocline extends from approximately 6 to 9 m, separating 16 to 18°C epilimnion waters from 5 to 10°C waters of the hypolimnion. Oxygen shows a consistent trend of decreasing concentration down the water column at all sites. The most pronounced oxygen depletion occurs at site 9302 where distinctly anoxic conditions exist in the hypolimnion, the ratio of bottom to surface oxygen concentration (expressed as a percentage) is only 9%. This is in contrast to relatively oxic conditions at the other two sites were bottom to surface oxygen ratios are 57 and 65 per cent.

Most of the other measured parameters, e.g. pH, conductivity and alkalinity, are similar within and between the sampling stations. Iron, Mn, and Mo exhibit the greatest variations. The higher concentrations of Fe and Mn in the bottom waters particularly at site 9302, may reflect the increased solubility of Fe and Mn compounds, both within the water column and surface sediments, under reducing conditions. A similar mechanism may account for the highly anomalous Mo concentrations in the bottom waters at all 3 stations. However, whatever the reason for the higher concentrations of Mo and other elements in bottom waters compared to surface waters, the data clearly show a vertical zonation for some elements in the Tatin Lake water column. This may be an important overlooked variable when using surface lake waters for mineral exploration and environmental studies (cf. Friske et al., 1994b).

Chemical composition of lake sediments

Major components

To assess differences in the chemical composition within and among the three sites, various plots and tables were prepared. For each site, "background" values were computed by averaging the concentration of all samples extending from 22 cm to the bottom of the core (Table 3). This reflects the composition of the relatively stable zone below the most intense diagenetic activity and, assuming a reasonable sedimentation rate of up to 2.5 mm/a (cf. Wong et al., 1984; Fortescue, 1988), predates any anthropogenic atmospheric component. Average composition of the surface sediments (0 to 10 cm) are also given in Table 3.

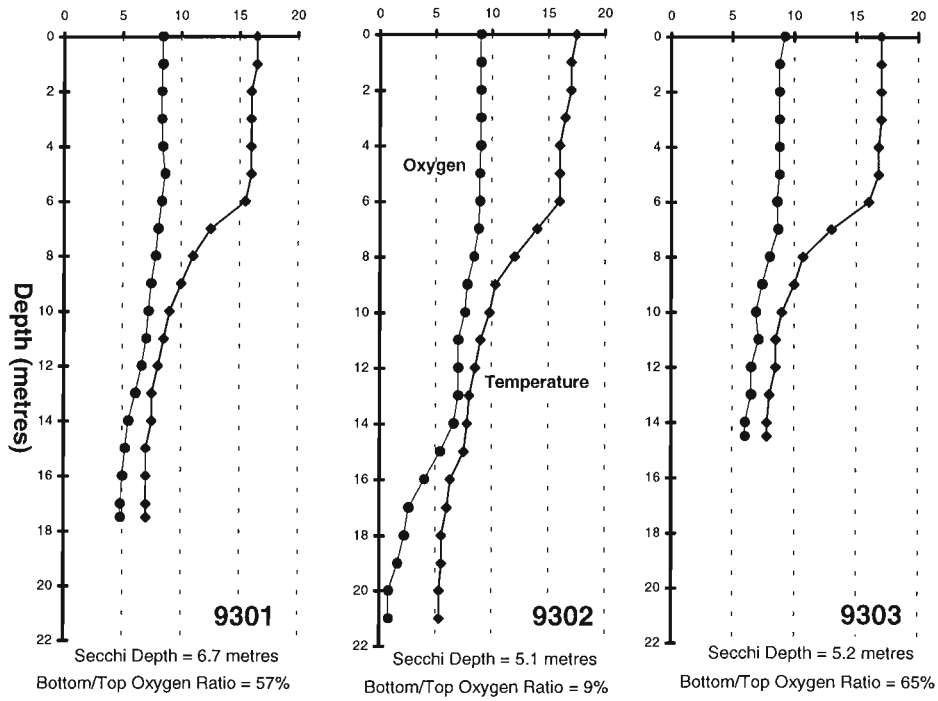

Figure 3. Water column profiles of dissolved oxygen (ppm) and temperature (°C).

Table 2. Summary of selected variables in surface and bottom water samples.

Site	Sample Depth (m)	pH	Specific Cond.	Total Alkalinity (ppm) Field	Total Alkalinity (ppm) Lab	Ca (ppm)	Na (ppm)	SO4 (ppm)	Fe (ppb)	Mn (ppb)	Mo (ppb)	Zn (ppb)	Cu (ppb)
9301	0.5	6.8	81.6	34	34	9.8	2.0	0.26	16	4	<5	6	2
	17.0	7.0	81.9	36	33	10.0	2.1	0.36	93	53	62	10	2
9302	0.5	7.6	77.7	32	34	9.6	2.0	0.26	31	4	<5	10	2
	20.5	7.6	114.7	37	35	9.9	2.1	0.37	192	324	81	5	2
9303	0.5	7.6	83.7	34	34	9.5	2.1	0.28	19	6	<5	4	4
	14.0	7.7	79.3	35	35	9.7	2.1	0.36	37	21	22	15	2

Table 3. Average concentrations of variables in surface (0-10 cm) and "background" (>22 cm) sections of the three Tatin Lake sediment cores. Also shown are the differences, expressed as a percentage, between the background and surface sections using Al normalized data.

			MAJOR COMPONENTS									TRACE ELEMENTS									
			LOI %	Al %	Ti %	K %	Na %	Mg %	Ca %	Fe %	Mn PPM	As PPM	Co PPM	Cr PPM	Cu PPM	Hg PPB	Mo PPM	Ni PPM	Sr PPM	V PPM	Zn PPM
Core		N	GRAV	ICP	ICP	ICP	ICP	ICP	ICP	AAS	AAS	ICP	AAS	ICP	AAS	AAS	AAS	AAS	ICP	AAS	AAS
9301	Av. 0-10 cm	5	34.1	3.0	0.15	0.6	0.9	0.3	1.2	10.5	3652	20	11	23	37	208	9	15	142	56	82
% Change	(Al normalized)		65		-4	-5	4	10	33	141	273	78	51	7	14	121	-15	7	25	2	24
BkGrnd	(22-50 cm)	7	30.7	4.5	0.23	1.0	1.3	0.4	1.3	6.4	1441	16	11	32	48	140	15	21	169	82	98
9302	Av. 0-10 cm	5	31.5	1.8	0.11	0.3	0.4	0.2	0.7	3.5	2468	4	5	20	36	150	21	14	75	55	56
% Change	(Al normalized)		-1		1	6	8	12	11	-36	-20	-30	-27	22	-10	24	-19	-21	9	-10	5
BkGrnd	(22-61 cm)	10	27.4	1.6	0.09	0.3	0.3	0.2	0.5	4.6	2535	5	6	15	35	106	23	15	61	54	47
9303	Av. 0-10 cm	5	40.2	3.5	0.20	0.8	1.0	0.4	1.5	2.6	1007	10	8	32	39	186	13	22	158	63	67
% Change	(Al normalized)		34		1	-26	-16	2	18	44	132	26	20	2	-3	55	23	30	8	2	2
BkGrnd	(22-55 cm)	8	33.0	3.9	0.22	1.0	1.4	0.4	1.4	2.0	484	9	8	35	44	134	11	18	162	69	73

Change +- >25 to 50 percent *Change +- >50 percent*

Aluminum and/or titanium are commonly used as immobile components against which other elements are normalized to evaluate observed compositional changes (Kemp et al., 1976; Johnson et al., 1986; Livett, 1988). Based on the raw compositional data both Al and Ti exhibit distinct changes in all 3 cores but most notably in 9301 (Table 3, Fig. 4) where background Al concentration is 4.5% compared to 3.0% in the surface sediments, a decrease of 33%. Titanium varies sympathetically decreasing from 0.23 to 0.15 per cent. These changes are largely attributable to dilution effects related to the diagenetic increase of Fe and Mn. Figure 5 shows the strong negative correlation ($r^2 = -0.93$) between total Fe plus Mn versus Al for core 9301 which has the largest Fe and Mn increase. A similar trend has been described by Cornwell (1985) in sediments from Toolik Lake in Alaska. Therefore, to evaluate the observed changes in chemical composition, the data have been normalized to Al to correct for dilution effects, assuming that Al was an immobile component. Consistent Ti to Al ratios in all 3 cores (Fig. 4) further supports the contention that Al and Ti have remained immobile during diagenesis of the Tatin Lake sediments. It is unlikely that two elements generally considered as immobile would vary sympathetically.

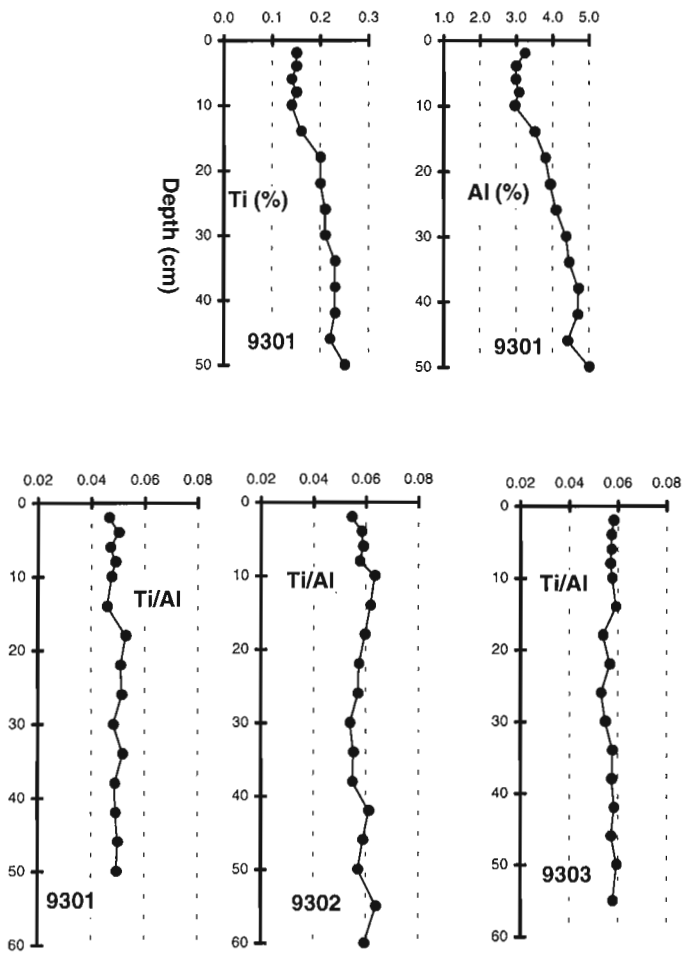

Figure 4. Down core profiles of Al and Ti (raw values) in core 9301 and profiles of Ti to Al ratios for all three cores.

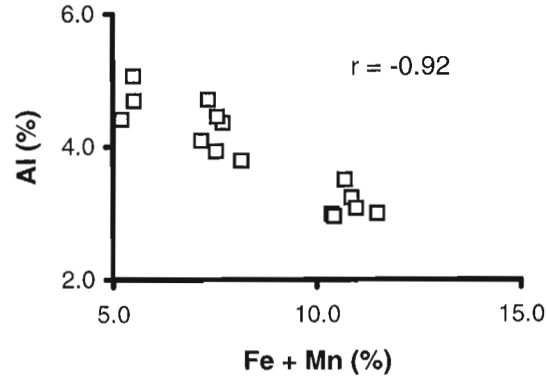

Figure 5. Scatterplot showing the strong negative correlation ($r^2 = -0.92$) between total Al versus total Fe plus Mn in samples from core 9301.

The most striking changes related to the major components (>0.1 wt. %) occur with Fe and Mn. Manganese concentrations in the upper sediments of cores 9301 and 9303 increase by 273% and 132% respectively compared to background (Table 3, Fig. 6). Enrichment in Fe is also considerable increasing 44% in core 9303 and 141% in 9301. In contrast, surface sediments from core 9302 have slightly lower Mn (-20%) and Fe (-36%) contents than the corresponding background sediments.

The spatial trends in Fe and Mn are consistent with the well documented behavior of these two elements in differing limnological environments (Jones and Bowser, 1978; Engstrom and Wright, 1984; Davison, 1985; Bendell-Young et al., 1989) similar to those encountered in Tatin Lake. Circumneutral hypolimnion waters that are relatively oxic throughout the year (site 9301 and 9303) tend to have significant enrichments of Fe and Mn in the upper sediments related to changes in physiochemistry as the sediment is buried. Sediments initially deposited in a relatively oxic environment, at the sediment water interface, are subjected to a more reducing conditions as the material is buried. Under these conditions Fe and Mn tend to migrate upwards through the sediment column, reprecipitating when an appropriate redox boundary is reached (Mortimer, 1941). This process of diagenetic cycling can lead to significant enrichment of Fe and/or Mn at the sediment water interface or upper portion of the sediment column. Site 9302 represents a different limnological situation, in which the hypolimnion is tending towards anoxic conditions for at least part of the year. Under these conditions Fe and Mn released during diagenesis diffuse freely into the overlying water column and no enrichment zone is created.

Loss-on-ignition (LOI) is similar for background samples at the 3 sites ranging from 27 to 33 per cent. The LOI shows a systematic increase (going up profile) of 34% and 65% for cores 9303 and 9301 respectively but no significant change in core 9302. This may reflect increased biological activity within the more oligotrophic portions of the lake during its natural aging process (eutrophication).

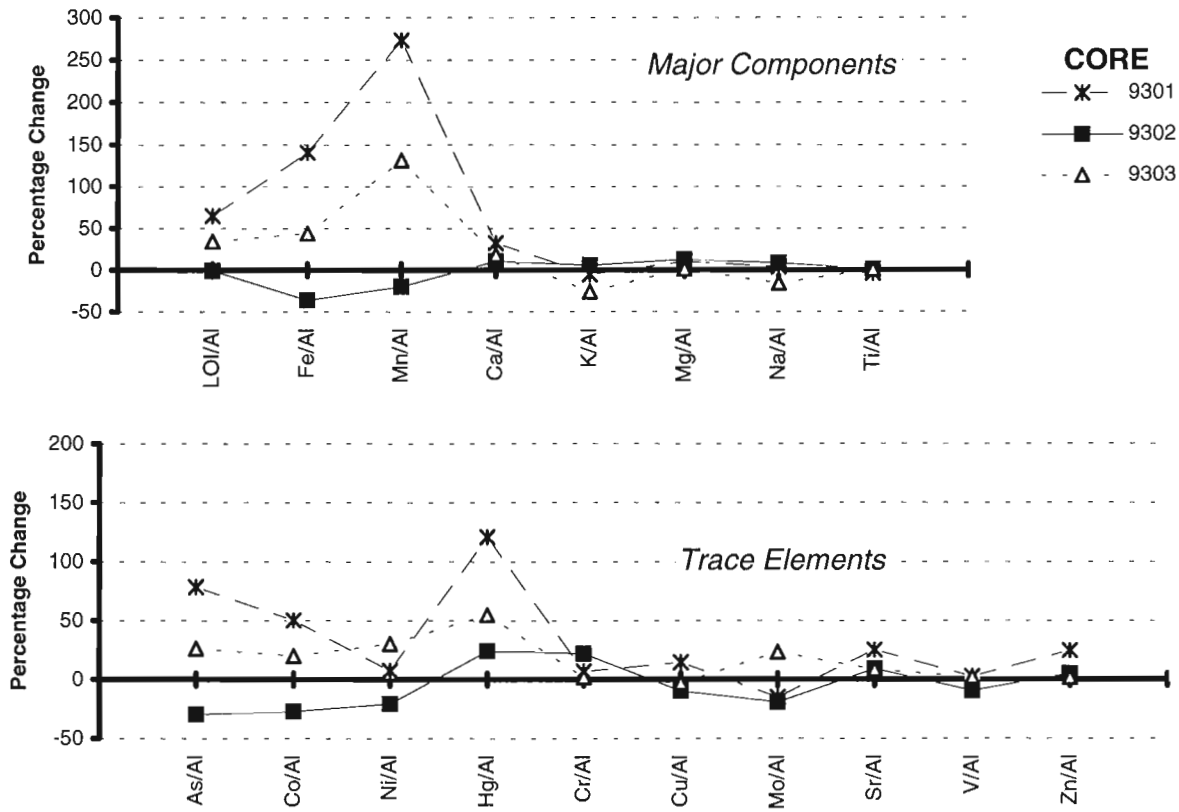

Figure 6. *Summary of changes between background and surface sediments for three cores. Changes based on Al normalized data.*

The remaining major components (K, Na, Mg, and Ca) do not exhibit significant down profile variations, indicating that they have not been affected by post depositional migration as have Fe and Mn (Fig. 6). There are, however, significant differences in the background values of these major components. Background concentrations in core 9302 are roughly 1/2 to 1/3 those encountered at the other 2 sites. This is similar to the difference in Al and Ti between the sites and indicates, as would be expected, that K, Na, Mg and Ca occur primarily in various silicate phases associated with the inorganic clastic fraction (Jones and Bowser, 1978; Engstrom and Wright, 1984).

Trace elements

Trace elements may be bound to a number of phases in lake sediments including silicates, oxides, sulphides, hydrous Fe and Mn oxides, carbonates and organic matter. Information on the speciation of trace elements, as obtained through sequential extractions and other procedures, is important in elucidating their provenance and diagenetic behavior. Only total extraction data are presently available for Tatin Lake sediments. However some general observations and interpretations of the trace element data can be made by evaluating them in the context of the major element data described above.

Of the 10 trace elements determined, the most significant down core changes occur with As, Co, Ni, and Hg. Trends of As, Co and Ni are similar to those of Fe and Mn, i.e. an enrichment in the surface sediments of cores 9301 and 9303 and depletion in 9302 (Table 3, Fig. 6). This suggests co-migration and enrichment of As, Co, and Ni along with Fe and/or Mn during diagenetic processes. Other studies have also documented marked enrichments of As (Azcue et al., 1994), Co (Cornwell, 1987; Williams, 1992) and Ni (Cornwell, 1987) in surficial sediments related to diagenetic cycling. However, in other studies, similar surficial enrichments of these and other elements have been ascribed to anthropogenic input. That the enrichments of As, Co, and Ni at Tatin Lake are related to diagenetic and not anthropogenic effects is indicated by 1) the absence of any definable anthropogenic point source for the 3 elements, 2) the close association of the elements with diagenetically recycled Fe and Mn, and 3) the lack of enrichment, in fact a depletion, at site 9302 because the limnological conditions are not conducive to mobilization and precipitation of hydrous oxides of Fe and Mn and associated trace elements.

Mercury shows an increase going up section in all 3 cores. The strong association of Hg with organic matter in lake sediments is well documented in the literature (Jonasson, 1976; Rasmussen, 1993). The greatest proportional increase in Hg occurs in core 9301 which also has the greatest increase in LOI in the surface sediments relative to background sediments (Table 3). However the increase in Hg by 24% in core 9302 where normalized LOI remained unchanged, suggests that factors other than organic content are controlling the vertical distribution. Rasmussen (1993) described similar enrichment of Hg in the top sediments of lakes from

Huntsville, Ontario, and attributes these to post depositional remobilization of Hg as either Hg°, organically-bound Hg-sulphide, or inorganic Hg-sulphide complexes that are less controlled by redox conditions.

In addition to the chemical changes in the sediment column, there are significant changes in the background concentration for many of the trace elements among the 3 sites. There are likely several factors accounting for these differences. Some of the changes may be related to compositional differences in the sediments as indicated by the major components (e.g. the 2- to 3-fold change in Cr and Sr levels parallel the change in Al). Assuming that Cr and Sr are primarily bound to silicate phases their background level variation may merely reflect changes in the abundance of silicates. Scavenging of trace metals by Fe and/or Mn may be another factor influencing the difference in trace element concentrations (Timperley and Allan, 1974; Coker and Nichol, 1975; Coker et al., 1979). Oxygenated hypolimnion waters (sites 9301 and 9303), as opposed to anoxic conditions, favour the formation and accumulation of Fe and Mn oxides from the water column. Significantly higher values of As, Co, and Ni occur at sites 9301 and 9303 compared to site 9302 where the hypolimnion is distinctly anoxic.

Implications for the use of lake sediment data

If a lake sediment survey were undertaken in the area following NGR protocols, samples would be collected from one or more of the three basins using a torpedo-like gravity sampler. The sampler is designed to collect a grab sample that excludes the upper 10 to 20 cm of the sediment column (Friske, 1991).

Table 4. Background concentration of selected elements at the three sampling stations and corresponding percentile level based on data from the Oosta NGR style lake sediment and water survey.

	As ppm	Co ppm	Cr ppm	Hg ppb	Mo ppm
9301	16 90 %tile	11 >99 %tile	32 85 %tile	140 70 %tile	15 >99 %tile
9302	5 15 %tile	6 60 %tile	15 20 %tile	106 50 %tile	23 >99 %tile
9303	9 60 %tile	8 90 %tile	35 90 %tile	134 65 %tile	11 99 %tile

Therefore NGR lake sediment samples collected from Tatin Lake would be compositionally similar to the "background" values determined for each core (>22 cm depth).

As described above there is considerable variation in the background trace element concentration among the three sites. To evaluate the significance of these differences the data are compared to data from an NGR style survey (Oosta survey) located just south of the study area.(Cook and Jackaman, 1994a). Tatin Lake background values and the corresponding percentile value, based on the Oosta survey data, are shown in Table 4. Data are shown for only 5 trace elements because the others were either not available or were determined using partial extraction procedures. Table 4 shows that the background variation between sites reflects a considerable range of values in the context of the Oosta survey. For example 5 ppm As from site 9302 corresponds to the 15th percentile value for the Oosta survey, whereas the 16 ppm value encountered at site 9301 corresponds to the 90th percentile. Molybdenum levels at all three sites are highly anomalous compared to the regional survey results, likely reflecting the presence of the Ken Mo-Cu occurrence just north of Tatin Lake (Fig. 2).

The variation in background trace element concentration between sites is generally considerably greater than the vertical variation. Table 5 shows that for all trace elements determined at Tatin Lake, except Hg, the range of values between sites (lateral variation) is greater, and often considerably so, than the range of values in the sediment column at a particular site (vertical variation calculated as the difference between surface sediment and background compositions). Therefore for Tatin Lake, because of the limnological differences, the selection of an NGR sample location would have a greater impact in terms of sample composition than the sample depth within the sediment column. Variation related to a grab sample inadvertently including surface sediment, would not be as significant as chemical variation between the sub-basins (Table 5).

The Tatin Lake data clearly show that variations in limnological conditions can affect the concentration of elements in lake sediments. It follows that limnological classification of the sub-basins where NGR samples were collected could be a useful variable for interpreting the lake sediment geochemistry. Lake classification systems are often based on the distribution of temperature and oxygen in the water column. Lakes with frequent or continuous mixing of the entire water column, without temperature stratification, are referred to as

Table 5. Ranges of within site (vertical) and between site (lateral) variations.

		As ppm	Co ppm	Cr ppm	Cu ppm	Hg ppb	Mo ppm	Ni ppm	Sr ppm	V ppm	Zn ppm
Within site range	9301	4	0	9	11	68	6	6	27	26	16
	9302	1	1	5	1	44	2	1	14	1	9
	9303	1	0	3	5	52	2	4	4	6	6
Between site range		11	5	20	13	34	13	6	108	28	51

polymictic lakes Dimictic lakes are characterized by a significant temperature stratification during the summer with free vertical mixing in spring and fall. Dimictic lakes can be further subdivided based on trophic state. Eutrophic lakes are nutrient rich lakes whose bottom waters are almost completely depleted in oxygen. Oligotrophic lakes are characterized by nutrient poor waters with relatively constant oxygen content with depth, and are generally larger and deeper than eutrophic lakes. Mesotrophic lakes are intermediate between the eutrophic and oligotrophic end-members.

Definition of the trophic state can be made on a number criteria including shape of the oxygen profile, nutrient concentrations, various measures of biomass or production. Unfortunately there is often no clear distinction based on a particular criterion and a lake may be oligotrophic by one criterion and eutrophic by another (Carlson, 1977). Earle (1993) classified the trophic status of lakes in the Nechako region of central British Columbia based on the ratio of bottom water to surface water oxygen levels (expressed as a percentage). Lakes with ratios less than 25% were classed as eutrophic, between 25% and 75% mesotrophic, and lakes with ratios greater than 75% were classed as oligotrophic. Using the oxygen profile data from site 9301 (bottom to top ratio: 57%), which is from the main basin, and the classification used by Earle (1993), Tatin lake is classified as mesotrophic (Fig. 3). Using available Ministry of Natural resources data Earle defined the lake as oligotrophic. This is based on top and bottom dissolved oxygen measurements of 9 and 8 ppm (ratio 89%). Regardless of which is correct, the classification of Tatin and other lakes based on data collected in only one or two parts of the lake may be misleading when extrapolated to other regions of the lake, particularly multi-basined lakes. Oxygen profile data from the far eastern basin (Fig. 3) indicate that this sub-basin is distinctly eutrophic.

This serves to illustrate the difficulties in using existing data on the trophic status of lakes to evaluate lake sediment geochemical data. What is required is not a classification of the lake from which a sample is collected but rather a classification of the depositional environment of each sample site. There are over 100 000 lake sediment samples taken across Canada as part of the NGR program. It is not feasible to return to each site and collect information such as oxygen profiles to determine the depositional environment. However there are considerable trace and major element data as well as unused pulps for all samples. With these it may be possible to reconstruct and classify the depositional environment using chemical (cf. Timperley and Allan, 1974; Hoffman and Fletcher, 1981; Earle, 1993) and/or mineralogical criteria (cf. Berner, 1981).

SUMMARY

The Tatin Lake study, clearly demonstrates that changing limnological conditions are important in controlling the composition of lake sediments. There are significant compositional differences between sediments collected from an anoxic sub-basin and two other sites where the hypolimnion is relatively oxygenated. The greatest differences occur with Fe and Mn. Sediments deposited in the relatively oxidizing environments have significant enrichments of Fe and Mn in the surface sediments due to diagenetic cycling. Trends in As, Co, and Ni are similar to Fe and Mn, suggesting vertical co-migration and enrichment of these elements during diagenesis. Concentrations of Cu, Cr, Mo, Sr, V, and Zn are not significantly different in the surface sediments compared to the background sediments indicating they have not been affected by post depositional migration. There are however significant differences in the background concentrations in most trace elements some of which possibly related to limnological factors other than post-depositional cycling.

It is evident that incorporating a limnological variable, would be useful in interpreting lake sediment data. However, lake classification schemes are commonly ambiguous and may not reflect conditions throughout a lake, particularly a multi-basined lake. To assist in the interpretation of NGR lake sediment data what is required is not the classification of the lake from which the sample was taken but rather a classification of the depositional environment of each site. There are considerable elemental data and unused pulps for each NGR sample and using these it may be possible to reconstruct and classify, based on chemical and/or mineralogical criteria, the depositional environment from which the sample was taken. A predictive model that incorporates a limnological factor may more clearly define trends and identify individual anomalies that are otherwise obscured because of combining data from different depositional environments. This would be particularly important for elements, shown to be particularly sensitive to changing limnological conditions, e.g. As, Co, and Ni .

Lake sediment data, primarily from cores, are widely used to monitor the effects of anthropogenic pollution. However, often these studies have only data for the trace elements being evaluated. As shown by the Tatin Lake data this could lead to erroneous interpretations. For example without major element data, such as Al, Fe and Mn, it would not be possible to determine whether compositional changes were related to any of a number of factors including post depositional migration, dilution effects and/or changes in metal loading. Limnological information would also be useful in determining the significance of observed variations in lake sediment profiles. Therefore any interpretation of trace element data from lake cores needs to be done in the context of a comprehensive framework of major element and limnological data.

ACKNOWLEDGMENTS

Martin McCurdy and Steve Day are gratefully acknowledged for their assistance in collecting the cores and related field information. Steve Cook is thanked for supplying previously collected lake sediment data that led to selecting the study area and also for interesting and informative discussions. Thanks are also expressed to Pat Rasmussen for helpful recommendations on the manuscript.

REFERENCES

Azcue, J.M., Mudroch, A., Rosa, F.
1994: Effects of abandoned gold mine tailings on the arsenic concentrations in water and sediments of Jack of Clubs Lake, B.C.; Environmental Technology, v. 15, p. 669-678.

Bendell-Young, L.I., Harvey, H.H., Dillon, P.J., and Scholer, P.J.
1989: Contrasting behavior of manganese in the surficial sediments of thirteen south-central Ontario lakes; The Science of the Total Environment, v. 87/88, p. 129-139.

Berner, R.A.
1981: A new geochemical classification of sedimentary environments; Journal of Sedimentary Petrology, v. 51, no. 2, p. 359-365.

Carlson, R.E.
1977: A trophic state index for lakes; Limnology and Oceanography, v. 22, no. 2, p. 361-369.

Coker, W.B. and Nichol, I.
1975: The relation of lake sediment geochemistry to mineralization in the northwest Ontario region of the Canadian Shield; Economic Geology, v. 71, p. 955-963.

Coker, W.B., Hornbrook, E.H.W., and Cameron, E.M.
1979: Lake sediment geochemistry applied to mineral exploration; in Geophysics and Geochemistry in the Search for Metallic Ores, (ed.) P.J. Hood; Geological Survey of Canada, Economic Geology Report 31, p. 435-477.

Cook, S.J. and Jackaman, W.
1994a: Regional lake sediment and water geochemistry of part of the Nechako River map area (93F/02, 03; 93F/06, 11, 12, 13, 14); British Columbia Ministry of Energy, Mines and Petroleum Resources, Open File 1994-19.
1994b: Regional lake sediment and water geochemistry surveys in the northern Interior Plateau, B.C.(93F/2,3,6,11,12,13,14); in Geological Fieldwork 1993; British Columbia Ministry of Energy, Mines and Petroleum Resources, Paper 1994-1, p. 55-61.

Cornwell, J.C.
1985: Sediment accumulation rates in an Alaskan arctic lake using a modified ^{210}Pb technique; Canadian Journal of Fisheries and Aquatic Science, v. 42, p. 809-814.
1987: Migration of metals in sediment pore waters: Problems for the interpretation of historical deposition rates; Heavy Metals in the Environment, New Orleans, p. 233-235.

Davison, W.
1985: Conceptual models for transport at a redox boundary; in Chemical Processes in Lakes, (ed.) W. Stumm; John Wiley and Sons, p. 31-54.

Earle, S.
1993: Assessment of the applicability of lake sediment geochemical surveys for mineral exploration in the Nechako Plateau area of British Columbia; in Exploration in British Columbia 1992; British Columbia Ministry of Energy, Mines and Petroleum Resources, p. 69-106.

Engstrom, D.R. and Wright Jr., H.E.
1984: Chemical stratigraphy of lake sediments as a record of environmental change; in Lake Sediments and Environmental History; (ed.) E.Y. Haworth and J.W.G. Lund, p. 11-67.

Fortescue, J.A.C.
1988: The use of geochemistry of long lake sediment cores for verification of regional geochemical results: Goudreau Lake area, District of Algoma; in Summary of Field Work and Other Activities, 1988; Ontario Geological Survey, Miscellaneous Paper 141, p. 482-488.

Friske, P.W.B.
1991: The application of lake sediment geochemistry in mineral exploration; Geological Survey of Canada, Open File 2390, Paper 4, p. 4-1 to 4-20.

Friske, P.W.B. and Coker, W.B.
in press: The importance of geological controls on the natural distribution of mercury in lake and stream sediments across Canada; Mercury in the Environment; Conference Proceedings, Whistler, B.C., July 1994.

Friske, P.W.B. and Hornbrook, E.H.W.
1991: Canada's National Geochemical Reconnaissance programme; Transactions of the Institution of Mining and Metallurgy, Section B; v. 100, p. 47-56.

Friske, P.W.B., McCurdy, M.W., Day, S.J., and Adcock, S.W.
1994a: National Geochemical Reconnaissance – Ontario Compilation: Distribution of Copper in 17,934 lake sediment samples; Geological Survey of Canada, Open File 2959a, 1 map (1:1 500 000).

Friske, P.W.B., Hall, G.E.M., and Day, S.J.A.
1994b: Comparison of trace element distributions in lake sediments and waters from the Florence Lake area, Labrador; in Current Research 1994-C; Geological Survey of Canada, p. 367-376.

Hoffman, S. J. and Fletcher, W.K.
1981: Detailed lake sediment geochemistry of anomalous lakes on the Nechako Plateau, central British Columbia – comparison of trace metal distributions in Capoose and Fish lakes; Journal of Geochemical Exploration, v. 14, p. 221.

Johnson, M.G., Culp, L.R., and George S.E.
1986: Temporal and spatial trends in metal loadings to sediments of the Turkey Lakes, Ontario; Canadian Journal of Fisheries and Aquatic Sciences, v. 43, p. 754-762.

Jonasson, I.R.
1976: Detailed hydrogeochemistry of two small lakes in the Grenville geological province; Geological Survey of Canada, Paper 76-13, 37 p.

Jones, B.F. and Bowser, C.J.
1978: The mineralogy and related chemistry of lake sediments; in Lakes – Chemistry, Geology, Physics, (ed.) A. Lerman; Springer-Verlag, p.179-235.

Kemp, A.L.W., Thomas, R.L., Dell, C.I., and Jaquet, J.M.
1976: Cultural impact on the geochemistry of sediments in Lake Erie; Journal of the Fisheries Research Board of Canada, v. 33, p. 440-462.

Livett, E.A.
1988: Geochemical monitoring of atmospheric heavy metal pollution: theory and applications; in Advances in Ecological Research, Volume 18, (ed.) M. Begon, A. Fitter, and A. MacFadyen; Academic Press, p. 65-175.

Lodder, W.
1969: Geological and geochemical report on the Tatin Lake molybdenite prospect; British Columbia Department of Mines and Petroleum Resources, Assessment Report 1871.

Mortimer, C.H.
1941: The exchange of dissolved substances between mud and water. I and II; Journal of Ecology, v. 30, p. 280-329.

Rasmussen, P.E.
1993: The environmental significance of geological sources of mercury: a Precambrian Shield watershed study; Ph.D. thesis, University of Waterloo, Waterloo, Ontario, 379 p.

Timperley, M.H. and Allan, R.J.
1974: The formation and detection of metal dispersion halos in organic lake sediments; Journal of Geochemical Exploration, v. 3, p. 167-190.

Tipper, H.W.
1971: Glacial geomorphology and Pleistocene history of central British Columbia; Geological Survey of Canada, Bulletin 196, 89 p.

Walsh, M.G.
1977: Tatin Lake; British Columbia Ministry of Environment, Lands and Parks; Fisheries Branch Internal Report.

Williams, T.M.
1992: Diagenetic metal profiles in recent sediments of a Scottish freshwater loch; Environmental Geology and Water Science, v. 20, no. 2, p. 117-123.

Wong, H.K.T., Nriagu, J.O., and Coker, R.D.
1984: Atmospheric input of heavy metals chronicled in lake sediments of the Algonquin Provincial Park, Ontario, Canada; in Geochronology of Recent Deposits, J.A. Roberts (ed.); Chemical Geology, v. 44, p. 187-201.

Geological Survey of Canada Project 850047

Site response modelling of the Fraser River delta, British Columbia: preliminary results from two deep boreholes

J.B. Harris, J.A. Hunter[1], J.L. Luternauer, and W.D.L. Finn[2]
GSC Victoria, Vancouver

Harris, J.B., Hunter, J.A., Luternauer, J.L., and Finn, W.D.L., 1995: Site response modelling of the Fraser River delta, British Columbia: preliminary results from two deep boreholes; in Current Research 1995-E; Geological Survey of Canada, p. 69-75.

Abstract: Preliminary one-dimensional dynamic analysis of two sites in the Fraser River delta using site models based on newly acquired geological and geophysical data, suggests that the response of the delta to earthquake loading can be significantly different than existing site models predict. Because the Quaternary sequence in the delta area is interpreted to be thicker than previously estimated, our models show that there is likely to be considerable long-period response (3.5 to 5.0 s). The presence of significant long-period ground motions has important implications for the stability of large structures on the delta (i.e. bridges, tall buildings, industrial facilities, pipelines) and, coupled with the complex geology of the delta area, suggests that multi-dimensional effects and surface-wave propagation are likely contributors to the seismic response of the delta.

Résumé: Selon une analyse dynamique unidimensionnelle provisoire de deux sites situées dans le delta du fleuve Fraser dans laquelle on utilise des modèles de sites basés sur des données géologiques et géophysiques récentes, la réponse du delta à une charge séismique peut significativement différer des prévisions obtenues par les modèles de sites actuels. Étant donné que la séquence quaternaire reposant dans la delta est évaluée plus puissante que prévu, nos modèles montrent que la réponse de longue période est considérable (entre 3,5 et 5,0 s). La présence de déplacements de terrain significatifs de longue période a des répercussions importantes sur le stabilité des grands ouvrages dans le delta (c'est-à-dire ponts, immeubles élevés, installations industrielles, pipelines) et, compte tenu de la géologie complexe du delta, on peut supposer que les effets multidimensionnels et la propagation des ondes de surface contribuent à la réponse séismique du delta.

[1] Terrain Sciences Division
[2] Department of Civil Engineering, University of British Columbia, Vancouver, British Columbia V6T 1W5

INTRODUCTION

Regions underlain by thick deposits of unconsolidated sediments, such as the Fraser River delta in southwestern British Columbia, are known to experience greater levels of earthquake damage due to amplification of seismic waves. The delta's architecture, its location within the most seismically active region in Canada, and the rapid growth of communities situated on the delta have raised concerns about the area's seismic vulnerability.

As part of a continuing effort to identify and help assess earthquake hazards of the Fraser delta, the Geological Survey of Canada (GSC) has initiated a project to model the response of the thick sediment deposits to earthquake ground motions. In the spring of 1994, scientists from the GSC and several Canadian universities completed two 300-m-deep geotechnical boreholes in the northern part of the Fraser River delta. The purpose of the work was to characterize the geology of the delta at two sites with contrasting geological settings (Dallimore et al., 1995), and provide in situ geological, geophysical, and geotechnical measurements of sediment properties at depths that had not previously been sampled. These new data can be used in more accurate dynamic modelling of the response of the thick sediments associated with the Fraser River delta to earthquake loading. This paper discusses preliminary one-dimensional site response modelling based on geological models constructed using these new data, and compares the results with the response of previously existing geotechnical models of the delta. The results demonstrate the importance of accurate geological characterization in site response modelling.

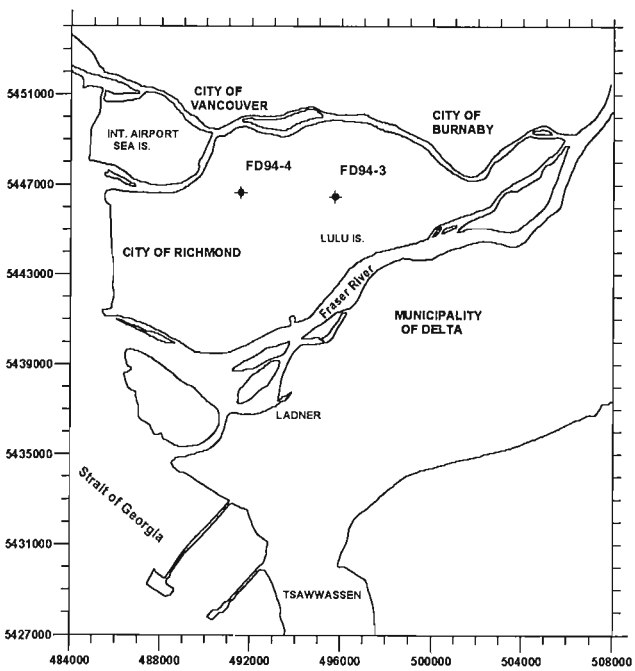

Figure 1. Map of the Fraser River delta showing the locations of boreholes FD94-3 and FD94-4 in eastern Richmond. The axes are in UTM co-ordinates.

GEOLOGICAL SETTING

The Fraser River delta, western Canada's largest, is composed of a thick sequence of unconsolidated sands and silts underlain by nonlithified glacial/interglacial sediments (Luternauer et al., 1994). The Quaternary deposits lie unconformably on a Tertiary bedrock with high relief: depth to bedrock ranges from hundreds of metres to more than 1000 m (Britton et al., 1995). Figure 1 shows the configuration of the Fraser River delta, and the locations of the two deep boreholes that were drilled by the GSC (Dallimore et al., 1995).

In borehole FD94-3, the Holocene-aged deltaic sequence is 19 m thick and is underlain by Pleistocene sands and clays. In contrast, the Holocene/Pleistocene boundary in borehole FD94-4 occurs at a depth of 240 m and is marked by a firm glacial till (no till was found in borehole FD94-3). Tertiary bedrock was not encountered in either borehole, a surprising result given previous estimates of depth to bedrock (Byrne and Anderson, 1987; Finn and Nichols, 1988; Lo et al., 1991; Sy et al., 1991).

SITE RESPONSE MODELLING

Computer modelling programs have been developed for site-response analysis of the sediment column on bedrock ground motions. The most widely used program is SHAKE (Schnabel et al., 1972), a one-dimensional site-response modelling routine designed to propagate vertically incident shear-waves from bedrock through a column of horizontally layered soil horizons. The key parameter in determining the dynamic response of a site to seismic loading is the low-strain shear modulus (G_{max}) of the individual layers making up the soil column. G_{max} can be calculated as the product of the soil layer's shear-wave (S-wave) velocity squared times its mass density. Other necessary parameters include layer thicknesses and estimates of the strain-dependant response of shear modulus and damping.

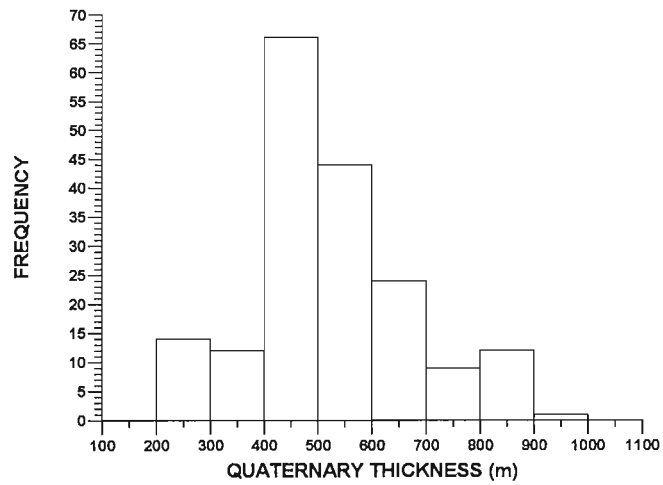

Figure 2. Histogram showing the distribution of Quaternary thicknesses in the delta area interpreted from seismic reflection data (182 observations).

Shear-wave velocities

Detailed downhole S-wave surveys were completed in boreholes FD94-3 and FD94-4 (Dallimore et al., 1995) with good-quality S-wave velocity measurements to a depth of 300 m at each site. Because Tertiary strata were not encountered in either borehole, depths to bedrock were estimated from industry seismic reflection data (Britton et al., 1995). Based on this newly available data set, Quaternary sediments are interpreted to be significantly thicker than have been previously considered in site response modelling of the Fraser delta area (Fig. 2). In an effort to assess S-wave velocities of the entire post-Tertiary sequence, an S-wave velocity estimation routine was established using the combined S-wave and compressional-wave (P-wave) velocity data that were recorded in boreholes FD94-3 and FD94-4 (Dallimore et al., 1995) and P-wave interval velocities that were available from the industry seismic reflection data (Hunter et al., in prep.). P/S velocity ratios were plotted against P-wave velocity for boreholes FD94-3 and FD94-4 (Fig. 3), and 182 individual "P-wave velocity panels" on 126 line-km of industry seismic reflection data (Fig. 4) were analyzed and converted to S-wave velocity using the relationship shown (4th-order polynomial fit). Because no S-wave velocity data were available for the Tertiary section, the last point on the curve was fixed using S-wave velocities from Tertiary rocks in the North Sea area (Reilly, 1994) that are similar to those that lie beneath the Fraser delta. Although there is significant scatter in the data in Figure 3, we believe that in the absence of any deep S-wave velocity information the relationship shown represents a reasonable estimate of the range of S-wave velocities likely to be encountered in Quaternary sediments beneath the delta, and is certainly more accurate than estimates currently being used by the geotechnical community. Figure 5 summarizes the range of S-wave velocities calculated using our estimation procedure.

Site models

Shear-wave velocity data (above) and density measurements from Dallimore et al. (1995) were used to calculate the variation in G_{max} versus depth for FD94-3 and FD94-4 (Fig. 6). Based on a new map of the Tertiary (bedrock) surface (Britton et al., 1995), the Quaternary section was estimated to be 495 m thick at FD94-3 and 700 m thick at FD94-4. Figure 6 also shows G_{max} versus depth for five "typical" models of the delta that have been published in the geotechnical literature (Byrne and Anderson, 1987; Finn and Nichols, 1988; Lo et al., 1991; Sy et al., 1991) and widely used in site response modelling for the delta. These models have been based primarily on shallow borehole information; in general using

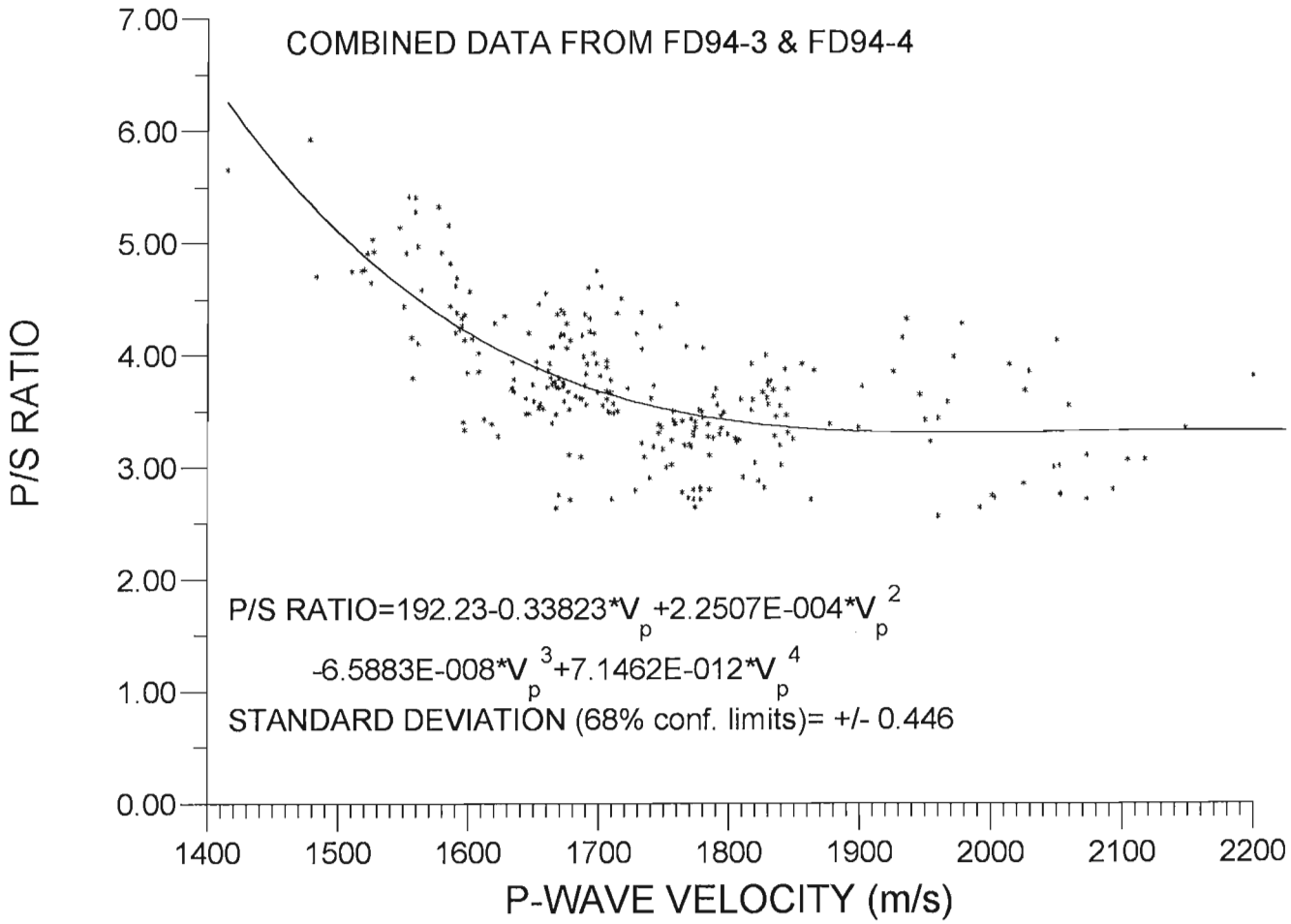

Figure 3. *Plot of P/S ratio versus P-wave velocity from measurements made in boreholes FD94-3 and FD94-4.*

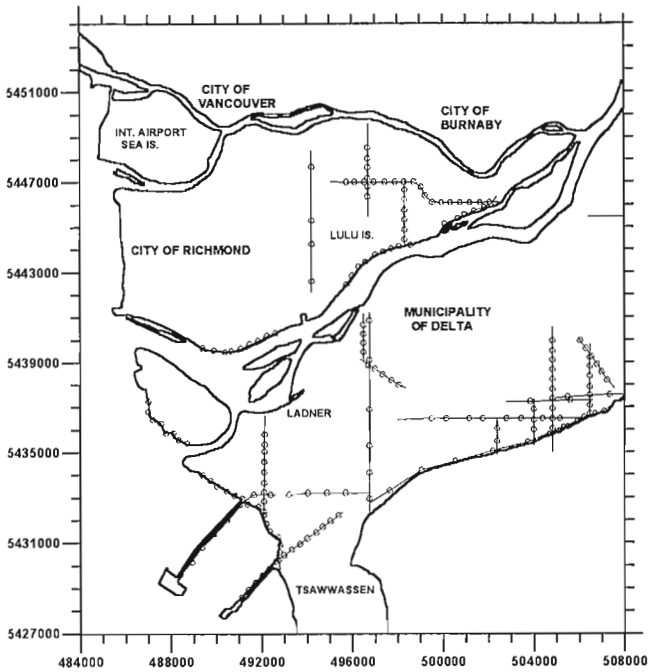

Figure 4. Locations of industry seismic reflection profiles (solid lines) and distribution of velocity analyses (open circles) used for this study. The axes are in UTM co-ordinates.

poorly supported estimates of geological conditions and geotechnical parameters below 100 m. However, when examined collectively the models shown in Figure 6 are an indication of the variability in site conditions that might be expected throughout the delta.

PRELIMINARY OBSERVATIONS

In a very preliminary site amplification analysis, two earthquake acceleration time-histories were propagated through the seven site models (FD94-3, FD94-4, and the five existing delta models) using WESHAKE (Sykora et al., 1991), an updated version of SHAKE (Schnabel et al., 1972) designed to run on personal computers. Acceleration records used were Castaic 021° (1971 San Fernando earthquake) and CUIP 270° (1985 Michoacan earthquake). The Castaic record (epicentral distance ≈30 km) was scaled to a peak acceleration of 0.21 g and the CUIP record (epicentral distance ≈375 km) was scaled to a peak acceleration of 0.035 g. The earthquake records and scaled acceleration values are consistent with those used in previous ground motion amplification studies of the Fraser delta (Byrne and Anderson, 1987; Finn and Nichols, 1988; Lo et al., 1991; Sy et al., 1991) and simulate seismic events [local (Castaic) and subduction zone (CUIP)] of primary concern to the Fraser delta area (Rogers, 1994). The modulus reduction and damping curves used in the site amplification analysis were from Sy et al. (1991).

In order to evaluate amplification as a function of period, spectral ratios (5% damped acceleration response spectra at the surface divided by 5% damped acceleration response spectra at bedrock) were calculated for each of the seven site models using both acceleration records. Figures 7 and 8 show spectral acceleration ratios of FD94-3, FD94-4, and the average of the five existing delta models for the Castaic 021° and CUIP 270° records, respectively. Spectral ratio peaks (site periods) for the average of the five existing delta models occur at periods shorter than 3.0 s (peak ratio of approximately 4), while site periods for FD94-3 and FD94-4 show significantly higher long-period response (peak ratios approaching 6 for periods longer than 3.5 s). Predominant site periods of 3.5 to 4.0 s are seen at FD94-3, and FD94-4 has a predominant site period of 4.5 s.

DISCUSSION AND RECOMMENDATIONS

New borehole information from the Fraser delta (Dallimore et al., 1995) shows that no bedrock was encountered in two 300-m-deep boreholes and a new map of the Tertiary (bedrock) surface beneath the delta (Britton et al., 1995) shows the bedrock surface to be in the order of two times deeper (on average) than has been previously modelled for geotechnical purposes. Preliminary ground motion amplification analysis using geotechnical site models based on this new geological and geophysical information suggests that significantly longer-period (3.5 s to 5.0 s) site response is likely for the Fraser delta. Existing geotechnical models of the delta (Byrne and Anderson, 1987; Finn and Nichols, 1988; Lo et al., 1991; Sy et al., 1991) do not predict this long-period response. Figure 9 shows the distribution of fundamental site periods calculated using the Quaternary thickness and S-wave velocity data presented in Figures 2 and 5. The figure shows the majority of fundamental site periods to be in the 4.0 s to 5.0 s range which is consistent with those seen on the spectral ratio plots for sites FD94-3 and FD94-4 (Fig. 7, 8). Not only does this long-period amplification potential have significant implications on the response of large structures (i.e. bridges, tall buildings, industrial facilities, pipelines) to earthquake ground motions, but it also calls into question the applicability

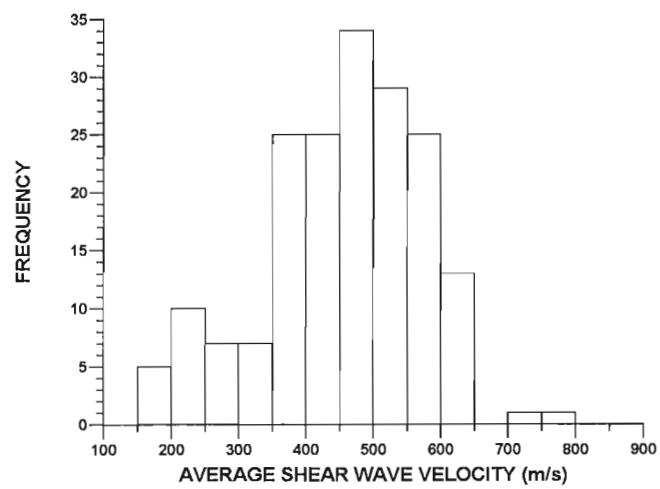

Figure 5. Histogram showing the distribution of Quaternary shear-wave velocities in the Fraser delta estimated from the velocity relationship shown in Figure 3 (182 observations).

of one-dimensional site response analysis (e.g. SHAKE modelling) for the Fraser delta. Sykora et al. (1991, p. 18) stated "... for periods greater than 4 sec, motions are likely to be significantly affected by two-dimensional effects and surface wave energy and are not well represented with SHAKE." The map of the bedrock surface (Britton et al., 1995) shows numerous structures that are likely to produce two- and three-dimensional effects such as trapping and focusing of seismic energy. In addition, the uplands surrounding the delta (Vancouver to the north, Surrey to the east, and Tsawwassen/ Point Roberts to the south) are likely boundaries for the conversion of body waves to surface waves which in turn would propagate through the delta. Spudich (1994, p. 13-9) reported that "... the bulk of seismological evidence indicates that it is quite common for surface waves to be generated at the edges of alluvial basins and propagate in the basins."

Although there are still many unresolved questions regarding the geology (e.g. the geometry and composition of the Pleistocene sequence) and seismic vulnerability (e.g. lack of strong-motion recordings) of the Fraser River delta, our picture of the delta and its potential seismic hazards is getting clearer. With new information on the subsurface geological structure and composition of the Fraser delta (Britton et al., 1995; Dallimore et al., 1995) available to the geotechnical

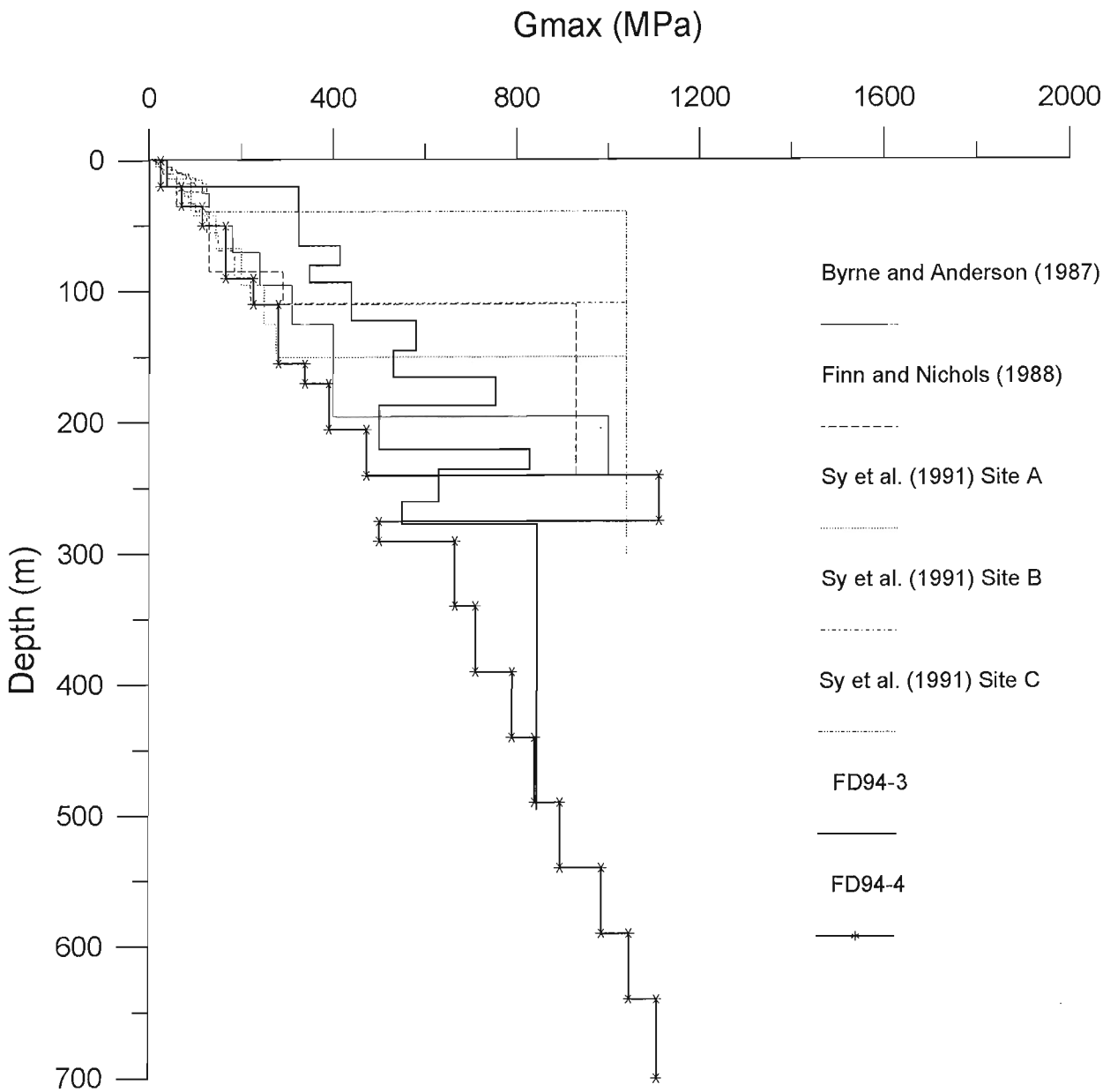

Figure 6. *G_{max} (low-strain shear modulus) versus depth for boreholes FD94-3, FD94-4, and five existing geotechnical models of the Fraser delta.*

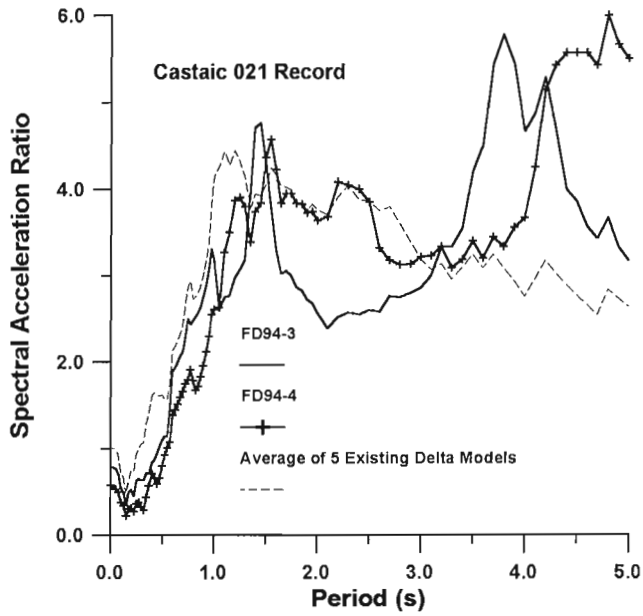

Figure 7. Spectral acceleration ratios for the models shown in Figure 6 using the Castaic 021° record.

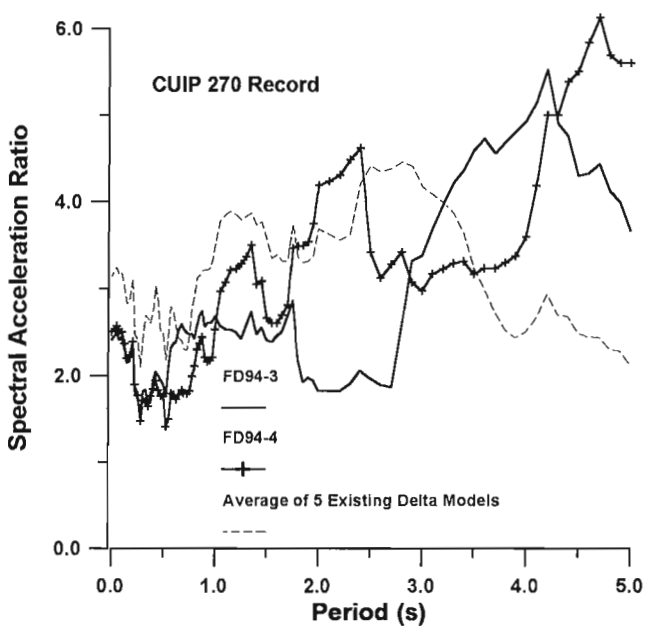

Figure 8. Spectral acceleration ratios for the models shown in Figure 6 using the CUIP 270° record.

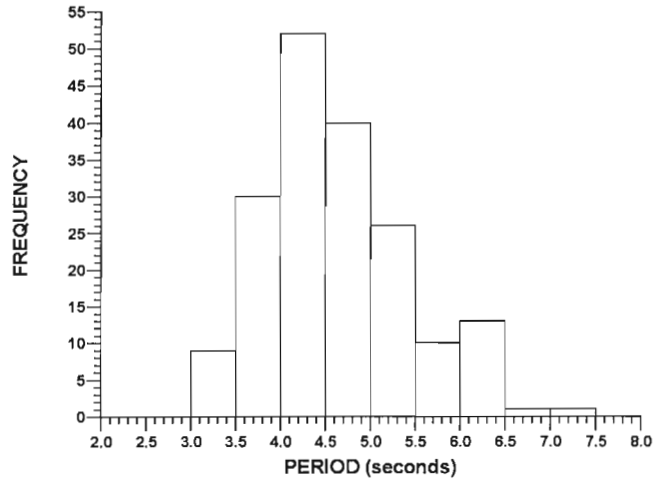

Figure 9. Histogram of fundamental site periods for the Fraser delta (182 observations). Calculations were made using the equation: $T = 4h/V_S$, where T = period, h = Quaternary thickness (from Fig. 2), and V_S = average Quaternary shear-wave velocity (from Fig. 5).

community working in the delta area, up-to-date earthquake hazard analyses and innovative ground motion modelling studies are expected in the near future.

ACKNOWLEDGMENTS

We thank Peter Mustard and Bev Vanlier (GSC, Vancouver) for their constructive reviews of the manuscript.

REFERENCES

Britton, J.R., Harris, J.B., Hunter, J.A., and Luternauer, J.L.
1995: The bedrock surface beneath the Fraser River Delta in British Columbia, based on seismic measurements; in Current Research 1995-E; Geological Survey of Canada.

Byrne, P.M. and Anderson, D.L.
1987: Earthquake design in Richmond, B.C., Version II; Department of Civil Engineering, University of British Columbia, Vancouver, British Columbia, Soil Mechanics Series No. 109.

Dallimore, S.R., Edwardson, K.A., Hunter, J.A., Clague, J.J., and Luternauer, J.L.
1995: Composite geotechnical logs for two deep boreholes in the Fraser River delta, British Columbia; Geological Survey of Canada, Open File 3018.

Finn, W.D.L. and Nichols, A.M.
1988: Seismic response of long-period sites: Lessons from the September 19, 1985, Mexican earthquake; Canadian Geotechnical Journal, v. 25, p. 128-137.

Lo, R.C., Sy, A., Henderson, P.W., Siu, D.Y., Finn, W.D.L., and Heidebrecht, A.C.
1991: Seismic site amplification study for Fraser delta, British Columbia; Proceedings, 6th Canadian Conference on Earthquake Engineering, Toronto, Ontario, p. 509-516.

Luternauer, J.L., Barrie, J.V., Christian, H.A., Clague, J.J., Evoy, R.W., Hart, B.S., Hunter, J.A., Killeen, P.G., Kostaschuk, R.A., Mathewes, R.W., Monahan, P.A., Moslow, T.F., Mwenifumbo, C.J., Olynyk, H.W., Patterson, R.T., Pullan, S.E., Roberts, M.C., Robertson, P.K., Tarbottom, M.R., and Woeller, D.J.
1994: Fraser River delta: Geology, geohazards, and human impact; in Geology and Geological Hazards of the Vancouver Region, Southwestern British Columbia, (ed.) J.W.H. Monger; Geological Survey of Canada, Bulletin 481, p. 197-220.

Reilly, J.M.
1994: Wireline shear and AVO modelling: Application to AVO investigations of the Tertiary, U.K. central North Sea; Geophysics, v. 59, p. 1249-1260.

Rogers, G.C.
1994: Earthquakes in the Vancouver area; in Geology and Geological Hazards of the Vancouver Region, Southwestern British Columbia, (ed.) J.W.H. Monger; Geological Survey of Canada, Bulletin 481, p. 221-229.

Schnabel, P.B., Lysmer, J., and Seed, H.B.
1972: SHAKE: A computer program for earthquake response analysis of horizontally layered sites; Earthquake Engineering Research Center, Berkeley, California, Report EERC-72/12.

Spudich, P.
1994: Recent seismological insights into the spatial variation of earthquake ground motions; Proceedings of ATC-35 Seminar on New Developments in Earthquake Ground Motion Estimation and Implications for Engineering Design Practice, Applied Technology Council ATC 35-1, p. 13(1-31).

Sy, A., Henderson, P.W., Lo, R.C., Siu, D.Y., Finn, W.D.L., and Heidebrecht, A.C.
1991: Ground motion response for the Fraser delta, British Columbia; Proceedings, 4th International Conference on Seismic Zonation, Stanford, California, v. 2, p. 343-350.

Sykora, D.W., Wahl, R.E., and Wallace, D.C.
1991: WESHAKE for personal computers; U.S. Army Corps of Engineers Geotechnical Earthquake Engineering Software, Instructional Report GL-91-1.

Geological Survey of Canada Project 860022

Borehole magnetic susceptibility measurements in unconsolidated overburden of the Fraser River delta, British Columbia

J.A. Hunter, R.A. Burns, R.L. Good, Yuchun Wang[1], and M.E. Evans[1]
Terrain Sciences Division

Hunter, J.A., Burns, R.A., Good, R.L., Wang, Y., and Evans, M.E., 1995: Borehole magnetic susceptibility measurements in unconsolidated overburden of the Fraser River delta, British Columbia; in Current Research 1995-E; Geological Survey of Canada, p. 77-82.

Abstract: Borehole magnetic susceptibility logging has been performed in four boreholes in the Fraser River delta. Good correlation was obtained between laboratory samples and in situ logging. The results suggest that the borehole magnetic susceptibility sonde can be utilized for lithological studies in overburden in this area. As well, there appears to be a significant difference in magnetic susceptibility between Holocene and Pleistocene materials, which suggests that such measurements may be useful in determining such a geological time boundary within the unconsolidated sediments of the delta area.

Résumé : Dans le delta du fleuve Fraser, on a effectué des diagraphies de la susceptibilité magnétique dans quatre trous de sondage. On a obtenu une bonne corrélation entre les échantillons de laboratoire et les diagraphies in situ. Les résultats indiquent que la sonde de susceptibilité magnétique peut être utilisée dans les études lithologiques des morts-terrains de cette région. De plus, il semble qu'il existe un différence importante de la susceptibilité magnétique entre les matériaux holocènes et pléistocènes, ce qui laisse supposer que ces mesures peuvent être utiles pour déterminer une telle limite géochronologique dans les sédiments non consolidés de la zone deltaïque.

[1] Institute of Geophysics, Meteorology, and Space Physics, University of Alberta, Edmonton, Alberta

INTRODUCTION

The magnetic susceptibility of a material is the degree to which it can be magnetized in the presence of an applied magnetic field; hence it is the ratio of the intensity of magnetization divided by the magnetic field strength (Telford et al., 1976, p.107).

The bulk magnetic susceptibilities of most unconsolidated sediments are relatively low, due to the absence of significant amounts of ferrimagnetic mineral grains. The most common minerals with significant grain magnetic susceptibility are the iron-titanium oxides; of these, magnitite has by far the highest susceptibility values (Lindsley et al., 1966). Hence, in Quaternary unconsolidated sediments, the measurement of the bulk magnetic susceptibility may effectively be a measure of the relative magnetite content.

In the past few years, the GSC has drilled several boreholes in the Fraser River delta area for geological and geophysical studies related to earthquake hazards. Some of these holes encountered a variety of sediment types in terms of age, grain size, and depositional environment. These holes afforded an opportunity to measure in situ magnetic susceptibility to assess the applicability of such measurements to lithological definition. Laboratory determination of magnetic susceptibility was also carried out on core from some of the holes to allow a comparison with in situ measurements. The locations of the boreholes discussed herein are shown in Figure 1.

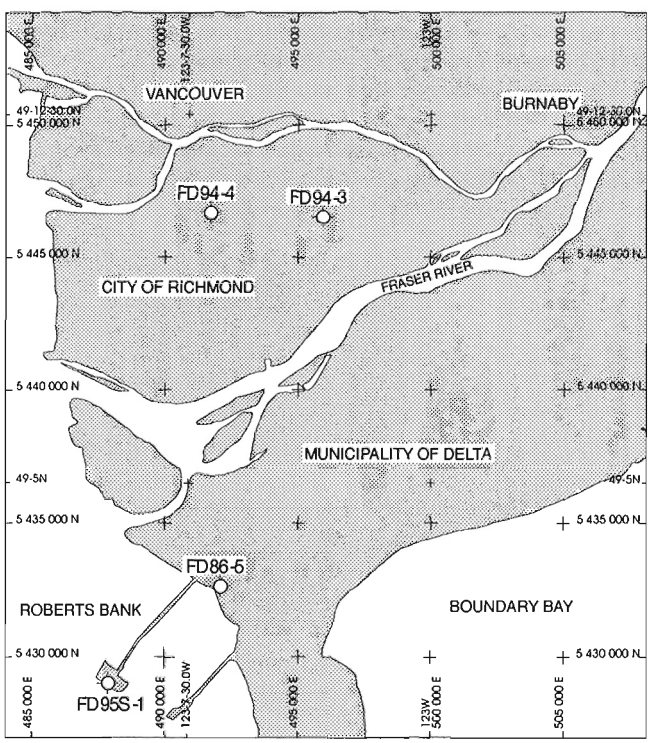

Figure 1. Locations of GSC Fraser delta boreholes discussed in this paper.

THE MAGNETIC SUSCEPTIBILITY LOGGING SYSTEM

The logging system used in this study was built by Geonics Ltd of Mississauga, Ontario. The EM39S magnetic susceptibility borehole sonde is fashioned after the Geonics EM-39 electrical conductivity sonde (Taylor et al., 1989) with identical physical dimensions but with differing sonde electronics. It consists of a self-contained magnetic dipole receiver coil and associated electronics that measure the inphase component of the secondary field response from the surrounding media, excited by the magnetic dipole receiver separated 50 cm from the receiver sensor. The inphase component of the secondary field, under the low induction number condition, is linearly proportional to the formation magnetic susceptibility. The EM39S probe does not include a focussing coil as used in the conductivity probe to reduce effects of borehole fluid and removal of the primary field, including the inphase component of the secondary field.

The data acquisition system used was that of the EM-39 conductivity logging unit with slight modifications of the electronics to accommodate calibration and acquisition of the magnetic susceptibility data.

Since large differences in magnetic susceptibility can be expected between soils and rocks, the data are recorded in two channels over two ranges: 0-30 x 10^{-3} S.I., and 0-300 x 10^{-3} S.I. with 14-bit digital resolution.

BOREHOLE MEASUREMENTS

Boreholes FD94-3 and Fd94-4, both drilled to 300 m depth, offered an excellent opportunity to test the system in differing Quaternary sediments and, since laboratory measurements of magnetic susceptibility were available from the core, to test the calibration of the system. The laboratory measurements were done on whole roundcore samples with a Barinton MS2C sensor system. Detailed geological, geophysical, and geotechnical information on these two boreholes are given by Dallimore et al. (1995).

The magnetic susceptibility results from in situ logging at 0.05 m intervals in FD94-3, is shown in Figure 2, along with the laboratory results and the generalized geology. The upper limit of logging data is defined by the base of the steel casing in the hole, since this equipment can only be run in open-hole or plastic-cased-hole conditions.

The general magnetic susceptibility response correlates extremely well with the lithological variations of FD94-3. Radiocarbon dates obtained from shell material from these units (Dallimore et al., 1995) would suggest that they are of Pleistocene age. The upper sand units have an average susceptibility of approximately 4-5 ppt, whereas some of the lower sand units reach values of 30-40 ppt, with the average in the 8 to 12 ppt range. The clayey silt units in the range of 150-180 m depth as well as in the range of 235-245 m depth have values that are close to zero (the zero calibration was

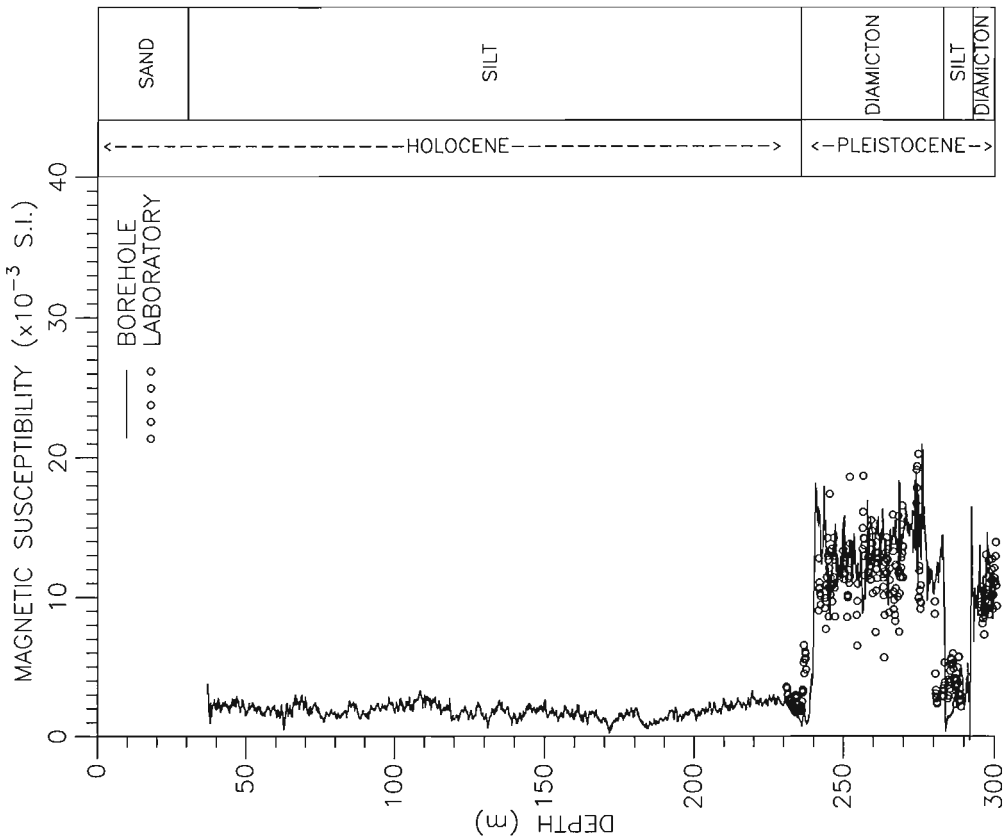

Figure 3. *Generalized geology, borehole and laboratory measurements of magnetic susceptibility for GSC borehole: FD94-4.*

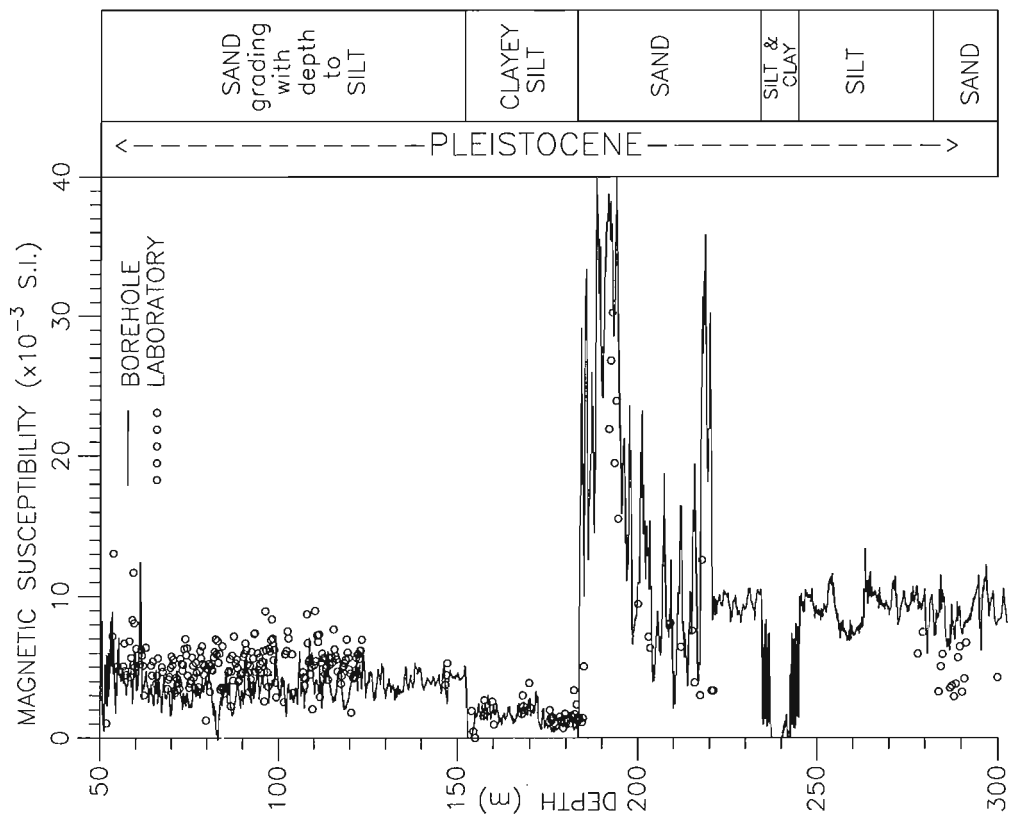

Figure 2. *Generalized geology, borehole and laboratory measurements of magnetic susceptibility for GSC borehole: FD94-3.*

done on site to an accuracy of approximately ±0.1 ppt S.I.). Hence it is probable that the fine grained units contain little or no magnetite.

The in situ magnetic susceptibility results from borehole FD94-4 are shown in Figure 3, along with the laboratory measurements and the generalized geology. Radiocarbon dates from this hole (Dallimore et al., 1995) would suggest the boundary between Holocene and Pleistocene sediments as shown. Within the inferred Holocene sediments, despite some variations in grain size, the magnetic susceptibility values are uniformly low and are in the range of 1-2 x 10^{-3} S.I.. From experience gained from measurements in several other Fraser Delta boreholes within Holocene sediments of variable grain size, this appears to be a diagnostic characterisitc. A large change in magnetic susceptibility can be seen to be associated with the inferred top of the Pleistocene sediments at approximately 236 m depth. In general, the magnetic susceptibility readings within the Pleistocene materials of both boreholes FD94-3 and FD94-4 are relatively high compared to those of Holocene sediments, and may reflect a higher magnetite content.

Although the magnetic susceptibility sonde was calibrated by the manufacturer using the GSC borehole calibration facilities in Ottawa (Bristow and Bernius, 1984), it is interesting to compare the in situ and laboratory results in the two boreholes. The correlation between the two sets of measurements is shown in Figure 4 along with the least squares linear fit. Although the bulk of the data is in the very low value range (<10 x10^{-3} S.I.) there appears to be a 1 to 1 relationship between the two data sets.

EXAMPLES OF APPLICATIONS

Borehole FD95S-1 was drilled by GSC for geotechnical and geological studies on the outer edge of the Roberts Bank Superport Facility (H. Christian, GSC Halifax, pers. comm.). The magnetic susceptibility log obtained in the hole, along with the generalized geology, are shown in Figure 5. Both the upper and lower sediments have a predominant coarse fraction (including the diamictons), yet, a distinct change in magnetic susceptibility is associated with the tentatively interpreted Holocene-Pleistocene boundary (H. Christian, GSC Halifax, pers. comm., 1995). The detailed mineralogy of the sediment column is not known at this time; however, it is suggested that increased abundance of magnetite within coarse grained Pleistocene sediments may be largely responsible for the magnetic susceptibility values.

Some years ago, borehole FD86-5 was drilled by GSC for geological studies (Clague et al., 1991) and was subsequently utilized for geophysical studies related to earthquake hazards. In particular, downhole shear wave velocities were obtained

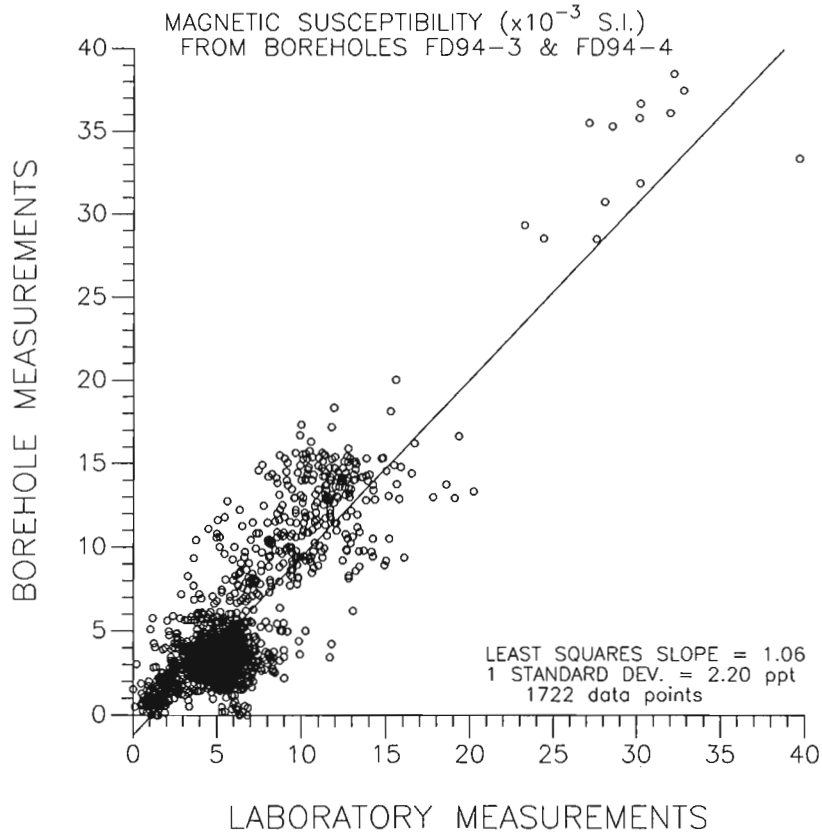

Figure 4. Comparison of borehole and laboratory measurements of magnetic suceptibility obtained from two GSC Fraser delta boreholes.

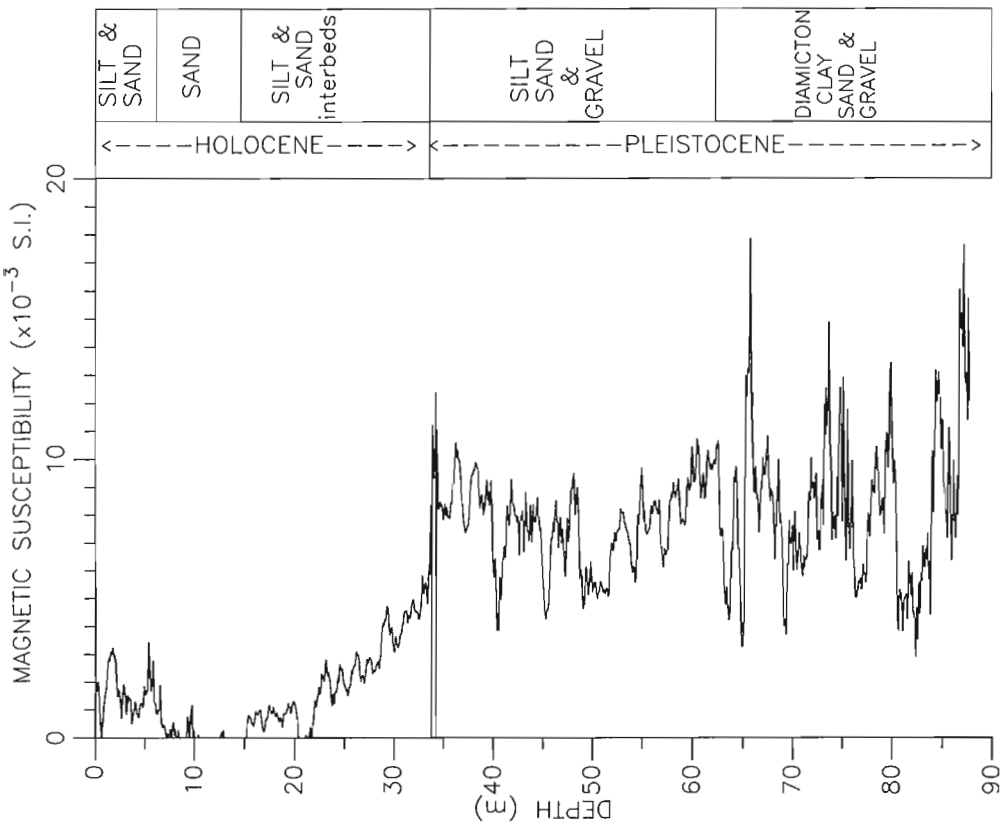

Figure 6. *Borehole magnetic susceptibility measurements and generalized geology for GSC borehole: FD86-5. The Holocene-Pleistocene boundary has been interpreted from the susceptibility log.*

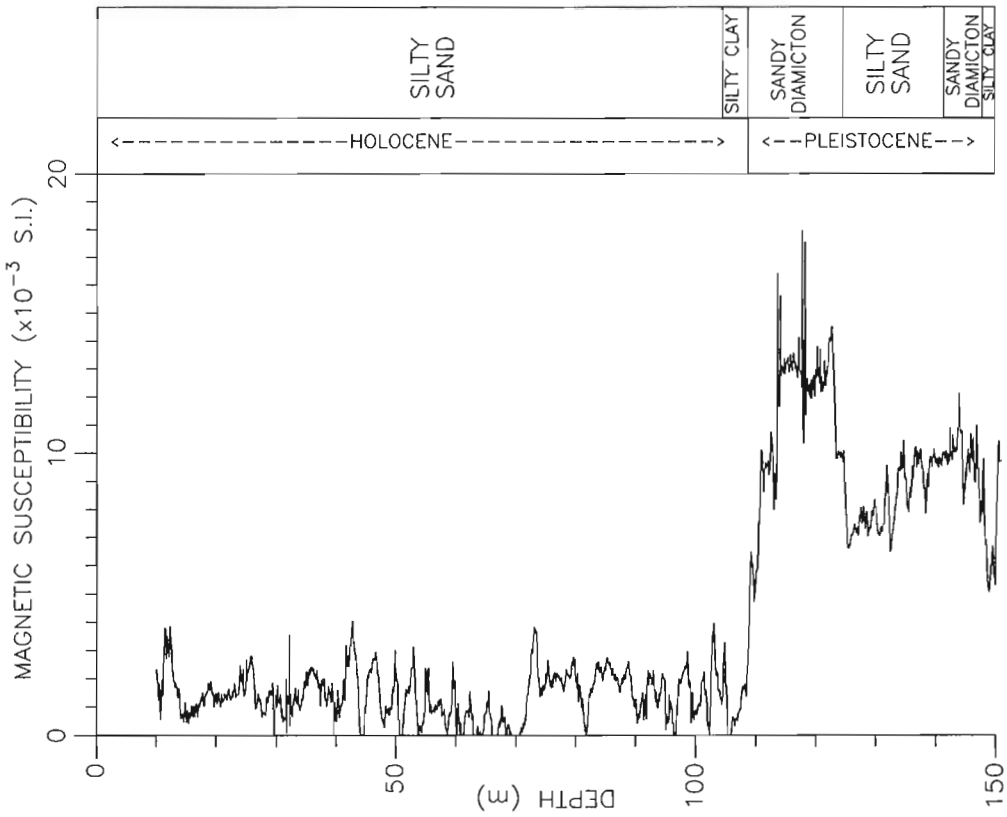

Figure 5. *Borehole magnetic susceptibility measurements along with the tentative geological interpretation (H. Christian GSC Halifax, pers. comm.) for GSC borehole: FD95S-1.*

which indicated anomalously high shear wave velocities within the basal Holocene sediments (Hunter et al., 1990). With lack of chronostratigraphy, there has always been an element of doubt in interpretation of the top of Pleistocene sediments at approximately 50 m depth in this particular hole (J. Luternauer, GSC, Victoria, pers. comm., 1995) since the top of the Pleistocene is not defined by a diamicton (the upper diamicton is at an approximate depth of 63 m). Figure 6 shows the in situ magnetic susceptibility measurements along with the generalized geology. Based on the previous experience on the magnetic susceptibility characteristics of the interpreted Holocene-Pleistocene boundary as discussed above, it is suggested that this boundary is probably at an approximate depth of 34 m in the hole. With this interpretation, the high shear wave velocities below this depth (Hunter et al., 1990) can be associated with Pleistocene age sediments, thus resolving a puzzling anomaly in earthquake hazard-related shear wave studies in the delta.

SUMMARY

Borehole magnetic susceptibility surveys have been conducted in the Fraser River Delta of British Columbia. Values of magnetic susceptibility of sediments are relatively low, but tend to reflect the lithology and probably mineralogy of the sediments. Because of a suggested difference in magnetite content between Holocene and Pleistocene sediments, this technique may possibly be used as an indicator of the Holocene-Pleistocene boundary in this geological environment. Future studies of the mineralogy of the boreholes discussed above are required before any firm conclusions can be reached.

REFERENCES

Bristow, Q. and Bernius, G.
1984: Field evaluation of a magnetic susceptibility logging tool; in Current Research, Part A; Geological Survey of Canada, Paper 84-1A, p. 453-462.

Clague, J.J., Luternauer, J.L., Pullan, S.E., and Hunter, J.A.
1991: Postglacial deltaic sediments, southern Fraser River delta, British Columbia; Canadian Journal of Earth Sciences, v. 28, p. 1386-1393.

Dallimore, S.R., Edwardson, K.A., Hunter, J.A., Clague, J.J., and Luternauer, J.L.
1995: Composite geotechnical logs for two deep boreholes in the Fraser river delta, British Columbia; Geological Survey of Canada, Open File 3018.

Hunter, J.A., Burns, R.A., and Good, R.L.
1990: Borehole shearwave velocity measurements, Fraser delta 1989; Geological Survey of Canada, Open File 2229.

Lindsley, D.H., Andreasen, G.E., and Balsley, J.R.
1966: Magnetic properties of rocks and minerals; in Handbook of Physical Constants; Geological Society of America, Memoir 97, Section 25, p. 543-552.

Taylor, K.C., Hess, J.W., and Mazzela, A.
1989: Field evaluation of a slim-hole borehole induction tool; Ground Water Monitoring Review, winter issue, p. 100-104.

Telford, W.M., Geldart, L.P., Sheriff, R.E., and Keys, D.A.
1976: Applied Geophysics; Cambridge University Press, Cambridge U.K., 860 p.

Geological Survey of Canada Project 890023

The bedrock surface beneath the Fraser River delta in British Columbia based on seismic measurements

J.R. Britton[1], J.B. Harris, J.A. Hunter, and J.L. Luternauer[2]
Terrain Sciences Division

Britton, J.R., Harris, J.B., Hunter, J.A., and Luternauer, J.L., 1995: The bedrock surface beneath the Fraser River delta in British Columbia based on seismic measurements; in Current Research 1995-E; Geological Survey of Canada, p. 83-89.

Abstract: Common depth point seismic data, collected as part of a hydrocarbon exploration program in the Fraser River delta has been interpreted to map the depth to bedrock, which coincides with the Pleistocene-Tertiary unconformity. A structure map of the surface shows northwest-trending highs and lows, ranging in depth from 200 to 1000 m. The development of a bedrock map forms a key component of the geological and geophysical framework relevant to geotechnical investigations focussing on the ground response to earthquake shaking.

Résumé : Pour cartographier la profondeur du substratum rocheux, qui coïncide avec la discordance pléistocène-tertiaire, on a interprété les données sismiques de point-miroir commun dans le cadre d'un programme d'exploration des hydrocarbures dans le delta du fleuve Fraser. Une carte structurale de la surface montre des crêtes et des creux à direction nord-ouest, variant de 200 à 1 000 m de profondeur. La cartographie du substratum rocheux constitue une composante clé du cadre géologique et géophysique nécessaire aux analyses géotechniques portant sur la réponse du sol aux secousses séismiques.

[1] Dynamic Oil Ltd., Vancouver
[2] Cordilleran Division, GSC, Vancouver

INTRODUCTION

The Fraser River delta is one of the most rapidly developing urban areas of Canada in the most seismically active region in Canada. To assess the impact of earthquakes on ground conditions, geotechnical studies require detailed knowledge of the geological materials and their structure from ground surface down to, and including the top of competent bedrock.

Although the geological and geotechnical properties of the near-surface are becoming well known, information about the unconsolidated overburden and bedrock at depth in the delta is relatively sparse. Although several gas exploration wells have been drilled in the area during the last century, most have been relatively shallow, and data on the depth to bedrock are known for only three of these.

This paper presents an interpretation of the bedrock topography beneath the Fraser River delta, from an analysis of conventional seismic data acquired by Dynamic Oil Ltd. of Vancouver.

GEOLOGICAL OVERVIEW

A brief description of the surface and subsurface geology of the Fraser River delta region can be obtained from excellent reviews by Monger and Journeay (1994), Mustard (1994), Mustard and Rouse (1994), Clague (1994), Luternauer et al. (1994), Monger et al. (in press), and Mustard et al. (in press). The older basement in the area consists mainly of Mesozoic volcanic and sedimentary rocks and granitic intrusions. Upper Cretaceous and Tertiary strata overlying these rocks were deposited within the Georgia Basin/Depression, the main depocentre in southwestern British Columbia into which the Fraser River delta is now prograding. The combined sequence of crystalline and sedimentary rocks were folded, faulted, and tilted during a period of major deformation occurring mainly during Eocene time. Geophysical surveys and physiographic lineaments within the Fraser Lowland suggest northeast-trending faults were active between 25 and 14 Ma ago, and possibly later. Regional topography, with well-defined northeasterly and northwesterly trends, was controlled by such tectonics as well as Neogene and Quaternary uplift and Pleistocene glacial and fluvial erosion. Locally variable Pleistocene glacial and interglacial sediments accumulated on eroded bedrock surfaces and were subsequently buried by Holocene Fraser River delta sediments which are documented to be as thick as 236 m (Dallimore et al., 1995) in places.

THE SEISMIC DATABASE

Over the past several years, Dynamic Oil Ltd. of Vancouver has acquired an extensive data bank of seismic reflection sections, as part of an on-going hydrocarbon exploration program in the lower mainland. This information was obtained using the current state-of-the-art geophysical surveying technology.

In the Fraser River delta, multichannel seismic surveys, using "common depth point" (CDP) techniques and environmentally benign multi-vibrator energy sources were conducted between 1977 and 1989. Within our area of concern, approximately 126 line-kilometres were obtained. The location of the seismic lines are shown in Figure 1.

The seismic field geometry of sources and geophones were designed to image structure within the Tertiary bedrock to a depth of several kilometres with a high signal-to-noise ratio. Hence, a typical survey geometry consisted of 120 channels of seismic traces per "shot", 9 equi-spaced geophones per group (or channel) and a group spacing of 17 m. Energy source spacings were arranged along the seismic lines to obtain 120-fold data (the number of summed or "stacked" traces per computer processed output trace using CDP analysis techniques).

In general, the seismic section quality is good, and structures within the bedrock are well-defined. As well, due to the large thickness of unconsolidated overburden in the delta, the overburden-bedrock boundary can be interpreted reliably in most of the sections. Figure 2 shows the upper portion of a seismic section down to, and including the top of bedrock obtained in the Boundary Bay area of the delta.

Because of the long spread lengths in the field seismic array, reflections from geological contacts within the overburden are often poorly delineated. This results from a decreased "fold" or stack since only the near-offset geophone

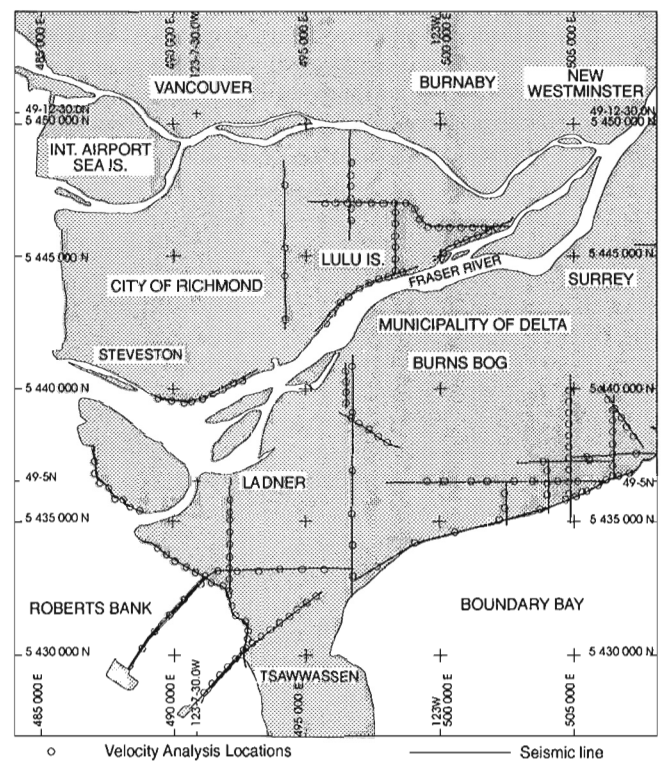

Figure 1. Location map of seismic lines and velocity panels in the Fraser River delta study area.

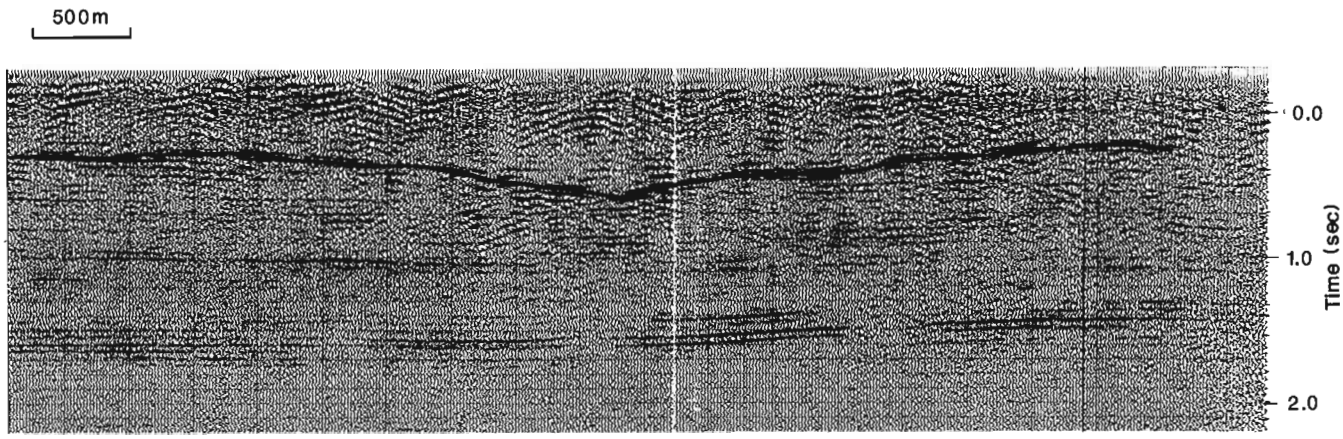

Figure 2. The upper portion of Dynamic Oil Ltd. seismic line 87-103 in the area of Boundary Bay showing the angular unconformity between Pleistocene and Tertiary sediments. Over 300 m of relief are interpreted along a horizontal distance of 4400 m.

groups can be utilized in processing for shallow reflections. Infra-overburden reflections can only be continuously and reliably observed in some areas of the delta where strong velocity contrasts are associated with major geological contacts.

To obtain proper input parameters for computer processing and to obtain two-way reflection travel-time to depth conversion for interpretation, velocity analyses were carried out at regular intervals along a seismic line (at approximately 500 to 1500 m spacings – see Fig. 1). These resulting "velocity panels" give the average compressional wave velocity from ground surface to a reflecting horizon at depth ("root-mean-square" or V_{rms}). An example of a velocity panel is shown in Figure 3. Using established methodology (Dix, 1955), this information can be used to compute the average compressional wave velocities between reflecting horizons known as the "interval velocity" (V_{int}). As well, the thickness of the "velocity layers" can also be calculated.

BEDROCK DEPTH INTERPRETATION TECHNIQUE

To obtain the two-way travel time to the top of the bedrock, an interpretation of the reflection associated with the overburden-bedrock interface was performed by one of us (JRB) on all seismic sections at an approximate surface distance spacing of 170 m (corresponding to every 10th geophone group spacing). The travel-times were compiled in map form and contoured as shown in Figure 4.

To obtain a generalized travel-time/depth conversion function, the travel-time and RMS velocity data for all velocity panels were compiled in one plot as shown in Figure 5. A least-squares best-fit polynomial curve was calculated as

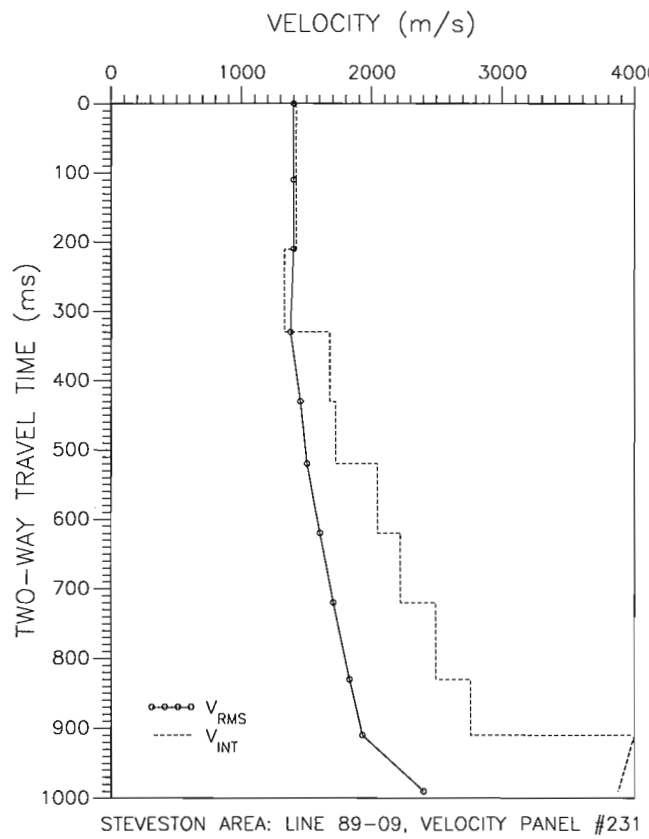

Figure 3. An example of a "velocity panel" showing RMS velocity interpretations from reflectors and the derived interval velocities. High velocities below 900 ms indicate Tertiary sediments.

shown. From this curve, the two-way travel-time/depth curve was calculated along with one standard deviation error limits as shown in Figure 6. The variation of the +/- one standard deviation (68% confidence limits) with depth is shown in Figure 7.

Conversion of two-way travel-time to depth for the bedrock surface was initially carried out using only the travel-time contour map, and was subsequently modified with the site-specific velocity panel information. The resulting depth map is shown in Figure 8. Solid contours in the vicinity of the seismic lines are used to indicate the confidence level of the interpretation. Dashed lines are used whenever long-range interpolation between lines was required and offer a largely speculative interpretation of the bedrock surface.

PROMINENT FEATURES OF THE BEDROCK SURFACE TOPOGRAPHY

From the contours shown in Figure 8, there appears to be a general northwest trend to the topographic highs and lows. Significant bedrock topographic highs occur in the eastern portion of the map, in the vicinity of Burns Bog, as well as on the eastern portion of Lulu Island. Prominent topographic lows are evident in the Boundary Bay area and on-strike from Ladner through to Steveston. See Figure 1 for place-name locations.

The narrow trough in the bedrock surface in the vicinity of Boundary Bay reaches a maximum depth of 1052 m, as determined from a velocity panel interpretation. The width of the valley is approximately 3 km (to the 500 m depth contour). The trend of the valley towards the northwest is speculative, due to lack of coverage in the Burns Bog area, but the interpretation is guided by the line coverage in the vicinity of the main arm of the Fraser River.

The broad northwest-trending trough in the Ladner-Steveston area is reasonably well-defined from seismic line coverage. The maximum depth to bedrock as determined from velocity panels is 890 m and is located on the seismic line in the Steveston area. Although no data are available farther to the northwest it is possible that this trend continues beneath the urbanized area of Richmond.

The nature of the bedrock topographic high (reaching 200 m depth) in the Burns Bog area is speculative, as only the southern edge is delineated from the seismic line coverage; however, the shape of the anomaly is constrained by a portion of one seismic line at the eastern boundary of the survey area, as well as more extensive line coverage which exists (but is not shown) immediately east of the survey area.

The topographic high in the east-central portion of Lulu Island is well defined from the seismic line coverage. Since this area was selected for a deep-drilling

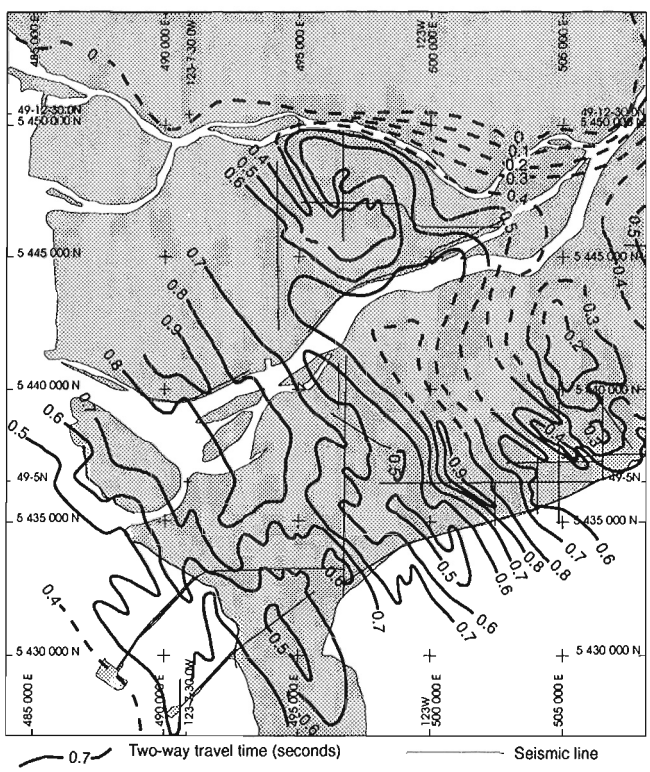

Figure 4. Two-way reflection travel time interpretation to the top of Tertiary sediments from analyses of the seismic sections.

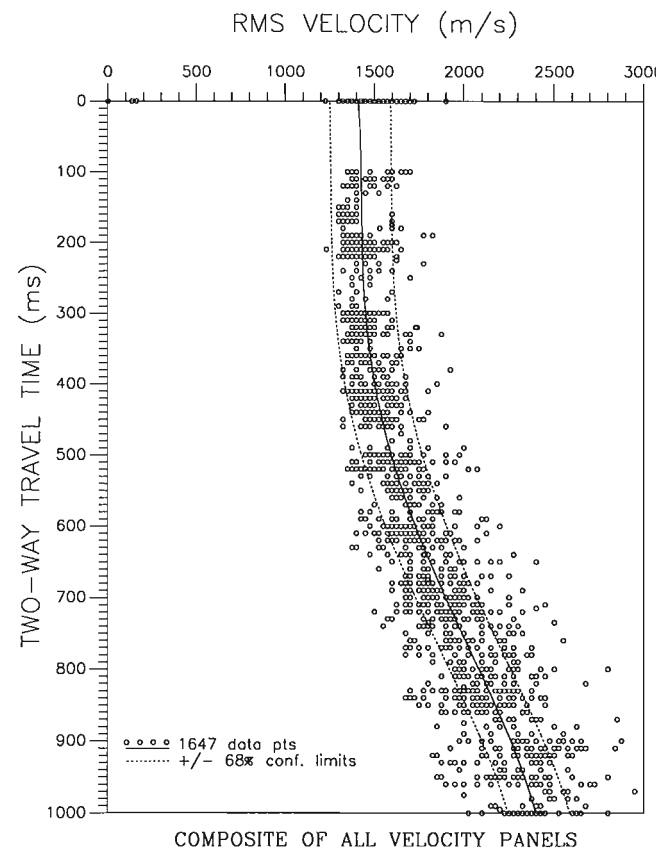

Figure 5. A least-squares polynomial fit to the composite data from 182 velocity panels from all seismic lines.

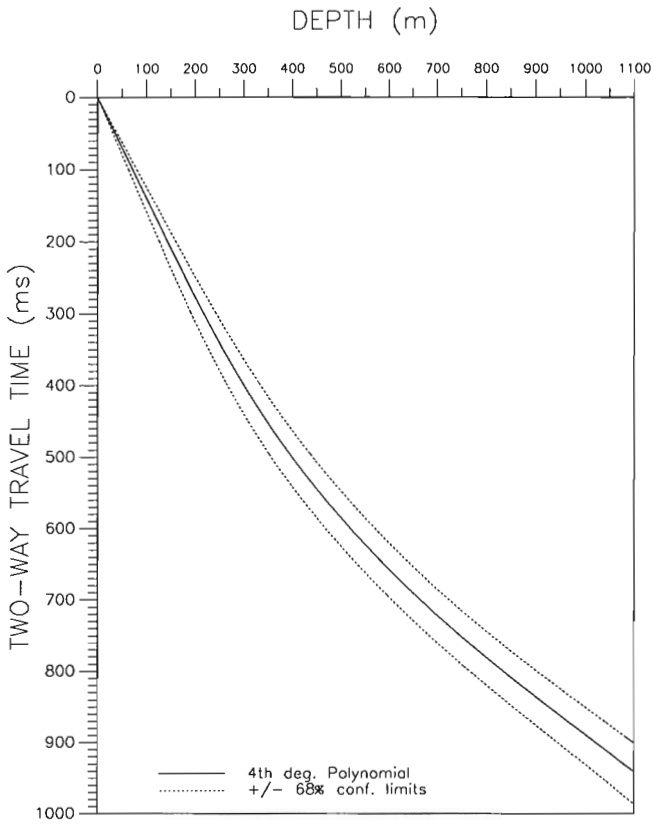

Figure 6. *Travel time-depth conversion of the least-squares fit shown in Figure 5.*

location for overburden studies (Dallimore et al., 1995), further detailed high-resolution seismic surveys are currently being carried out by GSC which will contribute greater detail of the structure of the bedrock surface in this area in the near future.

The shape of the bedrock surface in the northern portion of the map area is speculative, since no seismic line coverage exists. Armstrong and Hiscock (1976) indicated that Tertiary bedrock outcrops on the Pleistocene highlands north of the north arm of the Fraser River; the thickness of the Pleistocene sediments in that area is apparently poorly defined. However, Hunter et al. (1992) indicated the presence of high shear wave velocities at shallow depths (<30 m) in this area which suggests that the 0 depth contour, as indicated, is probably a reasonable interpretation for geotechnical modelling.

Perhaps another noteworthy trend of the topographic relief is the indication of relatively shallow bedrock depths seaward of Roberts Bank in the southeastern portion of the area. This trend is well defined by two seismic lines obtained along the two causeways extending across the intertidal zone.

For the purpose of providing an overview of bedrock depth variation within the Fraser River delta, a histogram of bedrock depths obtained from the complete velocity panel data is shown in Figure 9. The majority of computed bedrock depths are in the 400-600 m range. Since there is no obvious geological bias to the distribution of the seismic surveys, this histogram is probably a representative one for the Fraser River delta.

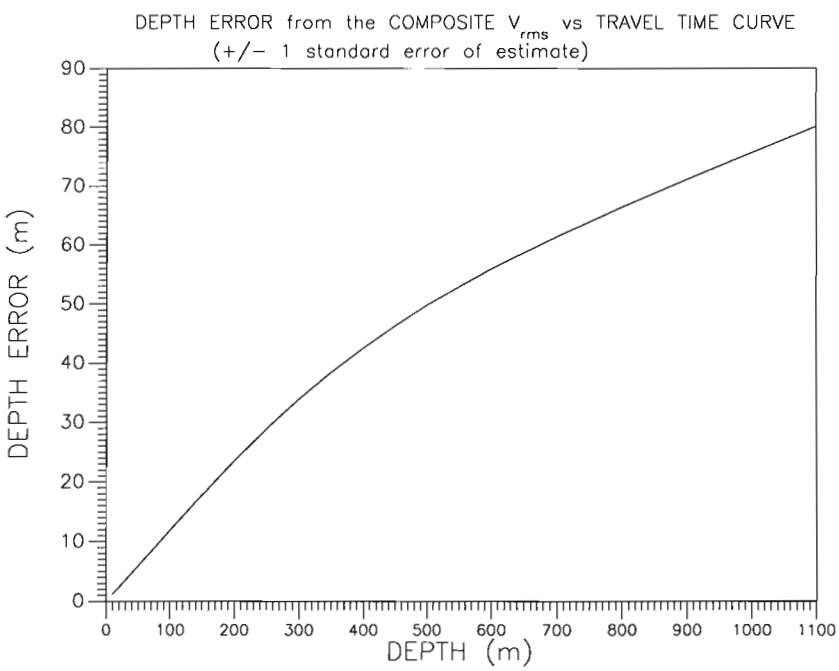

Figure 7.

The variation of statistical error with interpreted depth for 68% confidence limits for the travel time-depth curve of Figure 6.

GEOLOGICAL CHARACTER OF THE BEDROCK SURFACE

As mentioned above, faulting, glacial and fluvial erosion as well as uplift all contributed to the character of the present Tertiary bedrock surface and topography. Exploration wells indicate that, in the survey area, sediments underlying Pleistocene deposits include conglomerates, sandstones, coals, and shales as young as late Miocene in age. The Pleistocene-Tertiary angular unconformity therefore represents a depositional hiatus of approximately 6 Ma or more. Estimates of sediment compactions based on analyses of geophysical well logs by Dynamic Oil Ltd. suggest that 1800-2400 m of late Tertiary sediments were eroded from this region. Vertical relief (300 m across a 4400 m section displayed in Fig. 2) developed on the bedrock surface, is similar to that at the apex of the present delta between the Fraser River channel and adjacent uplands of New Westminster and Surrey.

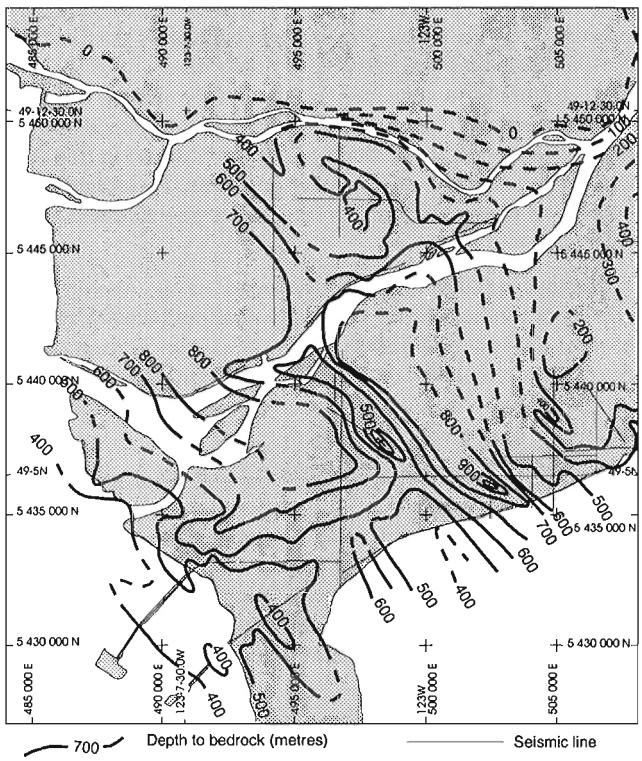

Figure 8. Interpreted bedrock depth map of the survey area based on combined travel-time picks and velocity panel data.

SUMMARY

Approximately 126 line-km of conventional CDP multichannel seismic reflection data have been interpreted to identify the Pleistocene-Tertiary unconformity (bedrock surface) beneath the Fraser River delta. Depths to this surface range between 200 and 1000 m, with an average bedrock depth in the range of 500 m. The northwest-trending topographic highs and lows dominate throughout the area. Although data coverage is missing in the urban areas of the city of Richmond, an apparent broad topographic low can be extrapolated beneath the city. In contrast, topographic highs can be interpreted in the east-central portion of Lulu Island, as well as the eastern portion of Burns Bog.

One of the major objectives of the GSC earthquake hazards program in the lower mainland is the establishment of the geological and geophysical framework relevant to geotechnical investigations. The interpretation offered here is one of the basic building blocks for the framework. It is hoped that this information will be of use to the geotechnical community in modelling ground response to earthquake shaking.

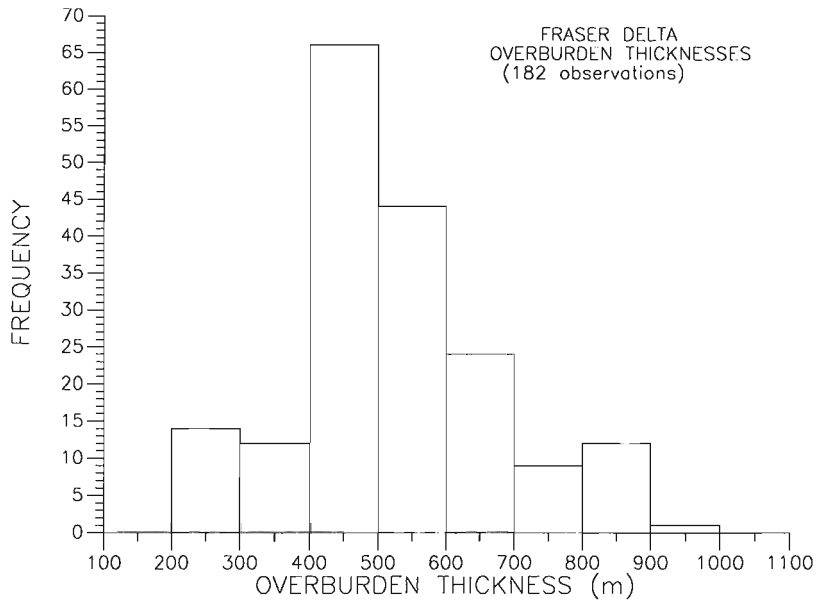

Figure 9.

Histogram of Quaternary overburden thicknesses from velocity panel and two-way travel time data.

ACKNOWLEDGMENTS

We wish to thank Dynamic Oil Ltd. and its partners for allowing the release of the travel-time interpretation and associated overburden velocity data. We appreciate the many hours of discussions with Wayne Babcock, president of Dynamic Oil Ltd., on the seismic and geological aspects of the delta, as well as his encouragement and support of this present work. P. Mustard (GSC Vancouver) kindly reviewed an earlier draft of this manuscript.

REFERENCES

Armstrong, J.E. and Hiscock, S.R.
1976: Surficial Geology, Vancouver British Columbia: Geological Survey of Canada, Map 1486A.

Clague, J.J.
1994: Quaternary stratigraphy and history of south-coastal British Columbia; in Geology and Geological Hazards of the Vancouver Region, Southwestern British Columbia, (ed.) J.W.H. Monger; Geological Survey of Canada, Bulletin 481, p. 181-192.

Dallimore, S.R., Edwardson, K.A., Hunter, J.A., Clague, J.J., and Luternauer, J.L.
1995: Composite geotechnical logs for two deep boreholes in the Fraser River delta, British Columbia; Geological Survey of Canada, Open File 3018.

Dix, C.H.
1955: Seismic velocities from surface measurements: Geophysics, v. 20, p. 68-86.

Hunter, J.A., Luternauer, J.L., Neave, K.G., Pullan, S.E., Good, R.L., Burns, R.A., and Douma, M.
1992: Shallow shear wave velocity-depth data in the Fraser Delta from surface refraction measurements 1989, 1990, 1991; Geological Survey of Canada, Open File 2504, 270 p.

Luternauer, J.L., Barrie, J.V., Christian, H.A., Clague, J.J., Evoy, R.W., Hart, B.S., Hunter, J.A., Killeen, P.G., Kostaschuk, R.A., Mathewes, R.W., Monahan, P.A., Moslow, T.F., Mwenifumbo, C.J., Olynyk, H.W., Patterson, R.T., Pullan, S.E., Roberts, M.C., Robertson, P.K., Tarbotton, M.R., and Woeller, D.J.
1994: Fraser River delta: geology, geohazards and human impact; in Geology and Geological Hazards of the Vancouver Region, Southwestern British Columbia, (ed.) J.W.H. Monger; Geological Survey of Canada, Bulletin 481, p. 197-220.

Monger, J.W.H., and Journeay, J.M.
1994: Basement geology and tectonic evolution of the Vancouver region; in Geology and Geological Hazards of the Vancouver Region, Southwestern British Columbia, (ed.) J.W.H. Monger; Geological Survey of Canada, Bulletin 481, p. 3-25.

Monger. J.W.H., Journeay, J.M., Currie, L., and Hamilton, T.
in press: Neogene tectonics of southwestern British Columbia; Geological Association of Canada, Annual Meeting, Abstract, May 1995.

Mustard, P.S.
1994: The upper Cretaceous Nanaimo Group, Georgia Basin; in Geology and Geological Hazards of the Vancouver Region, Southeastern British Columbia, (ed.) J.W.H. Monger; Geological Survey of Canada, Bulletin 481, p. 27-95.

Mustard, P.S. and Rouse, G.E.
1994: Stratigraphy and evolution of Tertiary Georgia Basin and subjacent Upper Cretaceous sedimentary rocks, southwestern British Columbia and northwestern Washington State: in Geology and Geological Hazards of the Vancouver Region, Southeastern British Columbia (ed.) J.W.H. Monger; Geological Survey of Canada, Bulletin 481, p. 97-169.

Mustard, P.S., Clague, J.J., Woodsworth, G.J., Hickson, C.J., Jackson, L.E., Luternauer, J.L., Monger, J.W.H., Ricketts, B.D., Turner, R.J.W., Hunter, J.A., and Monahan, P.A.
in press: Geology and Geological Hazards of the Greater Vancouver Area; in Urban Geology and geohazards of the greater Vancouver region; (ed.) P.F. Karrow and O.L. White; Geological Association of Canada, Special Publication.

Geological Survey of Canada Project 890023

Interior Plains and Arctic Canada

Plaines intérieures et région arctique du Canada

Proboscidean tusk of Middle Wisconsinan age from sub-till gravel, near Turtle Mountain, southwestern Manitoba[1]

R.J. Fulton
Terrain Sciences Division

Fulton, R.J., 1995: Proboscidean tusk of Middle Wisconsinan age from sub-till gravel, near Turtle Mountain, southwestern Manitoba; in Current Research 1995-E; Geological Survey of Canada, p. 91-96.

Abstract: An AMS radiocarbon age of 33 860 ± 330 BP was obtained for a partial tusk from a gravel pit on the northern flanks of Turtle Mountain, southwestern Manitoba. The tusk was not collected in place but was removed from a pile of spoils. Gravel in the pit is capped by till which is overlain by glacial lake silt and sand. The gravel was interpreted as an ice advance glacial deposit because it grades into overlying till and bedding is locally faulted and disrupted. It was hoped the age of the tusk would correspond closely to the beginning of overriding of the area by the last ice sheet (Late Wisconsinan). Because the age obtained is about 10 000 years older than was expected, it appears the tusk may have been incorporated from older deposits, or may come from an unrecognized, Middle Wisconsinan-aged gravel which underlies the gravel exposed immediately below the till.

Résumé : On a obtenu par spectrométrie de masse par accélérateur sur carbone radioactif un âge de 33 860 ± 330 B.P. pour une défense partielle provenant d'une gravière sur les flancs nord du mont Turtle dans le sud-ouest du Manitoba. La défense n'a pas été recueillie sur place mais dans un tas de déblais. Le gravier de la carrière est surmonté de till qui est à son tour recouvert de silt et de sable glaciolacustres. Le gravier est interprété comme un dépôt d'avancée glaciaire étant donné qu'il se transforme en till sus-jacent et que la stratification est localement faillée et perturbée. On espérait que l'âge de la défense correspondrait assez exactement au début du recouvrement de la région par la dernière calotte glaciaire (Wisconsinien supérieur). Puisque que l'âge obtenu est d'environ 10 000 ans plus ancien que prévu, il semble que la défense a pu être incorporée à partir de dépôts plus anciens ou qu'elle proviendrait d'un gravier non reconnu du Wisconsinien moyen qui s'étend sous le gravier exposé immédiatement sous le till.

[1] Contribution to the Southern Prairies NATMAP Project.

INTRODUCTION

A tusk fragment was discovered in 1981, in a gravel pit on the northern margin of Turtle Mountain in southwestern Manitoba (Fig. 1). Turtle Mountain is an upland remnant of early Tertiary sediments which is overlain by hummocky glacial deposits. The discovery gravel pit lies at the southern edge of a topographic bench which skirts the northern margin of the upland. Reports of seven other Manitoba[1] discoveries of proboscidean remains have been made in the literature (4 reported in Leith, 1949, 2 reported in Young, 1966, and 1 by Nielsen et al., 1988). Most of the previous finds were from gravel pits which were probably in glacial fluvial deposits related to retreat of the last ice sheet; the molar reported in Nielsen et al. (1988) is an exception as it is thought to have come from either Early Wisconsinan (65-80 000 years ago) or Sangamonian (80-130 000 years ago) age deposits. Two of the previously found fossils were tusks and the remaining 5 were teeth. Four of the teeth have been identified as *Mammuthus primigenius* (woolly mammoth) while the remaining one has been referred to by Young (1966) as *"Parelephas jeffersoni"*[2]. The tusks were not identified.

DISCOVERY

L. Black discovered the tusk fragment in 1981 while removing gravel from the municipal gravel pit on the land of J.S. Hammond (location: about 22 km southwest of Boissevaine, UTM zone 14, E406500, N5439300, NW06-02-21W1, Fig. 1). The tusk was not seen in place in the wall of the excavation but was found within an excavated pile of gravel lying about 6 m below the natural ground surface. Larry Black had no doubts that the tusk had come from the gravel which is exposed in the wall of the pit but the part of the pit from which the gravel was excavated is not presently exposed. The tusk material was white when it was dug up but after several days began to discolour and to crumble. It was taken to Brandon University where it was identified as "Mastodon", coated with white glue and eventually sent to the Moncur Museum in Boissevain.

HAMMOND PIT SITE

When visited in June 1994, little gravel had been removed from the pit for several years but good exposure persisted in several places (Fig 2). The description which follows is a "composite" section pieced together from exposures in various parts of the pit and was not seen as a single vertical succession (see Table 1).

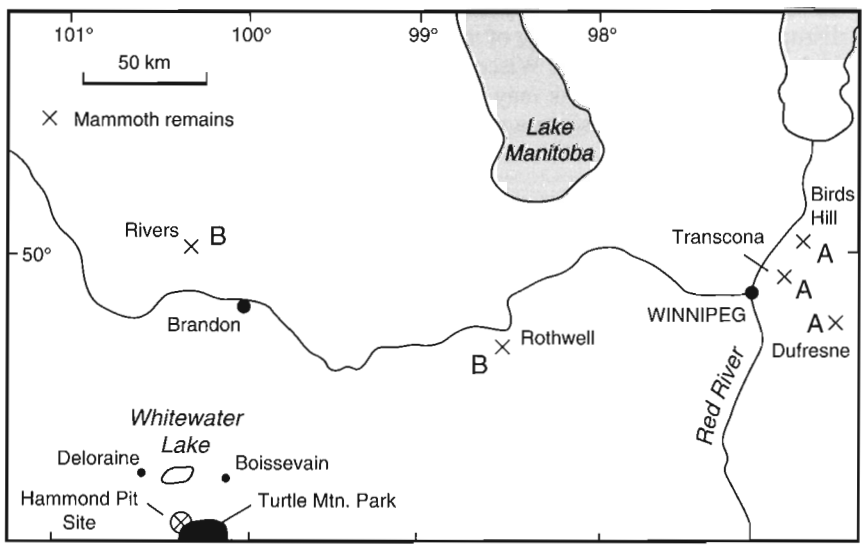

Figure 1.

Hammond pit site with location of other proboscidean remains in southern Manitoba (A – reported in Leith, 1949; B - reported in Young, 1966).

[1] Another finding is reported in unpublished field notes of J.A. Elson (Geological Survey of Canada, September 4, 1953). These record that R.A. MacNeish told Elson that a mammoth tooth had been found in a gravel pit 20 ft (6 m) below surface in SW35-02-12, 2 miles northwest of Crystal City. The pit wall was not exposed when Elson visited the site but he thought the gravel probably was outwash but might have been "Older Alluvium". I have no other information on this find.

[2] *"Parelephas jeffersoni"* is referred to as *Mammuthus jeffersonii* (Kurtén and Anderson, 1980) and is sometimes considered to be a progressive stage of *Mammuthus columbi* (Maglio, 1973) approaching *Mammuthus primigenius* in its advanced characteristics. Because of this, *Mammuthus jeffersonii* is not recognized by Maglio (1973), Agenlroad (1984), Harington (1984), or Graham (1986) as a valid species but as a variant of *M. Columbi.* . Harington and Ashworth (1986) indicated that "Woolly mammoth occupied discontinuous tundra-like range south of the ice sheets, extending from southern British Columbia to the Atlantic Coast ...roughly paralleling the southern margin of the Wisconsin ice sheets". According to that view, the Manitoba elephants might be best referred to woolly mammoths.

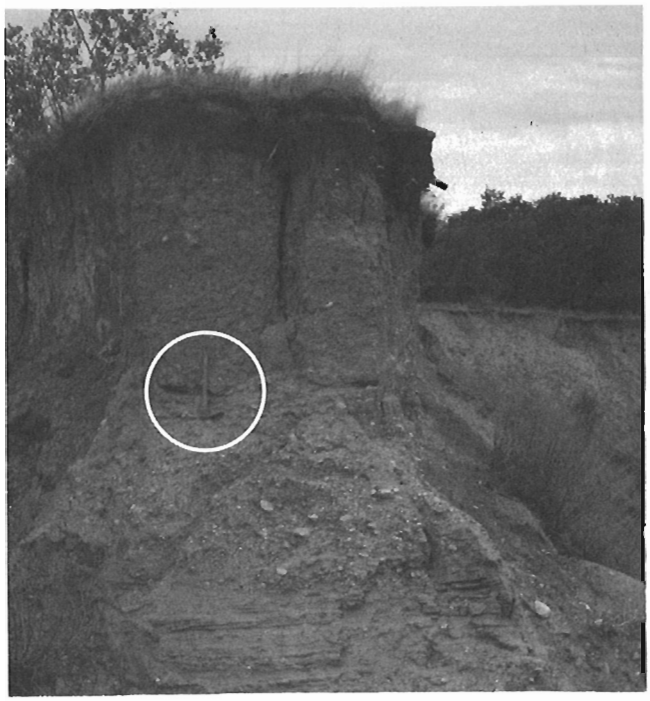

Figure 2. Hammond pit exposure, till over glaciofluvial gravel. Pick at base of till is 40 cm long.

RELATIONSHIP OF TUSK AND GRAVEL

The tusk fragment was found in gravel but was not abraded (Fig. 3) as would be expected if it had been transported by the stream which deposited the gravel. Also, no other large bones were found in the pit. These are contradictory observations as separation of the tusk from other remains would have required some transport by the stream. Three possible interpretations are: 1) the animal lived in the area as the last glacier was advancing and died near the Hammond pit site; the tusk was the only fossil that was rolled a short distance to this site; 2) the animal died and its bones (at least one tusk) were buried sometime before the last ice sheet advance; during ice advance a meltwater stream exhumed the remains and carried the tusk to this site; and 3) the gravels, which contained the tusk fragment, are not related to the glacial deposits which make up the upper part of the succession but were deposited in a normal stream during the nonglacial period which preceded the last glaciation; the animal, which carried the tusk, died and the tusk fragment was the only part of its skeleton deposited at this site.

TUSK DESCRIPTION

The partial tusk (Temporary Accession no. DgMb11) is about 60 cm long. The root or proximal end is about 9 cm in diameter and the other end is about 9.5 cm (Fig. 4). The piece curves gently and the cementum (the hard outer layer) is missing from the outer curve. The cementum is about 0.8 cm thick.

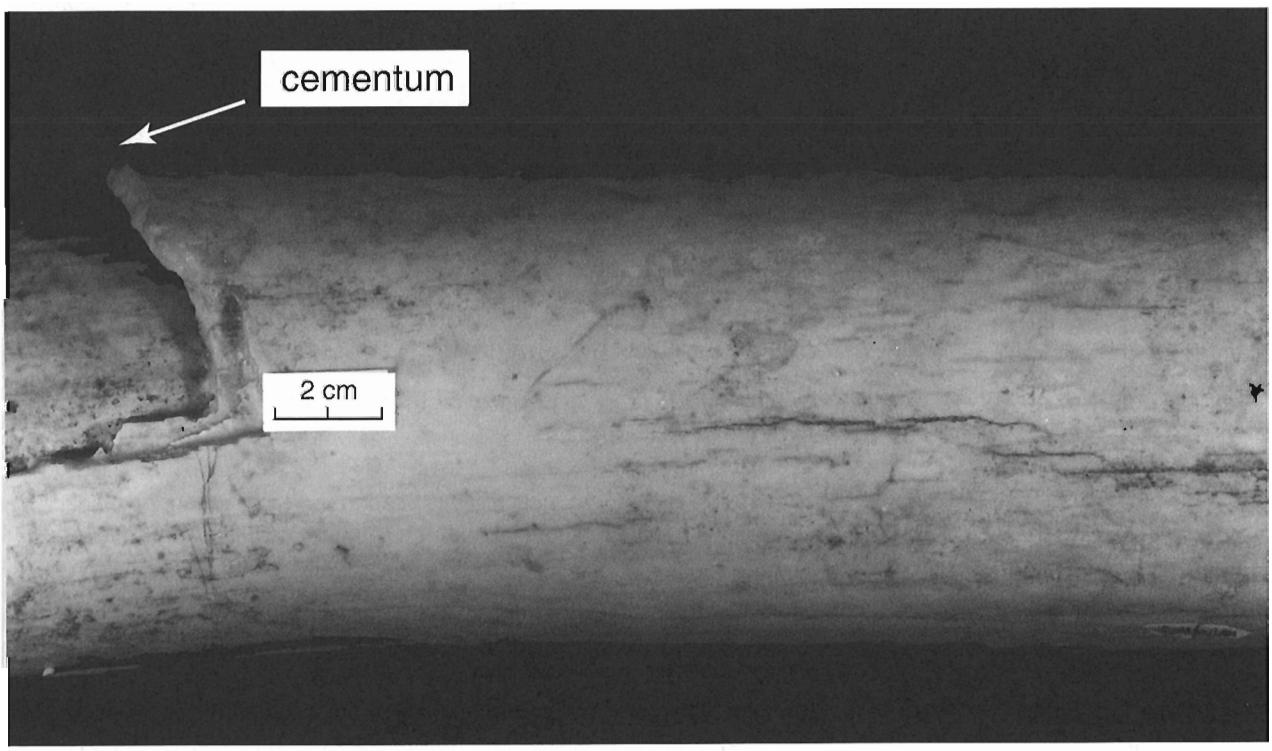

Figure 3. Hammond pit tusk showing unabraided surface.

Figure 4. Side view of Hammond pit tusk. The proximal (root) end is to the left.

The distal end is rounded and blunt suggesting that the tusk had been broken some time before death of the animal (Fig. 5).

IDENTIFICATION OF TUSK

The tusk was labelled as "Mastodon" in the museum, although it is not clear who provided the identification or what criteria were used. In 1994, D.C. Fisher, a vertebrate paleontologist at the Museum of Paleontology and Department of Geological Sciences, University of Michigan, was contacted for advice. He reported that it is very difficult to identify tusks, particularly when only a fragment is available. From the description given here, he said that this fragment probably came from a mature female (based on size, lack of a taper, and the fact that the tusk thickens beyond its growing margin). He also said that mammoth tusks tend to have thicker cementum (~1.2 cm) than do mastodon (~0.7 cm).

Because of problems with illegal ivory, considerable effort has been placed on developing techniques for differentiating modern from ancient ivory (Espinoza et al., 1990 and Espinoza and Mann, 1991). The best technique available involves measuring the Schreger angles (angle between crossing lines seen in cross sections of proboscidean ivory). This approach has been used in an attempt to differentiate mammoth tusks from mastodon but with limited success (D.C. Fisher, pers. comm., 1994). A crude attempt was made to measure the Schreger angles of the Hammond pit tusk. Eighteen measurements gave an average value of 108°, an angle which lies in an over-lap zone between those typical of modern elephant and those typical of mammoths (Espinoza and Mann, 1991).

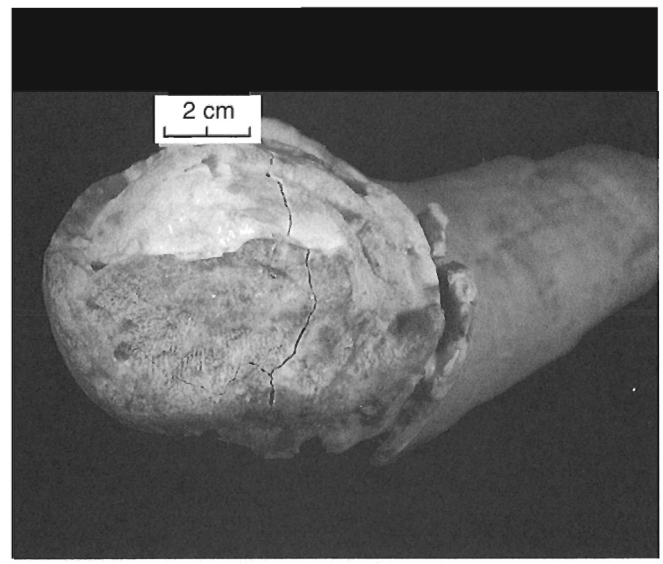

Figure 5. Blunt distal end of Hammond Pit tusk.

A clear identification therefore cannot be made. As mentioned above, the Hammond pit tusk has cementum ~0.8 cm thick suggesting that the tusk is from a mastodon. However, according to C.R. Harington (pers. comm., 1995), mastodon remains have generally been found in eastern and southern North America with mammoths totally dominating proboscidean finds in the northwestern part of the continent (see also the comments in footnote 2). In addition, if this is a mastodon tusk, it would be the first mastodon fossil identified in Manitoba. Hence, the tusk is best referred to "Proboscidea" and most likely represents a mammoth.

Table 1. Composite stratigraphic section for the Turtle Mountain Tusk site.

Unit	Material	Thickness	Interpretation
A	Laminated sandy silt	0-1 m	Sediment deposited in a small, shallow lake which was ponded between the glacier (to the north) and the hillside (to the south). The lake probably was present for only a few tens of years during retreat of the glacier ~12 000 years ago.
B	Massive sandy silt diamicton (till)	1.5-4 m	This compact, poorly sorted sediment was deposited by the last glaciers to override this area. The sediment consists of material, that was either plastered onto the underlying gravel by the overriding ice or melted out of the ice. The last glacier advanced over the area ~23 000 years ago.
C	Sandy gravel	>16 m	The stratification of this well sorted gravel is in places folded, faulted, and disrupted; suggesting that it was deposited as a kame terrace (gravel deposited by a glacier meltwater stream which flows between a glacier and the adjacent hillside); locally, gravel appears to grade into overlying till. At least the upper part of the gravel is thought to have formed as the last glacier began to override the area ~23 000 years ago.

AGE AND INTERPRETATION

An AMS radiocarbon age of 33 860 ± 330 BP on tusk material (TO-4639) indicates that the proboscidean lived during the Middle Wisconsinan nonglacial period prior to the last glacial advance.

The tusk came from a gravel which was thought to have been deposited as an ice-marginal, glaciofluvial deposit. This genetic interpretation of the gravel was based on disruption of the gravel stratification which was thought due to melting of adjacent ice and on an apparent local gradation from the gravel to the overlying till. Because of this interpretation, the gravel was thought to have been deposited as the last ice sheet moved into the area about 23 000 years ago. On the assumption that the proboscidean tusk dated back to this time, it was hoped that the age of the tusk would closely define the timing of glacier advance into this area. The radiocarbon age obtained is about 10 000 years older than the estimated time of ice advance (Fenton, 1984). This suggests that either the glacial stream eroded the tusk from an older deposit (interpretation #2 above) or that the origin of the gravel containing the tusk was incorrectly interpreted. Another possibility is that more than one gravel unit is present in this pit and the tusk came from a layer which was deposited during the nonglacial period (Middle Wisconsinan) which preceded the last glaciation (#3 above).

Deposits dating from the Middle Wisconsinan interval (23-65 000 years ago) have been reported from several places in the Canadian Prairie Provinces (Manitoba: Klassen, 1969; southern Alberta: Stalker, 1976: and central Alberta: Westgate et al., 1972, Lichti-Federovich, 1975, and Liverman et al., 1989). Only the southern Alberta deposits contains remains of large animals, among them mammoth. Climate during this nonglacial period has been interpreted as similar to or slightly cooler than present (Fenton, 1984).

CONCLUSIONS

1. Gravel, interpreted as being of ice-advance, glaciofluvial origin, is exposed beneath till in a gravel pit on the northern flanks of Turtle Mountain.
2. A partial tusk which came from the gravel (exact position unknown) provided an AMS radiocarbon age of 33 860 ± 330 BP.
3. As this age is about 10 000 years older than the advance of the last ice sheet, either it was incorporated from older gravels or the tusk comes from an unrecognized, Middle Wisconsinan-aged gravel which underlies the gravel exposed immediately below the till.
4. This find adds to earlier findings at Medicine Hat which indicate that large mammals were present in the southern part of the Canadian Provinces during Middle Wisconsinan.

ACKNOWLEDGMENTS

The Moncur Museum, Boissevain Manitoba and Bill Moncur made the tusk available to the Geological Survey of Canada and allowed the removal of material for dating. D.C. Fisher, University of Michigan, provided advice on the identification of tusk material. C.R. Harington, Canadian Museum of Nature reviewed an early version of this manuscript and provided information related to the classification of Proboscidea.

REFERENCES

Agenlroad, L.D.
1984: New world mammoth distribution; in Quaternary Extinctions – A Prehistoric Revolution, P.S. Martin and R.G. Klein (ed.); University of Arizona Press, p. 90-108.

Espinoza, E.O. and Mann, M.J.
1991: Identification guide for ivory and ivory substitutes; World Wildlife Fund and Conservation Foundation, Washington, D.C.. 35 p.

Espinoza, E.O.,Mann, M.J., LeMay, J.P., and Oakes, K.A.
1990: A method for differentiating modern from ancient Proboscidean ivory and worked objects; Current Research in the Pleistocene, v. 7, p. 81-83.

Fenton, M.M.
1984: Quaternary stratigraphy of the Canadian Prairies; in Quaternary Stratigraphy of Canada – A Canadian Contribution to IGCP Project 24, R.J. Fulton (ed.); Geological Survey of Canada, Paper 84-10, p. 57-68.

Graham, R.W.
1986: The Colby mammoth site - taphonomy and archeology of a Clovis kill in northern Wyoming; University of New Mexico Press.

Harington, C.R.
1984: Mammoths, bison and time in North America; in Quaternary Dating Methods, W.C. Mahaney (ed); Elsevier Science Publications B.V., Amsterdam, p. 299-308.

Harington, C.R. and A.C. Ashworth
1986: A mammoth (Mammuthus primigenius) tooth from Late Wisconsin deposits near Embden, North Dakota, and comments on the distribution of woolly mammoths south of the Wisconsin ice sheets; Canadian Journal of Earth Sciences, v. 23, p. 909-918.

Klassen, R.W.
1969: Quaternary stratigraphy and radiocarbon chronology of southwestern Manitoba; Geological Survey of Canada, Paper 69-27, 19 p.

Kurtén, B. and Anderson, E.
1980: Pleistocene Mammals of North America; Columbia University Press, 442 p.

Leith, E.I.
1949: Fossil elephants of Manitoba; Canadian Field-Naturalist, v. 63, p. 135-137.

Lichti-Federovich, S.
1975: Plant megafossils from Mid-Wisconsin sediments in west-central Alberta; in Report of Activities, Part C; Geological Survey of Canada, Paper 75-1, Part C, p. 85-90.

Liverman, D.G.E., Catto, N.R., and Rutter, N.W.
1989: Laurentide glaciation in west-central Alberta: a single (Late Wisconsinan) event; Canadian Journal of Earth Sciences v. 26, p. 266-274.

Maglio, V.J.
1973: Origin and evolution of the Elephantidae; Transactions of the American Philosophical Society, No. 63, 149 p.

Nielsen, E. Churcher, C.S. and Lammers, G.A.
1988: A woolly mammoth (Proboscidea, *Mammuthus promigenius*) molar from the Hudson Bay Lowland of Manitoba; Canadian Journal of Earth Sciences, v. 25, p.933-938.

Stalker, A. MacS.
1976: Quaternary stratigraphy of the southwestern Canadian Prairies; in Quaternary Stratigraphy of North America, W.C. Mahaney (ed.); Dowden, Hutchinson & Ross, Stroudsburg, Pa., p. 381-407.

Westgate, J.A.,Fritz, P., Matthews, J.V., Jr., Kalas, L., Delorme, L.D., Green, R., and Aario, R.
1972: Geochronology and palaeoecology of mid-Wisconsin sediments in west-central Alberta, Canada; 24th International Geological Congress (Montreal, Quebec), Abstracts, p. 380.

Young, H.R.
1966: Proboscidean molars from Manitoba; Canadian Field-Naturalist, v. 80, p. 95-98.

Geological Survey of Canada Project 910024

Age and stratigraphy of the Cass Fjord Formation, Arctic Canada

T. de Freitas and W.H. Fritz
GSC Calgary, Calgary

de Freitas, T. and Fritz, W.H., 1995: Age and stratigraphy of the Cass Fjord Formation, Arctic Canada; in Current Research 1995-E; Geological Survey of Canada, p. 97-104.

Abstract: Numerous Cambrian trilobites indicate a Late Cambrian age for the Cass Fjord Formation. The formation contains two unconformity-bounded members, a lower siliciclastic-rich dolostone member and a microbial bioherm, mudrock, limestone, and minor siliciclastic upper member. The contact between the two members is a hiatus representing up to four trilobite zones. The two members are completely exposed in east-central Ellesmere Island, whereas only the upper member is exposed in the western part of the island. In that area, the upper member is more than 1 km thick and was deposited during a basinward advance of a carbonate ramp.

Résumé : La présence de nombreux trilobites cambriens indique un âge du Cambrien tardif pour la Formation de Cass Fjord. La formation contient deux membres limités par une discordance, un membre inférieur dolomitique riche en roches silicoclastiques et un membre supérieur composé de bioherme microbien, de mudrock, de calcaire et d'un peu de roches silicoclastiques. Le contact entre les deux membres est un hiatus représentant jusqu'à quatre zones à trilobites. Les deux membres sont complètement exposés dans le centre est de l'île d'Ellesmere tandis que seul le membre supérieur affleure dans la partie occidentale de l'île. Dans cette région, le membre supérieur mesure plus de 1 km d'épaisseur; il s'est déposé durant la progression vers le bassin d'une rampe carbonatée.

INTRODUCTION

The Cass Fjord Formation has been investigated by numerous workers in North Greenland and Arctic Canada, but the age of the formation has only been established firmly in Washington Land, North Greenland (Palmer and Peel, 1981; Nowlan, 1985; Bryant and Smith, 1990). There, Palmer and Peel (1981, p. 6) noted that within the Cass Fjord Formation, a thin (30 m thick) interval is bracketed by fossils of the *Cedaria* and *Elvinia* zones. They pointed out that this interval "...is hardly enough to encompass three Upper Cambrian trilobite zones and that the interval is at the same position as a widespread disconformity in midcontinental United States".

During the summer of 1993, Geological Survey of Canada mapping activities in the vicinities of Vendom and Strathcona fiords and Makinson Inlet led to the discovery of abundant trilobite-bearing beds in the Cass Fjord Formation and the recognition of an extensive exposure of this unit in western Ellesmere Island (Harrison et al., 1994; Thorsteinsson et al., 1994). The following is a preliminary report of these new findings.

LITHOLOGY

The Cass Fjord Formation is exposed widely in two main, north-trending, outcrop belts, an almost continuously exposed eastern belt that includes stratigraphic sections 2, 3, and 4, and a more areally restricted western one including section 1 (Fig. 1). In the east, the formation is readily divided into two mappable, unconformity-bounded members (Fig. 2, members 1 and 2), but in the west, only member 2 is exposed.

Member 1

Member 1 is about 200 m thick in the eastern part of the report area. It rests disconformably on carbonates which include the Lower Cambrian Cape Leiper, Cape Ingersoll, Police Post, and Cape Kent formations, and the Middle Cambrian Cape Wood Formation (Fig. 2). The basal 0.2 m of the Cass Fjord Formation is a sandy, chert-pebble conglomerate, that is overlain by 10 to 30 m of locally fossiliferous, greyish-yellow weathering, dolomitic limestone and limestone with planar and wavy parallel lamination, intraclast conglomerates, and

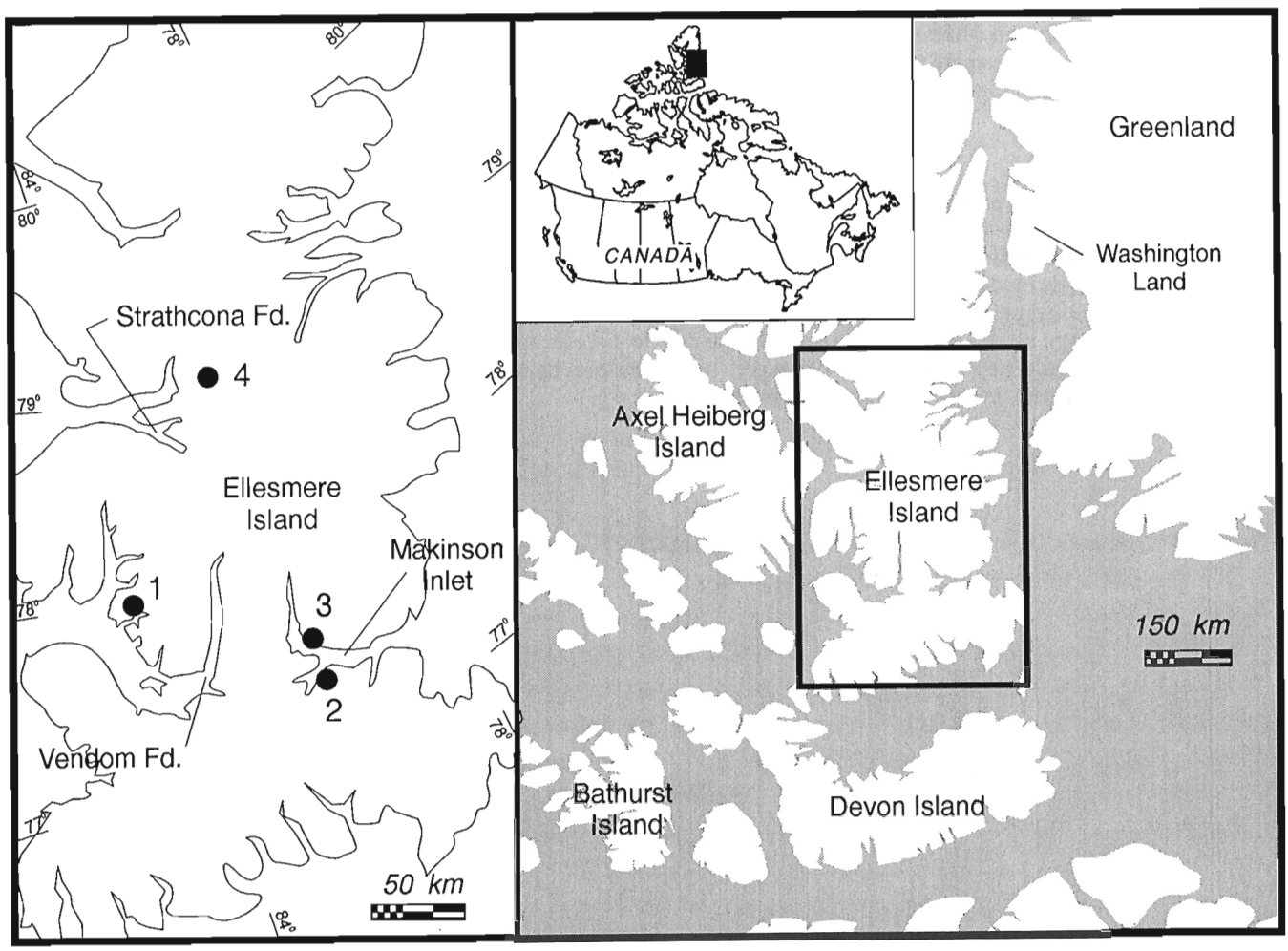

Figure 1. Location map. Black circles indicate measured sections shown in Figures 3 to 6.

rare burrows. These strata grade upward into red and orange weathering sandy dolostone, sandstone, and siltstone with ubiquitous polygonal mudcracks and intraclast conglomerates. Intraclast conglomerates are up to 0.6 m thick and contain tabular carbonate lithoclasts and a sandstone matrix with well-sorted, well-rounded, medium- to coarse-grained quartz sand grains.

Member 2

Member 2 is about 240 m thick in the eastern part of the report area. Its lower contact is disconformable and overlain by a 0.2 to 0.6 cm intraclastic pebble and cobble conglomerate with carbonate and minor chert lithoclasts in a medium- to coarse-grained sand matrix. The basal conglomerate is overlain by a succession of mudrock and limestone with locally large microbial buildups. The latter are oblate, up to 15 m thick structures composed of innumerable, closely but equally spaced, vertically oriented, 3 to 15 cm wide, digitate stromatolites. This is followed by a succession of calcimudstone, intraclast conglomerate, oolite, microbial boundstone, and silty laminated limestone. In the upper part of the member, sandstone is more common than in the lower part, and it consists of thin bedded, white and light grey weathering, intraclastic, well-sorted, fine- to medium-grained quartz arenite with polygonal mudcracks, symmetrical ripple marks, convolute lamination, burrows, and bi-directional cross-stratification.

The Cass Fjord-Cape Clay formational contact is not well exposed in most areas. On air photos and from a distance, the Cape Clay is cliff-forming and contrasts with the usually rubbly slopes underlain by the Cass Fjord Formation. At a close range, the contact is drawn up to 30 m below the abrupt increase in weathering slope angle. At section 4, the Cass Fjord-Cape Clay formational contact coincides with a marked

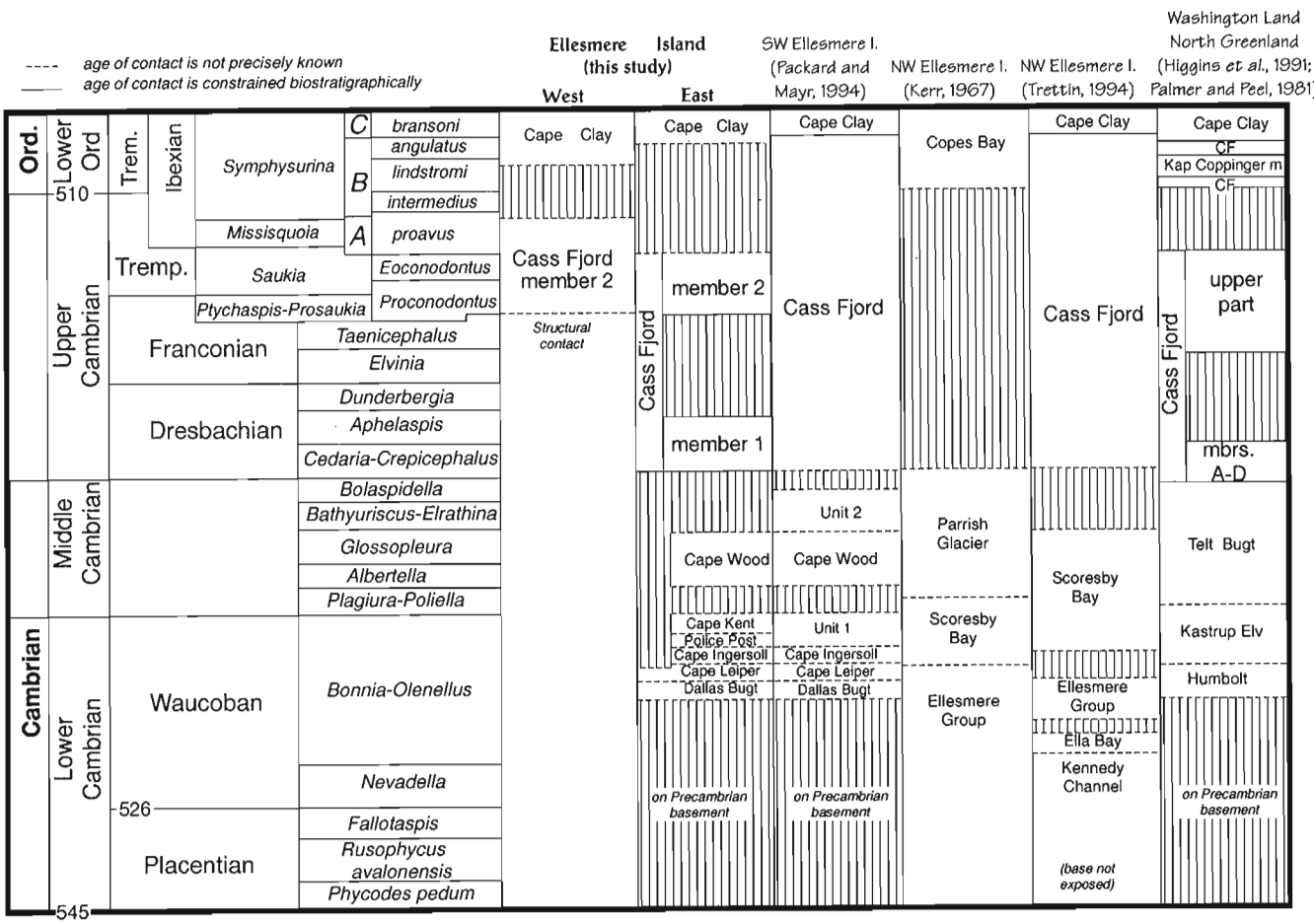

Figure 2. Correlation chart of Cambrian and lowest Ordovician strata in Ellesmere Island and North Greenland. Thompson and Pratt (1994) more completely described units stratigraphically underlying the Cass Fjord Formation. The level drawn for the Cambrian-Ordovician boundary is speculative. A formal level for this boundary has yet to be approved by the International Union of Geological Sciences. Kerr (1967, fourth column) assigned a Proterozoic age to the Ella Bay and Kennedy Channel formations, but these are now given an Early Cambrian age (Long, 1989). Trem., Tremadoc; Tremp., Trempealeauan. Lower Placentian ichnofossil biozones are from Landing (1994); body fossil zonation in upper Placentian, Waucobian, Middle and Upper Cambrian, and Lower Ordovician from Fritz et al. (1991) and Barnes et al. (1981).

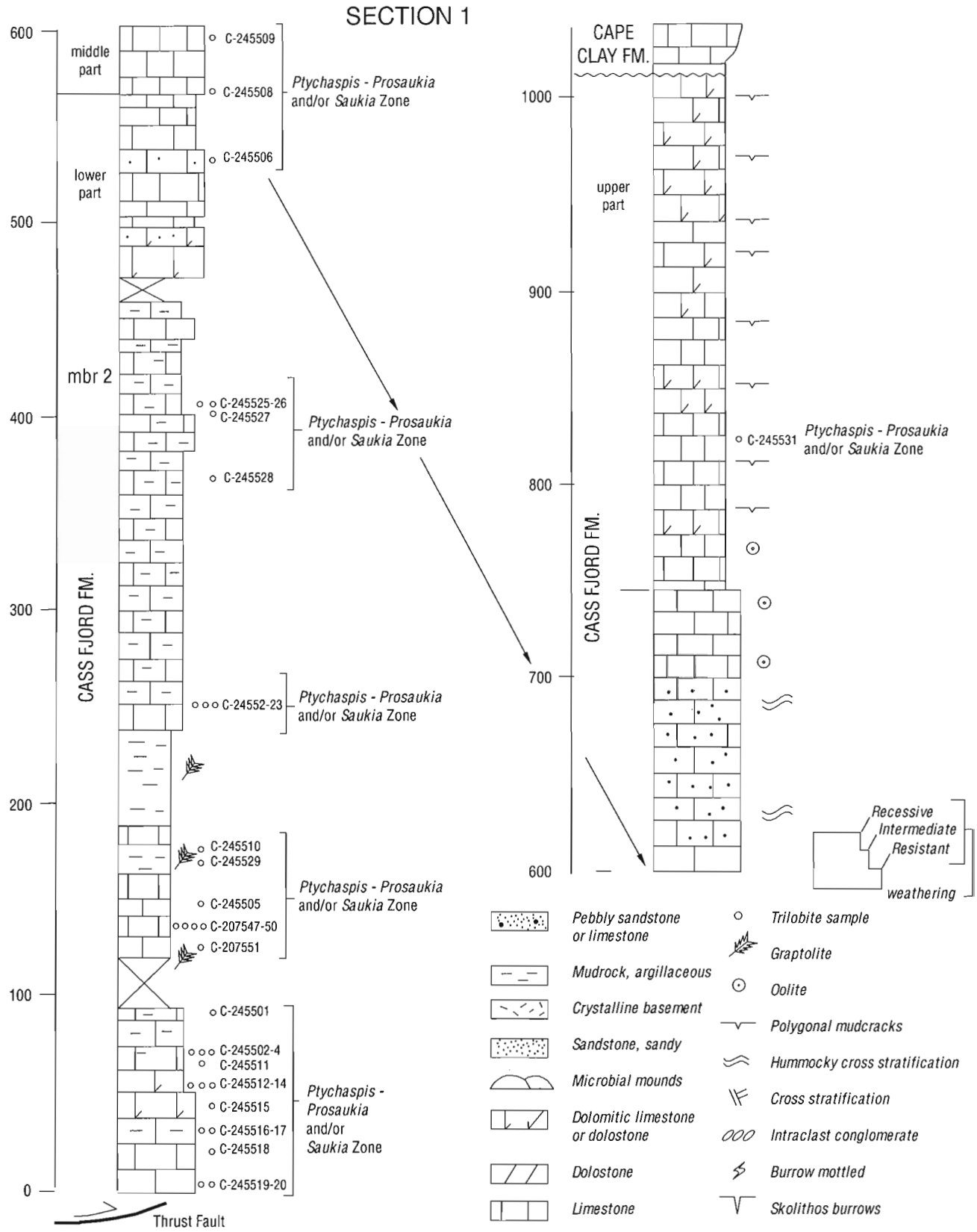

Figure 3. *Stratigraphic section of the Cass Fjord Formation, Troll Fiord, Figure 1, section 1.*

unconformity displaying up to 1 m of erosional relief. Strata above the unconformity consist of thickly bedded calcimudstone, interbedded with abundant intraclast conglomerates.

In the western part of the report area, member 2 is at least 1016 m thick and exposed in high, precipitous cliffs. The lower part of this member (at least 550 m thick) consists of a mixture of limestone and mudrock with abundant trilobites, brachiopods, and graptolites. Silicified trilobites, in particular, are abundant on many bedding surfaces. However, strong, high-angle cleavage makes it difficult to crack out fossil specimens. The mudrock and bioturbated limestone grade upward into very thick bedded, bioturbated, silty and sandy limestone (246 m thick, middle part, Fig. 3) with locally well-developed hummocky cross-stratification. These strata are overlain by a 288 m thick succession (upper part, Fig. 3) of thin- to medium-bedded, mudcracked dolostone and dolomitic limestone associated with small stromatolite mounds. This succession contains 28, metre-scale, upward shallowing sequences. The upper contact of this succession, which is the same as the Cass Fjord-Cape Clay formational contact, is a disconformity, overlain by a basal, 0.2 m thick, sandy carbonate conglomerate of the Cape Clay Formation. Above this, the Cape Clay Formation forms a resistant unit of bioturbated calcimudstone with locally well-developed microbial boundstone.

AGE AND CORRELATION

In eastern Ellesmere Island, trilobite-bearing beds in the Cass Fjord Formation are locally abundant (faunal list in GSC Paleontological Report ε1-1994-WHF). The occurrence of *Cedaria-Crepicephalus* Zone trilobites in the 1.2 to 50 m interval above the basal contact of the Cass Fjord Formation (Fig. 4, GSC loc. C-207453-458; Fig. 5, C-207400, C-207401, C-207402, C-207408) provides the most precise age information on this contact in the Canadian Arctic Islands. *Arapahoia*? sp., *Bonneterrina* aff. *B. greenlandica* Palmer, 1981, *Cedaria* sp., *Metisaspis*? sp., *Terranovella* cf. *T. arcuata* Palmer, 1981, and *Welleraspis* sp. are in this interval. These trilobites are evidence of a low position within the *Cedaria-Crepicephalus* Zone. Although the upper part of unit 1 is not well dated, it is considered that it too is within the same zone.

The basal part of the overlying member 2 in eastern sections 2 and 3 (Fig. 3, GSC loc. C-245502-504, C-245511, C-245512-514, C-24515-520; Fig. 4, GSC loc. C-207461; Fig. 5, C-207406) has yielded *Ptychaspis-Prosaukia* and/or *Saukia* Zone trilobites *Illaenurus*? sp., a saukiid? pygidium, and the brachiopod *Syntrophina* sp. In the western section (section 1), the basal exposures contain *Eurekia* sp. and the brachiopod *Finkelnburgia* sp. A comparison of the trilobite collections from member 1 with those from near the base of member 2 suggests that up to 4 biozones are missing at the unconformity that separates the two map units.

The upper contact of member 2 in the four Ellesmere Island sections is not well dated. The highest collection (Fig. 4, GSC loc. C-207465) does not contain diagnostic fossils; however, stratigraphically below this, at locality 3

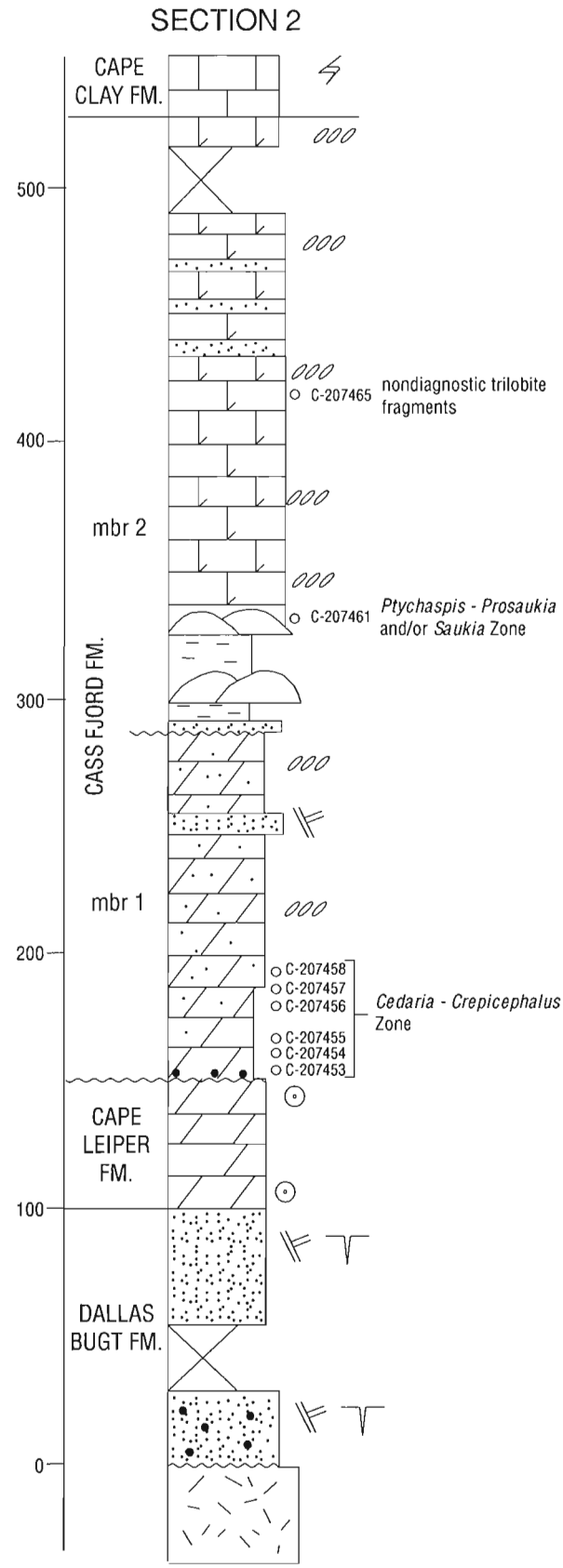

Figure 4. Stratigraphic section of the Cass Fjord Formation, south of Makinson Inlet, Figure 1, section 2. Legend as in Figure 3.

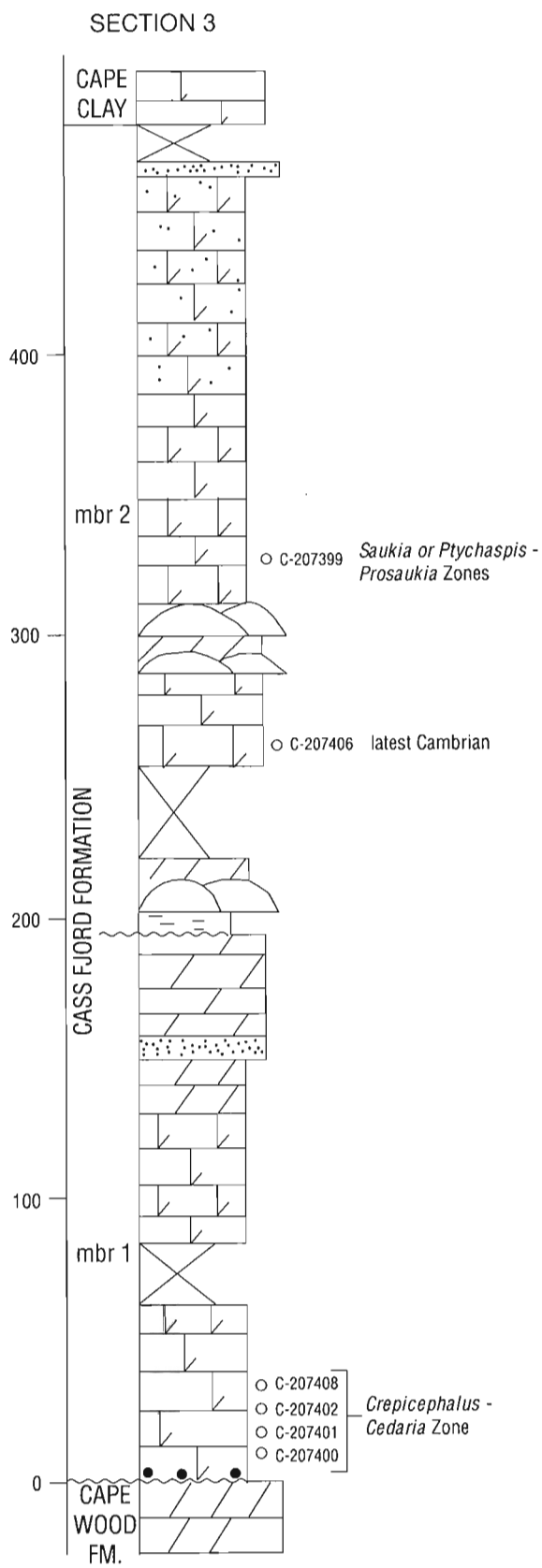

Figure 5. Stratigraphic section of the Cass Fjord Formation, Makinson Inlet, Figure 1, section 3. Legend as in Figure 3.

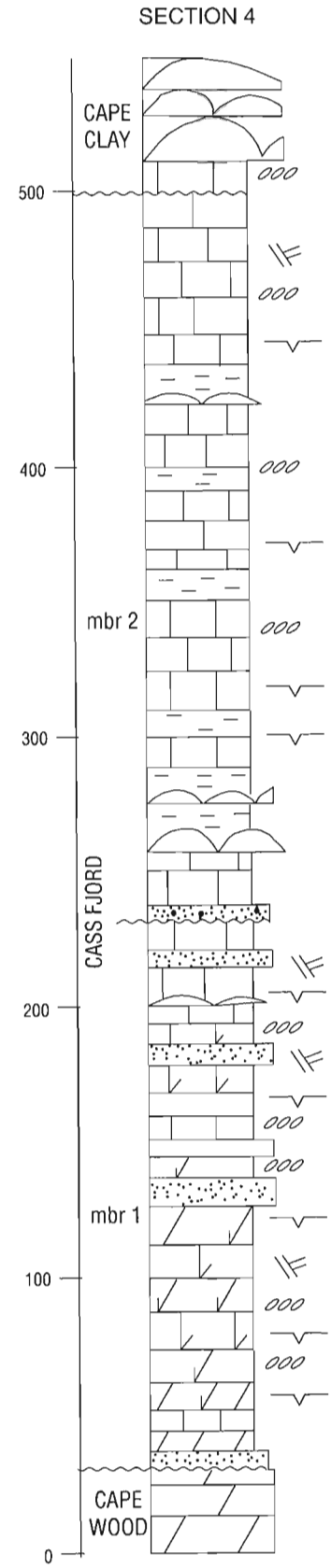

Figure 6. Stratigraphic section of the Cass Fjord Formation, Irene Bay, Figure 1, section 4. Legend as in Figure 3.

(Fig. 5, GSC loc. C-207399), the following fossils have been identified: cf. *Calvinella* sp. or *Briscoia* sp., *Plethometopus*? sp. (free cheek only), and the brachiopod *Glyptotrophia* sp., indicating the *Ptychaspis-Prosaukia* and/or *Saukia* Zone.

Fossils have not been collected from above the Cass Fjord-Cape Clay contact in the report area, except from about 30 km south of section 1. There, a collection from the lower Cape Clay Formation contains fossils of Early Ordovician age (faunal list in GSC paleontological report 0-2-BSN-1994 by B.S. Norford). Outside the report area, the base of the Cape Clay Formation has yielded fossils of the *intermedius* to *bransoni* zones (Nowlan, 1985; Bryant and Smith, 1990; Nowlan in Packard and Mayr, 1994; Nowlan in Trettin, 1994; Nowlan, pers. comm., 1995).

At stratigraphic section 1, member 2 is more than 1 km thick. Fossil beds containing *Ptychaspis-Prosaukia* and/or *Saukia* Zone fossils were collected within the interval 150 to 165 m below the top (Fig. 3). The lowest collections (Fig. 3, C-245511-520) contain *Eurekia* sp., *Idiomesis* sp., and *Finkelnburgia* sp., and about 600 m above this (Fig. 3, C-245509) *Eurekia* sp. and the brachiopod *Finkelnburgia* sp. occur. Faunal elements within the 0 to 600 m interval (*Elkanaspis* sp., *Kathleenella* sp., cf. *Lerifugula* sp., *Naustia*? sp., *Parabolinites* sp., and *Yukonaspis* sp.), and the local abundance of *Protospongia* sp. and fragmentary dendroid graptolites, suggest that deposition occurred in relatively deep water, on the outer part of a carbonate ramp.

DISCUSSION

The Cass Fjord Formation represents two thick transgressive-regressive (T-R) sequences in the Canadian Arctic Islands (de Freitas et al., 1994). Only member 1 is exposed in the eastern part of the report area. A substantial subaerial unconformity exists below its base, and several Lower and Middle Cambrian formations have been removed locally (Fig. 2). The initial transgression in lower Dresbachian time was widespread, and Cass Fjord Formation carbonate strata are now exposed in many of the Canadian Arctic Islands. In western North Greenland, the Cass Fjord yields trilobites questionably assigned to the late Middle Cambrian (Palmer and Peel, 1981, p. 13). If this assumption is correct, marine transgression happened slightly earlier in that area.

In eastern North Greenland, the Middle and Upper Cambrian sequence comprises three significant, basinward stepping progradational sequences (Peel, 1988). The upper T-R cycle, which began at the base of the Holm Dal Formation, appears to be the same age as the base of member 1 of the Cass Fjord Formation in Ellesmere Island.

Above the basal conglomerate in member 1, trilobite-bearing carbonates were deposited during maximum marine transgression. These strata are overlain by a thick carbonate and sandstone succession deposited in restricted, nearshore and perhaps also alluvial floodplain settings.

Although lower to middle Upper Cambrian strata are not preserved in the western part of the report area, member 2 of Trempealeauan age contains an apparently westward progradational carbonate ramp succession. The lowest trilobite-bearing carbonates (0-150 m) were deposited in an aerobic, storm-influenced outer shelf setting. Overlying unburrowed graptolitic mudrock and carbonate represent deeper water, perhaps dysaerobic to anaerobic, conditions that developed during maximum water depth (cf. Ekdale and Mason, 1988). Overlying strata show a gradual return to aerobic, then restricted, periodically exposed conditions in the highest beds of the member. The Cass Fjord Formation at section 1 is thus interpreted as a thick T-R package.

Member 2 of the correlative inner shelf (sections 2, 3, 4) is similarly a T-R sequence (Fig. 6). An unconformity at the base of the member, representing subaerial conditions, is overlain by a thin sandstone and conglomerate, perhaps deposited in a shoreface setting. Maximum transgression is represented by an overlying chert-rich mudrock with several large microbial bioherms. The regressive succession contains abundant intraclast conglomerates, laminated and mudcracked carbonates and minor sandstone, all of which were deposited under nearshore and intertidal conditions. Most of the Cass Fjord carbonate platform was exposed prior to the Cape Clay marine transgression in latest Cambrian to earliest Ordovician time.

CONCLUSIONS

The first extensive trilobite collections from Cass Fjord Formation in the Canadian Arctic Islands indicate a Late Cambrian age for the formation. It contains two mappable, unconformity bounded members, a lower one of Dresbachian age and an upper one of late Franconian to Trempealeauan age. These were deposited during two T-R marine cycles.

ACKNOWLEDGMENTS

We thank G.S. Nowlan for his careful review of the original typescript. The study also benefited from many discussions with R. Thorsteinsson.

REFERENCES

Barnes, C.R., Norford, B.S., and Skevington, D.
1981: The Ordovician System in Canada; International Union of Geological Sciences, Publication no. 8, 27 p.

Bryant, I.D. and Smith, M.P.
1990: A composite tectonic-eustatic origin for shelf sandstones at the Cambrian-Ordovician boundary in North Greenland; Journal of the Geological Society of London, v. 147, p. 795-809.

de Freitas, T., Harrison, J.C., and Mayr, U.
1994: Lower Paleozoic T-R sequence stratigraphy, central Canadian Arctic; Proceedings of the International Conference on Arctic Margins, Anchorage, Alaska, September, 1992, p. 123-128.

Ekdale, A.A. and Mason, T.R.
1988: Characteristic trace-fossil associations in oxygen-poor sedimentary environments; Geology, v. 16, p. 720-723.

Fritz, W.H., Cecile, M.P., Norford, B.S., Morrow, D., and Geldsetzer, H.H.J.
1991: Cambrian to Middle Devonian assemblages; in Geology of the Cordilleran Orogen in Canada, H. Gabrielse and C.J. Yorath (ed.); Geological Survey of Canada, Geology of Canada, no. 4, p. 151-218 (also Geological Society of America, The Geology of North America, v. G-2).

Harrison, J.C., Thorsteinsson, R., and de Freitas, T.A.
1994: Geology of the Strathcona Fiord map area (NTS 49E and part of 39F), District of Franklin, Northwest Territories, scale 1:250 000; Geological Survey of Canada, Open File 2881.

Higgins, A.K., Ineson, J.R., Peel, J.S., Surlyk, F., and Sønderholm, M.
1991: Lower Paleozoic Franklinian Basin of North Greenland; Grønlands Geologiske Undersøgelse, Bulletin 160, p. 71-139.

Kerr, J.W
1967: Stratigraphy of central and eastern Ellesmere Island, Arctic Canada. Part I. Proterozoic and Cambrian; Geological Survey of Canada, Paper 67-27, Part 1, 63 p.

Landing, E.
1994: Precambrian-Cambrian boundary stratotype ratified and new perspective of Cambrian time; Geology, v. 22, p. 179-182.

Long, D.G.F.
1989: Kennedy Channel Formation: key to the early history of the Franklinian continental margin, central eastern Ellesmere Island, Arctic Canada; Canadian Journal of Earth Sciences, v. 26, p. 1147-1159.

Nowlan, G.S.
1985: Late Cambrian and Early Ordovician conodonts from the Franklinian miogeosyncline, Canadian Arctic Islands; Journal of Paleontology, v. 59, p. 96-122.

Packard, J.J. and Mayr, U.
1994: Middle Cambrian to Upper Ordovician carbonate platform; in The Phanerozoic geology of southern Ellesmere and North Kent Island, Canadian Arctic Archipelago, U. Mayr, J.J. Packard, Q.H. Goodbody, A.V. Okulitch, R.J. Rice, F. Goodarzi, and K.R. Stewart (ed.); Geological Survey of Canada, Bulletin 470, p. 30-67.

Palmer, A. and Peel, J.S.
1981: Dresbachian trilobites and stratigraphy of the Cass Fjord Formation, western North Greenland; Grønlands Geologiske Undersøgelse, Bulletin 141, 46 p.

Peel, J.S.
1988: Stratigraphy and Palaeontology of the Holm Dal Formation (late Middle Cambrian), central North Greenland; Meddelelser om Grønland, Geoscience 20, 169 p.

Thompson, C.E. and Pratt, B.R.
1994: Preliminary stratigraphy of Lower and Middle Cambrian rocks, east-central Ellesmere Island, Canadian Arctic Islands; in Current Research 1994-E, Geological Survey of Canada, p. 165-168.

Thorsteinsson, R., Harrison, J.C., and de Freitas, T.A.
1994: Geology of the Vendom Fiord map area (NTS 49D), District of Franklin, Northwest Territories, scale 1:250 000; Geological Survey of Canada, Open File 2880.

Trettin, H.P.
1994: Pre-Carboniferous geology of the northern part of the Arctic Islands: Hazen Fold Belt and adjacent parts of Central Ellesmere Fold Belt, Ellesmere Island; Geological Survey of Canada, Bulletin 430, 248 p.

Geological Survey of Canada Project 860006

Triangle zone and foothills structures in the Turner Valley map area, Alberta[1]

D.A. Spratt[2], S. Chantraprasert[2], and P.A. MacKay[3]
Geological Survey of Canada, Calgary

Spratt, D.A., Chantraprasert, S., and MacKay, P.A., 1995: Triangle zone and foothills structures in the Turner Valley map area, Alberta; in Current Research 1995-E; Geological Survey of Canada, p. 105-111.

Abstract: New mapping of triangle zone and foothills structures, combined with well and proprietary seismic reflection data, constrain a new interpretation of the Turner Valley map sheet (82J/9). The Turner Valley Structure is not a fault propagation fold; it is a complexly faulted antiformal stack within a triangle zone wedge that has been shortened by 50 per cent. Folding of the upper detachment intensifies northward as displacement across the lower detachment increases. In the southern part of the map sheet, a relatively coherent beam of Paleozoic and Cretaceous rocks is inserted into the foreland along a detachment in the Bearpaw Formation. Near the Bearpaw Formation's zero edge in the north, detachment is transferred to the Wapiabi Formation and the wedge is complexly deformed into a composite duplex. Detachment occurs along four horizons, such that Mississippian, Blairmore and Alberta Group rocks comprise three levels of duplexes; higher levels are deformed as the underlying duplexes are emplaced.

Résumé : De nouveaux travaux de cartographie des structures de la zone triangulaire et des avant-monts, de même que des données tirées de puits et des données de sismique réflexion du domaine privé, permettent de réinterpréter la feuille de Turner Valley (82J/9). La structure de Turner Valley n'est pas un pli de propagation de faille; il s'agit plutôt d'un édifice anticlinal faillé de façon complexe au sein d'un biseau de zone triangulaire qui a subi un raccourcissement de 50 %. Le plissement du décollement supérieur s'intensifie vers le nord plus le déplacement s'accroît sur le décollement inférieur. Dans la partie sud de la feuille, un faisceau relativement cohérent de roches paléozoïques et crétacées est inséré dans l'avant-pays le long d'un décollement dans la Formation de Bearpaw. Près de l'endroit où la Formation de Bearpaw se termine au nord, le décollement se prolonge dans la Formation de Wapiabi et le biseau est déformé de façon complexe en un duplex composite. Il y a décollement le long de quatre horizons, de sorte que des roches du Mississippien, de Blairmore et du Groupe d'Alberta comportent trois niveaux de duplex; les niveaux plus élevés sont déformés à mesure que sont insérés les duplex sous-jacents.

[1] Contribution to the Eastern Cordillera NATMAP Project. Foothills Research Project Contribution No. 004
[2] Department of Geology and Geophysics, University of Calgary, Calgary, Alberta T2N 1N4
[3] Morrison Petroleums Limited, Suite 3000, 400-3rd Avenue S.W., Calgary, Alberta T2P 4H2

INTRODUCTION

The Turner Valley oil and gas field, discovered in 1913, was the first significant discovery of hydrocarbons in Canada and the largest producing field in the British Commonwealth until the end of World War II. The western portion of the Turner Valley sheet was mapped by Hume (1931) as part of a Geological Survey of Canada mapping program in the southern Alberta Foothills. Since then, numerous wells have been drilled, the fields of quantitative structural geology and reflection seismology have evolved, and the Turner Valley structure has been recognized as a triangle zone (Jones, 1982; MacKay, 1991). With these added constraints on its three-dimensional geometry, the entire Turner Valley map sheet (82J/9) is being remapped, reinterpreted and compiled at 1:50 000 scale as part of the Eastern Cordillera NATMAP project. The study area is located 30 to 60 km southwest of Calgary, Alberta, between latitudes 49°30'N and 49°45'N (Fig. 1).

A triangle zone is a structural complex, found at the foreland edge of a deformed belt, where foreland-dipping strata and hinterland-dipping strata are juxtaposed. The term "triangle zone" was introduced by Gordy et al. (1977) to describe the eastern limit of the orogenic wedge in the southern Canadian Rocky Mountains. The wedge comprises a lower detachment surface that separates deformed foreland-verging allochthonous strata in its hanging wall from autochthonous strata in its footwall, and an upper detachment surface that separates foreland-verging allochthonous strata in its footwall from hinterland-verging autochthonous strata in its hanging wall. Following the terminology of MacKay (1991), the upper and lower detachments define the top and base of an intercutaneous wedge. Simultaneous motion along these two surfaces allows the wedge to advance toward the foreland as it is emplaced between layers of relatively undeformed foreland basin strata (Price, 1981, 1986).

Three models have been proposed for the formation of triangle zones (Jones, 1982; Charlesworth and Gagnon, 1985; Jamison, 1993). All models show the lower detachment surface of the wedge with a ramp and flat geometry, cutting upsection toward the foreland; the models differ in their treatment of the upper detachment surface. Jones (1982) proposed that the upper detachment is parallel to bedding such that the wedge is simply a duplex. However, Charlesworth and Gagnon (1985) argued that the backthrust and the lower detachment must initiate as conjugate faults, with the backthrust at an angle of greater than 30° to the flat of the lower detachment. Jamison's (1993) finite element model predicted a range of possible backthrust ramp angles based on the strength of the rocks in the hanging wall of the upper detachment. None of the models addresses the problem of changes in geometry and kinematics along strike.

In Alberta, the surface expression of the triangle zone is an antiform developed between the western flank of the Alberta syncline in the Plains and the west-dipping thrusts of the Foothills Belt. At Turner Valley, oil and gas are produced from Paleozoic carbonates in the core of the triangle zone, but Cretaceous and Tertiary strata are the only rocks exposed in the Turner Valley map sheet. High quality seismic reflection data, abundant well data, and detailed geological mapping are instrumental in tying the exposed structures to those in the subsurface and constraining balanced cross-sections (Spratt et al., 1993).

STRATIGRAPHIC FRAMEWORK

A stratigraphic chart for the study area is given in Figure 2. The rocks exposed at surface are clastic and comprise the Lower Cretaceous Blairmore Group, the Upper Cretaceous Alberta (Blackstone, Cardium and Wapiabi formations) and Brazeau groups, and the Upper Cretaceous-Tertiary Coalspur (in the north) and Willow Creek (in the south) formations. Deep wells in the study area penetrate the Paleozoic carbonates. Detailed descriptions of the Cretaceous units that outcrop in the north half of Figure 1 are given by Olchowy and Spratt (1993). Jerzykiewicz and Norris (1993) have proposed new subdivisions of the Upper Cretaceous and Tertiary strata that can be applied to the relatively undeformed southeastern portion of the map sheet. Since the northern limit of the Upper Cretaceous Bearpaw Formation occurs just north of Longview, subdivision of the Brazeau Group is difficult north of Sheep River. A strong anisotropy is imparted by numerous weak shale and coal horizons, so the Upper Cretaceous sequence is disrupted by thrust faults and detachments at several stratigraphic levels (Fig. 2).

STRUCTURE

This study expands upon the work of MacKay (1991), who delineated structural variations in the triangle zone between Sheep Creek and Highwood River. Several key outcrops that constrain the interpretation of the triangle zone geometries are described in Spratt et al. (1993) and MacKay et al. (1994). During the summer and fall of 1994, the remainder of the deformed belt in the Turner Valley map sheet was mapped. Geological field data have been collected at various scales, ranging from 1:1 000 scale planetable maps to 1:25 000 scale enlargements of 1:50 000 scale NTS topographic basemaps. The data are digitized and compiled at 1:50 000 scale using FIELDLOG software (Brodaric and Fyon, 1989) interfaced with AutoCAD*. The digitization of different types of information as separate layers allows printing of the data, or portions thereof, at any scale (eg. Fig. 1).

Understanding the continuity of structures and the ways in which thrust faults merge on the map requires interpreting these features in three dimensions. The map interpretation and several serial cross-sections are constructed and balanced alternately, with many iterations, locally adding more seismic or well data to more precisely constrain the fault trajectories and positions of stratigraphic cutoffs. Two representative balanced sections across the deformed belt of the Turner

* AutoCAD is the registered trademark of Autodesk Inc.

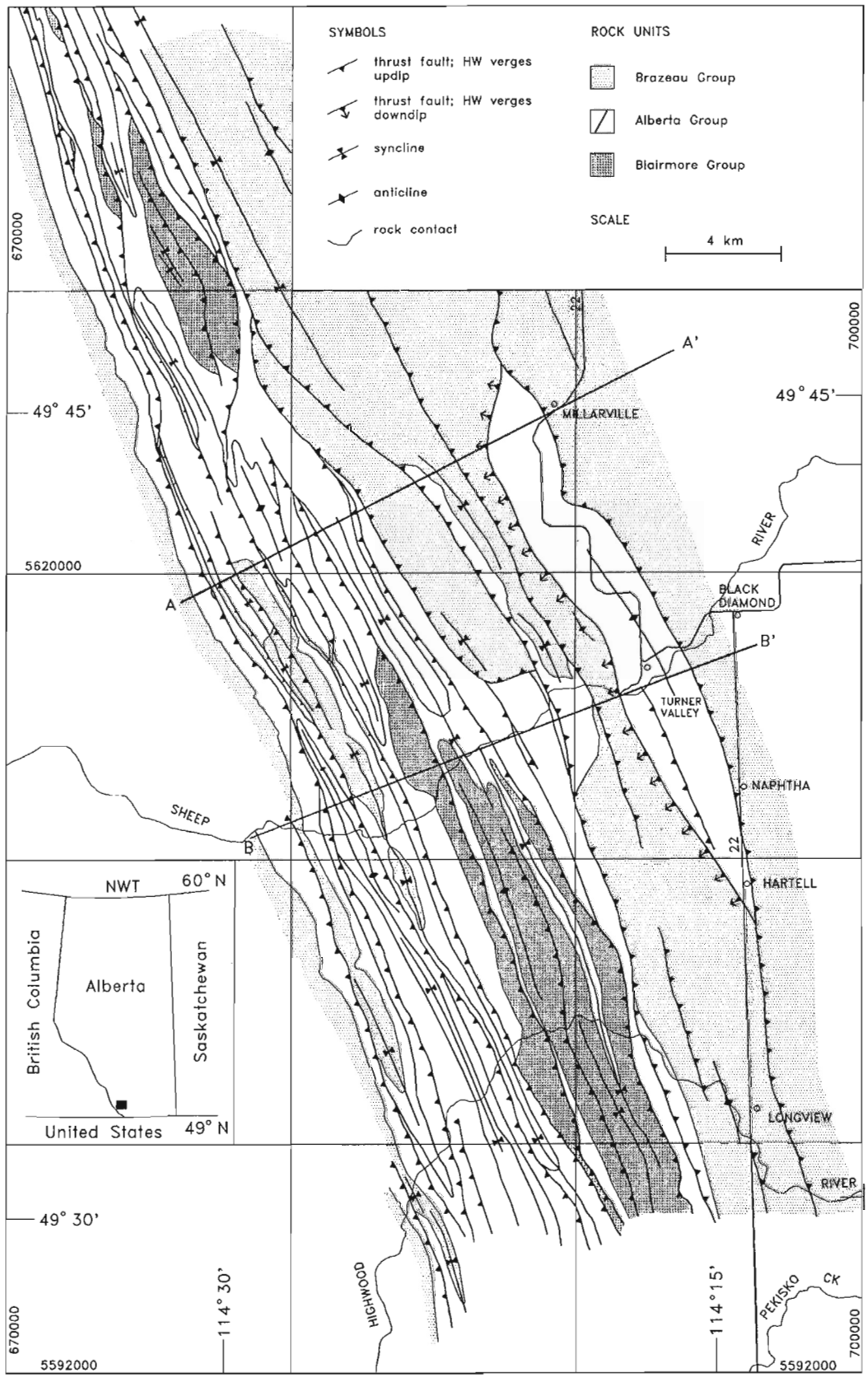

Figure 1. Geologic map of the Turner Valley area; UTM grid lines and positions of cross-sections A-A' and B-B' are delineated.

Valley map sheet are shown in Figure 3. They demonstrate the major changes in geometry and structural style along strike.

Three culminations are obvious on the map. Two involve the Blairmore Group: one occurs in the northwest corner of Figure 1, the other is found along strike to the southeast. The town of Turner Valley is centred on a third culmination, known as the Turner Valley Structure, that exposes Alberta Group rocks flanked by the Brazeau Group. Earlier workers (Hume, 1931; Gallup, 1951; Gordy et al., 1975) interpreted it to be an anticline, but seismic and well data combined with detailed mapping indicate that it is a complexly faulted antiformal stack within a triangle zone (Fig. 3, B-B'; MacKay, 1991). Thrust sheets normally verge up the dip of a fault, except where folded portions of a fault plunge back into the ground. Where vergence indicators exist in the study area, thrusts that are both west-verging and west-dipping are distinguished by special symbols (see legend, Fig. 1). The west-verging upper detachment is folded such that the Alberta Group rocks are exposed in an erosional window at Turner Valley (Fig. 1). The lower detachment has a typical ramp and flat geometry and carries a competent beam of Mississippian carbonates, which is offset by 4 km along the fault plane (Fig. 3, B-B'). As displacement of the Mississippian rocks decreases southward, the Turner Valley structure dies out and folding of the upper detachment decreases. South of Hartell, the upper detachment is not folded but has a smooth listric shape. The southern termination of Paleozoic involvement in the structure is marked by the southern end of the Turner Valley oil and gas field at Longview (Gordy et al., 1975; MacKay et al., 1994).

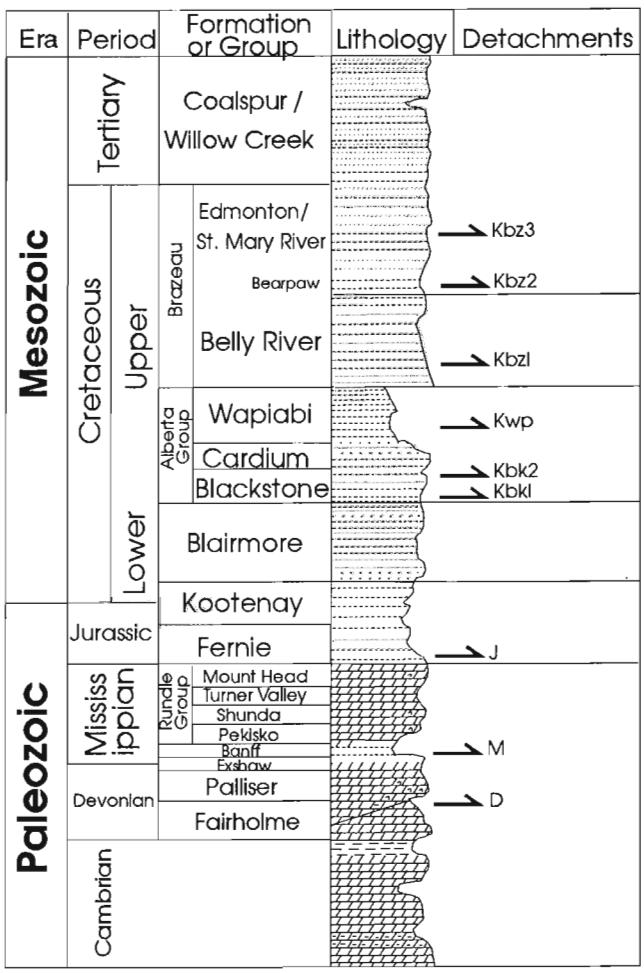

Figure 2. Generalized stratigraphic column for the Alberta Foothills with detachment levels identified: D, Devonian; M, Mississippian; J, Jurassic (Fernie); Kbkl, lower Blackstone; Kbk2, upper Blackstone; Kwp, Wapiabi; Kbzl, lower Brazeau (Belly River); Kbz2, middle Brazeau (Bearpaw or equivalent); Kbz3, upper Brazeau (St. Mary River, Edmonton, or equivalent). Lithological symbols: shales, dashes; siltstones, small dots; sandstones, large dots; limestones and dolostones, crosshatched.

West of Turner Valley, a similar Mississippian structure known as the Highwood Structure is developed in the subsurface (Fig. 3, B-B'; MacKay, 1991); it cores the Blairmore Group culmination that is exposed in the southern half of the map sheet (Fig. 1). Note that the Blairmore is repeated by several thrusts, such that the culmination is more precisely described as a hinterland-dipping duplex (Fig. 3, B-B'). At the Mississippian level, strata are offset by 6 km as a continuous beam that overrides a panel of relatively undeformed Blairmore and Alberta Group rocks. This significant change in structural style with depth occurs across a major detachment in the Jurassic Fernie Group (Fig. 2).

Major changes in structural style also occur along strike. The Highwood structural culmination plunges northward such that no Blairmore or older rocks are exposed along section line A-A' (Fig. 3). In section A-A', Mississippian strata within the Highwood Structure have not been translated 6 km as a continuous beam; instead they are repeated by several smaller thrusts that join to form an antiformal stack. Paleozoic rocks in the eastern culmination are also repeated by several thrusts, in contrast to the one major thrust seen at the base of the Turner Valley Structure in section B-B' (Fig. 3).

Shortening at the Paleozoic level is balanced by duplexes in the overlying Cretaceous rocks. In wells 11-27-20-4W5 and 5-35-20-4W5, at the west end of cross-section A-A' (Fig. 3), the Blairmore Group is structurally thickened to more than three times its normal stratigraphic thickness, indicating the presence of detachments above and below the Blairmore Group, in the Fernie Group, and in the Blackstone Formation (base of the Alberta Group). A third, higher detachment occurs in the Wapiabi Formation at the top of the Alberta Group. The Fernie and Wapiabi detachments continue to serve as major structural discontinuities in the eastern part of section A-A' and to the south in section B-B', but detachment in the Blackstone Formation is much less significant in these areas; Blairmore and Alberta Group rocks are deformed together conformably within the thrust sheets and structurally thickened by folding (Fig. 3).

DISCUSSION

The existence of a folded upper detachment was not recognized by previous workers (Hume, 1931; Gallup, 1951; Gordy et al., 1975), although Bally et al. (1966) did interpret the lower detachment as a blind thrust (it does not reach the ground surface). Building upon the interpretation of Gallup (1951), Dahlstrom (1970) inferred that the 4 km of displacement seen at the Mississippian level must therefore decrease to zero updip. Williams and Chapman (1983) went on to use the Turner Valley structure as an example of a fault propagation fold without questioning the interpretations shown on Hume's (1931) map or Gallup's (1951) rudimentary cross-section. Tippett et al. (1985) explained evidence refuting the interpretation of Williams and Chapman (1983), but Jamison (1987) and Mitra (1990) apparently missed this paper and continued to promote Turner Valley as a classic example of a fault propagation fold. The more recently available well information and good quality seismic reflection data, combined with detailed remapping at surface, indicate that the Turner Valley structure is definitely not a fault propagation fold. It is a complexly faulted antiformal stack within a

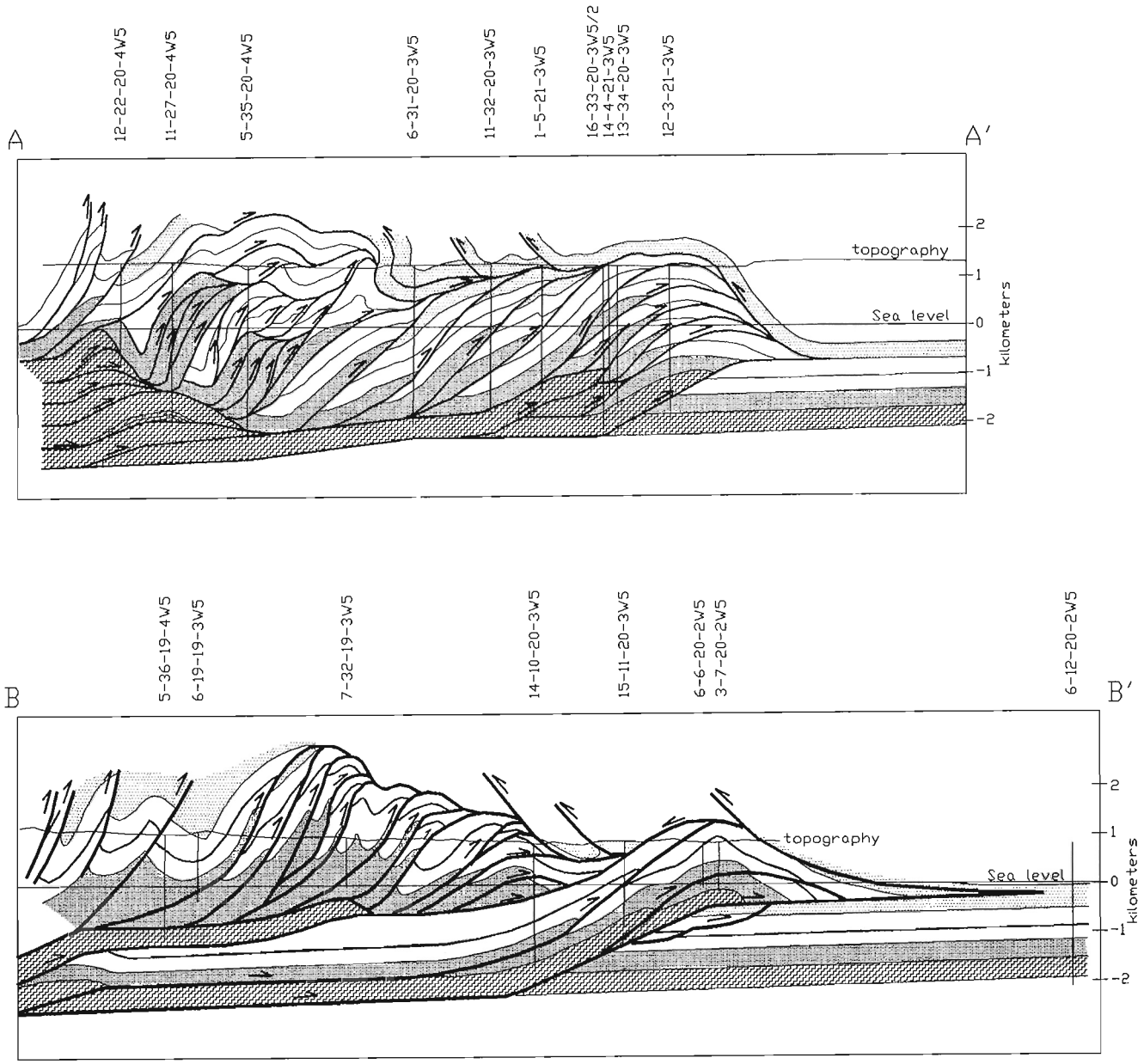

Figure 3. Balanced cross-sections A-A' and B-B'. See Figure 1 for locations. Wells occur along the lines of section or are projected from less than 1 km away. Brazeau Group, light stipple pattern; Alberta Group, white with internal Cardium marker shown as thin black line; Blairmore Group (+Kootenay and Fernie), dark stipple pattern; Mississippian, zig-zag pattern; Turner Valley Structure, eastern culmination cored by Mississippian; Highwood Structure, western culmination cored by Mississippian rocks.

triangle zone, and shortening within the wedge is much greater (50%) than previous workers thought (Fig. 3, B-B'; MacKay, 1991). Recognition of the upper detachment constrains the cross-sections such that they can be balanced without resorting to a sharp decrease in displacement along the lower detachment (Fig. 3).

The geometry of the wedge is seen to vary across the study area and the lower and upper detachments merge with a lower taper angle in section B-B' than in A-A' (Fig. 3). The detachments also merge in the foreland at different stratigraphic levels. In section A-A', they merge in the Wapiabi Formation, whereas in section B-B' they merge in the Bearpaw Formation. South of Turner Valley, to the U.S. border, the Bearpaw Formation is a regional shale marker and the major detachment horizon. The gradual merging of the upper and lower detachments in section B-B' is similar to that reported by Hiebert and Spratt (1991) and Lawton et al. (1994b). Since A-A' lies at or north of the zero edge of the Bearpaw Formation, the change in detachment level (to the Wapiabi Formation) is likely due to the facies change. Detachment in the Wapiabi Formation continues north of the study area to Jumpingpound (Olchowy and Spratt, 1993) and Wildcat Hills (Lawton et al., 1994a). However, in those areas detachment also occurs 350 m higher in the section (in coals and shales of the Brazeau Group), such that the taper angle of the wedge is nearly 0° and strain is dissipated between the detachments (Lawton et al., 1994a). By comparison, the taper angle of the wedge in A-A' appears anomalously large. This may reflect a higher frictional resistance to glide in the Wapiabi than in the Bearpaw or Brazeau shales; none of the faults in A-A' exhibit large displacements, and duplexing is pervasive across the section. North and south of A-A', the wedge has been inserted farther into the foreland along detachments in the Bearpaw Formation (Fig. 3, B-B') and Brazeau Group (Lawton et al., 1994b).

In the future we plan to model wedging in anisotropic media that have both vertical and lateral variations in rheology. Since other workers associated with the Eastern Cordillera NATMAP project are studying lithological changes within the Brazeau Group, we should soon have the information required to accurately model variations in its rheology and determine how they influence thrust sheet emplacement.

ACKNOWLEDGMENTS

Amoco Canada, Chevron Resources, Home Oil, and Mobil Canada have provided access to seismic data in the Turner Valley area during the last five years. Natural Resources Canada (Contract No. 23294-4-0568/01-XSG) funded 1994 fieldwork for this study. James Tolton assisted Sarawute Chantraprasert in the field.

REFERENCES

Bally, A.W., Gordy, P.L., and Stewart, G.A.
1966: Structure, seismic data, and orogenic evolution of the southern Canadian Rocky Mountains; Bulletin of Canadian Petroleum Geology, v. 14, p. 337-381.

Brodaric, B. and Fyon, J.A.
1989: OGS FIELDLOG: A microcomputer-based methodology to store, process and display map-related data; Ontario Geological Survey, Open File Report 5709, 73 p. and 1 magnetic diskette.

Charlesworth, H.A.K. and Gagnon, L.G.
1985: Intercutaneous wedges, the triangle zone, and structural thickening of the Mynheer coal seam at Coal Valley in the Rocky Mountain Foothills of central Alberta; Bulletin of Canadian Petroleum Geology, v. 33, p. 22-30.

Dahlstrom, C.D.A.
1970: Structural geology of the eastern margin of the Canadian Rocky Mountains; Bulletin of Canadian Petroleum Geology, v. 18, p. 332-406.

Gallup, W.B.
1951: Geology of the Turner Valley oil and gas field, Alberta, Canada; American Association of Petroleum Geologists Bulletin, v. 35, p. 97-821.

Gordy, P.L., Frey, F.R., and Norris, D.K.
1977: Geological guide for the Canadian Society of Petroleum Geologists and 1977 Waterton-Glacier Park Field Conference; Canadian Society of Petroleum Geologists, Calgary, 93 p.

Gordy, P.L., Frey, F.R., and Ollerenshaw, N.C.
1975: Road Log, Calgary – Turner Valley – Jumping Pound – Seebe; in Structural Geology of the Foothills between Savanna Creek and Panther River, S.W. Alberta, Canada, "Exploration Update '75" Guidebook, H.J. Evers and J.E. Thorpe (ed.); Canadian Society of Petroleum Geologists and Canadian Society of Exploration Geophysicists, p. 35-61.

Hiebert, S.N. and Spratt, D.A.
1991: Study of the triangle zone and Foothills structures near Pincher Creek, Alberta; in Current Research, Part B; Geological Survey of Canada, Paper 91-1B, p. 41-46.

Hume, G.S.
1931: Geology, Turner Valley sheet, Alberta; Geological Survey of Canada, Map 257A (scale 1:63 360).

Jamison, W.R.
1987: Geometric analysis of fold development in overthrust terranes; Journal of Structural Geology, v. 9, p. 207-220.
1993: Mechanical stability of the triangle zone: the backthrust wedge; Journal of Geophysical Research, v. 98, p. 20015-20030.

Jerzykiewicz, T. and Norris, D.K.
1993: Evolution of the Laramide foredeep and adjacent thrust belt in southern Alberta; Geological Survey of Canada, Open File 2663, 96 p.

Jones, P.B.
1982: Oil and gas beneath east-dipping underthrust faults in the Alberta Foothills; in Geological Studies in the Cordilleran Thrust Belt, R.B. Powers (ed.); Rocky Mountain Association of Geologists, v. 1, p. 61-74.

Lawton, D.C., Spratt, D.A., and Hopkins, J.C.
1994a: Tectonic wedging beneath the Rocky Mountain foreland basin, Alberta, Canada; Geology, v. 22, p. 519-522.

Lawton, D.C, Stockmal, G.S., and Spratt, D.A.
1994b: Seismic definition of the triangle zone east of Maycroft, Alberta; in Current Research 1994-E; Geological Survey of Canada, p. 109-116.

MacKay, P.A.
1991: A geometric, kinematic and dynamic analysis of the structural geology at Turner Valley, Alberta; Ph.D. thesis, University of Calgary, Calgary, 138 p.

MacKay, P.A., Spratt, D.A., Soule, G.S., and Lawton, D.C.
1994: The triangle zone of southern Alberta - geometry, lateral variations and associated oil and gas fields: Field Trip Guidebook; Canadian Society of Exploration Geophysicists/Canadian Society of Petroleum Geologists, Calgary, Alberta, 105 p.

Mitra, S.
1990: Fault propagation folds; geometry, kinematic evolution and hydrocarbon traps; American Association of Petroleum Geologists Bulletin, v. 74, p. 921-945.

Olchowy, B.M. and Spratt, D.A.
1993: Study of the Triangle Zone and Foothills structures in the Jumpingpound Creek area of Alberta; in Current Research, Part B; Geological Survey of Canada, Paper 93-1B, p. 45-50.

Price, R.A.
1981: The Cordilleran foreland thrust and fold belt in the southern Canadian Rocky Mountains; in Thrust and nappe tectonics, N.J. Price and K.R. McClay (ed.); Geological Society of London Special Publication 9, p. 427-448.

Price, R.A. (cont.)
1986: The southeastern Canadian Cordillera: Thrust faulting, tectonic wedging, and delamination of the lithosphere; Journal of Structural Geology, v. 8, p. 239-254.

Spratt, D.A., Lawton, D.C., and MacKay, P.A.
1993: The triangle zone and Turner Valley Structure west of Calgary; Geological Association of Canada and Mineralogical Association of Canada Field Trip A-1 Guidebook, 41 p.

Tippett, C.R., Jones, P.B., and Frey, F.R.
1985: Strains developed in the hanging walls of thrusts due to their slip/propagation rate: a dislocation model: discussion; Journal of Structural Geology, v. 7, p. 755-758.

Williams, G. and Chapman, T.
1983: Strains developed in the hanging walls of thrusts due to their slip/propagation rate: a dislocation model; Journal of Structural Geology, v. 5, p. 563-571.

Geological Survey of Canada Project 930006

Magnetic overprinting of the Neoproterozoic Shaler Supergroup, Amundsen Basin, Northwest Territories, Canada during the Franklin magmatic episode

John K. Park and Robert H. Rainbird
Continental Geoscience Division

Park, J.K. and Rainbird, R.H., 1995: Magnetic overprinting of the Neoproterozoic Shaler Supergroup, Amundsen Basin, Northwest Territories, Canada during the Franklin magmatic episode; in Current Research 1995-E; Geological Survey of Canada, p. 113-123.

Abstract: Paleomagnetic studies of the Neoproterozoic Shaler Supergroup of the Amundsen Basin, centred on the Amundsen Gulf of northwestern Canada, reveal a record of magnetic overprinting due to Franklin magmatism. Magnetic components B2 and B1 from Shaler strata agree closely with discreet magnetization directions from the Franklin igneous events, dated between 727 and 716 Ma. The new interpretation of B1 as other than primary obviates an earlier suggestion of relative rotation between the Brock Inlier of the Amundsen Basin and the Mackenzie Mountains of the northern Cordillera that was based on the geological correlation of the Shaler and Mackenzie Mountains supergroups. Other overprints in the Shaler Supergroup, being steeply directed, may relate to geological events both in late Neoproterozoic and in Cretaceous to Recent times.

Résumé : Des études paléomagnétiques du Supergroupe de Shaler du Néoprotérozoïque du bassin d'Amundsen, centré sur le golfe Amundsen dans le nord-ouest du Canada, révèlent une surimpression magnétique attribuable à un magmatisme franklinien. Les composantes magnétiques B2 et B1 des couches de Shaler correspondent étroitement à des directions distinctes de magnétisation à partir d'événements ignés frankliniens, datés entre 727 et 716 Ma. La nouvelle interprétation de B1 comme une composante autre que primaire s'éloigne d'une proposition antérieure voulant qu'il y ait eu une rotation relative entre la boutonnière de Brock du bassin Amundsen et les monts Mackenzie dans la Cordillère septentrionale basée sur la corrélation géologique des supergroupes de Shaler et de Mackenzie Mountains. D'autres surimpressions dans le Supergroupe de Shaler, étant très inclinées, peuvent être liées à des événements géologiques tant dans le Néoprotérozoïque tardif que dans l'intervalle allant du Crétacé à l'Holocène.

INTRODUCTION

Geological correlation between the Mackenzie Mountains Supergroup of the northern Cordillera and the Shaler Supergroup (change from group status proposed by Rainbird et al., 1994b) of the Amundsen Basin (Fig. 1) was proposed by Aitken et al. (1978) and subsequently refined by Young (1979), Jefferson and Young (1989), and Rainbird (1994). This correlation has been bolstered by sequence stratigraphic, geochronological, and biostratigraphic comparisons between the two areas (Rainbird et al., in press; Hofman and Rainbird, 1995).

Rainbird et al.'s (1994b) unification of the formational terminology from the various regions of the Amundsen Basin on the basis of field studies, now allows paleomagnetic results from these regions to be combined and a better comparison made with results from correlative units in the Mackenzie Mountains (Fig. 2). An earlier paleomagnetic study supported the geological correlation between the two regions (Park and Aitken, 1986a) using results from the lower clastic member of Reynolds Point Formation (now termed Grassy Bay Fm.) on Victoria Island (Palmer et al., 1983). A later study indicated a displacement of poles between unit P3 (now termed Nelson Head Fm.) in the Brock Inlier of the Amundsen Basin and the correlative Tsezotene and Katherine units of the Mackenzie Mountains (Fig. 2) (Park, 1992a), suggesting a relative rotation between these regions. The present study indicates that the apparent displacement is likely explained by overprinting of the original magnetization of the Shaler Supergroup during the Franklin magmatic episode.

GEOLOGY

Geological setting

The sedimentary rocks collected for this study belong to the Shaler Supergroup, which outcrops within a group of inliers that form part of the Proterozoic Amundsen Basin (Christie et al., 1972) (Fig. 1). Samples mainly were collected from the Minto Inlier on Victoria Island (Fig. 3) but also from the Coppermine area on the northern mainland (Fig. 1). The nomination 'Shaler Supergroup' was recently proposed as a consequence of the elevation to formation status of several informal members of the former 'Shaler Group' (Thorsteinsson and Tozer, 1962; Rainbird et al., 1994a). It is generally accepted that sedimentary strata of the Shaler Supergroup are of early Neoproterozoic age and belong to Sequence B of Young et al. (1979). These strata are considered to be

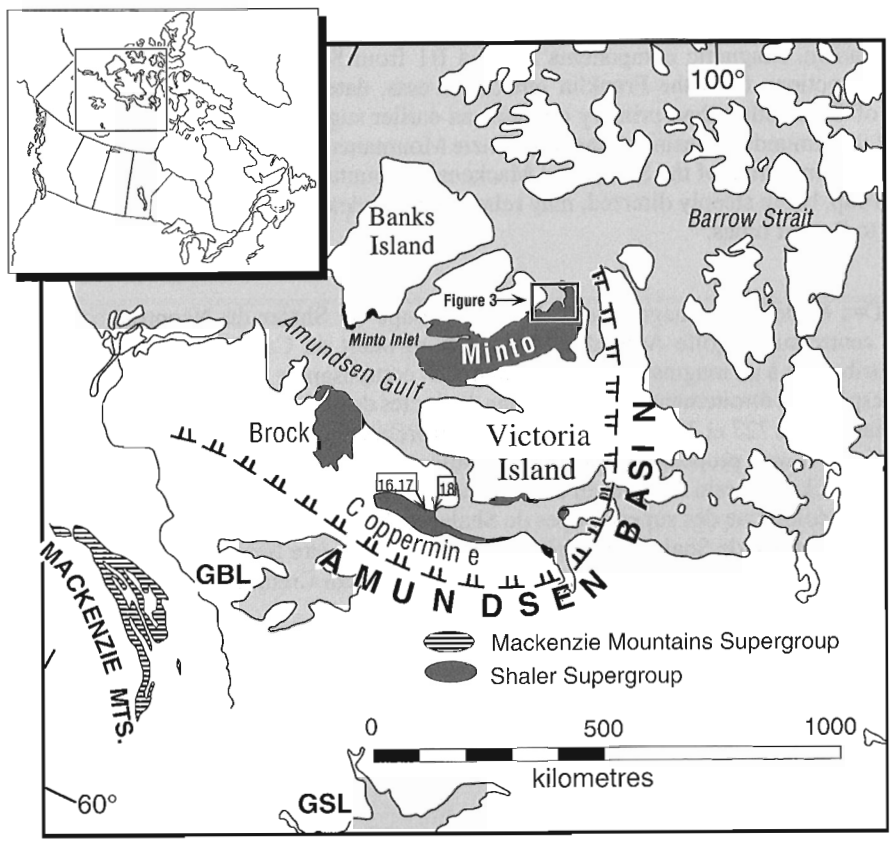

Figure 1. Regions of correlative Neoproterozoic rock units of northwestern Canada (inset). Paleomagnetic sampling sites from Coppermine area are shown. See Figure 3 for sites in Minto Inlier. Site co-ordinates are given in Tables 1 and 3.

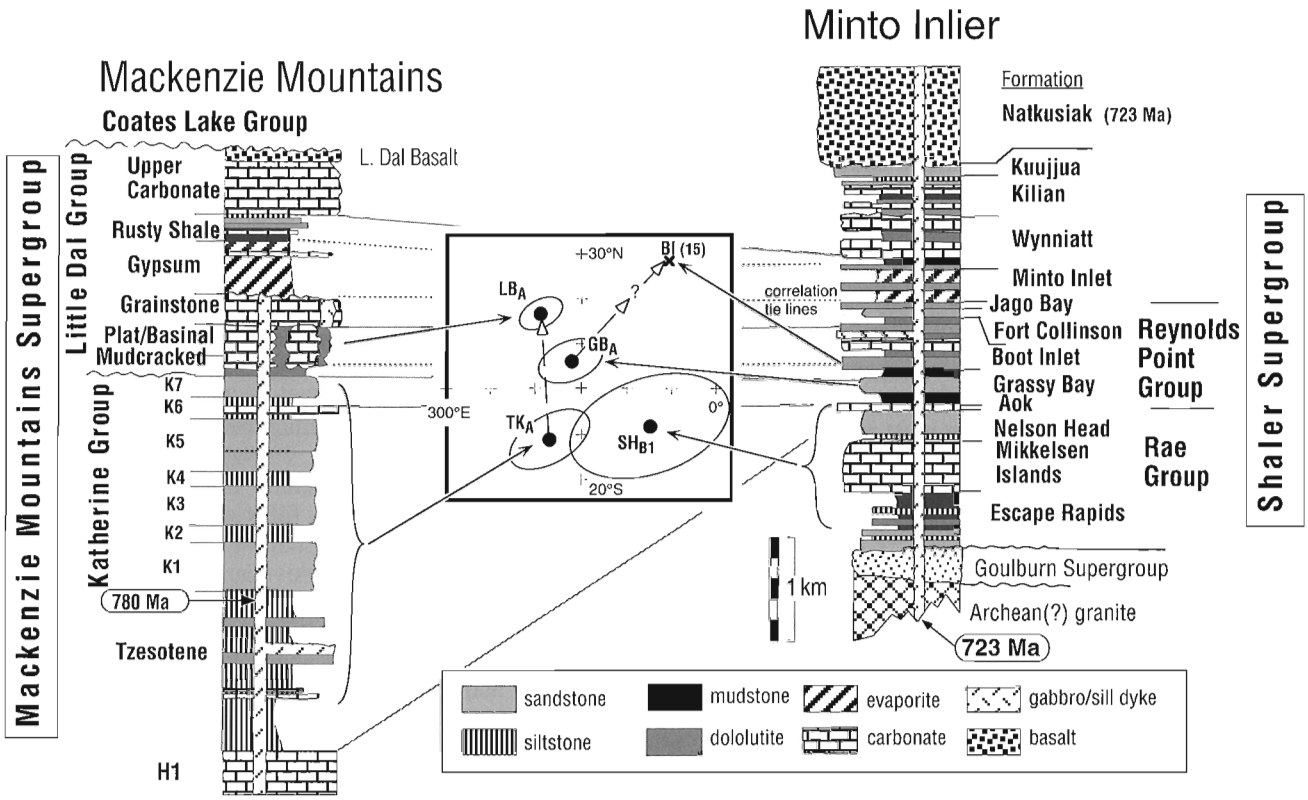

Figure 2. Comparison of paleopoles from the stratigraphically correlated Mackenzie Mountains and Amundsen Basin regions. See text and Table 4. The Boot Inlet pole is from a single site 15. Polar errors are $\delta p°$, $\delta m°$, the semi-axes of the oval of 95% confidence about the pole.

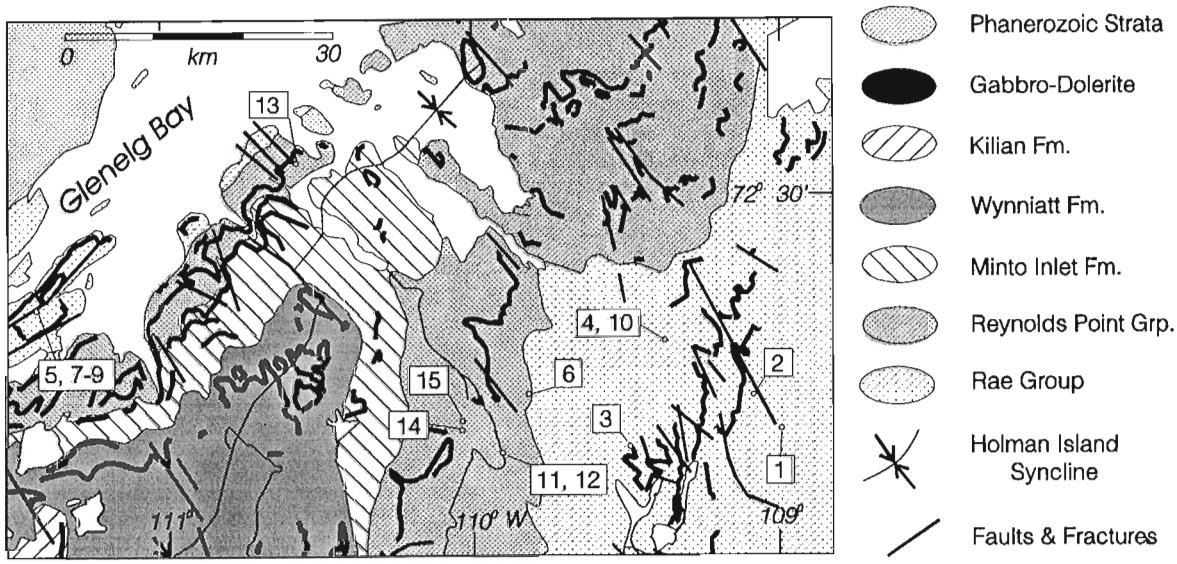

Figure 3. Paleomagnetic sampling sites from Minto Inlier. See Figure 1.

stratigraphically equivalent to the Mackenzie Mountains Supergroup in the northern Canadian Cordillera (Fig. 2) (Young, 1977; Aitken et al., 1978).

The Shaler Supergroup comprises an up to 5 km thick sequence of platformal marine carbonate, evaporite, and subordinate siliciclastic rocks overlain and underlain by fluvial and fluvio-deltaic sandstones (Young, 1981). It includes the formations, Escapes Rapids to Kuujjua (Thorsteinsson and Tozer, 1962; Young, 1981; Jefferson, 1985; Rainbird, 1991; Rainbird et al., 1994b) (Fig 2). The strata are intruded by numerous gabbroic sills of the Franklin igneous events, a mafic magmatic episode that affected a 2 000 000 km square area of northern (present coordinates) Laurentia at 723 + 4/-2 Ma (Heaman et al., 1992). The sills vary in thickness from less than 5 to more than 100 m, but most are less than 50 m. A few northwest-striking dykes intrude the sequence in northeast Minto Inlier.

In Minto Inlier, the Shaler Supergroup is overlain by the Natkusiak Formation, an up to 1100 m-thick sequence of flood basalt flows and minor volcaniclastic rocks that are the only known subaerial manifestation of the Franklin igneous events. A maximum age for the Shaler Supergroup of 1077 Ma has been determined from U-Pb analysis of detrital zircon from the Nelson Head Formation of the Rae Group (Rainbird et al., 1994b).

The Shaler Supergroup, unconformably overlies Paleoproterozoic sedimentary rocks of the Goulburn Supergroup (Campbell, 1981), which in turn overlie granite of suspected late Archean age on the northeast side of Minto Inlier (Thorsteinsson and Tozer, 1962). It also overlies Mesoproterozoic strata of the Coppermine River Group in the Coppermine area (Baragar and Donaldson, 1973).

Tectonic history

The Shaler Supergroup is affected by broad northeast and later northwest-striking open folds with dips generally less than 10 degrees (Thorsteinsson and Tozer, 1962), and a northeast-striking zone of block-faults that extend along the northwest side of Minto Inlier between Minto Inlet and Glenelg Bay (Rainbird et al., 1994a). The Minto and Brock inliers are presumably structural highs preserved by late Neoproterozoic deformation; folds and faults are erosionally bevelled beneath flat-lying shallow marine carbonates and quartzarenites of Cambro-Ordovician age (Thorsteinsson and Toszer, 1962). In the Brock Inlier, subsequent uplift and erosion occurred in the Early Cretaceous and regional unconformities occur below and above Lower Cretaceous rocks (Balkwill and Yorath, 1970). The hiatus between Lower Cretaceous rocks and Pleistocene glacial deposits (Balkwell and Yorath, 1970) may relate to postulated Eocene uplift in

Table 1. Magnetic components in Shaler Supergroup.

Si	Area	Treatment (°C)	*N*	*D°, I°*	*R*	*k*	α_{95}°	Cp
Boot Inlet Formation, Reynolds Point Group								
15	M	200-580	4	071, +41	3.93	42	14	?
Grassy Bay Formation, Reynolds Point Group								
8	M	100-665	4	092, +05	3.98	134	8	*B2*
9	M	NRM-500	5	116, +76	4.83	24	16	*C2*
		100-600	5	090, +35	4.83	24	16	*B2?*
Aok Formation, Rae Group								
6	M	100-450	3	270, -62	2.83	12	37	*C3*
		100-550	2	086, +13	-	-	-	*B2*
7	M	NRM-300	2	094, +75	-	-	-	*C2*
		200-550	3	078, +04	2.92	24	26	*B2*
11	M	450-660	5	290, -65	4.86	29	14	*C3*
18	C	NRM-400	2	034, +78	-	-	-	*C2*
		350-550	4	092, +04	3.98	155	7	*B2*
Nelson Head Formation, Rae Group								
16	C	200-600	5	085, +10	4.97	129	7	*B2*
Mikkelsen Islands Formation, Rae Group								
1	M	NRM-475	4	062, +86	3.95	66	11	*C2*
		300-655	5	089, +61	4.94	70	10	*C3*
		625-675	5	085, +39	4.89	35	13	*B2*
2	M	NRM-550	3	098, +73	2.97	75	14	*C2*

Notes: Si, site; *N* is the number of samples; *D°, I°* are the declination and inclination of magnetic direction, corrected for tilt; *R* is the vector resultant; *k* is the precision; α_{95}° is the error of 95% confidence about the direction; Cp is component. C, Coppermine area; M, Minto Inlier. Sites 4, 12, and 13 from the Nelson Head, Grassy Bay, and Fort Collinson formations, respectively, did not yield any useful data. Site co-ordinates are: 1 - 108°59'0"W, 72°16'15"N; 2 - 109°0'0"W, 72°16'40"N; 4 - 109°22'30"W, 72°19'30"N; 6 - 109°47'30"W, 72°18'15"N; 7 - 111°26'0"W, 72°24'40"N; 8, 9 - 111°26'0"W, 72°24'40"N; 11, 12 - 109°50'W, 72°12'40"N; 13 - 110°34'0"W, 72°32'30"N; 15 - 109°56'41"W, 72°17'14"N; 16 - 115°52'58"W, 67°54'23"N; 18 - 115°38'16"W, 67°56'16"N.

the Minto Inlier (Palmer et al., 1983) associated with the Eurekan Orogeny (Tozer, 1968, p. 585) in the Sverdrup Basin, northeast of the Minto Inlier, and with a related rifting episode (Kerr, 1977) centred around Barrow Straight to the northeast (Fig. 1).

METHODS

From three to five block samples, oriented by sun and magnetic compasses, were obtained at each site in the field by RHR. Samples were cored in the laboratory and cut into several specimens (2.2 cm in height, 2.5 cm in diameter). Natural remanent magnetizations (NRMs) were measured on commercial spinner magnetometers: sedimentary samples on a Geofyzika JR-4 and igneous diabase samples on a Schonstedt DSM. Samples were demagnetized by thermal (TH) and alternating field (AF) techniques to analyze the components of NRM. Thermal treatments were done by means of calibrated Schonstedt TSD-1 ovens and AF treatments by a Schonstedt GSD-1. In the latter instrument specimens were demagnetized along each of three axes in succession, and measured in two orientations after each measurement. Demagnetization axes were reversed on alternate AF treatment steps, with treatments ending when directions became 'unstable'. All experiments were carried out in a shielded room with ambient field less than 3000 ϒ's. Magnetic components were analyzed by means of vector diagrams and the LINEFIND program of Kent et al. (1983).

RESULTS AND ANALYSIS

Shaler Supergroup

Three magnetic components, B2, C2, and C3, were isolated from the NRMs using thermal demagnetization (Table 1) (Fig. 4). These are analyzed along with similar components and two additional ones, B1 and C1, identified from an earlier study in the Brock Inlier using TH, AF, and acid leaching (CH) methods (Park, 1992a). Mean directions, coercivities, unblocking temperatures (T_{UB}'s), and interpreted magnetic carriers for each of the Shaler Supergroup remanences isolated in the two studies are summarized in Table 2.

Magnetic components B1 and B2 have similar directions and magnetic characteristics. The earlier study distinguished between them in single specimens, where the distinctly directed B2 component was removed before B1 by both TH and CH experiments. Those experiments showed that B2 resided in diagenetic hematite and B1 in probable magnetite, and that the remanences probably predated quartz cementation. The present study shows that B2 also resides in probable magnetite as well as in hematite, making the difference between B1 and B2 less distinct. The possible meaning of these components is discussed below.

Magnetic components C1, C2, and C3 have steeply inclined directions (Fig. 5). C1 has a distinctly different direction and appears to reside in magnetite, whereas C2 and C3 have distinctly different magnetic characteristics from one another. All three components reside in magnetic carriers that appear to postdate quartz cementation (Park, 1992a).

A magnetization from site 15, an ooid grainstone from the younger Boot Inlet Formation, is not classified.

Magnetic components of the present study can generally be related to the magnetic mineral phases. Shaler Supergroup sites have varying amounts of opaque minerals, including common secondary hematite, sparse sulphides (sites 13, 15,

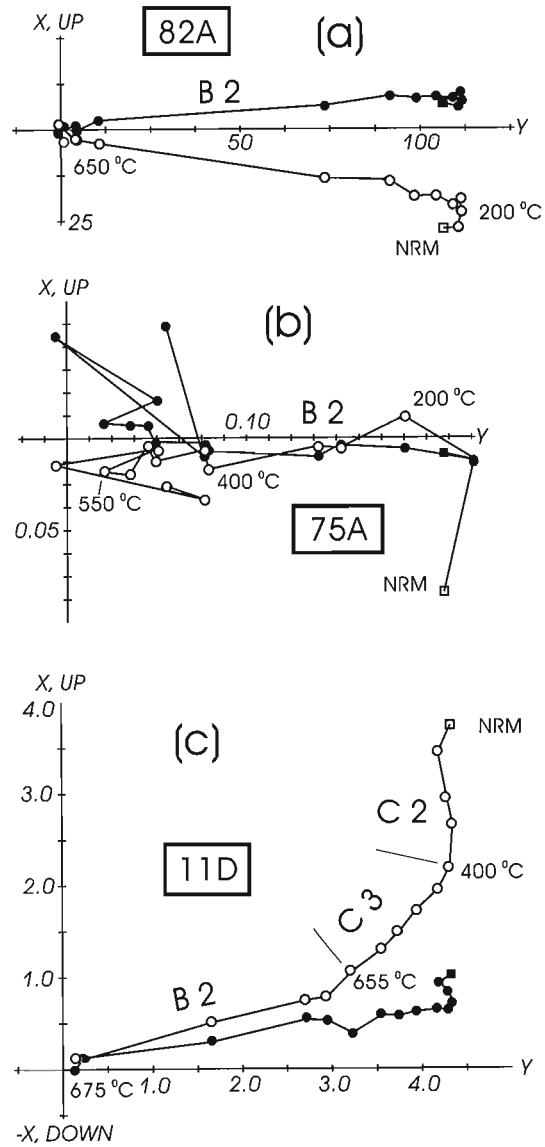

*Figure 4. Vector diagrams showing the decay of natural remanent magnetization under thermal treatment of specimens from the Grassy Bay (**a**), Aok (**b**), and Mikkelsen Islands formations (**c**). Vectors are depicted as closed circles on the horizontal (x-y) plane and as open circles on the vertical (up-y) plane. Directions are not tilt-corrected. Component ranges are approximately indicated.*

Table 2. Mean component directions from Shaler Supergroup.

Entry	Cp	Po	*D°, I°*	*N*	*R*	*k*	α_{95}°	Coercivities/T_{UB}'s mT,	°C	Magnetic carrier
1.	*B1*	M	081, -20	4	3.90	31	17	5- 75,	N-595	mt
2.	*B2*	N	080, +10	8[1]	7.81	36	10	5- 20,	100-550	mt
								- ,	500-675	ht
3.	*C1*	N	103, -76	12[2]	11.67	32	8	N- 60,	100-575	mt
4.	*C2*	N	072, +82	7	6.95	119	6	N- 175,	N-550	?
5.	*C3*	M	081, +62	4	3.97	91	10	65->270,	100-675	ht

Notes: See Table 1. Po, polarity: M, mixed; N, normal. Mt, magnetite; ht, hematite. Site or sample directions were recalculated at the reference coordinates (70°N, 116 °W) before mean calculated. All directions are corrected to the paleohorizontal, except *C2*. Selection criteria for sites: $N \geq 2$ samples and $\alpha_{95} \leq 40°$. Sites of Park (1992a) are preceded by R; other sites are in Table 1. In Park (1992a), *B1* is labeled *A* and B2, *B*. Entries: 1. Sites R4, R11, R13, and R17. 2. Sites R11, R12, 1, 6-9, 16, and 18. 3. Recalculated at reference coordinates (Park, 1992a). 4. Site R2, R4, 1, 2, 7, 9, and 18. 5. Site R2, 1, 6, and 11.
[1] Excluding site 9. The magnetite component may have a different origin because the site, 115m away from the nearest dyke, may not have been affected by the Franklin magmatism. [2] Samples from 5 sites.

18), and rutile. Rutile commonly replaces hematite phases to a lesser (site 1, 6, 13, 15) or greater degree (sites 4, 12, 16), including detrital hematite that was only identified at site 16. The B2 remanence at site 16 may relate to euhedral grains of possible magnetite. B2 and C3, as in the previous study (Park, 1992a), are generally identified with the secondary hematite pigment. Samples where C3 was revealed are distinguished by a dark red colour.

Fold tests (McFadden, 1990) were conducted on all components. C2 appears to be postfolding (ξ_2 = 3.690, tilt-corrected, compared to 95% critical value of 3.086; N = 7 sites) and C3, prefolding (ξ_2 = 2.529, in situ, compared to 95% critical value of 2.335), although there are only four sites for the latter test. Fold tests on C1, B1, and B2 gave equivocal results.

Franklin intrusions

Analysis of the Franklin diabase dyke sites yielded a soft, steep downward-directed magnetization E with T_{UB}'s to 500°C and a hard, characteristic, shallowly inclined east or west component A with T_{UB}'s in the magnetite range (Table 3).

DISCUSSION

Magnetic components of the Shaler Supergroup

The complex NRMs of the Shaler Supergroup comprise three steeply inclined (C1, C2, C3) and two shallowly inclined components (B1, B2). C2 is a postfolding magnetization. With a direction similar to the present Earth's field (PEF) direction in the region (Fig. 5), C2 probably relates to the Recent Epoch.

C1 and C3 have distinct directions located away from the PEF direction (Fig. 5). Magnetic characteristics suggest that they reside in different phases: C1 possibly in magnetite

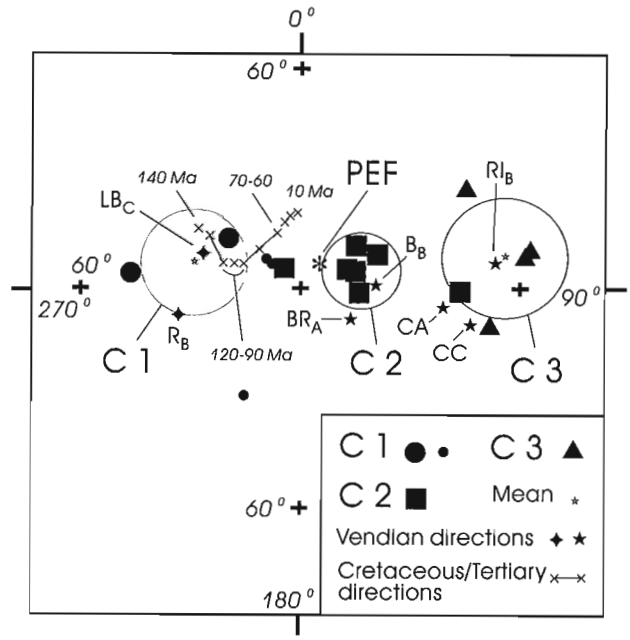

Figure 5. Stereographic projection (centred on 90° down) of steeply directed magnetic components, C1, C2, and C3, revealed within the Amundsen Basin. C1, which has been reversed, has only been found in the Brock Inlier. C1 and C3 are plotted with respect to the paleohorizontal; C2, with respect to the present horizontal. These directions are compared to overprint (B_B and RI_B, Park, in press; LB_C, Park, 1981a; R_B, Morris, 1977) and probable primary directions (BR_A, Park, 1992b; CA, Meert et al., 1994; CC, Symons and Chiasson, 1991) attributed to Neoproterozoic and Early Cambrian times, and to a path of Cretaceous and Tertiary directions (Irving and Irving, 1982). Small closed circles denote sites with only one sample. Error circles show α_{95}° values; that for C1 is based on samples (N=12) rather than sites. All directions have been recalculated to the reference co-ordinates (70°N, 116 °W).

Table 3. Magnetic directions in the Franklin diabase.

Si	Area	Treatment		N	D°, I°	R	k	α_{95}°	Cp
		AF (mT),	TH (°C)						
3	M	10->38,	200-580	5	078, +11		193	6	*A*
5	M	13->55,	520-580	5	095, -10		40	12	*A*
10	M	-	100-450	4	156, +73		48	13	*E*
		17->35,	500-560	4	258, +47		70	11	*A*
14	M	NRM- 13,	NRM-500	5	305, +85		287	5	*E*
		5->50,	500-560	4	260, +42		52	13	*A*
17	C	NRM- 8,	NRM-450	4	076, +77		163	7	*E*
		5->80,	450-570	5	086, +17		267	5	*A*

Notes: See Table 1. Component *A* is tilt-corrected; component *E* is *in-situ*. Site coordinates: 3 - 109°30'30"W, 72°15'30"N; 5 -111°26'0"W, 72°24'40"N; 10 - 109°22'30"W, 72°19'30"N; 14 - 109°55'47"W, 72°17'33"N; 17 - across the river from site 16 (Table 1).

(Park, 1992a) and C3 in authigenic hematite. There are several possible origins for C1. Because C1 lies near the trace of Cretaceous directions (140-65 Ma; Fig. 5) (Irving and Irving, 1982), it could be a prefolding component of Cretaceous age, perhaps related to faulting documented in the Early Cretaceous (Balkwill and Yorath, 1970). As a possible thermal overprint, it could relate specifically to the recorded hiatus following Early Cretaceous deposition (Balkwell and Yorath, 1970). Thus, C1 may have been blocked-in during cooling following uplift and erosion of the Coppermine area. Alternatively, C1, earlier assigned to the Neoproterozoic Era (Park, 1992a), could have formed during Neoproterozoic folding (Thorsteinsson and Tozer, 1962; Rainbird et al., 1994a). It plots with several directions (LB_C, Park, 1981a; R_B, Morris, 1977) (Fig. 5) that may represent the early part of the hiatus preceding latest Neoproterozoic rifting in the Cordillera (Park, 1994). If C1 is Cretaceous, its direction would need a slight correction, because the amount of folding apportioned between the latest Neoproterozoic and the Cretaceous is not known.

Component C3 appears to predate folding, which began in the latest Neoproterozoic. Its direction is distinct from Cretaceous and Tertiary directions of North America (Fig. 5) documented by Irving and Irving (1982) and lies near primary directions (CA, Meert et al., 1994; CC, Symons and Chiasson, 1991) from eastern North America associated with latest Neoproterozoic rifting at about 575 Ma. In addition, C3, like C1, also plots near overprint directions (B_B, RI_B; Park, in press) (Fig. 5) attributed to latest Neoproterozoic rifting in the northern Cordillera (Park, in press). Perhaps, C3 is a diagenetic overprint predating the sub-Paleozoic angular unconformity in the Amundsen Basin. Like C1, it may require a slight amount of tectonic correction.

B1 was earlier nominated as primary on the basis of a reversal at one site and on TH experiments on leached specimens that nominally identified magnetite as the carrier (Park, 1992a). B2 was considered to be secondary (Park, 1992a). However, both B1 and B2 agree with discreet directions from the Franklin magmatic episode, suggesting instead that they are both overprints. The magnetite of these components could have been chemically produced. As an example, magnetite was likely formed from hematitic redbeds of the Firstbrook Formation (Huronian Supergroup) by intrusion of the Nipissing Diabase (Buchan et al., 1989). Alternatively, these magnetite remanences may be thermal overprints, because all Shaler sites, except sites 8 and 9, were collected within about 50 m of Franklin diabase dykes and sills. This explanation is preferred, because the authigenic hematite subcomponent of B2, interpreted as a secondary CRM, would not have formed coevally with chemically formed magnetite. Poles are plotted in Figure 6.

Magnetic components and poles from diabases

Normal A components from diabase sills that intrude the Shaler Supergroup agree with previously determined normal directions from Franklin sills of the Amundsen Basin (Robertson and Baragar, 1972; Palmer and Hayatsu, 1975; Park, 1981b; Palmer et al., 1983) (compare pole entries 6 and 7, Table 4), indicating that A is primary. The reverse A directions from this study (entry 10) have only been identified at one other site (Park, 1992a) which does not meet the selection criteria (see Table 4). Normal poles from Franklin diabases of the Amundsen Basin (F_N, Fig. 6) (entry 6) are displaced from antiparallel poles from Franklin diabases outside the basin (entry 11, Table 4) (F, Fig. 6). The separation is mirrored by normal (entry 5) and reverse poles (entry 9, Table 4) of the Natkusiak basalt within the basin. This separation suggests that Franklin directions within the basin could be biased by a small unremoved secondary component.

Diabase sites of this study contain a viscous component E, similar to a steeply directed viscous component of Recent age determined from Franklin intrusions in the Brock Inlier (Park, 1981b). Several previous studies of Franklin diabase have revealed that in some cases the primary component was biased by a steeply directed down component (Fahrig et al., 1971; Palmer et al., 1983; Pehrsson and Buchan, 1994), similar to the C components uncovered in the Shaler sites of the present study. The steep overprints were variously ascribed to Cretaceous or Tertiary magnetizations, either to a partial thermal remagnetization (Fahrig et al., 1971) or CRM (Pehrsson and Buchan, 1994) formed during the opening of Baffin Bay, or to a viscous partial thermo-remanent magnetization caused by uplift, erosion, and cooling (Palmer et al., 1983) in response to the Eurekan orogeny. None of the

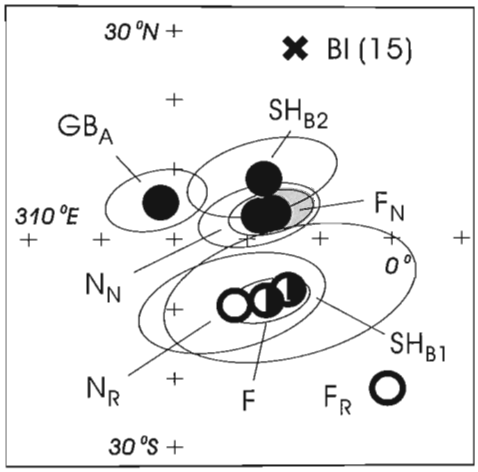

Figure 6. Comparison of Shaler Supergroup poles with those from the Franklin igneous episode (see Table 4). F_N, F_R, Franklin poles of Amundsen Basin; F, all Franklin poles from outside the Amundsen Basin; N_N, N_R, Natkusiak basalts normal, reverse; SH_{B1}, SH_{B2}, Shaler Supergroup B1 and B2 components. BI(15) is a site pole from the Boot Inlet Formation. See references to poles in Table 4.

supposedly affected data have been used in this study; nevertheless, there is the possibility that even the accepted Franklin data is slightly contaminated. It is of note that most Franklin samples in previous studies have been demagnetized at only one AF step, so that any remaining overprint, if present, would not be detected.

The directional separation of Franklin directions could, alternatively, indicate an age difference (Palmer and Hayatsu, 1975), although this was dismissed by Palmer et al. (1983) in favour of the bias interpretation. Precise dating of the Franklin diabases (Heaman et al., 1992) has suggested two ages of intrusion at 723 +4/-2 and 718 ± 2 Ma; however, because only one analysis gave the latter age, the difference, given the precision of analyses, may not be significant.

Comparison of Franklin and Shaler directions

The two discreet polar groupings from the Franklin diabase and Natkusiak basalt, as noted, appear to correspond with B2 and B1 directions from the Shaler Supergroup (Fig. 6). This prompts the questions: Are the interpreted overprints contaminated by an unremoved magnetization? or, Do they, in fact, support an age difference within the Franklin magmatic episode? Three pairs of shallowly and steeply inclined components, each pair with similar T_{UB}'s (Table 2), are compared to ascertain whether there is contamination: B2/C3 (hematite), B2/C2 (magnetite), and B1/C1 (magnetite).

Comparison of the B2 and C3 hematite components reveals that in individual specimens the respective T_{UB} ranges are reasonably well-defined with little overlap (see Fig. 4c). Furthermore, there is no evidence for C components in sites R11 and R12 where B2 hematite subcomponents were identified (Park, 1992a). With respect to the B2 and C2 magnetite components, there is a slight overlap of T_{UB} ranges where the components occur together in sites 7 and 8, with C2 having the lower T_{UB}'s (Table 1). However, the reasonable agreement between the B2 magnetite (D, I = 262°, -06°; N = 4 sites; a95 = 10°) and hematite directions (D, I = 257°, -13°; N = 4 sites; α_{95} = 20°) suggests that there is no bias in B2. This is consistent with the close agreement (7° difference) between the primary diabase direction at site 17 (Table 3) and the B2 direction at site 16 (Table 1), about 20 m away stratigraphically. In the case of B1 and C1, complementary magnetic coercivity and T_{UB} spectra in individual specimens, indicate, instead, that C1 may represent a later thermal overprint on the magnetic phase carrying B1. It appears then that B1, like B2, is not biased by steeply directed components.

However, on the other hand, uncertainties in the Shaler poles show that the separation of B1 from B2 is barely significant and that their poles could be coincident. The same applies to the Natkusiak poles; though separation due to contamination is also possible, as reverse poles from both the Natkusiak and Franklin units of the Amundsen Basin lie south of the normal poles (Fig. 6). The possibility of a distinct age difference of Franklin events is tantalizing; nevertheless, in view of the possible contamination of results in previous Franklin paleomagnetic studies and insufficient data from the Shaler Supergroup, it is not possible at present to explain the discrepancy between directions.

Comparison of paleopoles from the Amundsen Basin and the Mackenzie Mountains

Pole GB_A from the Grassy Bay Formation of the Shaler Supergroup (Palmer et al., 1983) is distinct from the normal Franklin poles. It is considered to be a primary pole on the basis of its latitudinal position between primary poles of bounding units from the stratigraphically correlated Mackenzie Mountains Supergroup (Fig. 2) (Park and Aitken, 1986a; Park, 1992a). The virtual normal geomagnetic pole from a single site of the Boot Inlet Formation is distinct both from any overprint poles in the Shaler Supergroup and from the reverse pole of a nearby diabase sill (site 14, Table 3), which has a stratigraphic separation of 50 m. It could be primary (Fig. 2).

Diabases of the Franklin igneous events do not intrude the Mackenzie Mountains Supergroup of the Mackenzie Mountains. Some overprints in the Mackenzie Mountains Supergroup are probably caused by magnetically distinctive 780 Ma mafic intrusions, which affected units of the Little Dal Group, including the Basinal sequence from which primary pole LB_A (Table 4, Fig. 2) is derived (Park, 1981a; Park and Jefferson, 1991). Other documented Neoproterozoic overprints in the Mackenzie Mountains Supergroup appear to relate to hiatuses in the geological record and to rifting (Park, 1994). None of the interpreted primary poles, including TK_A (entry 14, Table 4, Fig. 2) from the Mackenzie Mountains Supergroup, relate to the mafic intrusions. The discrepancy between the Shaler Supergroup pole (SH_{B1}) and the Tsezotene and Katherine formation poles (here combined in TK_A, Park and Aitken, 1986a, b) (Fig. 2, Table 4) from approximately correlative units, was attributed to possible

Table 4. Paleopoles of mean directions.

E	Unit	Sym	Cp	Pole (°E, °S)	N	δp°, δm°	λ° (°S)
Amundsen Basin							
1.	Shaler Sgp		*C2*	292, -68	7	10, 11	-73 ± 10
2.	Shaler Sgp		*C1*	000, +61	12[1]	14, 14	65 ± 14
3.	Shaler Sgp		*C3*	144, +43	4	12, 15	43 ± 12
4.	Gras. Bay	GB_A	*A*	327, +06	10	4, 7	8 ± 4
5.	Natkusiak	N_N	*N*	341, -03	11	4, 9	0 ± 4
6.	Franklin	F_N	*N*	340, -04	3	14, 27	-2 ± 14
7.	Franklin	F_N	*N*	343, -04	28	2, 5	0 ± 2
8.	Shaler Sgp	SH_{B2}	*B2*	342, -08	8	5, 9	-5 ± 5
9.	Natkusiak	N_R	*R*	338, +09	8	7, 13	10 ± 7
10.	Franklin	F_R	*R*	359, +21	2	-	29
11.	Franklin	F	*N, R*	342, +08	43	2, 5	11 ± 2
12.	Shaler Sgp	SH_{B1}	*B1*	346, +07	4	9, 18	11 ± 9
Mackenzie Mountains							
13.	Litt. Dal	LB_A	*A*	321, -16	14	3, 5	-14 ± 3
14.	Tsez/Kath	TK_A	*A*	323, +11	19	5, 10	11 ± 5

Notes: See Table 1. E, entry; Sym, pole symbol. N, normal; R, reverse. In this study, polarities of Precambrian poles are reversed from their conventional assignment (see Park, 1992b; Park, 1994). *N* is the number of sites; *δp°, δm°* are the semi-axes of the oval of 95% confidence about the pole; λ° is the paleolatitude of the reference sampling locality: 70 °N, 116 °W for the Amundsen Basin; 65 °N, 128 °W for the Mackenzie Mountains. Poles have been calculated from directions that have been recalculated at the reference coordinates. Selection criteria for Franklin data (entries 6, 7, 10, 11): sites have been included where $N \geq 3$ samples and $\alpha_{95} \leq 25°$. Because the amount of data from sedimentary sites is much less, in order to make reasonable estimates for discussion, selection criteria have been relaxed. Therefore, sites have been included where $N \geq 2$ samples and $\alpha_{95} \leq 40°$, except for entry 18 where 14 sites have only 1 specimen. Entries: 1. entry 4, Table 2. 2. entry 3, Table 2. 3. entry 5, Table 2. 4. Palmer et al. (1983), corrected for tilt. 5. 5 sites, Palmer and Hayatsu (1975); 6 sites, Palmer et al. (1983). 6. this paper. 7. Sites of Amundsen Basin: 2 sites, Fahrig et al. (1971); 8 sites, Robertson and Baragar (1972); 11 sites, Palmer and Hayatsu (1975); 4 sites, Park (1981b); 3 sites (Table 3). 8. entry 2, Table 2. 9. 8 sites, Palmer et al. (1983). 10. Sites of Amundsen Basin: 2 sites (Table 3). 11. Franklin sites outside Amundsen Basin: 19 sites, Fahrig et al. (1971); 10 sites, Fahrig and Schwarz (1973); 2 sites, Park (1974); 12 sites, Christie and Fahrig (1983). 12. entry 1, Table 2. 13. Park (1981a). 14. Combines primary components by site from Tsezotene Formation (Park and Aitken 1986b) and Katherine Group (Park and Aitken 1986a).
[a] 12 samples from 5 sites.

relative rotation between the Mackenzie Mountains and the Brock Inlier (Park, 1992a). However, the agreement between SH_{B1} and F, and lack of paleomagnetic (Park et al., 1989, in press) and structural evidence for rotations (Norris, 1972; Aitken and Long, 1978), suggests rather that the discrepancy between TK_A and SH_{B1} is due to overprinting by the Franklin intrusions.

CONCLUSIONS

1. Shaler Supergroup sedimentary rocks of this study contain magnetic overprints, B1 and B2, caused by Franklin intrusions, that mask or replace the primary magnetization.
2. The 20° difference between a primary pole from the Tsezotene and Katherine units of the Mackenzie Mountains and a previously inferred primary pole from correlative Shaler Supergroup sedimentary rocks of the Brock Inlier (Park, 1992a) is attributed to magnetic overprinting of the Shaler Supergroup by Franklin intrusions.
3. A steeply directed overprint C3 is attributed to latest Neoproterozoic diagenesis recorded during the sub-Paleozoic hiatus.

ACKNOWLEDGMENTS

We would like to thank Garry Freda who prepared the samples for study. Polar Continental Shelf Project provided logistical support in the field. Field assistance was provided by K. Telmer, J. Morin, J. Kimiksana, G. Green, and C.W. Jefferson. We thank K.L. Buchan for discussions and an internal review of the manuscript.

REFERENCES

Aitken, J.D. and Long, D.G.F.
1978: Mackenzie tectonic arc - reflection of early basin configuration; Geology, v. 26, p. 626-629.

Aitken, J.D., Long, D.G.F., and Semikhatov, M.A.
1978: Correlation of Helikian strata, Mackenzie Mountains-Brock Inlier-Victoria Island; in Current Research, Part A; Geological Survey of Canada, Paper 78-1A 178 p.

Balkwill, H.R. and Yorath, C.J.
1970: Brock River map-area, District of Mackenzie (97D); Geological Survey of Canada, Paper 70-32, p. 1-25.

Baragar, W.R.A. and Donaldson, J.A.
1973: Coppermine and Dismal Lakes map areas; Geological Survey of Canada, Paper 71-39, 20 p.

Buchan, K.L., Card, K.D., and Chandler, F.W.
1989: Multiple ages of Nipissing Diabase intrusion: paleomagnetic evidence from the Englehart area, Ontario; Canadian Journal of Earth Sciences, v. 26, p. 427-445.

Campbell, F.H.A.
1981: Stratigraphy and tectono-depositional relationships of the Proterozoic rocks of the Hadley Bay area, northern Victoria Island, District of Franklin; in Current Research, Part A; Geological Survey of Canada, Paper 81-1A, p. 15-22.

Christie, K.W. and Fahrig, W.F.
1983: Paleomagnetism of the Borden dykes of Baffin Island and its bearing on the Grenville Loop; Canadian Journal of Earth Sciences, v. 20, p. 275-289.

Christie, R.L., Cook, D.G., Nassichuk, W.W., Trettin, H.P., and Yorath, C.J.
1972: The Canadian Arctic Islands and Mackenzie region; 24th International Geological Congress, Montreal, Guide to Excursion A66, 146 pp.

Fahrig, W.F. and Schwarz, E.J.
1973: Additional paleomagnetic data on the Baffin diabase dikes and a revised Franklin pole; Canadian Journal of Earth Sciences, v. 10, p. 576-581.

Fahrig, W.F., Irving, E., and Jackson, G.D.
1971: Paleomagnetism of the Franklin diabases; Canadian Journal of Earth Sciences, v. 8, p. 455-467.

Heaman, L.M., LeCheminant, A.N., and Rainbird, R.H.
1992: Nature and timing of Franklin igneous events, Canada; Earth and Planetary Science Letters, v. 109, p. 117-131.

Hoffmann, H.J. and Rainbird, R.H.
1995: Carbonaceous megafossils from Neoproterozoic Shaler Supergroup, Victoria Island, Arctic Canada; Paleontology, v. 37, p. 721-731.

Irving, E. and Irving, G.A.
1982: Apparent polar wander paths, Carboniferous through Cenozoic and the assembly of Gondwana; Geophysical Surveys, v. 5, p. 141-188.

Jefferson, C.W.
1985: Uppermost Shaler Group and its contact with the Natkusiak basalts, Victoria Island, District of Franklin; in Current Research, Part A; Geological Survey of Canada, Paper 85-1A, p. 103-110.

Jefferson, C.W. and Young, G.M.
1989: Late Proterozoic orange-weathering stromatolite biostrome, Mackenzie Mountains and western Arctic Canada; Canadian Journal of Earth Sciences; in Reefs, Canada and adjacent Area, (ed.) H.H.J. Geldsetzer, N.P. James, and G.E. Tebbutt; Canadian Society of Petroleum Geologists, Memoir 13, p. 72-78.

Kent, J.T., Briden, J.C., and Mardia, K.V.
1983: Linear and planar structure in ordered multivariate data as applied to progressive demagnetization of paleomagnetic remanence; Geophysical Journal of the Royal Astronomical Society, v. 75, p. 593-621.

Kerr, J.W.
1977: Cornwallis fold belt and the mechanism of basement uplift; Canadian Journal of Earth Sciences, v. 14, p. 1374-1401.

McFadden, P.L.
1990: A new fold test for paleomagnetic studies; Geophysical Journal International, v. 103, p. 163-169.

Meert, J.G., Van Der Voo, R., and Payne, T.W.
1994: Paleomagnetism of the Catoctin volcanic province: a new Vendian-Cambrian apparent polar wander path for North America; Journal of Geophysical Research, v. 99, p. 4625-4641.

Morris, W.A.
1977: Paleolatitude of glaciogenic upper Precambrian Rapitan Group and the use of tillites as chronostratigraphic marker horizons; Geology, v. 5, p. 85-88.

Norris, D.K.
1972: En échelon folding in the northern Cordillera of Canada; Bulletin of Canadian Petroleum Geology, v. 20, p. 634-642.

Palmer, H.C. and Hayatsu, A.
1975: Paleomagnetism and K-Ar dating of some Franklin lavas and diabases, Victoria Island; Canadian Journal of Earth Sciences, v. 12, p. 1439-1447.

Palmer, H.C., Baragar, W.R.A., Fortier, M., and Foster, J.H.
1983: Paleomagnetism of Late Proterozoic rocks, Victoria Island, Northwest Territories, Canada; Canadian Journal of Earth Sciences, v. 20, p. 1456-1469.

Park, J.K.
1974: Paleomagnetism of miscellaneous Franklin and Mackenzie diabases of the Canadian Shield and their adjacent country rocks; Canadian Journal of Earth Sciences, v. 11, p. 1012-1017.
1981a: Analysis of the multicomponent magnetization of the Little Dal Group, Mackenzie Mountains, Northwest Territories, Canada; Journal of Geophysical Research, v. 86, p. 5154-5146.
1981b: Paleomagnetism of basic intrusions from the Brock Inlier, Northwest Territories, Canada; Canadian Journal of Earth Sciences, v. 18, p. 1637-1641.
1992a: Paleomagnetism of units P1-P3 of the Late Precambrian Shaler Group, Brock Inlier, Northwest Territories; in Current Research, Part C; Geological Survey of Canada, Paper 92-1C, p. 43-52.
1992b: Did Laurentia pass over the south pole during earliest Cambrian time?; in Current Research, Part E; Geological Survey of Canada, Paper 92-1E, p. 11-22.
1994: Palaeomagnetic constraints on the position of Laurentia from middle Neoproterozoic to Early Cambrian times; Precambrian Research, v. 69, p. 95-112.
in press: Paleomagnetism of the late Neoproterozoic Blueflower and Risky formations of the northern Cordillera, Canada; Canadian Journal of Earth Sciences, in press.

Park, J.K. and Aitken, J.D.
1986a: Paleomagnetism of the Katherine Group in the Mackenzie Mountains: implications for post-Grenville (Hadrynian) apparent polar wander; Canadian Journal of Earth Sciences, v. 23, p. 308-323.
1986b: Paleomagnetism of the Late Proterozoic Tsezotene Formation of northwestern Canada; Journal of Geophysical Research, v. 91, p. 4955-4970.

Park, J.K. and Jefferson, C.W.
1991: Magnetic and tectonic history of the Late Proterozoic Upper Little Dal and Coates Lake Groups of northwestern Canada; Precambrian Research, v. 52, p. 1-35.

Park, J.K., Buchan, K.L., and Harlan, S.S.
in press: A proposed radiating dyke swarm fragmented by the separation of Laurentia and Australia - based on paleomagnetism of ca. 780 Ma intrusions in western North America; Earth and Planetary Science Letters, in press.

Park, J.K., Norris, D.K., and Larochelle, A.
1989: Paleomagnetism and the origin of the Mackenzie Arc of northwestern Canada; Canadian Journal of Earth Sciences, v. 26, p. 2194-2203.

Pehrsson, S.J. and Buchan, K.L.
1994: Borden dykes interpreted as remagnetized Franklin dykes based on U-Pb baddeleyite geochronology and paleomagnetic re-interpretation; Geological Association of Canada Annual Meeting, University of Waterloo, Program with Abstracts, v. 19, A87.

Rainbird, R.H.
1991: Stratigraphy, sedimentology and tectonic setting of the upper Shaler Group, Victoria Island, Northwest Territories; Ph.D. Thesis, University of Western Ontario, London, Ontario, 257 p.
1994: Stratigraphy and correlation of the Neoproterozoic Shaler Supergroup, Amundsen Basin, northwestern Canada; in Proceedings of the 1992 International Conference on Arctic Margins, United States Minerals Management Service Outer Continental Shelf Study; (ed.) D.K. Thurston and K. Fujita, p. 117-122.

Rainbird, R.H., Hodgson, D.A., and Jefferson, C.W.
1994a: Bedrock and surficial geology, Glenelg Bay (78B/6), District of Franklin, Northwest Territories; Geological Survey of Canada, Open File 2920, Scale 1:50,000.

Rainbird, R.H., Jefferson, C.W., Hildebrand, R.S., and Worth, J.K.
1994b: The Shaler Supergroup and revision of Neoproterozoic stratigraphy in Amundsen Basin, Northwest Territories; in Current Research, Part C; Geological Survey of Canada, Paper 94-C, p. 61-70.

Rainbird, R.H., Jefferson, C.W., and Young, G.M.
in press: Early Neoproterozoic sequences on the northwest margin of Laurentia: correlations and paleogeographic significance; Geological Society of America Bulletin.

Rainbird, R. H., McNicoll, V. J., and Heaman, L. M.
1994c: Detrital zircon studies of Neoproterozoic quartzarenites from northwestern Canada: additional support for an extensive river system originating from Grenville orogen; Abstracts of the Eighth International Conference on Geochronology, Cosmochronology and Isotope Geology, Berkeley, California, United States Geological Survey Circular 1107, p. 258.

Robertson, W.A. and Baragar, W.R.A.
1972: The petrology and paleomagnetism of the Coronation sills; Canadian Journal of Earth Sciences, v. 9, p. 123-140.

Symons, D.T.A. and Chiasson, A.D.
1991: Paleomagnetism of the Callander Complex and the Cambrian apparent polar wander path for North America; Canadian Journal of Earth Sciences, v. 28, p. 355-363.

Thorsteinsson, R. and Tozer, E.T.
1962: Banks, Victoria and Stefansson Islands, Arctic Archipelago; Memoir 330, 85 p.

Tozer, E.T.
1968: Geology of the Arctic Archipelago; in Geology and Economic Minerals of Canada; (ed.) R.J.W. Douglas; Geological Survey of Canada, Economic Geology Report No. 1.

Young, G.M.
1977: Stratigraphic correlation of upper Proterozoic rocks of northwestern Canada; Canadian Journal of Earth Sciences, v. 14, p. 1771-1787.
1979: Correlation of middle and upper Proterozoic strata of the northern rim of the North American craton; Transactions of the Royal Society of Edinburgh, v. 70, p. 323-326.
1981: The Amundsen Embayment, Northwest Territories; relevance to the upper Proterozoic evolution of North America; in Proterozoic Basins of Canada; (ed.) F.H.A. Campbell; Geological Survey of Canada, Paper 81-10, p. 203-211.

Young, G.M., Jefferson, C.W., Delaney, G.D., and Yeo, G.M.
1979: Middle and Late Proterozoic evolution of the northern Canadian Cordillera and Shield; Geology, v. 7, p. 125-128.

Geological Survey of Canada Project 870002

Canadian Shield

Bouclier canadien

Thermal parameters in rock units of the Winter Lake-Lac de Gras area, central Slave Province, Northwest Territories – implications for diamond genesis[1]

P.H. Thompson, A.S. Judge[2], and T.J. Lewis[3]
Continental Geoscience Division

Thompson, P.H., Judge, A.S., and Lewis, T.J., 1995: Thermal parameters in rock units of the Winter Lake-Lac de Gras area, central Slave Province, Northwest Territories – implications for diamond genesis; in Current Research 1995-E; Geological Survey of Canada, p. 125-135.

Abstract: Radiogenic heat production varies with rock type from 0.1-0.8 μW/m^3 in amphibolite and tonalitic gneiss to 8.0-15.8 μW/m^3 in late granites. Metasedimentary rocks and other granitoid units fall between these extremes. Thermal conductivity ranges from 2.3 to 4.9 W/m•K. Conductivity parallel to planar foliation or layering is up to 1.6 times higher than that perpendicular to these features.

A simple conductive thermal model and the assumption that the lithosphere/asthenosphere boundary is a thermal feature (1300°C) suggests that decreasing heat production in the crust can account for the transition from barren lithosphere less than 100 km thick at the end of the Archean to a diamond-bearing lithosphere 200-225 km thick today. Lateral variations in this parameter may cause the thickness of diamond-bearing lithosphere beneath the Slave Province to change.

Consistency between the model results, surface geology, and the results of other modelling approaches suggests that crustal thermal parameters and their evolution with time should be part of any comprehensive hypothesis for formation and evolution of lithosphere beneath Archean cratons.

Résumé : La production de chaleur d'origine radioactive varie selon le type de roche, soit de 0,1-0,8 μW/m^3 dans l'amphibolite et le gneiss tonalitique à 8,0-15,8 μW/m^3 dans les granites tardifs. Les roches métasédimentaires et autres unités granitoïdes se situent entre ces deux extrêmes. La conductivité thermique varie entre 2,3 et 4,9 W/m•K. La conductivité parallèle à la foliation ou stratification planaire est jusqu'à 1,6 fois plus élevée que celle qui lui est perpendiculaire.

Selon un modèle simple de conductivité thermique et l'hypothèse selon laquelle la limite lithosphère-asthénosphère est une caractéristique thermique (1300°C), une diminution de la production de chaleur dans la croûte peut être à l'origine de la transition entre une lithosphère stérile de moins de 100 km d'épaisseur à la fin de l'Archéen et une lithosphère diamantifère de 200 à 225 km d'épaisseur aujourd'hui. Les variations latérales de ce paramètre peuvent modifier l'épaisseur de la lithosphère diamantifère au-dessous de la Province des Esclaves.

La cohérence entre les résultats obtenus par modélisation, les données géologiques sur les dépôts superficiels et les résultats obtenus par d'autres méthodes de modélisation fait supposer que les paramètres thermiques de la croûte et leur évolution dans le temps devraient être intégrés à toute hypothèse globale de la formation et de l'évolution de la lithosphère sous les cratons archéens.

[1] Contribution to the Slave NATMAP Project
[2] Terrain Sciences Division
[3] GSC Victoria, Sidney

INTRODUCTION

The strong influence of crustal radiogenic heat production and thermal conductivity on heat loss from the earth's interior has a significant effect on geothermal gradients in the lower crust and lithospheric mantle (Pollack and Chapman, 1977). Together with surface heat flow, these parameters are essential components of numerical models constructed to explain the thermal evolution and metamorphic history of any orogen. Of particular interest is the time at which the lithosphere beneath the Archean Slave Province, northwestern Canadian Shield, became thick and cool enough to contain diamonds. One school of thought maintains that the apparent lithospheric roots outlined by present day seismic tomography beneath Archean cratons formed at the same time as overlying crust (Jordan, 1988; Pearson et al., 1995). Other workers argue for progressive growth with time (Helmstaedt and Schultze, 1989; Ringwood, 1989; Abbot, 1991). Although ages of inclusions in individual kimberlite pipes that range from 3.2 to 1.2 Ga (Richardson et al., 1993; Pearson et al., 1995) can be attributed to a long history of metasomatic alteration of a very old root, the range could reflect the heterogeneity of material added to a progressively growing root. Neither side of the discussion has paid particular attention to the effect of crustal thermal parameters on the evolution of subcratonic roots.

Charles Fipke's discovery of 52 million year old diamond-bearing kimberlites (Northern Miner, 1993) and seismic tomography (Grand, 1987) are consistent with a thick (>120 km), cold lithosphere beneath the Slave Province today. In contrast, Archean low-pressure/high-temperature metamorphism and magmatism (Thompson, 1989; Thompson et al., 1995) and numerical modelling results (Thompson and Lucazeau, 1989) indicate that the late Archean geothermal gradients were high enough to intersect the base of the lithosphere at pressures too low for formation of diamonds. We use new thermal data from the Slave Province to investigate the possibility that decreasing crustal heat production was a factor in the lithospheric thickening required to explain the contrast between the Late Archean geological record and lithosphere today.

The definition of continental lithosphere remains controversial (Anderson, 1995). Jordan (1988) proposed that seismic tomographic roots 300-400 km thick correspond to a lithological or chemical mantle root that was depleted in basaltic components. Polet and Anderson (1995) discussed chemical roots of a "permanent" nature only 200 km thick that induce cold downwellings in the asthenosphere, thereby increasing their apparent depth by 100-200 km (i.e. 300-400 km). The modelling described here assumes that at 1300°C peridotite is close enough to its solidus that it flows on a scale that is characteristic of the asthenosphere, thereby defining the base of the lithosphere. This simplifying assumption does not consider the complications introduced by the effects of water, carbon dioxide, and increasing pressure on the solidus. Nor does it address compositional variations in the mantle.

A strong relationship between surface heat flow, crustal heat production, and temperature variations with depth in the continental lithosphere is not a new idea (Pollack and Chapman, 1977; Stein, 1995). In this paper, we extend the concept to consider changes in temperature with time in a stable craton due to a natural reduction of heat production in rocks (Jessop and Lewis, 1978). Moreover, we consider the possibility that lateral variations in this parameter affect the thickness of diamond-bearing lithosphere.

GEOLOGICAL SETTING

The Slave Province of the Canadian Shield (Fig. 1) is distinguished from classic Archean "granite-greenstone" terranes, like the Abitibi segment of the Superior Province or the Kaapvaal craton in South Africa, by the high proportion of sedimentary rocks in the supracrustal sequence, the limited occurrence of ultramafic igneous rocks, and abundant highly-evolved granitoid rocks (McGlynn and Henderson, 1972; Henderson, 1981; Padgham, 1990). Centred 250 km north of Yellowknife, the Winter Lake-Lac de Gras map area (11 000 km^2, Thompson and Kerswill, 1994; Thompson et al., 1995) is typical of Slave geology and contains parts of two major lithotectonic elements. Thin discontinuous volcanic belts (2.7 Ga; Villeneuve, 1993) separate a domain dominated by recrystallized, migmatitic and gneissic granitoid rocks from one dominated by metamorphosed greywacke-mudstone. The metamorphosed, heterogeneous, "older" granitoid rocks are interpreted to be, for the most part, crystalline basement beneath the supracrustal sequence (Yellowknife Supergroup of Henderson, 1970) on the basis of the map pattern, discordant metamafic dykes, the isograd pattern, and the change in structural style across the domain boundary (Thompson et al., 1995). "Younger" granitoids similar to those dated elsewhere in the Slave at 2.62-2.58 Ga (van Breemen et al., 1992 and references therein) intrude both domains. Peak metamorphic conditions were probably attained after 2.62 and before 2.58 Ga. The map area overlaps the western boundary of the BHP-Diamet property. A diamond-bearing kimberlite also occurs 40 km to the southwest and another 50 km south-southeast of the map area (Pell, 1995).

THERMAL PARAMETER DATA

In the course of the geological mapping of the Winter Lake-Lac de Gras (Thompson and Kerswill, 1994; Thompson et al., 1995), rock samples were collected from ten rock units for measurement of thermal conductivity and radiogenic heat production (Table 1). For comparison, heat production was also measured in 20 metasedimentary rocks from three other sedimentary domains in the Slave Province (Fig. 1). Rock units referred to in this paper are described by Thompson et al.(1994) and Thompson and Kerswill (1994). Prior to this study, the only published measurements of heat flow, heat production, and thermal conductivity in the craton were from a single site near Yellowknife (Lewis and Wang, 1992).

Laboratory methods

The concentrations of the naturally occurring, long-lived radioactive isotopes of uranium, thorium, and potassium and/or daughter products were determined by passive gamma-ray

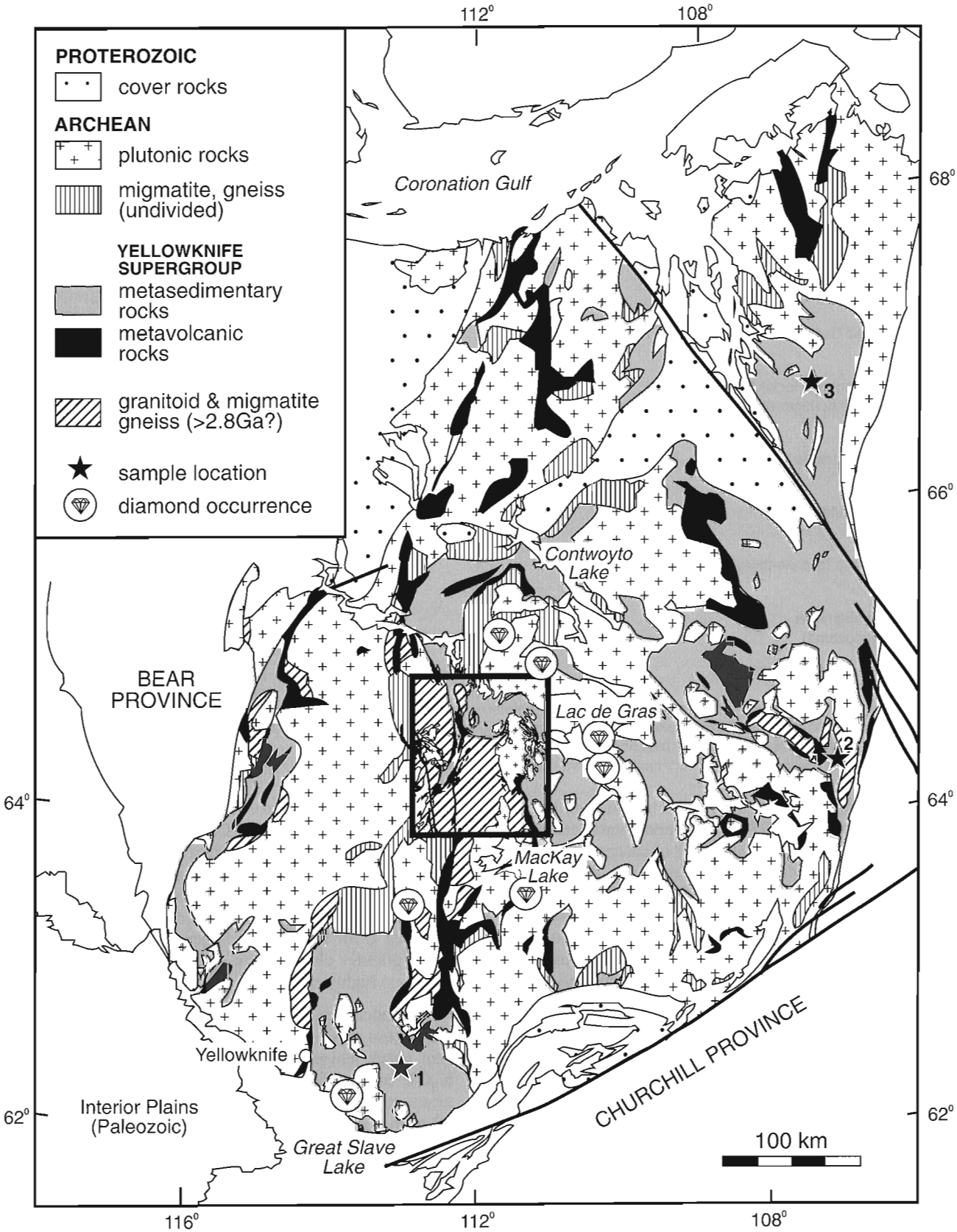

Figure 1. Simplified map of the Slave Province after McGlynn (1977) outlining location of the Winter Lake-Lac de Gras map area (rectangle) and other sampled sedimentary domains (1-Yellowknife, 2-Healey Lake, 3-Tinney Hills-Overby Lake).

Table 1. Radiogenic heat production and thermal conductivity of rock units in the Winter Lake-Lac de Gras map area.

Rock Type	Number of samples	Heat Generation ($\mu W/m^3$) average/range/standard dev. t = 0	Heat Generation ($\mu W/m^3$) average/range/standard dev. t = 2400 Ma	Thermal Conductivity (W/m•K) (no. samples)
Pink Biotite Granite	5	9.1 4.9-15.9	15.7 ± 8.7 8.1-29.1	nd
White Biotite Granite	8	6.4 5.3-8.1	10.5 ± 1.7 8.5-13.8	4.0 (3)
Biotite-magnetite Granodiorite	1	0.5	1.0	nd
Quartz Glob Granite	6	0.7 0.6-0.8	1.5 ± 0.2 1.4-1.7	3.5 (2)
Metasedimentary Rocks * (phyllite, schist, migmatite)	29	1.2 0.1-3.1	2.9 ± 1.2 0.2-5.9	3.3 (25) planar fabric para(5) 3.9 perp(5) 2.9
Mafic Metavolcanic Rocks (amphibolite)	3	0.5 0.1-0.8	0.9 0.3-1.4	planar fabric para(1) 2.8 perp(1) 2.3
Hornblende Metagranite	6	2.2 1.4-3.8	4.0 ± 0.2 2.8-6.7	4.5 (2)
Metagranitoid (granite-tonalite)	15	1.4 0.2-5.4	2.4 ± 2.1 0.5-8.7	3.4 (1)
Granitoid Migmatite (dyke/leucosome)	3 3	0.4 9.2	0.8 15.1	3.2 (1)
Quartzofeldspathic Gneiss	6	2.0 0.8-3.4	3.2 ± 1.4 1.3-4.3	planar fabric para(2) 4.1 perp(2) 3.5

* four sample domains (number samples, average heat production): 1) Yellowknife (7, 1.1 $\mu W/m^3$); 2) Healey Lake (9, 1.1 $\mu W/m^3$); 3) Tinney Hills-Overby Lake (8, 1.1 $\mu W/m^3$); 4)Winter Lake-Lac de Gras (5, 1.4 $\mu W/m^3$)

spectrometry using comparisons with internationally calibrated standards (Lewis, 1974). Heat generation is calculated from these concentrations on the basis of accepted values for half-lives and present day energy conversions. A density of 2.70 g/cm^3 is assumed. The assumption causes heat production to be overestimated in denser rocks and underestimated in less dense rocks by a few per cent. Thermal conductivity of the rock samples collected in the course of regional mapping was measured at room temperature using the divided bar steady state method (Jessop, 1970) on discs cut from 2 cm cores. Rocks containing a planar preferred orientation of minerals or compositional layering were cored parallel and perpendicular to the structure. Uncertainties of less than plus or minus five per cent are associated with heat production and thermal conductivity measurements.

Results

Radiogenic heat production in the different rock types of the Winter Lake-Lac de Gras area varies by a factor of 15 (Table 1). Metamorphosed sedimentary and mafic volcanic rocks are relatively low, as are the four components of the deformed and metamorphosed "older" granitoid-migmatite-gneiss suite. Similar heat production values were obtained from metasedimentary rocks in three other areas of the Slave Province (Table 1, Fig. 1). The Pink Granite and the White Granite of the younger, discordant granitoid suite are the most radiogenic. However, a discordant granitic dyke (20 cm thick) intruded into the granitoid migmatite and, locally, the leucosome in the migmatite, yielded values similar to those obtained from the most radiogenic granites. Compared to many granites elsewhere (e.g. Whalen, 1993), those in this study are highly radiogenic.

Chemical and petrographic studies indicate that the most radiogenic rocks sampled to date are true granites (>35 per cent alkali feldspar) with highly potassic (4.5-5.5 per cent K_2O), metaluminous compositions. In the Pink Granite, uranium ranges from 7.3 to 53 ppm and thorium from 29 to 59 ppm. Comparable thorium contents occur in the White Granite (30-63 ppm) but uranium is generally lower (4.9-15 ppm). Potassium feldspar and the common accessory minerals, allanite, monazite, and zircon are the most likely hosts of radioactive elements.

Radiogenic heat production in rocks decreases with time through a natural decay of the radioelements. At the time of latest granite intrusion in the Slave Province (e.g. 2620-2580 Ma, van Breemen et al., 1992 and references therein),

heat production of each of the rock units was almost double present day measurements. Table 1 includes values back-calculated to 2400 Ma.

Measurements of thermal conductivity ranged from 2.5 to 4.5 W/mK (Table 1). Conductivity parallel to foliation or gneissic layering is up to 1.6 times that perpendicular to these features. Regional dips at the surface tend to be moderate to steep. At depth, attitudes are not known.

THE MODEL

In the absence of non-conductive heat transfer within the lithosphere (i.e. crust + lithospheric mantle), the increase of temperature with depth in the lithosphere is a function of its thermal conductivity, heat derived from radioactive decay within the lithosphere, and heat coming from the underlying asthenosphere. Higher heat flow at the earth's surface corresponds to a higher geothermal gradient; that is, a larger temperature change through the lithosphere, and typically accompanies a thin or thinner lithosphere (Pollack and Chapman, 1977). This paper focuses on the influence of radiogenic heat production and thermal conductivity in the crust on lithospheric thermal regimes, both laterally within a craton today and with time since the end of the Archean 2500 Ma ago.

The present day situation

Present day temperature profiles with depth below the surface were calculated for a single site at Yellowknife and, using a weighted average, 65 sites for the Winter Lake-Lac de Gras area. The following equation was used assuming purely conductive heat transfer within the lithosphere and crust;

$$T = T_0 + qz/k - Az^2/2k$$

T = temperature at depth z, T_0 = surface temperature

q = surface geothermal flux (summation of crust and mantle contributions)

k = thermal conductivity

A = radiogenic heat production in a layer (per unit time per unit volume)

Model parameters are summarized in Table 2 and on schematic lithospheric columns (Fig. 2). An average thermal conductivity of 3.5 W/m·K was calculated for the surface rocks (Table 1). Dependence of conductivity on temperature takes the form, $k = k(T=0°)/(1 + cT)$, where T is temperature and c=.002 for the crust and c=.001 elsewhere. The base of the lithosphere is assumed to correspond to the 1300°C isotherm (i.e. lithosphere/asthenosphere boundary for this purpose is assumed to be thermal in nature), the crust to be 35 km thick (Barr, 1971), and heat production within the more

Table 2. Model parameters (estimated and assumed).

Parameters	Yellowknife		Winter Lake-Lac de Gras	
	t = 0 a	t = 2400 Ma	t = 0 a	t = 2400 Ma
Thickness (km)				
upper crust	10	10	10	10
middle crust	10	10	10	10
lower crust	15	15	15	15
Heat Production (μW/m³)				
upper crust	2.3	4.2	1.7	3.0
middle crust	1.0	2.0	1.0	2.0
lower crust	0.15	0.30	0.15	0.30
crustal average	1.0	1.9	0.8	1.6
lithospheric mantle	0	0	0	0
Thermal Conductivity (W/m·K)*				
surface rocks	3.5	3.5	3.5	3.5
Upper boundary, top of crust (°C)	0	0	0	0
Lower boundary base of lithosphere (°C)	1300	1300	1300	1300
Surface heat flow (mW/m²)	50	91	40	73
Derived mantle heat flow (base of lithosphere)	13	21	11	18

* conductivity(k) = k(T=0°)/(1 + cT), where T = temperature and c = .002 for crust and c = .001 for mantle

mafic (tonalitic?) middle and lower crust and the ultramafic upper mantle taken as 1.0, 0.15, and 0 $\mu W/m^3$, respectively. Recent heat flow and heat production measurements in the Basin and Range Province of the United States (Lachenbruch et al., 1994) support the assumption that radioactivity of rocks decreases with depth, at least within the crust. Our assumed middle and lower crustal values are similar to Drury's (1989) estimates for the Superior Province. Ashwal et al. (1987) estimated a mean value of about 1 $\mu W/m^3$ for middle and lower crust in the Kapuskasing Zone (Superior Province). Derived mantle fluxes of 13 and 11 mW/m^2 for the two areas (Table 2) are comparable to values of 10-14 mW/m^2 obtained for the Superior Province (Guillou-Frontier et al., 1994). Two lithospheric temperature profiles calculated from the weighted average of new heat production and conductivity data at Winter Lake-Lac de Gras (65 sites) and from the published data for a single site west of Yellowknife are considered to be two among a range of profiles that might be expected across the Slave Province. Yellowknife is included here because it is the only site for which surface heat flow data has been published.

Geothermal gradient **c** (Fig. 3) for the Yellowknife site is derived using an upper crustal heat production (2.3 ± 1.4 mW/m^3, Fig. 2) averaged from ten samples of surface granodiorite (Lewis and Wang, 1992). Their measured heat flow of 50 ± .18 mW/m^2 (Lewis and Wang, 1992) is somewhat higher than the average (42 ± 8 mW/m^2) for the Archean Superior Province of the Canadian Shield (Drury, 1991). Heat production in the granodiorite is near the low end of the range measured in granitoid rocks from the Winter Lake-Lac de Gras map area. Model gradient **c** (Fig. 3) implies a present day lithosphere 175 km thick with the lowermost 20 km in the stability field of diamond.

Geothermal gradient **b** representing the Winter Lake-Lac de Gras map area (11 000 km^2) incorporates an upper crustal heat production of 1.7 $\mu W/m^3$ based on the relative surface area of rock units and their average heat production (Table 1). To simplify the calculation, the less-radiogenic granitoids that intrude the volcano-sedimentary sequence were grouped together as granite/granodiorite (Fig. 2) as were all the units interpreted as older than the supracrustal rocks. In the absence of measurements of heat flow, 40 mW/m^2, a value close to the average for the Superior Province (Drury, 1991), was assumed

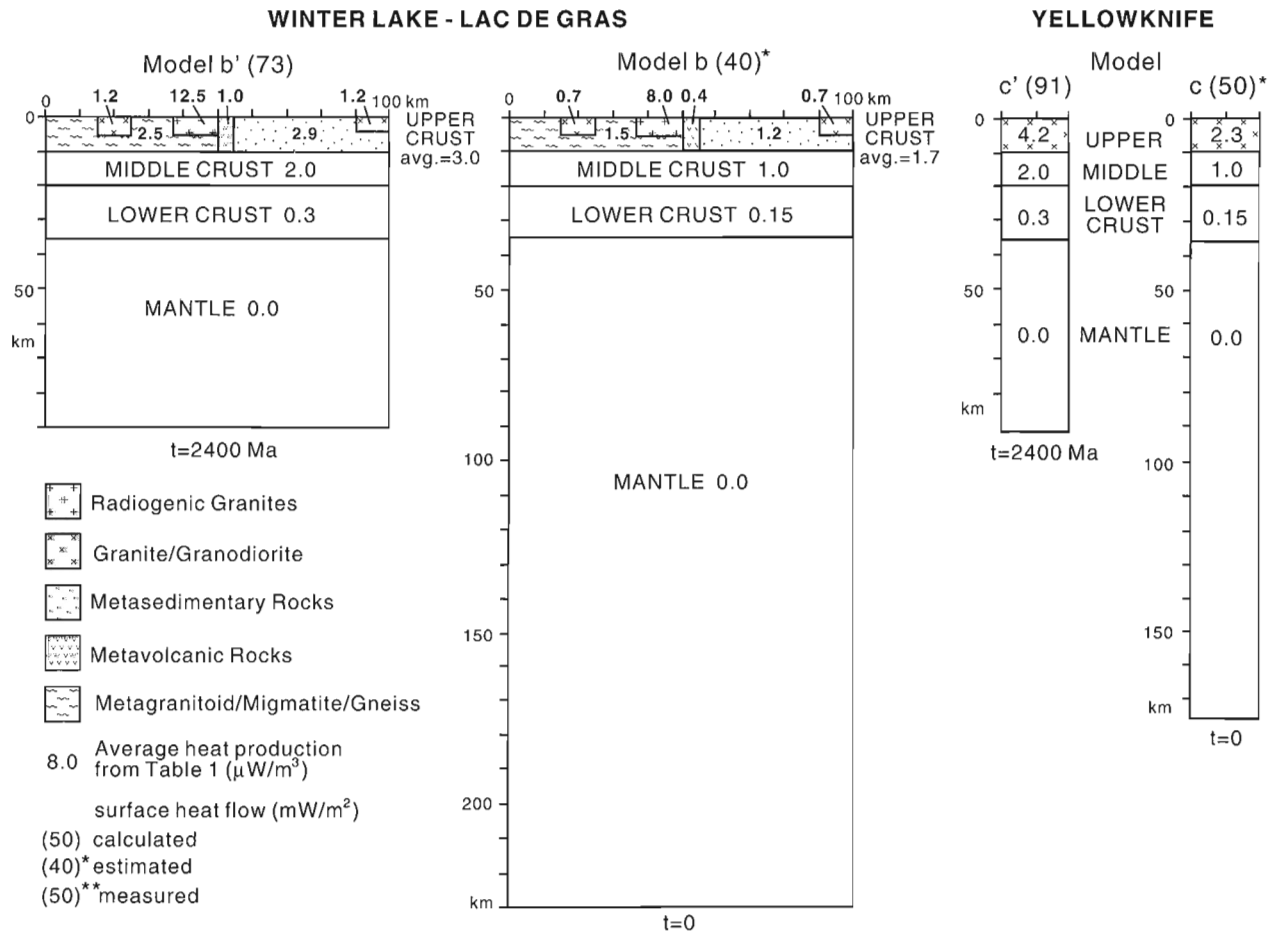

Figure 2. Schematic lithospheric columns corresponding to the geothermal gradients presented in Figure 3. For the purposes of modelling, the upper crust at the site west of Yellowknife was assumed to be composed entirely of the granodiorite present at the surface. See text for explanation of heat source distribution in upper crust representing Winter Lake-Lac de Gras area.

for the Winter Lake-Lac de Gras area where average heat production is significantly lower than it is at the Yellowknife site. With the assumed distribution of heat sources (Fig. 2) and this heat flow, the present base of the lithosphere (1300°C) occurs at a depth of 225 km and the lowermost 110 km fall in the diamond stability field (Fig. 3). On this basis, five times more lithosphere occurs within the diamond stability field beneath Winter Lake-Lac de Gras than beneath the Yellowknife locality.

These preliminary calculations show that if the average crustal heat production does, in fact, vary to the extent indicated in the schematic lithospheric columns, the thickness of lithosphere that falls within the diamond stability field may differ across the Slave Province. The single Yellowknife site is probably not representative of the surrounding region. There is, however, a radioactivity anomaly tens of kilometres wide located 100 km to the northeast (Darnley et al., 1986) that corresponds to regional heat production much higher

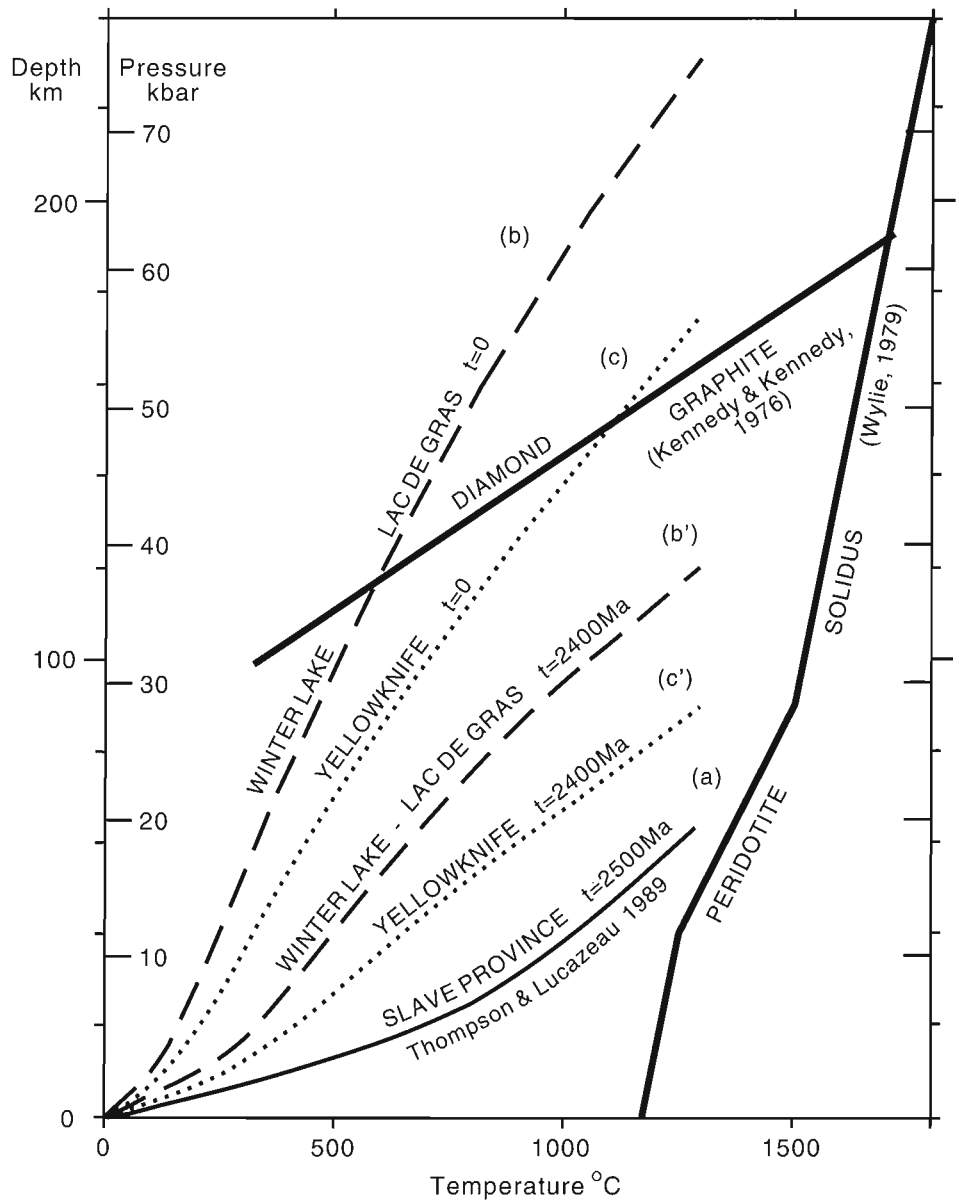

Figure 3. *Pressure(depth)-Temperature diagram of calculated geothermal gradients, graphite/diamond transition (Kennedy and Kennedy, 1976), and dry peridotite solidus (Wyllie, 1979). Geothermal gradient* ***a*** *after Thompson and Lucazeau (1989) is close to the gradient derived from metamorphic data in the Winter Lake-Lac de Gras area (Thompson et al., 1995) for the temperature range 0-900°C. See also Thompson (1989).*

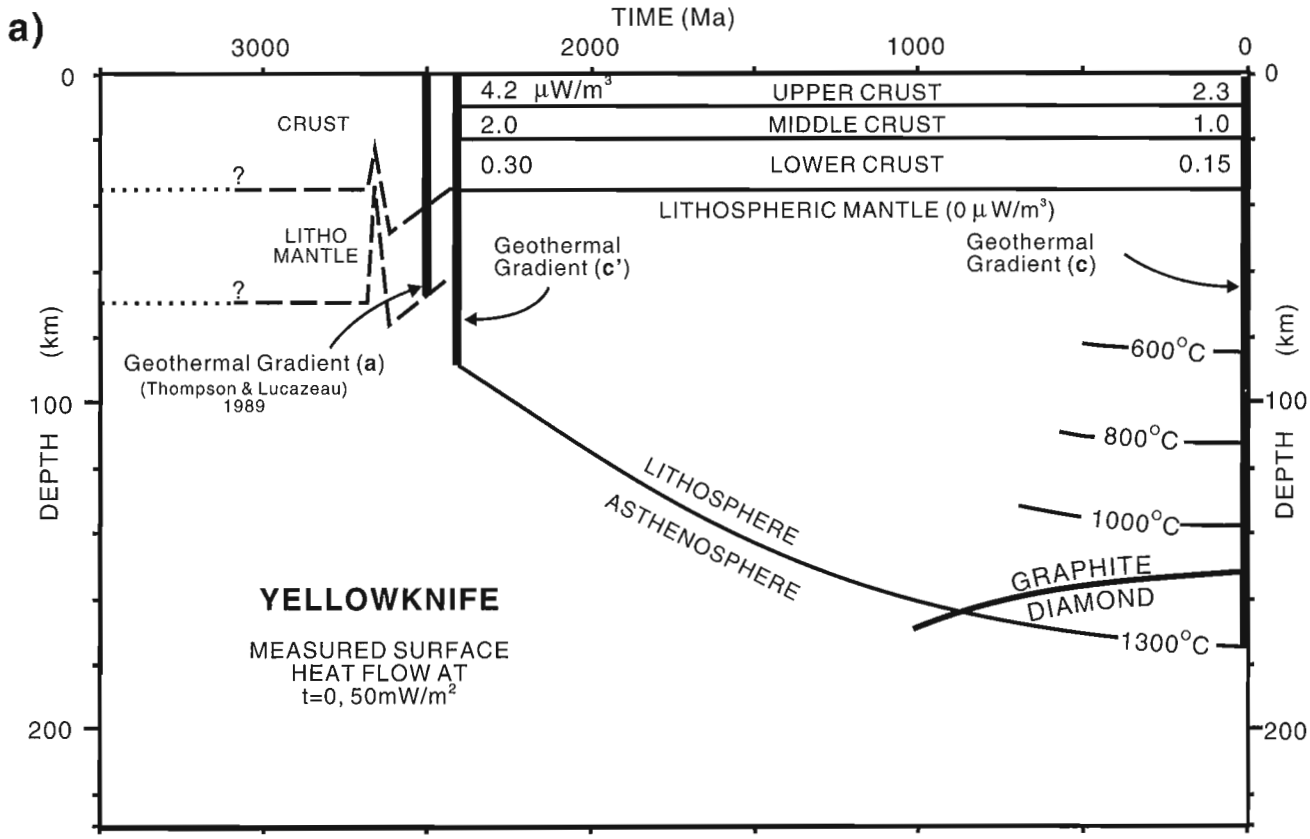
a)
TIME (Ma)
3000
2000
1000
0
4.2 μW/m³
UPPER CRUST
2.3
2.0
MIDDLE CRUST
1.0
0.30
LOWER CRUST
0.15
LITHOSPHERIC MANTLE (0 μ W/m³)
CRUST
LITHO MANTLE
Geothermal Gradient (c')
Geothermal Gradient (c)
Geothermal Gradient (a)
(Thompson & Lucazeau) 1989
600°C
800°C
1000°C
1300°C
LITHOSPHERE
ASTHENOSPHERE
GRAPHITE
DIAMOND
YELLOWKNIFE
MEASURED SURFACE HEAT FLOW AT t=0, 50mW/m²
DEPTH (km)
0
100
200

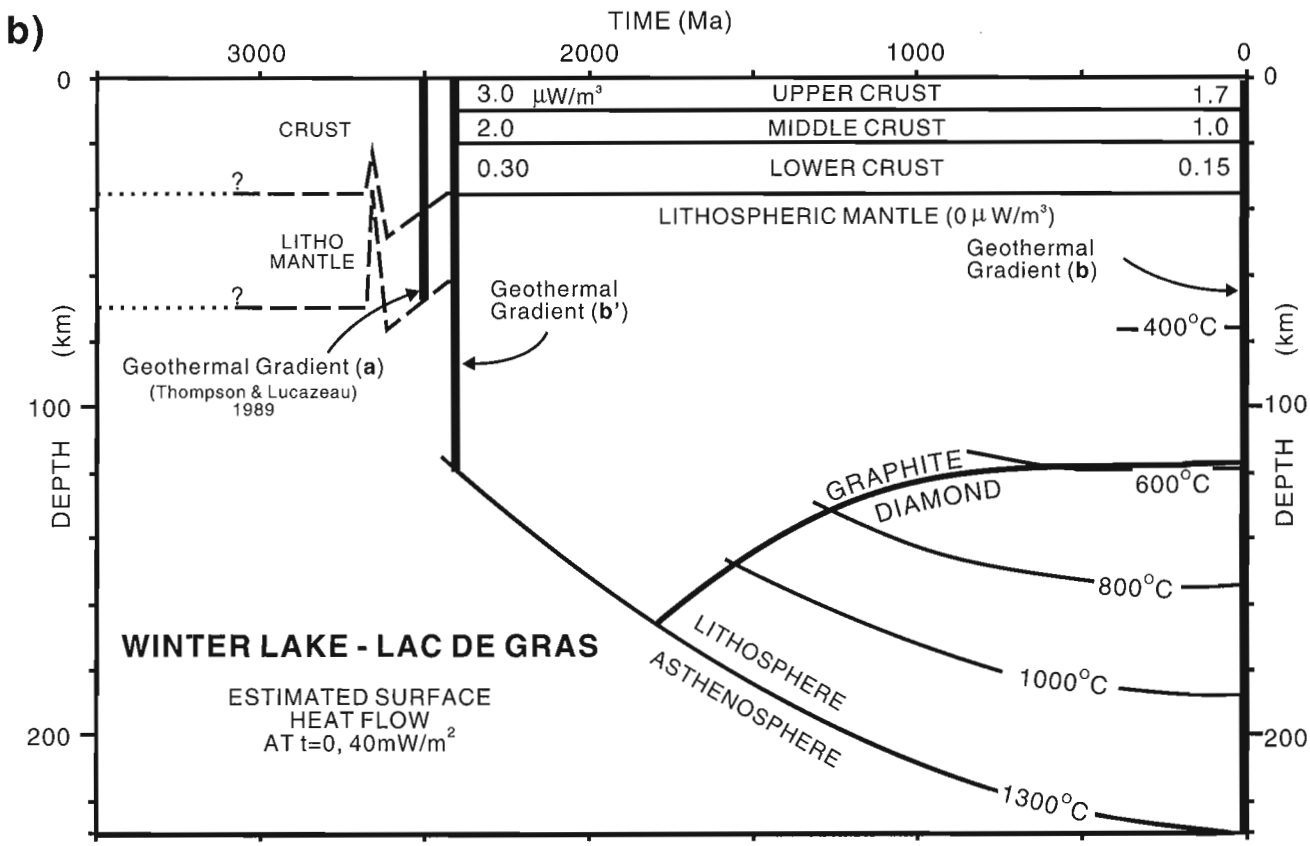
b)
TIME (Ma)
3000
2000
1000
0
3.0 μW/m³
UPPER CRUST
1.7
2.0
MIDDLE CRUST
1.0
0.30
LOWER CRUST
0.15
LITHOSPHERIC MANTLE (0 μ W/m³)
CRUST
LITHO MANTLE
Geothermal Gradient (b)
Geothermal Gradient (b')
Geothermal Gradient (a)
(Thompson & Lucazeau) 1989
400°C
600°C
800°C
1000°C
1300°C
GRAPHITE
DIAMOND
LITHOSPHERE
ASTHENOSPHERE
WINTER LAKE - LAC DE GRAS
ESTIMATED SURFACE HEAT FLOW AT t=0, 40mW/m²
DEPTH (km)
0
100
200

than that west of Yellowknife or that in the west half of the Winter Lake-Lac de Gras area. Different average heat production within zones that are more than 100 km wide, are more likely to have an effect on lithospheric thickness than are smaller scale variations present within the upper crust of a zone (e.g. column b, Fig. 2). If, as predicted by the model, such broad zones of high crustal heat production correspond to thinner lithosphere, the probability of a Cretaceous kimberlite picking up diamonds on its way through the Slave lithosphere may not have been everywhere the same.

2400 Ma before present

Geothermal gradients **b'** and **c'** calculated for 2400 Ma (Fig. 2, 3) correspond to gradients **b** and **c** at the present time. The only differences are caused by the calculated higher radiogenic heat production at that time due to the greater amounts of U, Th, and K present 2400 Ma ago. Related increases in surface heat flow and in derived mantle heat flow are indicated in Table 2. We assume, using simple models of thermal conduction in the crust and lithosphere, that uplift and erosion related to ca. 2.6 Ga Archean orogenesis had ceased 2400 Ma ago (Thompson, 1989) and that the present erosion surface is approximately the same as it was then. That is, burial of the present erosion surface beneath younger sedimentary cover (subsequently removed) was not more than one or two kilometres (Grotzinger and Royden, 1990; Nassichuk and McIntyre, 1995). Furthermore, we assume that Proterozoic orogenic events around the margins of the craton (McGlynn and Henderson, 1972) had little impact on the thermal regime in the central Slave Province. Any thermal effects associated with the diabase dyke swarms that intruded the Slave craton between 2.27 and 1.23 Ga (LeCheminant, 1994), are interpreted to be localized on the craton margins. Going back in time, as radiogenic heat production and hence, surface heat flow, increase, geothermal gradients for both areas are higher (Fig. 3, Table 2). Eventually, the calculated gradients for each area reach asthenospheric temperatures (1300°C for this model) without crossing the diamond stability field. The time at which this occurs is the maximum age for diamond growth in the model lithosphere.

Depth-time diagrams (Fig. 4) show the time dependence of lithospheric growth over 2400 Ma based on our proposed model for thermal evolution of the lithosphere. The model results are very sensitive to crustal heat flow and heat production. This is demonstrated by comparing the Yellowknife locality where upper crustal heat production increases from 2.3 to 4.2 $\mu W/m^3$ (Fig. 4a) with the Winter Lake-Lac de Gras area (1.7 to 3.0 $\mu W/m^3$, Fig. 4b). Surface heat flows of 50 and 40 mW/m^2, increase to 91 and 73 mW/m^2, respectively, 2400 Ma ago. In both cases, the increase in radiogenic heat production is sufficient to cause the model lithosphere to thin by more than 50 per cent. To the extent that the assumptions on which the modelling is based are valid, the results have a bearing on diamond stability in the lithosphere and on thickening of the lithosphere with time.

*Figure 4. Depth-time diagrams representing increasing depth to the base of the lithosphere (1300°C) as crustal radiogenic heat production decreases with time. Thermal evolution between 2700 and 2400 Ga is after Thompson (1989) and after a numerical model involving overthickening of previously-thinned crust/lithosphere (Thompson and Lucazeau, 1989). Geothermal gradients for time = 0 and time = 2400 Ma are from Figure 3. Diamond stability field after Kennedy and Kennedy (1976). **a)** Yellowknife heat flow site; **b)** Winter Lake-Lac de Gras map area.*

SUMMARY OF IMPLICATIONS

If the average crustal heat production and surface heat flow are as high as may be the case at Yellowknife (Fig. 4a), the amount of present day lithosphere within the diamond stability field is probably less than it would be at Winter Lake-Lac de Gras (Fig. 4b), thereby reducing the chance of a kimberlite picking up diamonds during ascent. Is it coincidental that many more diamond-bearing kimberlites have been reported from the Lac de Gras region? Moreover, the time at which the base of the lithosphere entered the diamond stability field occurs later where heat production is higher, and therefore the maximum age of diamond growth is younger, for example, 900 Ma (Fig. 4a) rather than 1850 Ma (Fig. 4b).

Model results 2400 Ma back in time (Fig. 3,4) show a tendency for the geothermal gradients to approach **a**, a gradient that intersects the base of the model lithosphere (1300°C), at a depth of 65 km, well before it encounters the stability field of diamond (Fig. 3). Ancient crustal geothermal gradients can be reconstructed from the metamorphic pressures and temperatures preserved in metamorphic terranes (Richardson, 1970; Thompson, 1977). Gradient **a** represents the thermal regime at 2500 Ma as derived from a kinematic numerical model of the 2.7-2.4 Ga thermal and tectonic history of the Slave Province (Thompson and Lucazeau, 1989). Gradient **a** is constrained by low-pressure/high-temperature metamorphic conditions attained during ca. 2.6 Ga orogenesis in the Slave Province (Thompson, 1989; Thompson et al., 1995). Both evidence of 2.6 Ga Archean metamorphism on the present erosion surface and the results of thermal modelling of the period 2700-2400 Ma are consistent with our results indicating that lithosphere thickness has more than doubled since the end of the Archean.

DISCUSSION

Our simple conductive model and the assumption of a thermal/mechanical definition for the base of the lithosphere suggests that the lithosphere beneath the Slave craton may have been less than half its present thickness prior to 2400 Ma ago. Thin lithosphere at 2.6 Ga is also a requirement of a lithospheric delamination hypothesis proposed by Davis et al., 1994) to explain late granite magmatism and metamorphism in the Slave. Furthermore, a lithosphere 115-150 km thick at 2.0 Ga (Fig. 4) is supported by Grotzinger and Royden (1990). They argued, on the basis of a flexural analysis of the Proterozoic Kilohigok sedimentary basin in the northern

Slave, that the elastic plate thickness at 1.96 Ga was about one tenth the present value and geothermal gradients were two to four times higher. Hoffman (1990) pointed out that these results are in direct disagreement with arguments (Jordan, 1988) supporting an Archean age for deep lithospheric roots beneath Archean cratons, and went on to suggest that models for progressive thickening of the lithosphere need consideration (e.g. Helmstaedt and Schulze, 1989).

Although age ranges of 3-1 Ga obtained from xenoliths and inclusions in diamonds from individual kimberlite pipes have been interpreted as evidence of alteration of a very old root (e.g. Richardson et al., 1993; Carlson et al., 1994; Pearson et al., 1995), they may also be consistent with progressive thickening of the lithosphere. Our model (Fig. 4) shows lithosphere thickening at an average rate of 40-50 m/Ma from less than 100 km at the end of the Archean to 200-225 km today. This implies that the age of the lithosphere should decrease with depth, presumably as progressively younger asthenosphere cools and accretes to the lithosphere. We predict that lithospheric xenoliths and diamonds found in kimberlite pipes in the Slave Province would have a range of ages with higher pressure xenoliths more likely to be younger.

More measurements of heat production and of heat flow across the Slave Province are desperately needed to explore the possibility that lithospheric thickness is affected by variations in upper crustal heat production. This can be done relatively cheaply by using the holes drilled for exploration although specialized borehole measurement techniques must be used to combat the presence of permafrost in these northern locales (Judge, 1973).

The simple thermal model presented here is obviously not the complete solution to the complex problem of the origin of subcratonic lithosphere which is both thermally and chemically controlled. Consistency between our model results, surface geology and the results of other modelling approaches leads us to suggest, however, that crustal thermal parameters and a consideration of thermal evolution with time should be part of any comprehensive model proposed for the formation and evolution of continental lithosphere beneath Archean cratons.

ACKNOWLEDGMENTS

We would like to thank Anne Wilkinson (Terrain Sciences Division), the Analytical Chemistry Section (Mineral Resources Division), and Wanda Bentkowski (GSC Victoria) for their laboratory work and Dianne Paul (Continental Geoscience Division) and Darren Viner (Geological Information and Communications Division) for drafting the diagrams. Comments and suggestions from the critical readers Malcolm Drury, John Henderson, and Steve Lucas improved the paper significantly. Tony LeCheminant's comments on a second related paper were also very helpful here.

REFERENCES

Abbot, D.
1991: The case for accretion of the tectosphere by buoyant subduction; Geophysical Research Letters, v. 18, p. 585-588.

Anderson, D.L.
1995: Lithosphere, asthenosphere, and perisphere; Reviews of Geophysics, v. 33, p. 125-149.

Ashwal, L.D., Morgan, P., Kelley, S.A., and Percival, J.A.
1987: Heat production in an Archean crustal profile and implications for heat flow and mobilization of heat producing elements; Earth and Planetary Science Letters, v. 85, p. 439-450.

Barr, K.G.
1971: Crustal refraction experiment: Yellowknife, 1966; Journal of Geophysical Research, v. 76, p. 1929-1947.

Carlson, R.W., Shirey, S.B., Pearson, D.G., and Boyd, F.R.
1994: The mantle beneath continents; Carnegie Institution Yearbook 93, The President's Report, p. 109-117.

Darnley, A.G., Richardson, K.A., Grasty, R.L., Carson, J.M., Holman, P.B., and Charbonneau, B.W.
1986: Radioactivity map of Canada; Geological Survey of Canada, Map 1600A (1:5 000 000).

Davis, W.J., Fryer, B.J., and King, J.E.
1994: Geochemistry and evolution of Late Archean plutonism and its significance to the tectonic development of the Slave craton; Precambrian Research, v. 67, p. 207-241.

Drury, M.J.
1989: The heat flow-heat generation relationship: implications for the nature of continental crust; Tectonophysics, v. 164, p. 93-106.
1991: Heat flow in the Canadian Shield and its relation to other geophysical parameters; in Exploration of the deep continental crust, V. Cermak, and L. Rybach (ed.); Springer-Verlag, Berlin, p. 317-337.

Grand, S.P.
1987: Tomographic inversion for shear velocity beneath the North American plate; Journal of Geophysical Research, v. 92, p. 14,065-14,090.

Grotzinger, J. and Royden, L.
1990: Elastic strength of the Slave craton at 1.9 Gyr and implications for the thermal evolution of the continents; Nature, v. 347, p. 64-66.

Guillou-Frontier, L., Mareschal, J.-C., Jaupart, C., and Gariépy, C.
1994: Heat flow, gravity, and structure of the lithosphere; Trans-Hudson Orogen Transect Lithoprobe Report #38, p.58-59.

Helmstaedt, H. and Schulze, D.J.
1989: Southern African kimberlites and their mantle sample: implications for Archean tectonics and lithosphere evolution; in Kimberlites and related rocks, J. Ross (ed.); Geological Society of Australia, Special Publication 14, p. 358-368.

Henderson, J.B.
1970: Stratigraphy of the Yellowknife Supergroup, Yellowknife Bay-Prosperous Lake area, District of Mackenzie; Geological Survey of Canada, Paper 70-26, 12 p.
1981: Archean basin evolution in the Slave Province, Canada; in Plate Tectonics in the Precambrian, A. Kroner (ed.); Elsevier, Amsterdam, p. 213-35.

Hoffman, P.A.
1990: Old and young mantle roots; Nature, v. 347, p. 19-20.

Jessop, A.M.
1970: The effect of environment on divided-bar measurements; Tectonophysics, v. 10, p. 39-49.

Jessop, A.M. and Lewis, T.J.
1978: Heat flow and heat generation in the Superior Province of the Canadian Shield; Tectonophysics, v. 50, p. 55-77.

Jordan, T.H.
1988: Structure and formation of the continental tectosphere; Journal of Petrology, Special Lithosphere Issue, p. 11-37.

Judge, A.S.
1973: Geothermal measurements in northern Canada; in Geology of the Canadian Arctic, J.D. Aitken, and D.J. Glass (ed.); Geological Association of Canada-Canadian Society of Petroleum Geologists, p. 301-312.

Kennedy, C.S. and Kennedy, G.C.
1976: The equilibrium boundary between graphite and diamond; Journal of Geophysical Research, v. 81, p. 2467-2470.

Lachenbruch, A.H., Sass, A.H., and Morgan, P.
1994: Thermal regime of the southern Basin and Range Province: 2. Implications for heat flow for regional extension and metamorphic core complexes; Journal of Geophysical Research, v. 99, p. 22, 121-22, 123.

LeCheminant, A.N.
1994: Proterozoic dyke swarms, Lac de Gras and Aylmer Lake areas, District of Mackenzie, Northwest Territories; Open File 2975, scale 1:125,000.

Lewis, T.J.
1974: Heat production measurements in rocks using gamma ray spectrometry and a solid state detector; Canadian Journal of Earth Sciences, v. 11, p. 526-538.

Lewis, T.J. and Wang, K.
1992: Influence of terrain on bedrock temperatures; Paleogeography, Paleoclimatology, Paleoecology (Global and Planetary Change Section), v. 98, p. 87-100.

McGlynn, J.C.
1977: Geology of Bear-Slave Structural Provinces, District of Mackenzie; Geological Survey of Canada, Open File 445.

McGlynn, J.C. and Henderson, J.B.
1972: The Slave Province; in Variations in Tectonic Styles in Canada, R.A. Price and R.J.W. Douglas (ed.); Geological Association of Canada, Special Paper 11, p. 506-526.

Nassichuk, W.W. and McIntyre, D.J.
1995: Cretaceous and Tertiary fossils discovered in kimberlites at Lac de Gras in the Slave Province, Northwest Territories; in Current Research 1995-B; Geological Survey of Canada, p. 109-114.

Northern Miner
1993: BHP-Diamet age of kimberlite; Northern Miner, v. 29, p. 1.

Padgham, W.A.
1990: The Slave Province, an overview; in Mineral deposits of the Slave Province, Northwest Territories (Field Trip 13), W.A. Padgham and D. Atkinson (ed.); Geological Survey of Canada, Open File 2168, p. 1-40.

Pearson, D.G., Shirey, S.B., Carlson, R.W., Boyd, F.R., Pokhilenko, N.P., and Shimizu, N.
1995: Re-Os, Sm-Nd, Rb-Sr isotope evidence for thick Archean lithospheric mantle beneath the Siberian craton modified by multistage metasomatism; Geochimica et Cosmochimica, v. 59, p. 959-977.

Pell, J.
1995: Kimberlites and diamond exploration in the central Slave Province, N.W.T.; NWT Geology Division, Indian and Northern Affairs Canada, EGS 95-1 (1:500,000 scale map).

Polet, J. and Anderson, D.L.
1995: Depth extent of cratons as inferred from tomographic studies; Geology, v. 23, p. 205-208.

Pollack, H.N. and Chapman, D.S.
1977: On the regional variation of heat flow, geotherms and thickness of the lithosphere; Tectonophysics, v. 38, p. 279-296.

Richardson, S.H., Harris, J.W., and Gurney, J.J.
1993: Three generations of diamonds from old continental mantle; Nature, v. 366, p. 256-258.

Richardson, S.W.
1970: The relation between a petrogenetic grid, facies series, and the geothermal gradient in metamorphism; Fortschritte Mineralogie, v. 47, p. 65-76.

Ringwood, A.E.
1989: Constitution and evolution of the mantle; in Kimberlites and related rocks, J. Ross (ed.); Geological Society of Australia, Special Publication 14, p. 456-485.

Stein, C.A.
1995: Heat flow of the earth; in Global earth physics: A handbook of physical constants, J.J. Ahrens (ed.); American Geophysical Union, Washington, p. 144-158.

Thompson, P.H.
1977: Metamorphic P-T distributions and the geothermal gradients calculated from geophysical data; Geology, v. 5, p. 520-522.
1989: Moderate overthickening of thinned sialic crust and the origin of granitic magmatism and regional metamorphism in low-P/high-T terranes; Geology, v. 17, p. 520-523.

Thompson, P.H. and Lucazeau, F.
1989: Lithospheric thermal regimes during Archean low-pressure/high-temperature orogenesis, Slave Province, Canadian Shield; EOS Transactions , American Geophysical Union, v. 70, no. 43, p. 1321.

Thompson, P.H. and Kerswill, J.A.
1994: Preliminary geology of the Winter Lake-Lac de Gras area, District of Mackenzie, Northwest Territories; Geological Survey of Canada, Open File 2740 (revised) 1:250 000 scale.

Thompson, P.H., Ross, D., and Davidson, A.
1994: Regional geology of the Winter Lake - Lac de Gras, central Slave Province, District of Mackenzie, Northwest Territories; in Current Research 1994-C; Geological Survey of Canada, p. 1-12.

Thompson, P.H., Russell, I., Paul, D., Kerswill, J.A., and Froese, E.
1995: Regional geology and mineral potential of the Winter Lake-Lac de Gras area (76D W1/2, 86A E1/2), central Slave Province, Northwest Territories; in Current Research 1995-C; Geological Survey of Canada, p.107-119.

van Breemen, O., Davis, W.D., and King, J.E.
1992: Temporal distribution of granitoid plutonic rocks in the Archean Slave Province, northwest Canadian Shield; Canadian Journal of Earth Sciences, v. 29, p. 2186-2199.

Villeneuve, M.
1993: Preliminary geochronological results from the Winter Lake -Lac de Gras Slave Province NATMAP project, N.W.T.; in Radiogenic Age and Isotopic Studies: Report 7; Geological Survey of Canada, Paper 93-2, p. 29-38.

Whalen, J.B.
1993: Geology, petrography, and geochemistry of Appalachian granites in New Brunswick and Gaspésie, Québec; Geological Survey of Canada, Bulletin 436, 124 p.

Wyllie, P.J.
1979: Petrogenesis and the Physics of the Earth; in The Evolution of the Igneous Rocks: fiftieth anniversary, perspective, H.S. Yodder (ed.); Princeton University Press, Princeton, p. 483-520.

Geological Survey of Canada Project 870008

Diverse metavolcanic sequences and late polymictic conglomerate-associated metasedimentary rocks in the Winter Lake supracrustal belt, Slave Province, Northwest Territories[1]

R.B. Hrabi[2], M.D. Nelson[2], and H. Helmstaedt[2]
Continental Geoscience Division

Hrabi, R.B., Nelson, M.D., and Helmstaedt, H., 1995: Diverse metavolcanic sequences and late polymictic conglomerate-associated metasedimentary rocks in the Winter Lake supracrustal belt, Slave Province, Northwest Territories; in Current Research 1995-E; Geological Survey of Canada, p. 137-148.

Abstract: Mafic volcanic sequences in the Winter Lake belt have a wider range in chemical composition than previously recognized, ranging from calc-alkalic to tholeiitic basalts. Trace element geochemistry indicates that some of the volcanic rocks, including pillowed komatiitic basalts, have been contaminated by crustal material while others do not show such contamination. The differences in the chemical composition, the sequence of volcanic units, and their contact relationships on opposite sides of the belt indicate that the volcanic rocks do not form a simple stratigraphic sequence.

Polymictic conglomerates and associated sandstones near Sherpa lake post-date the mafic volcanic rocks, are deformed about upright folds, and are preserved in a steeply south-plunging structural basin that is overturned at the south closure. Map-scale "interfingering" of the conglomerate and mafic volcanic rocks is a fold repetition of these units.

Résumé : Les séquences volcaniques mafiques dans la ceinture du lac Winter présentent un éventail de composition chimique plus étendu que d'abord établi, variant de basaltes calco-alcalins à basaltes tholéiitiques. L'analyse géochimique des éléments traces indique que certaines roches volcaniques, dont des basaltes komatiitiques en coussins, ont été contaminées par du matériau crustal tandis que d'autres ne l'ont pas été. Les différences de composition chimique, la séquence d'unités volcaniques et leurs relations par contact sur les côtés opposés de la ceinture indiquent que les roches volcaniques ne forment pas une séquence stratigraphique simple.

Les conglomérats polygéniques et les grès associés près du lac Sherpa sont postérieurs aux roches volcaniques mafiques, sont déformés autour des plis droits et sont conservés dans un bassin structural fortement incliné vers le sud et qui a été renversé à la fermeture sud. L'«interdigitation» d'échelle cartographique du conglomérat et des roches volcaniques mafiques est une répétition par plissement de ces unités.

[1] Contribution to Canada-Northwest Territories Mineral Initiatives (1991-1996), an initiative under the Canada-Northwest Territories Economic Development Cooperation Agreement
[2] Department of Geological Sciences, Queen's University, Kingston, Ontario K7L 3N6

INTRODUCTION

The Winter Lake supracrustal belt is located in the east half of the Winter Lake sheet (NTS 86A), central Slave Province (Fig. 1). Mapping at 1:50 000 scale of the belt was completed during the summers of 1992 and 1993 (Hrabi et al., 1993, 1994). During the summer of 1994 the areas west of Big Bear and Sherpa lakes were mapped in detail and critical contact relationships were re-examined in several other areas. The summary map (Fig. 2) includes changes made during mapping this summer and supersedes previous maps published by this project.

Previous work in the Winter Lake area includes 1:250 000 scale regional mapping by Fraser (1969) and detailed mapping of the sedimentary rocks southwest of Newbigging Lake (Rice et al., 1990). The 1:250 000 scale mapping was undertaken concurrently with this project by Peter Thompson (GSC, Ottawa) (Thompson, 1992; Thompson et al., 1993, 1994a, b). Mike Villeneuve (GSC, Ottawa) is responsible for the U-Pb geochronology studies associated with the project. Bill Davis (GSC, Ottawa) is undertaking Nd isotopic studies of the volcanic rocks in the belt.

The supracrustal rocks have been informally subdivided into three groups (Hrabi et al., 1993, 1994): 1) older felsic to intermediate volcanic rocks with distinctly different ages of ca. 3.1 Ga (Villeneuve et al., 1993) and ca. 3.3 Ga (M.E. Villeneuve, pers. comm., 1994) at the structural base of opposite sides of the belt; 2) mafic to intermediate volcanic rocks and turbiditic sedimentary rocks similar to units of the Yellowknife Supergroup (Henderson, 1970); and 3) a sequence of polymictic conglomerate and associated sedimentary rocks interpreted to post-date the mafic volcanic and turbiditic sedimentary rocks (Fig. 2).

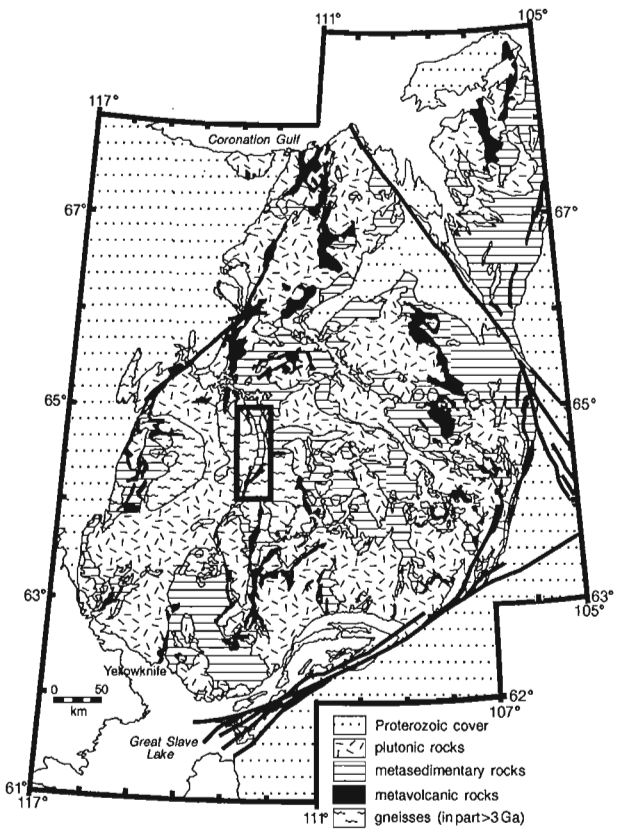

Figure 1. Location of the Winter Lake supracrustal belt (outlined) in the Slave Province. Modified after Hoffman (1989).

The purpose of this paper is to describe the differences in geochemistry and field relationships of some of the volcanic rocks in the Winter Lake belt that suggest the belt contains fragments of volcanic rock with significantly different origins. An equally important objective is to describe the geometry and sedimentology of the polymictic conglomerate-associated sedimentary rocks west of Sherpa lake to clarify the relative timing of deposition of these rocks. All rock types have been metamorphosed under greenschist or amphibolite facies conditions, but for clarity the prefix "meta" has been omitted in this paper.

MAFIC AND KOMATIITIC BASALT VOLCANIC ROCKS

Introduction

The Winter Lake belt has a broadly synformal geometry. The older felsic rocks present on both margins of the belt flank units of mafic volcanic rocks and the belt is cored by turbiditic sedimentary rocks. The apparent uniform nature of the mafic volcanic rocks that lie on either side of the belt resulted in these rocks being grouped together during previous mapping of the belt (Hrabi et al., 1993, 1994). More detailed mapping in 1994 southwest of Big Bear lake and west of Sherpa lake, together with the results of major and trace element geochemistry, suggest that the mafic volcanic rocks have a wider range in composition than was previously recognized.

Field observations

A relatively homogeneous sequence of pillowed mafic volcanic rocks is found on both sides of the belt. On the west side, this sequence forms an east-facing homocline of mafic volcanic rocks that immediately overlies the older (ca. 3.3 Ga) felsic volcanic rocks. On the east side, it is a folded sequence of mafic volcanic rocks that structurally overlies the older felsic rocks (ca. 3.1 Ga) along a highly strained contact. The belt has an overall southward-closing synformal outline north of the Snare River (Fig. 2), but the mafic volcanic sequence cannot be traced around this apparent hinge zone. Rather, the east and west limbs become parallel to the belt boundaries as the belt narrows to the south (Fig. 2), and it is probable that the eastern and western mafic sequences are not strictly correlative.

Several differences are noted between the two mafic sequences. Komatiitic basalts are found on both sides of the belt, but their stratigraphic position relative to the pillowed mafic volcanic rocks is different. On the east side, a thin unit of pillowed komatiitic basalt lies between the older felsic rocks and the mafic sequence. In contrast, the western mafic

sequence is separated from the older felsic rocks by a thin unit of iron-formation and orthoquartzite, and the komatiitic basalts form part of a diverse group of volcanic rocks, epiclastic rocks, and iron-formation structurally above the mafic rocks (Fig. 3).

The contact of the mafic sequences with the older felsic volcanic rocks also differs significantly. On the east side of the belt southeast of Sherpa lake, the ca. 3.1 Ga felsic volcanic rocks, pillowed komatiitic basalts, and the main mafic sequence are folded together around a series of large-scale F2 folds. In spite of the generally high state of strain in this area, an earlier foliation, parallel to the contact, can be traced around these folds. Furthermore, the foliation was best developed towards the contact. In contrast, along the west side of the belt southwest of Big Bear lake, layering in iron-formation and orthoquartzite lying along the upper contact of the older felsic rocks parallels the adjacent mafic sequence and these rocks are relatively undeformed at the contact with the underlying schistose felsic to intermediate volcanic rocks.

GEOCHEMISTRY

One of the most important differences between the east and west sequences of mafic rocks is their geochemical characteristics. The samples described are from the area south of Big Bear lake to the Snare River on the west side of the belt and from west of Sherpa lake south to the Snare River on the east side of the belt. In the following discussion, major elements are used to distinguish the major subdivision of rock types. Rare earth element (REE) patterns and Th-Nb-La systematics have been used in numerous studies to identify arc signatures in modern and ancient rocks (Briqueu et al., 1984; Swinden et al., 1990; Jenner et al., 1991) or to identify crustal contamination in komatiites (Jochum et al., 1991).

The geochemical composition of the mafic volcanic rocks on the east side is quite homogeneous. They range from Mg- to Fe-tholeiites (Fig. 4) when plotted on a Jensen Cation Plot (Jensen, 1976). On an extended REE plot they typically have flat to very slightly LREE-enriched profiles (Fig. 5a). Most samples have a small negative Nb-negative Th anomalies relative to La and these samples are therefore unlikely to have been contaminated by continental crustal material.

The geochemistry of the samples from the western mafic homoclinal sequence is more complicated. The samples analyzed to date from this sequence plot on a Jensen cation diagram in a dispersed region overlapping the tholeiitic basalt, tholeiitic andesite and calc-alkalic basalt fields (Fig. 4). A series of six analyses from a single vertical section through the homocline gives the best control on the vertical chemical variation of the sequence. All four samples from the base of the section are LREE-enriched and have a definite Th enrichment relative to La and the three samples analyzed for Nb have a Nb depletion relative to La (Fig. 5b). The two uppermost samples in the section have a flat REE profile or are slightly LREE-depleted and they have a negative Nb-negative Th anomaly relative to La (Fig. 5b). Of three samples from other locations in the western mafic sequence, one has characteristics similar to the samples from the base of section and two are similar to the samples from the top of the section. Additional analyses are in progress to test whether the LREE enrichment and negative Nb-positive Th anomalies are restricted to the lower part of the western mafic sequence. It is clear, however, that within this sequence some units have characteristics consistent with an arc signature (Briqueu et al., 1984; Swinden et al., 1990; Jenner et al., 1991) or with contamination by crustal material (Jochum et al., 1991).

The komatiitic basalt samples (as plotted on a Jensen cation plot, Fig. 4) from both sides of the belt are very similar, all showing LREE-enriched profiles and a strong negative Nb-positive Th anomaly relative to La (Fig. 5c). This strongly suggests that the komatiitic basalts contain a component of crustal material (Jochum et al., 1991).

BIG BEAR LAKE SECTION

The area southwest of Big Bear lake is well exposed and contains the widest variety of mafic and ultramafic rock types in the belt (Fig. 2, 6). As such, detailed mapping of the western volcanic section at 1:15 000 scale was undertaken in 1994 near Big Bear lake.

Strongly deformed quartz-biotite-plagioclase±hornblende schists identified by Fraser (1969) occur at the structural base of the section. These are interpreted to be felsic to intermediate volcanic rocks based on the common presence of monomictic quartz-phyric lapilli tuff and lapilli breccia within the unit.

A unit of sulphide iron-formation and orthoquartzite up to several metres thick is present along the upper contact of the schistose felsic section for at least 8 km. The iron-formation is generally strongly oxidized, but well-preserved nodular pyrite layers with thin chert layers were observed. The main mafic volcanic sequence, the east-facing homocline of tholeiitic to calc-alkalic basalts described previously, lies above and appears concordant to the iron-formation. The mafic sequence is up to 2 km thick, but is only 300-800 m thick in the Big Bear lake section. The pillowed rocks are intruded by fine- to medium-grained gabbroic dykes and sills.

The strain in the mafic rocks is relatively low through most of the Big Bear lake section including at the contact with the older felsic rocks. The felsic rocks, however, contain a strong foliation locally discordant to the contact, not observed in the mafic rocks. This relationship suggests that the older felsic rocks were deformed prior to the extrusion of the mafic volcanic rocks and that in this area the contact has not been significantly deformed since the extrusion of the pillowed rocks.

East of the mafic homocline is a heterogeneous group of interlayered volcanic rocks, chemical and clastic sedimentary rocks, and mafic to ultramafic intrusions. Part of this unit was mapped in detail at 1:1 000 scale where it is fault-bounded by extensions of late (Proterozoic?) faults (Hrabi et al., 1994) previously mapped to the south by Stubley (1990a, b). The sequence consists of mixed units of fine grained volcaniclastic rocks, lapilli tuffs, and serpentinized peridotites overlain by a series of thin flows of fine grained igneous rocks ranging from

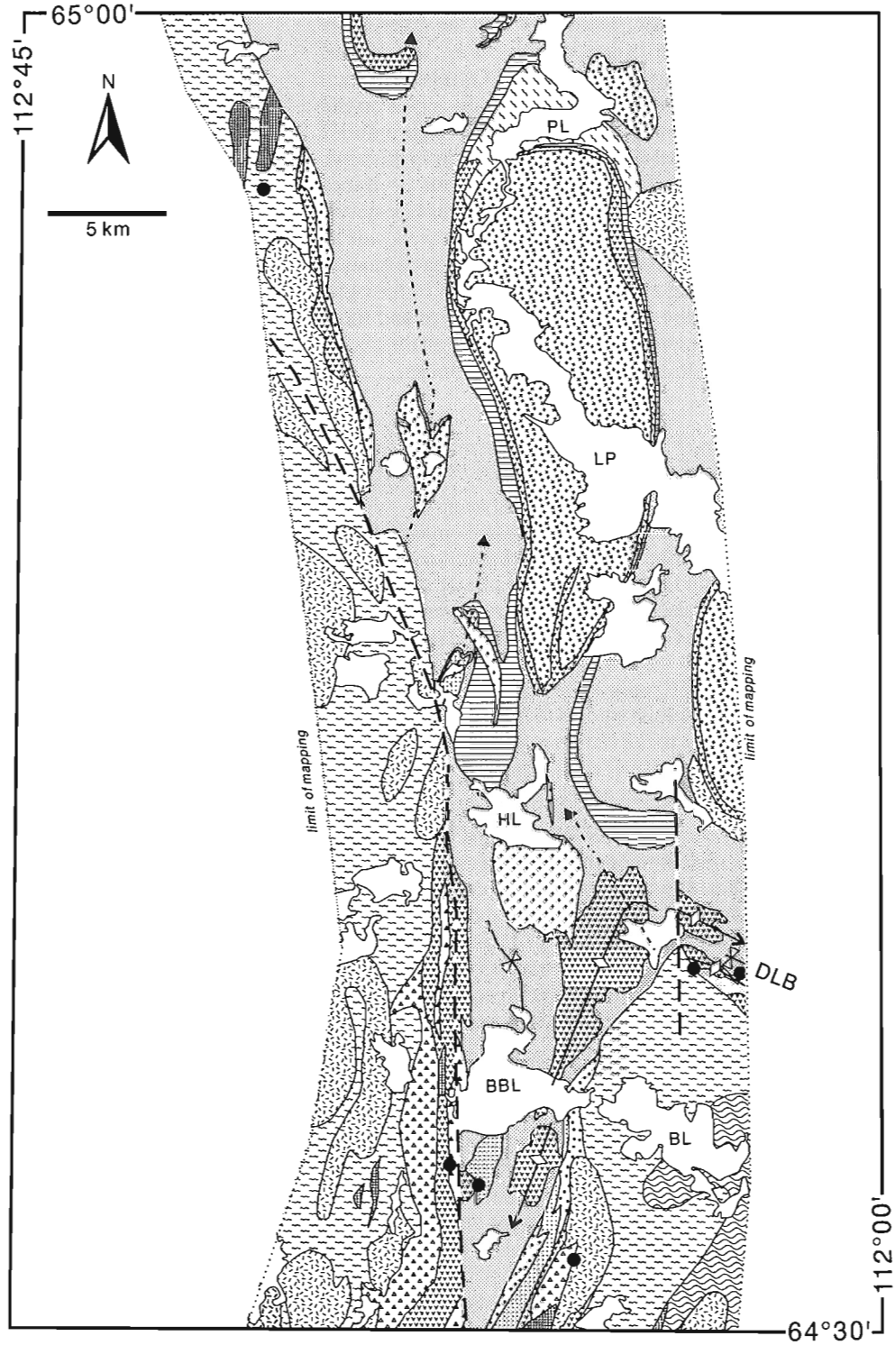

Figure 2.

Simplified geological map of the Winter Lake supracrustal belt.

BL – Beauparlant Lake,
BBL – Big Bear lake,
HL – Hopeless lake,
IL – Izabeau lake,
LP – Lake Providence,
LL – Left lake,
NL – Newbigging Lake,
PL – Point Lake,
ShL – Shallow lake,
SL – Sherpa lake,
SR – Snare River,
TL – Terminus lake.

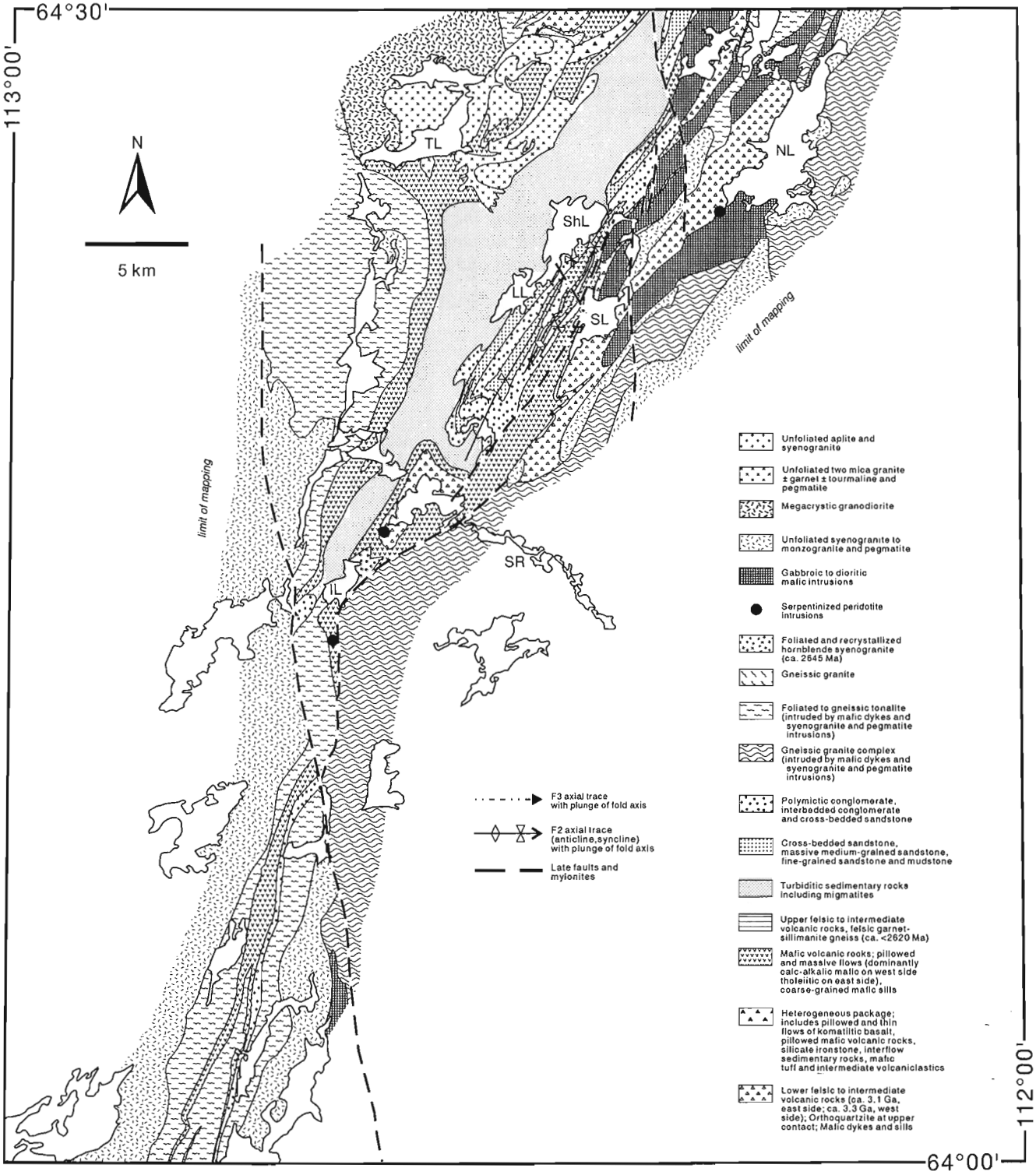

Figure 2 (cont.)

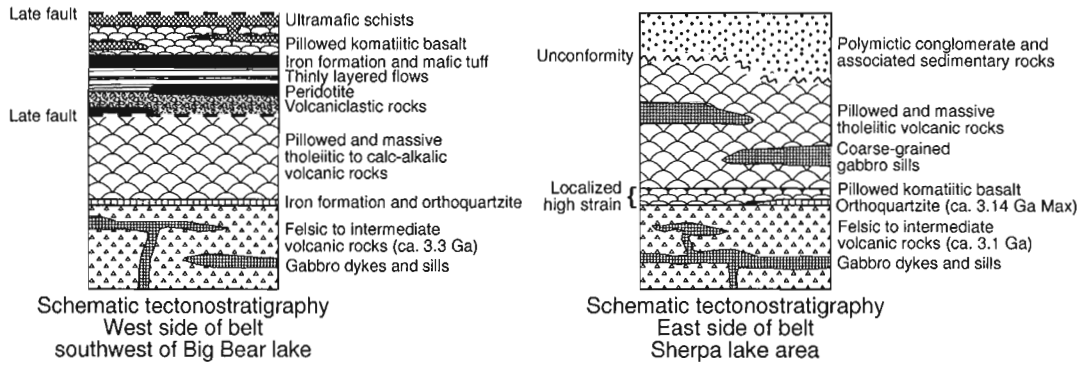

Figure 3. *Diagrammatic sections illustrating the differences in the mafic volcanic sections on the east and west sides of the supracrustal belt. Peridotites are found throughout the belt intruding most rock types and are not considered characteristic of the western section.*

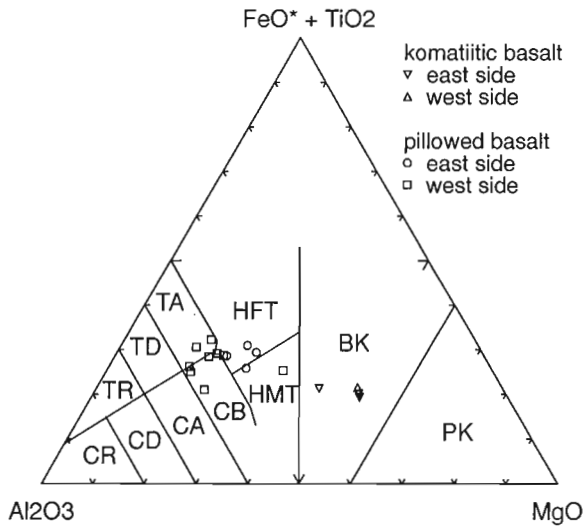

Figure 4. *Jensen Cation Plot of analyzed pillowed komatiitic basalts and pillowed basalts from the east and west sides of the belt.*

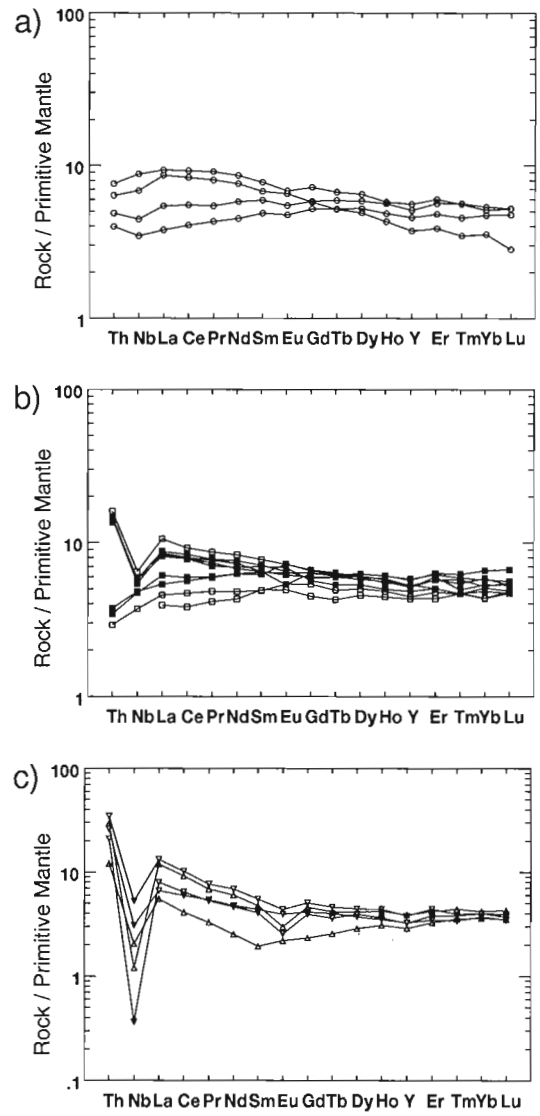

Figure 5. *Extended rare earth element spidergrams of* ***a)*** *pillowed mafic volcanic rocks, the east side of the supracrustal belt,* ***b)*** *pillowed mafic volcanic rocks, the west side of the belt, and* ***c)*** *pillowed komatiitic basalts from the east and west sides of the belt. Symbols as in Figure 4; filled squares in Figure 5b are from the single vertical section discussed in text. Primitive mantle normalizing values from Hofmann (1988).*

10 cm to 65 cm in thickness (Fig. 7a). When originally mapped at 1:50 000, these layers were thought to represent sheeted dykes. Stripping and washing of outcrops revealed units of silicate facies iron-formation (Fig. 7b) overlying the thin flows. The flows and iron-formation are folded, resulting locally in the near orthogonal orientation of the layered units to the regional strike of the mafic sequence that had been observed during regional mapping. Other evidence gathered during the detailed mapping to support the interpretation of these rocks as thin flows includes the presence of interlayered mafic tuffs/interflow sediments with the layered rocks (Fig. 7c, 7d) and the along-strike continuation of similar thin layered units with associated layers of iron-formation.

The iron-formation and mafic tuff units are intruded by medium grained black gabbros. These units are overlain by a thick sequence of fine grained cummingtonite- and/or tremolite-bearing volcanic rock, similar in appearance to the komatiitic basalts interlayered with strongly foliated, medium- to coarse-grained ultramafic schists of variable composition. In one outcrop of cordierite-anthophyllite-tremolite schist, poorly defined features resembling relict spinifex texture were observed (Fig. 8). Slabbed sections show that the features have irregular boundaries, and thin sections show the radiating features are composed of Mg-rich chlorite. While it appears that these could simply be alteration features, the possibility remains that some of the coarser ultramafic schists represent true komatiitic flows.

The contact relationships of the fine grained cummingtonite-tremolite-bearing rocks and the ultramafic schists are highly variable. In places, the schists can be mapped as both cross-cutting and forming concordant layers within coherent layers of pillowed flows. Elsewhere, variably-sized, isolated lozenges of pillowed flows were found within the coarser grained schists. Units consisting of thin, discontinuous layers of the fine grained volcanic rocks interfingered with strongly foliated schist are common. Close to the late fault on the east side of the detailed section the rocks are all schists. The two rock types are thought to represent two distinct protoliths. The coarser grained ultramafic schists may represent Mg-rich intrusions (+flows?) into komatiitic basalt flows. Partitioning

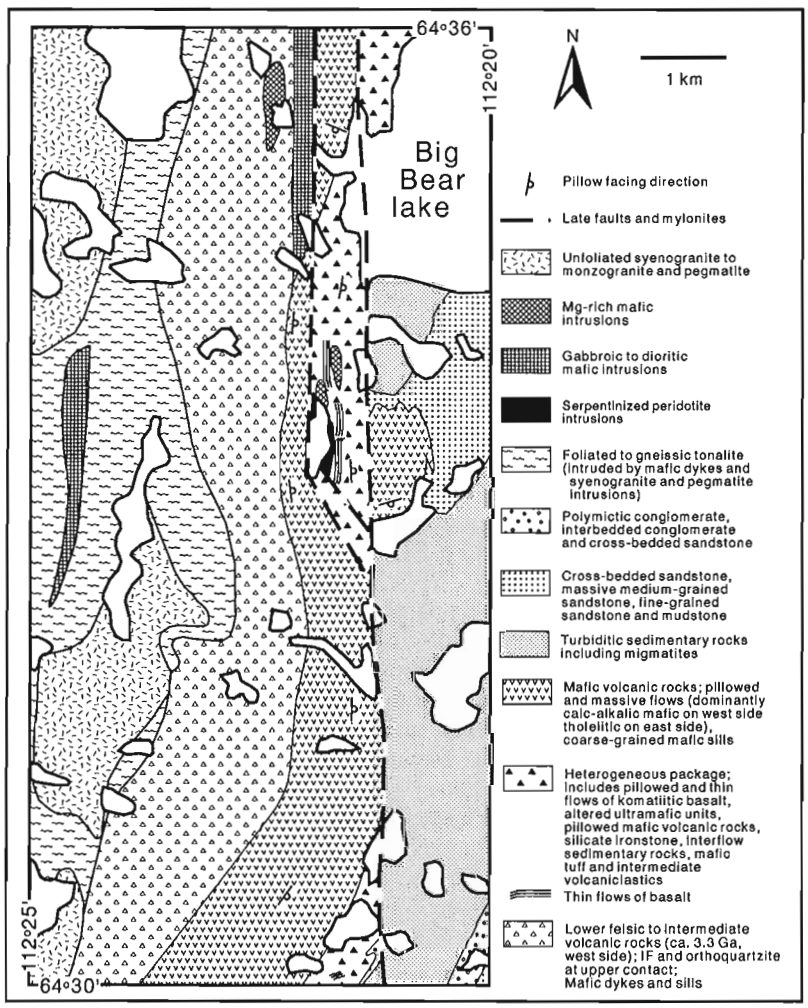

Figure 6.

Map of the supracrustal belt southwest of Big Bear lake.

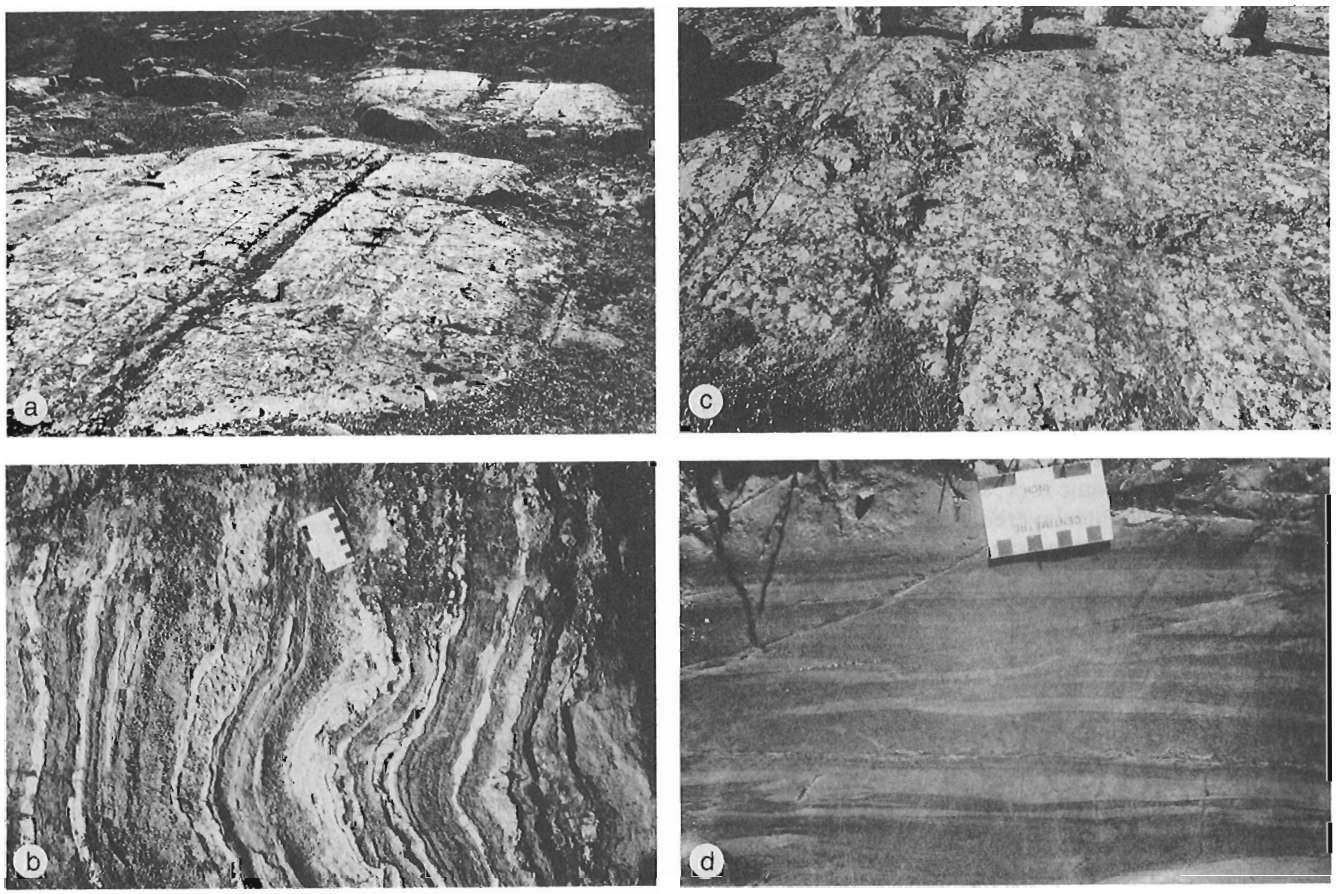

Figure 7. Representative units in the heterogeneous group of volcanic and sedimentary rocks. ***a****) Thin flows striking 070° with no interflow sediments between flows.* ***b****) Silicate facies iron-formation to east of thin flow unit.* ***c****) Interlayered flows and interflow sedimentary layers (uneven weathering layers).* ***d****) Close-up of one of layers of interflow sediment after stripping and washing of the outcrop.*

Figure 8. Radiating features resembling spinifex texture in a strongly altered rock that now contains a cordierite-anthophyllite-tremolite assemblage.

of strain during strong deformation could have resulted in the dismemberment of many of the flows and the development of the stronger fabric in the schists.

LATE COARSE SEDIMENTARY SEQUENCE

Mapping of the polymictic conglomerates and associated sandstones west of Sherpa lake (Sherpa lake sequence) (Fig. 2, 9) was undertaken to resolve controversy on the relative age and stratigraphic significance of these deposits. Rice et al. (1990) suggested that the entire Sherpa lake sequence is east facing and stratigraphically overlies the turbiditic sedimentary rocks to the west, based on younging indicators in the western part of the sequence. Mafic volcanic layers are interfingered with the sedimentary rocks and, in the absence of observed facing directions in these rocks, the mafic volcanic rocks were interpreted to be stratigraphically interlayered with the conglomerate sequence (Rice et al., 1990). Thompson et al. (1993, 1994a, b) concurred with this interpretation based on the apparent interlayering of the units and the concordant structures and similar metamorphic grade in the coarse sedimentary rocks and the surrounding units.

In contrast, Hrabi et al. (1993, 1994) interpreted the conglomerate-sandstone sequence to have been deposited unconformably on the volcanic-turbidite sequences. This interpretation was based on the very coarse and polymictic nature of the conglomerates, the recognition of folds in the underlying turbidites that were not recognized in the conglomerates and sandstones, and on local angular unconformable map relationships in which conglomerates overlap both turbiditic sedimentary rocks and the mafic volcanic rocks.

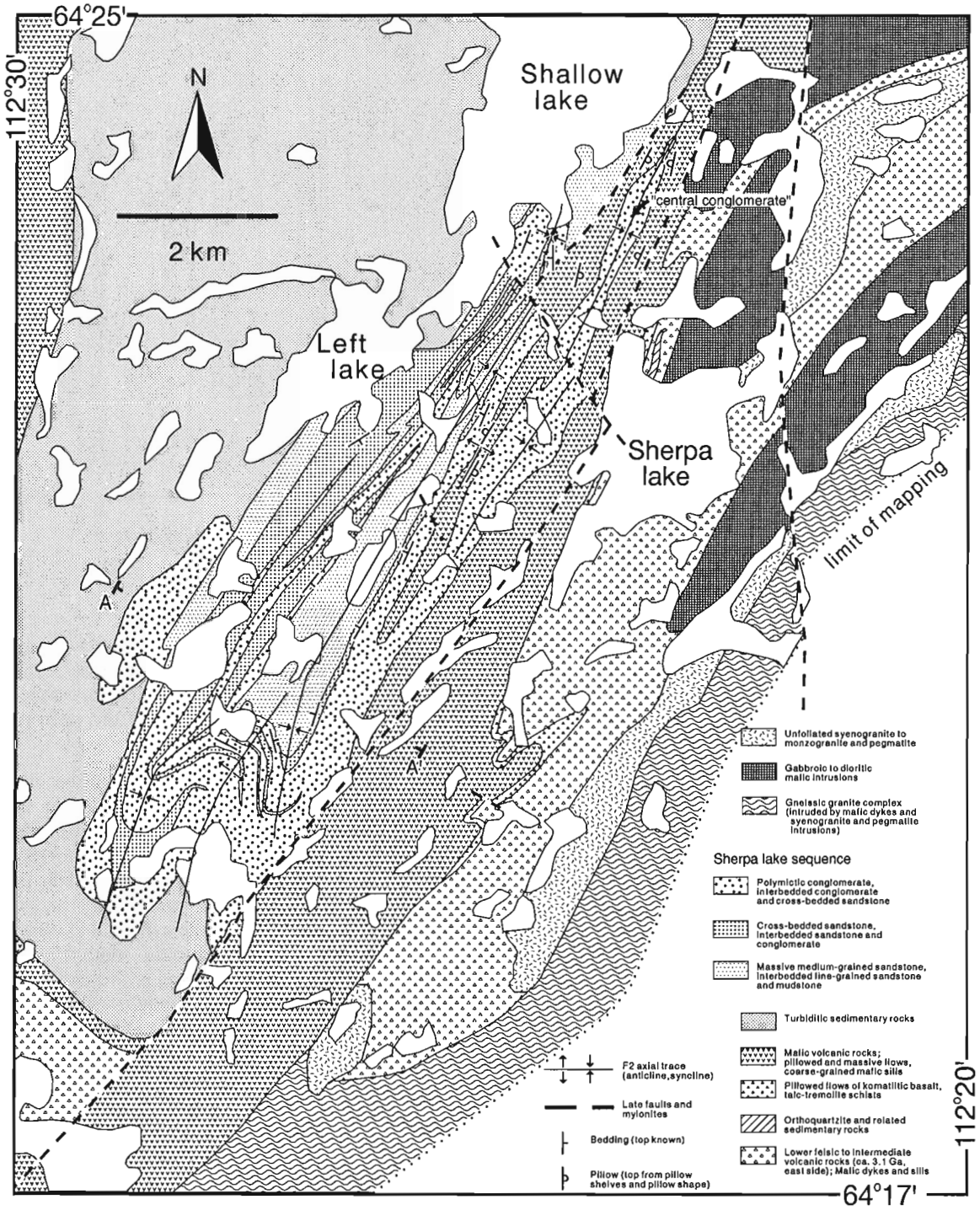

Figure 9. Map of the conglomerate associated sedimentary rocks west of Sherpa lake.

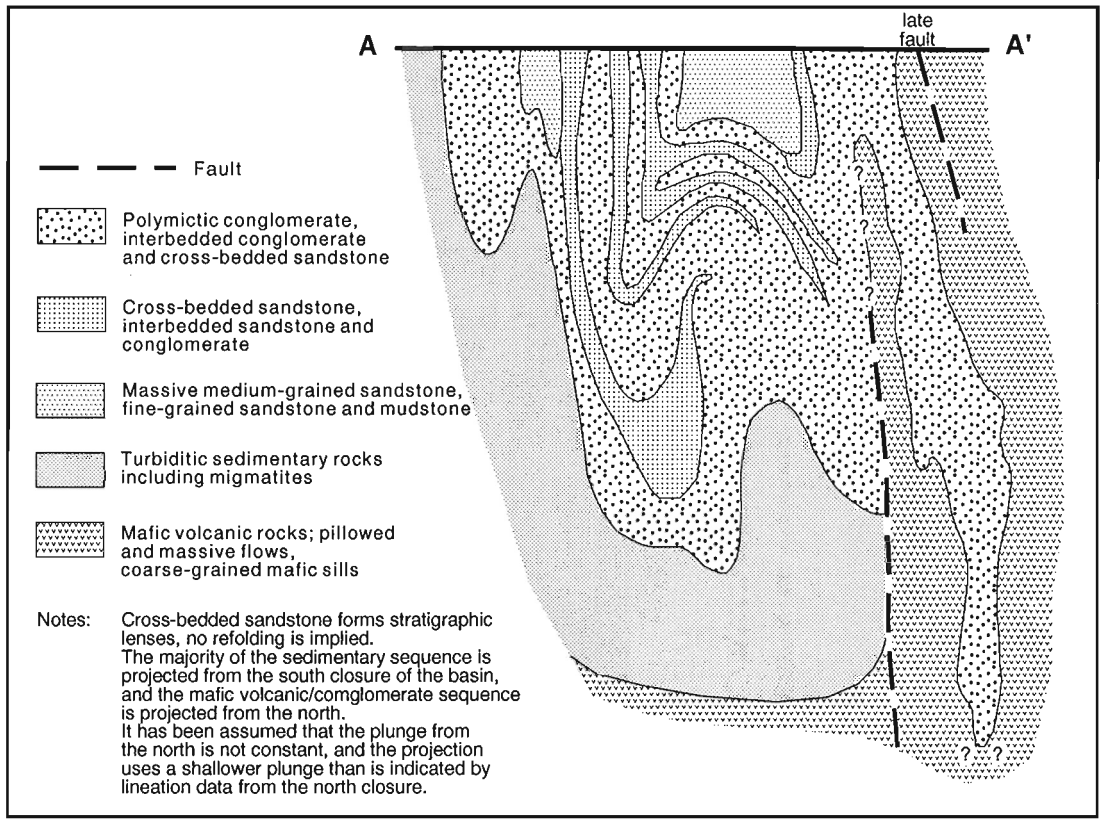

Figure 10. *Composite schematic section west of the Sherpa lake based on plunge projections from the south and north ends of the basin.*

Geometry

During previous mapping (Hrabi et al., 1993), it was recognized that the Sherpa lake sequence clearly closes in a synform north of the Snare River but this closure could not be traced northward due to the lack of west-facing top directions. Rare facing reversals did suggest, however, that the section to the north is not homoclinal. Part of the problem in determining the geometry of the rocks west of Sherpa lake was the lack of reliable facing indicators in the apparently "interlayered" mafic volcanic rocks and conglomerates ("central conglomerate") that occur east of the main part of the Sherpa lake sequence (Fig. 9). Considerable time this summer was spent cleaning outcrops and searching for unambiguous facing directions, usually in the form of consistent pillow shelves and pillow shapes.

Within the mafic flows around the northern closure of the central conglomerate, several unambiguous facing directions were found to indicate that these flows face inward toward the conglomerate that occupies the core of a syncline between two limbs of mafic rocks. At each contact (or "base") of the conglomerate, small-scale unconformable contacts cutting across mafic units can be observed. In addition, the conglomerate has a symmetrical distribution of units between the mafic limbs. The conglomerate is dominated by mafic clasts and has a mafic matrix composition at both contacts with the mafic flows. Towards the centre of the conglomerate unit this changes to a polymictic composition with a feldspathic arenite matrix. Within the conglomerate, facing indicators are rarely observed, but a few, thin, channel-shaped units of sandstone were found that support the interpretation of a synclinal geometry.

In the Sherpa lake sequence west of the infolded mafic volcanic rocks, most top directions face east. However, by concentrating in the area close to the mafic volcanic rocks, several well-preserved primary structures (crossbedding, normal grading, and channel shapes) reveal the presence of a narrow west-facing limb of sedimentary rocks. This limb represents the extension of the synclinal closure of the conglomerate sequence mapped to the south (Fig. 9). A pillow shelf in an outcrop of west-facing pillows was found near the west edge of the west finger of mafic volcanic rocks located midway between Sherpa lake and Left lake (Fig. 9). Although based on very limited data, we suggest that an anticlinal axial trace passes through the western finger of mafic volcanics. Units within the coarse grained sedimentary sequence are truncated at this contact and a well-developed schistosity is present along this contact. Together these observations suggest that the sedimentary sequence and mafic volcanics have been folded into an asymmetric antiform with a thin, west-facing limb, but a fault along or near the sedimentary-mafic contact modifies the fold and may be partly responsible for the thinness of the west-facing limb.

The Sherpa lake sequence is deformed by upright F_2 folds and occupies a canoe-shaped structural basin that is steeply overturned at its southern closure. A composite schematic section across the sequence based on plunge projections from the north and south closures of the basin is shown in Figure 10. The geometry of the mafic volcanic-sedimentary domain west of Sherpa lake clearly shows that the conglomerates are not synvolcanic. The coarse sedimentary rocks post-date the mafic volcanic rocks, but the absolute age difference between these different rock units has not yet been determined.

DISCUSSION

Volcanic sequences

Detailed mapping and the results of geochemical analyses indicate that the mafic volcanic sequences in the Winter Lake supracrustal belt have a wider range in composition than previously recognized. The trace element composition of the komatiitic basalts analyzed to date from both sides of the belt indicate that they have been contaminated by a component of pre-existing crustal material. In contrast, the mafic volcanic sequences have distinct geochemical signatures. On the east side of the belt, the tholeiitic mafic volcanic sequence have a MORB-like trace element pattern suggesting neither crustal contamination nor eruption in an arc setting. In the homocline on the west side of the belt, the geochemical nature of tholeiitic to calc-alkalic basaltic rocks changes from the bottom to the top of the section. At their base, the mafic rocks have negative Nb-positive Th anomalies and enriched LREE suggesting that these samples could also have been erupted through pre-existing crustal material. However, the trace element patterns of samples from the top of this section suggest little or no crustal contamination.

Consideration of the geochemical data in the context of the present distribution and contact relationships of the volcanic sequences poses several interesting problems. On the west side of the belt south of Big Bear lake, the mafic rocks are conformable with the iron-formation and orthoquartzites, the underlying older felsic volcanic rocks locally have foliation patterns discordant with the contact and there are preserved sections of the contact along which the overlying mafic rocks are not highly strained. These observations are consistent with the felsic rocks having been deformed prior to deposition of the mafic sequence above a disconformable contact with no significant post-mafic deposition structural reactivation along the contact. While the "crustally contaminated" geochemistry of the lower mafic sequence is consistent with such an interpretation, it is unclear why the upper part of the section is apparently not "contaminated".

The komatiitic basalts on the west side of the belt also have been influenced by pre-existing crustal material but overlie the top of the tholeiitic to calc-alkalic mafic homocline that has not been influenced by such material. The contact between these sequences, where not defined by late faults, is marked by a distinct topographic lineament and increased alteration. As the contact itself is generally covered, structural data suggesting a fault are not available. Although the difference in crustal contamination may be a function of the higher thermal erosive ability of the hotter komatiitic lavas, the observations are also consistent with a structural juxtaposition of the volcanic sequences.

On the east side of the belt, tholeiitic volcanic rocks, pillowed komatiitic basalts and older felsic volcanic rocks are separated by highly strained contacts which have been subsequently deformed during the first folding event recognized in all the supracrustal rocks (Hrabi et al., 1993). Whereas the komatiitic basalts directly above the older felsic volcanic rocks indicate contamination with older crustal material, the tholeiitic volcanic rocks do not. If the data are not simply reflecting the increased thermal erosive ability of the komatiitic basalt lavas, these observations are consistent with the tholeiitic rocks having formed in a different tectonic setting and subsequently faulted against the komatiites and older felsic rocks. Continued structural and geochemical analysis may help to answer some of these problems.

Sherpa lake sequence

Many uncertainties concerning the geometry of the Sherpa lake sequence and its relationship with the adjacent supracrustal rocks have been resolved. The apparent interlayering of the polymictic conglomerate with mafic volcanic rocks results from folding of the conglomerates and underlying mafic rocks. Facing directions in the pillowed volcanic rock and erosional features at the base of the conglomerates in the syncline show that these conglomerates post-date the adjacent mafic volcanic rocks.

On a map scale, the Sherpa lake sequence unconformably cuts through the adjacent turbiditic sedimentary rocks down to the mafic rocks and does not record the earliest folds observed in the underlying turbiditic sequence. This suggests that the conglomerate sequence not only post-dates the mafic volcanism but is significantly younger that the other supracrustal rocks. The absolute timing of deposition for these rocks, however, is still uncertain. U-Pb dating of detrital zircons and individual clasts has not established a young (i.e. <2605 Ma) depositional age as in the Jackson Lake Formation in the Yellowknife greenstone belt (Isachsen and Bowring, 1993) or the Kaycee conglomerates in the Anialik River belt (Villeneuve et al., 1993). In the Winter Lake belt, dating of detrital clasts and cross-cutting dykes so far has constrained the deposition of the group to between 2689 Ma and 2548 Ma.

A better bracket of the depositional age of the Sherpa lake sequence continues to be an important objective of the project. Structural analysis suggests that the conglomerates were deposited after a folding event recorded in the turbiditic sedimentary rocks but prior to two other major folding events (Hrabi et al., 1993). In addition, the conglomerate sequence has a similar metamorphic grade as the surrounding supracrustal rocks (Thompson et al., 1994b). A better defined age for the deposition of the conglomerates will therefore help to put absolute limits on the timing of the different deformation events and metamorphism in the Winter Lake supracrustal belt.

ACKNOWLEDGMENTS

Craig Nicholson provided excellent expediting services throughout the summer. Logistical support provided by Monopros Ltd. was much appreciated. Bill Davis, Peter Thompson, and Janet King each provided stimulating discussion in the field. A field visit by Warren Hamilton was particularly useful, and it was he who pointed out the distinctive textures in the ultramafic schists and, prior to our detailed mapping, suggested the layered units might be thin flows. The U-Pb dating completed by Mike Villeneuve has made a vital contribution to the understanding of the supracrustal belt. Peter Thompson, Janet King, Mike Villeneuve, Bill Davis, and Rob Harrap provided beneficial comments or reviews of this manuscript.

REFERENCES

Briqueu, L., Bougault, H., and Joron, J.L.
1984: Quantification of Nb, Ta, Ti and V anomalies in magmas associated with subduction zones: petrogenetic implications; Earth and Planetary Science Letters, v. 68, p. 297-308.

Fraser, J.A.
1969: Geology, Winter Lake, District of Mackenzie; Geological Survey of Canada, Map 1219A, scale 1:253 440.

Henderson, J.B.
1970: Stratigraphy of the Yellowknife Supergroup, Yellowknife Bay-Prosperous Lake area, District of Mackenzie; Geological Survey of Canada, Paper 70-26, 12 p.

Hoffman, P.F.
1989: Precambrian geology and tectonic history of North America; in The Geology of North America -An Overview, (ed.) A.W. Bally and A.R. Palmer; Geological Society of America, Boulder, Colorado, Volume A, p. 447-512.

Hofmann, A.W.
1988: Chemical differentiation of the Earth: the relationship between mantle, continental crust and oceanic crust; Earth and Planetary Science Letters, v. 90, p. 297-314.

Hrabi, R.B., Grant, J.W., Godin, P.D., Helmstaedt, H., and King, J.E.
1993: Geology of the Winter Lake supracrustal belt, central Slave Province, District of Mackenzie, Northwest Territories; in Current Research, Part C; Geological Survey of Canada, Paper 93-1C, p. 71-81.

Hrabi, R.B., Grant, J.W., Berclaz, A., Duquette, D., and Villeneuve, M.E.
1994: Geology of the northern half of the Winter Lake supracrustal belt, Slave Province, Northwest Territories; in Current Research1994-C; Geological Survey of Canada, p. 13-22.

Isachsen, C.E. and Bowring, S.A.
1993: U-Pb geochronology of the Yellowknife volcanic belt: 340 Ma of crustal evolution; Geological Association of Canada, Mineralogical Association of Canada, Joint Annual Meeting, Program and Abstracts, v. 18, p. A47.

Jenner, G.A., Dunning, G.R., Malpas, J., Brown, M., and Brace, T.
1991: Bay of Islands and Little Port complexes, revisited: age, geochemical and isotopic evidence confirm suprasubduction-zone origin; Canadian Journal of Earth Sciences, v. 28, p. 1635-1652.

Jensen, L.S.
1976: A New Cation Plot for Classifying Subalkalic Volcanic Rocks; Ontario Division of Mines, Miscellaneous Paper 66, 22 p.

Jochum, K.P., Arndt, N.T., and Hofmann, A.W.
1991: Nb-Th-La in komatiites and basalts: constraints on komatiite petrogenesis and mantle evolution; Earth and Planetary Science Letters, v. 107, p. 272-289.

Rice, R.J., Long, D.G.F., Fyson, W.K., and Roscoe, S.M.
1990: Sedimentological evaluation of three Archean metaquartzite-and conglomerate-bearing sequences in the Slave province, N.W.T.; in Current Research, Part C; Geological Survey of Canada, Paper 90-1C, p. 305-322.

Stubley, M.P.
1990a: Preliminary geology of the McCrea-Drybones lakes area (parts of NTS 85 P/9 and 10); Northwest Territories Geology Division, Department of Indian Affairs and Northern Development, Map EGS 1990-4, scale 1:50 000.
1990b: Preliminary geology of the Prang Lake area (parts of NTS 85P/15 and 16); Northwest Territories Geology Division, Department of Indian Affairs and Northern Development, Map EGS 1990-19, scale 1:50 000.

Swinden, H.S., Jenner, G.A., Fryer, B.J., Hertogen, J., and Roddick, J.C.
1990: Petrogenesis and paleotectonic history of the Wild Bight Group, an Ordovician rifted island arc in central Newfoundland; Contributions to Mineralogy and Petrology, v. 105, p. 219-241.

Thompson, P.H.
1992: The Winter Lake – Lac de Gras regional mapping project, central Slave Province, District of Mackenzie, Northwest Territories; in Current Research, Part A; Geological Survey of Canada, Paper 92-1A, p. 41-46.

Thompson, P.H., Ross, D., Froese, E., Kerswill, J.A., and Peshko, M.
1993: Regional geology in the Winter Lake-Lac de Gras area, central Slave Province, District of Mackenzie, Northwest Territories; in Current Research, Part C; Geological Survey of Canada, Paper 93-1C, p. 61-70.

Thompson, P.H., Ross, D., and Davidson, A.
1994a: Regional geology of the Winter Lake – Lac de Gras area, cental Slave Province, District of Mackenzie, Northwest Territories; in Current Research 1994-C; Geological Survey of Canada, p. 1-12.

Thompson, P.H., Ross, D.A., Davidson, A., Froese, E., Kerswill, J.A., and Peshko, M.
1994b: Preliminary geology of the Winter Lake - Lac de Gras area, District of Mackenzie, N.W.T.; Geological Survey of Canada, Open File 2740, scale 1:250 000 with marginal notes.

Villeneuve, M.E., Hrabi, R.B., Jackson, V., and Relf, C.
1993: Geochronology of supracrustal sequences in the central and northern Slave Province; in Exploration Overview 1993, (ed.) S.P. Goff, Northwest Territories Geology Division, p. 53-54.

Geological Survey of Canada Project 870008-KP

Structure and stratigraphy of the Indin Lake area, western Slave Province, Northwest Territories[1]

S.J. Pehrsson, J.W. Grant[2], A.C. Dorval[3], and M. Lewis[2]
Continental Geoscience Division

Pehrsson, S.J., Grant, J.W., Dorval, A.C., and Lewis, M., 1995: Structure and stratigraphy of the Indin Lake area, western Slave Province, Northwest Territories; in Current Research 1995-E; Geological Survey of Canada, p. 149-159.

Abstract: Lithological and structural mapping has determined that the Indin Lake greenstone belt comprises a mafic through felsic volcanic assemblage conformably overlain by turbidites. Homoclinal panels of mafic volcanic rock intercalated with the turbidites have strongly tectonized contacts. The structural geometry of the belt is characterized by regional scale, F_2/F_1 interference fold patterns involving both the turbidites and volcanic rocks, which have been refolded about an upright, steeply plunging F_3 synclinorium. The occurrence of downward-facing folds and kilometre-scale overturned panels implies that this possibly imbricated structural stack was in part overturned prior to D_3 deformation.

Granulite to uppermost-amphibolite-facies gneisses of the Cotterill Lake complex, east of the greenstone belt, include tonalite orthogneiss, migmatitic paragneiss, and diatexite. Preliminary age relationships and lithological similarities suggest the complex could represent mid-crustal rocks of the greenstone belt, that have been uplifted on a Late Archean to Paleoproterozoic oblique-normal fault

Résumé : La cartographie de la lithologie et de la structure de la ceinture de roches vertes d'Indin Lake a permis d'établir qu'elle se compose d'un assemblage volcanique intermédiaire à felsique surmonté en concordance de turbidites. Les panneaux homoclinaux de roches volcaniques mafiques intercalés avec les turbidites ont des contacts fortement tectonisés. La géométrie structurale de la ceinture est caractérisée par des plis d'interférence F_2/F_1 d'échelle régionale qui ont touché tant les turbidites que les roches volcaniques, lesquelles ont été repliées autour d'un synclinorium F_3 droit, à plongement raide. La présence de plis à vergence vers le bas et de panneaux déversés d'échelle kilométrique laisse supposer qu'une partie de cet édifice structural possiblement imbriqué a été renversée avant la déformation D_3.

Les gneiss du faciès des granulites au faciès sommital des amphibolites du complexe de Cotterill Lake, à l'est de la ceinture de roches vertes, incluent des orthogneiss tonalitiques, des paragneiss migmatitiques et de la diatexite. Les liens provisoires établis entre les âges et les similarités lithologiques portent à croire que le complexe pourrait représenter des roches de la croûte intermédiaire de la ceinture de roches vertes qui ont été soulevées sur une faille oblique-normale de l'Archéen terminal au Paléoprotérozoïque.

[1] Contribution to Canada-Northwest Territories Mineral Initiatives (1991-1996), an initiative under the Canada-Northwest Territories Economic Development Cooperation Agreement.
[2] Department of Earth Science, Queen's University, Kingston, Ontario, K7L 3N6
[3] Department of Earth Science, Carleton University, Ottawa, Ontario, K1S 5B6

INTRODUCTION

The Indin Lake area, situated in the western half of the Archean Slave Province (Fig. 1), is underlain by volcanic and sedimentary rocks of the Indin Lake greenstone belt and high grade gneisses of the Cotterill Lake complex (Fortier, 1949; Tremblay et al., 1953; Stanton et al., 1954; Frith, 1993). The present mapping project has been undertaken to update the geological understanding of the area and to provide a structural context for mineral occurrences in the Indin Lake greenstone belt. Field work in 1994 focused on structural and stratigraphic relationships within the greenstone belt and characterization of the gneiss complex.

This report contains: (1) an overview of the stratigraphy of the greenstone belt, (2) a description of the high grade gneiss domain, and (3) an overview of the structure of the area. Readers are referred to Pehrsson and Beaumont-Smith (1994) for a more complete description of rock units. All rock units described are metamorphosed to lower greenschist to granulite facies. For simplicity the prefix "meta" has been omitted.

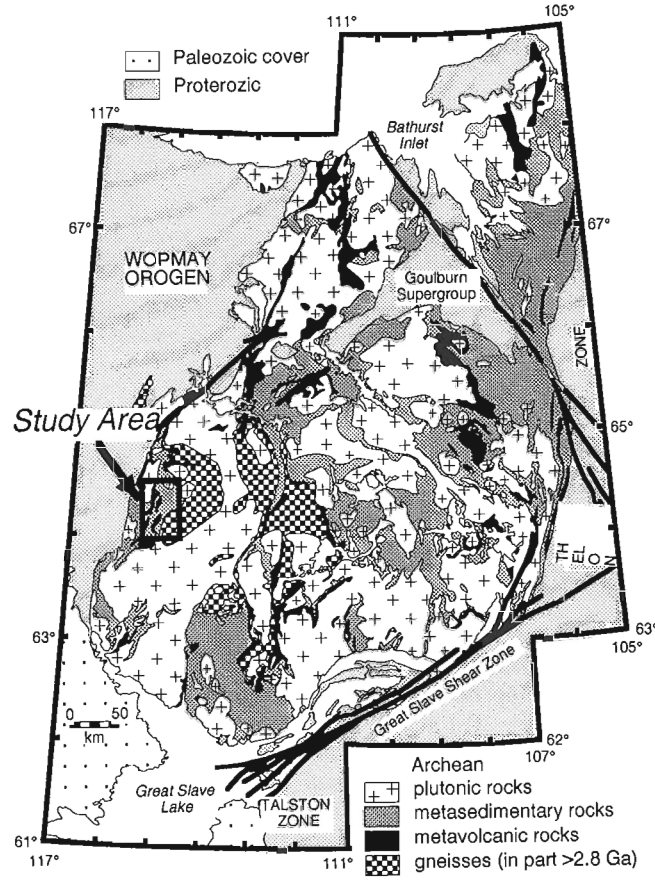

Figure 1. Location map of the study area within the Slave Province. IL=Indin Lake, PL=Point Lake.

INDIN LAKE GREENSTONE BELT

The Indin Lake greenstone belt comprises three intercalated lithostratigraphic units: i) turbiditic sedimentary rocks (hereafter referred to as turbidites), ii) Hewitt Lake assemblage volcanic and intrusive rocks, and iii) Leta Arm assemblage volcanic and intrusive rocks (Fig 2). All of these units are intruded by tonalite-granodiorite and granite plutons that have been described elsewhere (Pehrsson and Beaumont-Smith, 1994). A brief summary description of the volcanic assemblages and turbidites is given below.

Paleoproterozoic strike-slip fault

Intrusive units

- unfoliated monzo- and syenogranite, pegmatite
- foliated hbl-bio tonalite and granodiorite
- megacrystic monzogranite and porphyritic granite with numerous migmatite/gneiss inclusions

Supracrustal rocks

- turbiditic sedimentary sequences
- silicate, oxide-facies iron formation

Leta Arm assemblage

- felsic volcanic rocks including hypabyssal porphyry intrusions
- intermediate-mafic volcanic and volcaniclastic rocks, diorite sills, intruded by gabbro dykes and sills

Hewitt Lake assemblage

- felsic-intermediate volcanic and volcaniclastic rocks intruded by gabbro dykes and sills
- mafic volcanic rocks, gabbro dykes and sills

Cotterill Lake complex

- gt-cord-sill migmatite and diatexite, opx-cpx-plag migmatite
- banded tonalite orthogneiss, amphibolite, migmatitic paragneiss, foliated monzogranite
- biotite-in isograd
- cordierite-in isograd
- sillimanite-in isograd
- melt-in isograd
- granulite-facies assemblage occurrence

Legend for Figure 2.

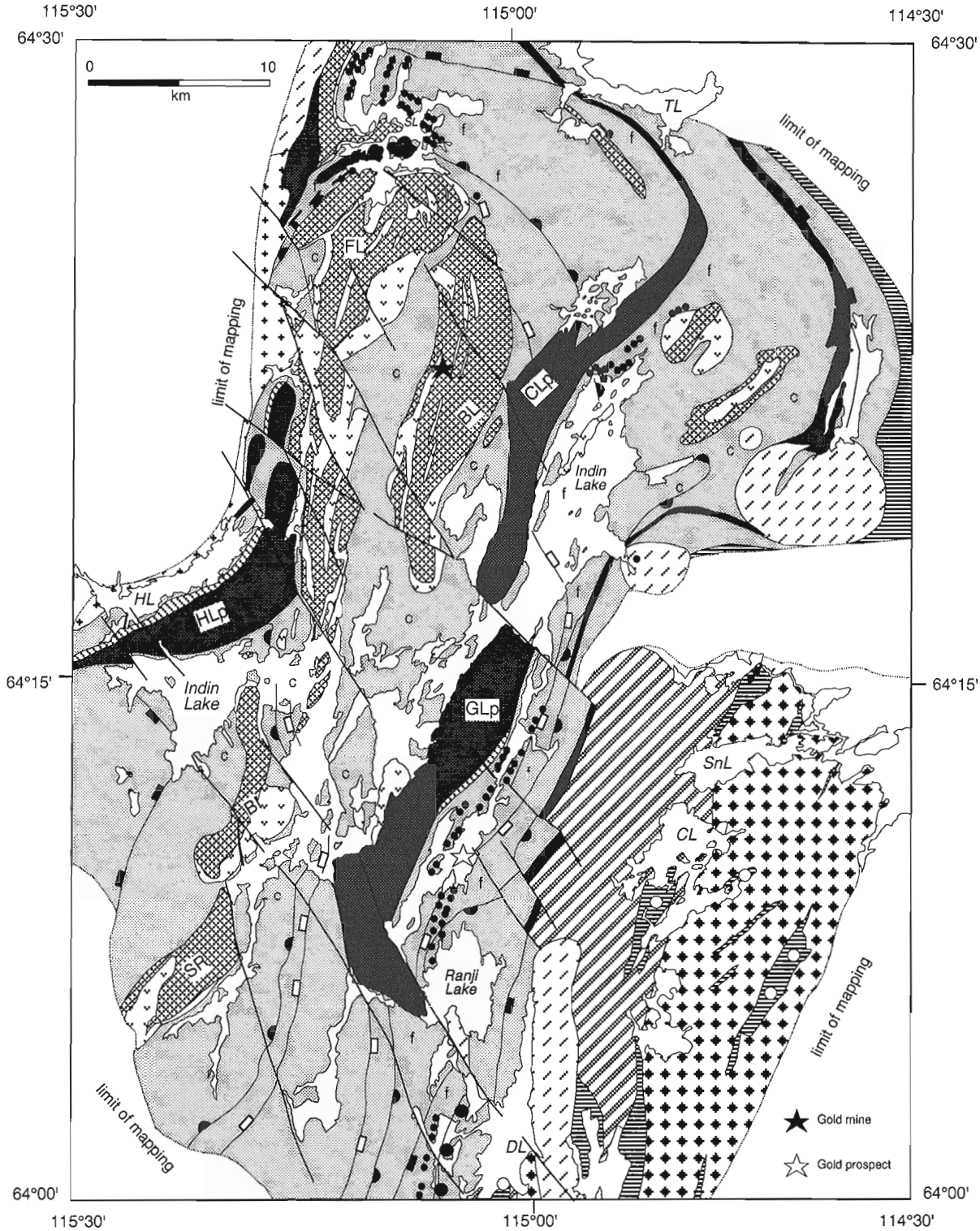

Figure 2. Simplified geological map of the Indin Lake area. 'c' and 'f' denote distribution of the coarse and fine facies turbidites. Large scale folded bodies of the Leta Arm assemblage are named as follows: BI=Burn Inlet body, BL= Baton Lake body, FL=Fortune Lake body, SR=Snare River body. Dominantly mafic volcanic rocks occur in the Hewitt Lake panel (HLp), the Gamey Lake panel (GLp) and the Chalco Lake panel (CLp). Lake abbreviations are as follows: CL-Cotterill Lake, DL-Daran Lake, HL-Hewitt Lake, SnL-Snare Lake, SL- Spider Lake, TL-Truce Lake.

Hewitt Lake assemblage

Mafic volcanic rocks of the Hewitt Lake assemblage occur in large (2-5 km thick, 10-40 km long) homoclinal panels or as thin (<1 km wide, 10-50 km long) units within the turbidite packages (Fig. 2). The assemblage comprises over 80% aphyric, pillowed and massive mafic volcanic flows, subordinate gabbro sills and minor mafic to felsic breccias and epiclastic sedimentary rocks. The mafic rocks are overlain by up to 200 m of felsic to intermediate flows and volcaniclastic rock within the Hewitt Lake and Gamey Lake panels (Fig. 2). These upper units are intruded by gabbro dykes and sills.

Leta Arm assemblage

The Leta Arm assemblage is characterized by mafic, intermediate and felsic composition volcanic and volcaniclastic rocks. The units within the assemblage are laterally discontinuous and heterogeneously distributed. Volcanic flows and fragmental units of felsic, intermediate and mafic composition are interlayered on a tens of metres to 500 m scale. Felsic to intermediate clast to matrix-supported breccias and lapilli tuffs commonly occur at the top of the Leta Arm assemblage panels. All units in this assemblage are intruded by gabbro dykes and sills, themselves deformed and metamorphosed.

Our work has shown that the Leta Arm assemblage panels are not predominantly underlain by mafic pillowed flows as previously suggested (Frith, 1993). Up to 25% of the units, formerly characterized as mafic, are composed of quartz and feldspar-phyric felsic lapilli and block sized clasts set in a chlorite, actinolite or hornblende-rich groundmass depending on metamorphic grade (Fig. 3). Cordierite-staurolite and cordierite-sericite quartzofeldspathic schists are associated with these volcaniclastic rocks. The patchy, irregular distribution of the Fe/Mg-rich groundmass at the outcrop scale, intermediate to felsic composition of the clasts, and unusual porphyroblasts suggest that these units are metamorphosed, metasomaticaly altered felsic to mafic volcanic rocks.

Figure 3. Felsic volcanic agglomerate with a recrystallized plagioclase-hornblende matrix. Patchy development of hornblende (note hbl poor areas above lens cap) can vary from 25-90% of the matrix at the outcrop scale. Lens cap is 5 cm wide. GSC 1994-734K

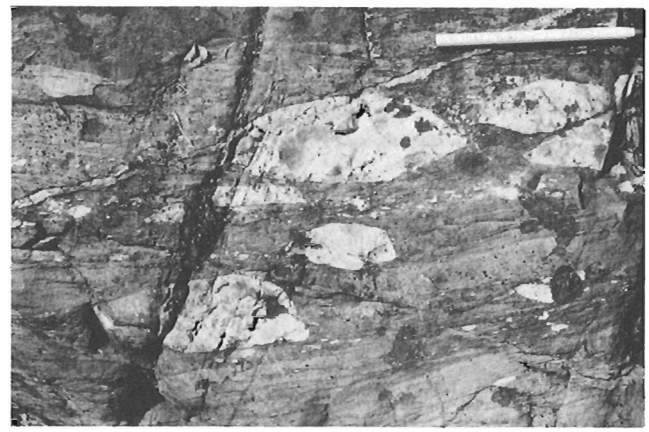

Figure 4. Felsic volcanic lapilli and blocks in bedded greywacke-siltstone. Pen is 15 cm long. GSC 1994-734J

Other felsic volcanic units

As described by Pehrsson and Beaumont-Smith (1994), felsic debris flows occur within the lower turbidite package. Additional rhyolite flows, tuffs, and debris flows have been found within this package. These comprise massive quartz-feldspar-phyric rhyolite flows with brecciated tops and associated, laterally discontinuous, beds of felsic volcanic granule to boulder conglomerate with a silt to ash matrix (Fig. 4). A preliminary age of 2670 ± 10 Ma has been obtained from one of the felsic debris flows (Pehrsson et al., 1994). The age of these felsic volcanic rocks relative to the Leta Arm assemblage is not presently known.

Turbidites

Based on work in 1993 the turbidites were subdivided into two facies (Fig. 2). The coarse facies is characterized by thick, graded greywacke to mudstone beds (15 cm to >1.5 m thick), with local massive greywacke channels greater than 10 m thick. Thin (<5m thick) beds of quartz-feldspar grit, granule conglomerate and volcanic pebble to boulder conglomerate are associated with this facies. The pebble to boulder conglomerates, dominated by rhyolite, dacite and quartz-porphyry clasts, occur as rare, discontinuous units at the Leta Arm assemblage contact and as beds within the turbidites.

The finer grained facies consists of 1-15 cm thick, laminated, graded beds of greywacke to mudstone, pyritic dark brown to black shales and 1-15 m thick units of silicate, oxide, and sulphide-facies iron-formation. At higher metamorphic grade the black shales are recognized as distinctive andalusite-garnet and staurolite-garnet schists.

Previous work suggested that the two facies were restricted to separate packages separated by the Hewitt Lake assemblage (Pehrsson and Beaumont-Smith, 1994). This year's work has revealed that the turbidite facies grade into one another laterally and vertically within both areas.

The centre of the greenstone belt predominantly comprises the coarse facies turbidites, which directly overlie the Leta Arm assemblage. The contact between the Leta Arm

assemblage and overlying turbidites is apparently conformable with consistent younging directions across the contact. The finer turbidites underlie a 2 to 6 km wide, 50 km long strip above the Hewitt Lake assemblage on the east side of the greenstone belt. The contact relationships of the turbidites with the Hewitt Lake assemblage will be discussed below.

Structure

The structure of the Indin Lake greenstone belt is dominated by fold interference patterns at all scales, involving both the turbidites and volcanic assemblages. Three regional sets of Archean structures have been observed in the turbidites, whereas two have observed in the volcanic rocks. An outline of these structural sets is presented here, along with a schematic cross-section and description of the regional structural geometry of the map area.

D_1 structures

Turbidites

The earliest recognized fabric in the turbidites, S_1, is a rare, bedding-parallel, slaty cleavage. It is defined by aligned biotite and muscovite and is commonly preserved within microlithons between the syn-thermal peak, S_2, cleavage surfaces. Throughout much of central Indin Lake it has been obliterated by strong development of the regional S_2 cleavage. At higher metamorphic grade S_1 is observed as crenulated inclusion trails within cordierite and andalusite porphyroblasts, suggesting its formation predates the metamorphic thermal peak.

Early folds of bedding, overprinted by the regional S_2 cleavage, are found in the turbidites throughout the map area. Hinges are rare and the folds are commonly recognized by changes in younging direction. They are tight to isoclinal folds with tens of metres to 100 m wavelength. The folds are moderately doubly-plunging (25-60°). The map trace of S_1 is axial planar to these folds, however, due to strong S_2 or later overprinting, S_1 has not been observed within the preserved F_1 hinges.

Recumbent isoclinal folds, with axial traces 5 to 10 km long have been identified in northeast and southwest Indin Lake (Fig. 5). The absence of an axial planar cleavage, and overprinting by S_2 cleavage leads us to infer that they are large-scale F_1 stuctures.

Volcanic rocks

The oldest recognized fabric in the volcanic rocks is a regional foliation defined by alignment of quartz and feldspar and the long axes of flattened volcanic clasts and pillows. A strong steeply plunging vesicle and clast elongation lineation is developed on S1. A spaced cleavage, concordant with S2 in the turbidites, locally overprints S1 in the volcanic rocks. At low metamorphic grade actinolite and chlorite overgrow or are aligned parallel to S1 . At higher grade garnet porphyroblasts and cummingtonite laths overgrow S1. Thermal peak minerals such as hornblende are concentrated within compositional bands defining S_1 folia but are not aligned within the plane of the foliation. These observations suggest that the metamorphic thermal peak outlasted S_1 formation in the volcanic rocks and it is therefore correlated with S_1 in the turbidites.

Regional F_1 folds of the volcanic rocks within the Leta Arm assemblage have been interpreted based on changes in facing direction and folding of S_1 in regional-scale fold interference patterns (see below).

Hewitt Lake assemblage-turbidite contacts

A penetrative S_1 cleavage, which locally obliterates primary features, occurs in the both the turbidites and volcanic rocks at the Hewitt Lake assemblage-turbidite contacts. It is subparallel to bedding in the turbidites and is associated with a greater than average concentration of bedding parallel quartz veins. These veins are boudinaged or completely pulled apart parallel to S_1. S_1 within the volcanic rocks intensifies at the contacts and an increased flattening of pillows, from equant in the horizontal plane to 10:1 or 20:1 attenuation, is observed. Unique intrafolial folds and an extreme boudinage of quartz veins are observed in the volcanic rocks. A strong, steeply north-plunging quartz-feldspar stretching lineation on S_1 is observed in both the turbidites and volcanic rocks in these zones of higher D_1 strain.

D_2 structures

The predominant fabric in the turbidites is a crenulation cleavage, S_2, which overprints the limbs and axial traces of the F_1 folds and refracts through graded beds. It is defined by aligned biotite and is both overgrown by, and wraps around, cordierite and andalusite porphyroblasts. These observations suggest that D_2 deformation was broadly coeval with the metamorphic thermal peak.

S_2 is axial planar to folds of bedding and S_1 in the turbidites that have wavelengths from tens to several hundreds of metres. Minor F_2 folds are moderate to tight with a predominant "Z" asymmetry. They have upright to slightly inclined, northeast-trending axial surfaces in central Indin Lake and are steeply north plunging (>65°). The S_2/S_0 intersection lineation is predominantly steeply north to northeast plunging. Local variations in this plunge direction are related to changes in bedding orientation around F_1 hinges. F_2 interference with east-west trending F_1 axial surfaces produces minor and meso-scale modified mushroom to heart shaped fold patterns (intermediate between type 2 and 3 of Ramsay (1967)).

A crenulation cleavage, interpreted to be S_2, is locally well-developed within the volcanic rocks and is particularly strong west of Indin Lake, and south of Spider Lake. It is axial planar to minor asymmetric folds of S_1. It is defined by aligned hornblende and actinolite and is concordant with S_2 of the turbidites, with which it is correlated. A steeply north-plunging lineation, defined by aligned and stretched feldspar and hornblende, is developed on S_2. It is subparallel to F_2 fold axes and S_2/S_0 intersection lineations.

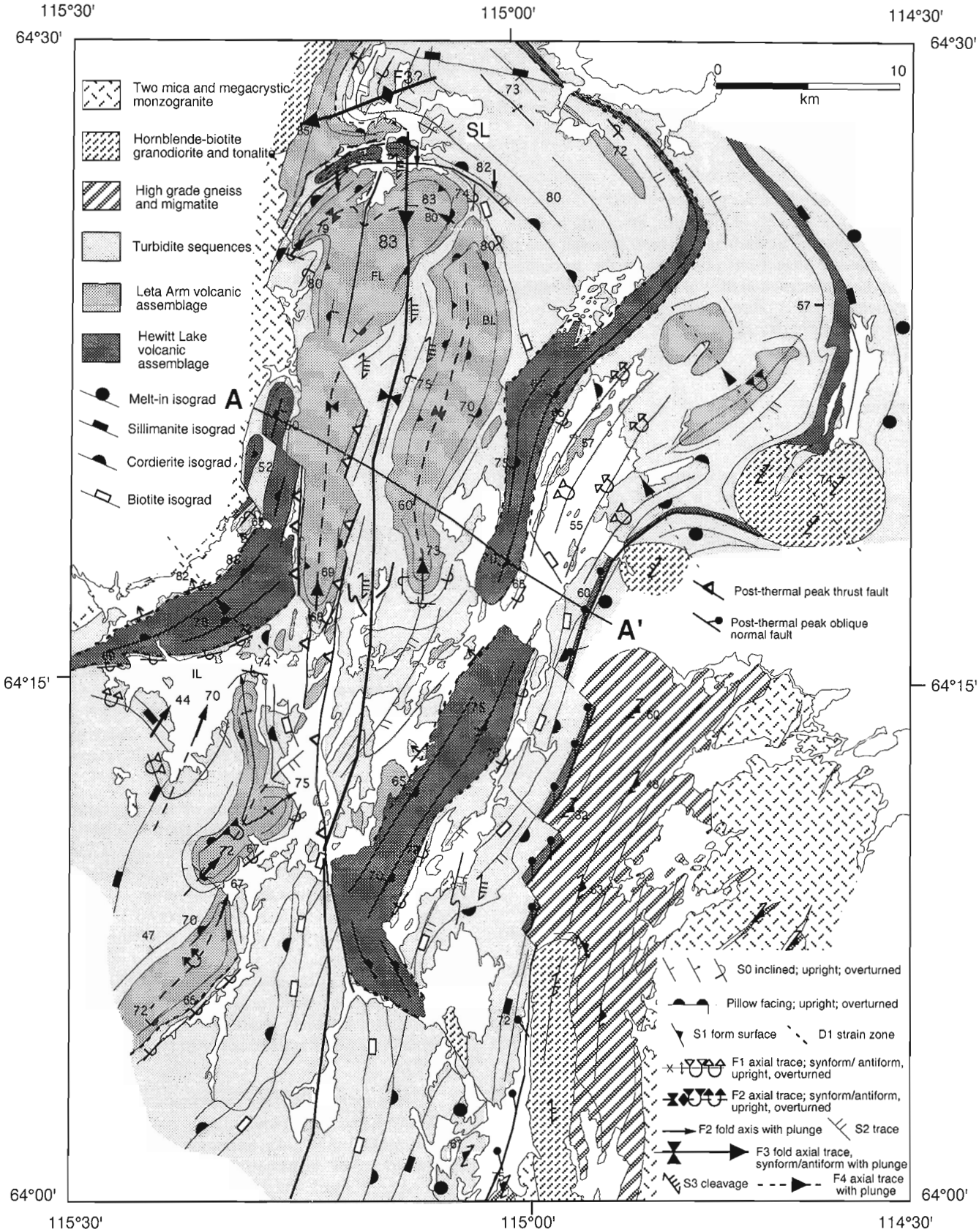

Figure 5. Simplified stratigraphy and structure of the Indin Lake area. Line A-A' is location of schematic section in Figure 7. See text for discussion. Abbreviations as in Figure 2.

The outcrop pattern of the Leta Arm volcanic assemblage defines four major, elliptical to irregular shaped bodies (Fig. 5). S1 foliation within the volcanic rocks and bedding within the turbidites are folded around these bodies. A crenulation cleavage correlated with S2 in the turbidites is axial planar to these folds, implying that they are regional scale F2 folds. The Fortune Lake and Burn Inlet bodies are doubly-plunging and mushroom to heart-shaped. They are interpreted to be regional scale interference patterns, similar to the meso-scale F2/F1 interference patterns observed in the turbidites. The southern hinges of the Baton Lake, Fortune Lake, and Burn Inlet bodies plunge steeply northward (Fig. 6A, B). L2 mineral alignment and stretching lineations and S2/S0 intersection lineations also plunge steeply north. These data imply that these folds are synforms. However, younging directions within these bodies and adjacent turbidites face outward, leading to the interpretation that the Leta Arm assemblage F2/F1 interference fold patterns are downward facing. This geometry could be due to preservation of only the overturned limb of regional-scale recumbent F1 folds within the Leta Arm assemblage. More work is required to characterize the geometry of these folds, particularly within the Baton Lake body, where the vertical plunge of the northern hinge precludes interpretation as a simple doubly-plunging F_2 synform.

D_3 and later structures

A locally developed, north-northeast trending S3 cleavage crenulates S2 in the Spider Lake and Indin Lake regions. It is preferentially developed in the pelitic portions of graded beds and is defined by aligned biotite. It wraps around cordierite and garnet porphyroblasts, suggesting that its development post-dated the metamorphic thermal-peak. S3 is axial planar to symmetric, open minor folds at Spider Lake, minor folds of "S" asymmetry east of Indin Lake and an upright large-scale fold of bedding, S_1 and S_2 (Fig. 5). These structures are interpreted to be F_3 folds. The regional F_3 fold is north- northeast trending and steeply south plunging (Fig. 6C), with a wavelength of over 10 km. S3 is clockwise to bedding on the east limb of this fold, but can only locally be differentiated from S_2 on the west limb, where it is counterclockwise to bedding. Minor F_3 fold axes and S_3/S_0 intersection lineations at Spider Lake plunge steeply to the south (Fig 6C). The cordierite-in and biotite-in regional metamorphic isograds in the turbidites are apparently folded by F_3. The south-plunging nature of this structure indicates that it is a synform. This has important implications for the overall regional geometry which will be discussed below.

A steep, northwest-trending, crenulation cleavage, S_4, (previously termed S_3, Pehrsson and Beaumont-Smith, 1994) overprints S_2, S_3, and both limbs of the major F_3 fold. It is locally the main fabric observed in turbidites on west and northeast Indin Lake. S4 is axial planar to upright, minor chevron folds and kinks and open, kilometre-scale folds of bedding, S_1, and S_2 in northeastern and western Indin Lake. These folds are interpreted to be northwest-trending, F4 cross-folds (Fig. 5). Continued study will focus on resolving the extent to which the F2/F1 interference fold patterns have been modified by F_3 and F_4 folding.

Latest Archean to Proterozoic structures

The map area is transected by two sets of latest Archean to Proterozoic faults. The first set comprises north-south trending, brittle-ductile, high angle reverse faults (Bay-Lex and Leta faults of Stanton et al., 1954). A younger set of northwest-trending brittle, strike-slip faults with sinistral map separations truncate all units in the map area. These faults are thought to be older than 1.84 Ga., as they are not known to cut the Proterozoic/Archean unconformity to the west, which

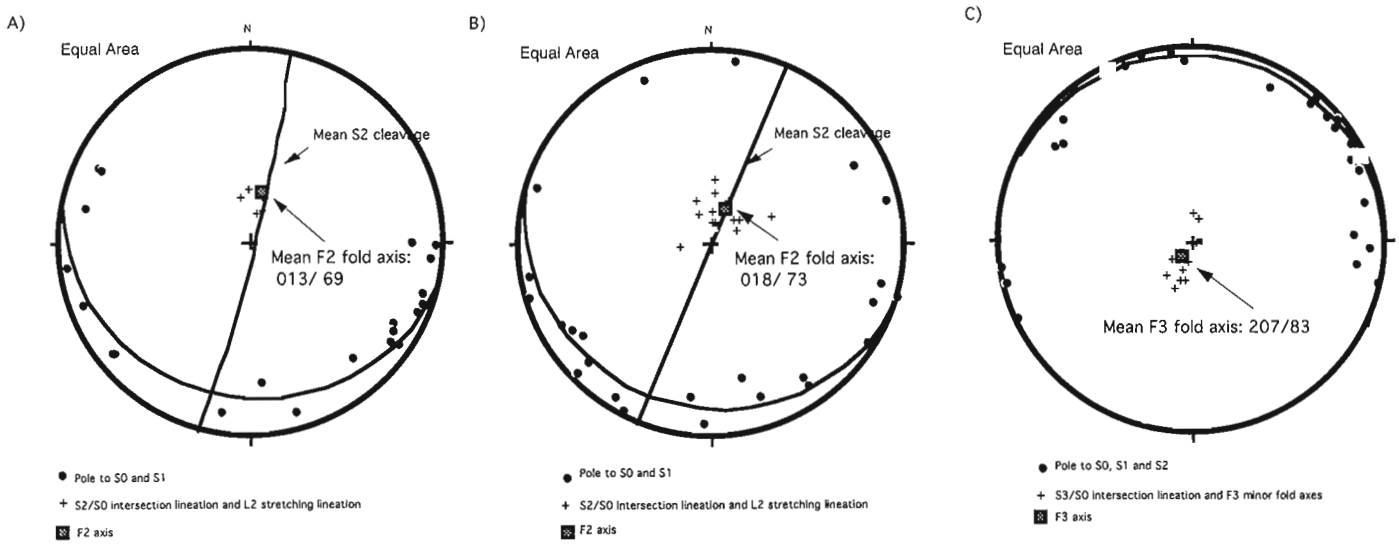

Figure 6. Equal area stereonet projections of selected data. F_2 and F_3 fold axes are defined by measured minor fold axes and stereonet fit of dispersion of S_0 and S_1 and S_2. A) southern Fortune Lake hinge, B) southern Baton Lake hinge, and C) Spider Lake area.

is offset by ca. 1.84 Ga strike-slip faults (Frith, 1993). As the north-south reverse faults are offset by the northwest faults and themselves truncate the regional metamorphic isograds, they are inferred to be Latest Archean to Paleoproterozoic in age.

Belt-scale geometry

A schematic cross-section parallel to the northwest-trending cross-folds has been constructed through the central, least deformed, part of the Indin Lake belt. (Fig. 7). It illustrates that the belt scale geometry is potentially affected by a regional F3 synform. Within the section the Leta Arm assemblage is preserved in steeply plunging, downward-facing F2 synforms, whereas the Hewitt Lake assemblage occurs as steeply overturned, homoclinal panels. Younging directions between intercalated volcanic assemblages and turbidites define a pre-F2 structural stack in which the lowest tectonostratigraphic unit of the greenstone belt is the Leta Arm assemblage and the highest unit is the turbidites stratigraphically overlying the Hewitt Lake assemblage (Fig. 2, 5). Age determinations of the two volcanic assemblages and turbidites are currently in progress to test this relative stratigraphic sequence inferred from the field observations.

EASTERN GNEISS DOMAIN

Mapping of the Daran Lake and Cotterill Lake areas outlined a domain of uppermost amphibolite to granulite facies gneisses and plutonic rocks (Fig. 2). The following description of the high-grade metamorphic mineral assemblages is based on field examination.

Cotterill Lake complex

The western half of the Cotterill Lake map sheet (86B/2) is predominantly underlain by a heterogeneous unit of banded gneiss. This unit was first outlined by Fortier (1949) and subsequently studied by Frith (1993) who interpreted it to be basement to the Indin Lake greenstone belt.

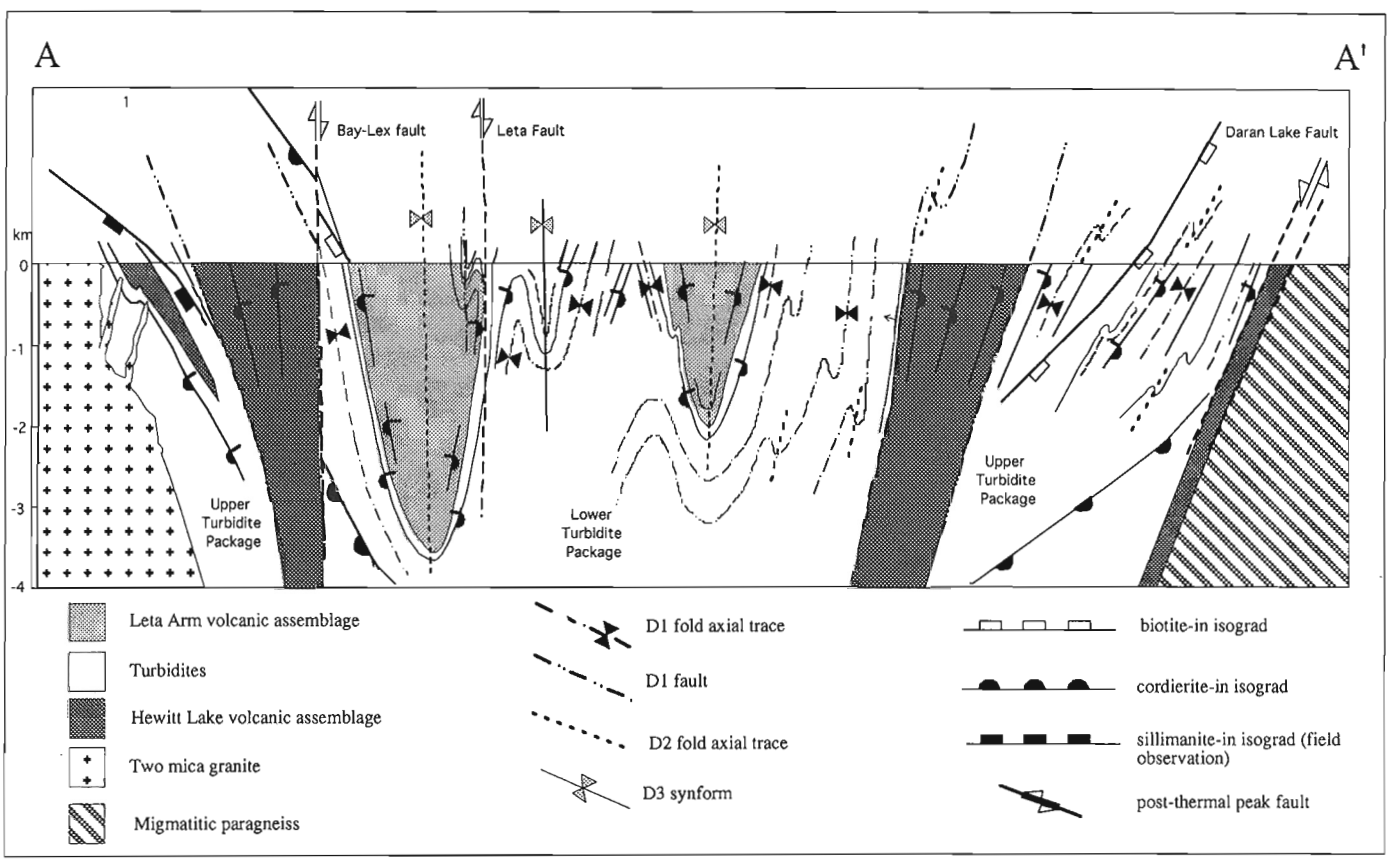

Figure 7. Schematic structural-section of the Indin Lake greenstone belt. Features shown are constructed from station observations on the line of section or by up- or down-plunge projection. Dip of isograds is constrained by drill data from the Damoti Lake gold prospect (H. Falck, pers. comm. 1994). The section illustrates the possible synformal nature of the F3 refold, and the overturning of units at the belt scale. No vertical exaggeration. Location of section shown in Figure 5.

The gneiss is characterized by a pronounced compositional layering composed of strongly foliated to gneissic tonalite, amphibolite, and weakly foliated to massive monzogranite. This layering is concordant with narrow (<50 m wide), anastomosing zones of high strain in which the unit develops a straight gneissic to mylonitic foliation. Monzogranite dykes crosscut the compositional banding but are transposed into the zones of high strain. Undeformed syenogranite and pegmatite dykes crosscut the foliation.

Coarse grained amphibolite increases in abundance (to 25% of the unit) adjacent to the greenstone belt. It carries white-weathering, zoned porphyroblasts of garnet surrounded by plagioclase feldspar, a typical metamorphic texture commonly related to decompression (Fig. 8A).

Panels (10 to >500 m wide) of dark-green weathering, fine grained amphibolite, talc schist, coarse amphibolite with subrounded quartzofeldspathic fragments, and migmatitic paragneiss with iron-formation can be mapped within the Cotterill gneiss. These units resemble the upper-amphibolite-facies mafic volcanic flows, felsic volcanic breccias and turbidites within the Indin Lake greenstone belt, and consequently are interpreted to be of supracrustal origin. A U-Pb zircon crystallization age of 2680 ± 5 Ma has been obtained from the foliated tonalite phase of the banded gneiss (Pehrsson et. al., 1994). This age is coeval with a preliminary age of a felsic volcanic rock obtained from the Leta Arm assemblage in the greenstone belt, suggesting that the tonalite gneiss may be largely synvolcanic.

Granulites and late granites

Granulite-facies gneisses and migmatites have been found on the south shore of Daran Lake and east of Cotterill Lake (Fig. 2). The Daran Lake unit is a hornblende-orthopyroxene-clinopyroxene-quartz-plagioclase migmatite with large porphyroblasts of orthopyroxene in the leucosome (Fig. 8B). The migmatite is cross-cut by narrow dykes of weakly foliated orthopyroxene-bearing monzogranite and is intruded along its eastern contact by this unit. The migmatite and foliated monzogranite are, in turn, intruded by a tabular shaped pluton of megacrystic granite. These units are the northern continuation of similar units found in the Wijinnedi Lake map area immediately to the south (Henderson and Schaan, 1993).

The eastern half of the Cotterill Lake area is largely underlain by megacrystic granite containing mappable enclaves of migmatitic paragneiss, diatexite, and tonalite gneiss (Fig. 2). The megacrystic granite locally shows waxy green feldspar on the fresh surface. The paragneisses and diatexite have the assemblage cordierite-garnet-kfeldspar-sillimanite. At the eastern limit of the map area the paragneiss contains rare orthopyroxene and is associated with orthopyroxene-clinopyroxene-plagioclase gneiss. A similar association of megacrystic granite, cordierite-garnet-Kfeldspar diatexite with orthopyroxene-bearing gneiss has been noted in the Wijinnedi Lake area where pressure-temperature determinations on the diatexite yield conditions of 750-800°C and 7 kbar (Chacko et al., 1995).

The megacrystic granite is associated with massive to weakly foliated monzogranite with a Kfeldspar porphyritic, magnetite-bearing phase. Both the megacrystic and magnetite-bearing monzogranite phases occur as veins in the migmatites. The magnetite-bearing monzogranite intrudes the tonalite orthogneiss.

An elongate body of coarse grained, foliated hornblende-biotite tonalite intrudes the gneiss complex east of Daran Lake, but is overprinted by a foliation parallel to the host gneissic foliation. Similar foliated tonalite occurs as inclusions and large enclaves within the megacrystic granite, indicating it predates intrusion of the megacrystic granite.

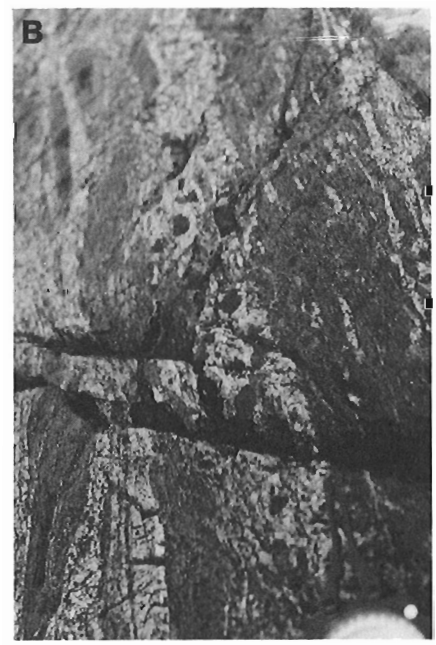

Figure 8. *A) Foliated spotted amphibolite. Black arrow points to a porphyroblast with a garnet core (grey) surrounded by a plagioclase rim (white). Pen is 15 cm long. GSC 1994-734D.* ***B)*** *Two-pyroxene-plagioclase migmatite from the Daran Lake area. Grey ovals are 2 cm orthopyroxenes. Brunton compass is 20 cm long. GSC 1994-734I*

Greenstone belt-gneiss domain contact

The contact between the Indin Lake greenstone belt and the high grade gneiss domain where observed, is a steeply west dipping, ductile shear zone (here informally termed the Daran Lake fault). Stretching lineations in the mafic mylonites along the Daran Lake fault plunge 65° to the north. Offset of the isograds, as well as one observation of asymmetric extensional shears give an oblique-normal (west-side down and north) sense of displacement. This is consistent with the juxtaposition of upper-amphibolite to granulite- facies rocks of the gneiss domain with greenschist to mid- amphibolite facies rocks of the greenstone belt. Pressure- temperature estimates for the amphibolite grade rocks in western Indin Lake are between 450-570°C and 2-3.5 kbar (Jones, 1994). Peak pressure estimates from granulite-facies units in the Wijinnedi Lake area correlative with those at Daran Lake, are ca. 7 kbar (Chacko et al., 1995). While more thermobarometric work is required to characterize the pressure jump at Daran Lake itself, the existing data suggest a difference of up to 3.5 kbar across the fault. The timing of the oblique-normal faulting is bracketed between the age of regional peak metamorphism (ca 2.6 Ga for the Wijinnedi Lake area, M. Villeneuve, pers. comm.) and the Paleoproterozoic northwest-trending strike-slip faults that offset the contact.

ASPECTS OF ECONOMIC INTEREST

Field work in 1994 has outlined new occurrences of iron-formation and the thinly bedded turbidites that host the Damoti Lake gold prospect (Fig. 2). Silicate-facies iron-formation extends to west of Daran Lake where it lies along strike of iron-formation units in the northern Wijinnedi Lake map area (Henderson and Schaan, 1994). Assays of sulphide-bearing iron-formation found on northeastern Indin Lake in 1994 have yielded anomalous gold values of >100 ppb.

Pyrrhotite- and arsenopyrite-bearing iron-formation occurs discontinuously along a strike length of nearly 7 km on north-central Spider Lake (Fig. 2). A trench exposes large quartz veins in this arsenopyrite-bearing occurrence. Assays of the iron-formation in the vicinity of the trench yield up to 500 ppb Au.

Iron-formation was traced northward to the limit of the map area, although the lower turbidite package continues for another 18 km to the north (Frith, 1993). These turbidites, in the Origin and Grenville Lake sheets, are considered highly prospective for sulphide-bearing iron-formation.

Volcaniclastic rocks of the Leta Arm assemblage in the Burn Inlet panel contain abundant sericite, cordierite, and staurolite (Fig. 2). These felsic schists are interpreted as metamorphosed, hydrothermally altered volcaniclastic rocks. Mineralogically similar altered volcanic rocks are associated with massive sulphide mineralization in the High Lake greenstone belt of the northern Slave Province (Henderson et al., 1994). The observations indicate that the Leta Arm assemblage may be a target for base-metal exploration.

DISCUSSION

Detailed study of the Indin Lake greenstone belt has shown that it has a complex structural geometry resulting from four generations of folding. The plunge direction of the regional F_3 fold and the F_2 interference patterns of the Leta Arm assemblage are critical to the interpretation of the belt-scale geometry. Current data suggest that the regional structural geometry can be explained by upright F_2 and F_3 refolding of recumbent F_1 folds and thrusts. Further work is required to test the geometry of the interference fold patterns and its implications. We suggest that given the tectonized nature of the Hewitt Lake assemblage contacts, similarity between the turbidites above and below the unit, and in the absence of evidence for a major unconformity within the turbidites themselves, it is unlikely that the currently preserved structural stack is an intact stratigraphic sequence. Intercalation of the Hewitt Lake assemblage with the turbidites and major thickness changes of the tectonostratigraphic units may have been a result of D_1 thrust imbrication.

Presence of supracrustal rocks similar to the Indin Lake greenstone belt in the Cotterill gneiss complex and the ca. 2.7 Ga date of tonalite crystallization imply that the upper-amphibolite to granulite facies Cotterill Lake gneisses may represent mid-crustal equivalents of the Indin Lake greenstone belt. These deeper crustal rocks were uplifted differentially in the Latest Archean to Early Proterozoic on an oblique-normal shear zone which marks the boundary between the Indin Lake greenstone belt and the Cotterill Lake complex.

ACKNOWLEDGMENTS

Christopher Johns is thanked for his entertaining assistance in the field and independent mapping contributions. We thank Craig Nicholson for his excellent expediting. Discussions and field trips with Herb Helmstaedt, Janet King, John Henderson, Tom Chacko, John Kerswill and Warren Hamilton were very helpful. Reviews by John Henderson, Janet King, Steve Lucas, Herb Helmstaedt, and Wouter Bleeker helped to significantly improve its clarity.

REFERENCES

Chacko, T. Creaser, R.A., Farquhar, J., and Muehlenbachs, K.
1995: The deep crust of the western Slave Province-initial petrologic and isotopic data from the high-grade rocks of the Ghost Domain; in Slave-Northern Cordillera Lithospheric Experiment (SNORCLE), Transect Meeting 1995 (April 8-9, 1995), compiled by F. Cook and P. Erdmer, University of Calgary, Alberta, Report No. 44, p. 4-7.

Fortier, Y.O.
1949: Geology, Indin Lake, E 1/2, District of Mackenzie; Geological Survey of Canada, Preliminary map 49-10a, scale 1:125 000.

Frith, R.A.
1993: Precambrian geology of the Indin Lake map area, District of Mackenzie, Northwest Territories; Geological Survey of Canada Memoir 424, 64 p.

Henderson, J.A., Henderson, M.N., and Kerswill, J.A.
1994: Geology and mineral occurrences of the central part of the High Lake greenstone belt, Archean Slave Province, Northwest Territories: a preliminary account of an unconformity between two volcanic sequences; in Current Research 1994-C; Geological Survey of Canada, p. 81-90.

Henderson, J.B. and Chacko, T.
1995: The high grade metamorphic terrane south of Ghost Lake, southwestern Slave Province, Northwest Territories; in Current Research 1995-C; Geological Survey of Canada, p. 77-86.

Henderson, J.B. and Schaan, S.E.
1993: Geology of the Wijinnedi Lake area: a transect into mid-crustal levels in the western Slave Province, District of Mackenzie, Northwest Territories; in Current Research 1993-C; Geological Survey of Canada, p. 83-92.

Jones, A.L.
1994: Metamorphism of the Yellowknife Supergroup at Indin Lake, western Slave Province, Northwest Territories; B.Sc. thesis, University of Alberta, Edmonton, Alberta, 27 p.

Pehrsson, S.J. and Beaumont-Smith, C.
1994: Preliminary report on the geology of the Indin Lake supracrustal belt, western Slave Province, Northwest Territories; in Current Research 1994-C, Geological Survey of Canada, p. 91-102.

Pehrsson, S.J., Helmstaedt, H., and King, J.E.
1995: Transect through the Indin lake area: a window on the upper to mid-crustal structure of an Archean greenstone belt; in Exploration Overview 1994, (ed.) R. Kusick and S. Goff; NWT Geological Mapping Division, Indian Affairs and Northern Development, p. 51.

Ramsay, J.G.
1967: Folding and Fracturing of Rocks; McGraw-Hill, New York, 586 p.

Stanton, M.S., Tremblay, L.P., and Yardley, D.H.
1954: Chalco Lake, District of Mackenzie, Northwest Territories; Geological Survey of Canada, Map 1023A, scale 1:63 360.

Tremblay, L.P., Wright, G.M., and Miller, M.L.
1953: Ranji Lake, District of Mackenzie, Northwest Territories; Geological Survey of Canada, Map 1022A, scale 1:63 360.

Geological Survey of Canada Project 870008

Controls on and geological setting of regional hydrothermal alteration within the Onaping Formation, footwall to the Errington and Vermilion base metal deposits, Sudbury Structure, Ontario[1]

D.E. Ames and H.L Gibson[2]
Mineral Resources Division

Ames, D.E. and Gibson, H.L., Controls on and geological setting of regional hydrothermal alteration within the Onaping Formation, footwall to the Errington and Vermilion base metal deposits, Sudbury Structure, Ontario; in Current Research 1995-E; Geological Survey of Canada, p.161-173.

Abstract: Comprehensive field evidence clearly indicates that the Early Proterozoic Onaping Formation is a hydrothermally altered sequence of pyroclastic fall and debris flow, hydroclastic breccia and pyroclastic flow deposits. A stacked, basin-wide, semi-conformable succession of altered tuff is well exposed in outcrop. From exposed base to top it comprises silicified, feldspathized, chloritized and carbonatized zones. Preliminary observations suggest that the basal, syndepositional silicification zone predates emplacement of the granophyre intrusion. Although the modes of brecciation and emplacement are similar to volcaniclastic deposits, the Onaping Formation is not a typical cauldron sequence, however it is not a suevite or meteorite fallback breccia. The exceptional preservation of one of the most extensive semi-conformable alteration systems known, permits detailed study of hydrothermal processes involved in generating the overlying replacive massive sulphide deposits hosted in carbonate sinter mounds.

Résumé : Les indices globaux recueillis sur le terrain indiquent clairement que la Formation d'Onaping du Protérozoïque précoce est une séquence altérée par des fluides hydrothermaux et composée de débris pyroclastiques de retombée et de coulée, de brèches hydroclastiques et d'ignimbrites. Une succession semi-concordante de tufs altérés empilés à l'échelle du bassin est bien exposée dans l'affleurement. De la base au sommet de l'affleurement, on observe des zones de silicification, de feldspathisation, de chloritisation et de carbonatation. Les observations préliminaires laissent supposer que la zone de silicification basale synsédimentaire précède l'intrusion de granophyre. Même si les modes de bréchification et de mise en place sont semblables à ceux de dépôts volcanoclastiques, la Formation d'Onaping ne constitue pas une séquence typique de chaudron, mais ce n'est pas non plus une brèche de retombée de suévite ou de météorite. La conservation exceptionnelle de l'un des systèmes d'altération semiconcordants les plus vastes connus permet d'étudier en détail les processus hydrothermaux participant à la mise en place des gisements de sulfures massifs de remplacement sus-jacents encaissés dans des monticules de tufs agglomérés.

[1] Contribution to Canada-Ontario Subsidiary Agreement on Northern Ontario Development (1991-1995), Canada-Ontario Economic and Regional Development Agreement.
[2] Geology Department, Laurentian University, Sudbury, Ontario P3E 2C6

INTRODUCTION

The study of regional semi-conformable alteration associated with volcanogenic massive sulphide (VMS) deposits is of prime interest to both the research community and the exploration industry as its characteristics, distribution, and interrelationships determine the nature of regional-scale hydrothermal systems. Although the spatial association between regional semi-conformable alteration and VMS deposits is recognized in such mining districts as Noranda, Sturgeon Lake, Snow Lake, Skellefte, Bergslagen and the Iberian Pyrite belt, the modes of formation and genetic relationships to the massive sulphide producers are poorly understood. Alteration systems in the Iberian Pyrite belt and Onaping Formation, Sudbury are an order of magnitude larger than those listed above.

The Onaping Formation is footwall to two known base metal deposits, the Errington and Vermilion mines containing 6.4 Mt grading 4.36% Zn, 1.37% Cu, 1.15% Pb and 55 g/t Ag (Jonasson and Gibson, 1993) and is host to numerous base metal prospects with lesser gold showings (Rousell, 1984). The Onaping Formation is optimum to study regional (approximately 53 X 17 X <3.5 km) semi-conformable silicification and carbonatization as two metamorphic and tectonic regimes are present: 1) greenschist facies, low strain rocks in the north range of the Sudbury structure and 2) amphibolite facies and high strain rocks in the south range.

This is a multi-year study of regional hydrothermal alteration within the Onaping Formation. It contributes to the origin of the Zn-Cu-Pb massive sulphide deposits and the nature of the Onaping Formation. The immediate objectives are to determine the spatial distribution, mineralogy, chemistry,

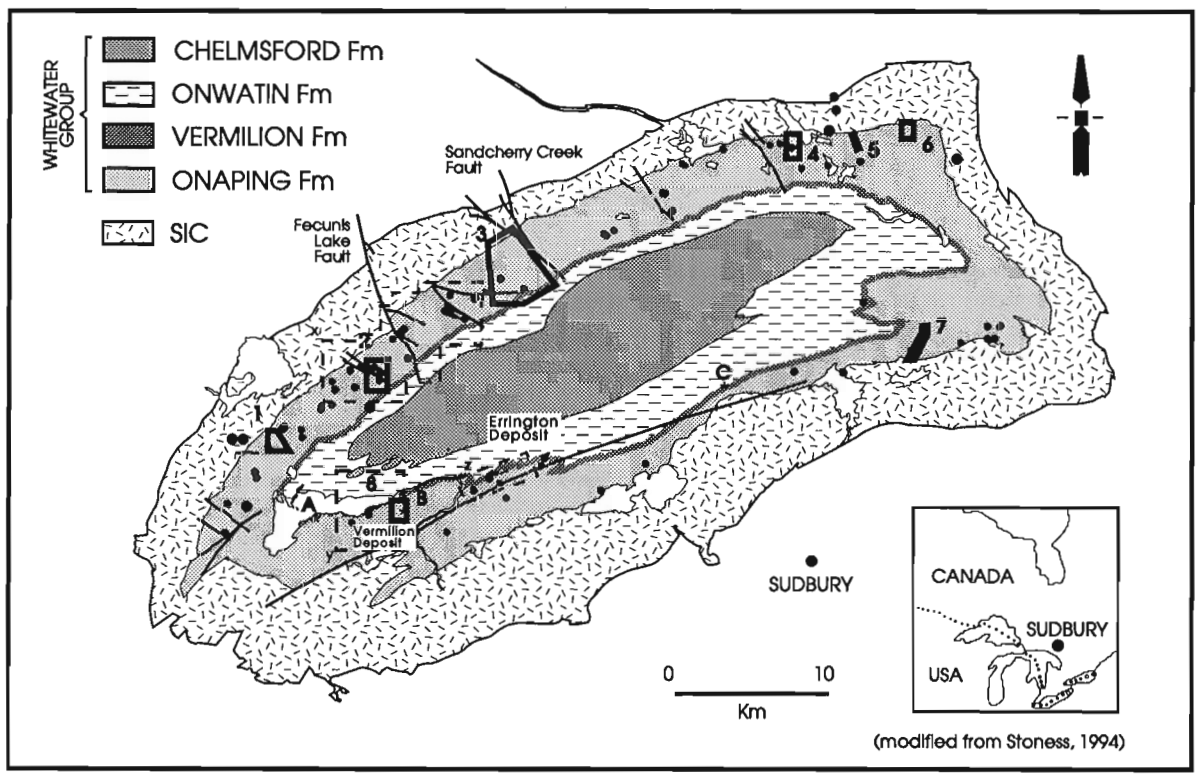

Regional Alteration and Stratigraphy

Map Area (1:2000)

1. Simmons 2. Cow Lake 3. Morgan 4. Joe Lake
5. Hanmer Powerline 6. Capreol 7. Garson Powerline
8. Gordon Lake Road

Peperite localities

* Detailed (1:200) map area

A. A+M showing B. Gordon Lake Road C.Azilda

Other Whitewater Group map areas

(1:5000-1:10000)

x. Gibbins et al, 1994
y. Gray et al, 1995
z. Paakki et al, 1992

Sulphide occurrences

Figure 1. Sudbury structure showing the location of 1993/1994 map areas in the Onaping Formation.

timing, and origin of "basin-wide" silicification, feldspathization, palagonitization/chloritization, and carbonatization and to determine the stratigraphic, syn- and post-depositional structural controls on alteration. A key is to distinguish which of the alteration types are related to intra-Onaping base metal occurrences, to the overlying Zn-Cu-Pb massive sulphide deposits, and perhaps, to both.

Detailed mapping (1:2000) of stratigraphy and alteration in each of the ten 1993-94 map areas (Fig. 1) encompassed:

1. complete transects through the Onaping Formation in the north range Morgan Township and south range Garson powerline transect (map areas 3 and 7);
2. three areas extending from the granophyre through the Sandcherry member strata and the contact unit of the overlying Dowling Member (map areas 4-6);
3. the upper Dowling Member (map areas 2,8);
4. intra Onaping mineralization including the Simmons Pb-Cu-Zn showing (map area 1), Limerick Cu-Zn showing (map area 3) (Fig. 1, 2, 3). Key areas mapped at 1:100 include those with critical stratigraphic relationships and the Cow Lake, McNunes and Ryan base metal occurrences (map areas A-C and 4) (Fig.1).

REGIONAL GEOLOGY

The 60 x 28 km, Sudbury Structure contains the outer Sudbury igneous complex (SIC), Sudbury breccia and the interior Whitewater Group that comprises (from oldest to youngest), the Onaping, Vermilion, Onwatin, and Chelmsford formations (Martin, 1957; Stoness, 1994). The Early Proterozoic Onaping Formation forms an inner annular rim around, and is intruded by the 1850 Ma Sudbury igneous complex (Krogh et al., 1984; Peredery, 1972; Muir and Peredery, 1984). The older age limit is constrained by the 2219 Ma Nipissing diabase dykes that do not intrude the Onaping Formation (Corfu and Andrews, 1986). Formation of the Sudbury structure was penecontemporaneous with a major tectono-metamorphic event termed the Penokean Orogeny which in the western Southern Province is a composite event attributed to multiple terrane collisions from 1.890 to 1.835 Ga (Van Schmus, 1980; Sims et al., 1989). In contrast, the Penokean orogeny in the Lake Huron region, is an event whose absolute age is not well established but, is broadly constrained as a post-Nipissing diabase (2219 Ma) and pre-Killarney (1750 Ma) deformational event (Card, 1992).

Onaping Formation

The Onaping Formation is controversial as to whether it is of impact or volcanic derivation. As with many impact structures (e.g. Ries, Germany; Mistassin Lake and Manicouagan, Canada) the fragmental succession of the Onaping Formation was initially mapped as ash-flow tuffs and lavas resulting from catastrophic volcanic eruptions during cauldron subsidence (Thompson, 1957; Williams, 1957; Stevenson, 1972, 1990; Muir, 1984). Others have interpreted the Onaping Formation as products from a meteorite impact including fallback breccias or suevite, melt bodies and wash-in from the crater walls (French, 1967; Dence, 1972; Peredery, 1972; Avermann, 1992).

The 1400 m Onaping fragmental sequence was until recently (Muir, 1984; Gibbins, 1994) considered a heterolithological chaotic mixture. Significant features first recognized by Muir (1983, 1984) include 1) the Onaping Formation is not chaotic and is bedded, 2) although the base is generally coarse and the top fine , it contains normally graded units with indistinct contacts, 3) the base of the so-called Black member is marked by an increase in the proportion of chloritic shards, and 4) carbon does not define the Black member because it is locally absent from the Black member and present in the Gray member.

Extensive mapping has defined a distinctive and consistent stratigraphic sequence with variations in shard morphology between blocky and lenticular, size and percentage of juvenile and lithic fragments, internal morphology, and contact relationships that are consistent with hydroclastic origin for the breccia (hyaloclastite, pyroclastic fall, flow or debris flow) (Gibbins, 1994) (Fig. 2a). Gibbins (1994) grouped these units into the Sandcherry member and Dowling member, the lower and upper part of the Onaping Formation, respectively. This change in terminology from Gray and Black member means that the newly defined contact marks a change in the morphology and size of shards, percentage of matrix and lithic fragments and is not due to a colour change or presence or absence of carbon (Gibbins, 1994). The terminology followed herein is based on Fisher's (1966) size classification of pyroclastic rocks with no genetic connotation.

Stratigraphy

The Onaping Formation consists of the Basal member (Muir, 1981, 1983; Muir and Peredery, 1984), the Sandcherry member composed of hydroclastic breccias with blocky shards and the Dowling member breccias produced by explosive eruptions (Gibson et al., 1994; Gibbins, 1994). The Basal member in the south range (Muir and Peredery, 1984) or quartzite breccias (Stevenson, 1961) outcrop only in the south and east range and lie stratigraphically below the Sandcherry member (Fig. 1, map area 7; Fig. 2a). This Basal member displays in situ brecciation of quartzite fragments with a cuspate, angular, chloritic matrix all intruded by granophyre. Due to intense deformation, primary relationships are obscured. Further mapping of this unit is required to understand the mechanisms of brecciation and its relationship to the basal intrusion and aphanitic dykes.

The Sandcherry member strata were grouped into two major rock types; 'Fluidal fragment', characterized by tabular flow banded shards and 'Shard-rich', characterized by equant plate-like shards. These are laterally discontinuous, matrix-poor and contain at least 60% shards. The base of the Dowling member is marked by the Contact unit (Gibbins, 1994) formerly the chlorite shard horizon (Muir and Peredery, 1984) or Green member (Avermann, 1992) and characterized by 20-45% lenticular chlorite shards that locally are incipiently

welded. The Dowling member contains matrix-rich (<40% glass shards) laterally continuous rock types stratigraphically grouped into lower, middle and upper units (Gibbins, 1994).

The majority of the Onaping formation (Sandcherry and Dowling member) has a very low average percentage of lithic fragments (<5% by volume), (Gibbins, 1994) although some units may display a block-rich base (30% by volume). In contrast the <150 m thick, Basal member on the southeast range comprises mainly lithic fragments (75-95% by volume) (Muir and Peredery, 1984).

Intrusions

The Onaping Formation is intruded by: 1) aphanitic, flow-banded dykes genetically related to fluidal fragments (Peredery, 1972; Gibbins, 1994) present in Sandcherry member rocks; 2) the 'Basal Intrusion' (Gibbins, 1994) that contains units previously described as Basal member and melt bodies (Peredery, 1972; Muir and Peredery, 1994); 3) the granophyric phase of the Sudbury igneous complex (Peredery, 1972); and 4) 1238 Ma Sudbury diabase dykes (Krogh et al., 1987) (Fig. 2a).

Syn-Onaping intrusions

Penecontemporaneous andesitic dykes were autobrecciated to form part of the Fluidal-fragment units and cut Shard-rich units in the Sandcherry member. Similar glassy andesitic dykes intrude the Onaping Formation at various stratigraphic levels with increasing vesicularity toward the top (Fig. 2a). Within the Contact unit, Middle units and Upper units are intrusive lobes (2.5 to 5 m) with annular, texturally variable bands. In general, the lobes have a massive core followed by spherulitic bands with variable amounts of hyaloclastite and an amygdaloidal rim (Fig. 3, 4).

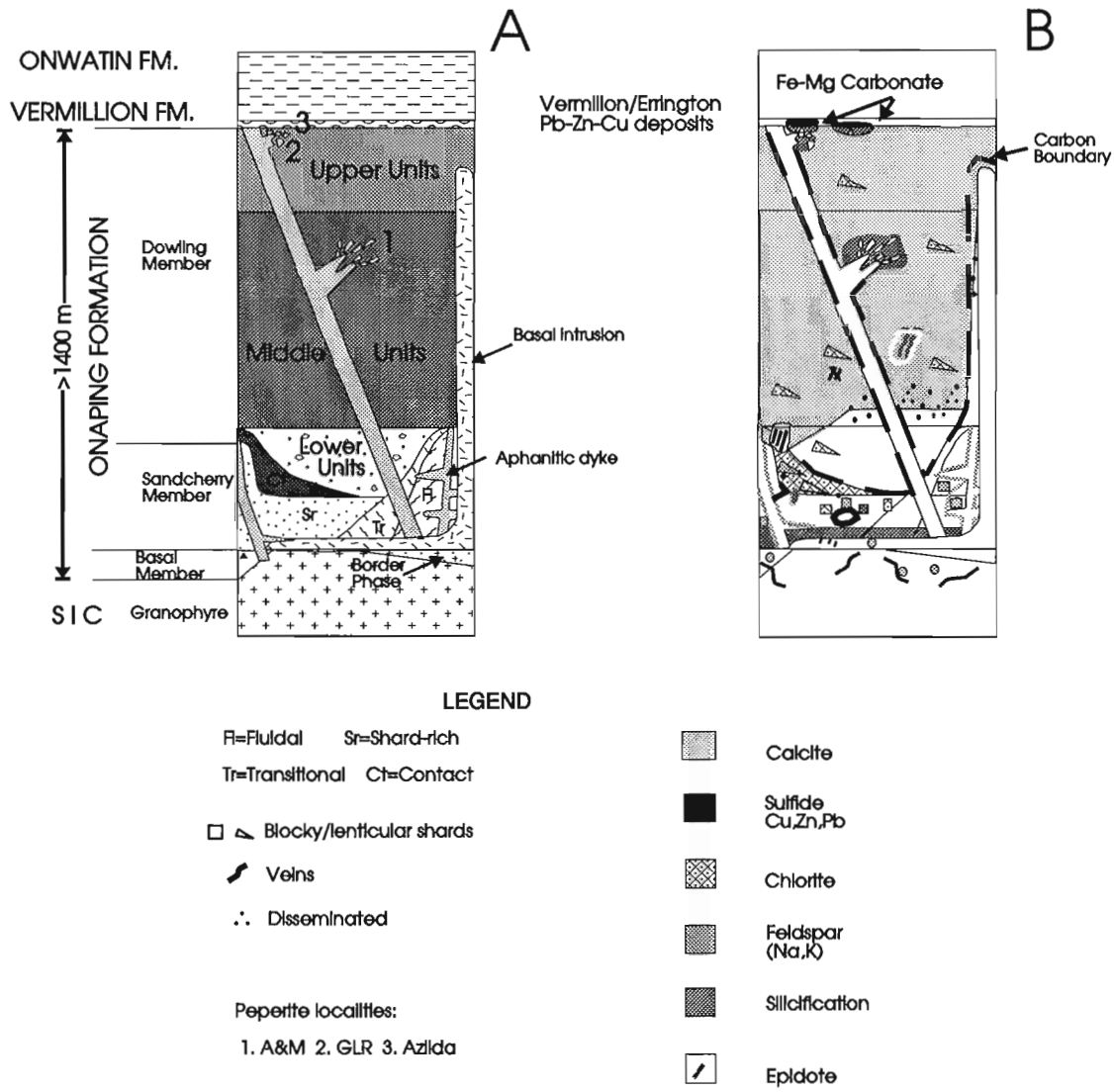

Figure 2. A) Simplified stratigraphic column of the Onaping Formation (modified after Gibbins, 1994; Muir and Peredery, 1984). B) Generalized alteration column through the Onaping Formation, showing alteration distribution and vertically stacked semi-conformable alteration zones.

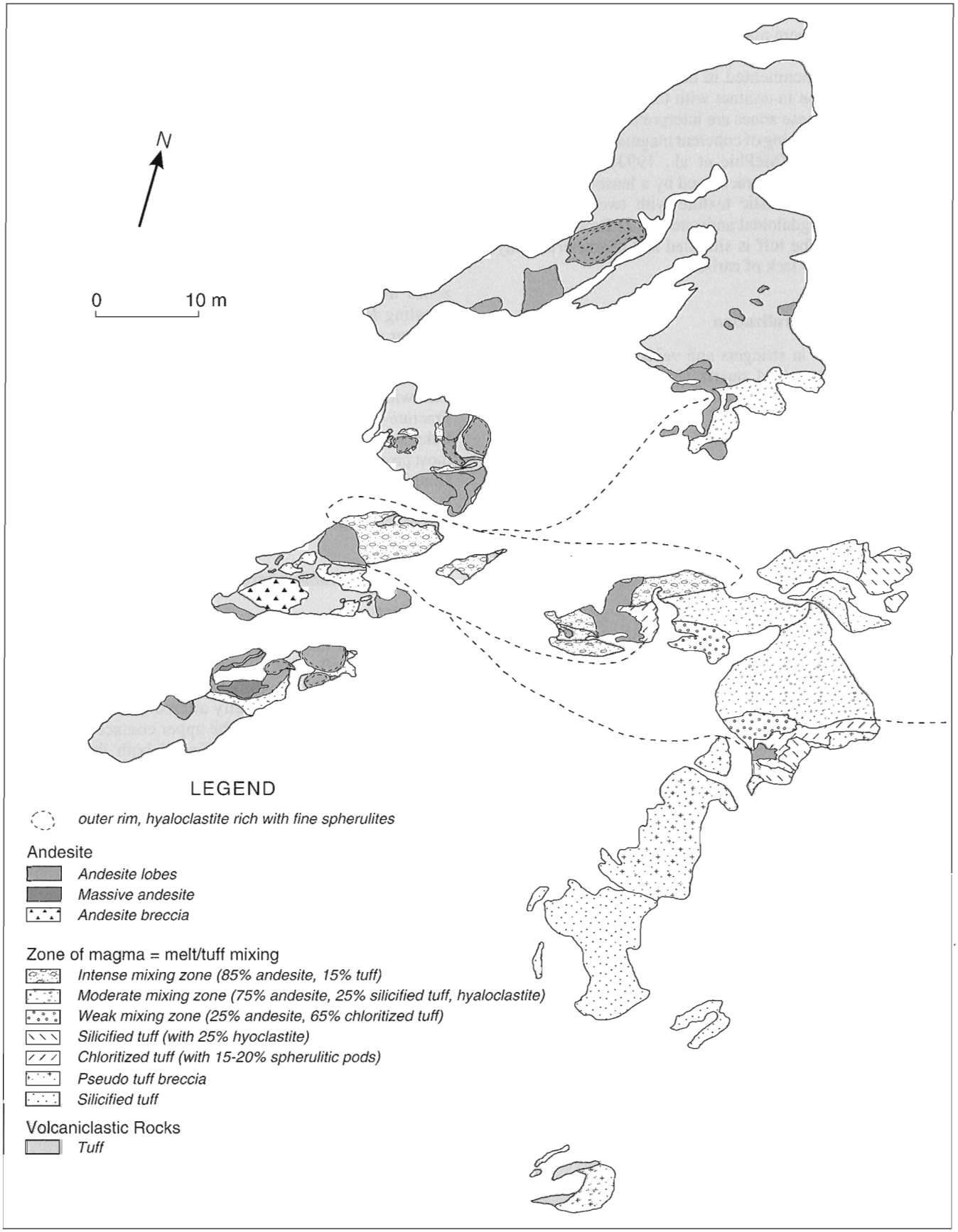

Figure 3. *Detailed geological map of A&M outcrops showing peperite crosscut by penecontemporaneous andesite lobes in the Middle unit, Dowling member, Onaping Formation.*

Zones of mixing between andesite dykes and tuff of the Dowling member were mapped (1:200 scale) in the middle units at the A&M showing, and in the upper units at Gordon Lake Road, and documented in drillcore at the top of the Onaping Formation in contact with the Vermilion Formation (Figs. 1-6). These zones are interpreted to be peperite, a rock generated by mixing of coherent magma with unconsolidated wet sediment (McPhie et al., 1993) (Fig. 5). The peperite exposures are characterized by a lensoidal (Fig. 6c) or blocky (Fig. 6a) clastic texture with two components 1) spherulitic, amygdaloidal andesite and 2) Dowling member tuff (Fig. 6). The tuff is silicified and characteristically light gray due to the lack of carbon.

Intra-Onaping mineralization

Base metals occur in stringers and veins of Cu, Zn, Pb, Fe sulphides, carbonate and quartz (Simmons and Limerick showings); reworked Cu, Zn, Pb, Fe and carbonate fragments (Cow Lake, McNunes area), and as sulphide replacements of lapillistone beds (Ryan) and shards, dominantly at the base of the Middle Units of the Dowling Member (Fig. 1). Sulphide is disseminated in the Middle and Upper units; the spatial association with synvolcanic faults, with or without dyke emplacement, can be documented in many areas.

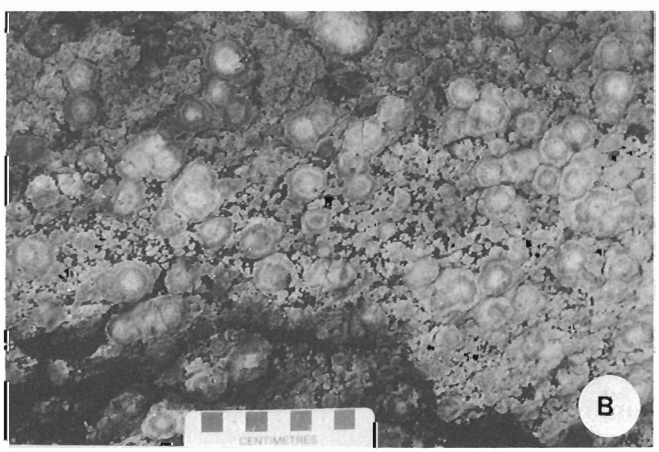

Figure 4. Outcrop photographs of A&M intrusive lobes. A) Andesite lobe with massive core, block rich zone and spherulitic, amygdaloidal outer margin. GSC 1995-077I B) Bimodal size population of spherulites within andesite lobe. GSC 1995-077J

HYDROTHERMAL ALTERATION

The relative distribution of vertically stacked semi-conformable alteration and disconformable alteration zones are simplified in Figure 2a. Silicification occurs as a basin-scale, semi-conformable zone of pervasive alteration at the exposed base of the Onaping Formation, as discordant fracture-controlled and pervasively silicified zones associated with high level dykes intermixed with Dowling Member tuff (i.e. peperite). Discordant zones of feldspar alteration are confined to Sandcherry member strata in association with hyaloclastite-rich margins to flow banded dykes and as mottled and pervasive zones in proximal breccias within feeder zones to the fluidal fragment breccias. Fracture-controlled feldspar-silicified zones are in the Joe Lake and Capreol map areas. Chlorite alteration of shards is most prominent in the contact unit but present throughout the Onaping Formation. Semi-conformable carbonate alteration is distinctive basin-wide in the upper part of the Onaping Formation (Fig 2b).

Semi-conformable alteration zones

Silicification

In the Morgan map area (Fig. 1), a 440 m map width of pervasive silicification was traced for 1300 m along the exposed base of the Onaping Formation. The lower contact is intruded by hydrothermally altered basal intrusion and unsilicified granophyre but the upper contact has not been observed. Silicification has affected both the shard-rich and fluidal-fragment lapilli tuffs in the Sandcherry member (Fig. 7). Relict, recessive weathering, blocky shard-like

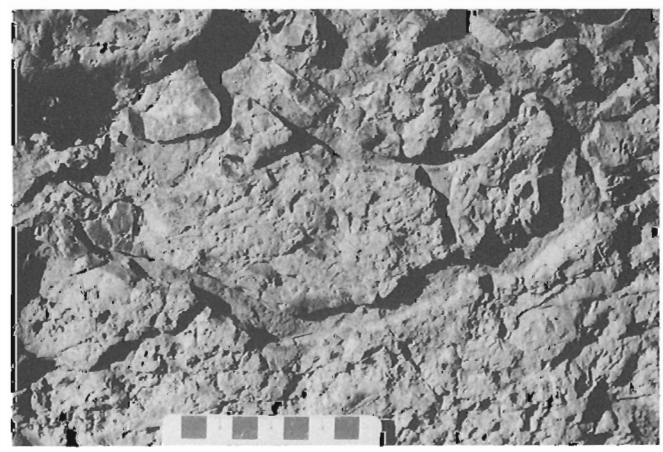

Figure 5. In situ brecciation of silicified (light gray) tuff separated by andesite. (GSC 1995-077P). This jigsaw-fit texture is characteristic of the "pseudo tuff breccia" exposed at the southern margin of the intense zone of mixing in Figure 3.

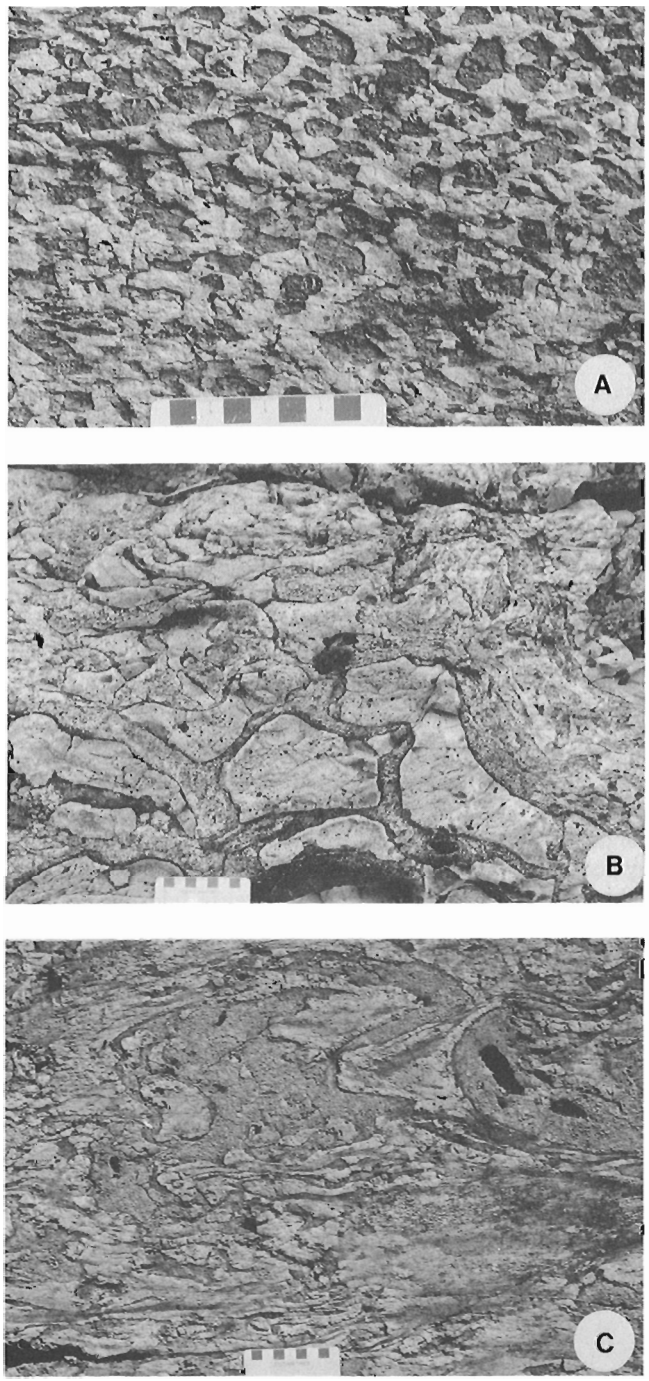

Figure 6. Outcrop photographs of peperite textures in the most intense and moderate zones of mixing. ***A)*** *Blocky peperite texture with clasts of andesite in silicified tuff. Representative of most intense mixing zone in the Upper units, Dowling member, Gordon Lake Road. GSC 1994-321* ***B)*** *Clasts of silicified tuff within matrix of spherulitic andesite in the most intense mixing zone, Middle units, Dowling member, A&M outcrops. GSC 1994-324* ***C)*** *Lensoidal-texured peperite with spherulitic amoeboid pods of andesite and dark gray hyaloclastite in silicified, light gray tuff. Moderate mixing zone in the Middle units, Dowling member, A&M outcrops. GSC 1994-316*

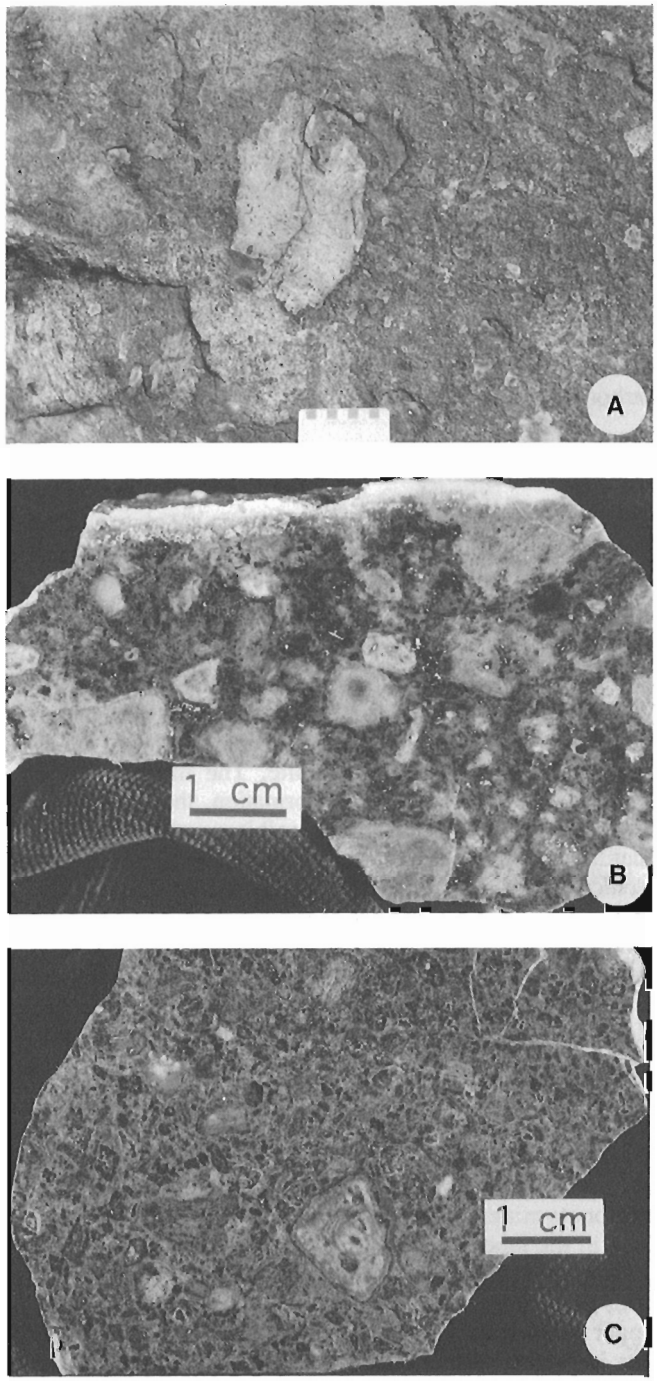

Figure 7. Photographs of basal silicification zone. ***A)*** *Fragment of previously silicified Shard-rich lapilli tuff within stratigraphically higher, relatively unaltered Shard-rich lapilli tuff. GSC 1995-077K Evidence for syn-depositional timing of basal silicification.* ***B)*** *Polished slab of intensely silicified Fluidal-fragment lapilli tuff. GSC 1995-077U* ***C)*** *Polished slab of intensely silicified Shard-rich lapilli tuff, note the relict blocky shard outlines. GSC 1995-077W*

outlines decorate buff weathering, orange and yellowish stained outcrop. Local, 30 cm pervasively silicified patches are scattered throughout the zone. The mineral assemblage is dominated by albite and quartz with lesser chlorite, titanite and pyrrhotite, pyrite and chalcopyrite. Fragments of previously metasomatized, lithified shard-rich tuff from the basal silicified zone were observed in a relatively unaltered shard-rich unit <200 m above the silicified zone (Fig. 7a). In other localities silicified fragments occur within a silicified fragmental matrix. In the Capreol and Joe Lake map areas, carbon-bearing shard-rich units outcrop near the granophyre contact. The carbon distribution is patchy, locally semi-conformable and has diffuse gradational contacts with carbon-poor strata.

Palagonitization/Chloritization

Chlorite pseudomorphs after palagonite in shards are distributed throughout the Onaping Formation but obscured in areas of most intense silicification or feldspathization. Feldspar and quartz also replace palagonite around the rims of chloritized shards.

In the basal silicification zone, relict chlorite cores some shards. In feldspathized zones the shards clearly indicate feldspar overprinting chlorite. Some chlorite shards are also partially overprinted by actinolite. The most prominent chloritic unit in the Onaping Formation, the Contact unit contains 20% (vol.) orthoclase+albite+quartz leucocratic shards and 40% chloritized, lenticular, locally incipiently welded shards. Patchy, diffuse feldspar+quartz alteration is common, at the base of the unit in blocky shards and localized lithophysae are found. The relative distribution, compositions, and importance of chlorite, feldspar and quartz alteration of palagonite are being determined.

Carbonatization

Regional carbonate alteration was studied in detail in the Cow Lake, Simmons, and Morgan map areas by mapping the presence or absence of calcite. Other (Fe, Mg, Mn) carbonate minerals compositions are currently being examined in the laboratory. Calcite is ubiquitous in shards and matrix, as rims on lithic fragments and locally as fragments with pyrrhotite, chalcopyrite, pyrite, and sphalerite in the upper 1400 m (apparent) of the Onaping Formation. Calcite is notably absent in areas of mineralization or discordant silicification. Both the upper and lower contacts of the carbonate alteration zone are slightly discordant to stratigraphy in detail. In the Morgan area, the uppermost exposed 100 m lacks calcite but the presence of other carbonate minerals cannot be ruled out. Distribution of such carbonate minerals may have important implications with respect to emplacement of sulphide mineralization.

Disconformable alteration zones

Epidotization

Vein controlled epidote is at the top of the granophyre in the Joe Lake and Capreol map areas (Fig. 8). The vein paragenesis from core to rim is quartz+potassium feldspar, epidote+actinolite or chlorite and quartz within a pyritic wallrock. Epidote is essentially lacking in the Onaping Formation, except for local microscopic metamorphic epidote in the Sandcherry member rocks. The carbonate-bearing environment of the Onaping Formation may have inhibited the formation of epidote.

Feldspathization

The only volumetrically significant discordant alteration is feldspathic within the Sandcherry member strata. Mapping of feldspathic alteration in the Morgan, Joe Lake, Hanmer Powerline, Capreol, and Garson powerline map areas defined at least two stages and three types. The Joe Lake area is the type area for feldspar alteration and exemplifies a pervasive syndepositional phase and a second, brittle fracture controlled alteration that postdates emplacement of the Basal intrusion and granophyre.

Type 1, feldspar alteration is genetically and spatially associated with the emplacement of flow banded aphanitic sills and dykes (Fig. 9a). These dykes are feeders to the Sandcherry member fluidal-fragment units and may display hyaloclastite margins, implying passive fragmentation in a subaqueous environment (Fig. 9). Intense feldspar replacement of shards within 1 m wide envelops around isolated dyke apophyses, attests to the syndepositional timing of stage 1 alteration. Above sills, intense alteration is aerially extensive and the density of sills and dykes affects the alteration distribution. The least altered units have dark green amphibole and chlorite shards in a greyish green matrix (Fig. 9b). With increasing alteration the shards contain variable proportions of actinolite+chlorite and feldspar+quartz whereas the fluidal fragments are preferentially and pervasively altered. In zones

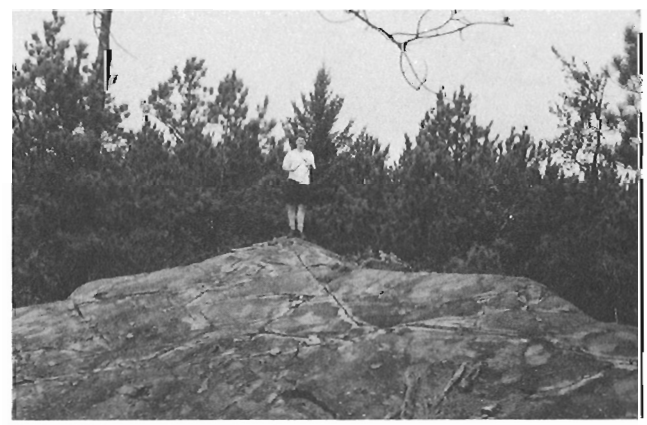

Figure 8. *Fracture controlled alteration within granophyre, Joe Lake map area. GSC 1995-077V*

of more intense stage 1 feldspar alteration the matrix is bleached; shards and flow banded lapilli fragments are pervasively replaced and lithic fragments are partly replaced. Quartzose lithic fragments are resistant to alteration (Fig. 9c). Within the most intense alteration adjacent to the flow banded sill-dyke complex, shard-rich lapilli tuff contains angular and spheroidal clots, with internally radiating amphibole enclosed by a 1-2 cm pinkish cream bleached halo and irregular, pervasively bleached, mottled patches in the tuff matrix (Fig. 9d, e).

Type 2, vein-controlled alteration is manifested by 1-2 cm actinolite vein cores surrounded by a halo of pinkish white, pervasively bleached feldspathic wallrocks (Fig. 10). Veins cut the 'Basal intrusion' and the surrounding lapilli tuff and also transect shard-rich tuff in the Joe Lake area. In the Capreol area a vertical pipe-like zone, containing at least 12 actinolite veins with silicified margins, is also spatially associated with a sill-dyke complex. These veins cannot be related to the syndepositional alteration associated with the intruding vent complex since they cut a younger intrusion.

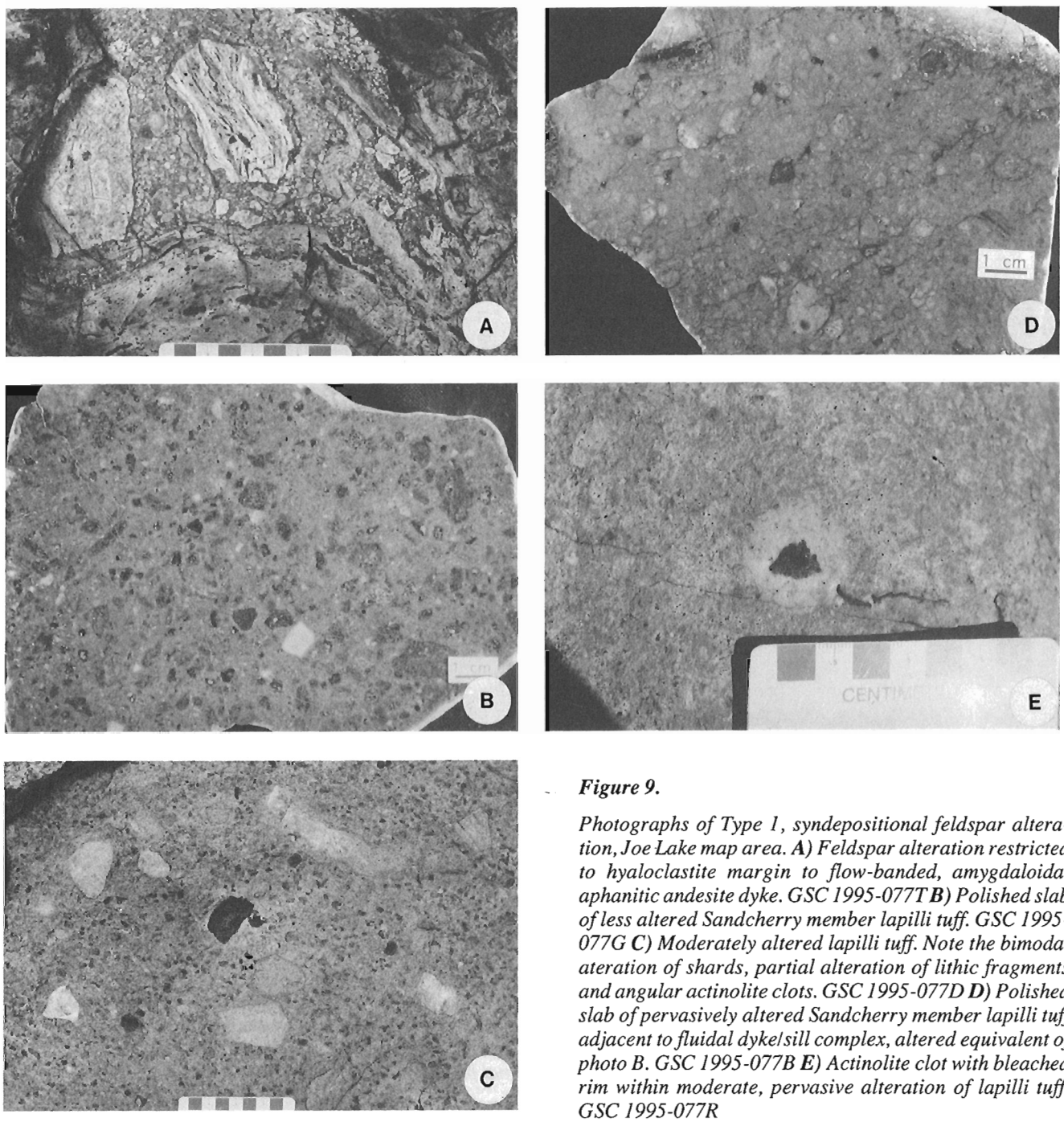

Figure 9.

Photographs of Type 1, syndepositional feldspar alteration, Joe Lake map area. ***A)*** *Feldspar alteration restricted to hyaloclastite margin to flow-banded, amygdaloidal aphanitic andesite dyke. GSC 1995-077T* ***B)*** *Polished slab of less altered Sandcherry member lapilli tuff. GSC 1995-077G* ***C)*** *Moderately altered lapilli tuff. Note the bimodal ateration of shards, partial alteration of lithic fragments and angular actinolite clots. GSC 1995-077D* ***D)*** *Polished slab of pervasively altered Sandcherry member lapilli tuff adjacent to fluidal dyke/sill complex, altered equivalent of photo B. GSC 1995-077B* ***E)*** *Actinolite clot with bleached rim within moderate, pervasive alteration of lapilli tuff. GSC 1995-077R*

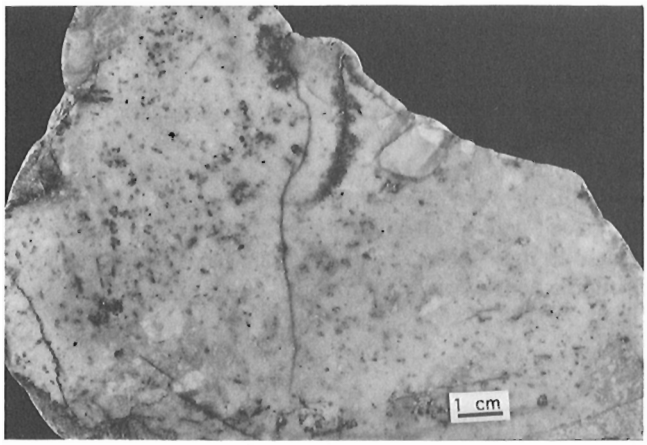

Figure 10. *Polished slab of Type 2, fracture controlled, pervasive feldspar/quartz alteration within Shard-rich tuff, Joe Lake map area. Note the relict quartzose lithic fragment. (GSC 1995-077A)*

Veins, stockwork breccias, and pegmatoid patches of quartz and pink weathering, potassium feldspar are characteristic of the third type of feldspar alteration (Fig. 11). A spectacular, 9 x 5 m stockwork breccia (Fig. 11) in the Joe Lake area is hosted by the Basal intrusion. This alteration is multi-staged as evidenced by early bleaching of the Basal intrusion and fragments which are derived by its brecciation, which are cut by a quartz+potassium feldspar veins which in turn are cut by a late quartz stage (Fig. 11). Pegmatoid quartz and potassium feldspar pods have been observed in the Onaping strata around the hydrothermal breccia and within a phase of the granophyre. A pipe-like body of potassium feldspar and quartz alteration observed in the granophyre at Joe Lake is of similar orientation to that in the Onaping Formation. Mineral chemistry, fluid inclusion, and oxygen isotope studies now underway should constrain the temperature of formation and genesis of the hydrothermal breccia, pegmatoid patches and veins. The timing of this alteration relative to stage 2 alteration is unknown but definitely postdates stage 1 syndepositional feldspathization.

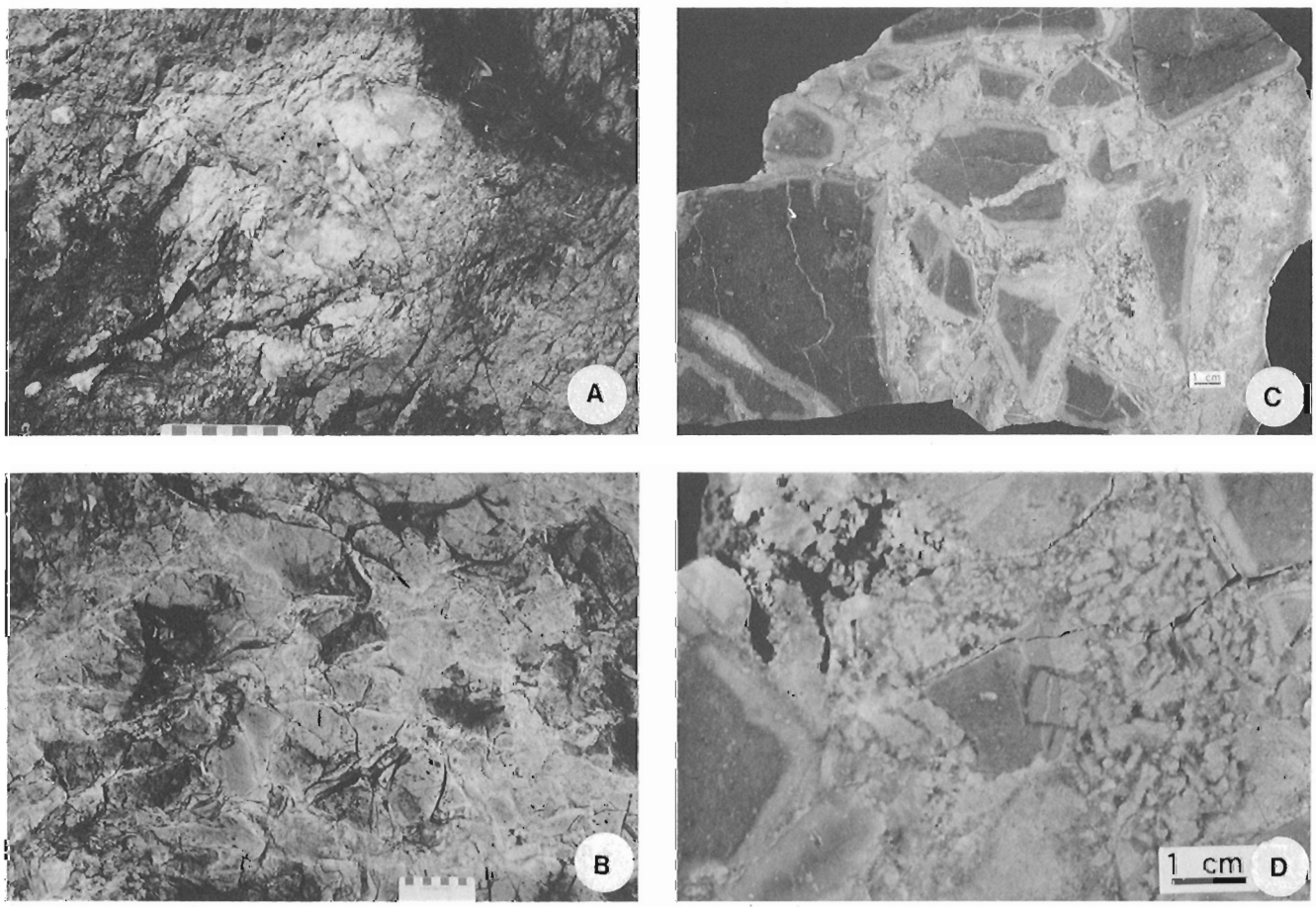

Figure 11. *Photographs of Type 3 feldspathization, Joe Lake map area.* ***A)*** *Quartz, potassium feldpar pegmatoid patch in Shard-rich unit. GSC 1995-077E* ***B)*** *Outcrop photograph of stockwork breccia cutting the Basal Intrusion. GSC 1995-077S* ***C)*** *Polished slab of stockwork breccia, note quartz-potassium feldspar veins (Stage 2) cut previously bleached fragments (Stage 1). GSC 1995-077H* ***D)*** *Late quartz (Stage 3) crosscuts quartz-potassium feldspar stage in hydrothermal breccia. GSC 1995-077F*

Silicification

Although disconformable silicification is associated with the feldspathization described above, there is a distinctively different style of quartz dominated fracture controlled silicification that pervasively replaces the matrix of lapilli-tuff units. This has been observed in the Morgan map area associated with a base metal showing in the Middle units of the Dowling member and in Hanmer powerline map area where it transgresses the Sandcherry member-Dowling member contact and is spatially associated with the emplacement of a flow banded, aphanitic dyke. The silicified tuff has a distinctive greyish quartzose matrix with cream weathering relict shards. This disconformable silicification clearly postdates the semi-conformable silicification zone.

Silicification is prominent at the A&M and Gordon Lake road peperite localities as pervasive alteration in the tuffaceous component of the peperite as well as in less dismembered tuff adjacent to zones of magma and wet tuff mixing. The silicified tuff is light grey due to the absence of carbon and increase in quartz.

Carbonatization

Discordant carbonate alteration is significant in close proximity to the carbonate-hosted Zn-Cu-Pb Errington and Vermilion deposits (Martin, 1957; Paakki, 1992; Gray et al., 1995; Gray and Gibson, 1993). Similarly the intra-Onaping base metal showings studied including Simmons, Cow Lake, McNunes, Ryan, Limerick, and unnamed occurrences show similar discordant Fe-Mg carbonate alteration. Minor carbonate alteration occurs in the basal zone of silicification and as amygdale fillings in peperite bodies within Dowling member strata.

DISCUSSION AND CONCLUSIONS

The Onaping Formation is not a fallback breccia nor a sequence of ash flow tuffs (Gibson et al., 1994) but neither is it a typical volcanic cauldron sequence. The entire 1400 m fragmental sequence including flow banded aphanitic dykes are compositionally similar (Gibbins, 1994), but cauldron sequences usually contain chemically variable lava flows, pyroclastic flows, domes, and debris flows. Single terrestrial calderas are smaller than the Sudbury structure.

Peperite bodies near the top of the Onaping Formation are significant in that magmatism continued throughout Onaping time, therefore deposition of the Onaping formation was not an instantaneous event. This is evidence against a meteorite fallback origin for the breccia. Zones of peperite have only been observed stratigraphically below known VMS deposits on the south-southwest part of basin and are associated with sericitization and silicification. Low confining pressures are required to form peperite bodies (Kokelaar, 1982) and thus peperites are suggestive of shallow water conditions.

Chlorite and calcite alteration minerals were previously observed within the Onaping Formation (Muir and Peredery, 1984). Schandl et al. (1986) documented compositional zoning in feldspar speciation from lower Na-rich feldspar to upper K-rich feldspars within the Onaping Formation, concluding that the alteration zonation was due to cooling of a single ignimbrite sheet. This hypothesis is weakened by field observations of: 1) type 3 feldspathization with microcline in the lower Sandcherry member rocks, coupled with preliminary microprobe results which indicate orthoclase and albite in the lower member rocks; 2) distinct different stratigraphic units; and 3) the distribution of alteration types.

Peredery (1972) interpreted complex glasses composed of mafic and felsic minerals as original heterogeneous features, atypical of volcanic glasses, formed during quenching of shock melted country rocks. In the light of extensive detailed field documentation of alteration in this study, the heterogeneous nature of glass shards is found to be due to devitrification, silicification, feldspathization, palagonitization, chloritization, and carbonatization.

The Onaping Formation is intruded at different stratigraphic intervals by granophyres of the Sudbury igneous complex (Muir and Peredery, 1984). In the north range the Sudbury igneous complex intrudes Sandcherry member strata whereas deeper stratigraphic levels are intruded in the south and east range, exposing the Basal member. The Onaping Formation on the north range could have been significantly thicker, with the base removed by the Sudbury igneous complex. The map distribution of the basal silicification zone, termed 'undefined units' by Gibbins (1994), is discontinuous along strike with intervening 'Basal intrusion and Fluidal-fragment' units and the Sudbury igneous complex. Various interpretations of the lower silicification zone based on the field observations outlined in this study and above are permissible. The upper contact of the silicified zone may represent: 1) a hiatus, between the silicified rocks and unaltered units that contain altered fragments, significant enough to allow deposition, metasomatism and lithification of the basal zone prior to rebrecciation; 2) syndepositional alteration with a progressive irregular, alteration front in which rocks, that have been silicified, brecciated and deposited in overlying sequences were subsequently silicified; 3) an early syndepositional silicification event that was originally discontinuous; or 4) continuous deposition but, subsequently intruded by aphanitic dykes and 'fluidal-fragment' units. There is no evidence of an erosional unconformity to support the first hypothesis but the others remain permissible; further field work will concentrate on this problem.

Many authors have suggested that the Sudbury igneous complex was the heat source for the Errington and Vermilion base metal deposits (Burrows and Rickaby, 1930; Martin, 1957; Card and Hutchinson, 1972; Paakki, 1992) but cross-cutting relationships show that a large hydrothermal alteration system was active prior to emplacement of the granophyre of the Sudbury igneous complex. Since the basal silicification is a syndepositional event it is not plausible that the intruding granophyre of the Sudbury igneous complex is the heat source. The patchy distribution of carbon in the Sandcherry member at Joe Lake and Capreol close to the granophyre contact, the removal of carbon within breccias adjacent to dykes, and the absence of carbon in silicified rocks in the Dowling member, suggest that carbon was once

ubiquitous throughout the Onaping Formation, but was subsequently oxidized and moved upward by a silica-rich hydrothermal fluid.

Determining the precise relationship between regional semi-conformable alteration and VMS deposits on the south range is inhibited by thrusting and intense deformation. Preliminary Pb-isotope studies of galena (Jonasson, pers. comm.) indicate that the Errington, Vermilion, and intra-Onaping base metal showings and deposits yield the same isotope signatures suggesting they formed during the same mineralizing event. Determining the genetic relationship between the intra-Onaping base metal showings and the types of regional alteration will enhance our knowledge of the processes involved in forming VMS related hydrothermal systems.

ACKNOWLEDGMENTS

Selection of the map areas was based on 2-km-spaced reconnaissance traverses mapped by Lori Nunes-Kormos, Stuart Gibbins (Falconbridge Ltd.) and Harold Gibson in 1990/91 and property maps; results from a joint venture agreement between Inco Ltd., Royal Oak, and Falconbridge Ltd. Field work was greatly aided by the assistance of N. Bernadetti, J. Stoness, C. Oreskovich, J. Fowler and S. Harding. Special thanks goes to I.R. Jonasson for discussion and critical review.

REFERENCES

Avermann, M.
1992: Die genese der allochthonen, polymikten breccien der Onaping Formation, Sudbury Struktur, Ontario, Kanada; Ph.D. thesis, Munster University, Munster, Germany, 170 p.

Burrows, A.G. and Rickaby, H.C.
1930: Sudbury basin area; Ontario Department of Mines, Annual Report for 1929, v.38, Part 3, 55 p.

Card, K.D.
1992: Circa 1.75 Ga ages for plutonic rocks from the Southern Province and adjacent Grenville Province: what is the expression of the Penokean Orogeny? Discussion; in Radiogenic Age and Isotopic Studies: Report 6; Geological Survey of Canada, Paper 92-2, p. 227-228.

Card, K.D. and Hutchinson, R.W.
1972: The Sudbury Structure: its regional geological setting; in New Developments in Sudbury Geology; Geological Association of Canada, Special Paper 10, p. 67-68.

Corfu, F. and Andrews, A.J.
1986: A U-Pb age for mineralized Nipissing Diabase, Gowganda, Ontario; Canadian Journal of Earth Sciences, v. 23, p. 107-109.

Dence, M.R.
1972: Meteorite impact craters and the structural geology of the Sudbury Basin; in New Developments in Sudbury Geology; Geological Association of Canada Special Paper 10, p. 7-18.

Fisher, R.V.
1966: Rocks composed of volcanic fragments and their classification; Earth Science Reviews, v. 1, p. 287-298.

French, B.M.
1968: Sudbury structure, Ontario: some petrographic evidence for and origin by meteorite impact; in Shock Metamorphism of Natural Materials, B.M. French and N.M. Short (ed.), Mono Book Corporation, p.383-412.

Gibbins, S.F.M.
1994: Geology, geochemistry, stratigraphy and mechanisms of emplacement of the Onaping Formation, Dowling Area, Sudbury Structure, Ontario Canada; M.Sc. thesis, Laurentian University, Sudbury, Ontario. 314 p.

Gibson, H.L., Gibbins, S.F.M., Gray, M.J., Stoness, J.A., Rogers, D., Jonasson, I.R., and Ames, D.E.
1994: Origin of the Onaping Formation and Zn-Cu-Pb massive sulphide deposits of the Proterozoic Sudbury Structure; in NODA (Northern Ontario Development Agreement) Summary Report 1993-1994; p. 90-94.

Gray, M., Bell, M., Tims, A., Wells, K., and Germundson, K.
1995: Vermillion central geology (map); in; The Geological Setting of the Vermilion Zn-Cu-Pb-Ag-Au Massive Sulphide Deposit, Sudbury Basin, Ontario, Canada; M.Sc. thesis (M. Gray, 1995), Laurentian University, Sudbury Ontario, p. 245.

Gray, M.J. and Gibson, H.L.
1993: Geological setting of the Vermilion Cu-Zn-Pb-Au-Ag massive sulphide deposit, Sudbury Basin in Joint Annual Meeting of the Geological Association of Canada/Mineralogical Association of Canada, Edmonton, Alberta, Program with Abstracts, p. A37.

Jonasson, I.R. and Gibson, H.L.
1993: Origin of the Onaping Formation and Zn-Cu-Pb massive sulphide deposits of the Proterozoic Sudbury Structure; in NODA (Northern Ontario Development Agreement) Summary Report 1992-1993; p. 93-96.

Kokelaar, B.P.
1982: Fluidization of wet sediments during the emplacement and cooling of various igneous bodies; Journal of the Geological Society of London, v. 139, 21-33.

Krogh, T.E., Davis, D.W., and Corfu, F.
1984: Precise U-Pb zircon and badeleyite ages for the Sudbury area; in The Geology and Ore Deposits of the Sudbury Structure; Ontario Geological Survey, Special Volume 1, p. 431-446.

Martin, W.G.
1957: Errington and Vermilion mines; in Structural Geology of Canadian Ore Deposits, 6th Commonwealth Mining and Metallurgical Congress, v. 2, p. 363-376

McPhie, J., Doyle, M., and Allen, R.
1993: Volcanic textures: a guide to the interpretation of textures in volcanic rocks; CODES Key Centre, University of Tasmania, 198 p.

Muir, T L.
1981: Geology of the Capreol Lake area, District of Sudbury; Ontario Geological Survey, Miscellaneous Paper 106, p. 76-79.
1983: Geology of the Morgan Lake-Nelson Lake area, District of Sudbury; Ontario Geological Survey, Open File Report 5426, 203 p.
1984: The Sudbury Structure: considerations and models for an endogenic origin; in The Geology and Ore Depositis of the Sudbury Structure; Ontario Geological Survey, Special Volume 1, p. 449-489.

Muir, T.L. and Peredery, W.V.
1984: The Onaping Formation; in The Geology and Ore Deposits of the Sudbury Structure; Ontario Geological Survey, Special Volume 1, p. 139-210.

Paakki, J. J.
1992: Geology of the Errington Mine Property #1 and #2 Shaft area-Sudbury Mining District (map); in The Errington Zn-Cu-Pb massive sulphide deposit, Sudbury, Ontario: Its Structural and Stratigraphic Setting and Footwall Alteration; M.Sc. thesis, Laurentian University, Sudbury, Ontario, 140 p.

Peredery, W.V.
1972: The origin of rocks at the base of the Onaping Formation, Sudbury, Ontario; Ph.D. thesis, University of Toronto, Toronto, Ontario, 366 p.

Rousell, D.H.
1984: Nature and origin of mineral occurrences inside the Sudbury Basin; Canadian Institution of Mining and Metallurgy, Bulletin 77, no.872, p. 63-75.

Rousell, D.H.
1984: Mineralization in the Whitewater Group; in The Geology and Ore Deposits of the Sudbury Structure, E.G. Pye, A.J. Naldrett and P.E. Giblin (ed.); Ontario Geological Survey, Special Volume 1, p. 219-232.

Schandl, E.S., Martin, R.F., and Stevenson, J.S.
1986: Feldspar mineralogy of the Sudbury igneous complex and the Onaping Formation, Sudbury, Ontario; Canadian Mineralogist, v. 24, p. 747-759.

Sims, P.K., Van Schmus, W.R., Schulz, K.J., and Peterman, Z.E.
1989: Tectono-stratigraphic evolution of the Early Proterozoic Wisconsin magmatic terranes of the Penokean Orogen; Canadian Journal of Earth Science, v. 26, p. 2145-2158.

Stevenson, J.S.
1972: The Onaping ash-flow sheet, Sudbury, Ontario; in New Developments in Sudbury Geology, J.V. Guy-Bray (ed.); Geological Association of Canada, Special Paper 10, p.41-48.

Stevenson J.S.
1990: The volcanic origin of the Onaping Formation, Sudbury, Canada; Tectonophysics, v. 171 (1-4), p. 249-257.

Stevenson, J.S.
1961: Recognition of the quartzite breccia in the Whitewater Series, Sudbury Basin, Ontario; Royal Society of Canada, Transctions, v. 55, series 3, p. 57-66.

Stoness, J.A.
1994: The stratigraphy, geochemistry and depositional environment of the Proterozoic Vermilion Formation, host to the Errington and Vermilion Zn-Cu-Pb massive sulphide deposits, Sudbury, Ontario; M.Sc. thesis, Laurentian University, Sudbury, Ontario, 205 p.

Thomson, J.E.
1957: Geology of the Sudbury Basin; Ontario Department of Mines, Annual Report for 1956, v. 65, part 3, p. 1-56.

Van Schmus, W.R.
1980: Chronology of igneous rocks associated with the Penokean orogeny in Wisconsin, Geological Society of America, Special Paper 182, p. 159-168.

Williams, H.
1957: Glowing avalanche deposits of the Sudbury Basin; Ontario Department of Mines, Annual Report for 1956, v. 65, part 3, p. 57-89.

Geological Survey of Canada Project 940002

Distribution and character of gold in surface till in the Flin Flon greenstone belt, Saskatchewan[1]

P.J. Henderson and M. Roy[2]
Terrain Sciences Division

Henderson, P.J. and Roy, M., 1995: Distribution and character of gold in surface till in the Flin Flon greenstone belt, Saskatchewan; in Current Research 1995-E; Geological Survey of Canada, p. 175-186.

Abstract: Gold distribution in till overlying the Flin Flon greenstone belt results from a combination of glacial transport and post-glacial weathering effects. On a regional scale, elevated gold values in the <0.063 mm fraction of till are found in areas of known gold mineralization. Ninety-three per cent of visible gold grains are in this size range and exhibit predominantly modified and pristine morphologies. In a detailed study conducted down-ice from a known gold occurrence, gold concentrations in weathered till (<0.063 mm fraction) are anomalous for the region. The size and morphology of gold grains in these samples are similar to the regional study. Pristine grains exhibit features observed in gold associated with pyrite and quartz in the mineralized bedrock. The presence of these grains in till suggests release from sulphides by post-glacial weathering processes. This observation questions the validity of using gold grain morphology in weathered till as an indicator of glacial transport distance.

Résumé : La distribution de l'or dans le till reposant sur la ceinture de roches vertes de Flin Flon est le résultat des effets combinés du transport glaciaire et de l'altération postglaciaire. À l'échelle régionale, les concentrations élevées d'or dans la fraction de <0,063 mm du till s'observent dans les zones de minéralisation aurifère connue. Quatre-vingt-treize pour cent des grains d'or visibles se situent dans cette fraction granulométrique et présentent surtout des morphologies inaltérées et modifiées. Dans une étude détaillée réalisée en aval-glaciaire d'un indice aurifère connu, les concentrations de l'or dans le till altéré (fraction de <0,063 mm) constituent une anomalie dans la région. La taille et la morphologie des grains d'or de ces échantillons sont semblables à celles établies dans l'étude régionale. Les grains inaltérés présentent des caractéristiques observées dans l'or associé à de la pyrite et du quartz dans le substratum rocheux minéralisé. La présence de ces grains dans le till incite à conclure qu'ils ont été arrachés des sulfures par des processus d'altération postglaciaires. Cette observation met en doute la validité d'utiliser la morphologie des grains d'or dans le till altéré comme indicateur de la distance du transport glaciaire.

[1] Contribution to Canada-Saskatchewan Partnership Agreement on Mineral Development (1990-1995), a subsidiary agreement under the Canada-Saskatchewan Economic and Regional Development Agreement.
[2] Département des Sciences de la Terre, Université du Québec à Montréal (UQAM), case postale 8888, succ. A, Montréal, Québec, Canada H3C 3P8

INTRODUCTION

Many researchers have examined the nature of gold distribution in till and addressed the difficulties associated with analytical techniques and reproducibility of results commonly involved in gold exploration using overburden (Lakin et al., 1974; DiLabio, 1985; 1990; Averill and Zimmerman, 1986; Rampton et al., 1986; Nichol et al., 1992; among others). These studies have identified many factors affecting gold concentrations in glacially derived sediments, particularly till. These factors include: 1) the degree of alteration of the till, 2) analytical techniques, 3) sample size, 4) the size range of gold in till, 5) the form of gold within the primary deposit, 6) the distribution of drift cover, and 7) the Quaternary history of the area. All studies emphasize the uniqueness of each mineralized region and the importance of developing exploration strategies specific to an area and/or deposit. In this paper we will concentrate on some of the factors affecting gold distribution in the Flin Flon greenstone belt, northern Saskatchewan, by examining the distribution of both visible gold grains and gold in the finer grained fractions of till. The size and morphology of gold grains will be characterized on a regional scale and the significance of these attributes to drift prospecting will be examined in a detailed study carried out in an area of known gold mineralization.

Studies focusing on drift prospecting with reference to gold in Canadian Shield areas of Saskatchewan include work by Averill and Zimmerman (1986), Schreiner (1986), Sopuck et al. (1986), and Campbell and Schreiner (1989). Campbell (1988) examined the gold distribution in tills in part of the Flin Flon greenstone belt included in this study. These last results will be integrated into this paper.

This project is part of a program which incorporates surficial geology mapping with geochemical studies of till and humus in the Amisk Lake-Annabel Lake area as part of the Canada-Saskatchewan Partnership Agreement on Mineral Development 1990-95 (Henderson and Campbell, 1992, 1994; Henderson, 1995). The study area (Fig. 1) is underlain by Proterozoic metavolcanic and metasedimentary rocks of the Flin Flon greenstone belt and the high grade metamorphic equivalent of the belt, the Kisseynew terrane, to the north. In the south, Canadian Shield rocks are unconformably overlain by Paleozoic dolomite and sandstone (Macdonald, 1987). The area has a high potential for gold and base metal mineralization (McDougall et al., 1982).

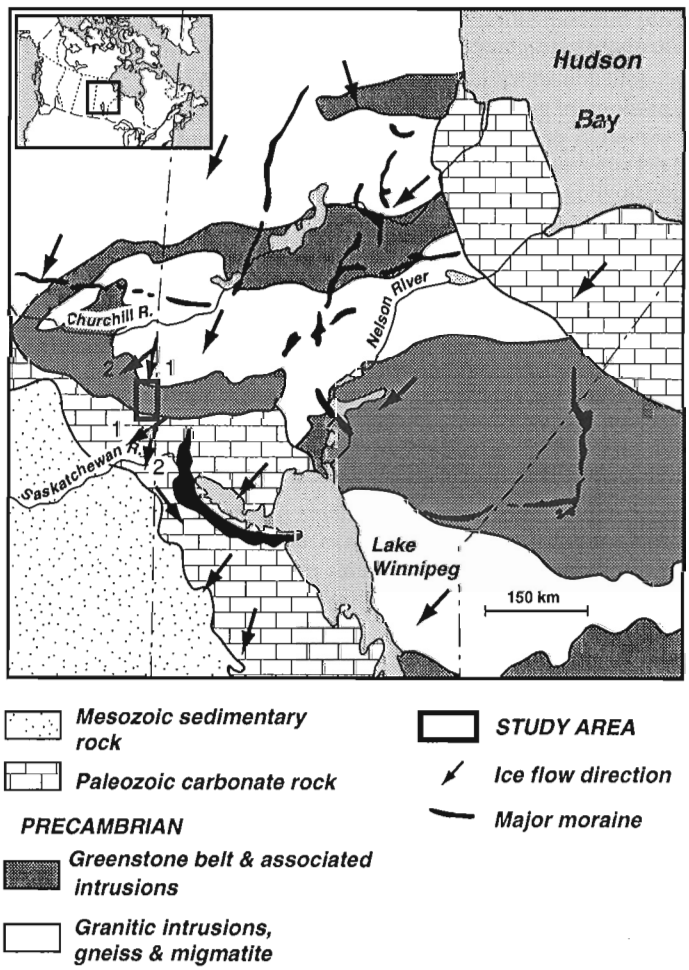

Figure 1. Location map showing major moraines and regional ice flow trends (after Prest et al., 1968). 1 = oldest relative age.

QUATERNARY GEOLOGY

The Quaternary geology of northern Saskatchewan has been mapped by Schreiner (1984). Surficial mapping has also been completed in the Flin Flon and Cormorant Lake areas (NTS 63K/12 and/13) (Clarke, 1989). More detailed Quaternary geology maps (scale 1:50 000) for the Amisk Lake-Annabel Lake area are presently in preparation (Campbell and Henderson, in prep.; Henderson, in prep.).

The region was glaciated by ice flow from a dispersal centre in the District of Keewatin (Prest et al., 1968). Dominant regional ice flow indicators in the study area trend south-southwest (190° to 206°) (Henderson and Campbell, 1994; McMartin, 1994; McMartin and Campbell, 1994; Nielsen, 1994) (Fig.1). Striations indicating an earlier ice flow (215° to 226°) are present within and east of Amisk Lake. A similar southwest ice flow trend (213° to 224°) recognized north of Creighton and Annabel Lake and in the eastern part of the area postdates the main south-southwest flow (190°-206°) and is interpreted as forming during a glacial readvance. During ice retreat, the entire area was inundated by Glacial Lake Agassiz and glaciolacustrine silt and clay are present in topographic depressions. Models for the deglaciation of northern Saskatchewan and Manitoba and the probable extent of Lake Agassiz are presented in Teller and Clayton (1983) and Schreiner (1984), among others.

On the shield, drift cover is thin (<2 m) and discontinuous with thicker accumulations occurring on the down-ice side of outcrops and in depressions; south of the shield margin, drift forms a thin, continuous blanket over dolomitic bedrock. Extensive deposits of glaciofluvial and glaciolacustrine origin are present north of Annabel Lake in an east-west-trending belt and as discontinuous, north-south-trending linear

features, east of Amisk Lake. These stratified sequences are interpreted as subaqueous outwash (Henderson and Campbell, 1994).

BEDROCK GEOLOGY AND GOLD MINERALIZATION

Bedrock mapping in the Annabel Lake-Amisk Lake area includes the work of Byers and Dahlstrom (1954), Byers et al. (1965), and Syme et al. (1993), among others. This discussion will focus on rocks of the Flin Flon greenstone belt which host the major gold occurrences in the area (Fig. 2).

The Flin Flon greenstone belt includes the Amisk Group, a metamorphosed assemblage of volcanic and associated sedimentary rocks, and the Missi Group, an overlying sequence of metamorphosed immature sandstones and conglomerates. These rocks have been intruded by a diverse suite of intrusive rocks, ranging from gabbroic to granitic composition, during various phases of deformation. East of Amisk Lake, the Amisk Group is composed primarily of subaqueous mafic to intermediate flows and pyroclastic rocks, with subordinate felsic to intermediate flows, volcaniclastic and sedimentary rocks. West of the lake, felsic to intermediate flows and pyroclastics predominate.

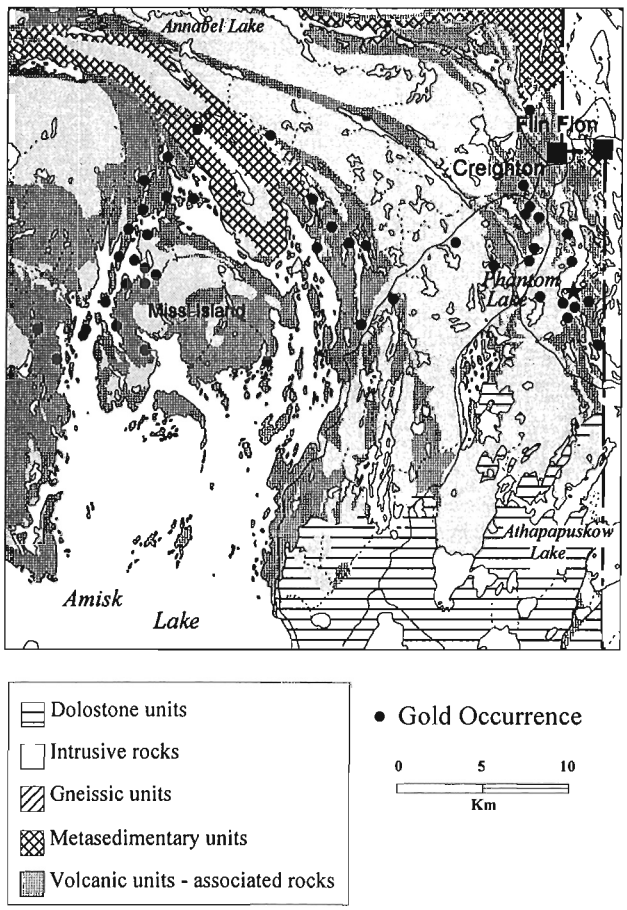

Figure 2. Distribution of known gold deposits and occurrences in the Annabel-Amisk Lake area (after Pearson, 1983). Star indicates the location of the detailed study. Geology simplified from Byers and Dahlstrom (1954) and Byers et al. (1965).

Gold occurs in two areas of the Flin Flon greenstone belt (Fig. 2): a) the Amisk Lake area, particularly the West Channel and Missi Island, and b) east of Amisk Lake in the vicinity of Creighton and Flin Flon (Coombe, 1984). The majority of these occurrences exhibit structural control, lying within fracture zones that are typically sulphide-bearing and may or may not be quartz-filled.

In the Amisk Lake area, all gold occurrences are hosted within Amisk Group metavolcanic rocks and associated intrusives and Missi Group metasedimentary rocks. Occurrences are commonly associated with widespread carbonatization, sericitization, silicification and tourmalinization of adjacent wall rocks. Associated mineralization may include pyrite, arsenopyrite, chalcopyrite, molybdenite, and galena (Pearson, 1980, 1983).

In the Creighton-Flin Flon area, occurrences are known in all rock types. Two generations of deposits have been recognized (Pearson and Galley, 1985). In the earlier generation deposits, quartz-sulphide veins, similar in mineralogy, lie within narrow alteration zones. Later generation deposits are more complex and exhibit differing ore mineralogy, host rock and alteration assemblages. Mineralization includes pyrite, chalcopyrite, arsenopyrite, molybdenite, and scheelite (Galley and Franklin, 1987). Associated alteration varies, but includes carbonatization, silicification, chloritization, and epidotization.

DRIFT PROSPECTING

Drift prospecting in the area is complicated by the presence of thick glaciolacustrine deposits which overlie previously deposited sediment in depressions and by extensive areas of ice marginal sedimentation. In upland areas or on the downice side of outcrops, a locally derived, commonly thin, till is present in depressions in the bedrock surface or buried beneath a thin glaciolacustrine cover. Striations on bedrock surfaces underlying this unit at several sites parallel the dominant ice flow trend. Since the composition and texture of the till is closely related to the lithology of the local bedrock, it is the optimal sampling unit for drift prospecting.

Samples were obtained primarily from pits dug to bedrock or 1.0 m depth and, in nearly all cases, were collected below the A and B soil horizon in order to minimize geochemical effects resulting from weathering processes. Over 400 6 kg till samples were collected at approximately 1-5 km spacing depending on access (Henderson, 1995). At selected sites, larger 10-12 kg samples were also collected for mineralogical analyses.

Analytical procedures

Gold was analyzed in the <0.063 mm (silt plus clay) fraction of till on a regional basis and, at the selected sites, by grain counts of visible gold. This analytical strategy was based on

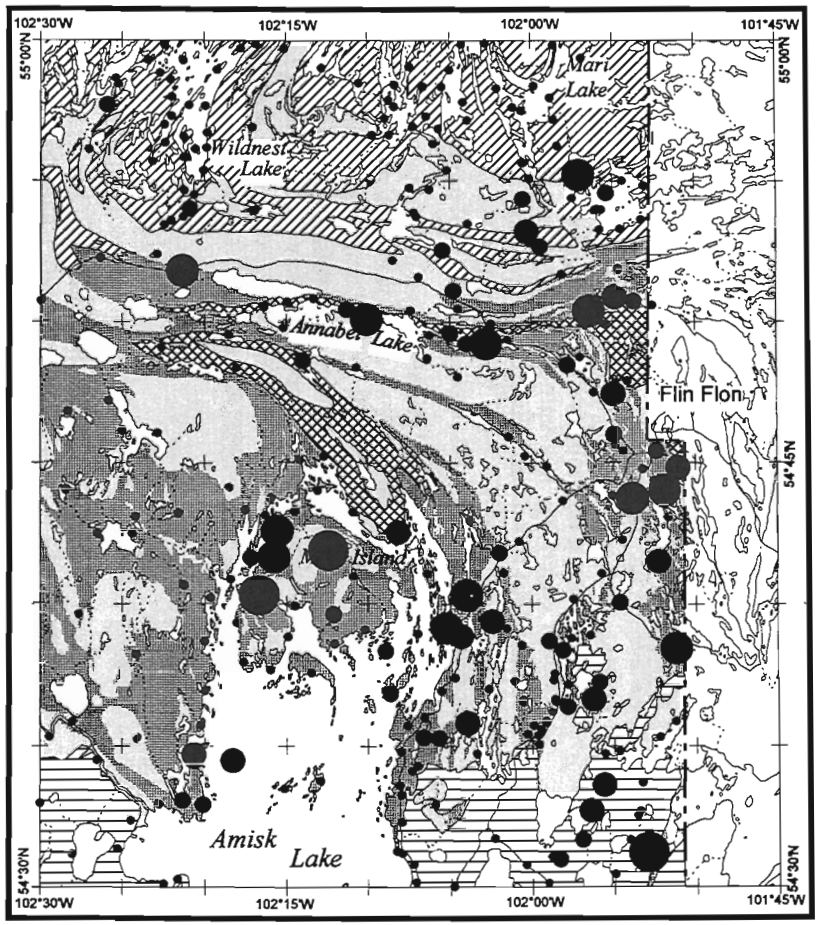

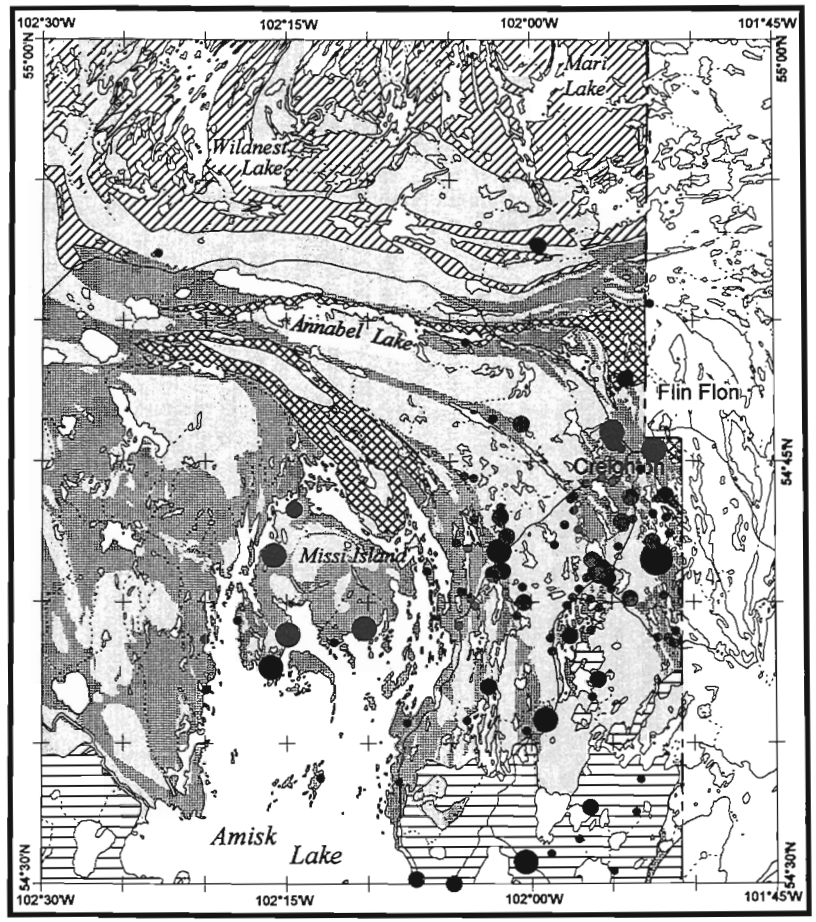

MIN ppb	MAX ppb	%TILE	#SAMP
1	9	78	275
10	16	10	41
17	26	4	17
27	50	3	14
51	148	0	3

Dolostone units
Intrusive rocks
Gneissic units
Metasedimentary units
Volcanic units - associated rocks

5 0 5 10 15
Km Km

Number of grains (10 Kg sample)

MIN grain	MAX grain	#SAMP
0	10	72
11	25	26
26	50	10
50	96	1

Data collected from this study
Data from Campbell, 1988

a) Gold in till (<0,063 mm fraction)

b) Visible gold grains in till (normalized to 10 kg < 2 mm table feed)

Figure 3a. *Regional distribution of gold in the <0.063 mm fraction of till. %tile = percentile.* ***b.*** *Distribution of the number of visible gold grains in till normalized to 10 kg <2 mm table feed.*

cost and on earlier work of Campbell (1988) and Schreiner (1986) which concluded that gold occurs predominantly in the fine fraction, generally <0.050 mm diameter. Nichol et al. (1992) concluded that <0.063 mm fraction is the optimum analytical fraction in gold prospecting. Gold grains extracted from till were examined to determine the number, character, and grain size distribution within the till.

The <0.063 mm fraction of till was separated by dry sieving. Au, Pt and Pd concentrations were determined by fire assay/atomic fluorescence spectrometry on approximately 30 g of this fraction by Chemex Inc., Vancouver, B.C. (Henderson, 1995, Appendix VI). Analytical accuracy and precision were monitored through duplicate analyses of submitted field samples and a laboratory standard. Results of analyses of the standard show good reproducibility; other duplicate analyses show poor reproducibility (Henderson, 1995, Appendix X). This inconsistency is common in gold analyses and has been attributed to the particulate nature in which gold occurs coupled with sample inhomogeneity (Lakin et al., 1974; Nichol et al., 1992). High gold values may be related to the presence of large grains in a subsample (the "nugget" effect). On a regional scale, however, gold analyses of the <0.063 mm fraction of till will highlight areas of potential mineralization, although at specific sites gold anomalies may be undetected or falsely represented.

Visible gold grains were extracted from the <2 mm fraction of the 10-12 kg till samples by Overburden Drilling Management Ltd., Nepean, Ont. using a shaker table followed by panning. Grains were counted and classified on the basis of size and morphology. Three categories based on morphology have been recognized: pristine, modified, and reshaped (DiLabio, 1990). These shape classes reflect the appearance and surface texture of the grain and have been used as an indication of distance of glacial transport (Averill and Zimmerman, 1986). Larger grains (>0.100 mm) were removed and examined under the SEM (scanning electron microscope) at the Geological Survey of Canada.

REGIONAL DISTRIBUTION OF GOLD

Till geochemistry

The regional distribution of gold in the <0.063 mm fraction is shown in Figure 3a. Within the area, gold values in this fraction range from below detection limit to 148 ppb. Values >10 ppb are considered significant (DiLabio, 1982); elevated values exceed the arithmetic mean by one standard deviation (s.d.) (>17 ppb); anomalous values by twice the s.d. (>27 ppb); and highly anomalous by three times the s.d.(>51 ppb) (Bird and Coker, 1987). Highest gold concentrations are clustered in four areas within the Flin Flon greenstone belt: 1) Missi Island, Amisk Lake, 2) the eastern shore of Amisk Lake, east of Missi Island, 3) south of Creighton-Flin Flon, and 4) along an east-west zone encompassing Annabel Lake. Extensive gold mineralization is known from three of these areas (Fig. 2). No known occurrences are reported in conjunction with anomalous concentrations (>27 ppb) present in the Annabel Lake zone, north-northwest of Creighton, and west of Athapapuskow Lake (cf. Fig. 2). However, the association between areas of known gold occurrences and gold concentrations in the <0.063 mm fraction of till indicates that gold is transported glacially from mineralized zones and till analyses can be an effective means of prospecting despite the limitations of gold analyses discussed in the previous section.

Visible gold grains

The distribution of visible gold grains extracted from bulk till samples (normalized to 10 kg <2 mm table feed) is shown in Figure 3b. In the present study, 48 samples were examined and 790 grains counted with the largest proportion (93%) <0.063 mm diameter (Table 1). The number of grains recovered from the tills ranges from 2 to 70 for an average of 17 grains per sample. This differs significantly from the study conducted by Campbell (1988) where the number of grains ranged from 0 to 13 and averaged 5 grains per sample from a

Table 1. Size distribution and morphology of visible gold grains extracted from till in the Amisk Lake-Annabel Lake area

a) Shape classification based on binocular microscope examination					
		Percentage of Visible Gold Grains			
Area	Grain size	Reshaped	Modified	Pristine	Total # Grains
Regional Study	<0.063 mm	53.9	34.2	12	735
(Henderson, 1995)	>0.063 mm	58.2	32.7	9.1	55
		Abraded	Irregular	Delicate	
East Amisk Lake	<0.063 mm	50.2	41.9	7.9	241
(Campbell, 1988)	>0.063 mm	27.8	57.4	14.8	54
b) Shape classification based on SEM examination					
		Percentage of Visible Gold Grains			
Area	Grain size	Reshaped	Modified	Pristine	Total # Grains
Regional Study	<2 mm	12.9	59.7	27.4	62

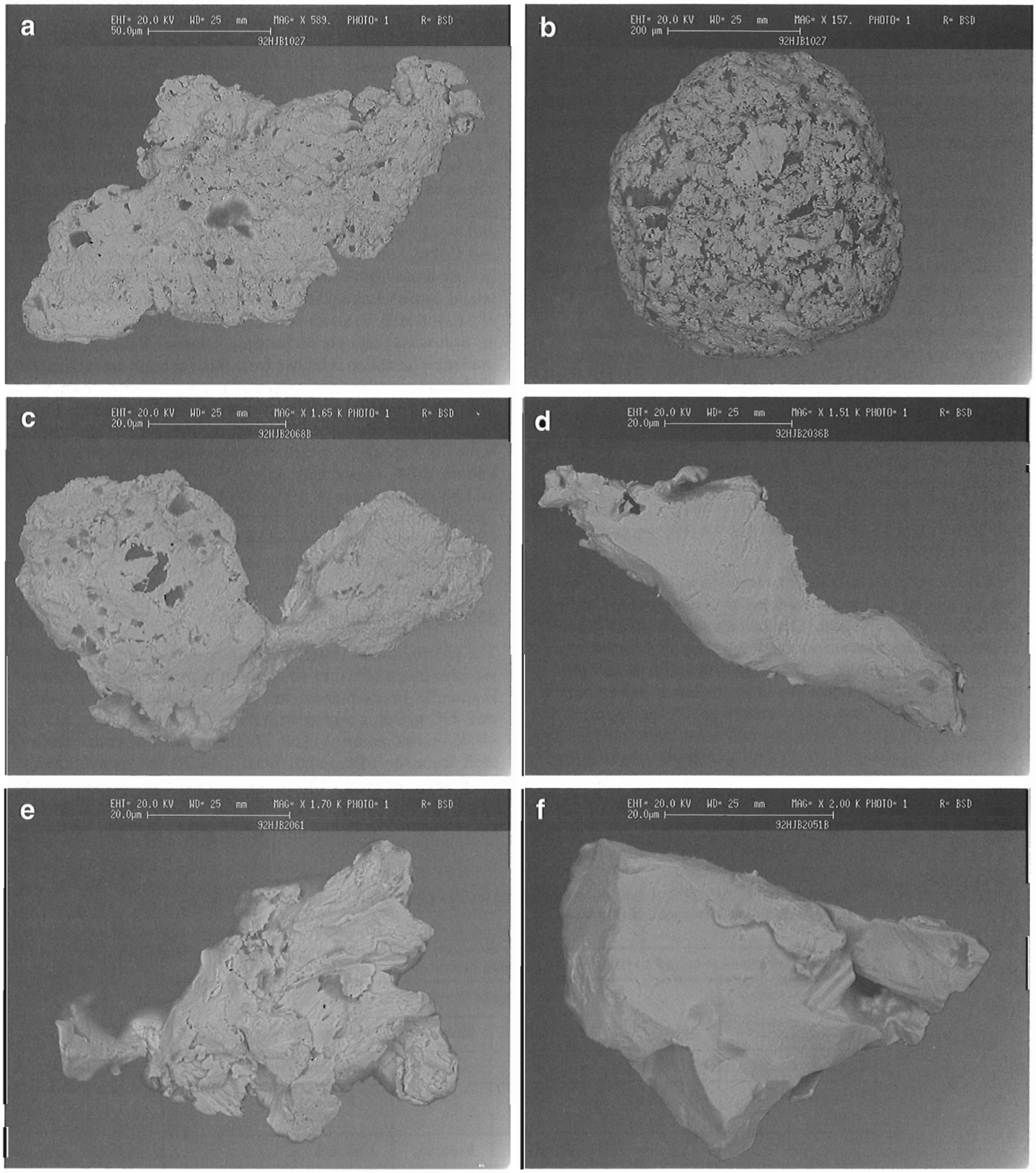

Figure 4. *Range of morphologies of gold grains extracted from the regional tills.* ***a,b****): Reshaped grains showing pitted and spongy surface. Folded protuberances are present at the grain edges (a).* ***c,d****): Modified grains with original shapes somewhat preserved. All edges appear curled, folded and/or blunted. Grain surfaces may be damaged (c).* ***e,f****): Pristine to slightly modified gold grains collected from till near Creighton. Crystal faces are preserved. Surfaces are smooth.*

similar amount of material. This discrepancy is most likely due to differences in sophistication of analytical procedures since the technique was in its infancy during the earlier study. Despite the differences, it is important to note that the highest number of gold grains for both studies is in the Flin Flon-Creighton area where gold mineralization is known. Significant concentrations are also present on Missi Island, Amisk Lake.

In the regional till database (Henderson, 1995), gold grain morphologies were classified through binocular microscope examination based on the scheme of DiLabio (1990) (Table 1a). Approximately half (54%) of the 790 grains extracted were classified as reshaped and 12% as pristine. The grains are predominantly silt-sized (54%) and compositions are mainly native gold with traces of silver. Examination with the SEM revealed a wide variety of grain shapes and considerable differences in the relative proportion of grains in each shape classification (Fig. 4). Based on SEM examination, the highest proportion of grains are described as modified (60%) and only 13% as reshaped (Table 1b). These observations question the reliability of binocular microscope classification for determining gold grain morphology.

Campbell (1988) used the terminology of Averill and Zimmerman (1986) to classify gold grains in the east Amisk Lake area using the binocular microscope. Approximately 46% of the 295 grains examined are described as reshaped, indicating some degree of reworking. Grains are predominantly fine (82% <0.063 mm) and, in contrast to the regional study, a higher proportion of coarser grains are classified as delicate in character (Table 1a).

DETAILED STUDY

A detailed study was conducted in the southeast end of Phantom Lake (cf. Fig. 2), in an area of known mineralization, the MacMillan prospect (Fig. 5). At this site, gold occurs in

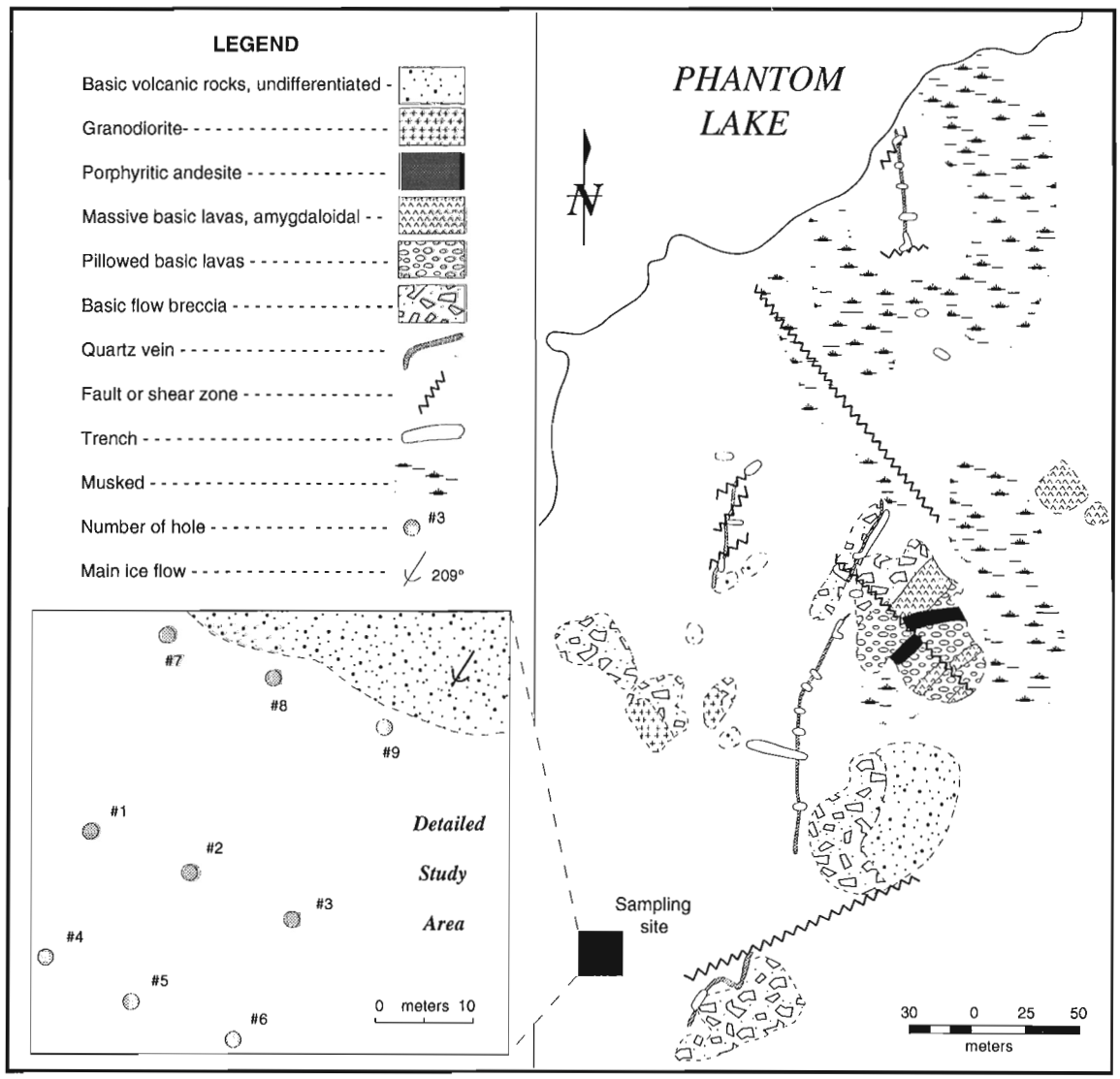

Figure 5. Geology of the MacMillan prospect showing location of detailed sampling grid (modified from Byers et al., 1965).

volcanic-hosted carbonate-quartz-sulphide zones (Pearson, 1983; Pearson and Galley, 1985). Four mineralized zones have been recognized (Byers et al., 1965). The mine is located in a quartz vein within massive and amygdaloidal basalts, flow breccias, and gabbro dykes. The vein is up to 60 cm wide, grey to white, and contains 5 to 10 per cent sulphides. The hangingwall rocks are altered to cherty quartz; footwall rocks are sheared and silicified. Pyrite, chalcopyrite, and galena are present in the quartz vein; pyrite, chalcopyrite, and gold in the cherty quartz.

Till distribution in the area of the deposit is discontinuous and occurs primarily on the flanks of outcrops. Depressions, including parts of the mineralized zone, are covered by thick deposits of glaciolacustrine sand and silt. Nine holes were dug in till on a grid (Fig. 5) in an area down-ice from the deposit. All holes were dug to bedrock and the degree of oxidation of the sediment varies from essentially unoxidized to highly oxidized. The pits were approximately 0.4 m diameter and ranged from 1.2 to 0.5 m depth. Each hole was sampled at 10 cm intervals. The <0.063 mm fraction of all samples was geochemically analyzed; the heavy mineral content and the composition and degree of weathering of clasts in the pebble fraction (4-8 mm) were determined to assess the degree of alteration of the sample medium (Roy, 1993). Finally, a bulk sample (10-12 kg) was taken at the base of each hole for visible gold analysis.

Table 2. Areal distribution of gold in the Phantom Lake sample grid

	Hole #7	Hole #8	Hole #9
<0.063 mm fraction (avg.) # visible gold grains	53.8 ppb 49	6.0 ppb 13	9.8 ppb 21
	Hole # 1	**Hole #2**	**Hole #3**
<0.063 mm fraction (avg.) # visible gold grains	32.0 ppb 36	29.6 ppb 44	25.3 ppb 45
	Hole #4	**Hole #5**	**Hole #6**
<0.063 mm fraction (avg.) # visible gold grains	37.0 ppb 62	37.5 ppb 70	30.2 ppb 40

Distribution of gold in till

The vertical distribution of gold in the <0.063 mm fraction of till collected in the Phantom Lake grid is variable (Roy, 1993). Gold values range from below detection limit to 88 ppb and average 30 ppb. This is significantly higher than the regional average (6.7 ppb), and is considered anomalous on that scale. With the exception of two holes, anomalous to extremely anomalous gold concentrations appear throughout or at some level within each hole although no consistent pattern is evident. This inconsistency is similar to that reported in previous studies examining the vertical variation in gold concentration in oxidized till (Rampton et al, 1986; DiLabio 1988).

The areal distribution of visible gold grains and the average gold concentration in the <0.063 mm fraction of till for each hole is given in Table 2. In both cases, absolute values increase in the down-ice direction (southwest to south-southwest): a result opposite to that expected in a classic dispersal train from the known deposit. Further detailed work is necessary to determine whether the observed pattern results from glacial processes peculiar to the site and/or represents an alternate source of gold mineralization.

Morphology and size of gold grains

Till

The size and morphology of gold grains extracted from till collected at the base of the holes in the sampling grid was examined. Of the 380 grains found, the bulk (94%) are in the <0.063 mm size range (Table 3). Grain morphologies are classified as dominantly reshaped and modified under the binocular microscope with the highest proportion of pristine grains in the finer size fraction. For the most part, a good correlation is present between the number of gold grains and gold concentration in the <0.063 mm fraction of till which suggests that the bulk of the gold is within the silt-size fraction.

Table 3. Distribution of the various gold grain morphologies in till collected in an area of bedrock mineralization

a) Shape classification based on binocular microscope examination					
Area	**Size Range**	**Percentage of Visible Gold Grains**			**Total # Grains**
		Reshaped	**Modified**	**Pristine**	
Phantom Lake	<0.063 mm	34.5	50.1	14.0	359
	>0.063 mm	66.7	28.6	9.5	21
b) Shape classification based on SEM examination					
Area	**Grain size**	**Percentage of Visible Gold Grains**			**Total # Grains**
		Reshaped	**Modified**	**Pristine**	
Phantom Lake	<2 mm	1.7	35.0	63.3	180

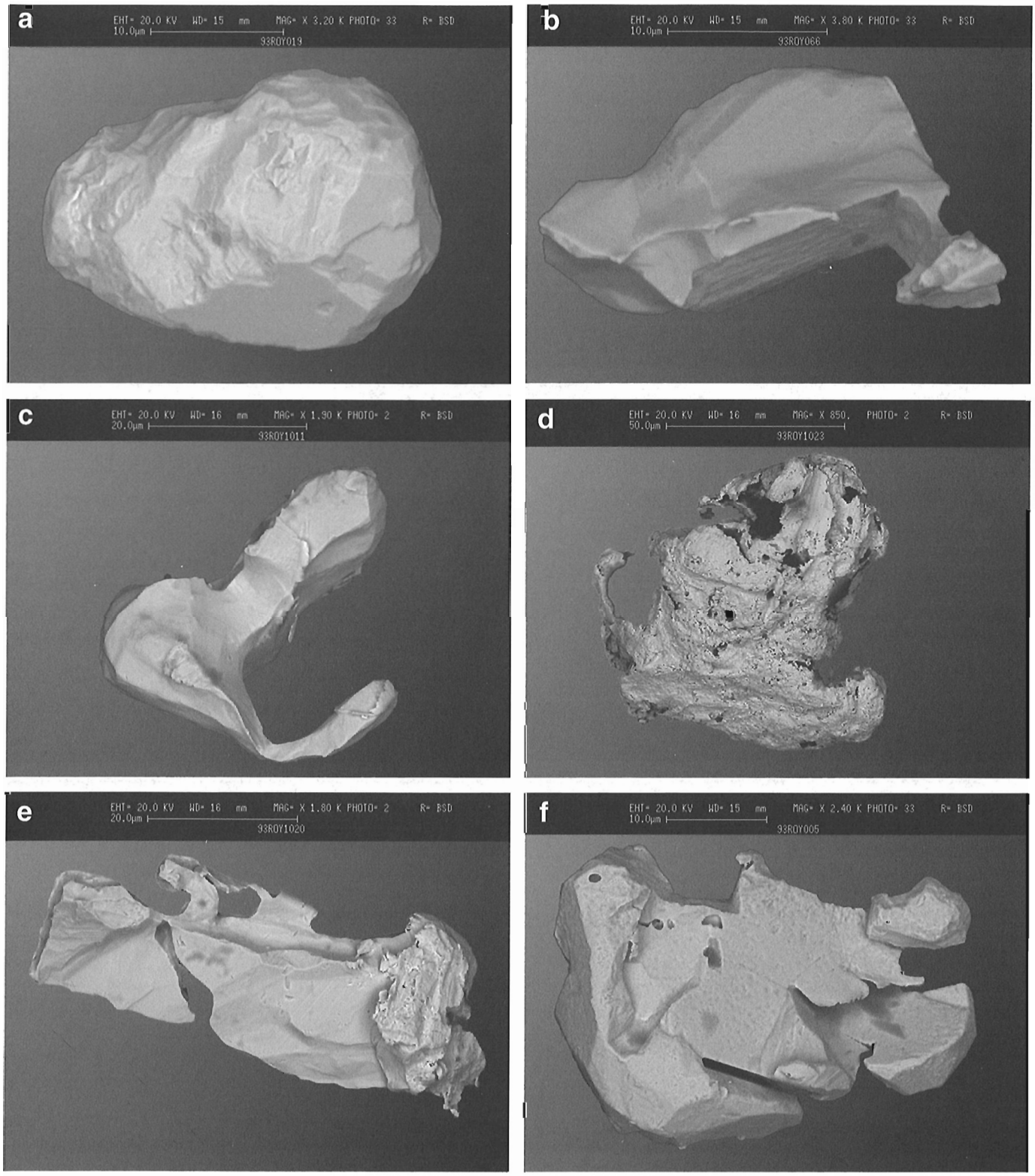

Figure 6. *Gold grains found in the till of the Phantom Lake area.* ***a,b):*** *Pristine grains showing crystal face and/or mold of the pyrite cubic crystal.* ***c,d):*** *Pristine to slightly modified grains with protruding wires folded or bent.* ***e,f):*** *Pristine grains showing void and indentations previously filled by quartz or sulphide.*

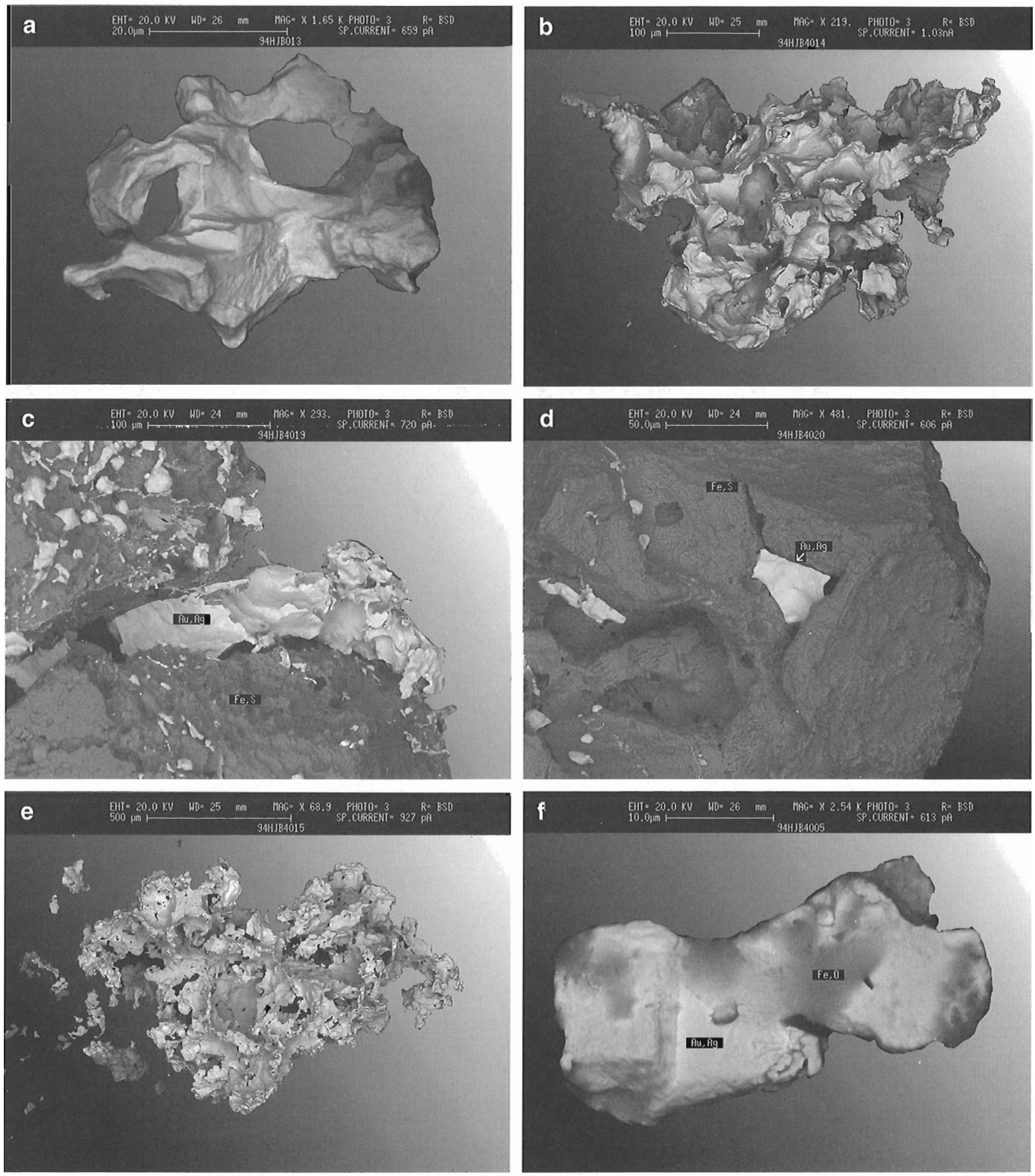

Figure 7. Gold grains extracted from a mineralized quartz vein in the Phantom Lake area. ***a,b):*** *Gold grain associated with quartz (note the sharp grain boundaries and remains of veinlets, now void).* ***c, d):*** *Gold grain associated with pyrite.* ***e):*** *Silt-sized flakes and large gold grain.* ***f):*** *Grain coating of iron oxide and incorporation of sulphides.*

Gold grains from till collected at the base of the holes have been examined under the SEM (Fig. 6). Single grains are primarily silt sized (94%). They are overwhelmingly classified as pristine (63%) and modified (35%) in shape, in contrast to the results obtained from binocular microscope examination (Table 3). The most common grain shape exhibits flat faces characteristic of crystal forms. These faces commonly have a cubic form and appear to represent a mold of part of the pyrite crystal with sharp edges (Fig. 6a,b). Protruding wires or projections which appear slightly folded or bent are also present (Fig. 6c,d). Voids or irregular shaped indentations suggest other primary mineralogical associations, likely with quartz (Fig. 6e,f). In occasional gold grains quartz was preserved in depressions in the grain surface. The composition of the gold grains is generally gold with a trace of silver.

Deposit

Several hand specimens containing visible gold were removed from the quartz vein at the MacMillan property and dissolved in hydrofluoric acid. In most cases, quartz was completely dissolved and resistate minerals, primarily sulphides, remained. This residual material was examined under a binocular microscope for hand-picking of gold grains and/or was panned and the heaviest grains were collected on a stub for examination under the scanning electron microscope.

Based on examination of 30 gold grains extracted from the quartz vein two associations of gold mineralization were recognized. The first type of gold occurs along quartz grain boundaries or as small veinlets or crystals within the quartz (Fig. 7a,b). It commonly exhibits void spaces, previously quartz filled, and extended protrusions with delicate terminations. The second type occurs as isolated grains or stringers within pyrite crystals (Fig. 7c,d). The size of primary gold grains occurs in two populations: the largest number averages 0.036 x 0.055 mm (silt size) and the other 0.7 x 1.0 mm (sand size). In some cases, the smallest grains appear to be derived from larger ones which are quite delicate and flaky, but generally similar in shape (Fig. 7e). Their surfaces are generally smooth and polished. Individual grains may be coated with iron oxides; cubic grain outlines suggest an association with sulphides such as pyrite or arsenopyrite during formation (Fig. 7f). As in the till, the composition of gold grains is generally gold with a trace of silver.

The similarity between the composition, size range, and morphology of grains extracted from the deposit and those found in till suggests that most pristine gold grains in the till are associated with the primary gold hosted in the mineralized quartz veins. In the deposit, gold grains are commonly associated with sulphides such as pyrite. In the till, no sulphides are present in the heavy mineral fraction due to the high degree of oxidation. If we assume that sulphides containing gold were originally within the till, it is conceivable that primary gold grains could have been released from the sulphide grains during the weathering process and exhibit no physical attributes resulting from glacial transport. In this instance, the shape of the grains has nothing to do with distance of glacial transport and everything to do with post-glacial weathering of the host minerals. The number of gold grains would be the best indication of closeness to the deposit.

SUMMARY

In the Amisk Lake-Annabel Lake area of the Flin Flon greenstone belt, gold occurs predominantly in the silt-size range. Therefore, analyses of the <0.063 mm fraction of till should give a reasonable indication of the gold mineralization in the area. This appears to be generally true on the regional scale and within the detailed study area; however, difficulties do exist in duplicating analytical results. These difficulties may result in undetected or falsely represented gold anomalies at specific sites, particularly at low gold concentrations.

The study indicates that pristine gold grains are released in till by post-glacial weathering of sulphides. This observation questions the validity of using gold grain morphology in weathered till as an indication of glacial transport distance; although shape classification can be a more useful tool in evaluating transport distances of gold grains in unweathered till. Comparison of the results of gold grain counts in the regional and detailed study indicates that the abundance of grains in till indicates closeness to mineralization, regardless of any secondary processes affecting the sample medium (Fig. 3b, Table 2).

The presence of modified or reshaped grains in till indicates glacial transport or post-depositional reworking of some kind. This includes pre-glacial weathering processes. If these grains occur in association with a considerable number of pristine grains, several explanations are possible: 1) the population represented by the pristine grains represents the post-glacial weathering of ore minerals such as sulphide, 2) the presence of multiple sources of mineralization in the area, and 3) the reworking of previously deposited material due to a shift in ice flow or a later glaciation.

ACKNOWLEDGMENTS

The authors would like to thank Janet Campbell, Saskatchewan Research Council, and the assistance of Chris Zdanowicz, Ly-shu Ramos Lam, Barbara Pierna and Marko Koprivnjak in sample collection. Special thanks to Richard Lamframboise for help with the detailed study and preparation of the dot diagrams; Barry Machin for conducting the laboratory work on the quartz vein; Bruce Ballantyne for numerous discussions and assistance; David Walker and Armand Tsai for providing their expertise on the SEM; Gordon McNeill for reproducing the gold grain figures; and Ron DiLabio for helpful comments and suggestions on the manuscript.

REFERENCES

Averill, S.A. and Zimmerman, J.R.
1986: The riddle resolved: the discovery of the Partridge gold zone using sonic drilling in glacial overburden at Waddy Lake, Saskatchewan; Canadian Geology Journal of the Canadian Institute of Mining and Metallurgy, v. 1, p. 14-20.

Bird, D.J. and Coker, W.B.
1987: Quaternary stratigraphy and geochemistry at the Owl Creek gold mine, Timmins, Ontario, Canada; Journal of Geochemical Exploration v. 28, p. 267-284.

Byers, A.R. and Dahlstrom, C.D.A.
1954: Geology and mineral deposits of the Amisk-Wildnest Lakes area, Saskatchewan; Saskatchewan Department of Mineral Resources, Report No. 14, 177 p.

Byers, A.R., Kirkland, S.J.T., and Pearson, W.J.
1965: Geology and mineral deposits of the Flin Flon area, Saskatchewan; Saskatchewan Energy and Mines, Report 62, 95 p.

Campbell, J.E.
1988: Preliminary report – Quaternary geology and till geochemistry – East Amisk Lake area, Saskatchewan; Saskatchewan Research Council, Report R-842-59-E-88, 31 p.

Campbell, J.E. and Schreiner, B.T.
1989: Quaternary geology and its implications to gold exploration in the La Ronge and Flin Flon domains, Saskatchewan; in Drift Prospecting, R.N.W. DiLabio, and W.B. Coker, (ed.); Geological Survey of Canada, Paper 89-20, p. 113-126.

Coombe Geoconsultants Limited
1984: Gold in Saskatchewan; Saskatchewan Energy and Mines, Open File Report 84-1, 134 p.

Clarke, M.D.
1989: Surficial geology, Cormorant Lake, Manitoba-Saskatchewan (63K); Geological Survey of Canada, Map 1699A, scale 1:125 000.

DiLabio, R.N.W
1982: Drift prospecting near gold occurrences at Onaman River, Ontario and Oldham, Nova Scotia; in Geology of Canadian Gold Deposits; Canadian Institute of Mining and Metallurgy, Special Volume 24.
1985: Gold abundance vs. grain size in weathered and unweathered till; in Current Research, Part A; Geological Survey of Canada, Paper 85-1A, p. 117-122.
1988: Residence sites of gold, PGE, and rare lithophile elements in till; in Prospecting in Areas of Glaciated Terrain – 1988; D.R. MacDonald and K.A. Mills (ed.); Canadian Institute of Mining and Metallurgy, p. 121-140.
1990: Classification and interpretation of the shapes and surface textures of gold grains from till on the Canadian Shield; in Current Research, Part C; Geological Survey of Canada, Paper 90-1C, p. 323-329.

Galley, A.G. and Franklin, J.M.
1987: Geological setting of gold, copper, tungsten and molybdenum occurrences in the Phantom Lake region; in Summary of Investigations 1987; Saskatchewan Geological Survey; Saskatchewan Energy and Mines, Miscellaneous Report 87-4.

Henderson, P.J.
1995: Surficial geology and drift composition of the Annabel Lake-Amisk Lake area, Saskatchewan (NTS 63L/9, L/16 and part of 63K/12 and K/13); Geological Survey of Canada, Open File 3026.

Henderson, P.J. and Campbell, J.E.
1992: Quaternary studies in the Annabel Lake-Amisk Lake area (NTS 63L/9, 63L/16, and part of 63K/12, K/13); in Summary of Investigations, 1992; Saskatchewan Geological Survey, Miscellaneous Report 92-4, p. 172-176.
1994: Surficial geology investigations related to drift prospecting in the Annabel Lake-Amisk Lake area, Saskatchewan (NTS 63L/9 and L/16 and part of 63K/12 and K/13); in Summary of Investigations; Saskatchewan Geological Survey, Miscellaneous Report 94-4, p. 75-78.

Lakin, H.W., Curtin, G.C., and Hubert, A.E.
1974: Geochemistry of gold in the weathering cycle; United States Geological Survey Bulletin 1330, 80 p.

Macdonald, R.
1987: Update on the Precambrian geology and domainal classification of northern Saskatchewan; in Summary of Investigations 1987; Saskatchewan Geological Survey, Miscellaneous Report 87-4, p. 87-104.

McDougall, F.H., Watters, B.R., and Parslow, G.R.
1982: Mineral occurrences in the Precambrian of NTS areas 62K and 63L, Saskatchewan; Saskatchewan Energy and Mines, Open File 82-6.

McMartin, I.
1994: Surficial geology investigations in the Athapapuskow Lake area (Parts of NTS 63K/11 and K/12); in Manitoba Energy and Mines, Report of Activities, 1995, p. 65-67.

Martin, I. and Campbell, J.E.
1994: Highlights of Quaternary geology investigations in the Sturgeon-Weir River area, near Flin Flon; in Summary of Investigations, 1995; Saskatchewan Geological Survey, Miscellaneous Report 94-4, p. 137-140.

Nichol, I., Lavin, O.P. , McClenaghan, M.B., and Stanley, C.R.
1992: The optimization of geochemical exploration for gold using glacial till; Exploration Mining Geology, v. 1, no. 4, p. 305-326.

Nielsen, E.
1994: Highlights of surficial geology and till geochemical sampling in the Flin Flon area (NTS 63K/13); in Manitoba Energy and Mines, Report of Activities, 1994, p. 81-82.

Pearson, J.G.
1980: The Flin Flon gold project; in Summary of Investigations 1980; Saskatchewan Geological Survey; Saskatchewan Energy and Mines, Miscellaneous Report 80-4, p. 70-80.
1983: Gold metallogenic studies: Flin Flon-Amisk Lake area; in Summary of Investigations 1983; Saskatchewan Geological Survey; Saskatchewan Energy and Mines, Miscellaneous Report 83-4, p. 67-74.

Pearson, J.G. and Galley, A.G.
1985: Gold deposits of the Flin Flon - Amisk Lake area; in Summary of Investigations 1985; Saskatchewan Geological Survey; Saskatchewan Energy and Mines, Miscellaneous Report 85-4, p. 83-89.

Prest, V.K., Grant, D.R., and Rampton, V.N.
1968: Glacial Map of Canada; Geological Survey of Canada, Map 1253A, scale 1:5 000 000.

Rampton, V.N., Gleeson, C.F. Thomas, R.D., and Paradis, S.
1986: Geochemical exploration in areas of shallow till: some case histories; Canadian Institute of Mining and Metallurgy Bulletin, v. 79, no. 896, p. 67-74.

Roy, M.
1993: Variations, lithologiques, granulométriques et géochimiques du till de surface de la région de Phantom Lake, Saskatchewan; Activité de Synthèse I, Université du Québec à Montréal, 37 p.

Schreiner, B.T.
1984: Quaternary geology of the Precambrian Shield, Saskatchewan; Saskatchewan Energy and Mines, Report 221, 106 p.
1986: Quaternary geology as a guide to mineral exploration in the southeastern shield, Saskatchewan; Saskatchewan Energy and Mines, Open File Report No. 86-5, 39 p.

Sopuck, V.J., Schreiner, B.T., and Averill, S.A.
1986: Drift prospecting for gold in the southwestern Shield of Saskatchewan, Canada; in Prospecting in areas of Glaciated Terrain - 1986; Institution of Mining and Metallurgy, London, p. 217-240.

Syme, E.C., Thomas, D.J., Bailes, A.H., Reilly, B.A. and Slimmon, W.L.
1993: Geology of the Flin Flon area, Manitoba and Saskatchewan (parts of NTS 63K and 63L); Geological Survey of Canada, Open File 2658, 1:50 000 scale map.

Teller, J.T. and Clayton, L.
1983: Glacial Lake Agasssiz; Geological Association of Canada, Special Paper 26, 451 p.

Geological Survey of Canada Project 920071

Till and stream sediment geochemistry near the Manitouwadge Greenstone Belt, Ontario[1]

I.M. Kettles[1], R.G. Garrett[2], and J.B. Murton[3]
Terrain Sciences Division

Kettles, I.M., Garrett, R.G., and Murton, J.B., 1995: Till and stream sediment geochemistry near the Manitouwadge Greenstone Belt, Ontario; in Current Research 1995-E; Geological Survey of Canada, p. 187-193.

Abstract: As part of the Northern Ontario Development Agreement (NODA) and in aid of mineral exploration, Geological Survey of Canada collected and analyzed 46 till samples from the vicinity of the Manitouwadge greenstone belt. Also analyzed were 98 till samples from a Carleton University study and 44 till and 109 stream sediments samples collected by Mineral Resources Division scientists in 1967. As would be expected, many till and stream sediment samples collected near the Manitouwadge mine sites have high concentrations of copper, zinc, and, in some cases, lead. Levels of the same elements are also high in stream sediments at three sites northwest of the Geco mine and in some till samples collected over or near the north-northeast-trending fault which extends from the eastern end of Manitouwadge Lake. Away from the mines in the detailed sampling area, there are few areas with high levels of copper or zinc in till or stream sediments. Elevated levels were detected in till at one site south of Little Mose Lake and at another south of Nama Creek. Some follow-up exploration work may prove worthwhile.

Résumé : Dans le cadre de l'Entente de développement du nord de l'Ontario et pour faciliter l'exploration minérale, la Commission géologique du Canada a analysé 46 échantillons de till recueillis dans les environs de la ceinture de roches vertes de Manitouwadge. De plus, on a analysé 98 échantillons de till utilisés dans une étude de l'Université Carleton et 44 échantillons de till et 109 échantillons de sédiments fluviatiles recueillis par des scientifiques de la Division des ressources minérales en 1967. Comme prévu, de nombreux échantillons de till et de sédiments fluviatiles prélevés près des sites miniers de Manitouwadge contiennent des concentrations élevées de cuivre, de zinc et, dans certains cas, de plomb. Les concentrations des mêmes éléments sont également élevés dans les sédiments fluviatiles à trois sites situés au nord-ouest de la mine Geco et dans certains échantillons de till prélevés au-dessus ou près de la faille à direction nord-nord-est qui s'allonge à partir de l'extrémité est du lac Manitouwadge. À une certaine distance des mines dans la région fortement échantillonnée, on observe quelques zones en hauteur où les concentrations de cuivre ou de zinc dans le till ou les sédiments fluviatiles sont élevées. Le plomb est présent dans le till d'un site au sud du lac Little Mose et d'un autre site au sud du ruisseau Nama. Un suivi des travaux d'exploration pourrait s'avérer valable.

[1] Contribution to Canada-Ontario Subsidiary Agreement on Northern Ontario Development (1991-1995), under the Canada-Ontario Economic and Regional Development Agreement.
[2] Mineral Resources Division
[3] Department of Geology, University of Wales, Cardiff, Wales

INTRODUCTION

As part of the Northern Ontario Development Agreement (NODA), the Geological Survey of Canada carried out a study of glacial sediments in the Manitouwadge area. Between 1991 and 1992, 616 till samples were collected (Kettles, 1993, 1994; Kettles and Murton, 1993). The purpose was to provide information about Quaternary geology, including ice flow directions and lithological and geochemical composition of glacial sediments, that would be valuable for drift prospecting. The survey included more detailed sampling in the vicinity of the Manitouwadge greenstone belt, especially near the Geco and several abandoned copper-zinc mines (46 samples) (Fig. 1). Other samples collected near Manitouwadge, including 98 till samples from a Carleton University study (Kettles and Murton, 1993) and 44 till and 109 stream sediments samples collected by Mineral Resources Division scientists in 1967, were also used (Garrett, 1969). Some preliminary results of the detailed survey are presented.

Field and analytical procedures

Till samples were collected from hand dug holes approximately 1 m deep. To minimize the effects of weathering on the geochemical composition of the till, care was taken to sample the least weathered till. Samples of fine sand to clay-sized materials were collected at or near the surface of stream beds at low energy sites. For both types of samples, the <0.063 mm fraction was obtained by dry sieving and analyzed for trace, minor, and major elements by Inductively Coupled Plasma Atomic Emission Spectroscopy (ICP-AES) methods, following an aqua regia partial extraction. Geochemical data were statistically analyzed using the computer software program Statview and were plotted using a computer program developed by Wyatt Geoscience, Ottawa.

Bedrock and surficial geology

The study area is underlain by Archean greenstone belts and granitoid plutons of the Wawa subprovince of the Canadian Shield (Williams and Breaks, 1990; Zaleski and Peterson, 1993; Ontario Geological Survey 1991; Fig. 2; Table 1). The

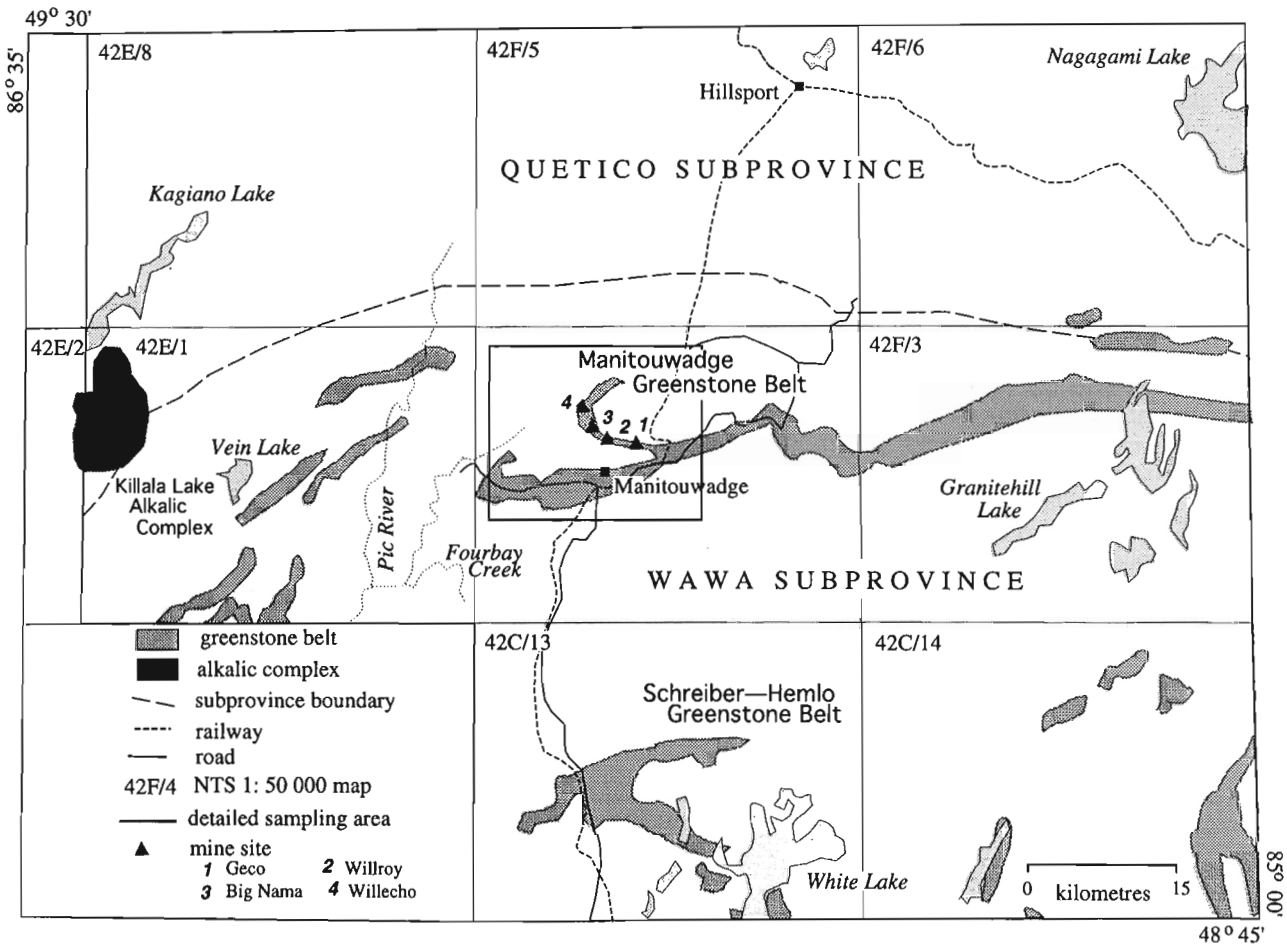

Figure 1. Project area, Manitouwadge-Hornpayne area. Area of more detailed sampling is outlined.

Manitouwadge greenstone belt, comprising highly deformed metavolcanic and metasedimentary rocks, hosts four known volcanogenic massive sulphide (VMS) deposits, the largest of which is the Geco copper-zinc-silver deposit (Fig. 1, 2; Friesen et al., 1982).

Detailed mapping of surficial deposits was undertaken in the area of the detailed survey by Kristjansson and Geddes (1986). All glacial sediments were deposited during the Late Wisconsinan. Striae measurements indicate that the predominant flow direction was 210-220°.

The most widespread glacial deposit is till, which commonly forms a thin, discontinuous veneer (up to 1.5 m thick), but in places exceeds 10 m in thickness. On account of poor exposure it was difficult to distinguish between till facies. However, where till was better exposed in road and stream cuts, the following three facies were observed and sampled (Kettles and Murton, 1993): (1) a compact diamicton enriched in Paleozoic carbonate clasts found on the down-ice slopes of certain hills and in some lowland sites; (2) a loose, sandy diamicton with low to high concentrations of Paleozoic clasts, it is the most widespread till, commonly forming discontinuous sheets of variable thickness (0.5-3.0 m); and (3) a loose, very sandy diamicton with high concentrations of angular clasts derived from the local Precambrain bedrock. It is common in areas of exposed bedrock.

Table 1. Bedrock geology legend

LEGEND

- Diabase
- Granitoid intrusive and gneissic rocks
- Metamorphosed iron formation
- Metasedimentary rocks
- Felsic to intermediate metavolcanic rocks
- Mafic to intermediate metavolcanic rocks

Geological contact . . . .

Fault . . . . . _____

Massive sulphide deposit X

Geology from Zaleski and Peterson, 1993

Glaciofluvial ice-contact and glaciolacustrine deposits also occur. Glaciolacustrine sediments have been observed as high as 325 m. (R. Geddes, unpublished report, 1987). Eolian dunes are found in some areas where glaciolacustrine sediments predominate, and alluvial sands and silts are well developed along major rivers and streams. Deposits of peat and organic muck are widespread, particularly in areas underlain by glaciolacustrine sediments.

TILL AND STREAM SEDIMENT COMPOSITION

Glacial sediments partially derived from local Precambrian units contain Paleozoic carbonate and Proterozoic metasedimentary rocks which were glacially transported at least 100 km southwestward from Hudson Bay Lowland (Kettles, 1993, 1994). Previous work on the granule-small pebble fraction (5.6-16.0 mm) of till samples from the detailed survey area (Kettles, 1993, 1994), indicated that 65% of the samples had greater than 20% Paleozoic carbonate clasts and only 7% of the samples had less than 5%. More than 50% of the samples also contained more than 10% Proterozoic metasedimentary clasts. In contrast, till samples with high concentrations of local Archean bedrock lithologies closely mirrored nearby outcrops.

The patterns of distribution of copper, lead, and zinc (Fig. 2,3,4) are similar in till and stream sediments, but levels of copper and zinc are generally higher in stream sediments (see statistical summaries). Similar patterns of regional distribution are expected since stream sediments are partially derived from till, and, as a result, their chemical characteristics are influenced by drift geochemistry. There are at least two explanations for the higher levels of copper and zinc in stream sediments within the detailed study area: 1) proportionally more stream sediment samples than till samples were collected from over bedrock units comprising the greenstone belt; 2) stream sediment samples are generally enriched in manganese compared to till samples, although they have similar levels of iron. Twenty five per cent of the till and stream sediment samples had manganese concentrations greater than 245 and 860 ppm, respectively. Stream sediments contain more by-products of postglacial weathering, such as oxides and hydroxides, which enhance their cation exchange capacity relative to the tills and, consequently, their cation concentrations.

High concentrations of Paleozoic carbonate in till and related sediments tend to suppress the geochemical signature of the fine fraction (Kaszycki, 1989), because unmetamorphosed carbonate bedrock contains low trace element concentrations with some exceptions (Mason, 1966, Table 6.5). Despite the effects of dilution resulting from long-distance transport of Paleozoic carbonate, the distribution of copper,

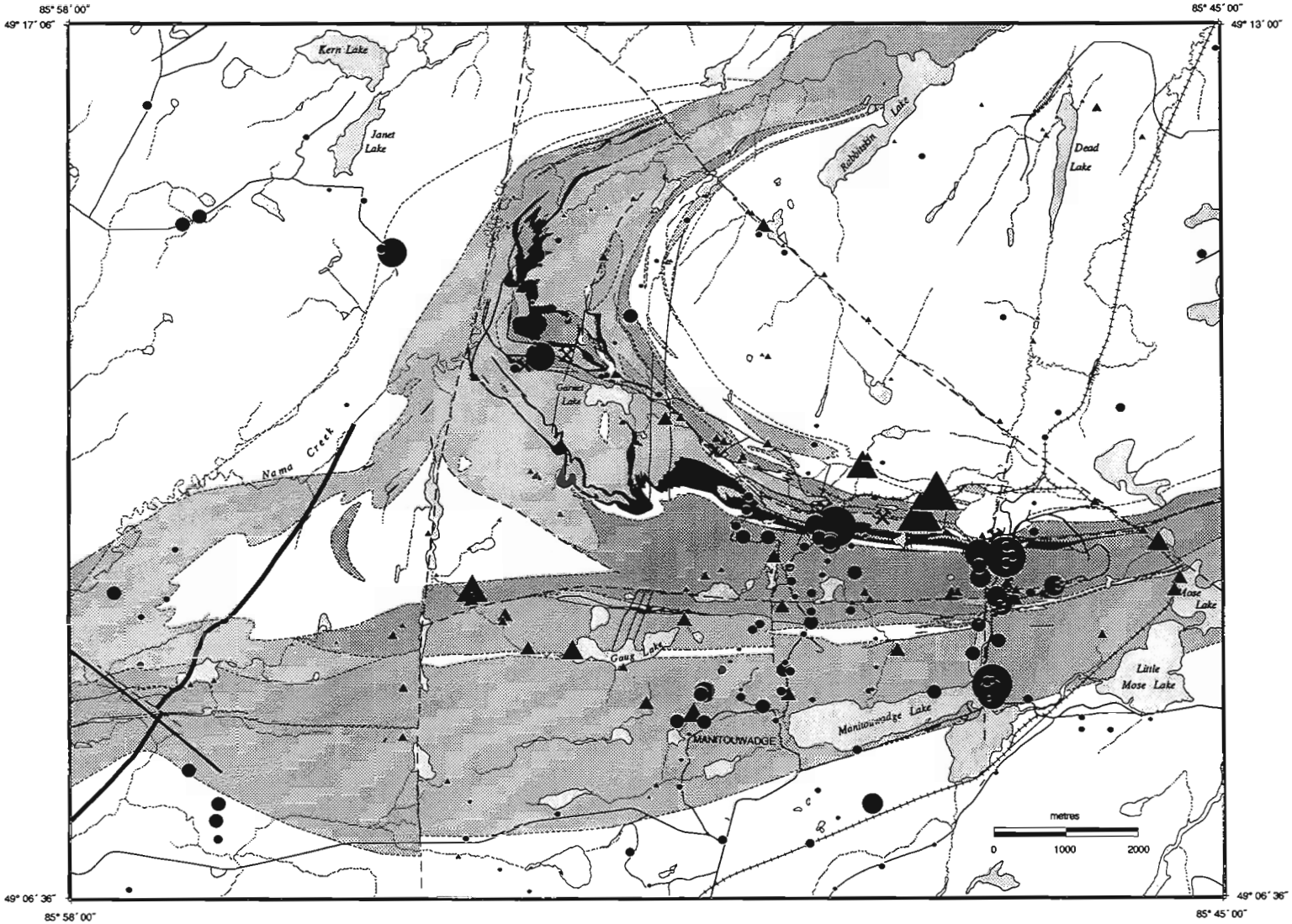

Copper (ppm) in the <0.063mm fraction of till

Symbol Legend

MIN.	MAX.	#SAMP	%TILE
2	7	42	26.9
7	11	41	53.2
11	18	35	75.6
18	36	23	90.4
36	55	8	95.5
55	95	4	98.1
95	1596	3	100

Summary Statistics

Number of Samples:	156
Minimum:	2
Maximum:	1596
Mean:	28.2
Median:	10.5
Standard Deviation:	128.7
Coefficient of Variation:	4.6

Copper (ppm) in the <0.063mm fraction of stream sediments

Symbol Legend

MIN.	MAX.	#SAMP	%TILE
3	10	28	25.7
10	19	28	51.4
19	43	26	75.2
43	88	16	89.9
88	125	6	95.4
125	230	3	98.2
230	449	2	100

Summary Statistics

Number of Samples:	109
Minimum:	3
Maximum:	449
Mean:	38.5
Median:	19
Standard Deviation:	56.7
Coefficient of Variation:	1.5

Cu

Figure 2. *Distribution of copper in the silt and clay-sized fraction (<0.063 mm) of Manitouwadge tills and stream sediments. Bedrock geology legend shown in Table 1.*

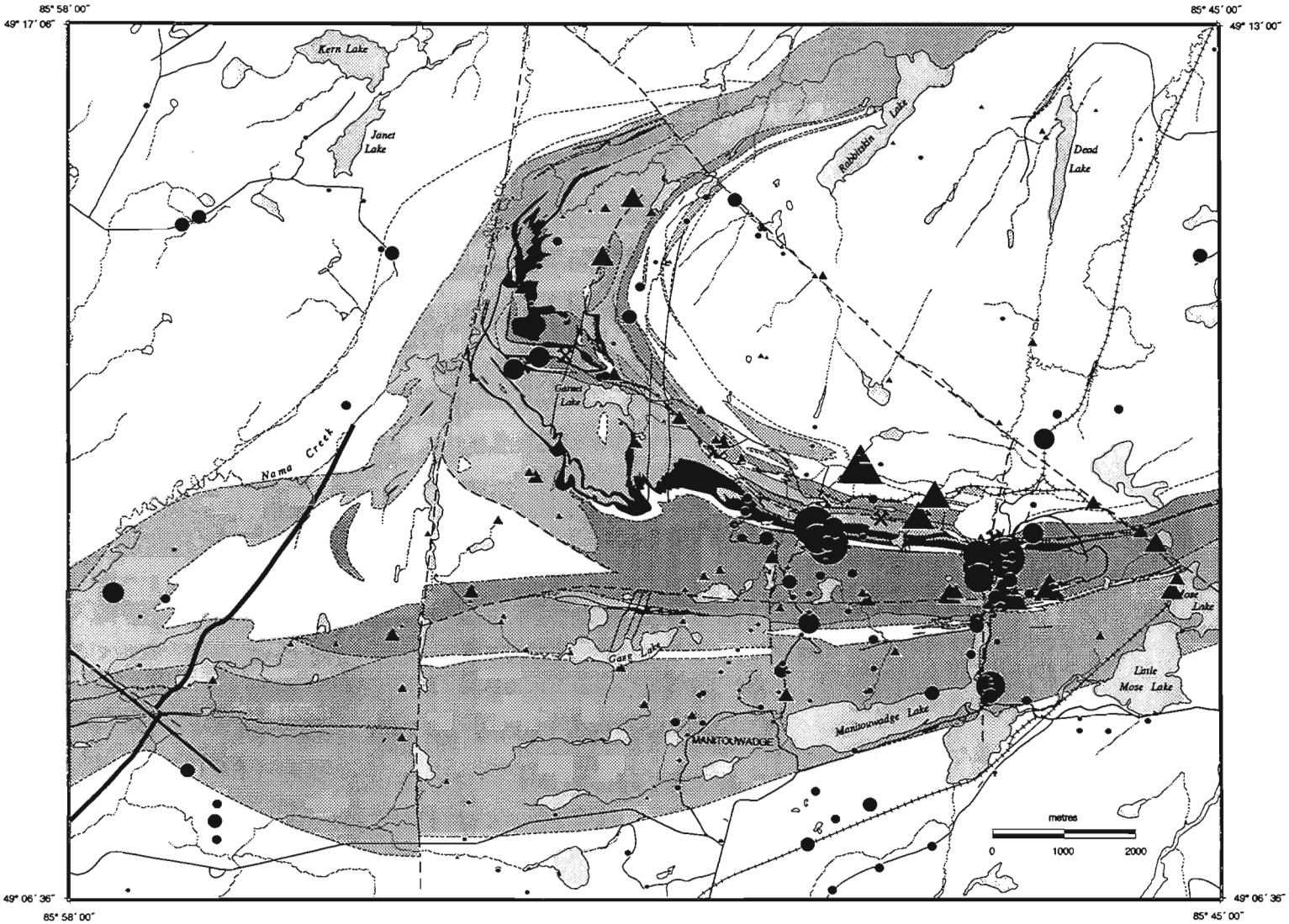

Zinc (ppm) in the <0.063mm fraction of till

Symbol Legend

MIN.	MAX.	#SAMP	%TILE
8	18	55	35.3
18	24	33	56.4
24	34	30	75.6
34	72	23	90.4
72	167	7	94.9
167	361	5	98.1
361	2589	3	100

Summary Statistics

Number of Samples:	156
Minimum:	8
Maximum:	2589
Mean:	57.7
Median:	23.5
Standard Deviation:	213.1
Coefficient of Variation:	3.7

Zinc (ppm) in the <0.063mm fraction of stream sediments

Symbol Legend

MIN.	MAX.	#SAMP	%TILE
12	34	30	27.5
34	70	25	50.5
70	122	28	76.1
122	279	15	89.9
279	881	6	95.4
881	3125	3	98.2
3125	3292	2	100

Summary Statistics

Number of Samples:	109
Minimum:	12
Maximum:	3292
Mean:	208.5
Median:	70
Standard Deviation:	548.3
Coefficient of Variation:	2.6

Zn

Figure 3. *Distribution of zinc in the silt and clay-sized fraction (<0.063 mm) of Manitouwadge tills and stream sediments. Bedrock geology legend shown in Table 1.*

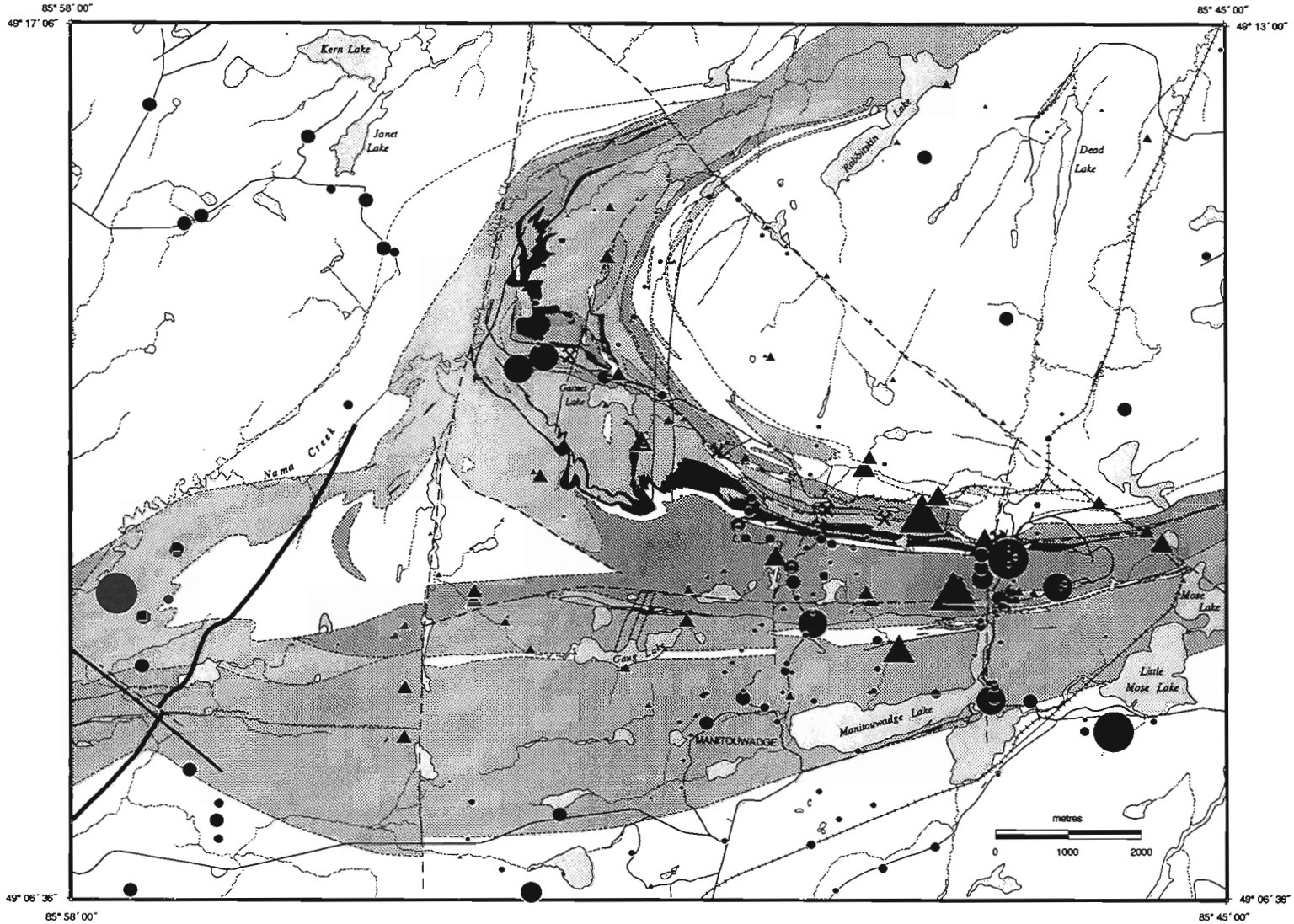

Lead (ppm) in the <0.063mm fraction of till

Symbol Legend

MIN.	MAX.	#SAMP	%TILE
1	4	53	34.0
4	8	37	57.7
8	17	29	76.3
17	23	27	93.6
23	27	2	94.9
27	59	5	98.1
59	224	3	100

Summary Statistics

Number of Samples:	156
Minimum:	1
Maximum:	224
Mean:	13.2
Median:	8
Standard Deviation:	22.5
Coefficient of Variation:	1.7

Lead (ppm) in the <0.063mm fraction of stream sediments

Symbol Legend

MIN.	MAX.	#SAMP	%TILE
2	4	48	44
4	6	19	61.5
6	10	16	76.1
10	19	15	89.9
19	30	6	95.4
30	56	3	98.2
56	134	2	100

Summary Statistics

Number of Samples:	109
Minimum:	2
Maximum:	134
Mean:	10.1
Median:	6
Standard Deviation:	15.5
Coefficient of Variation:	1.5

Pb

Figure 4. *Distribution of lead in the silt and clay-sized fraction (<0.063 mm) of Manitouwadge tills and stream sediments. Bedrock geology legend shown in Table 1.*

zinc, and lead in the <0.063 mm fraction of till and stream sediments may be related, in many areas, to local bedrock composition. As would be expected, many samples collected in the vicinity of the Manitouwadge VMS deposits have high concentrations of copper (>36 ppm for till, >88 ppm for stream sediments), zinc (>72 ppm for till, >279 ppm for stream sediments) and, in some cases, lead (>23 ppm for till, >19 ppm for stream sediments). Approximately 1 km northwest of the Geco mine, there are also high levels of the three elements in sediments from a stream which drains northward from the bedrock units associated with the VMS deposits. Likewise, sediments collected from a southward flowing stream 2 km northwest of the Geco site, are enriched in copper, zinc, and, to a lesser extent, lead. Although the latter sample site was located north of the bedrock units associated with the VMS deposits, it is within a kilometre of the Willroy mine and its associated mine waste. Hydromorphic geochemical dispersion is expected to be limited due to the high carbonate nature of the environment.

Levels of copper, zinc, and lead are also relatively high in a number of till samples collected over or near the fault which extends north-northeast from the eastern end of Manitouwadge Lake. The Geco mine site is located on the same fault. Other than in the vicinity of the mines, there are few areas with high levels of copper or zinc. However, till is enriched in lead at one site south of Little Mose Lake and at another site 12 km west of Manitouwadge. Where till or stream sediments are enriched in base metals some follow-up exploration work may prove worthwhile.

ACKNOWLEDGMENTS

The authors wish to thank the following: Steven Bauke and Kathryn Laurus for their able assistance in the field; K. Bell, Carleton University, for permitting use of samples obtained for a project funded by an NSERC strategic grant; Helena Karam for sample processing; Manfred Hebel for assistance with data compilation; Eva Zaleski for providing us with a digital bedrock map; D.B. McKay for helpful advice; the staff of the geology department of Noranda Geco mine for discussions and permission to sample near the mine; Northwood Geoscience for plotting the proportional symbol maps; and R.A. Klassen for reviewing the paper.

REFERENCES

Friesen, R.G., Pierce, G.A., and Weeks, R.M.
1982: Geology of the Geco base metal deposit; Geological Association of Canada, Special Paper 25, p. 343-363.

Garrett, R.G.
1969: Geochemical study, Manitouwadge, Ontario (42F/4); in Report of Activities, Part A; Geological Survey of Canada, Paper 69-1A, p. 47-48.

Geddes, R.S.
1987: Quaternary geology of the Hemlo region, Districts of Thunder Bay and Algoma; Ontario Geological Survey, unpublished report.

Kaszycki, C.M.
1989: Surficial geology and till composition, northwestern Manitoba; Geological Survey of Canada, Open File 2118, 150 p.

Kettles, I.M.
1993: Reconnaissance geochemical data for till samples from the Manitouwadge area, Ontario; Geological Survey of Canada, Open File 2616, 197 p.
1994: Till geochemistry in the Manitouwadge-Hornpayne region, Ontario; Geological Survey of Canada, Open File 2933, 287 p.

Kettles, I.M. and Murton, J.B.
1993: Till composition in the vicinity of the Manitouwadge greenstone belt, Ontario; in Current Research, Part C; Geological Survey of Canada, Paper 93-1C, p. 249-257.

Kristjansson, F.J. and Geddes, R.S.
1986: Quaternary geology of the Manitouwadge area, District of Thunder Bay; Ontario Geological Survey, Map P. 3055, scale 1: 50 000.

Mason, B.
1966: Principles of Geochemistry; Wiley, New York; 329 p.

Ontario Geological Survey
1991: Bedrock geology of Ontario, east-central sheet; Ontario Geological Survey, Map 2534.

Williams, H.R. and Breaks, F.W.
1990: Geology of the Manitouwadge-Hornpayne area; Ontario Geological Survey, Open File Map 142, scale 1: 50 000.

Zaleski, E. and Peterson, V.L.
1993: Geology of the Manitouwadge greenstone belt, Ontario; Geological Survey of Canada, Open File 2573, scale 1:25 000.

Geological Survey of Canada Project 910017

Formation resistivity factor of core samples from the Sudbury Structure, Ontario

T.J. Katsube, N. Scromeda, and M. Salisbury[1]
Mineral Resources Division

Katsube, T.J., Scromeda, N., and Salisbury, M., Formation resistivity factor of core samples from the Sudbury Structure, Ontario; in Current Research 1995-E; Geological Survey of Canada, p. 195-200.

Abstract: Formation resistivity factor (F) and pore surface resistivity (ρ_c) values were determined for 16 drillcore samples representing some of the major lithologies exposed in the Sudbury Structure (SS). The purpose was to provide basic information required to understand the electrical conductivity mechanisms of the structure.

Results indicate that F values obtained are within the range found in the literature for crystalline rocks (430-25 000). Preliminary examination of the relationship between these data for F and ρ_c and previous electrical resistivity (ρ_r) data suggest that several different characteristics exist. Some display characteristics likely due to the pore surfaces being fresh with little or no alteration, suggesting that pore structure has a dominant effect on ρ_r. Others display characteristics likely due to pore surfaces being highly altered, or completely or partially lined with conductive minerals, suggesting that pore structure has little effect on ρ_r. Some high ρ_r samples also display such characteristics.

Résumé : Les valeurs du facteur de formation (F) et de la résistivité de surface des pores (ρ_c) ont été déterminées pour 16 échantillons de carottes représentant quelques-unes des principales lithologies affleurant dans la structure de Sudbury (SS). Cette tâche avait pour but de fournir les informations de base nécessaires pour comprendre les mécanismes de conductivité électrique de la structure.

Les résultats indiquent que les valeurs obtenues pour F se situent dans l'intervalle donné pour les roches cristallines dans la documentation (430-25 000). L'analyse préliminaire de la relation entre ces données pour F et ρ_c et les données antérieures sur la résistivité électrique (ρ_r) révèlent qu'il existe plusieurs caractéristiques différentes. Certaines affichent des caractéristiques vraisemblablement attribuables aux surfaces des pores peu ou pas altérées, ce qui incite à proposer que la structure des pores a un effet dominant sur ρ_r. D'autres affichent des caractéristiques probablement attribuables à la forte altération des surfaces des pores ou au fait que ces surfaces sont complètement ou partiellement revêtues de minéraux conducteurs, indiquant que la structure des pores a peu d'effet sur ρ_r. Quelques échantillons à ρ_r élevé présentent également ces caractéristiques.

[1] GSC Atlantic, Dartmouth

INTRODUCTION

Formation resistivity factor, F, and pore surface resistivity, ρ_c, values have been determined for 16 drillcore samples representing some of the major lithologies exposed in the Sudbury Structure (Katsube and Salisbury, 1994). The purpose was to provide basic information required to understand the electrical conductivity mechanisms of the rocks constituting these lithologies.

Bulk rock electrical resistivity, ρ_r, and other physical properties have been measured on 52 drillcore samples (Scromeda et al., 1993) from the same lithologies to provide constraints on the interpretation of deep high electrical conductivity zones (Katsube and Salisbury, 1994) detected by surface electromagnetic surveys carried out across the southern part of the Sudbury Structure (Boerner et al., 1994). Samples with low resistivities unexpectedly found in cores (Katsube and Salisbury, 1994) from lower sections of the Sudbury Structure have provided some of these constraints (Boerner et al., 1994). Minor amounts of carbon were suggested as the likely cause of these low resistivities. However, the electrical conductivity mechanism of these rocks is not yet fully understood. The 16 samples used in this study are from the same suite of 52 samples.

The F and ρ_c values are determined by measuring bulk electrical resistivity (ρ_{rn}) of the rock samples for a multiple number of NaCl solutions with different values of pore fluid resistivity, ρ_{wn}, and then by inserting the results into the Patnode and Wyllie (1950) equation:

$$1/\rho_{rn} = 1/(F\rho_{wn}) + 1/\rho_c. \quad (1)$$

According to this equation, the relationship between the two variables, $1/\rho_{rn}$ and $1/\rho_{wn}$, should be linear. This linear relationship is used to determine F and ρ_c. This relationship, however, sometimes deviates from linearity and can become a source of reduced accuracy when determining F (Katsube and Scromeda, 1993). We normally use five different NaCl concentrations of 0.02 to 0.5 N (Katsube, 1981) to determine F and ρ_c. According to recent studies (Katsube and Scromeda, 1993; Katsube et al., 1995) on tight shales, the accuracy problem is usually eliminated by using NaCl concentrations greater than 0.02 N, and saturation times greater than 240 minutes.

Table 1. Formation-factor (F) and surface resistivities (ρ_c) for different NaCl solutions: boreholes 4301, 3502, 5601 and 52847

Sample	ρ_{rn} (x10^3 Ω-m)					F ±%	ρ_c ±%
ρ_{wn} (Ω-m) NaCl (N)	0.29± 0.001 0.5	0.61± 0.002 0.2	1.15± 0.003 0.1	2.09± 0.01 0.05	5.18± 0.03 0.02	(x10^2)	(x10^3) (Ω-m)
4301-1	1.61	4.20	6.51	11.5	68.8	55.0±0.5	***
4301-2	0.94	3.16	5.00	6.09	27.5	32.0±2.1	***
4301-3	1.35	4.33	5.58	6.86	31.0	47.4±2.5	***
4301-6	0.41	0.48	0.56	0.55	0.92	26.3±16	0.746±6.3
		X	X	X	X	14.7±21	0.870±11
4301-7	0.12	0.13	0.14	0.16	0.18	11.8±10	0.170±2.0
			X	X	X	4.27±0.0	0.196±0.0
3502-4	2.21	5.20	12.2	15.3	34.3	75.8±0.5	***
3502-5	0.75	0.90	1.02	0.93	1.18	73.0±8.8	1.13 ±1.8
5601-1	0.96	1.03	1.37	1.71	2.45	49.5±12	2.09 ±7.5
		X	X	X	X	26.4±1.1	2.69 ±0.9
5601-2	1.23	1.56	1.97	1.93	26.6	45.3±24	4.74 ±50
5601-6	0.33	0.37	0.39	0.38	0.73	20.5±42	0.553±18
52847-2	5.17	8.29	13.2	13.6	51.8	201±2.9	32.8 ±6.7
		X	X	X	X	151±7.5	50.5 ±25
52847-3	4.04	6.49	8.86	15.8	29.3	156±1.7	26.8 ±3.9
		X	X	X	X	118±2.1	42.0 ±6.3
52847-4	4.20	8.88	13.1	16.7	19.4	170±0.7	33.4 ±2.0
52847-5	9.73	27.1	19.4	46.0	54.0	382±7.0	87.0 ±27
52847-6	7.17	14.0	21.4	56.3	72.6	254±0.5	174 ±4.4
52847-7	3.44	6.78	11.1	15.7	17.7	135±0.3	31.9 ±0.9

ρ_{wn} = pore fluid resistivity
ρ_{rn} = bulk resistivity of the rock for solutions of different salinities
F = formation resistivity factor
ρ_c = surface resistivity
X = data points used for formation factor determination
*** = ρ_c values considered to be extremely large

We have published F data for various types of rocks (e.g. Katsube et al., 1991; Katsube and Mareschal, 1993), and have noticed this non-linearity problem existing in some cases other than tight shales. The measurement accuracy of these data were estimated to be ±50 % (Katsube, 1981). While this accuracy was considered to be adequate for obtaining reliable F data (Katsube et al., 1995), it is not sufficient for obtaining reliable pore surface resistivity (ρ_c) values (Katsube and Scromeda, 1993). However, it is not known whether the same procedure used to improve the accuracy for tight shales will apply to rocks from the Sudbury Structure. Therefore, the usual five different NaCl concentrations with saturation times larger than 240 minutes were used in this study, but with special attention given to the adequacy of these concentrations.

Bulk rock electrical resistivity (ρ_r) represents the in situ electrical resistivity of a rock when saturated with ground water or the natural pore water with an electrical resistivity of ρ_w. Since ρ_{rn} and ρ_{wn} can be replaced by ρ_r and ρ_w in equation (1), it indicates that the following relationship should exist:

$$\rho_r < \rho_c. \qquad (2)$$

However, actual measurements do not always produce such results (Katsube et al., 1995). Therefore, a check on whether ρ_c is larger than ρ_r is a good guide to improving measurement accuracy.

METHOD OF INVESTIGATION

The 16 samples are discs of 0.45-0.87 cm in thickness, cut from 2.54 cm (1 inch) diameter horizontal minicores obtained from approximately vertical drillcores (4 drillholes: 4301, 3502, 5601, 52847 in Tables 1 and 2), representing sequential depths of 200-2,720 m in the Sudbury Structure (Scromeda et al., 1993; Katsube and Salisbury, 1994). They are the same samples that were used for ρ_r measurements in the previous studies (Scromeda et al., 1993). F has been determined for only 16 out of the 28 samples previously studied from these 4 drillholes. This is because the rest display ρ_r values below 50 Ωm. We experience difficulty in obtaining reliable F values at low resistivities, since a high resistivity measuring system is used in these studies (Katsube et al., 1995).

Table 2. Formation-factor (F), surface resistivity (ρ_c) and bulk resistivities (ρ_r) for different NaCl solutions: boreholes 4301, 3502, 5601 and 52847

Sample	Sequence Depth (m)	Formation	ρ_r (x10^3 Ω-m)	F ±% (x10^2)	ρ_c (x10^3 Ω-m)
4301-1	206	Chlm-Gw	17.1 ± 0.6	55.0 ± 0.5	***
4301-2	275		7.7 ± 0.05	32.0 ± 2.1	***
4301-3	388		10.1 ± 0.8	47.4 ± 2.5	***
4301-6	484		0.75± 0.066	14.7 ± 21	0.870 ± 11
4301-7	478		0.24± 0.004	4.27 ± 0.0	0.196 ± 0.0
3502-4	1,260	Onp-Tf	30.2 ± 0.4	75.8 ± 0.5	***
3502-5	1,300		0.94± 0.004	73.0 ± 8.8	1.13 ± 1.8
5601-1	1,590	Onp-Tf	1.81± 0.17	26.4 ± 1.1	2.69 ± 0.9
5601-2	1,700		1.66± 0.01	45.3 ± 24	4.74 ± 50
5601-6	2,100		0.43± 0.00	20.5 ± 42	0.553 ±18
52847-2	2,450	Onp-Tf.bl	53.0 ± 1.2	151 ± 7.5	50.5 ± 25
52847-3	2,480	Onp-Tf.gr	19.8 ± 0.5	118 ± 2.1	42.0 ± 6.3
52847-4	2,570		17.8 ± 1.9	170 ± 0.7	33.4 ± 2.0
52847-5	2,650	Onp-Bsl	50.6 ± 2.8	382 ± 7.0	87.0 ± 27
52847-6	2,690		65.6 ± 0.4	254 ± 0.5	174 ± 4.4
52847-7	2,720	Grp	18.2 ± 3.8	135 ± 0.3	31.9 ± 0.9

Petrophysical Parameters
- ρ_r = bulk rock electrical resistivity
- F = formation resistivity factor
- ρ_c = pore surface resistivity

Formations
- Chlm = Chelmsford
- Onwt = Onwatin
- Onp = Onaping

Rock Types
- Gw = greywacke
- Tf = Tuff
- Bsl = Basal
- Grp = Granophyr

Colour
- bl = black
- gr = grey

All 16 samples are of tight solid material with no visible fractures, and with no visible sulphides present. Further details on the texture are described in the literature (Scromeda et al., 1993; Katsube and Salisbury, 1994). Information on the formations and rock types that these samples represent are listed in Table 2. Further details of the geological environment and rock types can be found in the literature (Scromeda et al., 1993; Katsube and Salisbury, 1994).

Further details of the measurement procedures used to determine F and ρ_c, using the five different NaCl concentrations of 0.02 to 0.5 N, are also described in the literature (Katsube and Scromeda, 1993).

EXPERIMENTAL RESULTS

Results of the ρ_m measurements used for F and ρ_c determination are listed in Table 1. The results of the F and ρ_c determinations using the Patnode and Wyllie equation (Katsube and Scromeda, 1993) are listed in the last two columns of this table. The reduced major axis (RMA) is used in these determinations. The percentage errors, listed in these columns, are determined by taking the differences in the F and ρ_c values obtained by using the different regression lines (Fig. 3, 4): the RMA and the normal regression lines (NRL). The two different NRLs, in each case, are derived by interchanging the data sets which are used as the dependent and independent variable. The principles of the RMA are described in Davis (1986), and examples of related applications are found in Katsube and Agterberg (1990). These F and ρ_c values are also listed in Table 2 which includes ρ_r values obtained by previous studies (Katsube and Scromeda, 1993; Katsube and Salisbury, 1994) for comparison.

Four types of $1/\rho_m$ versus $1/\rho_w$ relationships (equation 1) have been observed in these data, as shown in Figures 1 to 4a. No non-linear relationships, similar to those observed for shales (Fig. 5), showing deviations from linearity at the lower NaCl concentrations (lower $1/\rho_w$ values) have been seen in this study. A case where a good linear relationship exists between $1/\rho_m$ and $1/\rho_w$ is shown in Figure 1 for sample 52847-6. All three regression lines are represented by a single solid line in this figure, because the correlation coefficient (r) is close to unity in this case. A similar example, but displaying a negative $1/\rho_c$ value is shown in Figure 2 (4301-1). In this case, the RMA is interpreted to intersect the origin within the

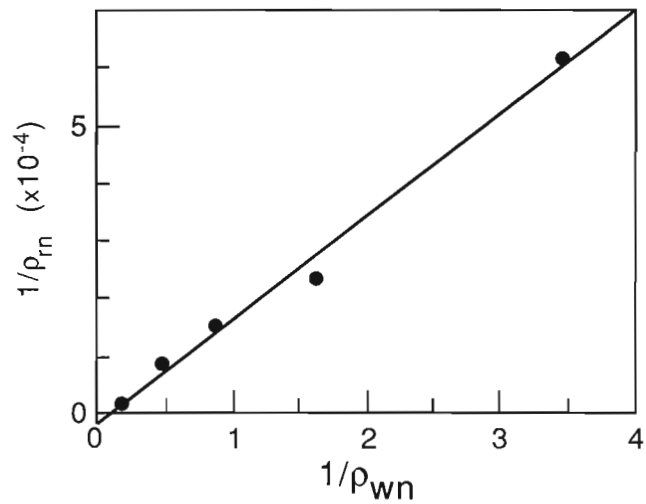

Figure 2. Typical example of $1/\rho_m$ as a function of $1/\rho_w$ for sample 4301-1, displaying a good linear relationship but with a negative $1/\rho_c$ value. The solid line represents the RMA and the two NRLs, which are coincident in this case.

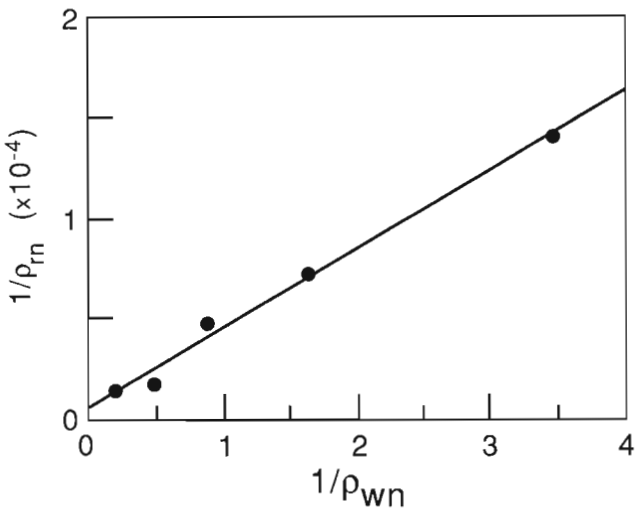

Figure 1. Typical example of $1/\rho_m$ as a function of $1/\rho_w$ for sample 52847-6, displaying a good linear relationship. The solid line represents the reduced major axis (RMA) and the two normal regression lines (NRL), which are coincident in this case.

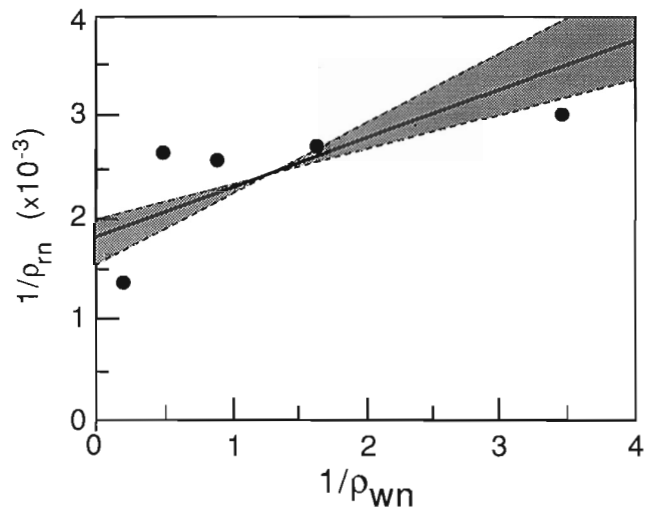

Figure 3. Typical examples of the $1/\rho_m$ as a function of $1/\rho_w$ for sample 5601-6, displaying considerable scatter. The solid line represents the RMA, and the broken lines represent the two NRLs.

range of measurement error. As a result, ρ_c is interpreted to be infinite. The "***s" in Table 1 represent such values for ρ_c. An example displaying considerable scatter is shown in Figure 3 (5601-6). An example interpreted to display non-linearity, due to data points deviating from linearity at the higher NaCl concentrations (higher $1/\rho_w$ values), is shown in Figure 4 (5601-1). This is in contrast with the non-linearity of the shales (Fig. 5) where deviations at the lower NaCl concentrations were the cause.

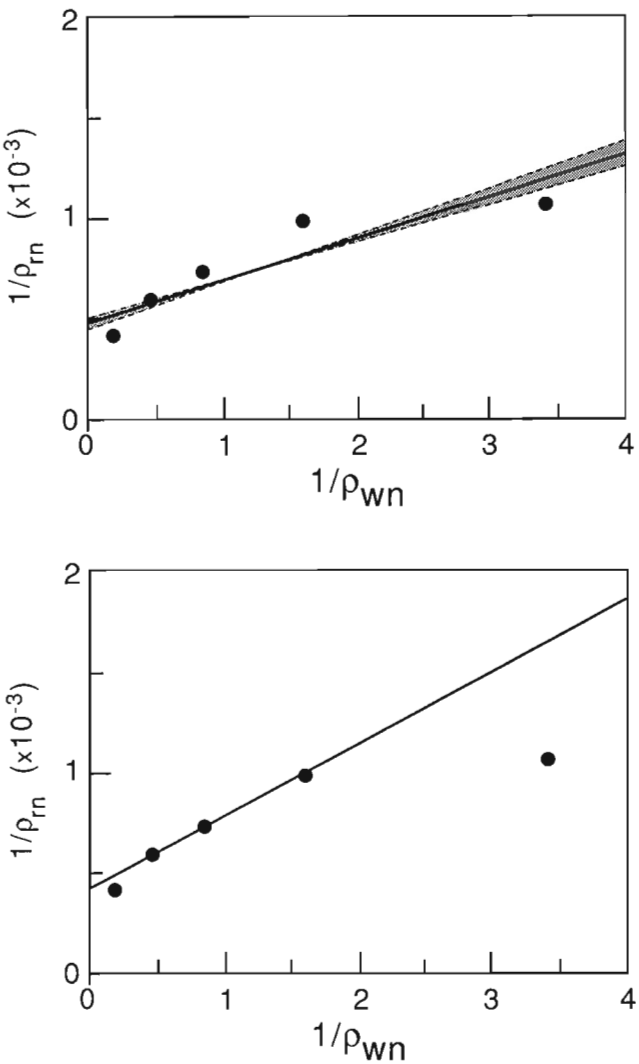

Figure 4. *Typical examples of the $1/\rho_{rn}$ as a function of $1/\rho_w$ for sample 5601-1 showing a poor linear relationship. Data point is interpreted to deviate from linearity at the highest NaCl concentrations (largest $1/\rho_w$ value).* (**a**) *The case where all five data points were used to determine F and ρ_c. The solid line represents the RMA, and the broken lines represent the two NRLs.* (**b**) *The case where the data point that deviated from the linear relationship (largest $1/\rho_w$ value) was eliminated to determine F and ρ_c. The solid line represents all three regression lines (RMA and NRLs), which are coincident in this case.*

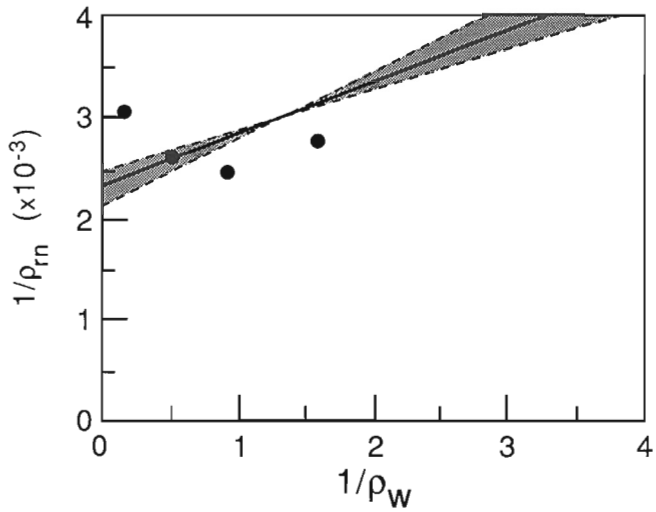

Figure 5. *Example of $1/\rho_{rn}$ as a function of $1/\rho_w$, showing poor linear relationship for a shale sample (Katsube et al., 1995). This is a case where progressive deviation from linearity is seen with decreasing NaCl concentrations (decreasing $1/\rho_w$ values), and only the three data points with the larger values of $1/\rho_w$ have been used to determine F and ρ_c. The solid line represents the RMA, and the broken lines represent the two NRLs.*

Samples displaying the first three $1/\rho_{rn}$ versus $1/\rho_w$ characteristics (Fig. 1-3) satisfy equations (1) and (2). Samples displaying the fourth characteristic (Fig. 4a), generally, have not satisfied equation (2). Only the data points with the smaller $1/\rho_w$ values have been interpreted to display a linear relationship and used to determine F and ρ_c for these cases. Figure 4b displays an example (5601-1) where the data point that deviated from the linear relationship (largest $1/\rho_w$ value) was eliminated. The data points used to determine F and ρ_c are represented by "Xs" in Table 1. There are five such cases listed in this table. Only the results that satisfy equation (2) are listed in Table 2 (columns 3 and 4). Although elimination of data points for high NaCl concentrations has resulted in an increase of ρ_c for these five samples, it has resulted in complete conformity with equation (2) for only three of the five samples (Tables 1 and 2). It did not result in acceptable conformity for the two Samples 4301-7 and 52847-2. However, since the two values are very close for these two samples, they are interpreted to be almost equal due to $1/(F\rho_w) \ll 1/\rho_c$ in equation (1). Consequently, they are interpreted to satisfy equation (2).

DISCUSSION AND CONCLUSIONS

The F values obtained in this study (Tables 1, 2) are in the range of 430-25 000. This is within the range found in the literature for crystalline rocks (Katsube and Mareschal, 1993). The infinite ρ_c values obtained for four of the samples (4301-1 to 4301-3 and 3502-4 in Table 2) are likely due to the pore surfaces being very fresh with little or no alteration. The two

samples (4301-7 and 52847-2), displaying ρ_c values close to those of ρ_r, likely have pore surfaces that are highly altered, or are completely or partially lined with conductive minerals of some kind.

A preliminary examination of the data for F and ρ_c suggest that several different characteristics can be seen in these rock samples. Samples from drillhole 52847 tend to show ρ_c values substantially larger than those of ρ_r (Table 2), except for sample 52847-2. This implies that the pore surface conditions for samples from this hole generally have only a minor effect on their ρ_r values. The fact that the ρ_r value of sample 52847-2 is dominated by ρ_c and that the sample has a blackish colour, suggests that although it has a very large ρ_r value, whatever electrical conduction is seen in that rock sample is probably due to carbon deposited on the pore surface with very minor effects from the pore structure.

Samples from drillholes 4301 and 3502 tend to display ρ_r values related to those of ρ_c (Table 2) with little effect from F, suggesting that pore surface conditions have a major influence on ρ_r for these samples. For samples from drillhole 4301, both pore surface ρ_c and F appear to influence ρ_r. This suggests that both pore structure and pore surface conditions influence the ρ_r values for these samples. Further analysis of these data is scheduled.

ACKNOWLEDGMENTS

The authors are grateful to R. Iuliucci (University of Dalhousie, Nova Scotia) for preparing the samples used in this study. The authors are also very grateful to Q. Bristow (Geological Survey of Canada, Ottawa) for critically reviewing this paper and for his useful suggestions.

REFERENCES

Boerner, D.E., Kellett, R., and Mareschal, M.
1994: Inductive source EM sounding of the Sudbury Structure; Geophysical Research Letters (GRL), v. 21, p. 943-946.

Davis, J.C.
1986: Statistics and Data Analysis in Geology; John Wiley & Sons, p. 200-204.

Katsube, T.J.
1981: Pore structure and pore parameters that control the radionuclide transport in crystalline rocks; Proceedings of the Technical Program, International Powder and Bulk Solids Handling and ProceSudbury Structureing, Rosemont, Illinois, p. 394-409. (Available from: CAHNERS Exposition Group, 222 West Adams Street, Chicago, Illinois 60606 U.S.A.).

Katsube, T.J. and Agterberg, F.P.
1990: Use of statistical methods to extract significant information from scattered data in petrophysics; in Statistical Applications in the Earth Sciences, (ed.) F.P. Agterberg and G.F. Bonham-Carter; Geological Survey of Canada, Paper 89-9, p. 263-270.

Katsube, T.J. and Mareschal, M.
1993: Petrophysical model of deep electrical conductors; Graphite lining as a source and its disconnection due to uplift; Journal of Geophysical Research, v. 98, B5, p. 8019-8030.

Katsube, T.J. and Salisbury, M.
1994: Implications of laboratory electrical measurements on interpretation of EM-surveys and origin of the Sudbury Structure; Geophysical Research Letters, v. 21, p. 947-950.

Katsube, T.J. and Scromeda, N.
1993: Formation factor determination procedure for shale sample V-3; in Current Research, Part E; Geological Survey of Canada, Paper 93-1E, p. 321-330.

Katsube, T.J., Best, M.E., and Mudford, B.S.
1991: Petrophysical characteristics of shales from the Scotian shelf; Geophysics, v. 56, p. 1681-1689.

Katsube, T.J., Scromeda, N., and Williamson, M.A.
1995: Improving measurement accuracy of formation resistivity factor measurements for tight shales from the Scotian Shelf; in Current Research 1995-D; Geological Survey of Canada, p. 65-71.

Patnode, H.W. and Wyllie, M.R.J.
1950: The presence of conductive solids in reservoir rocks as a factor in electric log interpretation; Transactions of the American Institute of Mining, Metallurgical and Petroleum Engineers, v. 189, p. 47-52.

Scromeda, N., Katsube, T.J., and Salisbury, M.
1993: Electrical resistivity and porosity of core samples from the Sudbury Structure; in Current Research, Part C; Geological Survey of Canada, Paper 93-1C, p. 279-285.

Geological Survey of Canada Project 870057

Quaternary geology and implications for drift prospecting in the Napaktulik Lake, Point Lake, and Contwoyto Lake map areas, northwest Slave Province, Northwest Territories[1]

D.E. Kerr, L.A. Dredge, B.C. Ward, and J.S. Gebert[2]
Terrain Sciences Division

Kerr, D.E., Dredge, L.A., Ward, B.C., and Gebert, J.S., 1995: Quaternary geology and implications for drift prospecting in the Napaktulik Lake, Point Lake, and Contwoyto Lake map areas, northwest Slave Province, Northwest Territories; in Current Research 1995-E; Geological Survey of Canada, p. 201-209.

Abstract: As a contribution to Slave NATMAP Project, three 1:250 000 map areas (NTS 86I, 86H, and parts of 76E) were mapped to provide fundamental regional baseline data of surficial materials for drift prospecting, integrated environmental planning, and assessment studies for future development. This report documents some of the preliminary results from the 1994 field season. One till sheet was identified, and till blankets and veneers are the most common surficial sediments. An exception is the eastern half of 86I where the granitoid bedrock has little or no overburden. Dominant ice flow directions range from west to northwest in the Point Lake and Contwoyto Lake areas, and from northwest to north in the Napaktulik Lake region. Glacial transport distances were evaluated based on pebble lithologies in till. Although erratics have been traced for tens of kilometres, the majority of pebbles appear to have travelled less than 10-15 km.

Résumé : Comme contribution au projet CARTNAT dans la Province des Esclaves, trois régions ont été cartographiées à l'échelle de 1/250 000 (cartes 86I, 86H et des parties de la carte 76E de la SNRC), afin d'obtenir des données de base régionales sur les matériaux superficiels aux fins de la prospection glacio-sédimentaire, de la planification environnementale intégrée et des études d'évaluation nécessaire aux mises en valeur futures. Le présent rapport documente certains résultats préliminaires recueillis durant la campagne de 1994. Une nappe de till a été identifiée; les couvertures et les placages de till sont les sédiments superficiels les plus répandus. On note une exception dans la moitié orientale de la carte 86I où le substratum granitoïde est peu ou pas recouvert de morts-terrains. Les directions dominantes de l'écoulement glaciaire varient d'ouest à nord-ouest dans les régions du lac Point et du lac Contwoyto et du nord-ouest au nord dans la région du lac Napaktulik. On a évalué les distances du transport glaciaire en se basant sur la lithologie des cailloux contenus dans le till. Même si l'on a retracé des blocs erratiques sur des dizaines de kilomètres, la majorité des cailloux semblent avoir parcouru moins de 10 à 15 km.

[1] Contribution to the Slave NATMAP Project

[2] Energy, Mines and Petroleum Resources, Government of Northwest Territories, P.O. Box 1320, Yellowknife, Northwest Territories X1A 2L9

INTRODUCTION

The Slave Province National Mapping Program (NATMAP) is a multi-disciplinary project which provides fundamental regional baseline data of surficial materials for ongoing development in the Slave Structural Province (Fig. 1). The discovery of diamonds by drift prospecting in the Lac de Gras region of the central Slave, and the possibility of a diamond mine, in addition to the gold and base metal potential of the area, have resulted in the need for a better understanding of the local and regional glacial geology. Stimulated by exploration and discovery interest and the fact that detailed knowledge of the glacial geology of the area was lacking, Terrain Sciences Division carried out intensive fieldwork during 1994 in three 1:250 000 map areas: Napaktulik (86I), Point Lake (86H) and south and west parts of Contwoyto Lake (76E), (Fig. 1, 2). This region is north of the three map areas mapped in 1993: Winter Lake (86A) (Kerr et al., 1994a), Lac de Gras (76D) (Ward et al., 1994b), and Aylmer Lake (76C) (Dredge et al., 1994a), east of the Coppermine River area mapped by St-Onge (1988), and west of the preliminary surficial maps of the Contwoyto Lake area (Hart et al., 1989).

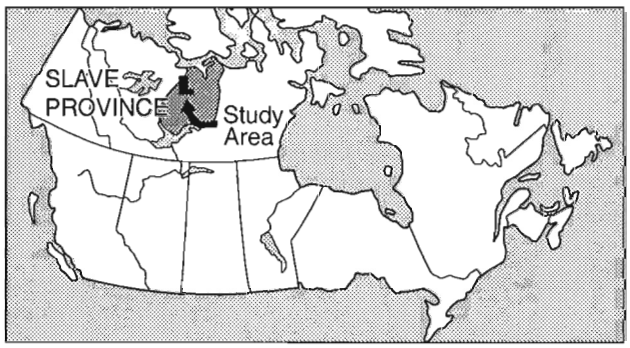

Figure 1. Location of Slave Province and study area.

The investigation involved interpretation of 1:60 000 scale airphotos, ground mapping, striation measurements, pebble lithology analysis, and mineralogical and geochemical analysis of till for gold, base metals, and kimberlite indicator minerals. Mineralogical and geochemical results will be released in separate publications in a similar format as that covering Winter Lake (Kerr et al., 1994b), Lac de Gras (Ward et al., 1994c), and Aylmer Lake (Dredge et al., 1994c).

METHODS

The area was mapped by traversing with helicopter, and by interpretation of 1:60 000 airphotos. Approximately 510 till samples of 3 kg were taken for grain size and trace element geochemical analysis. At each site, 50 pebbles (2 to 4 cm in diameter) were collected for provenance investigations, and

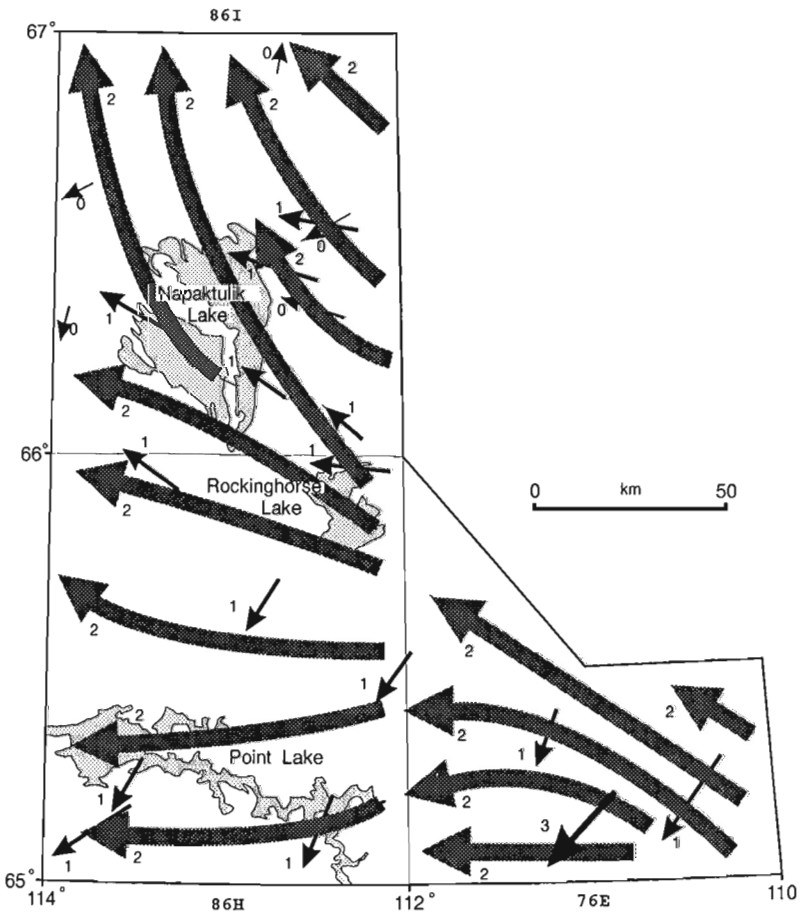

Figure 2.

Summary ice flow diagram for the study area. The flow events are numbered according to age. The thickness of the line gives the relative affect of the flow on transport of debris and on modifying the landscape; the thickest arrows represent the dominant flow, most responsible for the transport of glacial debris.

the nature of the bedrock was noted. In addition, 210 10 kg samples of till were taken for analysis of kimberlite indicator minerals to document their range and background concentrations. Till was collected predominantly from pits dug in mud boils for ease of sampling, at depths of 40 cm to 90 cm. Frozen ground was encountered at depths as shallow as 15 cm below the surface in peat in early to mid July. The active layer in till and glaciofluvial sediments was at least 90 cm deep in late summer. Detailed till sampling of glacial dispersal trains from two kimberlite sources was also undertaken in order to document their characteristics. Striation trends were measured and where possible, their relative ages determined to document ice flow history. Major stratigraphic sections along streams were also logged.

BEDROCK GEOLOGY

The study area straddles the northeast-trending boundary between the Archean Slave Province and the Proterozoic sedimentary cover (see bedrock geology map in pebble lithology section below) to the west (Gebert and Jackson, 1994). An isolated remnant of Proterozoic cover is found in the northeast quadrant of 86H. Archean rocks underlie much of the study area and consist of supracrustal rocks of the Yellowknife Supergroup (ca. 2.71 to 2.65 Ga; Mortensen et al., 1988), younger granitoid rocks, and more rarely granitoid and gneissic rocks pre-dating the Yellowknife Supergroup. Archean volcanic rocks of predominantly mafic composition form a thin north trending belt that is referred to as the Point Lake volcanic belt in the south (86H) and the Napaktulik Lake volcanic belt in the north (86I). Felsic volcanic rocks with numerous gossans are common in northeast-trending arms of the belts.

Slave Province greywacke-mudstone turbidites are found in the metasedimentary domain bordering the Point Lake volcanic belt. The turbidites are bordered by granitoid rocks, most commonly biotite-hornblende granite to granodiorite; gneissic granitoid rocks are common in the Napaktulik Lake sheet (86I). Proterozoic rocks record two sequences grading from clastic to carbonate rocks (Epworth and Recluse groups), overlain by fine grained clastic rocks of the Takiyuak Formation. The study area is transected by a variety of diabase dykes of which the north-northwest-trending Mackenzie swarm is most prominent. Thick diabase sheets (Morel Sills) lie along the Archean/Proterozoic boundary. Important volcanogenic base metal deposits (IZOK, Hood, Gondor) and iron-formation hosted gold deposits (REN) occur within the study area.

NATURE AND DISTRIBUTION OF SURFICIAL SEDIMENTS

Tills

As in the Winter Lake (86A), Lac de Gras (76D), and Aylmer Lake (76C) areas to the south, till is the most extensive surficial sediment in the mapping area (Dredge et al., 1994b; 1995; Kerr et al., 1995; Ward et al., in prep.) and is attributed to the Late Wisconsinan Laurentide Ice Sheet. The till consists of a matrix-supported diamicton, with a sandy silt to sand matrix, and exhibits low to high compaction. Clasts are generally subrounded to subangular and average 2-4 cm in diameter. Matrix grain size varies according to bedrock source; till derived from granitoid rocks is sandy whereas sedimentary and volcanic rocks produced a more silty till. Locally, in the Napaktulik Lake area, many of the fines were removed by meltwater, resulting in isolated lag deposits consisting of pebble to boulder-sized clasts <2 m diameter. In many cases, the upper 0.5 m to 1 m of till has been extensively modified by cryoturbation and solifluction, destroying primary sedimentary structures such as layers or lenses. Organic matter has sometimes been incorporated by cryoturbation to depths of 70-80 cm.

Till deposits are subdivided according to thickness and surface morphology: veneer, blanket, and hummocky. Till veneer is generally <2 m thick, rarely continuous over large areas containing bedrock outcrops and felsenmeer, and conforms to underlying bedrock morphology (Fig. 3A). Till veneer occurs throughout the study area. It is generally loose to compact, with high concentrations of cobbles and boulders at the surface; where veneer is thin and discontinuous, structural bedrock features are usually visible on airphotos. Till veneer was likely deposited during deglaciation, possibly as ablation till. Till blankets are generally >2 m thick and either drape the underlying bedrock, forming undulating till plains, or are low to moderate-relief drumlinoid and crag-and-tail features (Fig. 3B). These tills tend to be relatively compact, contain fewer boulders than till veneer and may represent lodgement till deposited directly by ice. Till blankets and associated crag and tails occur throughout the study area (Fig. 3C). A stark contrast in till thickness and landforms exists between regions underlain by Proterozoic cover and parts of the Slave Province; this is most noticeable in the eastern half of the Napaktulik Lake map area where granitoid bedrock is essentially devoid of any surficial sediment. In the western region which is underlain by Proterozoic bedrock, till plains, drumlinoid landforms and crag-and-tail features are common. Hummocky till is variable in thickness and forms hummocky topography with irregular mounds a few metres high. In the central Napaktulik Lake map area, they are sometimes associated with small rock outcrops or isolated kames, whereas they form an extensive area east of Point Lake. They range from firm to compact, and represent a form of ablation till, possibly associated with stagnant ice.

Glaciofluvial sediments

Glaciofluvial sediments consist of eskers, kames, and proglacial outwash commonly containing kettle lakes. The eskers have a sinuous to linear form and generally trend west, northwest, and north. Cobble and boulder lags are associated with the sides of eskers as well as bedrock surfaces between esker segments. Eskers range from small, sinuous ridges a few tens of metres long, to large, more linear features up to 30 m high and over 25 km in length, such as those occurring north and south of Napaktulik Lake (Fig. 3D). Sandy lateral nodes may occur at intervals along their length. Sediment texture and internal structures are variable, and grain size may change

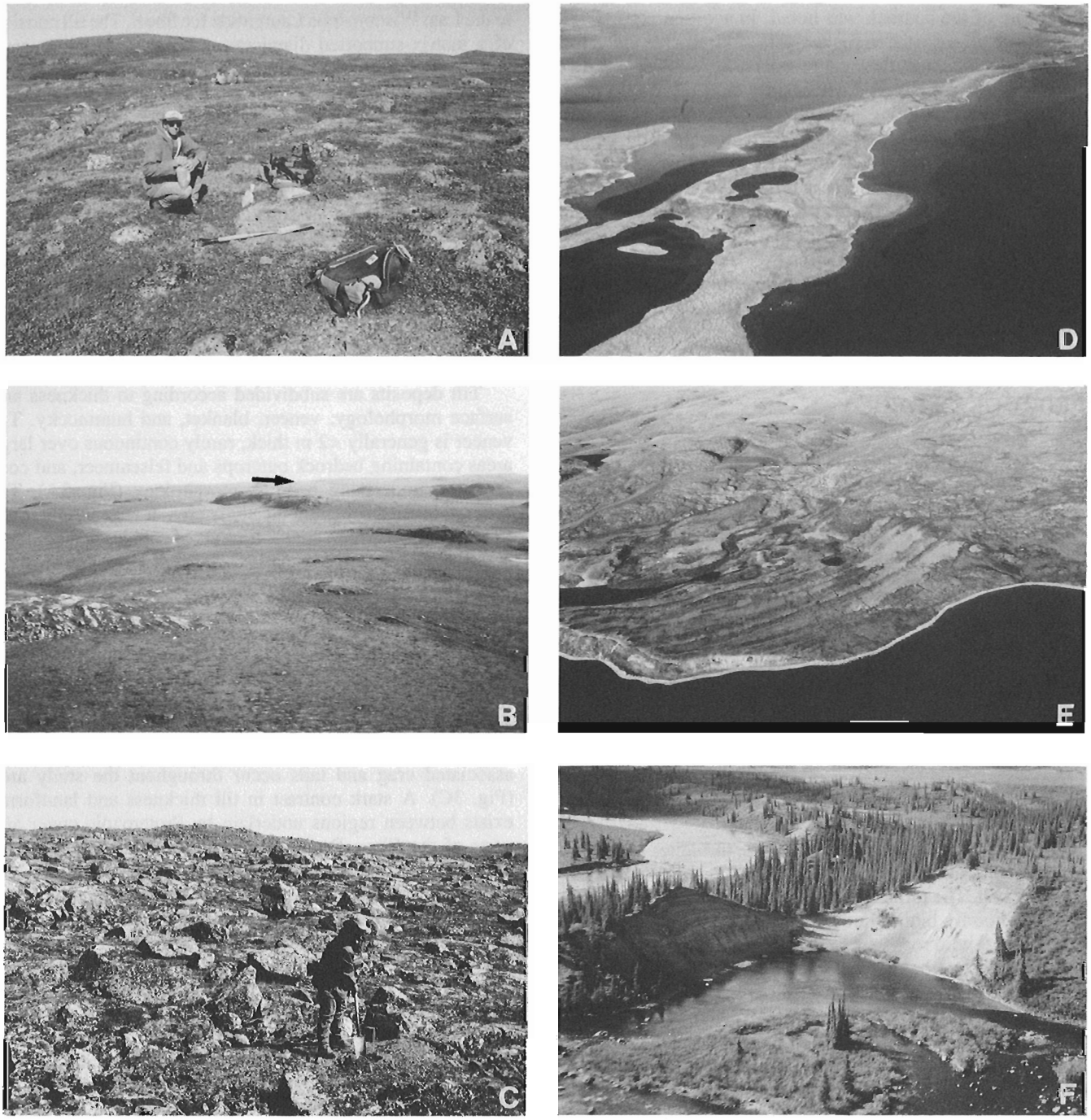

A. Boulder-till veneer overlying flat bedrock outcrops in the southeast quadrant of Napaktulik Lake map area (GSC 1995-081A);

B. Rolling till plains with rock outcrops and crag-and-tail features. Arrow indicates ice flow direction. (GSC 1995-081I);

C. Rock outcrop with veneer of boulders, eastern Napaktulik Lake map area (GSC 1995-081J);

D. Large esker complex exhibiting raised beaches on east (left) side, trending northwest, northern Napaktulik Lake map area (GSC 1995-081L);

E. Raised beaches up to 426 m a.s.l. (32 m above lake level), southern Napaktulik Lake (GSC 1995-081C);

F. Glaciolacustrine sediments exposed along the White Sandy River, southwest quadrant of Napaktulik Lake map area (GSC 1995-081B).

Figure 3.

rapidly over short distances. Very fine- to coarse-grained sand may be capped by a thin layer of gravel. Sedimentary structures consist dominantly of climbing ripples, planar bedding, and trough and planar crossbedding.

Flat-topped kame terraces and outwash plains scarred by braided channels are associated with the esker complexes but may also occur within structurally controlled bedrock gorges which served as meltwater drainage channels during ice retreat. Some of these sand and gravel outwash plains are more than 20 km long and up to 5 km wide. They are more common in the study area than the Winter Lake, Lac de Gras, and Aylmer Lake map areas to the south. As with eskers, their composition is variable, but finely laminated and cross laminated fine sand and silt are common. In many localities, the flanks of sharp crested eskers are surrounded by the terraces and outwash plains. The relative timing of esker development appears to have preceded that of the surrounding kame terraces and outwash plains which exhibit evidence of subaerial deposition. Glaciofluvial deposits are potential resources for large volumes of granular materials.

Glaciolacustrine sediments

Isolated deltas, raised beaches, and wave-washed benches on the flanks of reworked eskers and kames provide evidence for the existence of glacial lakes. Lake sediments were only identified in a few localities and consist of fine to coarse sand, pebbles, and cobbles forming deltas and beach ridges (Fig. 3E). With the exception of the Contwoyto Lake map area which extends outside the study area, the largest glacial lake appears to have been formed in the Napaktulik Lake basin. Abandoned shorelines are well developed in the north-central and eastern parts of Napaktulik Lake, north of the large peninsula which dissects the lake. They are generally absent from the northwest, west, and southwest regions of the lake, except for a few sites on the southern and western shores of the peninsula.

Craig (1960) reported raised beaches along the southeastern shore of Napaktulik Lake at 425 m a.s.l., about 30 m above the present lake level (394 m a.s.l.). During the present investigation, beaches and wave-washed zones were found up to 440 m on the eastern shores. In the southwest Napaktulik Lake map area, along the White Sandy River valley, isolated deposits at 360 m a.s.l. forming a 16 m coarsening-upward sequence (Fig. 3F) of rhythmically bedded, normally graded fine sand capped by clay drapes, climbing ripples, and coarse sand and gravel may represent deposits of Glacial Lake Coppermine (St-Onge et al., 1981; St-Onge, 1988) which occur immediately to the west of the study area. There is also evidence for recessional lakes around the west and south parts of Point Lake, up to 50 m above present lake level. In the Contwoyto Lake basin, Blake (1963) and Hart et al., (1989) reported well-developed abandoned glaciolacustrine shorelines above present lake level. No fine grained sediments are associated with this glacial lake but till near present lake level commonly appears washed with many of the fines being removed.

ICE FLOW PATTERNS

Figure 2 is a summary diagram of flow direction based on air photo interpretation and over 500 striae points, and on regional observations made by Craig (1960), Blake (1963), and Bostock (1980). However, some of the striae observations made by Bostock (1980) around Point Lake could not be confirmed.

In the Napaktulik map area, large-scale ice flow indicators (drumlins and crag and tails), together with well-defined and abundant striae reflect a dominant flow (2 in Fig. 2) to the northwest in the east, to the north-northwest and north in the northwest, and to the west-northwest in the southwest. In the Point Lake map area, the dominant flow as indicated by drumlins and the majority of striae (2 in Fig. 2) was generally west-southwestward and westward in the southern and south-central region, and west-northwestward in the north. In the Contwoyto Lake map area, dominant ice flow directions (2 in Fig. 2) are northwestward and more westward in the southwest quadrant.

At a few locations throughout the study area, isolated striae (1 in Fig. 2), cross-cut by the dominant striae, record a west-northwestward flow in the Napaktulik Lake region, southwestward and west-northwestward flow in the Point Lake map area, and a southwestward flow in the Contwoyto Lake map area; a similar southwestward striae pattern is recorded farther south (Ward et al., 1994a). At a limited number of sites in the Napaktulik map area, rare striae (0 in Fig. 2) record flow directions towards the southwest and northeast which deviate from and are cross-cut by dominant patterns (2 in Fig. 2), and, in one instance, are cross-cut by striae 1 (Fig. 2). Limited to the south-central region of the Contwoyto Lake map area, there is local evidence of a younger southwest ice flow (3 in Fig. 2) cross-cutting the dominant flow to the northwest and west.

GLACIAL HISTORY

All ice flow indicators are thought to represent flow directions relating to the Late Wisconsinan glaciation. The Napaktulik, Point Lake, and Contwoyto Lake map areas lie 600-700 km west of the M'Clintock Ice Divide of the Laurentide Ice Sheet (Dyke and Prest, 1987; Dyke and Dredge, 1989). This region was likely still ice covered by about 10 500 BP and became ice-free by about 9000 BP, at which time the ice margin lay 150-200 km to the east. Some aspects of the ice flow history can be determined by the relative age of striations, as well as large-scale indicators such as drumlinoid landforms, roches moutonnées, and crag and tails.

The oldest reported striae (0 in Fig. 2) represent ice flow prior to the establishment of the dominant regional patterns as they are cross-cut by flows '1' and '2'. Alternatively, they represent local, topographically controlled ice flow either during ice build-up, full glacial conditions, or early in the

deglaciation phase. If the second youngest set of striae (1) correlate, they may represent radial flow related to the advance of Laurentide Ice prior to the last, strongest flow (2 in Fig. 2). If striae (1) do not correlate throughout the study area, the southwestward flow in Point Lake area and the northwestward flow in Napaktulik areas could relate to different events.

The striation arrangement could represent the following sequence of events (Fig. 2) if striae 1 correlate throughout the study area and relate to the oldest flow: 1) in the central and southern region of the Napaktulik and Point Lake and southern Contwoyto Lake map areas, ice advanced from the northeast, east, and southeast; 2) a subsequent westward flow in the southern part of Point Lake and southwest part of Contwoyto Lake map areas with a shift to northwestward flow over northern Point Lake and southern Napaktulik Lake and much of the rest of the Contwoyto Lake map areas. This clockwise shift in flow continued with a north-northwestward and northward flow in the central and northwest region of Napaktulik Lake. However, there was northwestward flow in the northeast part of the Napaktulik Lake map area. All these flows (2 in Fig. 2) are dominant flows attributed to the last stages of glaciation; and 3) a younger, local flow towards the southwest in the southeast region of the Contwoyto Lake map area which may be related to reorientation of ice in the period of ice retreat.

During deglaciation a glacial lake formed in the Napaktulik Lake basin. The maximum elevation of wave-washed zones at 440-438 m a.s.l. (Fig. 4A) may reflect the first phase of a lake, herein called glacial lake Napaktulik. Its

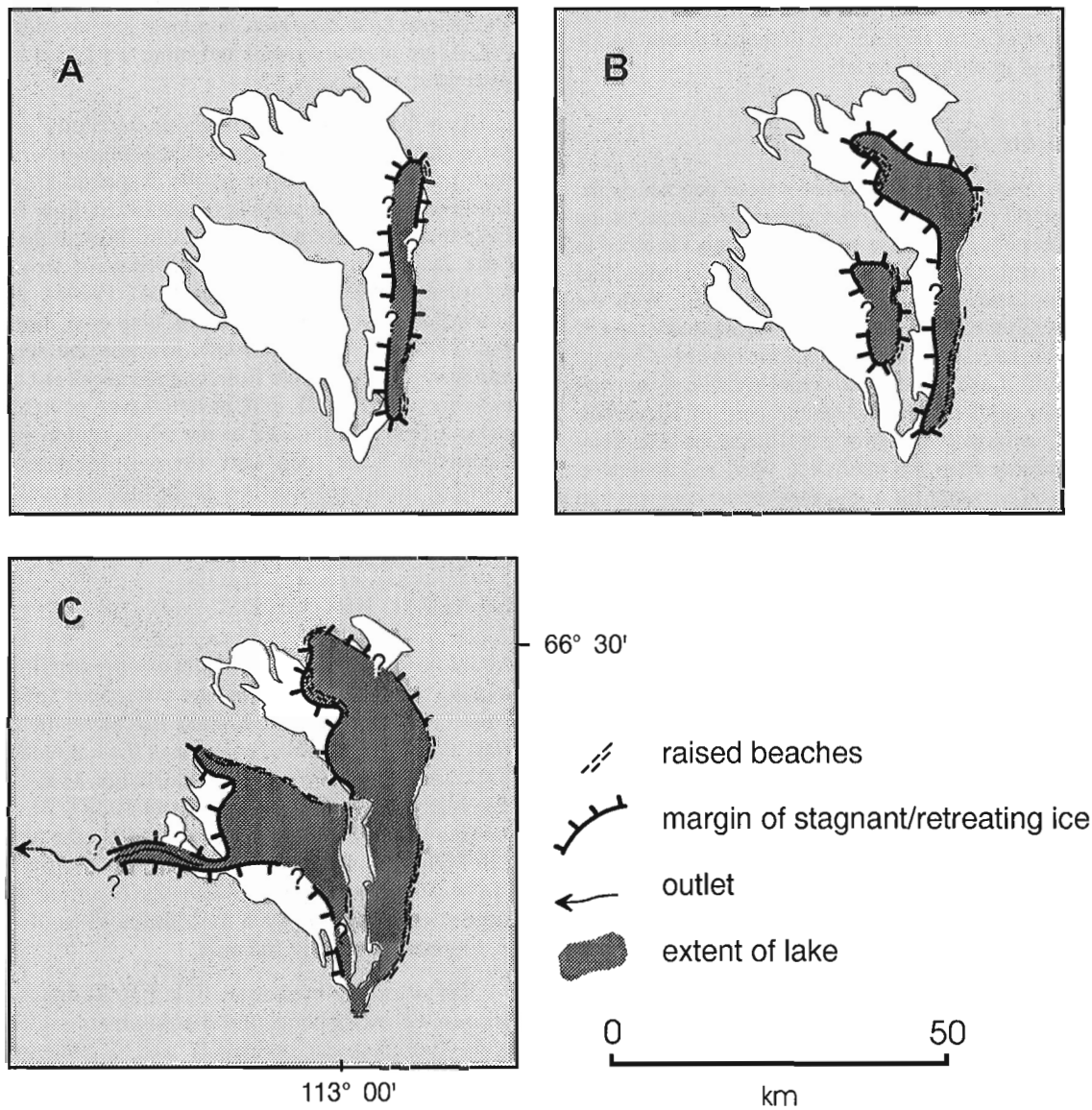

*Figure 4. Maps illustrating the evolution of glacial lake Napaktulik. Extent of the lake is extrapolated between isolated beaches at the same or similar elevations. **A)** 440-438 m; **B)** 426-420 m; **C)** 410-400 m.*

extent is defined on the basis of isolated beaches at similar elevations, and on the premise that areas which do not exhibit evidence of washing or wave action were ice-covered. As ice receded, the lake dropped to a second lower phase at 426-420 m a.s.l and expanded into two bodies of water separated by the large peninsula dissecting the lake (Fig. 4B). A northwest-trending esker with beaches on its northeast flank and ice-contact collapse structures on the opposite side indicate the ice margin was to the west. With continued deglaciation to the north, south, and northwest during phase three, glacial lake Napaktulik increased in area as evidenced by numerous beaches at 410-400 m a.s.l. (Fig. 4C). Melting of ice and/or ice retreat permitted waters to drain westward into the Coppermine River to the west of the study area.

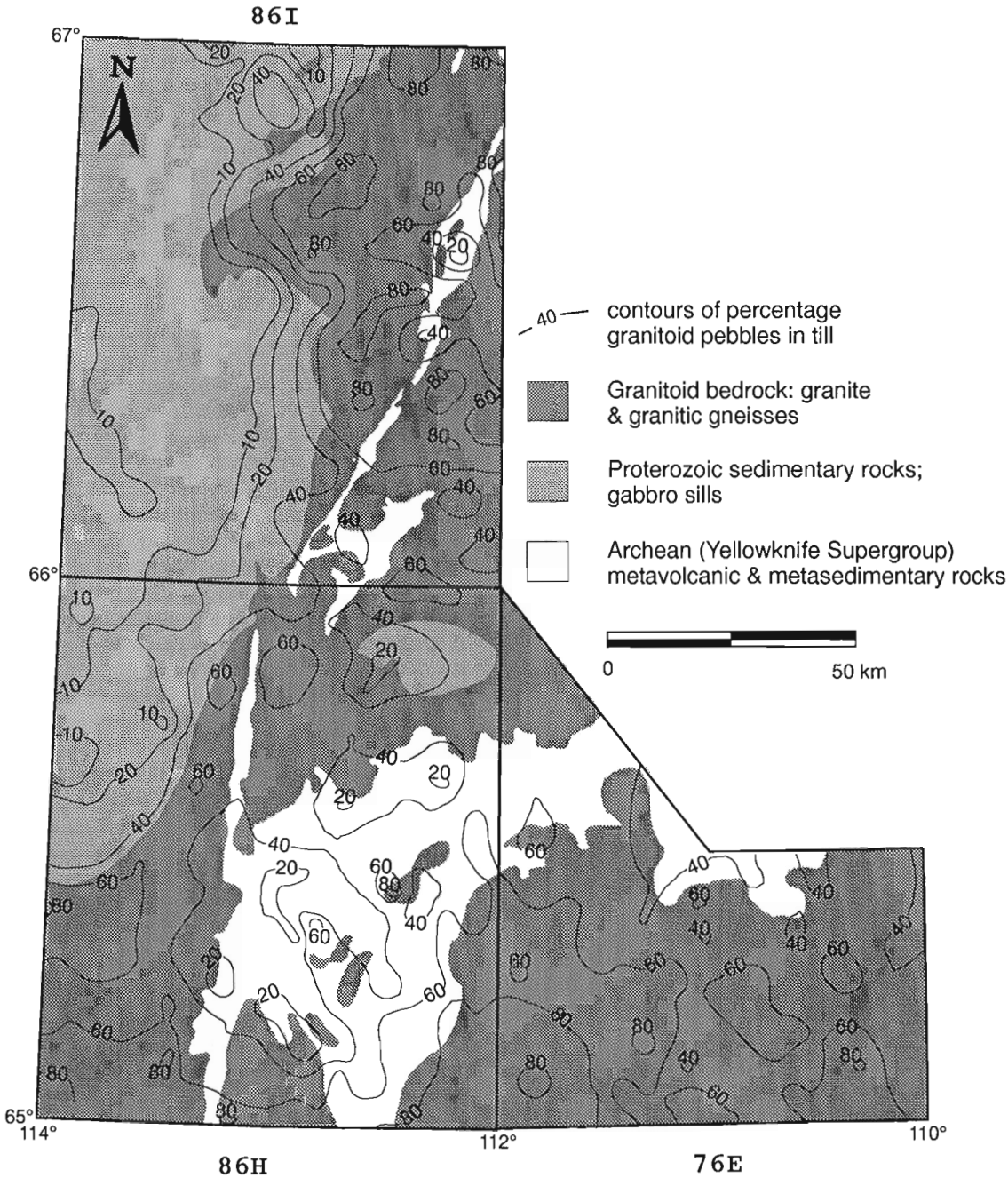

Figure 5. Clast lithology map showing the regional contoured percentages of granitoid pebbles in till from 86I, 86H and 76E. Dominant ice flows are summarized in Figure 2. Generalized bedrock geology modified from Gebert and Jackson (1994).

PEBBLE LITHOLOGY PROVENANCE STUDIES AND TRANSPORT DISTANCES IN TILL

A regional provenance study based on the lithology of pebbles in till and field observations on boulder lithologies was undertaken to determine the relation between till and bedrock, to estimate transport distances and directions as an aid to mineral exploration, as well as to contribute to the ice flow history. In planning a drift prospecting program in the map area, the 'dominant' ice flow, corresponding to the most prominent and frequent striae and orientation of drumlins and crag and tails, is the most important direction of till transport. The direction of dominant flow varies throughout the area with three broad zones recognized (Fig. 2): 1) a westward flow across the southern portion of Point Lake and southwest Contwoyto Lake map area; 2) a northwestward flow over much of the Contwoyto Lake, northern Point Lake and southern and northeast Napaktulik Lake map areas; and 3) a north-northwest and north flow in the central and northwest region of Napaktulik Lake.

This area provides the opportunity to determine patterns of drift transport because many of the bedrock contacts run perpendicular to dominant ice flow directions. Figure 5 shows the percentage and distribution of granitoid (granite and gneiss) pebbles in till over granitoid, sedimentary, metasedimentary, volcanic, and metavolcanic bedrock in the three map areas. To illustrate patterns of glacial dispersal, granitoid rock was chosen over other lithologies as an indicator lithology because of clearly defined source areas and because it can be easily distinguished as clasts compared to other rock types. Granitoid pebbles occur at almost all sites, although a number of sites underlain by sedimentary rocks in the western half of 86I contain no granitoids.

The expected distribution pattern of granitoid pebbles was one of consistently decreasing clast concentration down-ice (i.e. west, northwest, and north) of the source rock and bedrock contact, as illustrated by Shilts (1975) and other workers. The distribution map of Figure 5 illustrates a similar trend for granotoid clasts in the western region of 86I and the northwest region of 86H. However, the predicted pattern of clast-content attenuation is not as evident where different types of bedrock occur as small, disjointed bodies and where contacts are convoluted, as in the eastern half of 86H and the northern half of 76E.

As expected, the highest concentrations of granitoid clasts occur in areas underlain by granitoid bedrock. The highest reported concentration of these clasts is 94% in northeastern and east-central 86I, and regions containing 60% to over 80% are common. The sharpest decrease is noted in the western region of 86I and the northwest region of 86H where transport distances can be estimated along dominant ice flow pathways. In the down-ice direction to the northwest, concentrations fall to 40% within 5 km of granitoid bedrock, to 20% within approximately 15 km of granitoid bedrock, and to 10% or less from as little as 10 to 50 km of the bedrock source. At several sites in the west half of 86I, granitoid clasts (2-4 cm) are absent 20-35 km down-ice of the contact between non-granitoid and granitoid bedrock. They occur at greater distances as erratics up to several metres in diameter.

At the north end of Napaktulik Lake and the west margin of Rockinghorse Lake 5 to 6 km down-ice of non-granitoid bedrock sources, sites overlying granitoid bedrock contain as little as 4 to 14% granitoid clasts. The low concentrations can be interpreted on the basis of dominant ice flow directions. At the north end of Napaktulik Lake, 40 to 90% of clasts are non-granitoid in nature and were carried by ice northward onto granitoid terrain. Conversely, in the southeast quadrant of 86H, one site on non-granitoid bedrock contains up to 74% granitoid clasts, and is 8 km down-ice of a large granitoid complex.

The results from this study differ from those in the Aylmer Lake area (76C) to the southeast (Dredge et al., 1994b) where sites more than 20 km down-ice of a source rock contact commonly retained greater than 40% source rock (metasedimentary and metavolcanic) clasts, indicating a greater distance of glacial transport. The nature of the bedrock and till thickness may be factors contributing to a relatively well defined dispersal pattern observed on a regional scale in this study area. The sharp decrease of granitoid pebbles, and hence sharp increase in non-granitoid pebbles northwest of the main north-trending bedrock contact in the centre of 86I, may reflect differences in the break-down habits between sedimentary and volcanic rocks and granitoid rocks. The former fracture readily along planes into thin segments and are prone to break quickly into pebble-sized components creating a dilution effect, whereas granitoid rocks are coarsely jointed and break into blocks and boulders before comminution to pebble sizes (Dredge et al., 1994b). Areas of till veneer exhibit high concentrations of locally derived pebbles and relatively low concentrations of non-local clasts, although this difference in till thickness did not consistently account for pebble distribution. It is difficult to assess the effects of an earlier ice flow on pebble dispersal patterns in this region because distribution strongly reflects the predominant westward, northwestward, and northward flows. Lower granitoid concentration overlying granitoid bedrock in the central Contwoyto map area may result from the dilution of granitoids by sedimentary/volvanic clasts originating from the north-central regions of the map area during earlier flow.

CONCLUSION

This preliminary description of surficial sediments, striation patterns, till lithology, and glacial transport distances provides important implications for drift prospecting in this area. The recognition of one till sheet consisting of distinct till blankets, veneers and hummocky till is consistent with other regional studies in adjacent areas. Ice flow history and the three zones representing dominant ice flow directions relate to the main period of most till transport. Provenance investigations are summarized as follows: (1) the dominant clast content in till generally reflects the nature of the underlying bedrock; (2) sites overlying granitoid bedrock typically contain at least 40-50% granitoid clasts and generally 60-80% or

more; (3) the regional dispersal train resulting from erosion of granitoid bedrock forms a relatively narrow 10-20 km wide rim (from 50% down to 10%) in the down-ice direction along the length of the main western Proterozoic/granitoid bedrock contact; and (4) pebble distribution appears to suggest that dispersal trains from exploration targets are likely to be linear features parallel to the dominant ice flow patterns. Additional provenance studies are required to determine if volcanic or sedimentary rocks show similar distribution trends and more detailed orientation surveys are needed to accurately determine surficial sediment types and local ice flow patterns for effective drift prospecting.

ACKNOWLEDGMENTS

Thanks are extended to Jennifer Adams, Matt Caddel, and Ray Roberts who were field assistants on this project. Figures were produced with the assistance of Stephen Wolfe and Craig Nicholson. Polar Continental Shelf Project provided helicopter and partial fixed-wing support, and Craig Nicholson maintained radio contact and expediting facilities based out of Yellowknife. The authors would also like to thank S. Wolfe for insightful comments.

REFERENCES

Blake, W.
1963: Notes on glacial geology, northeastern District of Mackenzie; Geological Survey of Canada, Paper 63-28, 12 p.

Bostock, H.H.
1980: Geology of the Itchen Lake area, District of Mackenzie; Geological Survey of Canada, Memoir 391, 101 p.

Craig, B.G.
1960: Surficial geology of the north-central District of Mackenzie, Northwest Territories; Geological Survey of Canada, Paper 60-18, 8 p.

Dredge, L.A., Kerr, D.E., and Ward, B.C.
1995: Surficial geology, Point Lake, District of Mackenzie (86H), Northwest Territories; Geological Survey of Canada, Open File 3085, scale 1: 125 000. (in press)

Dredge, L.A., Ward, B.C., and Kerr, D.E.
1994a: Surficial geology, Aylmer Lake, District of Mackenzie (76C), Northwest Territories; Geological Survey of Canada, Open File 2798, scale 1: 250 000.
1994b: Glacial geology and implications for drift prospecting in the Lac de Gras, Winter Lake and Aylmer Lake map areas, central Slave Province, Northwest Territories; in Current Research 1994-C; Geological Survey of Canada, pp. 33-38.
1994c: Till geochemistry, Aylmer Lake, District of Mackenzie, Northwest Territories (NTS 76 C). Geological Survey of Canada, Open File 2867, 42p.

Dyke, A.S. and Dredge, L.A.
1989: Quaternary geology of the northwestern Canadian Shield; in Quaternary Geology of Canada and Greenland, (ed.) R.J. Fulton; Geological Survey of Canada, Geology of Canada, Geology of Canada, no. 1, p. 189-214; (also Geological Society of America, The Geology of North America, v. K-1).

Dyke, A.S. and Prest, V.K.
1987: The Late Wisconsinan and Holocene history of the Laurentide Ice Sheet; Géographie physique et Quaternaire, v. 41, p. 237-263.

Gebert, J.S. and Jackson, V.A.
1994: Preliminary compilation of the Point-Contwoyto-Napaktulik-Kathawachaga Lakes area (NTS 86H, 76E, 86I and 76L); Indian and Northern Affairs Canada, EGS 1994-2, scale 1: 250 000.

Hart, B.R., Avery, R.W., DiLabio, R.N.W., and Cocker, W.B.
1989: Surficial geology, Contwoyto Lake (76E/5 to 16), Northwest Territories; Geological Survey of Canada, Open File 2018, 6 sheets, scale 1: 50 000.

Kerr, D.E., Dredge, L.A., and Ward, B.C.
1995: Surficial geology, Napaktulik Lake, District of Mackenzie (86I), Northwest Territories; Geological Survey of Canada, Open File 3032, scale 1: 125 000.

Kerr, D.E., Ward, B.C., and Dredge, L.A.
1994a: Surficial geology, Winter Lake, District of Mackenzie (86A), Northwest Territories; Geological Survey of Canada, Open File 2891, scale 1: 125 000.
1994b: Till geochemistry, Winter lake, District of Mackenzie (NTS 86A), Geological Survey of Canada, Open File 2908, 34 p.

Mortensen, J.K., Thorpe, R.I., Padgham, W.A., King, J.E., and Davis, W.J.
1988: U-Pb zircon ages for felsic volcanism in the Slave Province, NWT; in Radiogenic Age and Isotopic Studies, Report 2; Geological Survey of Canada, Paper 88-2, p. 85-95.

Shilts, W.W.
1975: Principles of geochemical exploration for sulphide deposits using shallow samples of glacial drift; Canadian Institute of Mining and Metallurgy Bulletin, v. 68, p. 73-80.

St-Onge, D.A.
1988: Surficial geology, Coppermine River, District of Mackenzie, Northwest Territories; Geological Survey of Canada, Map 1645A, scale 1:250 000.

St-Onge, D.A., Geurts, M.A., Guay, F., Dewez,V., Landriault, F., and Léveillé, P.
1981: Aspects of the deglaciation of the Coppermine River region, District of Mackenzie; in Current Research, Part C; Geological Survey of Canada, Paper 81-1A, p. 327-331.

Ward, B.C., Dredge, L.A., and Kerr, D.E.
1994a: Ice flow indicators, Winter Lake (86A, Lac de Gras (76D), and Aylmer Lake (76C), District of Mackenzie, Northwest Territories; Geological Survey of Canada, Open File 2808, scale 1: 250 000.
1994b: Surficial geology, Lac de Gras (76D), District of Mackenzie, Northwest Territories; Geological Survey of Canada, Open File 2928 (supercedes Open File 2680), scale 1: 125 000.
1994c: Till geochemistry, Lac de Gras, District of Mackenzie, Northwest Territories (NTS 76 D); Geological Survey of Canada, Open File 2868, 42p.

Geological Survey of Canada Project 920072

Eastern Canada and National and General Programs

Est du Canada et programmes nationaux et généraux

A Paleogene radiolarian event of the South Mara unit, Banquereau Formation, Jeanne d'Arc Basin, offshore Newfoundland, and its implications

F.C. Thomas
GSC Atlantic, Dartmouth

Thomas, F.C. 1995: A Paleogene radiolarian event of the South Mara unit, Banquereau Formation, Jeanne d'Arc Basin, offshore Newfoundland, and its implications; in Current Research, 1995-E; Geological Survey of Canada, p. 211-220.

Abstract: During micropaleontological analysis of 15 wells in the Jeanne d'Arc Basin, large numbers of spumellarian radiolarians were found to be present in Paleocene to Lower Eocene sections in most sites. This event coincides with the deposition of the prodeltaic South Mara unit, a sandy/silty member of the otherwise shaly Banquereau Formation. The restricted range of these taxa within this interval suggests that their preservation may have been a function of the higher sedimentation rate represented by the South Mara unit. At least five different taxa appear in the interval, based on gross morphology. These are largely similar or identical to coeval types described and illustrated in the literature from the nearby DSDP Site 384 and some North Sea locations.

Résumé: Au cours de l'analyse micropaléontologique de 15 puits forés dans le bassin de Jeanne d'Arc, on a découvert un grand nombre de radiolaires spumellariens dans des profils du Paléocène à l'Éocène inférieur dans la plupart des sites. Leur présence coïncide avec le dépôt de l'unité prodeltaïque de South Mara, un membre sableux/silteux de la Formation de Banquereau autrement shaleuse. L'intervalle restreint de ces taxons durant cette période laisse supposer que leur conservation peut être due à la vitesse de sédimentation plus élevée représentée par l'unité de South Mara. En se basant sur la morphologie générale, on dénombre au moins cinq taxons différents dans l'intervalle. Ils sont en grande partie semblables ou identiques aux types contemporains décrits et illustrés dans la documentation portant sur le site 384 du PSFM situé dans le voisinage et sur certains endroits dans la mer du Nord.

INTRODUCTION

This paper describes the occurrences of several taxa of large spumellarian radiolarians in lower Paleogene sediments of the Jeanne d'Arc Basin, offshore Newfoundland, particularly the South Mara unit.

This basin has been the site of exploratory hydrocarbon drilling since 1971 and at present over 60 wells have been completed there, usually targeted on Mesozoic hydrocarbon-bearing zones.

In much of the basin, the overlying Cenozoic deposits together commonly total more than 1500 m in thickness. Cuttings samples from the Cenozoic sections of 15 wells have been analyzed for micropaleontological study (Thomas, 1994), and contain rich foraminiferal assemblages ranging from Paleocene to Late Miocene, based on the quantitatively derived scheme for the Eastern Canadian Margin devised by Gradstein and Agterberg (1982).

During the course of analysis, numbers of spumellarian radiolarians were encountered in 13 wells at levels usually dateable as Early Eocene. Until recently, these forms had not been identified definitely as radiolarians due to their usually poor state of preservation. In studies of individual wells in the region (Thomas, unpublished data), and a regional compilation (Thomas, 1994), these taxa were informally termed "balls", although their shapes actually ranged from spherical to lenticular, discoid and spindle-shaped.

All samples were prepared originally for foraminiferal analysis, not radiolarian research. Therefore, only relatively large radiolarian taxa would have been recovered. Nevertheless, to this author's knowledge, no work has yet been published on samples from this basin prepared specifically for radiolarian study, so the present survey represents baseline research for this field. This paper outlines the distribution and stratigraphy of these occurrences, and presents tentative identifications of these forms.

GEOLOGICAL SETTING

The Jeanne d'Arc Basin lies in the northeastern part of the Grand Banks of Newfoundland, a large eastward extension of the continental shelf (Fig. 1, Table 1). It has its origins in the early Mesozoic, but by the end of the Cretaceous it had stabilized to its present dimensions and attitude, and was being buried by marine shelf deposits. The structural highs that define the basin are the Outer Ridge Complex to the east and south and the Bonavista Platform to the west.

During the Tertiary the Jeanne d'Arc Basin was the site of apparently near-continuous deposition, usually as shales, with minor chalk and siltstones. The lithological unit encompassing the Tertiary in the Jeanne d'Arc Basin, as elsewhere on the Grand Banks and Scotian Shelf is the Banquereau Formation (McIver, 1972). A local feature of the Banquereau widespread in this basin is the Paleocene and Lower Eocene South Mara unit (also sometimes called the South Mara member), a

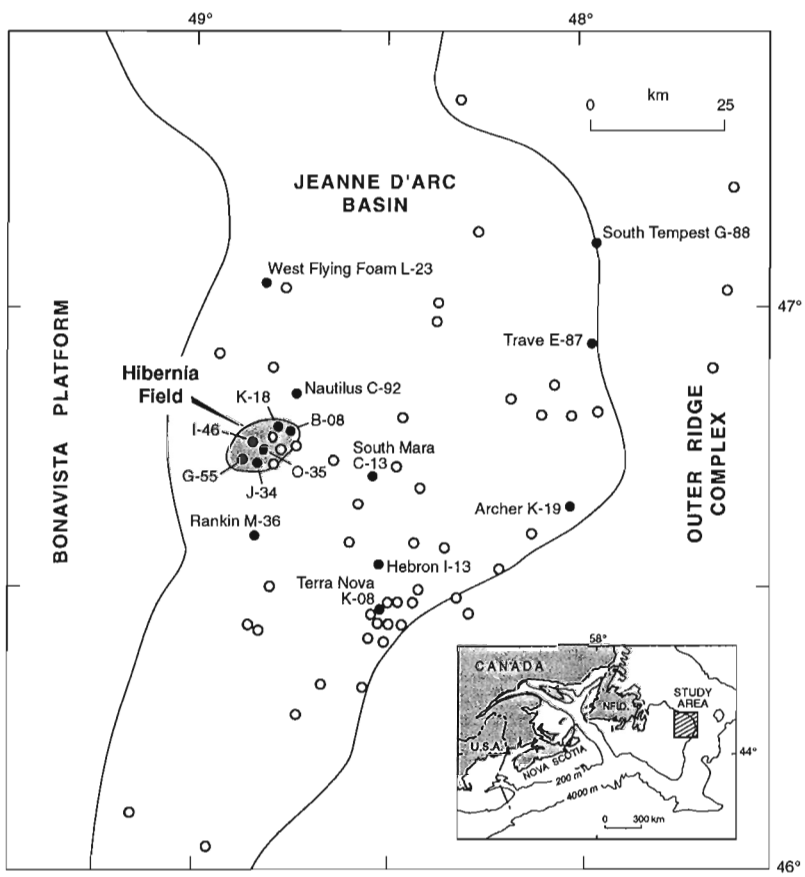

Figure 1.

Location map of Jeanne d'Arc Basin, showing well locations and structural features. Open circles show location of other wells not yet examined.

relatively silty/sandy unit derived from eroding Upper Cretaceous deposits near the western margin of the basin (Sinclair, 1988). A compilation of lithostratigraphic picks for 59 wells in this basin (McAlpine, 1989) defines top and bottom boundaries of the South Mara unit in the 15 wells analyzed in this paper.

In previous literature the South Mara unit has been characterized as principally Paleocene in age (Sinclair, 1988; McAlpine, 1989, 1990). Undoubtedly the deposition of this unit began in the Paleocene, but this study suggests deposition of the South Mara unit continued into the earliest Eocene in many sites. Figure 2 compares lithostratigraphy of the Banquereau Formation in the literature with this revised age of the South Mara unit.

Table 1. Technical data of 15 Jeanne d'Arc Basin wells.

WELL	Location Latitude Longitude
Husky-Bow Valley *et al.* Archer K-19	46°38'43.17"N 48°02'18.42"W
Mobil *et al.* Hebron I-13	46°32'33.95"N 48°31'45.47"W
Mobil *et al.* Hibernia B-08	46°47'06.36"N 48°45'29.87"W
Mobil *et al.* Hibernia G-55	46°44'17.07"N 48°53'10.75"W
Mobil *et al.* Hibernia I-46	46°45'40.74"N 48°51'17.20"W
Mobil *et al.* Hibernia J-34	46°43'33.84"N 48°50'13.00"W
Mobil *et al.* Hibernia K-18	46°47'34.69"N 48°47'17.05"W
Mobil *et al.* Hibernia O-35	46°44'54.92"N 48°49'53.74"W
Mobil *et al.* Nautilus C-92	46°51'03.55"N 48°44'20.64"W
Mobil *et al.* Rankin M-36	46°35'46.58"N 48°50'56.26"W
Mobil *et al.* South Mara C-13	46°42'01.07"N 48°32'19.63"W
Mobil *et al.* South Tempest G-88	47°07'19.92"N 47°57'30.48"W
Petro-Canada *et al.* Terra Nova K-08	46°27'31.60"N 48°30'59.60"W
Husky-Bow Valley *et al.* Trave E-87	46°56'17.56"N 47°58'09.74"W
Mobil *et al.* West Flying Foam L-23	47°02'43.81"N 48°49'17.02"W

Near the end of the Mesozoic, the sedimentary processes taking place in the Jeanne d'Arc were producing overlapping deltaic sequences with distal turbidites in the shallower southern and western areas and deeper-facies, chalky limestones in the northwest (Grant and McAlpine, 1990). By the Early Eocene, infilling during the Mesozoic had caused the Jeanne d'Arc to nearly cease being a distinct basin at all, and the whole structure was subsiding in concert with the entire Grand Banks area. The South Mara unit encountered in wells over much of the basin, seems to represent delta-front turbidites, deposited as distinct, episodic and intermittent events and appears in seismic lines as prograding wedges (Agrawal, pers. comm., 1994).

Seismic data show overlying strata of the Banquereau Formation to consist of mostly flat-lying, laterally continuous sheets with only minor local faulting. The regional subsidence of the Grand Banks area continued throughout the Cenozoic, roughly keeping pace with sediment deposition. Later Cenozoic depositional history and paleoceanographic events in this basin, as indicated by the foraminiferal faunas of the Hibernia area in the western part of the basin, have been documented elsewhere (Thomas, 1994).

METHODS

The samples used in this study were derived entirely from ditch cuttings. These were composite samples derived from two or three sample intervals which have been recombined to represent an interval of, usually, 10 m. There are normally 20 or even 30 m gaps between samples.

The raw samples ranged from 100 to 250 g, and were disaggregated by soaking for 24 to 48 hours (including an hour or so of heat and mechanical agitation) in an aqueous solution of Quaternary O, a commercial surfactant. They were washed through a 63 μm sieve, and the residues oven-dried. The microfossils were then hand-picked in a semi-quantitative way, as follows:

1. Residues were dry-screened in a stack of sieves with openings of 850 μm, 250 μm, and 150 μm.
2. Two picking trays of each of the three fractions were picked clean of microfossils, which were placed in 60-grid slides. The fraction less than 150 microns was not usually picked.
3. In cases where the faunas were very rich, less than two trays of each mesh size were picked, and this information was noted on the slide.

In this way, a roughly similar amount and microfossil size distribution of each sample was examined, allowing reasonable sample-to-sample comparisons for richness and species diversity.

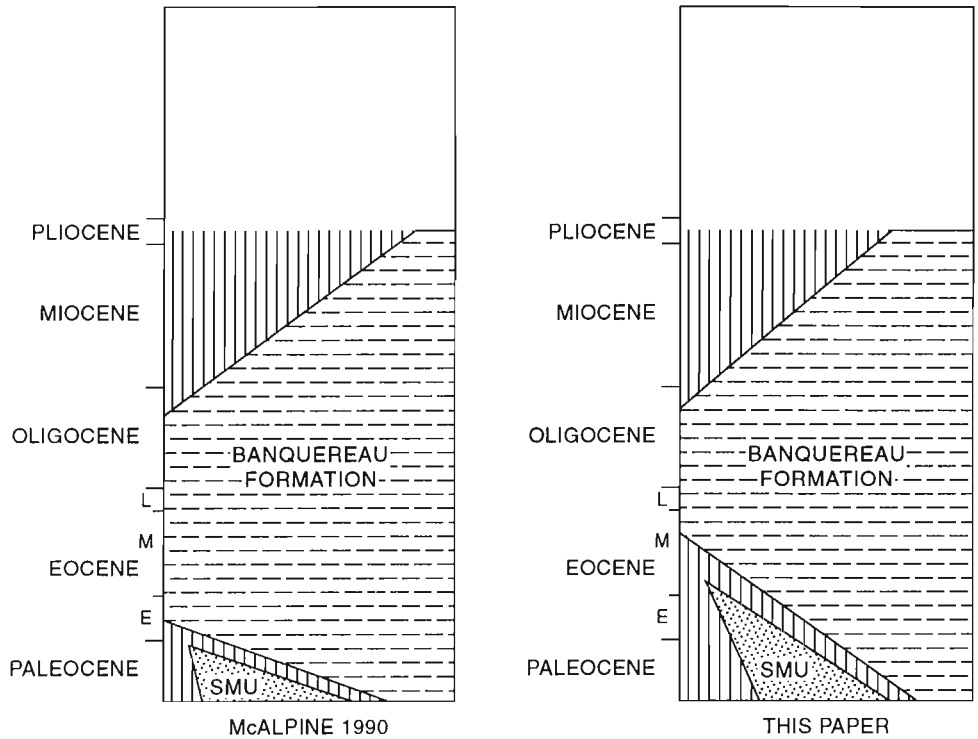

Figure 2. *Lithostratigraphy of Banquereau Formation and South Mara unit (SMU) as illustrated by McAlpine (1990) and as revised by recent micropaleontological work.*

Detailed species lists and gross biostratigraphic picks of the 15 wells of this survey have been documented elsewhere (Thomas, 1994).

The micrographs were taken on the Enviroscan environmental scanning electron microscope at the Geological Survey of Canada office in Dartmouth.

RESULTS

The constraints described above unquestionably affect the precision of paleoecological interpretations and stratigraphic correlation of the microfossil assemblages encountered. Yet the well-to-well comparisons of coeval assemblages in the lower Paleogene of these wells reveal both basin-wide events and local variances and permit some detail in outlining the deposition and preservation of the radiolarian event during this interval.

In general, the radiolarian event appears to correlate in time to the deposition of the South Mara unit, roughly spanning the Paleocene/Eocene boundary, and probably continuing for the first part of the Early Eocene. In a few cases, radiolarians appear in cuttings samples just above the upper boundary of the South Mara unit as defined by electrical logs, and more often, in samples from below the lower boundary. This latter case, however, can almost certainly be ascribed to downhole caving.

The size of the study area and distribution of sampled sites warrants division into three sections; western, south-central, and eastern.

Western

In the western half of the study area, represented by West Flying Foam L-23, Nautilus C-92, the six Hibernia wells (B-08, G-55, I-46, J-34, K-18, and O-35), and Rankin M-36, the South Mara unit can be dated by diagnostic planktic and/or benthic foraminifera (Fig. 3). In the Hibernia field, these dates are; Early Eocene in G-55, J-34, O-35; probably Early Eocene in I-46, and ?Paleocene to Early Eocene in B-08 and K-18. In all Hibernia wells, radiolarians appear at or near the top of the South Mara unit, and usually continue on for one or two samples below it, almost certainly as part of a substantial cavings component containing many demonstrably younger taxa.

North of this field, Nautilus C-92 contains some 180 m of sediments defined as the South Mara unit, Early Eocene in age, but completely devoid of preserved radiolarians. North of Nautilus, West Flying Foam L-23 contains a thinner, 90 m South Mara unit of Paleocene age, with small numbers of radiolarians.

South of the Hibernia field, Rankin M-36 contains significant numbers of these taxa in a 50 m span of undated, though pre-Late Eocene, sediments.

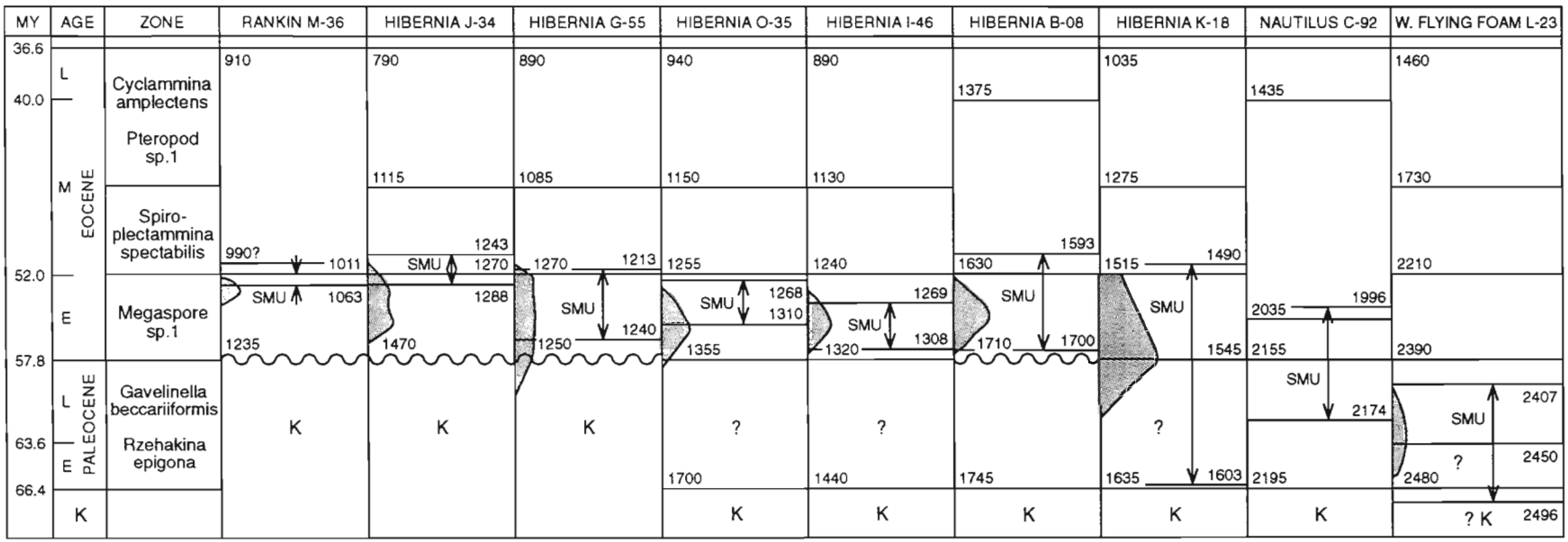

Figure 3. Positions of South Mara unit (SMU, from McAlpine, 1989) and radiolarian event in nine wells in western portion of Jeanne d'Arc Basin. Chronostratigraphy is from Palmer (1983), zonation is from Gradstein and Agterberg (1982).

South-Central

Three wells, Terra Nova K-18, Hebron I-13, and South Mara C-13 lie in the southern and central portion of the study area (Fig. 4). Hebron and Terra Nova both contain numbers of radiolarians within the South Mara unit, which is dated as Early Eocene. In both wells, thin beds of probable Paleocene age lie well under the lower boundary of the South Mara unit. The South Mara C-13 well contains no preserved radiolarians in its 120 m of this unit.

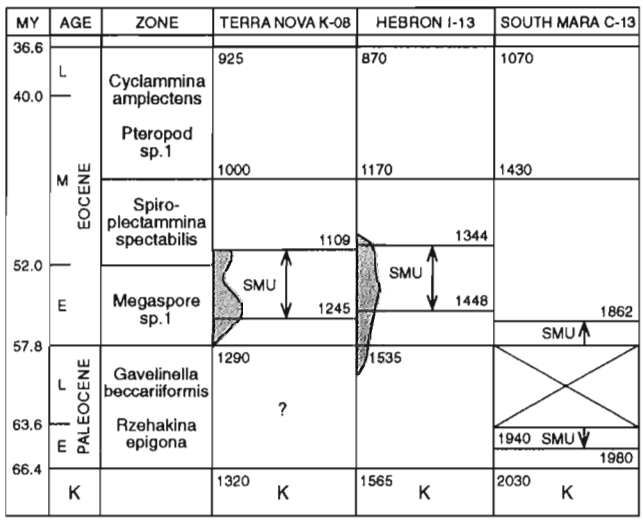

Figure 4. Positions of South Mara unit (SMU, from McAlpine, 1989) and radiolarian event in three south-central wells in Jeanne d'Arc Basin. Chronostratigraphy is from Palmer (1983), zonation is from Gradstein and Agterberg (1982).

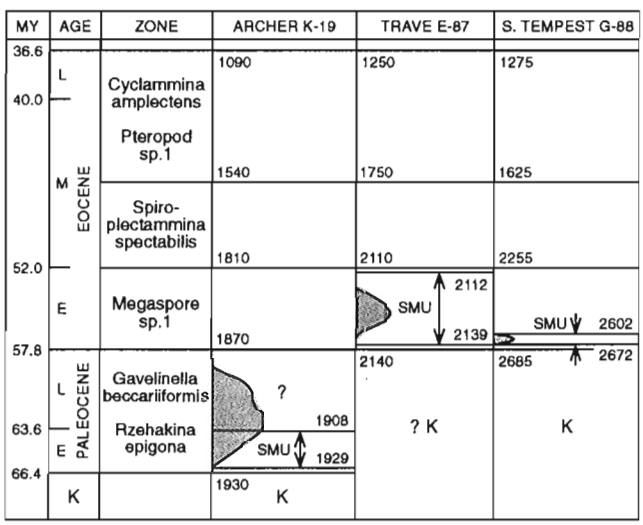

Figure 5. Positions of South Mara unit (SMU, from McAlpine, 1989) and radiolarian event in three eastern Jeanne d'Arc Basin wells. Chronostratigraphy is from Palmer (1983), zonation is from Gradstein and Agterberg (1982).

Eastern

On the eastern flank of the basin, Trave E-87 and South Tempest G-88 contain small numbers of radiolarians in somewhat condensed South Mara unit sections, both datable as Early Eocene (Fig. 5). Anomalously, Archer K-19, in the southeast corner of the basin, contains some of these taxa in a 50 m interval of questionable Paleocene or Early Eocene age just above the South Mara unit, also of the same uncertain age.

DISCUSSION

Stratigraphy

The relatively large numbers of radiolarians so widespread in this one chronolithological unit in the Jeanne d'Arc Basin is unique in the area's Cenozoic history. Except for those in the South Mara unit, very few radiolarians have ever been reported from this basin, usually as occasional isolated specimens (Thomas, 1994). Undoubtedly, this near-total absence can be ascribed at least in part to the fact that the samples were not specifically prepared for radiolarians, thus probably missing most of these taxa, which are normally somewhat smaller than most foraminifera. Significantly, the radiolarian taxa under discussion here are relatively large, easily within the size range of microfossils recovered in the original foraminiferal studies. Notwithstanding, some comments can still be made about the apparent radiolarian event in the South Mara unit.

The key to the restricted stratigraphic range of these taxa probably lies in the prodeltaic nature of the South Mara unit. This unit appears to have been deposited as episodic, instantaneous events, possibly in the form of turbidites. This interpretation is supported by the unit's appearance in seismic lines, its expression on electric logs, and by its coarser sediment size, compared to overlying strata (McAlpine, 1990).

Supporting evidence comes from the foraminiferal data. In many sites, the micropaleontological record in the South Mara unit is marked not only by the appearance of the radiolarians, but by a marked diminution in the numbers and diversities of the foraminiferal assemblages, compared to overlying material. In most of the studied sites, foraminiferal assemblages in levels just above the South Mara unit are primarily agglutinated "flysch-type" similar to those reported by Gradstein and Berggren (1981). The dilution of foraminiferal assemblages in situations of very rapid sedimentation is in keeping with similar locales and Cenozoic sections on the Canadian Atlantic Margin (Thomas, in press, and unpublished data).

According to Sanfilippo et al. (1985) radiolarians are commonly only preserved in situations where burial is rapid, unless bottom and interstitial water is saturated with respect to silica. Following this line of reasoning, the South Mara unit may represent the only time during the Cenozoic that these conditions were met on a regional scale before the gradually infilling basin became too shallow to support the ecological requirements of radiolarians.

In only two sites, Nautilus C-92 and South Mara C-13, are radiolarians missing from the South Mara unit. One possible explanation is that the more distal positions of these sites from sources of the South Mara unit may have resulted in their receiving smaller pulses of sediment containing more clays (and less free silica) than wells closer to the sources. Consequently, radiolarians may not have been preserved. Depth of burial is probably not a factor since present subsea depths of the South Mara unit are the same or greater in some of the more peripherally located wells.

Paleoecology

The presence of spumellarian radiolarians in the South Mara unit reveals little about the paleoecology of the basin during the early Paleogene. Sanfilippo et al. (1985) stated that radiolarians were probably widespread in all Cenozoic ocean waters of normal marine salinity, in a wide range of latitudes, and that their irregular distribution in marine sediments is usually a function of preservation.

The foraminiferal types co-occurring with these radiolarians are largely the species one would expect to find in mid- to upper-bathyal water depths (approximately 200-1000 m) in this latitude. Species lists for Lower Eocene and Paleocene sections for each site are published in Thomas (1994).

In a study of microfossils from wells in the North Sea, Jones (1988) reported large spherical radiolarians possibly conspecific with at least some of the South Mara unit fauna in basin floor assemblages from paleodepths of 1000-1500 m.

Taxonomy

Due to the usually poor preservation of the radiolarians in the South Mara unit, definitive identifications of the various morphological types represented are not practical at the present time. Interior structures, critical for reliable diagnosis in many radiolarian species, have been completely obliterated in the fossilization process. Also, in many cases secondary silica overgrowth seems to have occurred, obscuring surface details. However, since resemblances do exist to certain species recently reported from other Paleogene North Atlantic and North Sea sediments, especially among better-preserved specimens, some tentative suggestions as to the taxonomic positions of these species can be made.

Since all forms seem to exhibit a more or less spherical or ovoid outer structure, their taxonomic positions all appear to fall within the radiolarian order Spumellaria.

Grossly, the morphotypes observed are: a) spherical to ovoid, b) lenticular, and c) spindle-shaped.

Spherical to ovoid

Many of these forms bear a resemblance to *Cenosphaera lenticularis* (Grzybowski), a species figured by Jones (1988, Pl. 2, fig. 7) and described as common in Paleocene basin floor assemblages (1000-1500 m) of the Viking Graben, North Sea. The specimens from the Jeanne d'Arc basin are somewhat smaller than Jones's illustrated example, but are otherwise similar (see Pl. 1, fig. 1 and 4). A few show evidence of a single opening or depression somewhere on the otherwise finely reticulate surface, and may represent *Diploplegma* (?) sp. aff. *D. somphum* Sanfilippo and Riedel. illustrated by Nishimura (1992, Pl. 2, fig. 6, 10; Pl. 11, fig. 10) from DSDP Site 384, some 800 km to the south of the Jeanne d'Arc Basin (see Pl. 1, fig. 3, 5, 8). A few specimens showed regular polyhedral openings and a few triangular spines, allowing a very preliminary assignment to the genus *Pseudostaurosphaera* (Pl. 1, fig. 7). A few specimens were flattened into a discoid form, but poor preservation prevented determination whether these were actual discoid species or merely diagenetically flattened spheres. (Flattening of certain foraminiferal tests was not uncommon in many samples.)

Lenticular

Some specimens exhibited a biconvex, lenticular shape, with a finely reticulate surface visible in the SEM (see Pl. 1, fig. 6, 9).

Spindle-shaped

In some sites spindle-shaped individuals were seen, usually poorly preserved. The illustrated specimen (Pl. 1, fig. 10), in anomalously good condition, closely resembles *Spongurus* (?) *irregularis* as illustrated by Nishimura (1992, pl. 2, fig. 7, 8, 9).

FUTURE WORK

Since this study constitutes the first and only published work on radiolarians from offshore eastern Canadian sites, the scope for future work in the region on this class of microfossils is virtually unlimited. Analysis of smaller grain sizes in the cuttings samples of many sites may yield more Cenozoic (and Mesozoic) radiolarian assemblages, particularly in sections characterized by accelerated rates of deposition.

Realistically, however, it is probably not scientifically or economically rewarding enough to begin such a large undertaking in an area in which good biostratigraphic zonations and databases already exist for several microfossil groups including foraminifera (e.g. Ascoli, 1976; Gradstein and Agterberg, 1982; Thomas, 1994),palynology (e.g. Barss et al., 1979; Williams et al., 1990),and nannofossils (Doeven et al., 1982).

CONCLUSIONS

The data contained in the present study suggest the following points about the Paleogene history of the Jeanne d'Arc Basin:

PLATE 1

Figure 1. ?*Cenosphaera lenticularis* (Grzybowski) from Terra Nova K-08, 1120-1130 m. Actual diameter 0.187 mm. GSC specimen number 111002.

Figure 2. Ovoid form from Terra Nova K-08, 1120-1130 m. Actual diameter 0.176 mm. GSC specimen number 111003.

Figure 3. ?*Diploplegma* (?) sp. aff. *D. somphum* Sanfilippo and Riedel from Trave E-87, 2120-2130 m. Actual diameter 0.204 mm. GSC specimen number 111004.

Figure 4. ?*Cenosphaera lenticularis* (Grzybowski) from Rankin M-36, 1075-1085 m. Actual diameter 0.225 mm. GSC specimen number 111005.

Figure 5. ?*Diploplegma* (?) sp. aff. *D. somphum* Sanfilippo and Riedel from Archer K-19, 1900-1910 m. Actual diameter 0.296 mm. GSC specimen number 111006.

Figure 6. Lenticular form from Rankin M-36, 1115-1125 m. Actual diameter 0.270 mm. GSC specimen number 111007.

Figure 7. ?Pseudostaurosphaera sp. from Terra Nova K-08, 1120-1130 m. Actual diameter 0.173 mm. GSC specimen number 111008.

Figure 8. ?*Diploplegma* (?) sp. aff. *D. somphum* Sanfilippo and Riedel from Hibernia I-46, 1400-1410 m. Actual diameter 0.262 mm. GSC specimen number 111009.

Figure 9. Lenticular form (probably same species as 6) from Archer K-19, 1870-1880 m. Actual diameter 0.279 mm. GSC specimen number 111010.

Figure 10. *Spongurus* (?) *irregularis* Nishimura from Trave E-87, 2120-2130 m. Actual length 0.238 mm. GSC specimen number 111011.

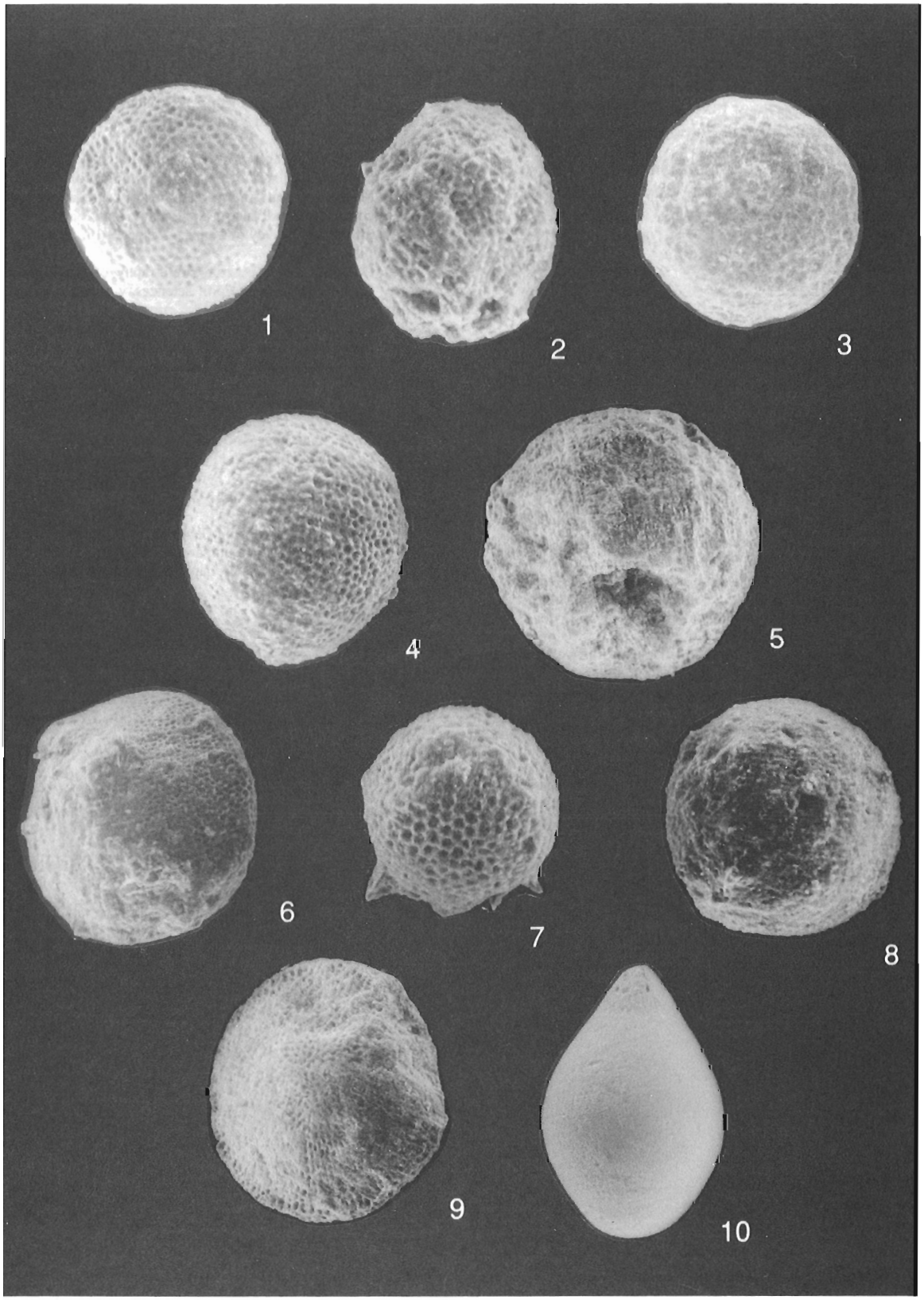
1
2
3
4
5
6
7
8
9
10

1. Based on the restricted range of preserved radiolarian species, the South Mara unit probably represents the single most rapid period of deposition in the basin during the Paleogene.
2. At least five different species of spumellarian radiolarians are probably present in the South Mara unit, and are comparable to some coeval taxa from DSDP Site 384 to the south, and possibly some Paleocene North Sea sites.
3. Future discoveries of these or similar taxa in other stratigraphic levels in the region may signal heightened depositional rates for these intervals.

ACKNOWLEDGMENTS

Many thanks to K.D. McAlpine and M.A. Williamson (GSC, Atlantic) for critical review of the manuscript. Also thanks to N. Koziel (GSC, Atlantic) for wordprocessing and R. Coulstring who drafted the figures.

REFERENCES

Ascoli, P.
1976: Foraminiferal and ostracod biostratigraphy of the Mesozoic-Cenozoic, Scotian Shelf, Atlantic Canada; in Proceedings of the 1st International Symposium on Benthonic Foraminifera of Continental Margins, Part B: Paleoecology and Biostratigraphy; Maritime Sediments Special Publication 1, p. 653-771.

Barss, M.S., Bujak, J.P., and Williams, G.L.
1979: Palynological zonation and correlation of sixty-seven wells, eastern Canada; Geological Survey of Canada, Paper 78-24, 118 p.

Doeven, P.H., Gradstein, F.M., Jackson, A., Agterberg, F.P., and Nel, L.D.
1982: A quantitative nannofossil range chart; Micropaleontology, v. 28, no. 1, p. 85-92.

Gradstein, F.M. and Agterberg, F.P.
1982: Models of Cenozoic foraminiferal stratigraphy, Northwestern Atlantic Margin; in Quantitative Stratigraphic Correlation, (ed.) J.M. Cubitt and R.A. Reyment; John Wiley & Sons Ltd., Chichester, U.K., p. 119-172.

Gradstein, F.M. and Berggren, W.A.
1981: Flysch-type agglutinated foraminifera and the Maestrichtian to Paleogene history of the Labrador and North Seas; Marine Micropaleontology, v. 6, p. 211-268.

Grant, A.C. and McAlpine, K.D.
1990: The continental margin around Newfoundland. Chapter 6 in Geology of the Continental Margin of Eastern Canada, (ed.) M.J. Keen and G.L. Williams; Geological Survey of Canada, Geology of Canada, no. 2, p. 239-292.

Jones, G.D.
1988: A paleoecological model of Late Paleocene "flysch-type" agglutinated foraminifera using the paleoslope transect approach, Viking Graben, North Sea; Abhandlungen der Geologisches Bundes-Andestalt Vienna, v. 41, p. 143-153.

McAlpine, K.D.
1989: Lithostratigraphy of fifty-nine wells, Jeanne d'Arc Basin; Geological Survey of Canada, Open File 2201, 97 p.
1990: Mesozoic stratigraphy, sedimentary evolution, and petroleum potential of the Jeanne d'Arc Basin, Grand Banks of Newfoundland; Geological Survey of Canada, Paper 89-17, 50 p.

McIver, N.L.
1972: Cenozoic and Mesozoic stratigraphy of the Nova Scotia shelf; Canadian Journal of Earth Sciences, v. 9, no. 1, p. 54-70.

Nishimura, A.
1992: Paleocene radiolarian biostratigraphy in the northwest Atlantic at Site 384, Leg 43, of the Deep Sea Drilling Project; Micropaleontology, v. 38, no. 4, p. 317-362.

Palmer, A.R.
1983: The Decade of North American Geology, 1983 geologic time scale; Geology, v. 11, p. 503-504.

Sanfilippo, A., Westberg-Smith, M.J., and Riedel, W.R.
1985: Cenozoic radiolaria; in Plankton Stratigraphy, (ed.) H.M. Bolli, J.B. Saunders, and K. Perch-Neilsen; Cambridge University Press, Cambridge, U.K., p. 631-712.

Sinclair, I.K.
1988: Evolution of Mesozoic-Cenozoic sedimentary basins in the Grand Banks area of Newfoundland and comparison with Falvey's (1974) rift model; Bulletin of Canadian Petroleum Geology, v. 36, no. 3, p. 255-273.

Thomas, F.C.
1994: Preliminary Cenozoic micropaleontological biostratigraphy of 16 wells, Jeanne d'Arc Basin, Grand Banks of Newfoundland; Geological Survey of Canada, Open File 2799, 53 p.
in press: Cenozoic micropaleontological stratigraphy of LASMO/NSRL Cohasset Producer CP1 P-51, Scotian Shelf; Atlantic Geology.

Williams, G.L., Ascoli, P., Barss, M.S., Bujak, J.P., Davies, E.H., Fensome, R.A., and Williamson, M.A.
1990: Biostratigraphy and related studies, Chapter 3 in Geology of the Continental Margin of Eastern Canada, (ed.) M.J. Keen and G.L. Williams; Geological Survey of Canada, Geology of Canada, no. 2, p. 87-137.

Geological Survey of Canada Projects 710065, 850055, 920058

Stratigraphy of the Central Maritimes Basin, eastern Canada: non-marine sequence stratigraphy

T.A. Rehill[1], M.R. Gibling[1], and M.A. Williamson
GSC Atlantic, Dartmouth

Rehill, T.A., Gibling, M.R., and Williamson, M.A., 1995: Stratigraphy of the Central Maritimes Basin, eastern Canada: non-marine sequence stratigraphy; in Current Research 1995-E; Geological Survey of Canada, p. 221-231.

Abstract: The Maritimes Basin of Atlantic Canada covers an area of 210 000 km^2. However, with more than 70% of the basin lying offshore, relatively little is known about its regional stratigraphic history. Offshore studies of the Upper Viséan to Lower Permian strata have identified the presence of five major depositional cycles of second order duration. The cycles are bounded by regionally identifiable, conformable to unconformable sequence boundaries. Each cycle consists of a basal coarse grained facies with an overlying finer grained facies. The basal facies are interpreted to be forestepping systems tracts, developed in response to increased sedimentation rates and decreased accommodation space. This caused braidplain fan deltas to prograde basinward. Backstepping systems tracts overlie both the basal unit and a transgressive surface. These tracts developed in response to decreasing sediment supply and increasing accommodation space. This resulted in a relative rise of base level, allowing finer grained sedimentation on the basin flanks.

Résumé : Le Bassin des Maritimes dans l'Atlantique au large du Canada s'étend sur une superficie de 210 000 km^2. Cependant, comme plus de 70 % du bassin est situé au large des côtes, on connaît relativement peu son histoire stratigraphique régionale. L'étude des couches du Viséen supérieur au Permien inférieur reposant au large a permis de relever cinq cycles de sédimentation importants de durée de second ordre. Les cycles sont limités par des limites de séquences concordantes à discordantes identifiables à l'échelle régionale. Chaque cycle est composé d'un faciès basal à grain grossier sur lequel repose un faciès à grain plus fin. Le faciès basal est interpreté comme un couloir de systèmes transgressifs, formés par un accroissement des vitesses de sédimentation et une diminution de l'espace disponible, causant la progradation vers le bassin des cônes de déjection de plaine anastomosée. Les couloirs des systèmes régressifs surmontent à la fois l'unité basale et une surface de transgression. Ces couloirs se sont formés en réaction à une diminution de l'apport sédimentaire et à une augmentation de l'espace disponible. Une hausse relative du niveau de base a suivi, favorisant une sédimentation à grain plus fin sur les flancs du bassin.

[1] Department of Earth Sciences, Dalhousie University, Halifax, Nova Scotia B3H 3J5

INTRODUCTION

Since the mid 1800s, geologists have studied eastern Canadian upper Paleozoic continental strata (Fig. 1). The strata, Late Devonian to Permian in age (Hacquebard, 1986), outcrop throughout northern Nova Scotia, southeastern and central New Brunswick, Prince Edward Island, southwestern Newfoundland, southeastern Gaspésie, and the Îles de la Madeleine. Offshore, in the Central Maritimes Basin (CMB) (Fig. 1), the strata underlie the southern Gulf of St. Lawrence and near the depocentre reach thicknesses of more that 12 km.

Over the last few decades, multiple depocentres have been recognized as sub-basins of a larger, regional Maritimes Basin (Fig. 2) (Williams, 1973). It has been suggested that during the Carboniferous the Maritimes Basin was composed of a complex series of interconnected sub-basins and platforms (Howie and Barss, 1975). However, although the Maritimes Basin is one of the largest preserved Late Paleozoic basins in North America, it is only an erosional remnant of a much larger basin that originated after the Acadian Orogeny (Gibling et al., 1992). Recent studies suggest that 1-4 km of strata have been removed since the Early Permian (Ryan and Zentilli, 1993)

The mapping of a thick upper Carboniferous coal-bearing package underlying much of the Gulf of St. Lawrence (Grant and Moir, 1992) provoked a new look at the resource potential of the offshore. Recent studies suggest that these coal measures have the potential to source hydrocarbons (Mossman, 1992). Traditionally, the depositional setting of most of the Central Maritimes Basin strata was thought to be fluvio-lacustrine (Howie and Barss, 1975). However, studies of agglutinated foraminifera now indicate that sections of the Coal Measures were deposited in marine influenced environments, enhancing the possibility of sourcing hydrocarbons from Type II and III kerogens (Wightman et al, 1994). The detection of marine foraminifera within the Coal Measures also supports recent suggestions of cyclothemic deposition in the Maritimes Basin (Grant, 1994).

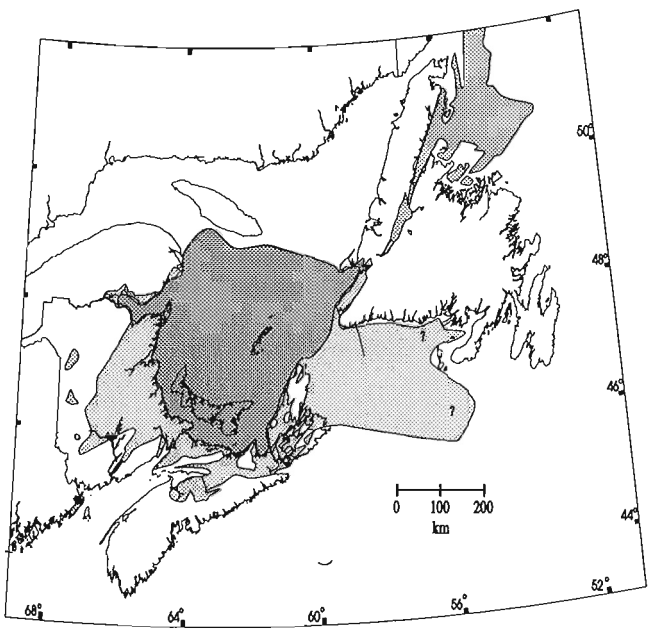

Figure 1. Map showing the distribution of upper Paleozoic strata location of the Maritimes Basin (shaded areas). The darker grey area is the Central Maritimes Basin (CMB).

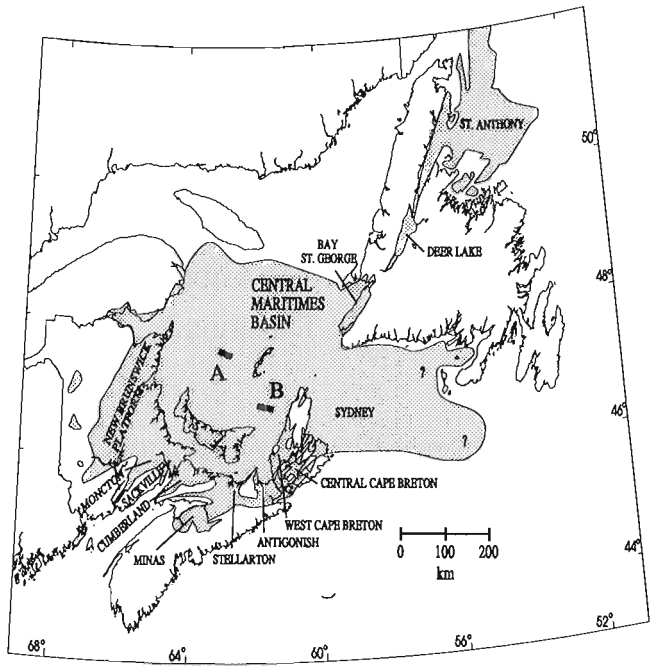

Figure 2. Map showing the distribution of sub-basins and platform areas which make up the composite Maritimes Basin. Seismic line locations are shown (A and B): see Figure 6.

The problem?

The Maritimes Basin of Atlantic Canada (Fig. 1) (Williams, 1973) covers approximately 210 000 km^2. With more than two thirds of the basin lying beneath the Gulf of St. Lawrence and Laurentian Channel, relatively little is known about regional stratigraphy, tectono-stratigraphic history, and hydrocarbon potential.

It is not surprising that with such a large composite, predominantly offshore basin, a complex stratigraphic nomenclature and tectonic history has evolved. Due to the offshore nature of the basin, geological studies of Carboniferous basin fill have tended to focus on the onshore. Over the last century, the stratigraphy and sedimentology of onshore strata have been well documented (Belt, 1964, 1965; Kelly, 1967; Ryan et al., 1991). In general, these studies have dealt with the tectonics and stratigraphy of each subbasin. The results of such studies were then applied to the regional basin framework. As a result, a unique stratigraphic nomenclature has become associated with each sub-basin, and although quite effective at the local scale, they typically cannot be applied and correlated basin wide.

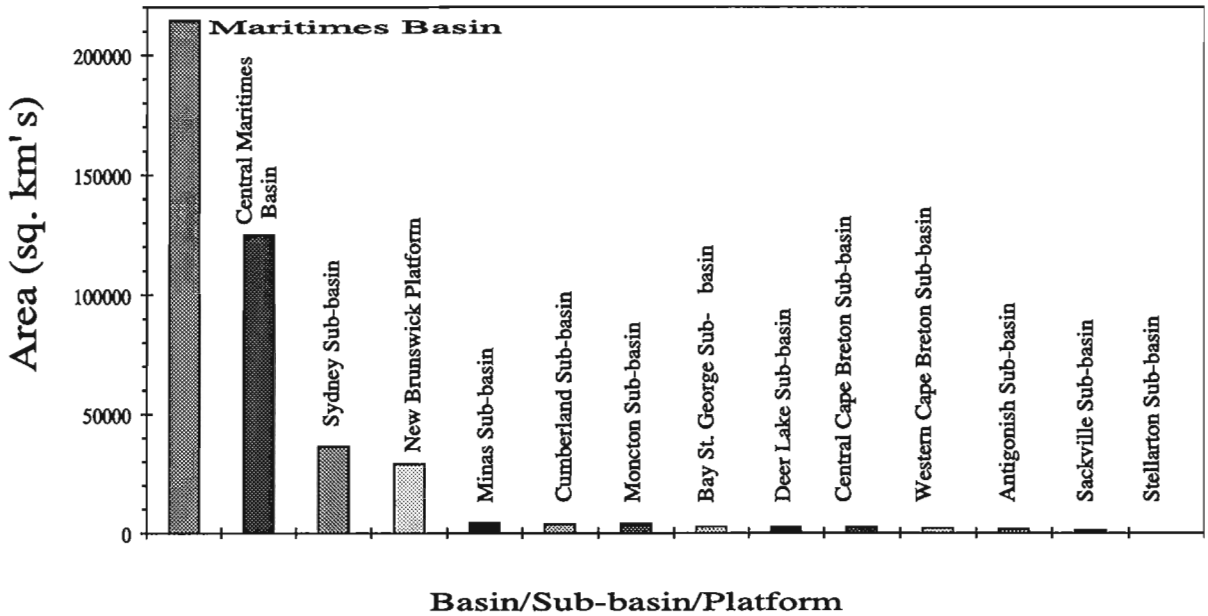

Figure 3. Plot of basin, sub-basin, and platform areas. The indicated sub-basins and platforms correspond to Figure 2.

Not only do these sub-basins and platform areas represent a very small portion of the total Maritimes Basin area (Fig. 3), the onshore record is further complicated by a complex history of local tectonic activity, that on the scale of the basin as a whole may in fact simply represent noise on the true basin fill record. The important question is whether the Maritimes Basin onshore exposures are representative of what underlies the Gulf of St. Lawrence. Until recently, any detailed stratigraphy of the offshore portion of the Maritimes Basin was restricted to areas of interest to the petroleum industry and published primarily in company well history reports. Ryan et al. (1991) and Hacquebard (1986) tied onshore Maritimes Basin stratigraphy to the offshore basin fill using changes in lithological colour and coal spores, respectively.

An offshore Central Maritimes Basin database has been compiled to assist in advancing our understanding of the geological framework of the Maritimes Basin region. This study includes: 1) reconnaissance surveys of Cape Breton Island, Prince Edward Island, Newfoundland, and northern Nova Scotia exposures; 2) the linking of stratal units and isolated wells by seismic data; and 3) analysis of well logs for lithology, correlation and sedimentologic trends. Our objective is to develop a regional Central Maritimes Basin stratigraphic framework to underpin our efforts to understand the stratigraphic and sedimentological history of the Maritimes Basin region.

METHODS OF STUDY

Geological data

The primary data sets for most offshore basin studies are geophysical wireline logs and seismic data. The presence of oil seeps in coeval onshore strata, sourced from the lower

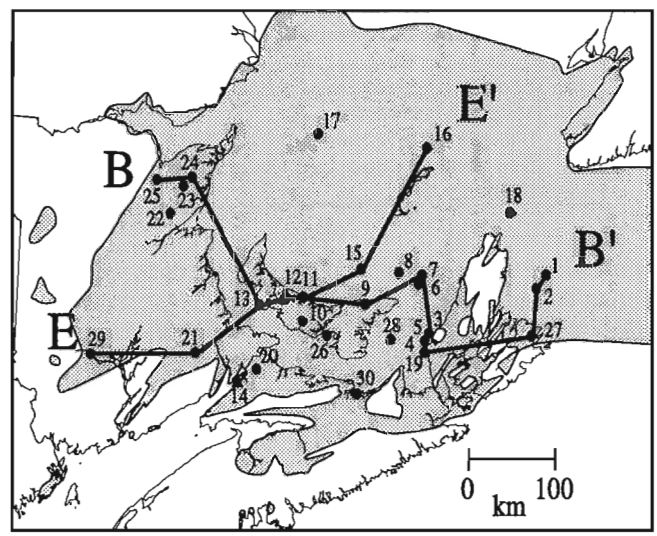

Figure 4. Map showing the location of study wells, coastal sections, and geological cross-sections: see Figure 5 and Table 1.

Carboniferous Horton Group, led to the drilling of 20 deep exploration wells in the Central Maritimes Basin. Most of the wells had gas shows, but all were classified dry and abandoned, except the East Point E-49 gas discovery. These 20 wells, along with 8 onshore wells and 2 coastal sections, were chosen for this study (Table 1). The two key prerequisites for well selection were that wireline logs had to be available and the well must have penetrated Late Carboniferous basin fill.

Geological cross-sections were constructed both across and parallel to the southwest-northeast orientated basin axis (Fig. 4, 5). Correlations were made between wells using

Table 1. List of wells and coastal sections providing subsurface data on Maritimes Basin fill: see Figures 4 and 5. In addition to geophysical well logs, types of supporting data for each well are indicated. Brackets indicate poor data, multiple "X's" indicate multiple data sets.

Well #	Well Name	Spud Date	Micropaleontological	Rockeval Data	SOQUIP Mineralogy	Foraminifera Data
1	Murphy et al. North Sydney P-05	10-Aug-74	XX		X	
2	Shell et al. North Sydney F-24	09-Jun-75	XX	X		
3	Mabou Coastal Section					
4	NSDME Borehole M-1	1978	X			
5	NSDME Borehole M-2A	1978	X			
6	Hudson's Bay et al. East Point E-47	09-Jun-80	X			
7	Hudson's Bay-Fina East Point E-49	26-Jun-70	XX		X	X
8	Hudson's Bay et al. Beaton Point F-70	01-Aug-80	XX	X		
9	Soquip et al. Naufrage No.1	29-Aug-75	XX	X	X	
10	Soquip et al. Tyrone No.1	26-Feb-75	XX		X	
11	Hudson's Bay-Fina Green Gables No.1	04-Jun-72	XX		X	
12	Hudson's Bay-Fina Irishtown No.1	24-Jan-72	XX		X	
13	Imperial Wellington Station No.1	03-Mar-58	X			
14	Cumberland Coastal Section	23-Sep-93	(X)			
15	Irving-Chevron-Texaco Cable Head E-95	26-Jun-83	XX	X		X
16	Sarep H.Q. Brion Island No.1	18-Sep-70	XX		X	X
17	Shell-Soquip-Amoco Bradelle L-49	07-Sep-73	XXXX	X	X	X
18	Petro-Canada et al. St. Paul P-91	02-Sep-83	(X)	X		
19	NSDME PH-3	1975	X			
20	Gulf et al. Hastings No.1	11-Jun-75	X	X		
21	Irving Chevron et al. Middlesex #1	24-Aug-82	(X)			
22	Hudson's Bay Bartibog No.1	06-Aug-67				
23	Hudson's Bay St. Isidore No.1	29-Jun-67				
24	Hudson's Bay St. Isidore No.2	29-Aug-67				
25	Hudson's Bay Blanchard No.1	16-Jul-67	(X)			
26	Island Development Company Hillsborough No.	11-Oct-43	(X)X			
27	Murphy et al. Birch Grove No.1	02-Feb-68	X			
28	Hudson's Bay et al. Northumberland Strait F-25	07-Apr-70	X		(X)	
29	Seru Nucleaire Canada Ltee. Fredericton 2	26-Apr-79	(X)			
30	NSDME P-58	11-Jun-86	X			

wireline log signature data, tied to seismic data, while honouring the supporting data identified in Table 1. In addition, where possible, the offshore wells were correlated to representative onshore sections surrounding the Central Maritimes Basin.

Seismic data

The seismic database in the Maritimes Basin is extensive. Over the last 30 years, 80 000 line-km of industry seismic data and several government lithoprobe and high resolution seismic surveys have been shot over much of the Central Maritimes Basin. All of the data are available to the general public.

Twenty-eight lines were chosen from the larger data set to complement the offshore well data set. These lines were investigated to determine the seismic character of the overall basin fill and more importantly, to tie the study wells to basin fill farther away from the well bore locations.

The lines were chosen specifically to get a regional view of basin fill across dip and strike, similar to the geological cross sections. Each line was examined for characteristic seismic reflector patterns (seismic facies) of the basin fill and when possible was tied to well bore data using synthetic seismograms.

RESULTS

Cross-sections

Six cross-sections were constructed; three across the basin axis and two parallel to the basin axis. Representative of both strike sections, section E-E' (Fig. 5) originates onshore on the New Brunswick Platform and extends 517 km towards the basin depocentre. The most obvious feature of this section is the areal extent of the subsurface units. Individual units (as described here, all units should be considered as informally named) and the surfaces which bound them are correlatable over large distances. On the New Brunswick Platform, the units are generally flat-lying and can be traced considerable distances with minor changes in thickness. However, once into the Central Maritimes Basin, the thickness of the units increases rapidly over a short distance. Through these changes, the units and bounding surfaces are still correlatable over tens to hundreds of kilometres. Close to the basin axis, and closest to the depocentre, units 3A and 3B appear in well #15. Unit 2A, in several locations, primarily near the onshore/offshore transition zone, eroded into units 1A and 1B. Unit 4A erodes into unit 2B on the basin flanks and on the New Brunswick Platform.

The B-B' section (Fig. 5) is a 737 km long cross-section that was constructed to show the geometries of stratal packages across the basin axis from onshore the New Brunswick

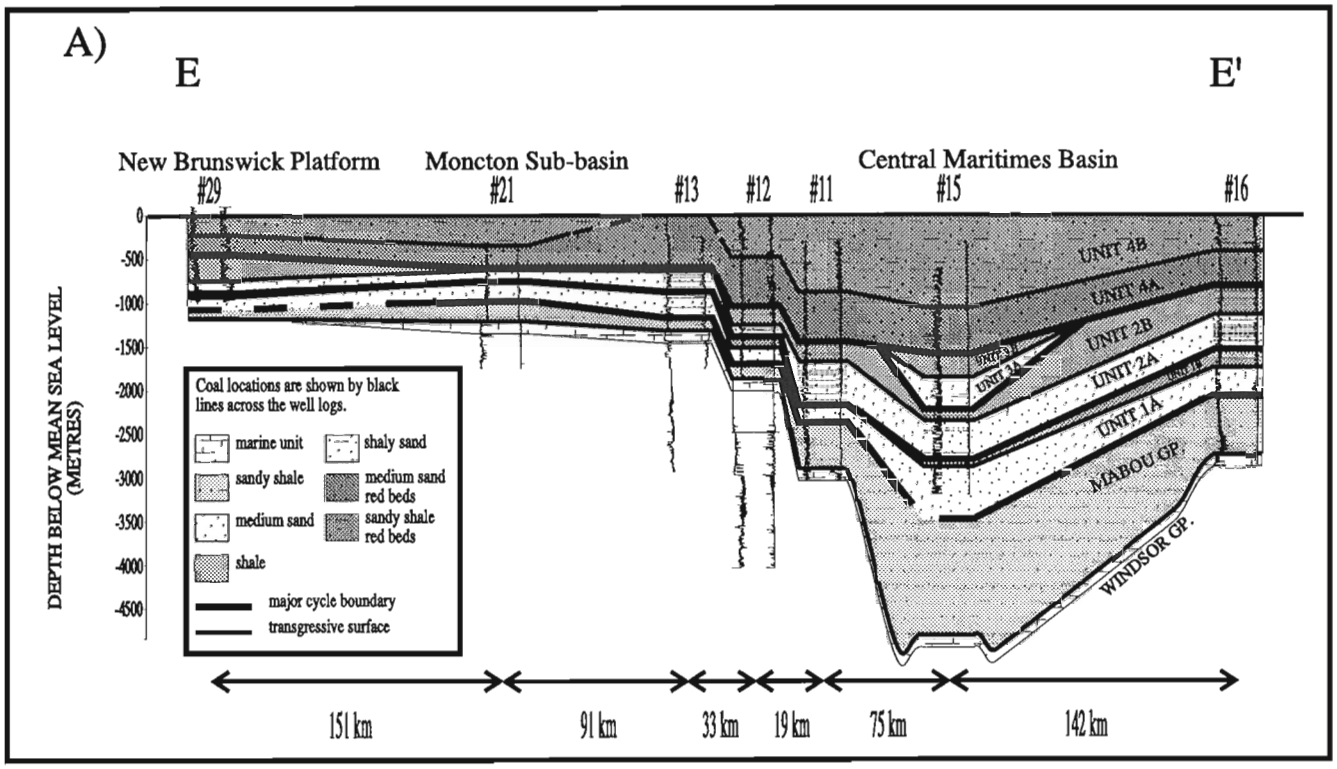

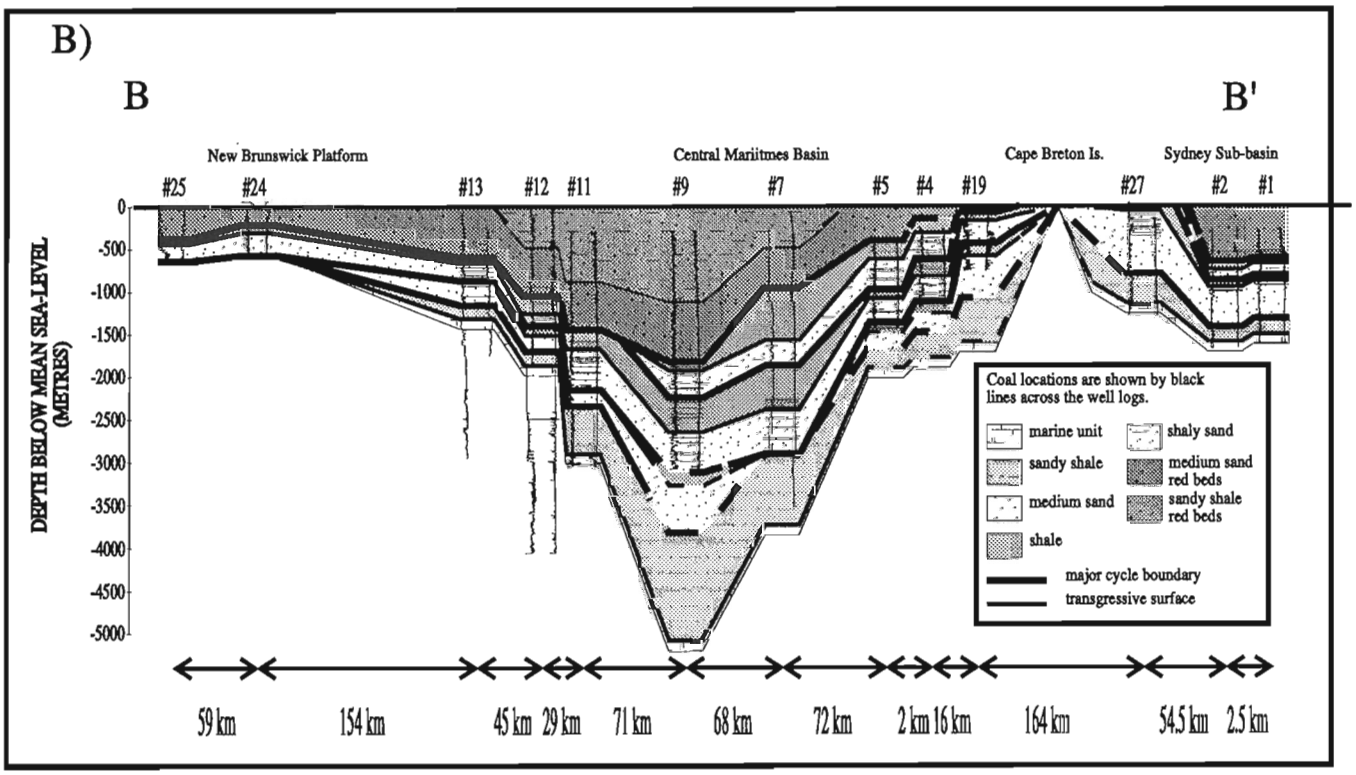

Figure 5. *Geological cross-sections across the Maritimes Basin (locations shown in Fig. 4).* ***A)*** *Cross-section EE' which parallels the northeast orientated basin axis.* ***B)*** *Cross-section BB' which lies perpendicular to the main basin axis (units of EE' are same for section BB').*

Table 2. List of seismic units and their characteristics identified in the Central Maritimes Basin (CMB) fill. The underlined units are aerially restricted to the basin depocentre and along the basin axis. These units are shown in Figure 6B, as unit 3A and unit 3B. The units are shown in descending order.

Seismic Unit	Character	Comments
Top high energy package	chaotic to weakly stratified high amplitude reflections	Located high in the section, seismic multiples often interfere with a full interpretation, however progradational reflections may be present. The underlying contact with either the second or third low energy zones is sharp to gradational.
Third "dead zone"	low energy, reflections may be chaotic to weakly stratified	This facies unit is restricted to the southern portion of the CMB.
East Point Wedge	high amplitude, acoustically well stratified reflections, similar to the Coal Measures facies	This facies unit is restricted to the southern portion of the CMB, near the depocentre, along the basin axis. The facies wedges out into chaotic to weakly stratified reflections towards the basin flanks. It overlies the second low energy zone below sharply to gradationally.
Second "dead zone"	low energy, reflections may be chaotic to weakly stratified	The weak/chaotic reflections are found in discrete groups in what appear to be specific zones on the seismic lines.
Coal Measures package	high amplitude, acoustically well stratified reflections	The package shows clear evidence of reflection progadation and shingling, the contact with upper and lower zones is sharp to gradational.
First "dead zone"	low energy, reflections may be chaotic to weakly stratified	
Top Windsor Group	strong, high amplitude reflection	Easily identified at the base of the section due to the high density contrast with overlying strata.

Platform, through the Central Maritimes Basin, over Cape Breton Island and into the Sydney sub-basin. Again the most obvious feature is the large areal extent of the basin fill units and bounding surfaces. Towards the basin axis (between wells #9 and #7), all unit thicknesses increase and units 3A and 3B appear. This cross section shows that the distribution of units 3A and 3B seems to be restricted to the southeastern portion of the Central Maritimes Basin and the Sydney sub-basin. units 1A and 1B have been completely removed by erosion in well #7 and in the Sydney sub-basin.

Seismic analysis

In general, the Central Maritimes Basin fill has a characteristic "cyclic" signature which is shown on almost all of the lines examined (Table 2) (Fig. 6). The most prominent reflections tend to be associated with the top of the Windsor Group, found at the base of the section and the "Coal Measures" facies mapped by Grant and Moir (1992). Low energy seismic zones are found both above and below the Coal Measures package. Contacts between the units are sharp to gradational. At the top of the section, another high amplitude reflection package has been identified. It has a sharp to gradational contact with the underlying seismic packages.

An additional facies was interpreted (Table 2) on several lines closer to the basin depocentre, along the main basin axis. This facies is similar in character to the Coal Measures facies but lies above the second low energy zone. The facies is composed of high amplitude, well-stratified reflections. This facies wedges out into more weakly stratified to chaotic reflections away from the basin axis. Lying above this unit but below the high amplitude reflection zone at the top of the section, is a third zone of low energy reflections. This zone is much like the previous two "dead zones" and periodically has weakly stratified to chaotic reflections.

In support of the seismic facies interpretation, sonic and density logs from wells #7, #15, #8 and #17 were used to construct synthetic seismograms, which linked well facies to seismic facies (Fig. 6). Dominantly coarse clastic packages (units 1A, 2A, 3A, and 4A) correspond to the units that were composed of high amplitude, well stratified reflections. The low energy, "dead zones" correspond to the dominantly shale units identified on the cross sections (Mabou, units 2B, 3B and 4B).

STRATIGRAPHIC FRAMEWORK

The geological cross-sections, supported by independent geological evidence and tied to the seismic database, allow the development of a representative Central Maritimes Basin stratigraphic column (Fig. 7). The units are described below.

Central Maritimes Basin Mabou Group equivalent?

Age: Late Viséan/Early Namurian to Early Westphalian

Distribution: Found throughout the offshore area, pinches out toward the New Brunswick Platform.

Description: Composed of interbedded sandstones, siltstones, and shales with thin limestones and marlstones. The sandstones are light grey to buff, very fine grained to fine grained, subangular and well to medium sorted. The sand units tend to increase in grain size and bed thickness upsection. The sandstones are cemented by a mixture of silica and calcite. The shales are red to grey to green, silty, micaceous and redden upsection. The thin limestones are light brown, silty, slightly dolomitic and grade into marlstones. Thin stringers and traces of coal increase in abundance towards the top of the section. The unit has an overall sand/shale ratio of 1.13.

Bounding surfaces: The unit conformably to unconformably overlies the Windsor Group. It also occasionally unconformably overlies the Acadian basement. It conformably to unconformably underlies unit 1A and unit 2A.

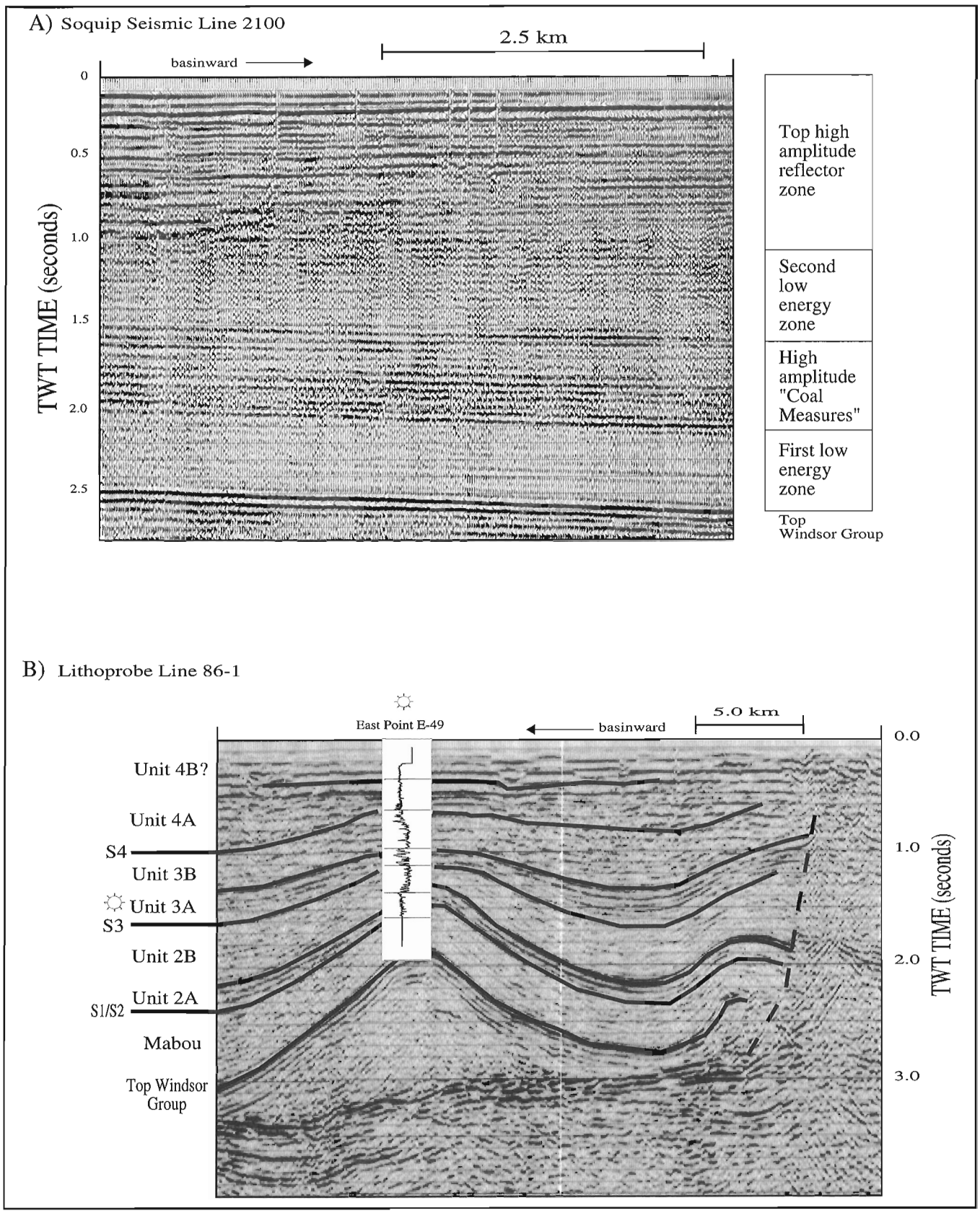

Figure 6. *Seismic records representative of the Maritimes Basin fill (locations shown in Fig. 2)* ***A)*** *Record showing cyclic nature of basin fill and the seismic facies identified.* ***B)*** *Well data unit top picks tied to the seismic data set.*

Seismic facies: The Mabou Group is associated with the first low energy reflector zone. It periodically has chaotic to weakly stratified reflector packages.

Onshore equivalent: Mabou Group ?

Unit 1A

Age: Early Westphalian A to Early Westphalian B

Distribution: The unit is widely distributed around the flanks of the Central Maritimes Basin. It generally is thicker around the southern rim of the Central Maritimes Basin. The unit is absent closer towards the depocentre, along the basin axis, and in the offshore Sydney sub-basin.

Description: Dominantly sandstones with grain size and bed thickness increasing upwards. The sandstones are light grey to light green to light red, medium grained to coarse grained, subangular and poor to medium sorted. Quartz pebbles are common throughout the section. Cements are dominantly silica in nature. The overall feldspar content of the unit decreases upsection. Shales in the unit tend to be grey-green-red, silty, micaceous and "grey" upwards. Thin stringers and traces of coal can be found towards the top of the section. The unit has a sand/shale ratio of 2.75.

Bounding surfaces: Unconformably to conformably overlies the Mabou Group, conformably overlain by unit 1B, unconformably overlain by unit 2A.

Seismic facies: The unit is represented by high amplitude reflectors that may weaken towards the base. This unit is the basal portion of the "Coal Measures" identified by Grant and Moir (1992). The reflectors commonly show a progradational or shingled geometry.

Onshore Equivalents: Enrage Formation/claremont Formation/ Boss Point Formation?

Unit 1B

Age: Early Westphalian B to Late Westphalian B – Early Westphalian C

Distribution: The unit is widely distributed around the flanks of the Central Maritimes Basin. It is absent near the depocentre, along the basin axis, and in the Sydney sub-basin.

Description: Dominantly composed of shales that are grey-green-dark brown/red, micaceous, waxy and silty. They also contain siltstone stringers and grey upwards. The thin sandstones found in this unit are very fine grained to fine grained, subangular, silty, silica cemented, argillaceous and medium to well sorted. The sands become more dolomitic towards the top of the section. Thin coal stringers and traces are found at the top and bottom of the section. Thin, white to light brown, argillaceous, silty limestones occur near the base of the section. The unit has a sand/shale ratio of 0.50.

Bounding surfaces: It lies conformably over unit 1A and conformably to unconformably underlies unit 2A.

Seismic facies: This unit is not distinguishable due to the dominant "Coal Measures Facies" Grant and Moir (1992).

Onshore Equivalent: ?

Unit 2A

Age: Late Westphalian B – Early Westphalian C to Early Westphalian D

Distribution: Widely distributed across the entire study area.

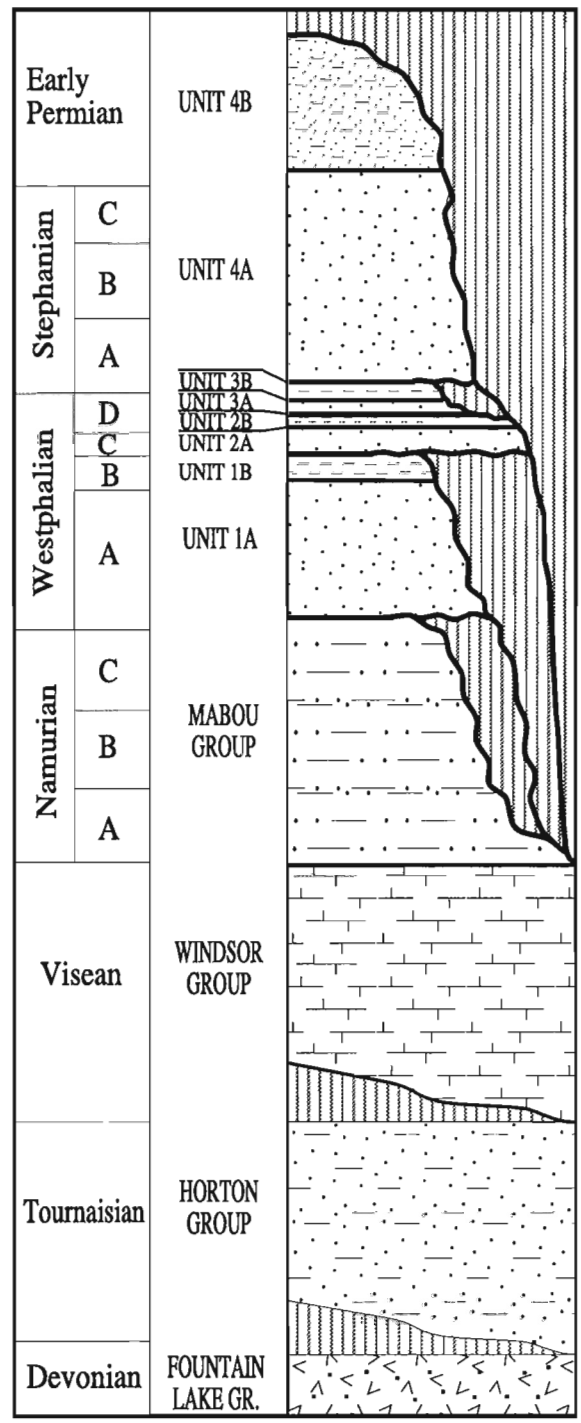

Figure 7. *Stratigraphic column for the Central Maritimes Basin: see Figure 5 for unit lithologies.*

Description: It is composed of dominant sandstones with minor interbeds of shales and coals. The sandstones are light green to light brown, fine grained to medium grained, subangular, siliceous, and medium sorted. Quartz pebbles are commonly found at the base of the section. The sandstones tend to increase in grain size and decrease in bed thickness upsection. Glauconite, kaolinite, and feldspar content increases upsection as does the shale content. The shales are dark green to grey to red, silty, micaceous and redden upwards. Beds, thin stringers, and traces of coal increase towards the top of the section. The sand/shale ratio is 2.93.

Bounding surfaces: The unit unconformably to conformably overlies unit 1B, unconformably overlies unit 1A, Mabou Group equivalent strata and occasionally basement. It is overlain conformably by unit 2B.

Seismic facies: This is the top section of the "Coal Measures Facies" mapped by Grant and Moir (1992). It is composed of high amplitude reflectors which are well stratified. The reflector packages periodically have progradational and shingled geometries.

Onshore equivalents: Malagash Formation/Inverness Formation/South Bar Formation/Salisbury Formation ?

Unit 2B

Age: Early Westphalian D to Mid Westphalian D

Distribution: As with unit 2A, unit 2B is widely distributed through the study area.

Description: Dominantly shale. The shales are interbedded with minor sandstone and coal beds. Limestones are occasionally found at the base of the section. The shales are grey to red, micaceous, silty, waxy, slightly dolomitic and contain stringers of siltstone, coal and limestone. The unit shales upwards. The sandstones are light brown to grey to light red, very fine grained to fine grained, subangular, argillaceous, medium to well sorted, and have a mixture of calcitic and silica cements. The coal beds, stringers, and traces are generally found at the base of the section. The thin beds and stringers of limestone are brown, argillaceous and silty. The unit has a sand/shale ratio of 0.41.

Bounding surfaces: The package conformably overlies unit 2A and conformably to unconformably underlies unit 3A, unit 3B, and unit 4A.

Seismic facies: This unit is the second low energy reflector zone. Periodically the unit has weakly stratified to chaotic reflectors.

Onshore equivalent: ?

Unit 3A

Age: Late Westphalian D to Late Westphalian D

Distribution: This unit is restricted to the southeastern portion of the Maritimes Basin, close to the basin axis and depocentre.

Description: The unit is composed of dominant sandstones basinward but becomes shalier towards the basin flanks. The unit contains minor coal and limestone beds. The sandstones are light green to grey to pink, fine grained to medium grained, subangular, siliceous, argillaceous, and medium to well sorted. The unit occasionally contains quartz pebbles. Feldspar content is up to 40% at base of the section and decreases upwards. Calcite cementation increases upsection. Shales are green to grey to red, silty, micaceous, dolomitic and contain stringers of coal and siltstone. The shales redden upwards. The thin beds and stringers of coal are found throughout the section. Limestones tend to be thin beds and stringers, light brown, argillaceous and silty. They are found generally at the base and middle of the section. The sand/shale ratio of unit 3A is 1.10.

Bounding surfaces: Unit 3A unconformably to conformably overlies unit 2B and is conformably overlain by unit 3B.

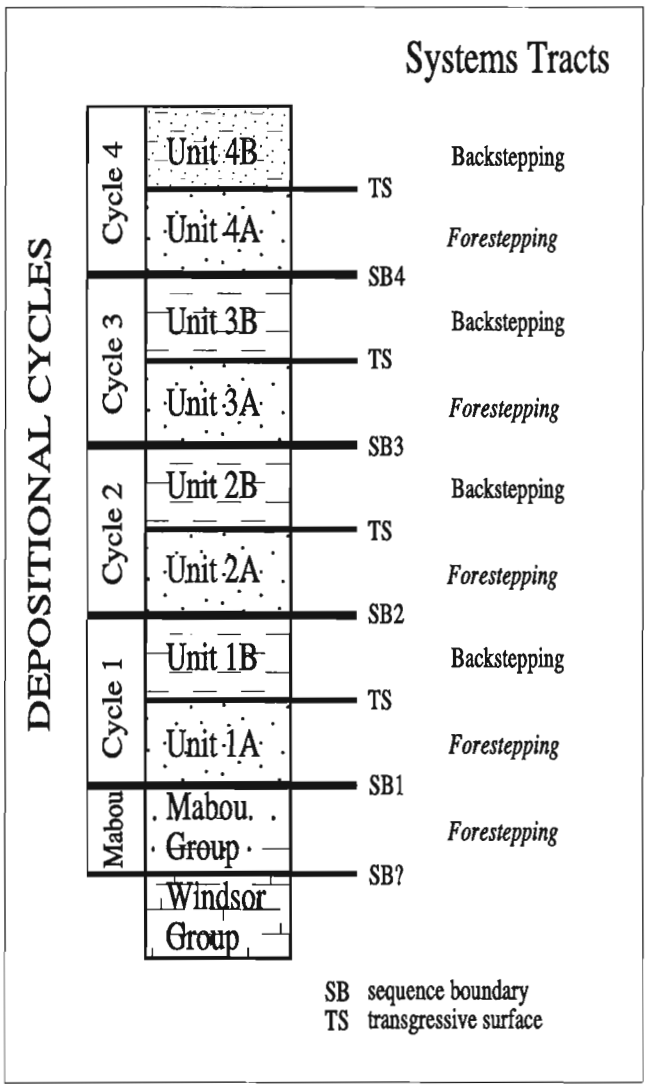

Figure 8. Sequence stratigraphic framework for the late Paleozoic Central Maritimes Basin fill: see Figure 5 for unit lithologies.

Seismic facies: This unit has high amplitude, well stratified reflectors basinward but they wedge out into weaker stratified/chaotic units.

Onshore equivalent: none ?

Unit 3B

Age: Late Westphalian D to Early Stephanian

Distribution: Like unit 3A, this unit is restricted to the southeastern portion of the Central Maritimes Basin.

Description: Dominantly shales with interbedded sandstones and thin limestone beds. Thin bed, stringers, and traces of coal are periodically found at the base of the section. The shales are red to green to grey, silty, calcareous, micaceous and contain siltstone, coal, limestone stringers. The sandstones are light grey to light pink, fine grained to medium grained, subangular, silty, calcite cemented, argillaceous, and medium to well sorted. Thin beds and stringers of limestone are grey to light brown, argillaceous, fossiliferous, and found at the base of the section. Unit 3B has a sand/shale ratio of 0.66.

Bounding surfaces: This unit conformably overlies unit 3A and conformably to unconformably underlies unit 4A.

Seismic facies: The unit is represented by the third low energy reflector zone. Like the other two low energy zones, this unit occasionally has weakly stratified to chaotic reflectors.

Onshore equivalent: none ?

Unit 4A

Age: Early Stephanian to Early Permian

Distribution: The unit is widely distributed throughout the basin.

Description: It is composed of dominant sandstones with interbedded shales and traces of coal. The sandstones are dark red to red to light brown, fine grained to medium grained, subangular grading to subrounded upwards, medium grading to well sorted upwards, and argillaceous. The sands coarsen upwards and there are occasional rusty brown quartz pebbles at the top of the section. Feldspar seems to be absent from this unit but there is an increase upwards in glauconite and kaolinite. The entire unit is dominantly calcite cemented and there are traces of fracture porosity. The shales are dark red to red grey, silty, micaceous, mottles and redden upwards. They contain abundant plant fragments and have thin siltstone and limestone stringers. The thin beds, stringers and traces of coal are found throughout the section. The units has a sand/shale ratio of 2.25.

Bounding surfaces: Unit 4A unconformably to conformably overlies units 2B and 3B. It is overlain conformably by unit 4B.

Seismic facies: This unit consists of high amplitude, chaotic to weakly stratified reflectors. The facies is commonly masked by surface noise and multiples of seismic energy.

Onshore equivalents: Balfron Formation/"Unnamed Redbeds"/ Tormentine Formation ?

Unit 4B

Age: Early Permian to Late Early Permian

Distribution: The unit is widely distributed throughout the entire Central Maritimes Basin.

Description: The unit is dominantly sandstone with interbedded shales and occasional limestones. The sandstones are red brown to light green, fine grained to medium grained, subangular grading upwards to subround, medium grading upwards to well sorted, and contain some quartz pebbles. The sands tend to increase in grain size and bed thickness upsection. There is an increase in chert, glauconite, and kaolinite upwards. The sandstones are cemented with calcite. The shales are red brown to light brown, silty, micaceous, and contain both limestone and siltstone stringers. The limestones are red, argillaceous, dolomitic, silty, and found at the base and middle of the section. It has a sand/shale ratio of 0.90.

Bounding surfaces: The unit conformably overlies unit 4A. The top of the section represents a major regional unconformity.

Seismic facies: This unit is masked by surface multiples and noise.

Onshore equivalents: Prince Edward Island Redbeds?

DISCUSSION

The development of a detailed stratigraphic framework and the identification of the surfaces which bound the units have helped us to recognize that the Central Maritimes Basin fill is cyclic in nature. We have identified that the basin fill is composed of five major depositional cycles, or sequences, of second order duration. We interpret the cycle bounding surfaces as sequence boundaries, regionally identifiable, conformable to unconformable in nature.

Foraminifera (Wightman et al., 1994) and seismic (Grant, 1994) studies indicate that there may have been marine incursions into the Maritimes Basin during the Late Carboniferous. We however, chose to apply nonmarine sequence stratigraphic tools to the basin fill package because of the basins overall nonmarine late Paleozoic character. The characteristic prograding/shingling nature of seismic reflectors, high sand/shale ratios, coarsening upwards nature and multistoried channel fill/deltaic log signatures of the coarser grained, basal units (units 1A, 2A, 3A, and 4A) have led us to interpret them as forestepping systems tracts as outlined by Legarreta et al. (1993). Deposition proceeded in response to an increase in coarse clastic sediment supply to the Maritimes Basin. This resulted in a decrease in accommodation space, causing the progradation of the forestepping systems tracts basinward. These prograding deposits for the reasons above are further interpreted to be a series of prograding braidplain fan delta systems.

The presence of limestones in nonmarine settings are sometimes indicators of transgressive surfaces (Shanley and McCabe, 1994). In addition, well developed coals commonly are formed during the late stages of lowstand and the early stages of relative base level rise (Beaubouef et al., 1995). The location of limestones at the base of the finer grained unit and the presence of coals at both the base of the finer grained units and tops of coarser grained units, indicate a transgressive surface at the boundary between the two units.

The fine grained units overlying the transgressive surfaces are interpreted to be backstepping systems tracts as outlined by Legarreta et al. (1993). These systems tracts developed primarily in response to a decreased sediment supply to the Maritimes Basin. The decreased sedimentation rates were followed by increases in regional accommodation space and a relative rise in relative base level causing the transgressive, backstepping, deposition of finer grained strata back onto the basin flanks.

SUMMARY

- A stratigraphic framework has been developed for the Central Maritimes Basin which has implications for regional studies of the Maritimes Basin.
- The new framework has been used to identify five major depositional cycles of second order duration.
- Each cycle is bounded at the top and bottom by regionally identifiable sequence boundaries.
- Each cycle is composed of a coarse grained basal member, overlain by a finer grained member.
- The basal members are Forestepping Systems Tracts which resulted from an increase in sediment supply, a decrease in accommodation space, and a relative lowering in base level. These system tracts are interpreted to be prograding braidplain fan delta deposits.
- Overlying the Forestepping Systems Tracts are transgressive surfaces, above which lie the finer grained Backstepping Systems Tracts. These deposits resulted from a decrease in sediment supply, an increase in accommodation space, and a relative rise in base level.

ACKNOWLEDGMENTS

This research was funded by an NSERC grant (through M. Gibling), by the GSC Atlantic and Dalhousie University's Industry Research Associate Scheme, and the GSC Atlantic's Hydrocarbon Charge Modelling Project, the Geological Society of America, and the Canadian Society of Petroleum Geologists. Thanks are due Paul Durling, Ken Skene, and Al Grant for many discussions which benefitted this project. Reviews by Al Grant and Phil Moir are much appreciated.

REFERENCES

Beaubouef, R.T., McLaughlin, P.P., Bohacs, K.M., and Devlin, W.J.
1995: Sequence Stratigraphy of Coal-Bearing Strata, Upper Cretaceous, Washakie Basin, SW Wyoming; American Association of Petroleum Geologists, Annual Convention, Program with Abstracts, p. 7A.

Belt, E.S.
1964: Revision of Nova Scotia Middle Carboniferous units; American Journal of Science, v. 262, p. 653-673.

Belt, E.S.
1965: Stratigraphy and palaeogeography of Mabou group and related Middle Carboniferous facies, Nova Scotia, Canada; Geological Society of America Bulletin, v. 76, p. 777-802.

Gibling, M.R., Calder, J.H., Ryan, R., Van De Poll, H.W., and Yeo, G.M.
1992: Late Carboniferous and Early Permian drainage patterns in Atlantic Canada; Canadian Journal of Earth Sciences, v. 29, p. 338-352.

Grant, A.C.
1994: Aspects of seismic character and extent of Upper Carboniferous Coal Measures, Gulf of St. Lawrence and Sydney Basins; Palaeogeography, Palaeoclimatology, Palaeoecology, v. 106, p. 217-285.

Grant, A.C. and Moir, P.N.
1992: Observations on coalbed methane potential, Prince Edward Island; in Current Research, Part E; Geological Survey of Canada, Paper 92-1E, p. 269-278. Hacquebard, P.A.
1986: The Gulf of St. Lawrence Carboniferous Basin; the largest coalfield of Eastern Canada; Canadian Institute of Mining Bulletin, v. 79, p. 67-78.

Howie, R.D. and Barss, M.S.
1975: Upper Paleozoic rocks of the Atlantic Provinces, Gulf of St. Lawrence, and adjacent continental shelf; Geological Survey of Canada, Paper 74-30, v. 2, p. 35-50.

Kelly, D.G.
1967: Some aspects of Carboniferous stratigraphy and depositional history in the Atlantic Provinces; Geological Association of Canada, Special Paper 4, p. 213-229.

Legarreta, L., Uliana, M.A., Larotonda, C.A., and Meconi, G.R.
1993: Approaches to nonmarine sequence stratigraphy – theoretical models and examples from Argentine Basins; in Subsurface Reservoir Characterization from Outcrop Observations, R. Eshard, and B. Doligez (ed.); Proceedings of the 7th IFP Exploration and Production Research Conference, Scarborough, April 12-17, 1992, p. 125-144.

Mossman, D.J.
1992: Carboniferous source rocks of the Canadian Atlantic margin: in Basins on the Atlantic Seaboard; in Petroleum Geology, Sedimentology and Basin Evolution, J. Parnell (ed.), Geological Society of America, Special Publication No. 62, p. 25-34.

Ryan, R.J. and Zentilli, M.
1993: Allocyclic and thermochronological constraints on the evolution of the Maritimes Basin of Eastern Canada: Atlantic Geoscience Society, Annual Colloquium and Symposia, Halifax, Nova Scotia, Program with Abstracts.

Ryan, R.J., Boehner, R.C., and Calder, J.H.
1991: Lithostratigraphic Revisions of the upper Carboniferous to lower Permian strata in the Cumberland Basin, Nova Scotia and the regional implications for the Maritimes Basin in Atlantic Canada; Bulletin of Canadian Petroleum Geology, v. 39, no. 4, p. 289-314.

Shanley K.W. and McCabe, P.J.
1994: Perspective on Sequence Stratigraphy of Continental Strata; American Association of Petroleum Geologists Bulletin, v. 78, p. 544-566.

Wightman, W.G., Grant, A.C., and Rehill, T.A.
1994: Paleontological evidence for marine influence during deposition of the Westphalian Coal Measures in the Gulf of St. Lawrence-Sydney Basin region, Atlantic Canada; in Current Research 1994-D; Geological Survey of Canada, p. 41-50.

Williams, E.P.
1973: St. Lawrence Lowlands, Gaspe, and Gulf of St. Lawrence Areas; in The Future Petroleum Provinces of Canada – Their Geology and Potential, R.G. McCrossan (ed.); Canadian Society of Petroleum Geologists, Memoir 1, p. 561-587.

Geological Survey of Canada Project 920058

The geological significance of the alkalic gabbro in the immediate hanging wall to the Brunswick No. 12 massive sulphide deposit, Bathurst, New Brunswick[1]

David R. Lentz[2], Wayne D. Goodfellow, and Carolyn E. Moore[3]
Mineral Resources Division

Lentz, D.R., Goodfellow, W.D., and Moore, C.E., 1995: The geological significance of the alkalic gabbro in the immediate hanging wall to the Brunswick No. 12 massive sulphide deposit, Bathurst, New Brunswick; in Current Research 1995-E; Geological Survey of Canada, p. 233-243.

Abstract: A small gabbro lopolith straddles the footwall-hanging wall contact at the north-end of the Brunswick No. 12 massive sulphide deposit. It is plagioclase-phyric in the core and fine grained along the margins. It is chemically unzoned and compositionally similar to the margins of the discordant porphyry dyke that cuts the mine sequence and the Brunswick alkalic basalts. Like the dyke, the gabbro probably represents a high-level subvolcanic intrusion to those basalts. The gabbro is relatively unaltered except by seawater spilitic processes, i.e. Mg and Na enrichment localized along its margin. The high Fe content is a primary feature of this alkalic gabbro suggesting that the very high Fe content of the basal Brunswick alkalic basalts is also a primary feature related to rift magmatism along the margin of the back-arc basin, rather than being related to late-stage hydrothermal alteration above the deposit.

Résumé : Un petit lopolite de gabbro chevauche le contact entre le mur et le toit à l'extrémité nord du gisement de sulfures massifs Brunswick n° 12. Son noyau est constitué de phénocristaux de plagioclase et ses bords de grains fins. Il est chimiquement non zoné et de composition semblable aux marges du dyke de porphyre discordant qui recoupe la séquence minière et les basaltes alcalins de Brunswick. Comme le dyke, le gabbro représente probablement une intrusion hypovolcanique de niveau élevé par rapport à ces basaltes. Le gabbro est relativement inaltéré sauf par des processus spilitiques en présence d'eau de mer, c'est-à-dire un enrichissement localisé en Mg et Na le long de sa bordure. La forte teneur en Fe est une caractéristique principale de ce gabbro alcalin indiquant que la très forte teneur en Fe des basaltes alcalins de la base du gisement de Brunswick est également une caractéristique primaire plutôt liée à un magmatisme de rift le long de la marge du bassin d'arrière-arc qu'à une altération hydrothermale de stade tardif au-dessus du gisement.

[1] Contribution to the 1994-1999 Bathurst Mining Camp, Canada-New Brunswick Exploration Science and Technology (EXTECH II) Initiative.

[2] New Brunswick Geological Surveys Branch, P.O. Box 50, Bathurst, N.B. E2A 3Z1
[3] Geological Consultant, 840 Grandview Street, Bathurst, N.B. E2A 3R7

INTRODUCTION

One of the challenges in studying ore deposits, especially in complexly deformed terranes like the Bathurst Mining Camp, is separating primary features related to the ore formation, i.e. geology, textures, and alteration, from those related to deformation and metamorphism. This is done through careful consideration of all available evidence. As an example, Lentz and van Staal (in press) used the general absence of alteration in a composite porphyry dyke, interpreted to be synvolcanic to the Boucher Brook alkalic basalts, to help constrain the timing and origin of hanging wall and footwall alteration at the Brunswick No. 12 deposit. A similar approach was followed in this study, where several samples were taken from across a small gabbro body located at the north end of the No. 12 deposit. This was done to constrain the chemical affinity and degree of alteration of this mafic intrusion, as well as to determine if the Fe-rich nature of the overlying spilitic alkalic basalts is a result of hanging wall-related alteration associated with the waning stages of massive sulphide formation, as previously suspected, or is a primary characteristic of these basalts. This paper describes these geochemical results and their implications with respect to primary and alteration features at the Brunswick No. 12 deposit.

GENERAL GEOLOGY

Middle Ordovician gabbros ranging from Mid Ocean Ridge Basalt (MORB) to alkalic compositions occur throughout the Bathurst Mining Camp in the Miramichi, Tetagouche, and Fournier groups (Hill, 1974; Janes, 1976; Whitehead and Goodfellow, 1978; van Staal, 1987; Paktunc, 1990; van Staal et al., 1991; Winchester et al., 1992). The alkalic gabbros in the Miramichi and Tetagouche groups, are related to back-arc rifting of a magmatic arc similar to the interpretation for the alkalic basalts (van Staal et al., 1991).

The gabbro body examined in this study (Fig. 1) straddles the contact between the stratigraphic footwall and hanging wall sequence of the No. 12 deposit (1000 m level) at its northern-most end and lies beneath the rift-related Brunswick alkalic basalts (Whitehead and Goodfellow, 1978; van Staal, 1987; van Staal et al., 1991). The geology is extremely complex at the 1000 m level of the mine because the main F_1 fold changes in plunge in this area (van Staal and Williams, 1984). The gabbro body seems to be a lopolith that intruded along the contact between the slates and wackes of the Patrick Brook and the rhyolites and related sedimentary rocks of the Flat Landing Brook formations (Lentz and Goodfellow, 1992). The Nepisiguit Falls Formation, including the ore horizon, is absent at this location, i.e. its stratigraphic position is occupied by the gabbro. The occurrence of an alkalic gabbro directly beneath the Brunswick alkali basalts of similar composition supports a para-autochthonous relationship of these basalts to the underlying sequence.

The gabbro is generally fine grained with a light to medium green mottled texture along its margin (quenched?) with very minimal fabric development unlike the much thinner porphyry dyke (Lentz and van Staal, in press). Primary mineralogy nor textures are preserved along the margin of the body due to replacement by amphiboles with minor carbonate. The central part of the body is coarser grained than the margin with both intergranular and glomeroporphyritic plagioclase crystals (<0.5 cm) that are weakly altered (Fig. 2). The pyroxenes seem to be, at least in part, replaced by amphibole that is coarser grained than those on the margins of the body. Disseminated hexagonal pyrrhotite platelets also

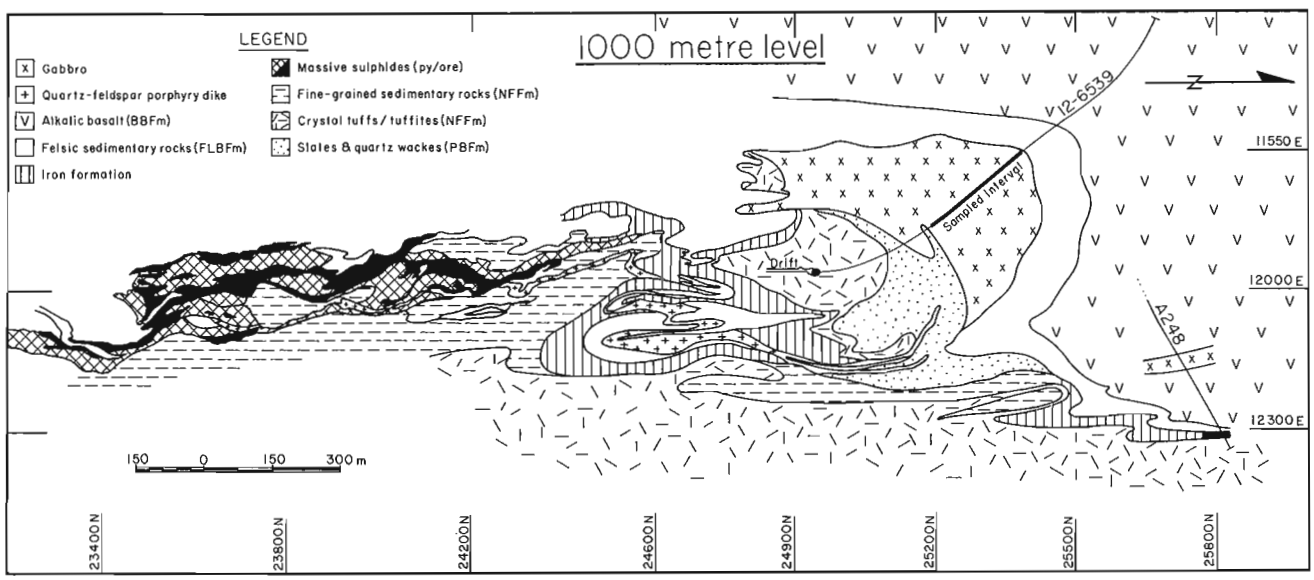

Figure 1. Geology of the 1000 m level of the Brunswick No. 12 deposit, Bathurst, New Brunswick (courtesy of Rheal Godin and Bill Luff of Brunswick Mining and Smelting Corporation). Diamond-Drill Hole 12-6539 was sampled between 261.2 m (near drift) to 533 m (upper contact) near the Brunswick alkalic basalts.

occur but are generally less than 1% of the mode. Overall, however, the petrographic evidence shows that the gabbro is not very altered or deformed.

This gabbro has been intersected four times in drillholes on the 1000 m level of the mine to the west of the deposit and, like the body sampled, is not in direct contact with the Boucher Brook alkalic basalts. However, there are very similar fine- to medium-grained, medium to dark green, plagioclase-phyric gabbros that occur locally at the base of, as well as within, the Boucher Brook alkalic basalts suggesting that they are comagmatic with the basalts. It was originally thought that the alkalic gabbro described herein was compositionally similar to other medium grained gabbros along the Brunswick Belt, in particular the medium grained tholeiitic gabbros that intrude the hanging wall of both the Brunswick No. 6 massive sulphide deposit and the Austin Brook iron-formation (see van Staal, 1987; and samples 45 and 48 of Paktunc, 1990). The gabbro cuts the Flat Landing Brook Formation (FLB rhyolites - 466 ± 5 Ma; Sullivan and van Staal, 1990; van Staal and Sullivan, 1992) but is cut by a thin porphyry dyke (459 ± 2 Ma; van Staal and Sullivan, 1992) that crosscuts the mine sequence (Lentz and van Staal, in press) indicating the gabbro has an approximate age of 464 to 460 Ma.

The localization of F_2 folding at the north end of the deposit is related to the occurrence of this large competent body similar to the control that the large porphyry dyke has on the localization of F_2 folds also in the north end of the deposit.

GEOCHEMICAL SYSTEMATICS

The major- and trace-element chemical compositions of the seven gabbros analyzed in this study are presented in Table 1. Chemical profiles from the lower Patrick Brook contact (261 m) to the upper Flat Landing Brook contact (533 m), from southeast to northwest in Figure 1, were generated (Fig. 3) to determine if there is any chemical zonation within the gabbro, as well as to ascertain the extent of alteration within the body. Primary compositional characteristics and chemical affinity of the gabbro are discussed and compared with other gabbros and alkalic basalts from the Bathurst Camp reported in the literature. This is followed by a description of the alteration features within the body.

Analytical methods

Seven samples were taken from diamond-drill hole (DDH) 12-6539 that cuts the gabbro body and analyzed in the geochemical laboratory of the Geological Survey of Canada (Table 1). Major elements were determined by X-ray fluorescence spectroscopy on fused disks, ferrous iron was determined by titration with ammonium metavanadate (modified Wilson method), and S, CO_2, and H_2O were determined by infra-red spectrometry of combustibles. Trace elements were analyzed by Inductively Coupled Plasma Emission Spectroscopy (ICP-ES) and mass spectroscopy (ICP-MS). The accuracy of these analyses was determined by comparing the internal standard MRG-1 with the accepted values (Abbey 1979; Govindaraju, 1994). The highest errors are typically associated with the elements of lowest abundance, i.e. near detection limits, although many of the elements that are low in MRG-1 are high in the Brunswick gabbro samples. A "?" designates uncertianty in the CANMET standard (Abbey, 1979). The relative per cent error based on comparison with MRG-1 are: <2% - SiO_2, TiO_2, Al_2O_3, FeO_t, MnO, MgO, CaO, Sr, Zr, Ce?, Pr?, Dy?, Ho?, Er?, and Lu?; <5% - H_2O, CO_2, Co, Hf?, Nb?, Sc?, and Sm?; <15% - K_2O, P_2O_5, S_t, Cr, Cs?, Cu, Pb, Rb, U?, V, Y?, La?, Nd?, Eu?, and Gd?; <25% -Na_2O, Ag?, Ni, Th?, Zn, Tb?, and Yb?;> 25% - Ba?, Be?, Mo?, Ta?, and Tm?.

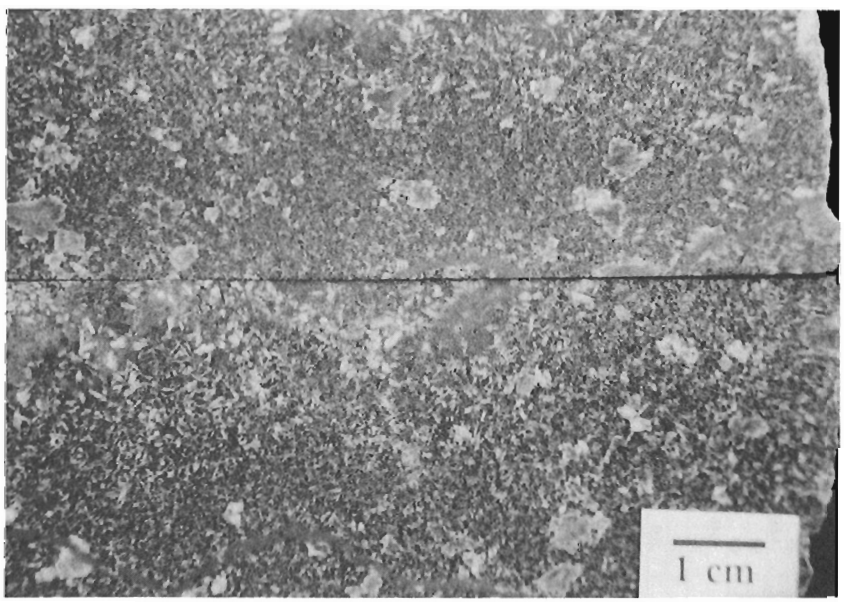

Figure 2.

Photograph of plagioclase porphyritic (meta)gabbro (GB-4; DDH 12-6539 @ 396.9 m) from sampled interval (see Fig. 1).

Table 1. Major-, trace-, and rare-earth-element composition of gabbro sampled (GB-) in this study and selected mafic rocks in the Bathurst Mining Camp.

SAMPLE	GB-1	GB-2	GB-3	GB-4	GB-5	GB-6	GB-7	DIKE1	DIKE2	DIKE3	GBstd	BRUN	CCL	CB	EMB	BER	ROB	KA	Gabbrol		Gabbroll	
DDH	6539	6539	6539	6539	6539	6539	6539	1277	1277	3027		avg	avg	avg	avg	avg	avg	avg	avg	std	avg	std
m	263.3	293.9	329.1	396.9	464.8	499.3	528.4															
wt.%	Ref.1	Ref.1	Ref.1	Ref.1	Ref.1	Ref.1	Ref.1	Ref.2	Ref.2	Ref.2	Ref.1	Ref.3	Ref.3	Ref.3	Ref.3	Ref.3	Ref.3	Ref.4	Ref.5		Ref.5	
SiO_2	43.20	45.60	48.40	49.60	49.90	47.70	46.90	42.80	40.40	49.80	48.60	46.78	47.40	47.60	46.20	46.60	49.50	42.18	47.48	2.17	46.58	0.97
TiO_2	2.32	2.32	4.10	2.34	1.84	4.29	2.79	2.66	2.72	2.49	2.63	3.06	3.21	3.27	2.82	2.67	2.22	2.44	1.61	0.48	3.31	0.20
Al_2O_3	12.10	15.30	12.90	15.10	16.10	11.90	14.90	13.70	13.30	13.30	15.80	14.93	15.92	13.58	14.97	15.98	14.85	14.98	14.78	1.70	13.84	0.27
Fe_2O_3	1.60	1.30	1.80	2.30	2.00	1.80	1.80	2.40	2.40	1.40	3.40	3.75	2.46	4.67	5.80	2.24	3.61	3.40	2.16	0.84	3.08	0.35
FeO	11.50	9.10	12.60	8.20	7.90	12.30	10.50	19.70	21.10	9.30	7.70	8.45	8.73	7.64	6.61	7.61	6.54	8.68	8.74	1.26	9.94	0.24
MnO	0.30	0.14	0.35	0.21	0.16	0.26	0.30	0.16	0.19	0.86	0.25	5.72	5.88	4.86	5.62	4.62	2.85	7.03	0.21	0.03	0.24	0.04
MgO	13.60	5.73	4.96	4.74	5.07	5.79	7.71	10.80	8.57	6.31	3.79	0.26	0.19	0.18	0.17	0.23	0.17	0.42	7.57	2.91	5.59	0.40
CaO	7.04	7.69	5.99	8.51	8.11	6.53	5.36	0.37	1.15	4.45	7.57	7.18	6.48	6.99	8.86	6.80	7.17	7.97	9.16	1.20	8.14	0.94
Na_2O	1.00	3.50	4.30	4.10	4.30	4.00	4.10	0.00	0.00	2.00	4.10	3.52	4.28	4.26	4.12	4.24	5.27	1.50	2.96	0.70	3.87	0.38
K_2O	0.08	0.66	0.91	0.49	0.58	0.92	0.41	0.01	0.08	1.28	1.99	0.88	0.30	1.22	0.47	1.51	1.75	1.29	0.46	0.31	0.75	0.37
P_2O_5	0.27	0.26	0.47	0.29	0.24	0.43	0.34	0.30	0.31	0.30	0.94	0.41	0.50	0.69	0.36	0.53	0.56	0.36	0.15	0.05	0.41	0.03
H_2Ot	5.90	4.30	3.20	2.70	2.80	3.40	4.20	7.70	7.50	4.20	3.20	4.83	4.91	4.86	3.91	6.90	5.50	4.98	3.44	1.16	3.44	0.83
CO_2t	1.70	4.70	0.70	1.90	1.00	1.10	0.80	0.00	2.70	3.20	0.20	-	-	-	-	-	-	4.96	0.83	1.15	0.59	0.46
St	0.02	0.15	0.07	0.22	0.18	0.25	0.41	0.63	0.17	0.17	0.14	0.03	0.02	0.03	0.01	0.02	0.03	0.03	0.17	0.28	0.11	0.06
Sum	100.6	100.8	100.8	100.7	100.2	100.7	100.5	101.2	100.6	99.1	100.3	99.8	100.3	99.9	99.9	100.0	100.0	100.2	99.7		99.9	
ppm																						
Ag	0.10	0.29	0.10	0.18	0.15	0.10	0.16	-	-	-	0.05	-	-	-	-	-	-	1.00	-	-	-	-
Ba	80	300	300	200	210	280	180	40	130	1400	360	244	113	237	103	362	797	496	142	62	180	64
Be	1.60	1.40	2.50	1.40	1.10	2.70	1.90	-	-	-	2.0	-	-	-	-	-	-	2.00	-	-	-	-
Co	58	40	48	37	37	52	47	-	-	-	29	-	-	-	-	-	-	45	-	-	-	-
Cr	69	75	5	29	36	5	59	21	28	65	33	80	33	5	65	72	7	193	204	166	48	13
Cs	0.45	1.20	11.00	0.49	0.54	7.40	0.47	-	-	-	0.21	-	-	-	-	-	-	1.63	-	-	-	-
Cu	35	52	27	25	38	21	51	76	35	36	18	46	46	42	87	32	21	21	-	-	-	-
Ga	16	19	21	19	18	20	21	-	-	-	24	-	-	-	-	-	-	-	-	-	-	-
Hf	3.6	3.8	6.2	5.3	4.4	6.0	4.4	-	-	-	7.9	7.00	7.60	6.60	5.00	6.40	9.90	3.75	2.79	0.93	5.20	0.67
Mo	1.0	1.2	2.2	1.9	1.1	1.6	1.4	-	-	-	3.6	-	-	-	-	-	-	0.50	-	-	-	-
Nb	19	19	35	28	22	32	24	37	20	26	67	28	35	39	26	47	58	23	5	2	28	8
Ni	110	39	5	16	18	5	35	35	34	37	5	42	89	17	55	33	10	103	93	89	28	5
Pb	10	8	12	6	7	4	11	13	15	34	7	16	21	13	13	12	12	1	-	-	-	-
Rb	2	14	45	8	8	33	5	6	9	50	24	-	-	-	-	-	-	15	22	20	30	9
Sc	28	30	31	29	30	38	32	-	-	-	20	31	34	27	31	25	15	31	35	5	26	15
Sr	64	330	92	230	340	110	100	13	41	190	490	284	209	212	367	263	336	138	196	104	603	806
Ta	1.9	1.8	1.9	2.1	1.5	2.6	1.7	-	-	-	4.2	2.5	3.3	2.3	1.6	3.4	4.8	1.25	0.43	0.22	1.26	0.33
Th	2.1	2.1	4.1	4.4	3.2	3.5	2.7	-	-	-	7.1	4.4	3.8	5.7	1.6	5.2	7.5	1.75	1.10	0.75	1.66	0.21
U	0.57	0.59	1.10	1.10	0.81	0.96	0.72	-	-	-	1.9	-	-	-	-	-	-	0.65	-	-	-	-
V	270	280	370	290	260	430	330	260	260	250	180	384	386	306	331	272	148	266	-	-	-	-
Y	21	21	35	30	25	33	26	45	45	37	45	37	42	45	30	34	49	27	32	11	33	7
Zn	78	64	58	52	52	89	60	240	230	120	84	115	110	126	114	97	128	115	-	-	-	-
Zr	160	160	300	250	200	260	210	260	240	250	380	236	224	289	194	237	359	198	99	33	213	20
La	14	14	26	22	18	23	19	39	36	31	55	32.4	19.3	31.8	11.5	37.9	59.3	17.05	7.4	2.7	19.5	2.4
Ce	36	35	63	54	43	56	46	81	74	-	120	70.7	45.0	73.9	30.5	81.6	120.1	38.25	18.2	6.4	47.8	4.9
Pr	4.3	4.3	7.7	6.4	5.1	6.9	5.6	-	-	-	13.0	-	-	-	-	-	-	-	3.0	0.5	16.9	14.2
Nd	20	20	35	29	23	33	26	44	41	-	57.0	39.0	37.0	42.6	28.4	44.2	60.3	19.75	15.5	4.5	35.4	3.5
Sm	4.8	4.7	8.4	6.6	5.4	7.7	6.2	11.0	10.0	-	12.0	8.0	11.85	8.80	6.50	8.70	11.30	4.68	3.8	1.3	6.8	0.5
Eu	1.7	1.8	2.7	2.0	1.7	2.5	2.2	2.5	3.1	-	3.7	2.6	3.40	2.70	2.20	2.80	3.40	1.68	1.3	0.4	2.3	0.3
Gd	5.5	5.6	8.8	7.1	6.0	8.7	6.7	10.0	9.3	-	11.0	-	-	-	-	-	-	-	5.1	1.7	7.8	1.2
Tb	0.84	0.82	1.40	1.10	0.94	1.30	1.00	-	-	-	1.7	-	-	-	-	-	-	0.68	0.99	0.16	1.10	0.00
Dy	4.3	4.3	7.1	5.9	5.0	6.9	5.4	10.0	9.1	-	8.7	-	-	-	-	-	-	-	5.58	1.85	6.88	0.35
Ho	0.84	0.83	1.40	1.20	1.00	1.30	1.00	-	-	-	1.7	-	-	-	-	-	-	-	1.26	0.26	1.16	0.06
Er	2.1	2.2	3.6	3.1	2.5	3.4	2.6	-	-	-	4.4	-	-	-	-	-	-	-	3.51	0.84	2.95	0.15
Tm	0.33	0.34	0.57	0.48	0.42	0.53	0.41	-	-	-	0.7	-	-	-	-	-	-	-	0.46	0.15	0.35	0.05
Yb	2.7	2.6	3.9	3.3	3.0	3.7	3.0	3.9	4.1	3.1	4.2	3.2	5.1	3.4	2.1	2.9	4.1	2.38	2.97	1.13	2.86	0.47
Lu	0.28	0.30	0.50	0.43	0.38	0.47	0.37	-	-	-	0.65	0.50	0.80	0.50	0.30	0.40	0.60	0.34	0.55	0.19	0.35	0.01

NOTES: Ref. 1 - this study; Ref. 2 - Lentz and van Staal (in press); Ref. 3 - van Staal et al. (1991); Ref. 4 - Lentz (1995); Ref. 5 - Paktunc (1990). - = no analysis.

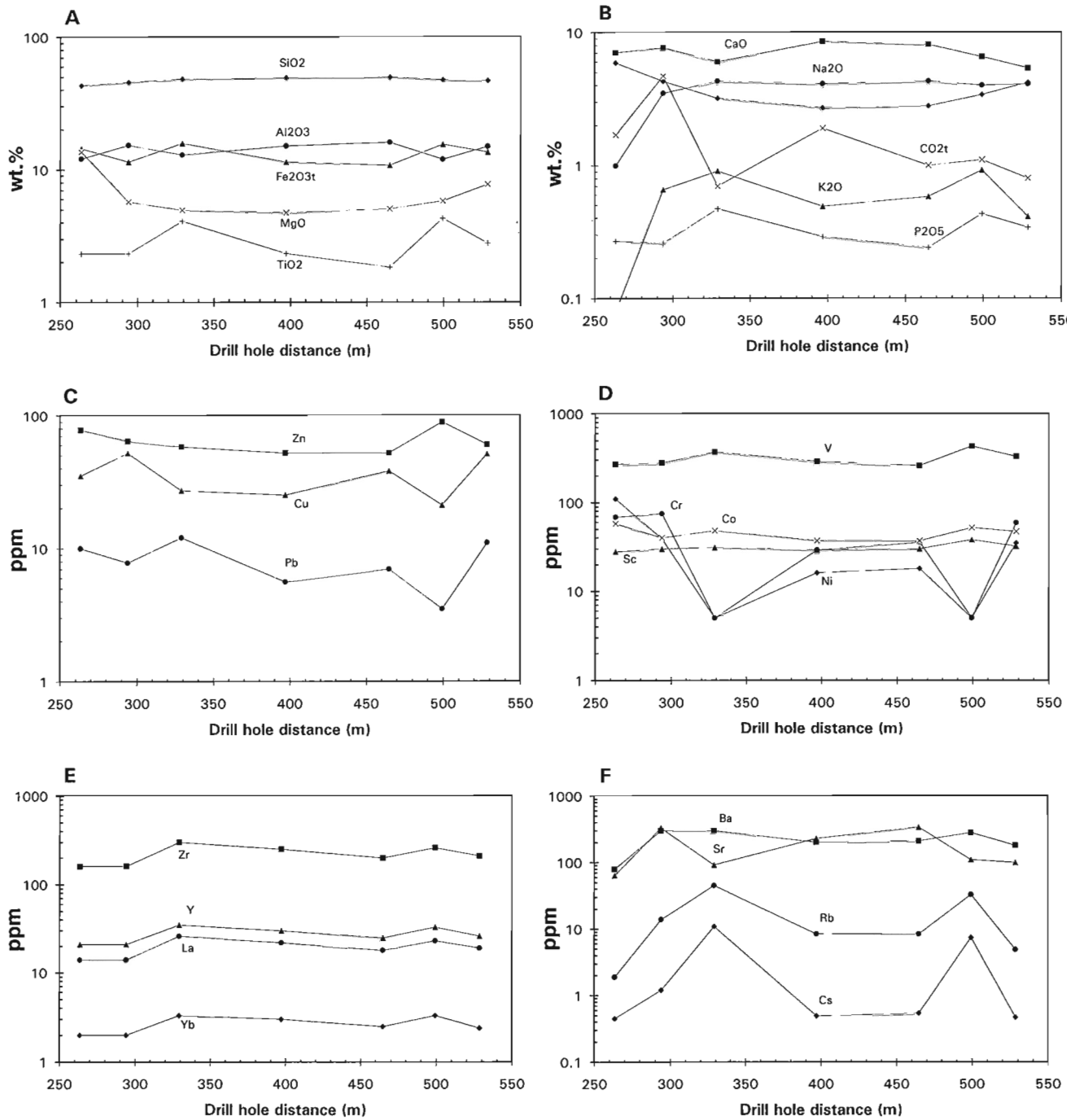

Figure 3. *Major- and trace-element geochemical profiles from the stratigraphic and structural base (261.2 m) to the top (533 m) of the gabbro body from Diamond-Drill Hole 12-6539 located at the northern-most end of the deposit.*

Primary compositional systematics and chemical affinity

There seems to be only minor alteration along the margins of the gabbro body (discussed later), so most element systematics reflect the primary chemical variability of the gabbro body. The intrusion is inherently Fe-rich like the overlying basalts. TiO_2 is somewhat irregular with values ranging from 1.8 to 4.3 but at the scale sampled, no zoning is evident (Fig. 3A). Except on the margin, Na_2O, CaO, Al_2O_3, P_2O_5, V, Co, and Sc are relatively uniform across the body (Fig. 3A and 3B). Similarly, Zn, Cu, and Pb are low and moderately uniform (Fig. 3C). The two samples with high TiO_2 also have low Cr and Ni contents (Fig. 3D) and high Zr, Y, La, and Yb (Fig. 3E) indicative of a high degree of fractionation. Many of the alkalic elements (Ba, Sr, Rb, Cs; Fig. 3F) are quite irregular, particularly on the margins but the highest Cs and Rb are in the the two most fractionated samples.

The gabbro samples are very similar to the mafic end-member of the composite porphyry dyke that cross cuts the mine sequence (Lentz and van Staal, in press), the Brunswick alkalic basalts (Whitehead and Goodfellow, 1978; van Staal et al., 1991) and the alkalic gabbros (van Staal, 1987; Paktunc, 1990) that occur throughout most of the Tetagouche Group (Table 1). The similarity of the gabbro composition to the basalts and the minimal evidence of local fractional crystallization enables the application of petrogenetic diagrams normally applied to mafic volcanic rocks (cf. van Staal, 1987; Paktunc, 1990). Considering the minimal carbonate alteration, the elements traditionally considered immobile, i.e. the high-field-strength elements (HFSE) (Davies et al., 1979; Davies and Whitehead, 1980; Hynes, 1980; Dostal and Strong, 1983) are used to determined the chemical affinity of these gabbros. Using the Zr/TiO_2 - Nb/Y discrimination plot (Fig. 4; Winchester and Floyd, 1977), the gabbro samples, as well as many of the other alkalic mafic rocks (Whitehead and Goodfellow, 1978; van Staal, 1987; van Staal et al., 1991; Lentz and van Staal, in press) and fine grained alkalic gabbros (van Staal, 1987; Paktunc, 1990) plot within the alkalic basalt field compared to the medium grained tholeiitic gabbros of Paktunc (1990). The TiO_2 - Zr plot (Fig. 5a; Pearce and Norry, 1979) illustrates the tight clustering of alkalic mafic rocks in the within-plate lava field. Based on the TiO_2-Zr/P_2O_5 plot (Fig. 5b; Winchester and Floyd, 1976), the body has a transitional composition between alkalic and tholeiitic end-members, although leaching of P_2O_5 (cf. van Staal, 1987) from the base of the body could account for the anomalous samples in the tholeiitic field (Fig. 5b). The gabbro samples plot well within the within-plate environment on the Zr/Y-Zr discrimination diagram (Fig. 5c; Pearce and Norry, 1979) with the alkalic gabbros and Brunswick alkalic basalts, i.e. distinctly separate from the group I tholeiitic gabbros. This is confirmed further by the compositional distribution on the Zr-Ti-Y (Fig. 5d; Pearce and Cann, 1973), Zr-Nb-Y (Fig. 5e; Meschede, 1986), and Th-Hf-Ta (Fig. 5f; Wood, 1980) discrimination diagrams and their overlap with the Brunswick alkalic basalt data (van Staal et al., 1991) and the group II gabbros (Paktunc, 1990). On the Th-Hf-Ta discrimination diagram, most of the gabbro samples plot along the line between the E-MORB field (B) and the alkalic basalt field (A), whereas the tholeiitic gabbros plot within the N-MORB field.

The chondrite-normalized rare-earth-element (REE) patterns (Fig. 6) of the Brunswick gabbros (this study), Brunswick alkalic basalts and dyke (Lentz and van Staal, in press), and group II gabbros (Paktunc, 1990) are virtually identical in slope with a La_N/Lu_N ranging from 48 to 52. However, there are substantial changes in absolute REE abundance among these units. There is a minor variation in the Eu anomaly from slightly positive to slightly negative indicating no obvious plagioclase fractionation. The negative Eu anomaly for sample GB-1 may be caused by hydrolysis of plagioclase feldspar, although the slight negative Eu anomaly in sample GB-5 is probably primary. The Zr-La variations (Fig. 7a) indicate a slightly different mantle source protolith for the Brunswick alkalic rocks (i.e., Zr/La >10) compared to other mafic rocks in northern New Brunswick (Zr/La <10). Although the Cr-Y diagram of Pearce (1982) (Fig. 7b) suggests that there is considerable fractionation of these magmas subsequent to partial melting, the total variation in REE abundance (Fig. 6), in particular Zr, Y, and La (Fig. 7a, b, c) seems greater than can be explained by fractional crystallization. Alternatively, disequilibrium (?) behaviour of Cr during partial melting or early Cr fractionation could help explain the incompatible element variations with respect to Cr. If correct, these incompatible element variations could then simply represent slightly variable degrees of partial

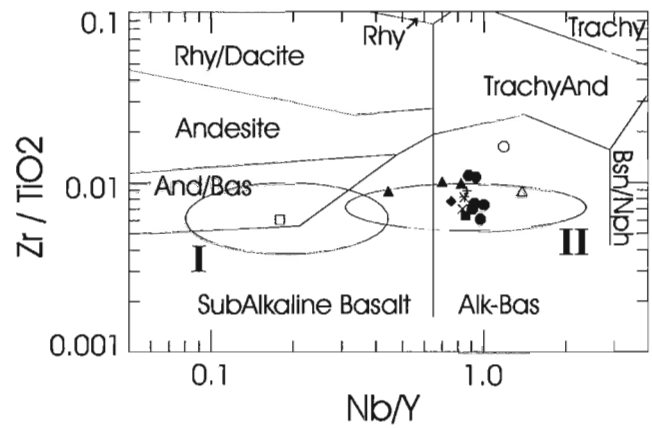

*Figure 4. Zr/TiO_2 versus Nb/Y compositional discrimination plot of Winchester and Floyd (1977) illustrating the compositional similarity of gabbro samples to the porphyry dyke and the Brunswick alkalic basalts. I = Group I medium grained tholeiitic gabbros and II = Group II fine grained alkalic gabbros (Paktunc, 1990). Gabbros – ● (this study); Brunswick porphyry dyke – ▲ (Lentz and van Staal, in press); Key Anacon average basalt – * (Lentz, 1995); averages for the Brunswick basalt – ◆; Canoe Landing Lake basalt – x; Camelback basalt – +; Eighteen Mile Brook basalt – ◊; Beresford average basalt – △; Robertville basalt – ○ (van Staal et al., 1991); Group I gabbros – □; Group II gabbros - ■ (Paktunc, 1990).*

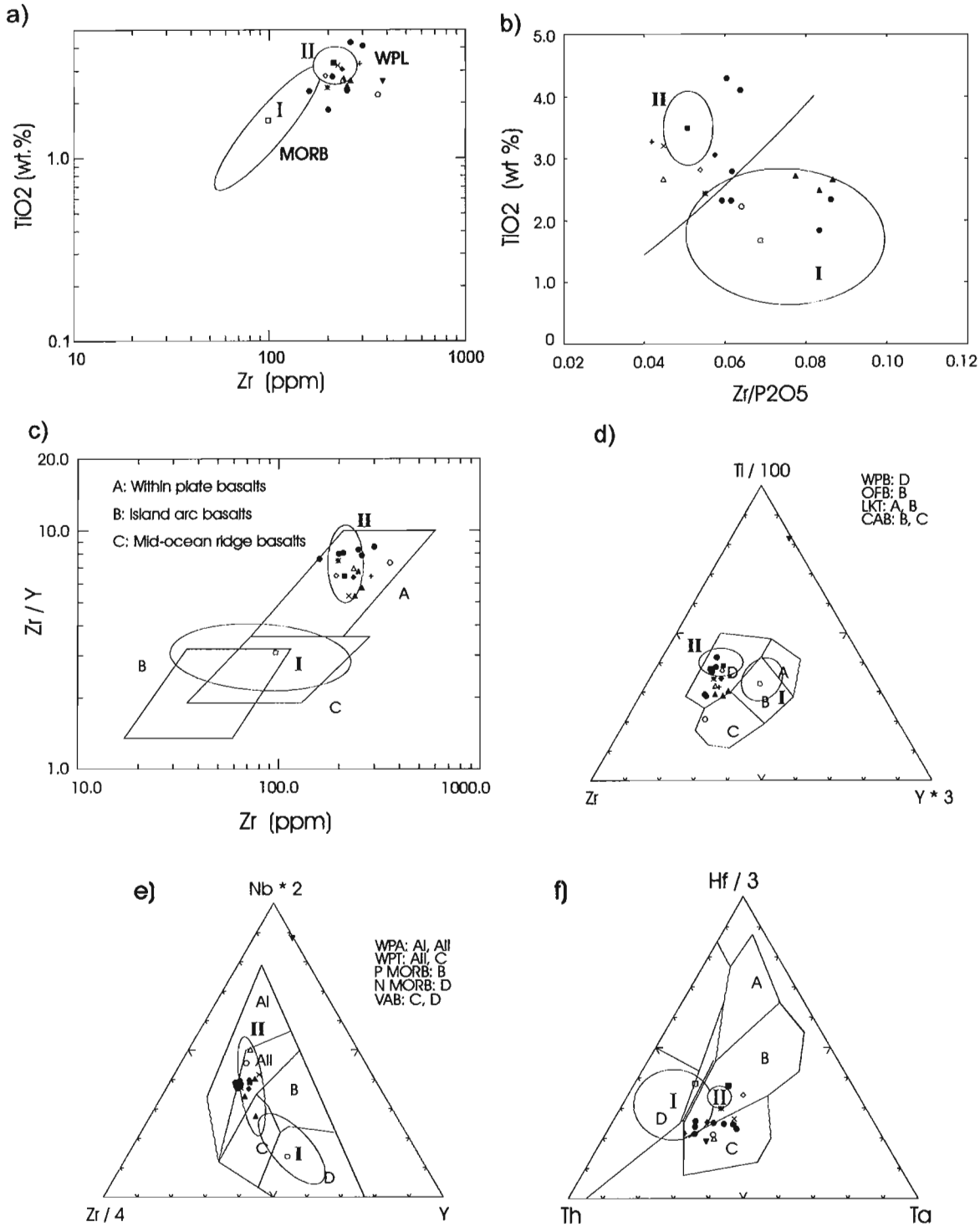

Figure 5. Geochemical tectonic discrimination diagrams illustrating the compositional similarity of the gabbro samples in this study to the porphyry dyke and Brunswick alkalic basalts and their tectonic setting. ***a)*** *Pearce and Norry (1979);* ***b)*** *Winchester and Floyd (1976);* ***c)*** *Pearce and Norry (1979);* ***d)*** *Pearce and Cann (1973), fields: within-plate basalt (D), Ocean-floor basalt (B), low K tholeiite (A,B), calcalkaline basalt (B, C);* ***e)*** *Meschede (1986), fields: within-plate alkalic (AI, AII), within-plate tholeiite (AII, C), P-MORB (B), N-MORB (D), volcanic-arc (C, D);* ***f)*** *Wood (1980), fields: A – N-MORB, B – E-MORB, C – Alkalic, D – calcalkaline basalt. Symbols are as in Figure 4.*

melting. Overall, these REE variations are different than the group I gabbros, which have flatter REE profiles (Fig. 6). The anomalous Yb values compared to the REE profile in this data set are consistent with the poor precision of the Yb data determined above.

Alteration systematics

There is minimal evidence of feldspar-destructive alteration (local saussuritization) of the gabbro except along the lower margin of the gabbro body (GB-1) (Fig. 8a) where the primary mineralogy and textures are destroyed. Coincidentally, this sample (GB-1) has the highest MgO, MnO, Ni, and H_2O with the lowest Na_2O and K_2O (Rb, Cs, etc) contents, which is similar to hydrothermal alteration observed in the hanging wall to the massive sulphide deposit (Goodfellow, 1975; Lentz and Goodfellow, 1994) as well as along the margins of the composite porphyry dyke that crosscuts the mine sequence (Lentz and van Staal, in press). For the remaining gabbro samples, the high proportion of Na relative to Ca (Fig. 8a; Graham, 1976; Stillman and Williams, 1979) and K (Hughes, 1973) suggests they are weakly spilitized. The trend of decreasing CaO with increasing MgO, in these rocks, may indicate minor plagioclase fractionation but a component is related to Na metasomatism (Stillman and Williams, 1979), as mentioned previously, with weak Mg metasomatism. The CO_2 contents are usually less than 2 wt.%, although GB-2 has 4.7 wt.% CO_2 but does not seem to be related to other geochemical variations. GB-1 (margin) has the lowest CO_2 and S contents. The coincidence of Mg and Na metasomatism are indicative of low-temperature seawater alteration (Hughes, 1973; Graham, 1976) of this gabbro body, which also affects the overlying Brunswick alkalic basalts (Whitehead and Goodfellow, 1978; van Staal, 1987). The correlation between Fe and Mg may be primary (Fig. 8c), although the Brunswick basalts contain less Ca than can be explained by plagioclase fractionation. The ferric- ferrous ratio seems to be unaffected by alteration processes with the most altered sample (GB-1) having a low ratio (Fe^{3+}/Fe^{2+} <0.15). The very magnetite-rich basalts at the base of the Brunswick alkalic basalt sequence are interpreted as sodic spilites (Whitehead and Goodfellow, 1978) and in mine terminology are commonly referred to as basic iron-formation (see Saif, 1980). The absence of Fe enrichment on the margin of the gabbro suggests that the Fe-rich nature of the gabbro and the associated basalts is related to their initial composition and is not caused by hydrothermal alteration related to the waning stages of massive sulphide deposition at the base of the mafic sequence.

There is no evidence of HFSE mobility in the gabbro with all variations explainable by primary processes. For example, the consistent LREE to HREE ratio (La_N/Lu_N) indicates negligible differential REE mobility compared to basaltic spilites with high fluid-rock ratios (Humphris, 1984). Al_2O_3 variations are related to the proportion of plagioclase within the gabbro and not related to mass gain/loss during alteration. Also, there is no correlation between REE and Al_2O_3, further suggesting that variation in ΣREE is not a function of mass gain/loss if Al is considered immobile.

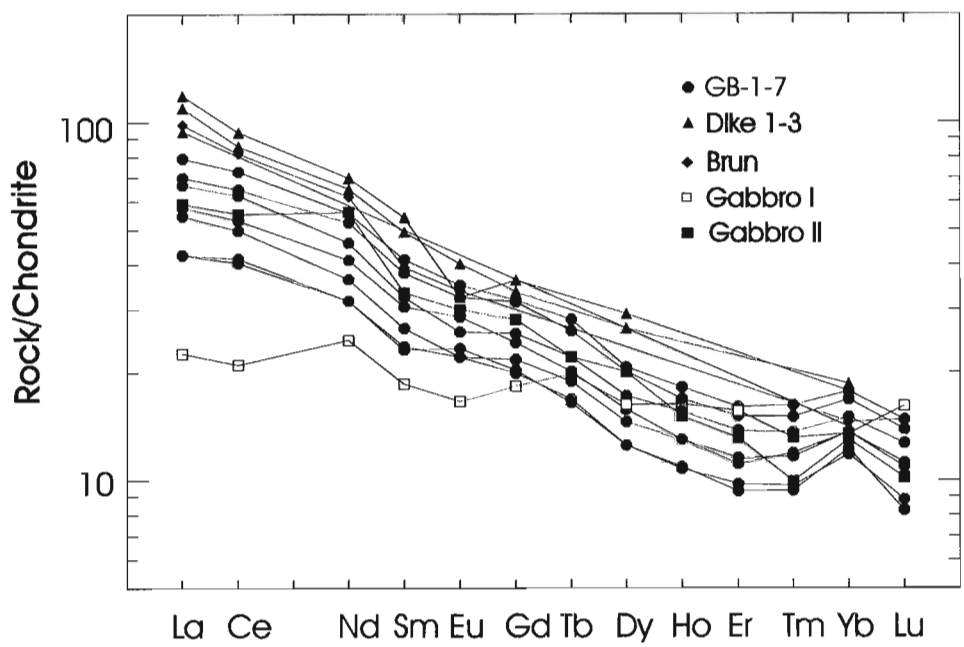

Figure 6. Chondrite-normalized rare-earth-element diagram illustrating the compositional similarity of the gabbro samples, dyke samples, and Brunswick basalts. Chondrite normalization factor from Anders and Ebihara (1982). Symbols are as in Figure 4.

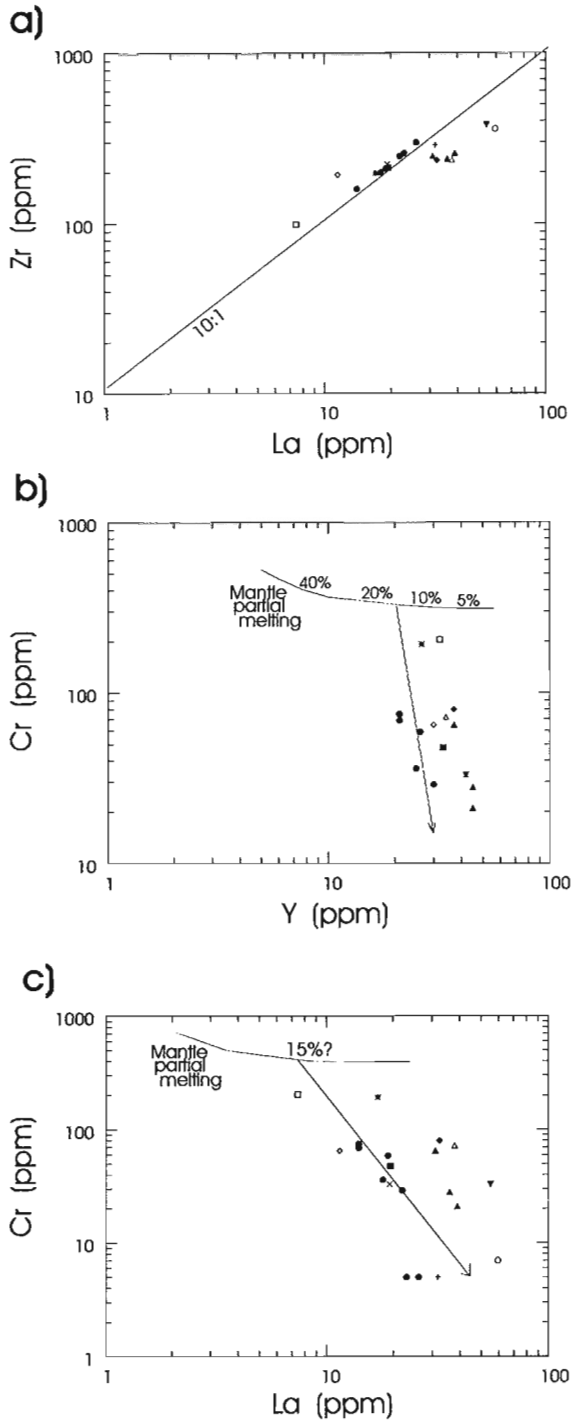

Figure 7. Trace-element geochemical variations illustrating differing chemical affinities between the gabbros and other alkalic basalts in the Bathurst Camp. ***a)*** *Zr versus La;* ***b)*** *Cr versus Y (Pearce, 1982);* ***c)*** *Cr versus La, the partial melting curve is hypothetical. Symbols are as in Figure 4.*

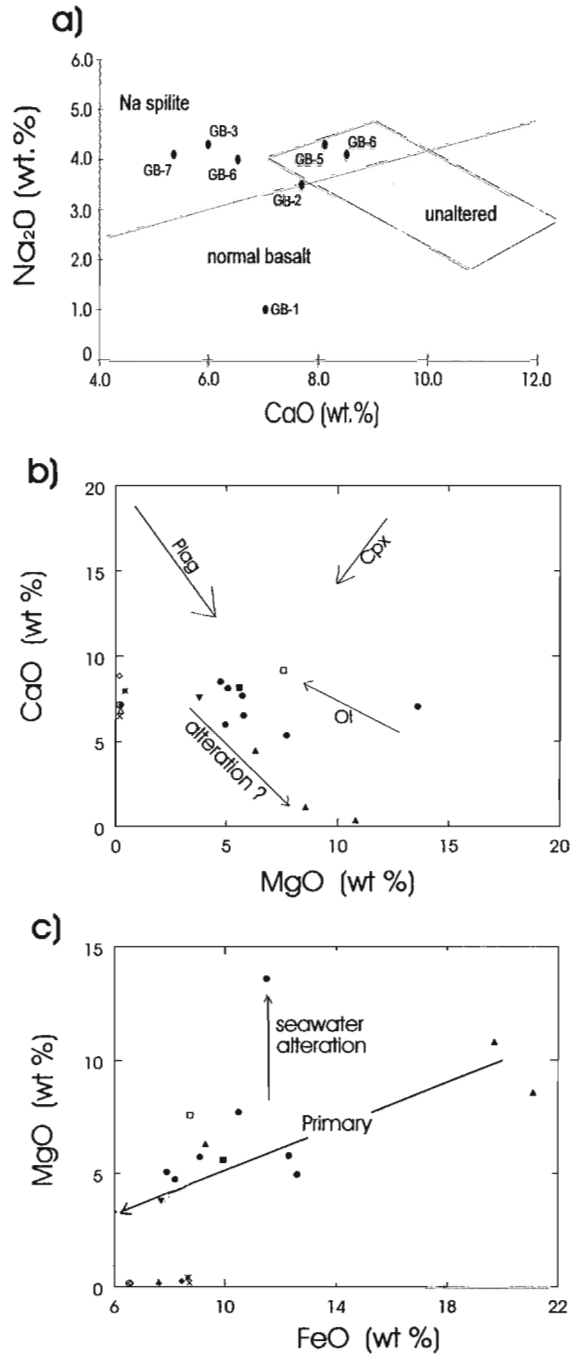

Figure 8. Major-element variations illustrating the various effects of seawater alteration on the gabbro and their variations with respect to other volcanic rocks. ***a)*** *Na_2O versus CaO illustrating the field of unaltered mafic rocks versus "normal" basalt and Na spilitic basalts (Graham, 1976; see van Staal, 1987);* ***b)*** *CaO versus MgO illustrating primary fractionation trends of plagioclase (Plag), olivine (Ol), and clinopyroxene (Cpx) and a possible alteration trend related to chloritization (Mg) of plagioclase;* ***c)*** *MgO versus FeO with a hypothetical primary trend and a seawater alteration trend. Symbols are as in Figure 4.*

DISCUSSION

The alkaline composition of the composite porphyry dyke and the gabbro, which cut the mine sequence, provide additional evidence for the autochthonous relationship of the Brunswick alkalic basalts to the mine sequence. The highly alkalic mafic composition of these rocks compared to other mafic rocks in the Bathurst Camp, as well as other deposits, which have autochthonous alkalic mafic volcanic rocks in their hanging wall, like the Canoe Landing Lake massive sulphide deposit (Walker and McDonald, 1995) and the Key Anacon massive sulphide deposits (Lentz, 1995), empirically links rift magmatism with massive sulphide genesis during both initial back-arc rifting (i.e. Canoe Landing Lake Formation alkalic basalts and rhyolite; 470 Ma; Sullivan and van Staal, 1993) and later rifting on the margin of a back-arc basin (i.e. Brunswick basalts; 457 Ma). The association of VMS deposits to alkalic mafic volcanism is two fold; 1) their subvolcanic equivalents, i.e. deep- to shallow-seated gabbros, may be responsible for developing large high-temperature hydrothermal circulation systems, and 2) the mafic volcanism may be occurring along rift structures that were previously hydrothermally active. Interestingly, the composite porphyry dyke at Brunswick No. 12 is situated within the stockwork zone of the deposit, which is inferred to be the paleofault that focussed fluids responsible for the formation of the deposit (Lentz and van Staal, in press). This is somewhat analogous to the rifted island-arc setting inferred for the Kuroko deposits (Cathles et al., 1983), as well as the role that subvolcanic intrusions play in the formation of some VMS deposits (Campbell et al., 1981).

CONCLUSIONS

1. The alkalic mafic composition of this gabbro is strong evidence that it represents a subvolcanic intrusion co-magmatic with the Brunswick alkalic basalts and suggests an autochthonous relationship of those basalts with the mine sequence.
2. This, together with the compositional systematics from the porphyry dyke, provides further evidence that the basalts are more or less autochthonous to the mine sequence.
3. Although this individual gabbro was not responsible for the hydrothermal system that formed Brunswick No. 12, similar intrusions at depth may have generated an anomalous thermal gradient during upwelling of the mantle.
4. The genetic link between highly alkalic mafic volcanism and the spatially associated Brunswick ore bodies is integral to understanding their paleoenvironment within the rift system but also determining the heat source that was responsible for the convecting hydrothermal system.

ACKNOWLEDGMENTS

We thank the staff at Brunswick Mines, in particular Bill Luff and Rheal Godin, for their help orienting us to the complex mine geology. The manuscript was critically reviewed by Steve McCutcheon (NBGSB) and Cees van Staal (GSC).

REFERENCES

Abbey, S.
1979: Reference Materials - Rock Samples SY-2, SY-3, MRG-1; CANMET Report 79-35, 66 p.

Anders, E. and Ebihara, M.
1982: Solar-System abundances of the elements; Geochimica et Cosmochimica Acta, v. 46, p. 2363-2380.

Campbell, I.H., Franklin, J.M., Gorton, M.P., Hart, T.R., and Scott, S.D.
1981: The role of subvolcanic sills in the generation of massive sulfide deposits; Economic Geology, v. 76, p. 2248-2253.

Cathles, L.M., Gruber, A.L., Lenagh, T.C., and Dudas, F.Ö.
1983: Kuroko-type massive sulfide deposits of Japan: Products of an aborted island-arc rift; in The Kuroko and related Volcanogenic Massive Sulfide Deposits, (ed.) H. Ohmoto and B.J. Skinner; Economic Geology Monograph 5, p. 96-114.

Davies, J.F. and Whitehead, R.E.S.
1980: Further immobile element data from altered volcanic rocks, Timmins mining area, Ontario; Canadian Journal of Earth Sciences, v. 17, p. 419-423.

Davies, J.F., Grant, R.W.E., and Whitehead, R.E.S.
1979: Immobile trace elements and Archean volcanic stratigraphy in the Timmins area, Ontario; Canadian Journal of Earth Sciences, v. 16, p. 305-311.

Dostal, J. and Strong, D.F.
1983: Trace-element mobility during low-grade metamorphism and silicification of basaltic rocks from Saint John, New Brunswick; Canadian Journal of Earth Sciences, v. 20, p. 431-435.

Goodfellow, W.D.
1975: Major and minor element halos in volcanic rocks at Brunswick no. 12 sulphide deposit, N.B., Canada; in Geochemical Exploration 1974, (ed.) I.L. Elliot and W.K. Fletcher; Association of Exploration Geochemistry, Special Publication No. 2, Elsevier, Amsterdam, p. 279-295.

Govindaraju, K.
1994: Compilation of working values and sample description for 383 geostandards; Geostandards Newsletter, v. 18, p. 1-158.

Graham, C.M.
1976: Petrochemistry and tectonic significance of Dalradian metabasaltic rocks of the S.W. Scottish Highlands; Journal of the Geological Society of London, v. 132, p. 61-84.

Hill, J.D.
1974: The petrology of the basic intrusions of the Bathurst-Newcastle area, New Brunswick; M.Sc. thesis, Acadia University, Wolfville, Nova Scotia.

Hughes, C.J.
1973: Spilites, keratophyres, and the igneous spectrum; Geological Magazine, v. 6, p. 513-527.

Humphris, S.E.
1984: The mobility of rare earth elements in the crust; in Rare Earth Element Geochemistry, (ed.) P. Henderson, Developments in Geochemistry 2, Elsevier, Amsterdam, p. 317-342.

Hynes, A.
1980: Carbonatization and mobility of Ti, Y, and Zr in Ascot Formation metabasalts, SE Quebec; Contributions to Mineralogy and Petrology, v. 75, p. 79-87.

Janes, P.A.
1976: Geochemistry of the altered volcanic and intrusive rocks of the Bathurst district, New Brunswick; M.Sc. thesis, University of Montreal, Montréal, Quebec.

Lentz, D.R.
1995: Stratigraphy and structure of the Key Anacon massive-sulphide deposits compared with the Brunswick deposits, Bathurst Mining Camp, New Brunswick; in Geoscience Research 1994, (ed.) J.P. Langton; New Brunswick Department of Natural Resources and Energy, Minerals and Energy Division, Miscellaneous Report 15, p. 23-44.

Lentz, D.R. and Goodfellow, W.D.
1992: Re-evaluation of the petrology and depositional environment of felsic volcanic and related rocks in the vicinity of the Brunswick No. 12 massive sulphide deposit, Bathurst Mining Camp, New Brunswick; in Current Research, Part E; Geological Survey of Canada, Paper 92-1E, 333-342.
1994: Character, distribution, and origin of zoned hydrothermal alteration features at the Brunswick No. 12 massive sulphide deposit, Bathurst Mining Camp, New Brunswick; in Current Research, (ed.) S.A. Abbott; New Brunswick Department of Natural Resources and Energy, Minerals Resources, Information Circular 94-1, p. 94-119.

Lentz, D.R. and van Staal, C.R.
in press: Predeformational origin of massive sulfide mineralization and associated footwall alteration at the Brunswick No. 12, Pb-Zn-Cu deposit, Bathurst, New Brunswick: evidence from the porphyry dyke; Economic Geology, v. 90, No. 2.

Meschede, M.
1986: A method of discriminating between different types of mid-ocean ridge basalts and continental tholeiites with the Nb-Zr-Y diagram; Chemical Geology, v. 56, p. 207-218.

Paktunc, A.D.
1990: Geochemical constraints on the tectonic setting of the mafic rocks of the Bathurst Camp, Appalachian Orogen; Canadian Journal of Earth Sciences, v. 27, p. 1182-1193.

Pearce, J.A.
1982: Trace element characteristics of lavas from destructive plate boundaries; in Andesites: Orogenic Andesites and Related Rocks, (ed.) R.S. Thorpe; John Wiley and Sons, U.K., p. 525-548.

Pearce, J.A. and Cann, J.R.
1973: Tectonic setting of basic volcanic rocks determined using trace element analysis; Earth and Planetary Science Letters, v. 19, p. 290-300.

Pearce, J.A. and Norry, M.J.
1979: Petrogenetic implications of Ti, Zr, Y, and Nb variations in volcanic rocks; Contributions to Mineralogy and Petrology, v. 69, p. 33-47.

Saif, S.I.
1980: Petrographic and geochemical investigation of iron formation and other iron-rich rocks in Bathurst District, New Brunswick; in Current Research, Part A; Geological Survey of Canada, Paper 80-1A, p. 309-317.

Stillman, C.J. and Williams, C.T.
1979: Geochemistry and tectonic setting of some Ordovician volcanic rocks in east and southeast Ireland; Earth and Planetary Science Letter, v. 41, p. 288-310.

Sullivan, R.W. and van Staal, C.R.
1990: Age of metarhyolite from the Tetagouche Group, Bathurst, New Brunswick; from U/Pb isochron analyses of zircons enriched in common Pb; in Radiogenic age and isotopic studies: Report 3; Geological Survey of Canada, Paper 89-2, p. 109-117.

Sullivan, R.W. and van Staal, C.R. (cont.)
1993: U-Pb age of the Canoe Landing Lake Formation, Tetagouche Group, New Brunswick; from U/Pb isochron analyses of zircons enriched in common Pb; in Radiogenic age and isotopic studies: Report 7; Geological Survey of Canada, Paper 93-2, p. 39-43.

van Staal, C.R.
1987: Tectonic setting of the Tetagouche Group in northern New Brunswick: implications for plate tectonic models in the northern Appalachians; Canadian Journal of Earth Sciences, v. 24, p. 1329-1351.

van Staal, C.R. and Sullivan, R.W.
1992: Significance of U-Pb zircon dating of silicic volcanic rocks associated with the Brunswick-Type massive sulphide deposits of the Tetagouche Group [abs.]; Geological Association of Canada/Mineralogical Association of Canada Joint Annual Meeting, Program with Abstracts, v. 17, p. A112.

van Staal, C.R. and Williams, P.F.
1984: Structure, origin, and concentration of the Brunswick #12 and #6 orebodies; Economic Geology, v. 79, p. 1669-1692.

van Staal, C.R., Winchester, J.A., and Bedard, J.H.
1991: Geochemical variations in Middle Ordovician volcanic rocks of the northern Miramichi Highlands and their tectonic significance; Canadian Journal of Earth Science, v. 28, p. 1031-1049.

Walker, J.A. and McDonald, S.M.
1995: Preliminary investigation of the Canoe Landing Lake massive-sulphide deposit, NTS 21 O/8e; in Geoscience Research, (ed.) J.P. Langton; New Brunswick Department of Natural Resources and Energy, Minerals and Energy Division, Miscellaneous Report 15, p. 78-99.

Whitehead, R.E.S. and Goodfellow, W.D.
1978: Geochemistry of volcanic rocks from the Tetagouche Group, Bathurst, New Brunswick, Canada; Canadian Journal of Earth Science, v. 15, p. 207-219.

Winchester, J.A. and Floyd, P.A.
1976: Geochemical magma type discrimination: application to altered and metamorphosed basic igneous rocks; Earth and Planetary Science Letters, v. 28, p. 459-469.
1977: Geochemical discrimination of different magma series and their differentiation products using immobile elements; Chemical Geology, v. 20, p. 325-343.

Winchester, J.A., van Staal, C.R., and Langton, J.P.
1992: The Ordovician volcanics of the Elmtree-Belledune Inlier and their relationship to the northern Miramichi Highlands, New Brunswick; Canadian Journal of Earth Sciences, v. 29, p. 1430-1447.

Wood, D.A.
1980: The application of a Th-Hf-Ta diagram to problems of tectonomagmatic classification and to establishing the nature of crustal contamination of basaltic lavas of the British Tertiary volcanic province; Earth and Planetary Science Letters, v. 50, p. 11-30.

Geological Survey of Canada Project 940001

Stratigraphy and structure of the Glover Group, Grand Lake-Little Grand Lake area, Newfoundland[1]

Adam Szybinski[2], Steve House[2], and G.A. Jenner[2]
Continental Geoscience Division

Szybinski, A., House, S., and Jenner, G.A., 1995: Stratigraphy and structure of the Glover Group, Grand Lake-Little Grand Lake area, Newfoundland; in Current Research 1995-E; Geological Survey of Canada, p. 245-251.

Abstract: The Glover Group comprises a lower Kettle Pond Formation characterized by felsic schists and an upper Tuckamore Formation consisting entirely of mafic volcanic and subvolcanic rocks. The boundary between the Kettle Pond and Tuckamore formations is drawn at the highest felsic horizon. A prominent and widespread horizon of metaconglomerate (Basal Conglomerate Member), separates the Kettle Pond Formation from the underlying ophiolitic Grand Lake Complex. The structure of south-central Glover Island is controlled by complicated fold interference patterns, resulting from the overprinting of D_2-related folds by D_3 folds.

Résumé : Le Groupe de Glover comprend la formation inférieure de Kettle Pond caractérisée par des schistes felsiques et la formation supérieure de Tuckamore constituée entièrement de roches volcaniques et hypovolcaniques mafiques. La limite entre les formations de Kettle Pond et de Tuckamore est tracée à l'horizon felsique le plus élevé. Un horizon métaconglomératique étendu et visible (Membre conglomératique basal) sépare la Formation de Kettle Pond du complexe ophiolitique sous-jacent de Grand Lake. La structure du centre sud de l'île Glover est contrôlé par des schémas complexes d'interférence de plis résultant de la surimpression de plis associés D_2 par des plis D_3.

[1] Contribution to Canada-Newfoundland Cooperation Agreement on Mineral Development (1994-1995), a subsidiary agreement under the Canada-Newfoundland Economic and Regional Development Agreement.
[2] Department of Earth Sciences, Memorial University of Newfoundland, St. John's AIB 3X5

INTRODUCTION

This report presents preliminary results from the mapping project carried out on rocks of the Glover Group (Knapp, 1982) during 1994. Mapping was confined to rocks of the group on Glover Island (Fig. 1a),where exposure is poor, (see also Cawood and van Gool, 1994) and concentrated on rocks in the interior of the island. In particular,emphasis was on the immediate area of Kettle Pond in the south-central part of Glover Island, in which the quantity and quality of outcrop is somewhat improved thanks to rugged topography and efforts of geologist(s) from Newfoundland Gold Bar Ltd. This area is located within the nose of a regional scale fold (the Glover Anticline of Knapp, 1982; Cawood and van Gool, 1993, 1994). The Glover Anticline represents one of several large structures, reflecting interference patterns produced by intensive overprinting of structural elements produced during different deformational events. Observations from this area were extrapolated southwest and northeast of the pond, where only subcrop and limited outcrop were found.

PREVIOUS WORK

The term Glover Group was applied by Knapp (1982) to a unit which was originally introduced by Riley (1957) as the Glover Formation. Knapp (1982) divided the group into the Kettle Pond (quartz-sericite-schist, metaconglomerate) and Tuckamore (variably interfingered silicic and mafic schists, volcanic and volcaniclastic rocks) formations, and excluded from it several rock types previously included by Riley (1957) in the Glover Formation. The excluded rock units were assigned by Knapp (1982) to the Grand Lake Complex (variably serpentinized and carbonitized ultramafic rocks, gabbro, trondhjemite, sheeted dykes, greenschist), Otter Neck Group (sheeted dykes, pillow lava), and Red Point (metasandstone and metaconglomerate, phyllite) and Corner Pond (metasandstone, metaconglomerate, pillow lava) formations. All of Knapp's (1982) lithostratigraphic divisions are considered informal.

Cawood and van Gool (1993, 1994) abandoned the Kettle and Tuckamore formations of Knapp (1982) and returned to the term Glover Formation (cf. Riley, 1957), but applied it only to mafic igneous rocks east of the Grand Lake Complex. Rocks included previously in the Kettle and Tuckamore formations are considered by these authors to form a large folded shear zone, the Kettle Pond shear zone, dividing the Grand Lake Complex and the Glover Formation.

The Newfoundland Gold Bar Ltd. geologists working on Glover Island use a modified version of the lithostratigraphic scheme of Knapp (1982) and presently recognize three formations, namely the Kettle Pond, Tuckamore and Glover formations (D. Barbour, pers. comm.). These include rocks previously included in the Glover Group, with rocks of the former Tuckamore Formation split between the modified Tuckamore (schistose felsic and mafic volcanic and volcaniclastic rocks) and Glover (predominantly mafic igneous rocks) formations.

PRESENT MAPPING

Our recent mapping on Glover Island (Fig. 1b) provided data that permit several changes to both presently used lithostratigraphic divisions (Knapp, 1982; Cawood and van Gool, 1993, 1994) and allows better understanding of structural evolution of the Kettle Pond area. Our field observations disagree with the outcome of work by Cawood and van Gool (1993, 1994), and allow us to conclude that the Kettle Pond and the Tuckamore formations represent stratigraphic units rather than a large shear zone. These observations support the validity of the lithostratigraphic divisions proposed by Knapp (1982), and we continue to use the name Glover Group as defined by Knapp (1982), as well as the names Kettle Pond and Tuckamore formations. However, we suggest some modifications, namely that all felsic rocks (schistose and apparently less metamorphosed or deformed varieties) previously included in the Tuckamore Formation should be removed from this formation and included in the Kettle Pond Formation, for reasons described below. A brief description of formations included in the Glover Group and of the associated Grand Lake Complex are given below.

Grand Lake Complex

The Grand Lake Complex (Knapp, 1982) is exposed northwest of Kettle Pond, where it consists of ultramafic rocks (represented by variably serpentinized pyroxenites and peridotites), fine- to coarse-grained gabbro (that intrudes the ultramafic rocks), diabase, greenschist, and sporadic mafic dykes. Small trondhjemitic and dioritic intrusions are found exclusively near the fault(?) contact between the Grand Lake Complex and Glover Group and are included in the complex, although their relationship to the complex is not clear at the moment. An outcrop of rocks believed to be sheeted dykes and included in the Grand Lake Complex (Knapp, 1982) was found to be altered ultramafic characterized by a layering of obscure origin.

Kettle Pond Formation

The Kettle Pond Formation is exposed best east and southeast of Kettle Pond. The southwestern shoreline of the pond is underlain by a distinct horizon of clast supported polymictic metaconglomerate that forms the lowermost rock unit of the Kettle Pond Formation along its contact with the Grand Lake Complex. It is here referred informally to as the Basal Conglomerate member. Our mapping indicates that exposure of this conglomerate extends northeast well beyond area previously mapped by Knapp (1982). The actual contact between the Kettle Pond Formation and the Grand Lake Complex has not been observed, and in all outcrops in which rock types of both units are exposed together, they appear to be divided by a shear zone or gap in exposure. In places, this contact is marked by slivers of mafic schist interpreted by some workers (D. Barbour and T. Calon, pers. comm.) as strongly deformed mafic dykes intruding the contact, although we feel that the mafic schist could represent a schistose equivalent of otherwise more massive mafic intrusive or volcanic (?) rocks of the Grand Lake Complex.

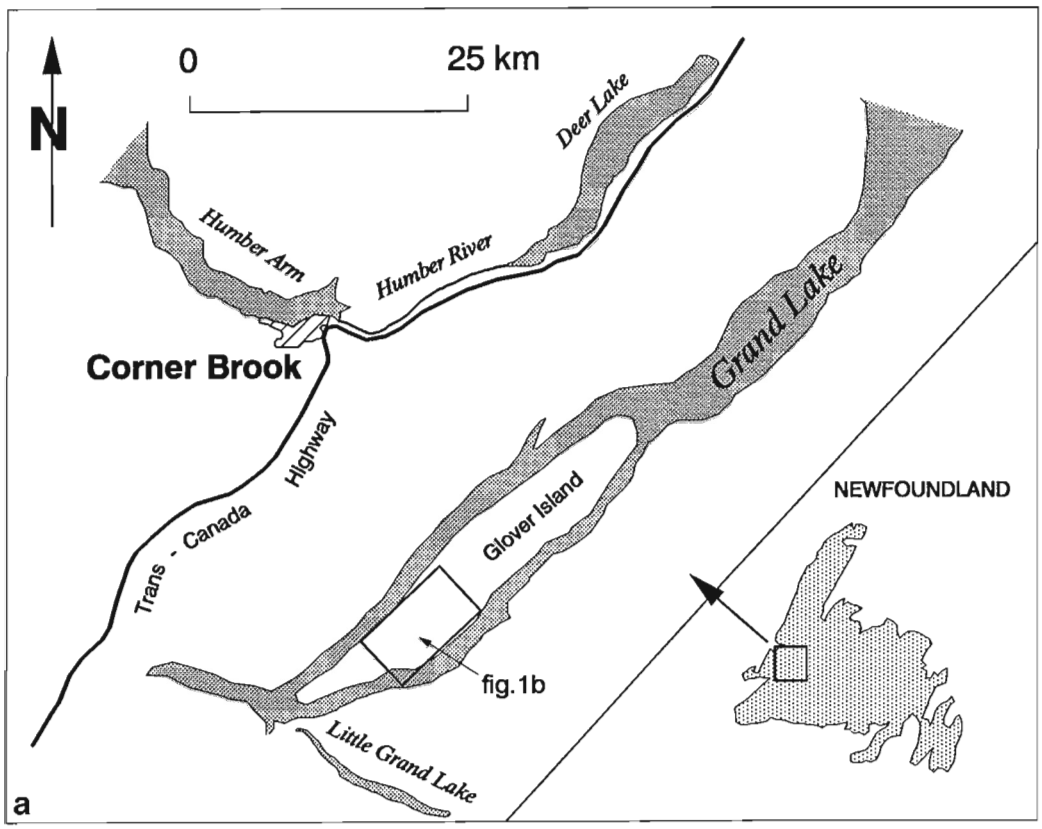

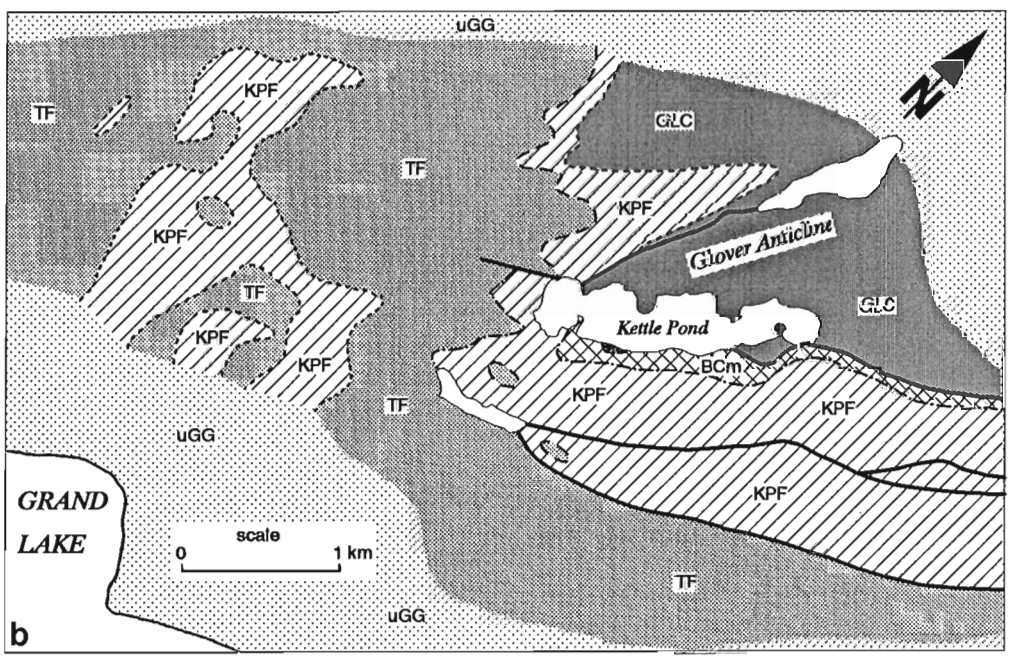

Units:

uGG - undivided Glover Group
TF - Tuckamore Formation
KPF - Kettle Pond Formation
BCm - Basal Conglomerate member
GLC - Grand Lake Complex

Symbols:

geological boundary
known
approximate
assumed

fault

*Figure 1. Location of the map area in western Newfoundland (**a**), and schematic geological map of the Kettle Pond area in southern Glover Island (**b**).*

Two endmember types of the conglomerate are present, one which contains predominantly clasts of various (fine grained to pegmatitic) types of trondhjemite surrounded by a felsic matrix, and the other type which consists mainly of hornblende gabbro and diabase cobbles immersed in a mafic matrix. However, most of the Basal Conglomerate member is transitional between these two end-members, and contains mixture of clasts in a composite matrix. The matrix of this conglomerate was probably tuffaceous sedimentary material. Locally it is strongly schistose and thinly laminated consisting of quartz-plagioclase laminae divided by sericite-chlorite films, and associated clasts are commonly stretched. Sparse massive mafic flows are present near the base of the member.

The Basal Conglomerate is overlain by thinly laminated quartz-sericite (± plagioclase and chlorite) schist, which in places contains variable amounts of trondhjemite and lesser felsic volcanic clasts, and sparse gabbro and reddish-grey hematitic chert. Locally, aggregates of fuchsite are present in the schist, probably derived from the underlying Grand Lake Complex. The presence of fuchsite and hematitic chert clasts in siliceous schist is used by exploration geologists in the area as a method of identifying the Kettle Pond Formation schist, and separating it from an apparently similar schist that forms the base of the Tuckamore Formation, as defined by Knapp (1982) (D. Barbour, pers. comm.). We feel that the somewhat erratic presence of the chert and fuchsite is a feature inadequate to warrant the division of siliceous schists between these two formations. The only major difference seen in the field between siliceous schists included in the Kettle Pond Formation and those formerly in the Tuckamore Formation is the presence of probable subvolcanic massive sills intruding the latter unit, particularly northeast of Kettle Pond. Taking under consideration the overall similarity of felsic rocks in both formations, felsic rocks of the Tuckamore Formation as defined by Knapp (1982), including those interlayered with the mafic schistose tuffs, are included here in the Kettle Pond Formation. The highest horizon of felsic schist in the Kettle Pond Formation is considered here to form the boundary between these formations.

Tuckamore Formation

As we have redefined the Tuckamore Formation, it consists of schistose mafic tuffs, less deformed pillowed to massive and locally brecciated flows, and fine- to medium-grained, frequently plagioclase-phyric, mafic intrusive rocks. The lowermost part of the Tuckamore Formation is strongly schistose in places (in particular where it interleaves with the felsic schists of the Kettle Pond Formation), but otherwise bedded to massive mafic tuffs are interbedded with sparse lenses of pillow lava and/or pillow breccia. The interleaving of siliceous felsic schists of the Kettle Pond Formation with mafic schistose tuffs of the Tuckamore Formation (as defined by Knapp, 1982) was observed only south and southwest of the pond. The contact between rocks of these formations east and northeast of Kettle Pond is commonly faulted, and here mainly intrusive mafic rocks of the Tuckamore Formation are juxtaposed with siliceous schists of the Kettle Formation. The main part of the Tuckamore Formation is made up of poorly pillowed to massive mafic volcanic and subvolcanic rocks.

PRELIMINARY PALEOTECTONIC DIVISIONS

The preliminary results of a geochemical sampling of volcanic, subvolcanic, and volcaniclastic rocks within the southern part of Glover Island indicate that rocks in this area formed in at least two distinct tectonic settings. This is reflected in a relatively wide range of Ti, Zr, and V abundances and immobile elements ratios as illustrated by the Ti-V and Zr-Ti diagrams (Fig. 2a, b). On the Ti-V diagram, samples have a relatively broad range of Ti and V abundances and Ti/V ratios between 20-50, similar to that expected in Mid Ocean Ridge Basalts (MORB). The same set of samples plots within the ocean floor basalt (OFB) field and beyond (towards ocean island basalt (OIB) compositions) on the Zr-Ti diagram, which supports their non-arc oceanic affinity. However, some samples plot mainly in the arc field on the Zr-Ti diagram, as calc-alkalic basalts (CAB) and low-K tholeiites (LKT). These geochemical relationships are consistent with, although not definitive of, an arc tectonic setting.

To test the validity of this division into arc and non-arc types based on Ti-V-Zr, the next step was to determine if samples in these sets have developed the more definitive arc geochemical signature, i.e. Nb depletion with respect to Th. On the Th-Zr-Nb diagram of Wood (1980) (Fig. 2c), samples that already revealed a non-arc affinity on the basis of the Ti-V and Ti-Zr variations display relatively high Nb/Th ratios and plot within the MORB field, however one sample that previously revealed the non-arc affinity plots within the arc field. This same sample plots in the arc field on the Th/Nb-Nb/Yb diagram of Pearce (1983) (Fig. 2d) and appears to possess geochemical signatures which are transitional between arc and non-arc.

The Glover Group/Grand Lake Complex volcanic rocks can be divided into two major types displaying diverse tectonic affinities: **NA-type:** non-arc volcanic rocks that include samples identified as having oceanic affinity on most of tectonic discrimination diagrams; **A-type:** arc volcanic rocks encompassing samples of clearly defined arc affinity. There is the possibility of a third **TR-type** of rocks transitional in geochemical characteristics between rocks erupted in non-arc and arc settings.

STRUCTURE

The main problems with establishing a definitive lithostratigraphic framework for the southern part of Glover Island stems from the locally intense and strongly heterogeneous brittle and plastic deformation that has predominantly affected rocks of the Kettle Pond Formation, as well as adjacent rocks of the Tuckamore Formation and Grand Lake Complex. Strain has been partitioned heterogenously between the locally isotropic to highly anisotropic conglomerates, and the overlying, isotropic to partially anisotropic felsic tuffs of the Kettle Pond Formation, and the interbedded mafic tuff facies. Felsic tuffs and sparse dykes form aspectrum of final lithological products that vary from brecciated felsic protolith to a widespread mylonite represented by quartz-sericite schist. A whole range of structures can be seen in pillowed

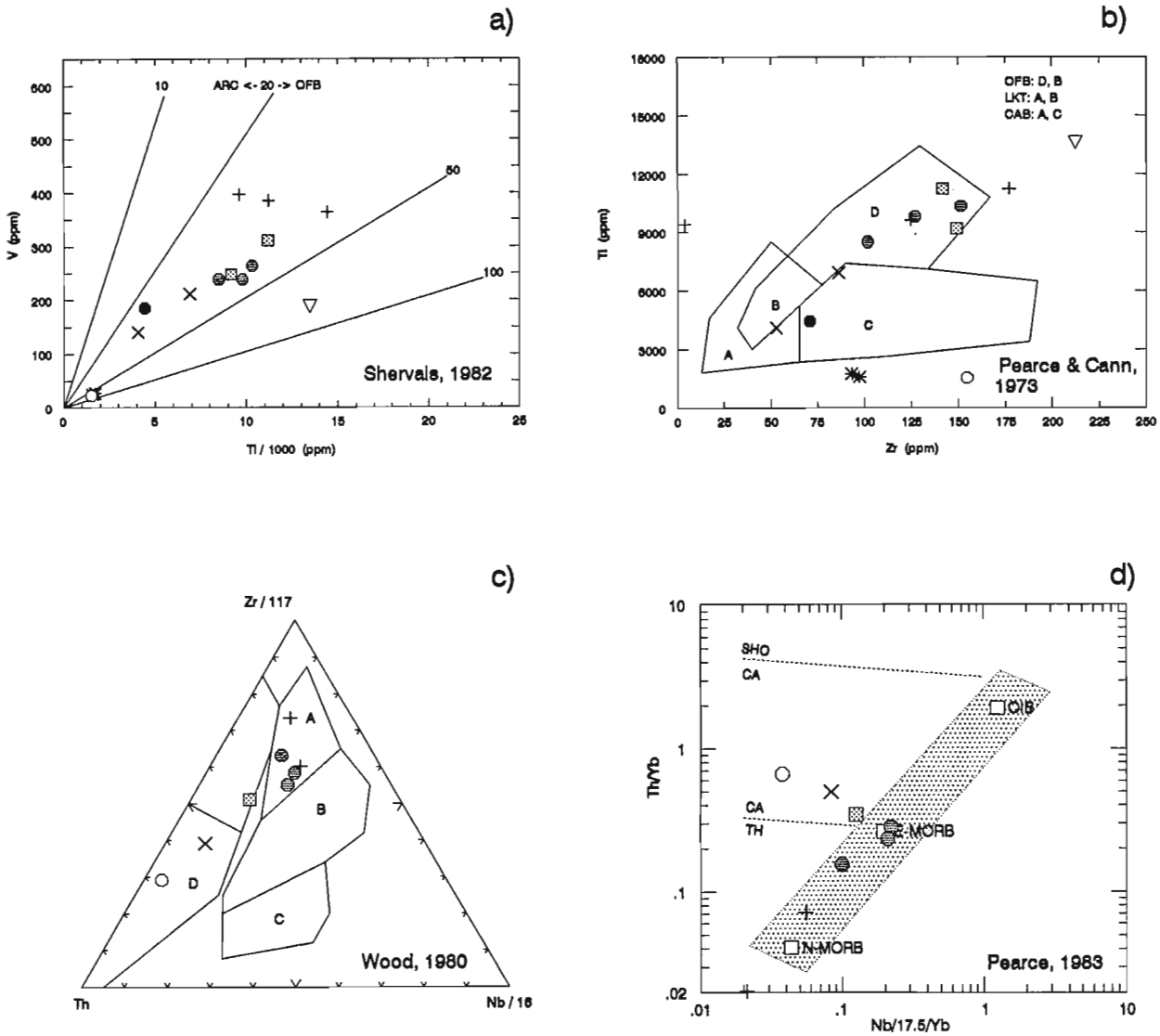

Legend of symbols:

- ● calc-alkalic pillow basalt, Tuckamore Fm.
- ⊗ non-arc pillow basalt, Tuckamore Fm.
- ⊠ massive flows, Kettle Pond Fm.
- ○ felsic tuff, Kettle Pond Fm.
- × sill, Kettle Pond Fm.
- ▽ mafic sill, Tuckamore Fm.
- + gabbro and diabase, Grand Lake Complex
- ✳ trondhjemite, Grand Lake Complex (?)

Figure 2. *The Ti/1000-V diagram (**a**) and Zr-Ti diagram (**b**) indicate two broad tectonic settings (non-arc and arc), in which the mafic (and one felsic) volcanic rocks of the Glover Island formed. The Th-Zr-Nb diagram (**c**) and Nb/Yb-Th/Yb diagram (**d**) provide, as well, division of the samples into the arc and non-arc types, and indicate an extistence within the samples of a third type with the transitional character. Fields A, B, and C in Figure 2c are non-arc,while field D is arc. Abbreviations are defined in text.*

and massive flows, and mafic tuffs of the Tuckamore Formation resulting from the brittle fracturing, as well as from a higher degree of penetrative strain.

At least three events were identified in the deformational history of the Kettle Pond area on the basis of structural and geological observations, but timing of these events is unclear. These events are described briefly below and a summary of structural elements recognized in the field is given in Figure 3. D_1 deformation is a regionally penetrative event that produced the dominant fabric seen in the rocks, i.e. S_1 foliation. The strongly mylonitic S_1 foliation appears to parallel S_0. The S_1 fabric is refolded by folds associated with at least two following major events, giving a wide distribution of normal to S_1 planes around the edges of a stereonet (Fig. 3). The S_1 foliationis associated with a locally well developed mineral lineation, that is moderately to steeply plunging and slightly oblique to the azimuth of the S_1 fabric. However, distribution of this lineation on the stereonetis suprisingly clustered (Fig. 3), suggesting possible association with one of the younger events postdating D_1. S_1, best developed in rocks of the Kettle Pond Formation, is heteregenously distributed and decreases in intensity away from rocks of this formation, but it is present as well in the Grand Lake Complex and the Tuckamore Formation rocks.

The D_2 and D_3 deformational events fold the S_0/S_1 fabric and produce complex large scale fold interference patterns. The most prominent fold produced is the F_2/F_3 half-dome and the surrounding basin-type folds in the Kettle Pond area (Fig. 1b). A more complex, "mushroom"– type fold interference pattern, that results from the overprint of the F_2 fold by the F_3 structure, is developed southwest of Kettle Pond (Fig. 1b).

On outcrop scale both the F_2 and F_3 events produced similar, frequently chevron-style folds and associated wide-spaced crenulation cleavage. However, features resulted from the D_2 and D_3 are rarely exposed together in single outcrop, and there is some overlap in orientation of the S_2 and S_3 foliations, which display azimuths between 120-240° and 70-150°, respectively.

SUMMARY

This mapping supports, in general, the stratigraphic divisions of Knapp (1982). Some changes to that scheme include removal of all felsic rocks from the Tuckamore Formation, and placing them together with felsic schists of the Kettle Pond Formation. In our version of the stratigraphy of central Glover Island, the Tuckamore Formation consists only of

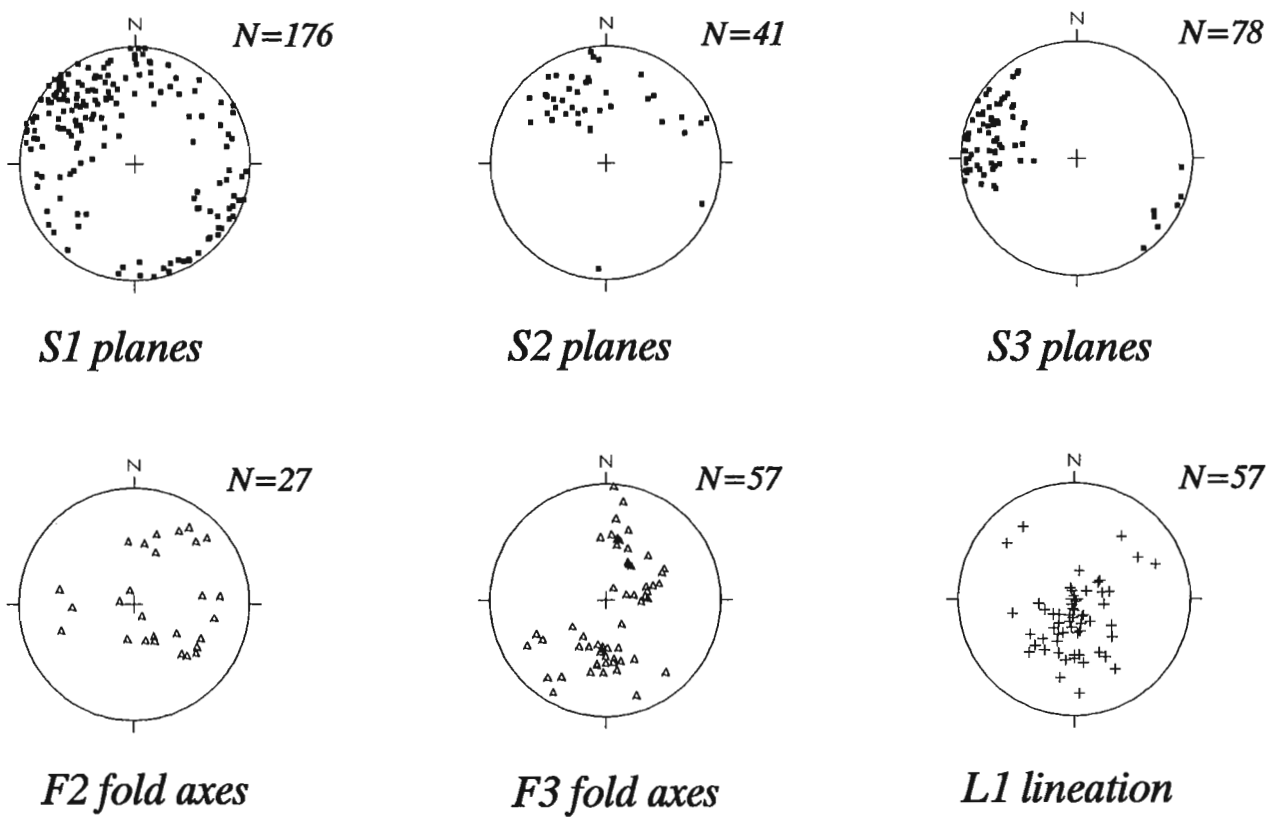

Figure 3. *Structural orientation data for the map area presented in Figure 1b. Poles to planes (S_1, S_2 and S_3), and linear structural elements (F_2, F_3, L_1) are plotted on equal-area projection and lower hemisphere stereo plots.*

mafic volcanic and subvolcanic rocks, and the boundary between the Kettle Pond and Tuckamore formations is drawn at the highest felsic horizon. The prominent horizon of polymictic to monomictic, clast supported metaconglomerate on the contact between the Grand Lake Complex and the Kettle Pond Formation is raised to the member level and appropriately named the Basal Conglomerate Member. The area of outcrop of this conglomerate was found to be much larger than previously found by Knapp (1982).

The structure of south central Glover Island is much more complex than indicated by previous studies (Knapp, 1982; Cawood and van Gool, 1993, 1994) and is controlled by complicated fold interference patterns, resulting from the overprinting of D_2 related folds by D_3 folds.

ACKNOWLEDGMENTS

This project is a part of the Canada-Newfoundland Mineral Development Agreement 1994-1995. Ken L. Currie acts as scientific authority for the project and we thank him for his support. We particularly thank D. Barbour for the insightful introduction into geology of the Kettle Pond area and stimulating discussions in the field, and T. Calon for similarly helpful comments afterwards. We are indebted to V. French for allowing us to set our tents in the relative safety of his camp. Andrea Mills provided capable assistance in the swamps of Glover Island.

REFERENCES

Cawood, P.A. and van Gool, J.A.M.
1993: Stratigraphic and structuralrelations within the western Dunnage Zone, Glover Island region, western Newfoundland; in Current Research, Part D; Geological Survey of Canada, Paper 93-1D, p. 29-37.

Cawood, P.A. and van Gool, J.A.M.
1994: Geology of the Corner Brook Lake region, Corner Brook, Newfoundland; Geological Survey of Canada, Open File 2830, scale 1:50 000.

Knapp, D.A.
1982: Ophiolite emplacement along the Baie Verte-Brompton Line at Glover Island, western Newfoundland; Ph.D. thesis, Memorial University of Newfoundland, St. John's, 338 p.

Pearce, J.A.
1983: Role of the sub-continental lithosphere in magma genesis at active continental margins; in Continental Basalts and and Mantle Xenoliths; by C.J. Hawkesworth and M.J. Norry (ed.); Nantwich, Shiva, p. 230-249.

Pearce, J.A. and Cann, J.R.
1973: Tectonic setting of basic volcanic rocks determined using trace element analyses. Earth and Planetary Science Letters, v. 19, p. 290-300.

Riley, G.C.
1957: Red Indian Lake (west half), Newfoundland; Geological Survey of Canada, Map 8-1957.

Shervais, J.W.
1982: Ti-V plots and the petrogenesis of modern and ophiolitic lavas. Earth and Planetary Science Letters, v. 59, p. 101-118.

Wood, D.A.
1980: The application of a Th-Hf-Ta diagram to problems of tectonomagmatic classification and to establishing the nature of crustal contamination of basaltic lavas of the British Tertiary volcanic province; Earth and Planetary Scince Letters, v. 50, p. 11-30.

Geological Survey of Canada Project 730044

Phase equilibrium constraints on the stability of biotite. Part 1: Mg-Al biotite in the system K_2O-MgO-Al_2O_3-SiO_2-H_2O-CO_2

R.G. Berman, L. Ya Aranovich[1], M. Genkin[2], U.K. Mader[3]
Continental Geoscience Division

Berman, R.G., Aranovich, L. Ya, Genkin, M., and Mader, U.K., 1995: Phase equilibrium constraints on the stability of biotite. Part 1: Mg-Al biotite in the system K_2O-MgO-Al_2O_3-SiO_2-H_2O-CO_2; in Current Research 1995-E; Geological Survey of Canada, p. 253-261.

Abstract: The stability of Mg-biotite has been determined from two sets of reversed phase equilibrium data. First, the equilibrium: phlogopite+quartz=enstatite+sanidine+H_2O has been reversed in pure H_2O and mixed H_2O-CO_2 fluid. Second, tight brackets define constant Al saturation at 1.62 ± 0.06 Al pfu (12 anion formula) in Mg-biotite in equilibrium with sillimanite+sanidine+quartz+H_2O over the P-T range 1.1-3.2 kbar and 650-750°C. The experimental data indicate significantly lower Al contents in Mg-biotite and a larger phlogopite stability field than predicted by Holland and Powell's (1990) data set, but agree reasonably with phlogopite stability based on Berman (1988). Thermodynamic properties refined from the new data for the biotite endmembers, phlogopite and eastonite, when combined with constraints on Fe-endmembers provide for more accurate construction of petrogenetic grids and thermobarometric calculations involving biotite.

Résumé : À partir de deux ensembles de données sur l'équilibre de phase inversé, on a déterminé la stabilité de la biotite-Mg. En premier lieu, l'équilibre phlogopite+quartz=enstatite+sanidine+H_2O a été inversé en H_2O pure et en fluide H_2O-CO_2 mélangé. En deuxième lieu, les expériences ont permis de définir une saturation en Al constante à 1,62 ± 0,06 unité par formule de Al (formule à 12 anions) dans la biotite-Mg en équilibre avec sillimanite+sanidine+quartz+H_2O dans l'intervalle de pression de 1,1-3,2 kbar et de l'intervalle de température de 650-750 °C. Les données expérimentales indiquent un abaissement significatif des teneurs en Al dans la biotite-Mg et un champ de stabilité de la phlogopite plus vaste que prévu par les ensembles de données de Holland et Powell (1990), mais elles correspondent raisonnablement avec la stabilité de la phlogopite selon Berman (1988). Les propriétés thermodynamiques établies avec plus de précision à partir des nouvelles données obtenues pour les membres extrêmes de la biotite, soit la phlogopite et l'eastonite, lorsque combinées aux données sur les membres extrêmes à Fe, permettent de dresser des grilles pétrogénétiques plus exactes et d'effectuer des calculs thermobarométriques incluant la biotite.

[1] Inst. Experimental Mineralogy, Chernogolovka, Russia
[2] Department of Geology, University of Ottawa, Ottawa, ON K1N 6N5
[3] Dept. Mineralogie, Bern Universität, Bern, Switzerland

INTRODUCTION

Over the past five years, the thermodynamic data sets of Berman (1988) and Holland and Powell (1990) have been used extensively for thermobarometric and phase diagram calculations. In addition to these tectonic/petrological applications, investigations of a number of other problems in the earth sciences, such as ore genesis/exploration, waste disposal, and other environmental issues depend critically on the availability of accurate, internally consistent sets of thermodynamic data for minerals, aqueous species, and gases. Because internal consistency is not a guarantee of accuracy (Berman, 1988), continuing efforts are needed to test and improve the accuracy of thermodynamic data sets. A significant step in this direction has been taken recently by including nonideal mixing models into the derivation of an updated thermodynamic data set for minerals (Berman and Aranovich, in press). The present two-part contribution was designed to improve thermodynamic data for biotite.

Biotite is particularly important in petrogenetic grids for pelitic rocks because of its occurrence in a wide range of bulk compositions, metamorphic grades, and numerous important uni- and divariant equilibria that serve as major metamorphic facies boundaries. In spite of its obvious importance, quantitative calculations involving biotite continue to be relatively uncertain, as evidenced by major differences in computed petrogenetic grids (Spear and Cheney, 1989; Powell and Holland, 1990) and thermobarometric formulations involving biotite (Ferry and Spear, 1978; Dasgupta et al., 1991). Much of this uncertainty stems from incomplete knowledge of the stability of the most important biotite endmembers, Phl and Ann (see Table 1 for abbreviations). Data in the Fe-system are discussed in Part 2 (Berman et al., 1995). In the Mg-system, experimental results on the stability field of Phl+Qz relative to En+Sa in pure H_2O (Wood, 1976; Wones and Dodge, 1977; Peterson and Newton, 1989) are compatible

Table 1. Abbreviations and chemical formulas.

Name	Abbrev	Formula
Annite	Ann	$K(Fe_3)(AlSi_3)O_{10}(OH)_2$
Phlogopite	Phl	$K(Mg_3)(AlSi_3)O_{10}(OH)_2$
Phlogopite$_{45}$	Phl$_{45}$	$K(Mg_{2.45}Al_{0.55})(Al_{2.55}Si_{1.45})O_{10}(OH)_2$
Eastonite	East	$K(Mg_2Al)(Al_2Si_2)O_{10}(OH)_2$
Siderophyllite	Sdr	$K(Fe_2Al)(Al_2Si_2)O_{10}(OH)_2$
Muscovite	Ms	$K(Al_2)(AlSi_3)O_{10}(OH)_2$
Enstatite	En	$MgSiO_3$
Sanidine	Sa	$KAlSi_3O_8$
Sillimanite	Si	Al_2SiO_5
Quartz	Qz	SiO_2

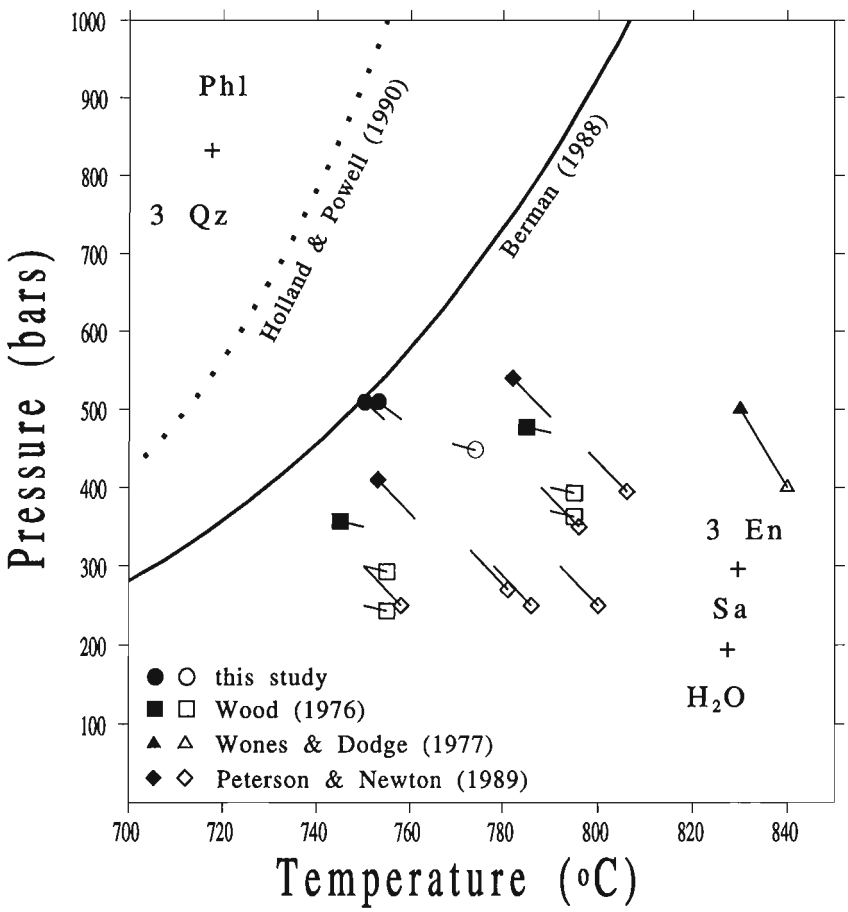

Figure 1.

P-T diagram showing experimental data for equilibrium A in pure H_2O along with its position calculated with thermodynamic data of Berman (1988; solid curve) and Holland and Powell (1990; dotted curve). Symbols show experimental data after adjustment for experimental uncertainties, while ends of connected lines show nominal experimental conditions. Solid and open symbols show growth of low-T and high-T assemblages, respectively.

with one another (Fig. 1), but all are discordant with results in mixed H_2O-CO_2 fluids (Bohlen et al., 1983) that suggest a smaller stability field for phlogopite.

Much more severe uncertainties attend calculations involving the aluminous biotite endmember, eastonite. The primary cause of these uncertainties is that pertinent phase equilibrium data (Robert, 1976) are unreversed. Nevertheless, these data show the important effect of excess Al expanding the thermal stability of biotite, an effect that explains some differences between petrogenetic grids computed with excess Al in biotite (Powell and Holland, 1990) and without excess Al in biotite (Spear and Cheney, 1989).

The present contribution represents the first of a two-part experimental study aimed at resolving some of the deficiencies and discrepancies cited above. In this paper (part 1) we (a) resolve the above noted discrepancy regarding endmember phlogopite stability by presenting new experimental data in both mixed H_2O-CO_2 and pure H_2O fluids on the equilibrium:

$$\text{Phl} + 3\ \text{Qz} = 3\ \text{En} + \text{Sa} + H_2O \qquad \text{(A)}$$

and (b) determine the stability of the eastonite endmember by presenting reversals of the equilibrium:

$$3\ \text{East} + 6\ \text{Qz} = 2\ \text{Phl} + 3\ \text{Si} + \text{Sa} + H_2O \qquad \text{(B)}$$

Results are used to derive new thermodynamic data for eastonite and phlogopite, which, when combined with constraints on Fe-biotite stability (Part 2, Berman et al., 1995) can be used to improve geothermobarometric calculations, to construct more accurate petrogenetic grids, and to perform forward modelling for any given rock composition (Spear and Florence, 1992; Berman and Aranovich, in prep.).

EXPERIMENTAL METHODS

Hydrothermal Apparatus

All experiments were conducted in cold-seal hydrothermal apparatus, with pressure vessels made from Haynes Alloy #25 (stellite) or Rene' 41, and H_2O as the pressure medium. Each pressure vessel was monitored by a 60 000 psi digital strain sensor (± 0.2% linearity), calibrated to a Heise burdon-tube gauge certified by the manufacturer as accurate to ± 0.1% of full scale (0-50 000 psi). The Heise gauge was maintained at 1 atm except when calibrating the transducers. Reported pressures are believed to be accurate to within ± 15 bars.

Temperatures were controlled and continuously monitored by a digital data acquisition and control system made by Sciemetric Inc., Ottawa, Ontario. Temperatures were measured using chromel-alumel thermocouples sheathed in inconel, inserted into a 2 cm well adjacent to the experimental charge. Each thermocouple was calibrated against a lab standard periodically in order to check for thermocouple drift with extended use. The lab standard was calibrated against the melting points of Zn (440.3°C), Al (660.8°C), and Ag (960.8°C). Offsets of measuring thermocouples relative to a "standard" thermocouple placed within the pressure vessels were less than 5°C at 1 atmosphere. Measurements at 1 atm indicate that temperature gradients were between 1.5 and 3°C over a distance of 3.0 cm. Temperature uncertainties reported in Tables 2 and 3 represent the sum of uncertainties due to fluctuations over the duration of the experiment, thermocouple calibration uncertainties (1°C), temperature gradients over the length of run capsules, and the temperature gradient across the Sciemetric control unit in which the zero point emf correction is made (1°C).

Table 2. Experiments on equilibrium A; Phl + 3 Qz = 3 En + Sa + H_2O.

Run #	Time (days)	T(°C)	P(kbar)	X_{CO_2} (initial)	X_{CO_2} (final)	Stable Assemblage	% Reaction Observed
2	25	780 ± 5.0	2.56 ± 0.08	0.79	nd	En + Sa	100
3	18	782 ± 6.0	2.49 ± 0.05	0.67	0.65	En + Sa	100
5	23	772 ± 4.0	2.53 ± 0.06	0.35	0.38	Phl + Qz	90
8	22	696 ± 6.0	2.54 ± 0.04	0.50	0.51	Phl + Qz	100
10	22	756 ± 5.0	2.47 ± 0.03	0.50	0.47	Phl + Qz	90
11	22	810 ± 6.0	2.49 ± 0.08	0.50	0.47	?	0
12	22	771 ± 7.0	2.61 ± 0.09	0.50	0.39	Phl + Qz	100
14	21	757 ± 7.0	1.76 ± 0.02	0.45	0.45	Phl + Qz	30
15	18	782 ± 6.5	1.74 ± 0.03	0.45	0.45	En + Sa	70
18	21	768 ± 4.0	1.74 ± 0.02	0.45	0.49	En + Sa	40
19	21	760 ± 4.0	1.74 ± 0.02	0.45	0.49	Phl + Qz	50
20	23	769 ± 5.0	0.46 ± 0.01	0.0	0.0	En + Sa	60
21	24	758 ± 6.0	0.49 ± 0.02	0.0	0.0	Phl + Qz	80
22	23	755 ± 5.0	0.49 ± 0.02	0.0	0.0	Phl + Qz	70

All fluid compositions represent initial compositions based on weighed amounts of $Ag_2C_2O_4$ + H_2O, except for runs # 14-19 in which oxalic acid was used, and # 20-22 which used pure H_2O; P-T uncertainties represent the sum of both precision and accuracy

Run Procedures

Experiments with H_2O-CO_2 fluid used 3 mm O.D. (0.1 mm wall) Au or 3.5 mm O.D. (0.2 mm wall) Pt capsules, containing about 5 mg of either $Ag_2C_2O_4$+H_2O (carefully weighed to yield specific fluid compositions) or oxalic acid (for fluid compositions of Xco_2 = 0.45), together with about 5 mg of mineral mix A. This mix contained about 10 wt.% of the low temperature assemblage of equilibrium A (with molar proportions Phl:Qz = 1:3) and 90% of the high temperature assemblage (with molar proportions (En:Sa = 3:1), homogenized by light grinding for about 10 minutes in an agate mortar. Experiments on equilibrium A in pure H_2O used 2 mm O.D. (0.1 mm wall) Au capsules, containing about 5 mg H_2O and 5 mg of mineral mix A. To study equilibrium B, two capsules were used in each experiment, one with low-Al biotite (Phl) and the other with high-Al biotite (Phl_{45}), both mixed in subequal weight proportions with Si, Sa, and Qz. Each capsule contained about 5 mg of mix and 5 mg of H_2O. All minerals used in the above mixes are described below. In all experiments, capsules were placed within a cavity in the end of steel filler rod. The opposite (cold) end of the filler rod was tapped and threaded in order to facilitate its removal with the sample capsules at the conclusion of each experiment.

Experiments were held at elevated pressure and temperature for durations of 18-29 days, and then quenched in a jet of compressed air to less than 100°C within 3 minutes. Samples were examined optically, by XRD, SEM, and microprobe. For equilibrium A, reversals were obtained by comparison of the intensities of non-overlapping XRD peaks (001 for Phl; 610 for En; $\bar{1}30$ for Sa) of the run product with the starting material. A half-bracket was considered successful if more than 30% change in peak ratios was observed. Fluid compositions determined after each experiment could not be used as reliable monitors of reaction direction because the observed changes were of the same magnitude as the analytical uncertainties (see below). For equilibrium B, reversals were obtained from electron microprobe analysis of the compositions of biotites in run products. Successful runs produced similar biotite compositions from the starting mixes with Phl and Phl_{45}.

Table 3. Experimental data for the assemblage Mg-biotite-Si-Sa-Qz-H_2O.

Run #	Time (Days)	T(°C)	P(kbar)	Initial Al[1]	Final Al
23	24	700 ± 4	1.24 ± 0.07	1.0	1.38-1.64
24	24	700 ± 4	1.24 ± 0.07	2.1	1.68-1.63
25	24	647 ± 4	1.12 ± 0.03	1.0	1.34-1.61
26	24	647 ± 4	1.12 ± 0.03	2.1	1.72-1.64
30	24	755 ± 4	1.12 ± 0.03	2.1	1.58-1.62
29	24	755 ± 4	1.12 ± 0.03	1.0	1.74-1.62
21	29	702 ± 4	3.20 ± 0.05	1.0	1.46-1.62
22	29	702 ± 4	3.20 ± 0.05	2.1	1.99-1.59

Al values are the # of cations based on 12 anion formula
[1] Initial biotites have Al = 1.0 (Phl) or 2.1 (Phl_{45})

Analytical methods

For cell refinements, X-ray diffraction scans were made over the 2θ range 5 to 90° with a Phillips automated diffractometer, using a step size of 0.01° 2θ, and Cu radiation. Si metal (a = 5.43054 A°) was used as an internal standard in each run. Cell refinements were performed using the computer program of Appleman and Evans (1973).

Fluid compositions of the run products of experiments on equilibrium A were determined by the method of Johannes (1969). CO_2 was first determined by the weight lost upon puncturing sample capsules. H_2O was then determined by the additional weight lost after drying of the capsule at 120°C. To minimize the escape of H_2O along with CO_2, capsules were centrifuged prior to puncture. Blank experiments, performed to check for absorbed H_2O or breakdown of the silver oxalate through exposure to light, indicate reproducibility in determining fluid compositions near Xco_2 = 0.5 of about ± 2 mol per cent. Blank experiments with oxalic acid reproduced the theoretical value of Xco_2 = 0.45 ± 0.02.

For SEM and microprobe analysis, samples were disaggregated by very light grinding with ethyl alcohol, finely dispersed by pipette on a polished graphite disc, and carbon coated. Analyses were collected on a CAMECA SX-50 electron microprobe operated at 15 kV and 10 nA sample current in wavelength dispersive mode. Analytical totals for synthetic biotites (see below) ranged between 52-86 wt. %, the lower totals being associated with much thinner biotite grains. Oxide sums did not, however, show any apparent correlation with Al contents calculated on a fixed anion basis.

RESULTS

Synthesis and characterization of starting materials

Phl and Phl_{45} were synthesized from stoichiometric mixtures of MgO, γ-Al_2O_3, K_2CO_3, and cristobalite. γ-Al_2O_3 and cristobalite were prepared by firing $Al(OH)_3$ and silicic acid, respectively, at 1000°C for 20 hours. The MgO was also heated at 1000°C for 20 hours to dry it completely. Between 120-150 mg of the starting mixture was sealed in 4 mm O.D. - 3.8 mm I.D. Au capsules and held for 7-8 days at 2 kbar and 750°C or 650°C for Phl or Phl_{45}, respectively. Powder X-ray diffraction patterns, as well as optical and SEM examination indicated complete reaction of the starting materials. Microprobe analysis was hindered by the extremely fine grained nature of the synthetic materials (1-5 μm), but showed no significant deviation from the expected stoichiometry. XRD analyses indicated the presence of both 1M and 3T polytypes. Unit cell parameters are similar to those obtained in other studies (Hewitt and Wones, 1975; Bohlen et al., 1983; Peterson and Newton, 1989).

Enstatite was synthesized from stoichiometric mixtures of MgO and cristobalite, prepared as described above. Complete reaction of starting mixtures was obtained in experiments at 2 kbar and 800°C for 3 days.

Sanidine was synthesized from a stoichiometric mixture of K_2CO_3, $Al(OH)_3$, and cristobalite, reacted hydrothermally at 775°C - 1 kbar for 3 days. Measurement of the (060-$\bar{1}$13) peak position difference (Hovis, 1989) indicated that the synthesis product was approximately 12% ordered.

Natural quartz (Lisbon) and sillimanite (Brandywine) were used in all experiments.

Experimental Data for equilibrium A

Experimentally determined half-brackets are listed in Table 2, and plotted in Figures 1 and 2. Complete reaction of Phl+Qz to En+Sa was observed in four experiments interpreted to be quite far from the equilibrium position. All other experiments except one (# 11) produced strong (>30%) changes in relative peak intensities, making interpretation of run direction unambiguous.

The new experimental data bracket the equilibrium in mixed volatiles at ~2.5 and ~1.75 kbar, and are particularly constraining at the latter pressure (#s 18 and 19). Using the calculated curve of Berman (1988) as a reference for interpolation (Fig. 1, 2), these data are in excellent agreement with the 5 kbar bracket of Bohlen et al. (1983), and with the computed curves of Berman (1988). On the other hand, the high T half-bracket in pure H_2O (# 20) clearly contradicts the results of Wones and Dodge (1977) and Wood (1976) (Fig. 1). These observations support the conclusion based on the mixed volatile data that the position of equilibrium A lies at lower T than determined in earlier studies.

To compare rigorously experimental results in pure H_2O and H_2O-CO_2 fluids, thermodynamic properties for phlogopite were derived from the phase equilibrium data presented above, making use of auxiliary data for minerals from Berman (1988) and P-V-T properties of H_2O and H_2O-CO_2 mixtures from the equations of state of Haar et al. (1984) and Kerrick and Jacobs (1981), respectively. With the experimental data adjusted for uncertainties described above, the two sets of new data are narrowly inconsistent: the data obtained in pure H_2O indicate a slightly expanded stability field (about 5°C) for Phl compared to the mixed volatile data. At the present time, it is not known whether the discrepancy is due to larger experimental uncertainties than estimated, to inaccuracies in the equations of state for H_2O and H_2O-CO_2 mixtures, or to a combination of both these possibilities.

Experimental Data for equilibrium B

Experimental half-brackets are listed in Table 3. All run products contained 2-5 µm biotite along with Si, Sa, Qz, and H_2O with no additional phases. Analyses of 6-14 grains were collected for each sample. Core to rim zonation in biotite Al content was not discernible. In all run products, biotite composition was significantly shifted from the starting composition (Fig. 3). The compositional variation between different

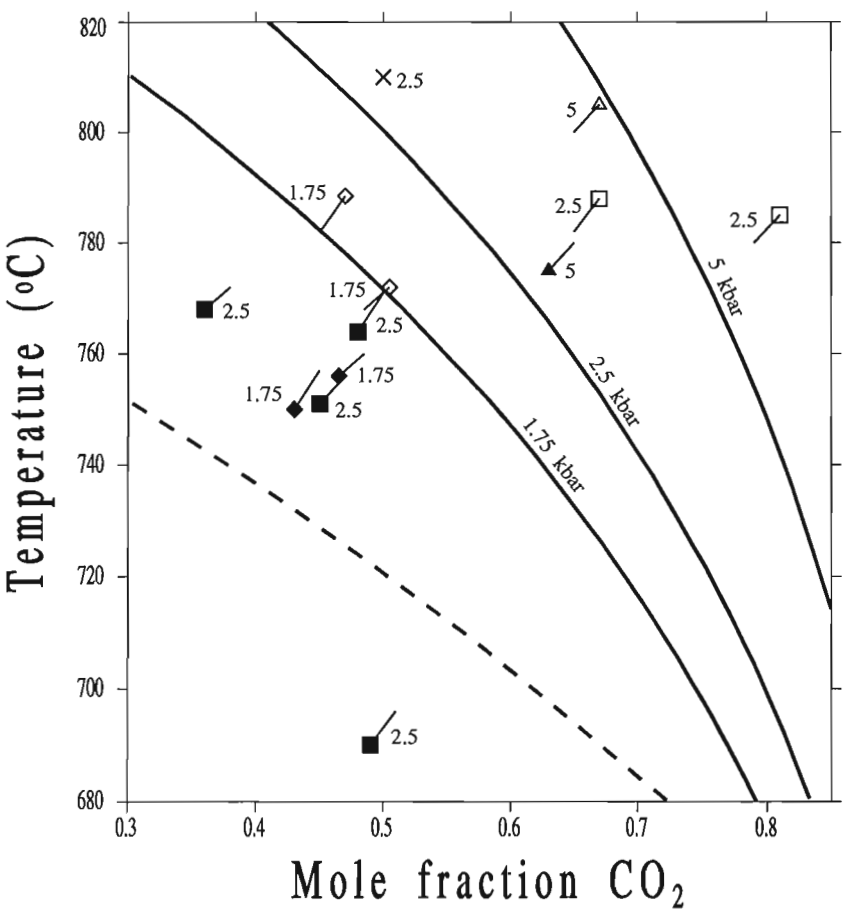

Figure 2.

T-X_{CO_2} diagram showing experimental data for equilibrium A along with its position at 1.75 kbar, 2.5 kbar, and 5 kbar, calculated with thermodynamic data of Berman (1988). Symbols as in Figure 1, with data from this study at 1.75 kbar (diamonds) and 2.5 kbar (squares; x = no reaction), and from Bohlen et al. (1983) at 5 kbar (triangles). Numbers beside data points indicate pressure (kbar) of experiments. Dashed curve is 1.75 kbar curve of Holland and Powell (1990).

grains in a single sample was generally in the range 0.15-0.25 Al pfu (12 anion formula), with no recognizable correlation with grain size. These observations suggest that the dominant mechanism of biotite equilibration was via dissolution and regrowth, rather than by diffusional reequilibration.

We interpret the compositional variations observed in each experimental product as representing differing degrees of approach towards equilibrium, which implies that the Al content most different from that of the starting biotite is closest to the equilibrium value. A complicating factor, however, is the possibility of overstepping the equilibrium Al content, as has been observed in experiments on Al solubility in orthopyroxene (Perkins et al., 1981). Tabulated Al values (Table 3) represent averages based on the 2 or 3 compositionally most advanced (most different from starting composition) grains within each run product. All pairs of experiments at a specific P-T produced tightly convergent compositional brackets, with only minor overlap (<0.02 Al pfu). These data indicate that the assemblage Bi-Si-Sa-Qz-H_2O buffers the Al content of biotite to a constant value of 1.62 ± 0.03 Al pfu over this P-T range.

Although total Al contents could be determined with confidence, imprecision in Si analyses due to fine grain size and surface irregularities, made it impossible to unambiguously determine octahedral versus tetrahedral Al contents. The analytical data obtained to date suggest some decoupling of octahedral and tetrahedral Al that can be expressed in terms of a Tschermak's exchange ($^{[6]}Mg^{[4]}Si = {}^{[6]}Al^{[4]}Al$), relating Phl and East components, and a dioctahedral exchange ($3^{[6]}Mg = 2^{[6]}Al^{[6]}\square^{[6]}$) relating Phl and Ms components. Compositional trends in experimental studies (Robert, 1976; Patino-Douce et al., 1993) and natural biotites (Guidotti, 1984) can be interpreted similarly. Synthesis experiments of Robert (1976) suggested a maximum of about 8 % Ms component in Mg-biotites at 600°C, a value compatible with the present results.

DISCUSSION

The combined set of new experimental data on equilibrium A lends support to the position of this equilibrium computed with the thermodynamic data of Berman (1988), with the mixed volatile and pure H_2O data indicating a slightly less stable and more stable phlogopite, respectively. In contrast, the data of Holland and Powell (1990), based primarily on their interpretation of natural assemblages, and of Circone and Navrotsky (1992), based on heat of solution measurements, both indicate a much lower breakdown temperature of Phl+Qz (Fig. 1). This reduced Phl stability is one major contributing factor to computed biotite stability fields (Powell and Holland, 1990) that are smaller than can be reconciled easily with observations based on natural assemblages (see also Berman et al., 1995).

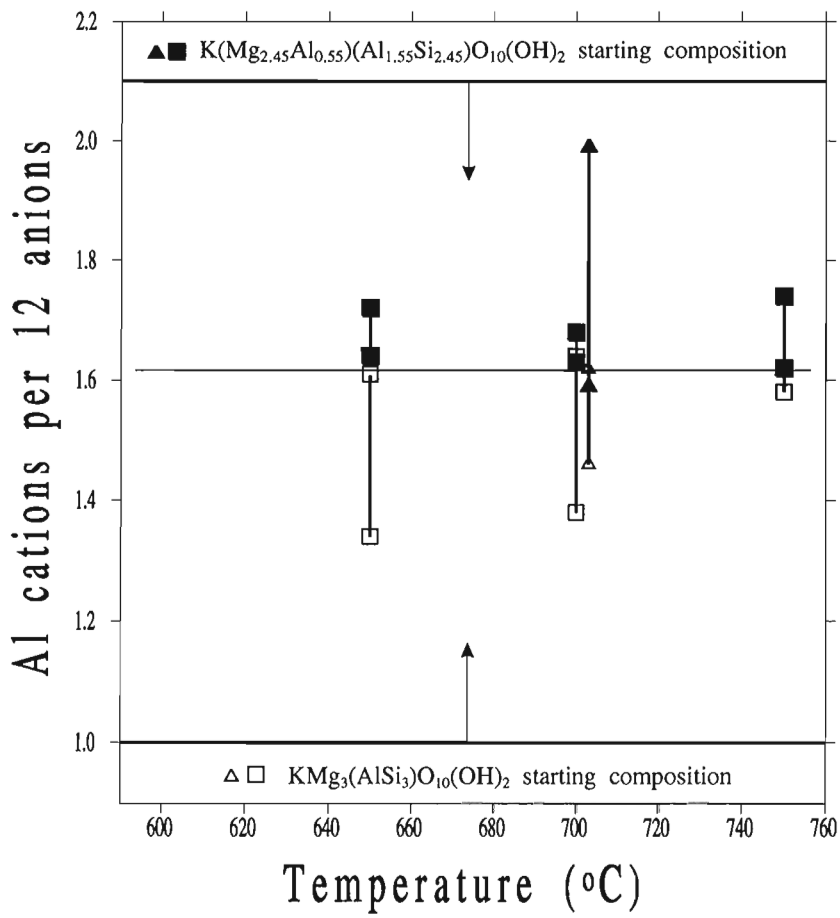

Figure 3.

Al content (per 12 anions) of Mg-biotites determined in this study (Table 3). Paired symbols show the range of Al content observed in different biotite grains of the same run product. Open and closed symbols represent the results of experiments starting with low-Al biotite (Phl) and high-Al biotite (Phl_{45}), respectively. Squares and triangles represent low pressure (~2 kbar) and high pressure (~3.4 kbar) experimental data, respectively.

The new data for equilibrium B represent the first set of reversed experiments defining Al solubility in Mg-biotite, and allow direct determination of the thermodynamic properties of eastonite. The enthalpy of formation we derive (Berman and Aranovich, in prep.) is approximately 30 kJ/mol less stable than that determined calorimetrically by Circone and Navrotsky (1992), and about 8 kJ/mol less stable than retrieved by Holland and Powell (1990) from experiments of Massonne and Schreyer (1987) on the phengite+Mg-biotite+Qz assemblage. The consequence of the latter difference is that Powell and Holland (1990) predicted Al saturation levels in Mg-biotite that are approximately 0.4 Al pfu greater than determined in this study.

The present experimental results, combined with those in Part 2 (Berman et al., 1995), tightly constrain the energetics of the reciprocal internal equilibrium:

$$2\ \text{Phl} + 3\ \text{Sdr} = 3\ \text{East} + 2\ \text{Ann} \qquad \text{(C)}$$

in the range 6-7 kJ/mol, assuming ideal on-site mixing. This enthalpy change reflects the lower solubility of Al in Mg-biotite than in Fe-biotite (part 2), a difference that is completely compatible with observations of natural biotite compositions which show approximately 0.2 less Tschermak's component in Mg-rich compared to Fe-rich biotites (Cheney and Guidotti, 1975). Natural Mg-rich biotites coexisting with Si or staurolite contain 1.65-1.70 Al (Cheney and Guidotti, 1975), in reasonable accord with the value (1.62 Al) determined in the present experimental results. The small amounts of octahedral Ti and Fe^{3+} in natural Mg-rich biotites (each about 0.05 cations/12 anions, Cheney and Guidotti, 1975), does not seriously affect this comparison (see part 2).

Results presented in part 2 demonstrate that Al solubility results in a marked increase in the stability of Fe-biotite, although the lower saturation levels in Mg-biotite lead to a smaller stability difference in the Mg system. Most importantly, derived thermodynamic properties for East and Sdr (part 2) permit prediction of stable biotite compositions in any KFMASH assemblage. When combined with the improved data on endmember stability presented above and in part 2, petrogenetic grids and thermobarometers involving biotite can be computed with much more confidence. Such predictions are explored in detail elsewhere (Berman and Aranovich, in prep.), and only two examples, computed with the THERIAK software (de Capitani and Brown, 1987) will be briefly discussed here.

In the KFMASH system, the upper thermal stability of Bi+Si+Qz is marked by the transition to Gt+Cd+Sa+H_2O. Figure 4 shows the computed univariant equilibrium in this system, along with predicted Gt and Bi compositions. Gt becomes increasingly Fe-rich with decreasing temperature until it reaches the Alm composition at the singular point at 688°C and 2.4 kbar. The position of this equilibrium is in fair agreement with Spear and Cheney's grid, but their Gt compositions are about 20 mol % richer in Mg. Our curve lies about 50°C higher than that of Holland and Powell (1990). The present results confirm that the Gt+Cd+Sa assemblage is

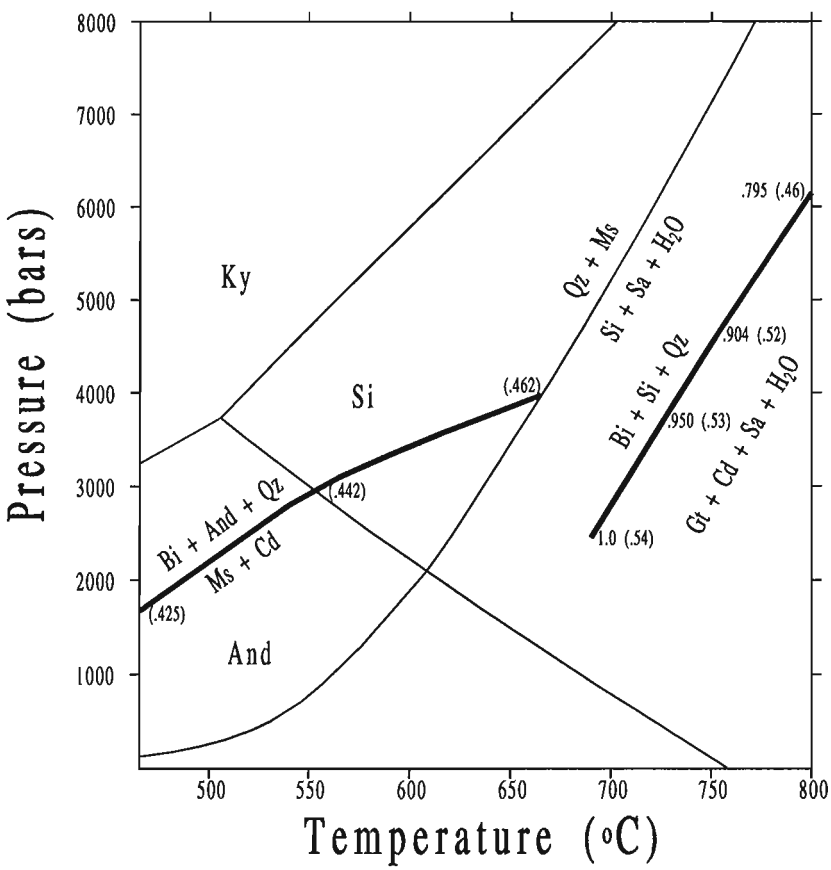

Figure 4.

P-T diagram showing computed position of KFMASH equilibria (heavy curves) discussed in text. Numbers beside calculated curves are X_{Alm} *and octahedral Al per 12 anion biotite formula (in parentheses).*

a good indicator of metamorphic grade that can be used to mark the amphibolite - granulite transition in pelites. The new data also allow for a wide stability field for the Bi+And+Qz assemblage observed in low pressure terrains worldwide. On the other hand, to allow for the occurrence of rare Gt-Cd-Ms assemblages, or of almandine-rich Gt in amphibolite facies rocks, Mn and/or Ca must be included in our calculations because of their large effect in expanding the calculated stability field of Gt (Spear and Cheney, 1989; Symmes and Ferry, 1992).

A final example involves the slope of the divariant KFMASH equilibrium:

$$Cd + Ms = Bi + Si + Qz \qquad (D)$$

which has been the subject of some debate because of its importance in constraining P-T-time paths (e.g. Pattison and Tracy, 1991) in low P terrains like the Slave Province. Our new experimental results provide thermodynamic properties for Mg-Fe-Al biotites that can be confidently used to predict the position of this equilibrium. As shown in Figure 4, the computed curve has a positive slope, in contrast with conclusions of Pattison and Tracy (1991) based primarily on interpretations of natural assemblages. Further calculations are needed to explore the sensitivity of these results to different cordierite hydration models, but the present results suggest that individual samples that show progressive development of Bi+Si from Cd+Ms are most easily reconciled with counterclockwise P-T paths.

ACKNOWLEDGMENTS

The results presented in this contribution could not have been obtained without the generous technical support of many GSC personel to whom we extend our most sincere gratitude: Steve Banszky and Sean Going who ensured that the lab stayed fully operational, John Stirling for assistance with microprobe analysis, Armand Tsai for his patient SEM work, and Bob Dilabio for running many XRD scans. We also thank Corinne Bensimon of the University of Ottawa who collected XRD data for cell refinements, and M.R. St.-Onge who provided a very helpful review of this manuscript.

REFERENCES

Appleman, D.E. and Evans, T.H., Jr.
1973: Job 9214: indexing and least-squares refinement of powder diffraction data.; National Technical Information Services, United States Department of Commerce, Springfield, Virginia.

Berman, R.G.
1988: Internally-consistent thermodynamic data for minerals in the system Na_2O-K_2O-CaO-MgO-FeO-Fe_2O_3-Al_2O_3-SiO_2-TiO_2-H_2O-CO_2; Journal of Petrology, v. 29, p. 445-522.

Berman, R.G. and Aranovich, L.Y.
in press: Optimized standard state and mixing properties of minerals: I. Model calibration for olivine, orthopyroxene, cordierite, garnet, and ilmenite in the system FeO-MgO-CaO-Al_2O_3-SiO_2-TiO_2; Contributions to Mineralogy and Petrology, (accepted for publication, March 1995).

Berman, R.G., Aranovich, L.Y., and Rancourt, P.
1995: Phase equilibrium constraints on the stability of biotite Part 2: Fe-Al biotite in the system K_2O-FeO-Al_2O_3-SiO_2-H_2O; in Current Research 1995-E; Geological Survey of Canada, this volume.

Bird, G.W. and Fawcett, J.J.
1973: Stability relations of Mg-chlorite-muscovite and quartz between 5 and 10 kb water pressure; Journal of Petrology, v. 14, p. 415-428.

Bohlen, S.R., Wall, V.J., and Clements, J.D.
1983: Stability of phlogopite-quartz and sanidine-quartz: a model for melting in the lower crust; Contributions to Mineralogy and Petrology, v. 83, p. 270-277.

Cheney, J.T. and Guidotti, C.V.
1975: Interrelationship between Mg/Fe ratio and octahedral Al content in biotite; The American Mineralogist, v. 60, p. 849-853.

Circone, S. and Navrotsky, A.
1992: Substitution of Al-6,Al-4 in Phlogopite: High temperature solution calorimetry, heat capacities, and thermodynamic properties of the phlogopite-eastonite join; The American Mineralogist, v. 77, p. 1191-1205.

Dasgupta, S., Sengupta, P., Guha, D., and Fukuoka, M.
1991: A refined garnet - Biotite Fe - Mg exchange geothermometer and its application in amphibolites and granulites; Contributions to Mineralogy and Petrology, v. 109, p. 130-137.

de Capitani, C. and Brown, T.H.
1987: The computation of chemical equilibrium in complex systems containing non-ideal solutions; Geochimica et Cosmochimica Acta, v. 51, p. 2639-2652.

Ferry, J.M. and Spear, F.S.
1978: Experimental calibration of the partitioning of Fe and Mg between biotite and garnet; Contributions to Mineralogy and Petrology, v. 66, p. 113-117.

Guidotti, C.V.
1984: Micas in metamorphic rocks; in; Micas, P.H. Ribbe (ed.); Reviews in Mineralogy, Mineralogical Society of America, p. 357-468.

Haar, C., Gallagher, J.S., and Kell, G.S.
1984: NBS/NRC Steam Tables. Thermodynamic and transport properties and computer programs for vapor and liquid states of water in SI units; Hemisphere Publishing Co, Washington.

Harley, S.L.
1989: The origins of granulites: a metamorphic perspective; Geological Magazine, v. 126, p. 215-247.

Hewitt, D.A. and Wones, D.R.
1975: Physical properties of some synthetic Fe-Mg-Al trioctahedral biotites; The American Mineralogist, v. 60, p. 854-862.
1984: Experimental phase relations of the micas; in; Micas, P.H. Ribbe (ed); Reviews in Mineralogy, Mineralogical Society of America, p. 201-256.

Holland, T.J.B. and Powell, R.
1990: An internally consistent thermodynamic dataset with uncertainties and correlations: the system K_2O-Na_2O-CaO-MgO-MnO-FeO-Fe_2O_3-Al_2O_3-Ti O_2-SiO_2-C-H_2O_2; Journal of Metamorphic Geology, v. 8, p. 89-124.

Hovis, G.L.
1989: Effect of Al-Si distribution on the powder-diffraction maxima of alkali feldspars and an easy method to determine T1 and T2 site occupancies; Canadian Mineralogist, v. 27, p. 107-118.

Johannes, W.
1969: An experimental investigation of the system MgO-SiO_2-H_2O-CO_2; American Journal of Science, v. 267, p. 1083-1104.

Kerrick, D.M. and Jacobs, G.K.
1981: A modified Redlich-Kwong equation for H_2O, CO_2, and H_2O-CO_2 mixtures at elevated pressures and temperatures; American Journal of Science, v. 281, p. 735-767.

Massonne, H.-J. and Schreyer, W.
1987: Phengite geobarometry based on the limiting assemblage with K-feldspar, phlogopite, and quartz; Contributions to Mineralogy and Petrology, v. 96, p. 212-224.

Patino Douce, A.E., Johnston, A.D., and Rice, J.M.
1993: Octahedral excess mixing properties in biotite: a working model with applications to geobarometry and geothermometry; The American Mineralogist, v. 78, p. 113-131.

Pattison, D.R.M. and Tracy, R.J.
1991: Phase equilibria and thermobarometry of metapelites; in; Contact Metamorphism, P.H. Ribbe (ed); Reviews in Mineralogy, Mineralogical Society of America, p. 105-206.

Perkins, D., Holland, T.J.B., and Newton, R.C.
1981: The Al_2O_3 Contents of Enstatite in Equilibrium with Garnet in the System $MgO-Al_2O_3-SiO_2$ at 15-40 kbar and 900-1600C; Contributions to Mineralogy and Petrology, v. 78, p. 99-109.

Peterson, J.W. and Newton, R.C.
1989: Reversed experiments on biotite-quartz-feldspar melting in the system kmash: implications for crustal anatexis; Journal of Geology, v. 97, p. 465-485.

Powell, R. and Holland, T.
1990: Calculated mineral equilibria in the pelite system, KFMASH ($K_2O-FeO-MgO-Al_2O_3-SiO_2-H_2O$); The American Mineralogist, v. 75, p. 367-380.

Robert, J.L.
1976: Phlogopite solid solutions in the system $K_2O-MgO-Al_2O-SiO_2-H_2O$; Chemical Geology, v. 17, p. 195-212.

Rutherford, M. J.
1973: The phase relations of aluminous iron biotites in the system $AlSi_3O_8-KAlSiO_4-Al_2O_3-Fe-O-H$; Journal of Petrology, v. 14, p. 159-180.

Selverstone, J. and Chamberlain, C.P.
1990: Apparent isobaric cooling paths from granulites: two counterexamples from British Columbia and New Hampshire; Geology, v. 18, p. 307-310.

Spear, F.S. and Cheney, J.T.
1989: A petrogenetic grid for pelitic schists in the system $SiO_2-Al_2O_3-FeO-MgO-K_2O-H_2O$; Contributions to Mineralogy and Petrology, v. 101, p. 149-164.

Spear, F.S. and Florence, P.
1992: Thermobarometry in granulites: pitfalls and new approaches; Precambrian Research, v. 55, p. 209-241.

Symmes, G.H. and Ferry, J.M.
1992: The effect of whole-rock MnO content on the stability of garnet in pelitic schists during metamorphism; Journal of Metamorphic Geology, v. 10, p. 221-237.

Wones, D.R. and Dodge, F.C.W.
1977: The stability of phlogopite in the presence of quartz and diopside; in Thermodynamics in Geology, D.G. Fraser (ed); Reidel Publishing Company, p. 229-247.

Wood, B.J.
1976: The reaction phlogopite+quartz=enstatite+sanidine+H_2O; Progress in Experimental Petrology, Natural Environment Research Council, Ser. D, p. 17-19.

Geological Survey of Canada Project 880014

Phase equilibrium constraints on the stability of biotite. Part 2: Fe-Al biotite in the system K_2O-FeO-Al_2O_3-SiO_2-H_2O

R.G. Berman, L. Ya Aranovich[1], and D.G. Rancourt[2]
Continental Geoscience Division

Berman, R.G., Aranovich, L. Ya, and Rancourt, D.G., 1995: Phase equilibrium constraints on the stability of biotite. Part 2: Fe-Al biotite in the sytem K_2O-FeO-Al_2O_3-SiO_2-H_2O; in Current Research 1995-E; Geological Survey of Canada, p. 263-270.

Abstract: The stability of aluminous Fe-biotite has been determined from two sets of reversed phase equilibrium data. First, tight brackets define constant Al saturation at 2.08 ± 0.05 Al pfu (12 anion formula) in Fe-biotite in equilibrium with sillimanite+sanidine+quartz+H_2O over the P-T range 2-3.5 kbar and 600-700°C. Second, breakdown of Al-saturated Fe-biotite via the univariant reaction: biotite+sillimanite+quartz=almandine+sanidine+H_2O has been reversed at ~2.4 kbar between 691 and 709°C. Thermodynamic analysis indicates that our data conflict with petrogenetic grids proposed by Spear and Cheney (1989) and Powell and Holland (1990), both of which result in expanded almandine stability fields. Quantification of biotite - almandine stability fields represents an important step towards accurate positioning of equilibria involving biotite in petrogenetic grid as well as thermobarometric calculations.

Résumé : À partir de deux ensembles de données sur l'équilibre de phase inversé, on a déterminé la stabilité de la biotite-Fe alumineuse. En premier lieu, les expériences permettent de définir la saturation en Al constante à 2,08 ± 0,05 unités par formule de Al (formule à 12 anions) dans la biotite-Fe en équilibre avec sillimanite + sanidine + quartz + H_2O dans l'intervalle de pression de 2-3,5 kbar et l'intervalle de température de 600-700°C. En deuxième lieu, le fractionnement de la biotite-Fe saturée en Al par le biais de la réaction univariante biotite + sillimanite + quartz = almandin + sanidine + H_2O a été inversé à environ 2,4 kbar entre 691 et 709°C. L'analyse thermodynamique indique que nos données ne sont pas en accord avec les grilles pétrogénétiques proposées par Spear et Cheney (1989) et Powell et Holland (1990), qui dans les deux cas donnent des champs de stabilité de l'almandin plus étendus. La quantification des champs de stabilité de la biotite et de l'almandin représente une importante étape vers le positionnement exact de l'équilibre incluant la biotite dans la grille pétrogénétique ainsi que les calculs thermobarométriques.

[1] Institute of Experimental Mineralogy, Chernogolovka, Russia
[2] Department of Physics, University of Ottawa, Ottawa, Ontario K1N 6N5

INTRODUCTION

This paper represents the second of a two-part experimental study on biotite stability, aimed at providing greater accuracy in construction of petrogenetic grids and in thermobarometric calculations involving biotite. In Part 1 (Berman et al., 1995), data pertaining to the stability of Mg-biotite endmembers, phlogopite and eastonite, are presented. In this contribution, we examine Fe-biotite stability relations in the KFASH system which is more directly relevant to petrogenetic grids for pelitic rocks because of their Fe-rich bulk compositions.

In spite of their importance, Fe-biotite phase relations are poorly constrained by existing experimental data, probably because of the added experimental difficulty of controlling oxygen fugacity and measuring Fe^{3+} contents of run products in Fe-bearing systems. One equilibrium that has been studied (Holdaway and Lee, 1977) and which is important in amphibolite-granulite grade pelites is (see Table 1 for abbreviations):

$$\text{Fe-biotite} + \text{Si} + \text{Qz} = \text{fCd} + \text{Sa} + H_2O \qquad \text{(A)}$$

Whereas the early grid of Harte and Hudson (1979) incorporated these experimental data, more recent grids (Spear and Cheney, 1989; Powell and Holland, 1990; Xu et al., 1994) are at odds with these results. Spear and Cheney (1989) rejected these data because, when combined with Holdaway and Lee's data for the equilibrium:

$$\text{fCd} = \text{Alm} + \text{Si} + \text{Qz} \qquad \text{(B)}$$

they limit almandine stability to temperatures above about 750°C. Powell and Holland (1990) also show a large stability field for almandine, a factor contributing to the exclusion from their grid of the KFMASH assemblage And + Bi + Qz commonly observed in low pressure terranes worldwide.

Clearly there is a need to resolve these differences both among various computed petrogenetic grids and between the calculations and experimental observations. There are two facets to this problem. The first is to determine the overall stability of Bi + Si + Qz relative to higher temperature, anhydrous assemblages. Before this can be achieved, however, the aluminum content of biotite buffered by the breakdown assemblage must first be defined, because solution of excess Al increases the thermal stability of biotite. These problems are addressed in this contribution through experimental determination of the Al content of Fe-biotite, buffered by the equilibrium

$$\text{Ann} + \text{Si} + \text{Sa} + H_2O = \text{Sdr} + \text{Qz} \qquad \text{(C)}$$

and the stability of Fe-biotite via the equilibrium:

$$\text{Fe-biotite} + \text{Si} + \text{Qz} = \text{Alm} + \text{Sa} + H_2O \qquad \text{(D)}$$

Table 1. Abbreviations and chemical formulae.

Name	Abbreviation	Formula
Annite	Ann	$K(Fe_3)(AlSi_3)O_{10}(OH)_2$
Phlogopite	Phl	$K(Mg_3)(AlSi_3)O_{10}(OH)_2$
Siderophyllite	Sdr	$K(Fe_2Al)(Al_2Si_2)O_{10}(OH)_2$
$Annite_{20}$	Ann_{20}	$K(Fe_{2.2}Al_{0.8})(Al_{1.8}Si_{2.2})O_{10}(OH)_2$
$Annite_{20}$	Ann_{45}	$K(Fe_{2.45}Al_{0.55})(Al_{1.55}Si_{2.45})O_{10}(OH)_2$
Almandine	Alm	$Fe_3Al_2Si_3O_{12}$
Fe-cordierite	fCd	$Fe_2Al_4Si_5O_{18}$
Sanidine	Sa	$KAlSi_3O_8$
Sillimanite	Si	Al_2SiO_5
Quartz	Qz	SiO_2
Eastonite	East	$K(Mg_2Al)(Al_2Si_2)O_{10}(OH)_2$

PREVIOUS EXPERIMENTAL WORK

Over the last 30 years, a number of experimental studies have been performed in order to define the major controls on biotite stability (see review by Hewitt and Wones, 1984). For the Fe-system, variable Fe^{3+} and uncertainties in hydrogen buffer calibrations and efficiency (Chou and Cygan, 1990) have contributed to significant uncertainty regarding annite stability over a range of oxygen fugacities. Recent work by Cygan et al. (in press) on the equilibrium:

$$\text{Ann} = \text{Magnetite} + \text{Fayalite} + \text{Sa} + H_2 \qquad \text{(E)}$$

appear to have resolved these problems. Rutherford (1973) studied Al solubility in the Fe-system, and obtained some reversals which show the increased stability of Fe-Al biotite relative to assemblages involving spinel solid solution, sanidine, and leucite. Quantitative calculations based on these data are hindered by the lack of reversed compositional data for spinel and biotite solid solutions. Studies by Partin (1984) and Rebbert (1986) place important constraints on the Fe^{3+} contents of Fe-Al biotites as a function of hydrogen fugacity. Holdaway and Lee (1977) presented data on equilibrium A, but the biotite composition produced in their experiments was not determined, and their synthetic fCd had impurities of hercynite.

EXPERIMENTAL METHODS

Description of experimental procedures are given in Part 1. Additional details specific to the results presented here are described below. Oxygen fugacity was controlled in all experiments using the C-CH_4 buffer (Eugster and Skippen, 1967). To study equilibrium C, two capsules were used in each experiment, one with low-Al biotite (Ann), the other with high-Al biotite (Ann_{20}), each mixed with subequal proportions by weight of sanidine, quartz, and sillimanite. For equilibrium D, we used a mineral mix consisting of subequal molar proportions of the low and high temperature assemblage. The biotite composition in this mix, Ann_{45}, was that determined to be stable after studying equilibrium C. In all experiments, each capsule contained approximately 5 mg mix and 5 mg of H_2O. Minerals used in each mix are described below. Reversals for equilibrium C were obtained from electron microprobe analysis of the compositions of biotites in run products. Reaction direction for equilibrium D was determined

by changes (>30%) in the ratios of X-ray diffraction peak heights (001 for Bi; 400 for Alm; (1 30 Sa) of run products compared to the starting mix.

Transmission Fe-57 Mössbauer spectra were collected for synthetic biotites at 22°C using a ~10 mCi Co-57 rhodium-matrix single-line thin source on a velocity range of ±4 mm/s with a constant acceleration drive. Data were acquired on 1024 channels and folded to give a flat background and a zero velocity position corresponding to the centre shift of metallic α-Fe at 22°C in the 512-channel spectrum. The absorber thickness was 40 mg sample per cm^2.

RESULTS

Synthesis and characterization of starting materials

Annite was synthesized from stoichiometric mixtures of $KSi_3O_{6.5}$ glass, prepared by the method of Schairer and Bowen (1955), with iron oxalate ($FeC_2O_4.2H_2O$), and γ-Al_2O_3. Aluminous biotites were synthesized from iron oxalate, γ-Al_2O_3, K_2CO_3, and cristobalite, mixed to give the compositions $K(Fe_{2.2}Al_{0.8})(Al_{1.8}Si_{2.2})(OH)_2$ (Ann_{20}) and $K(Fe_{2.45}Al_{0.55})(Al_{1.55}Si_{2.45})(OH)_2$ (Ann_{45}). γ-Al_2O_3 and cristobalite were prepared by firing $Al(OH)_3$ and silicic acid, respectively, at 1000°C for 20 hours. Between 120 to 150 mg of each mixture was sealed in 4 mm O.D. - 3.8 mm I.D. Au capsules and held for 7-13 days at 2 kbar and either 700°C (Ann) or 650°C (Ann_{20} and Ann_{45}). Hydrogen fugacity was buffered by the C-CH_4 assemblage (Eugster and Skippen, 1967), but no attempt was made to ascertain the attained fugacity values which depend on the rate of H_2 diffusion out of the pressure vessels (Chou and Cygan, 1990).

Powder X-ray diffraction patterns, as well as optical and SEM examination, indicated almost complete reaction of the annite starting materials. Minor amounts of fayalite and magnetite were discernible in XRD scans of Ann, which had a grain size between 2-20 μm (Fig. 1a). Similar impurities are reported in annite syntheses of Hewitt and Wones (1975), Partin (1984), and Rebbert (1986). Microprobe analyses showed no significant deviation from the expected stoichiometry.

Syntheses of aluminous biotites, Ann_{20} and Ann_{45}, produced 1-10 μm biotite grains (Fig. 1b) with several corundum grains as the only detectible (by SEM) impurities. Microprobe analyses of the more aluminous material range between 0.72-0.78 octahedral Al pfu (12 anion basis), and indicate that the stoichiometric mix composition, with 0.8 octahedral Al, was closely approached. Mössbauer analysis of the less aluminous material, which is very close to the equilibrium composition for the experimentally studied assemblage (see below), shows approximately 4% total Fe^{3+}, of which 2% is in tetrahedral and 2% in octahedral coordination. Mössbauer analysis of the synthetic annite indicated 12% total Fe^{3+} of which approximately 8% is in tetrahedral coordination. These data are very similar to wet chemical and Mössbauer data of other synthetic annites and Fe-Al biotites (Partin, 1984; Rebbert, 1986).

XRD analysis of all synthetic biotites indicated the presence of both 1M and 3T polytypes. Unit cell parameters were indexed on 17-18 peaks, assuming 1M polytype. Previous experimental work (Rutherford, 1973; Hewitt and Wones, 1975; Partin, 1984; Rebbert, 1986) has shown that the molar volume decreases with both increasing Al and increasing Fe^{3+} in biotite (Fig. 2). Our results are in excellent agreement with volumes determined from the most reduced biotites studied previously (Fig. 2), consistent with the Mossbauer measurements described above.

Synthetic sanidine and natural sillimanite and quartz starting materials are described in Part 1 (Berman et al., 1995).

Experimental data

Equilibrium C

Experimental data bracketing equilibrium C are presented in Table 2. All run products contained the assemblage biotite-Si-Sa-Qz-H_2O with no additional phases, except for

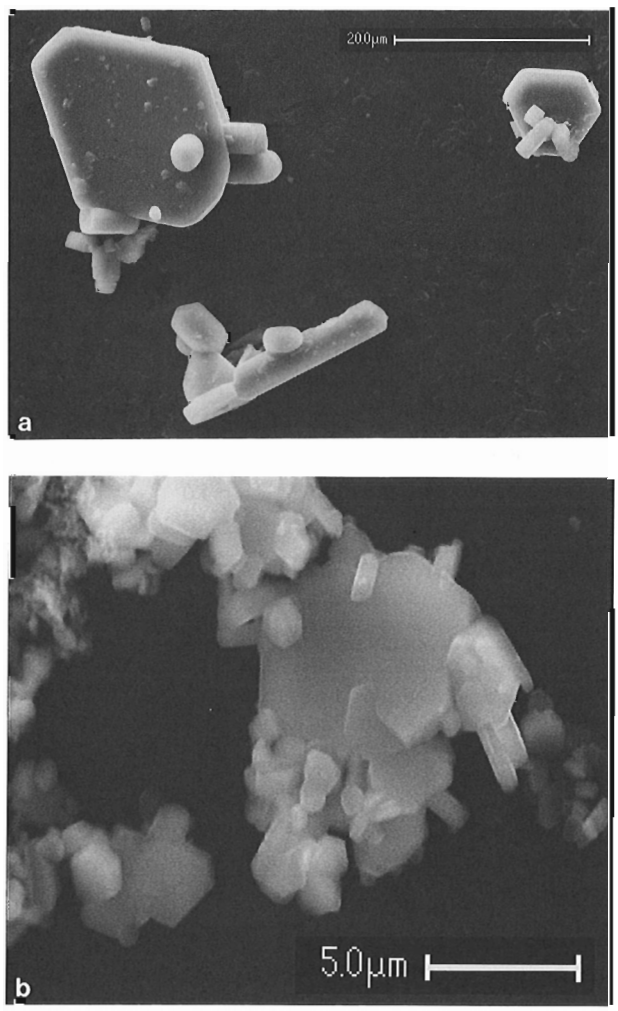

Figure 1. *Secondary electron images showing the range of crystal size and morphology of Fe-biotite in starting materials with annite (**a**) and with Ann_{20} (**b**).*

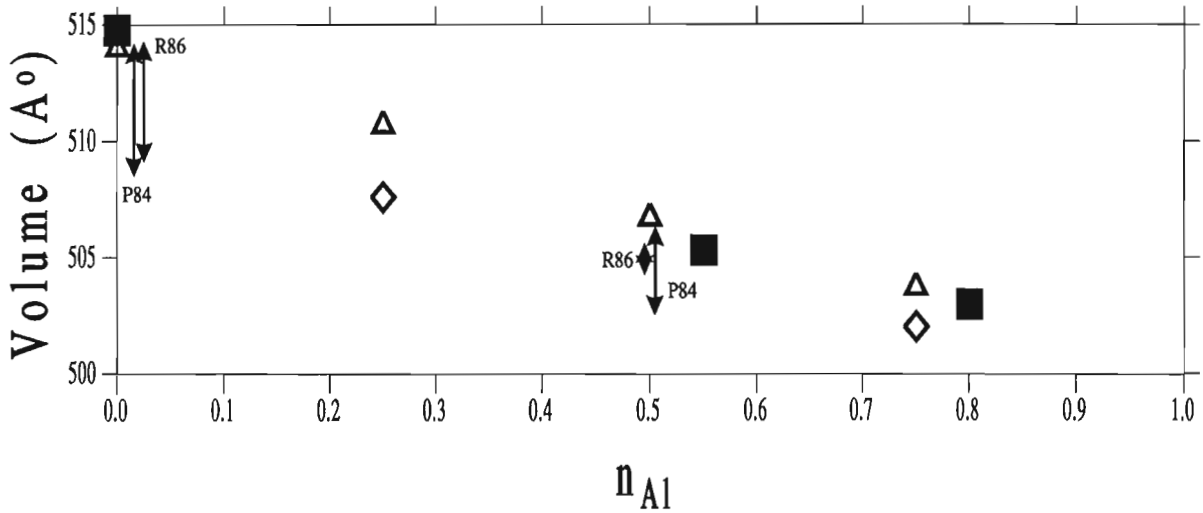

Figure 2. Variation of Fe-biotite molar volumes with n_{Al} (=$^{[4]}$Al-1=$^{[6]}$Al). Experimental data from this study (solid squares) are in good agreement with data of Rutherford (1973; diamonds) and Hewitt and Wones (1975; triangles). Paired arrows show range of volumes measured at different hydrogen pressures (see text) by Partin (1984; P84) and Rebbert (1986; R86).

Table 2. Experimental data for equilibrium C.

#	T(°C)	P (bars)	Al[1] initial	Al[1] Final
1	699±5	1.97±0.09	1.0	1.88-2.08
2	699±5	1.97±0.09	2.6	2.30-2.10
3	647±4	2.05±0.03	1.0	1.87-2.05
4	647±4	2.05±0.03	2.6	2.36-2.10
5*	777±5	2.03±0.07	2.6	
6*	777±5	2.03±0.07	1.0	
7	606±4	2.06±0.06	2.6	2.40-1.94
8	606±4	2.06±0.06	1.0	1.92-2.08
9	698±5	3.51±0.13	1.0	1.97-2.14
10	698±5	3.51±0.13	2.6	2.38-2.11
11[$]	597±3	3.67±0.05	1.0	1.83-1.84
12	597±3	3.67±0.05	2.6	2.14-1.92

Al pfu (12 anion formula)
[1] Initial biotites have Al = 1.0 (annite) or 2.6 (Ann_{20})
* Bi replaced by Alm + Si + Qz + hercynite + melt
[$] Most Bi replaced by fayalite

experiments #5 and 6 in which biotite reacted to form almandine (cordierite) + hercynite + melt, and experiment #11 in which most biotite reacted to form fayalite. Representative textures of run products are shown in Figure 3. Analyses of 10-22 grains were collected for each sample, with the exception of run #11 in which only 3 biotite grains were found.

Accepted analyses of biotite in run products have oxide totals between 85-96%, and K between 0.85-1.0 pfu (12 anion formula). No correlation was apparent between oxide sums and calculated cation contents. Replicate analyses of the same biotite grains in synthesis products and standards suggest that Al contents of individual grains are reproducible within ±3%. In all experiments, core to rim zonation in biotite Al content was negligible. The compositional variation between different grains in a single sample (Fig. 4) was generally in the range 0.15-0.25 Al pfu, with no recognizable correlation with grain size. Smaller variations were observed in run products which used the less aluminous starting biotite (Fig. 4). The largest variation (~0.45 Al) was found in the lowest P-T experiment using the more aluminous starting biotite.

As discussed in Part 1, the Al content of product biotite that was most different from that of the starting biotite was considered to be closest to the equilibrium value. The 6 experiments at temperatures above 606°C produced tightly convergent compositional brackets, with minor overlap (0.03 Al pfu) of the final compositions of experiments # 9 and 10. These data indicate that the assemblage Bi-Si-Sa-Qz-H_2O buffers Fe-biotite composition to a constant value of 2.08 ± 0.05 Al pfu over this P-T range.

The experimental results at ~600°C are more ambiguous due to the increased sluggishness of Al re-equilibration at lower temperature. Significant compositional overlap was produced in the experiments at 2 kbar. The much smaller variation between grains in the experiment with the Al-poor starting biotite (# 8) and the consistency of these compositions with those produced at higher temperatures (Fig. 4) suggest that this half-bracket is more reliable. The experimental results at 597°C and 3.7 kbar are the least reliable of all the data because only 3 biotite grains were found in experiment #11 in which most biotite reacted to form fayalite.

As was found in the Mg-system (Part 1), total Al contents could be determined with confidence, but octahedral versus tetrahedral Al contents could not be defined accurately. The analytical data obtained to date indicate operation of both Tschermak's and muscovite substitutions, with tetrahedral Al

increasing slightly and octahedral Al decreasing with increasing temperature. Patino Douce et al. (1993) observed similar results in unreversed experiments involving the assemblage Mg-Fe-Ti biotite-garnet-Si-Qz. Synthesis experiments of Rutherford (1973) suggested a maximum of 10-12% Ms component in Fe-biotites at 600°C, a value in reasonable agreement with that found in this study.

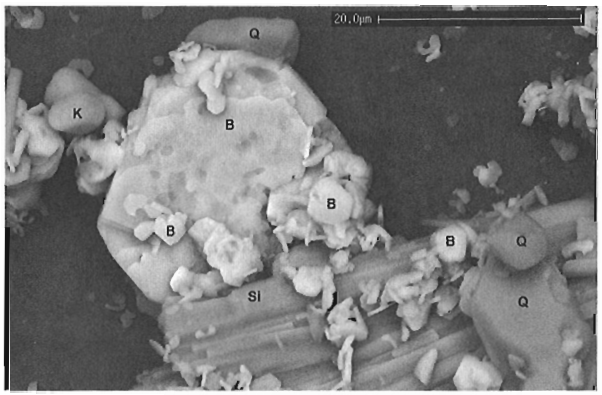

Figure 3. Secondary electron image of run product of experiment # 8 for equilibrium C. Mineral abbreviations: B = biotite; Si = sillimanite; Q = quartz; K = sanidine.

The total Al contents determined above are in excellent agreement with compositional data for natural biotites if the natural data are corrected for Ti and Fe^{3+}. Fe-rich biotites coexisting with sillimanite generally contain about 1.75 Al pfu (Cheney and Guidotti, 1975; Guidotti, 1984), with Fe^{3+} ~0.15 (assuming Fe^{3+}=10% of Fe, Guidotti and Dyar, 1991), and Ti ~0.1-0.2. The sum of these components (~2.05) is almost identical to the experimental Al values (~2.08). Crystal chemical arguments (Bailey, 1984) indicate that Fe^{3+} and Ti are octahedrally coordinated in biotite, and the above comparison suggests that these components may directly compete with Al for occupancy of octahedral sites.

Equilibrium D

Experimental data bracketing equilibrium D were obtained at ~2.4 kbar (Table 3). All run products contained the assemblage Bi-Alm-Si-Sa-Qz-H_2O, with no additional phases identified by XRD, SEM, or optically. XRD patterns of run products showing strong biotite growth exhibit stronger peaks at 17.54 and 45.00 2θ than Ann_{45} used in starting materials. These peaks are very close to the positions of (002) and (005) Ms peaks, but no muscovite was found in detailed SEM imaging, and all experiments were run at temperatures exceeding Ms + Qz stability. We interpret these changes in XRD peak intensities to indicate increase in the amount of Ms component in the product biotite.

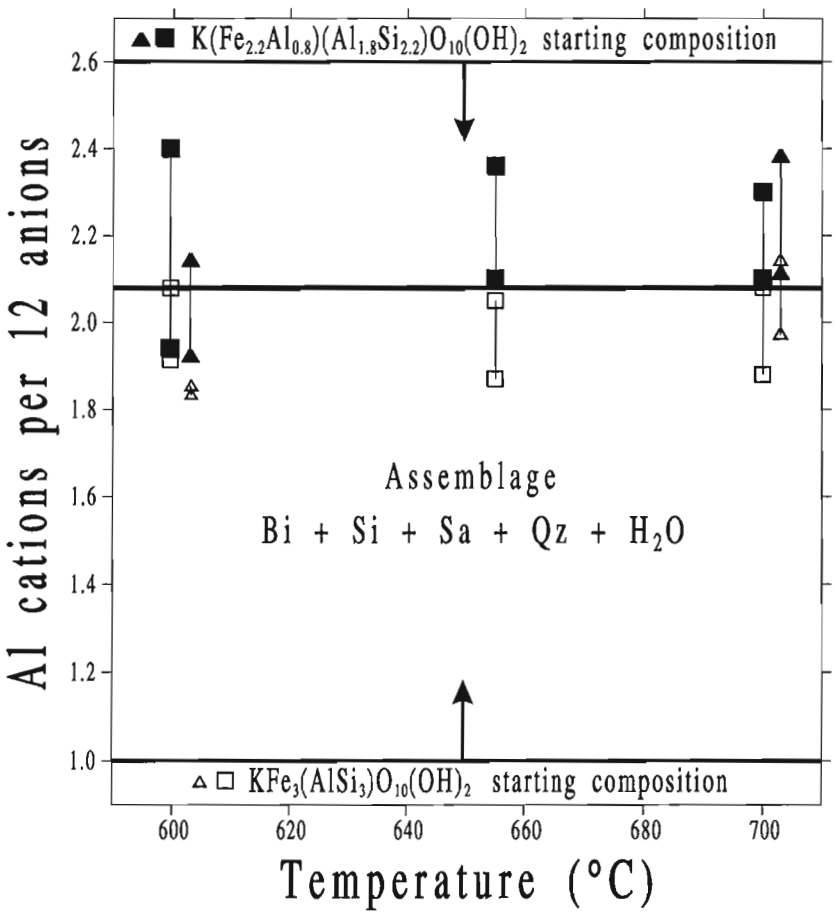

Figure 4.

Al content of Fe-biotites determined in this study (Table 2). Paired symbols show the range of Al content observed in different biotite grains of the same run product. Open and closed symbols represent the results of experiments starting with low-Al biotite (annite) and high-Al biotite (Ann_{20}), respectively. Squares and triangles represent low pressure (~2 kbar) and high pressure (~3.5 kbar) experimental data.

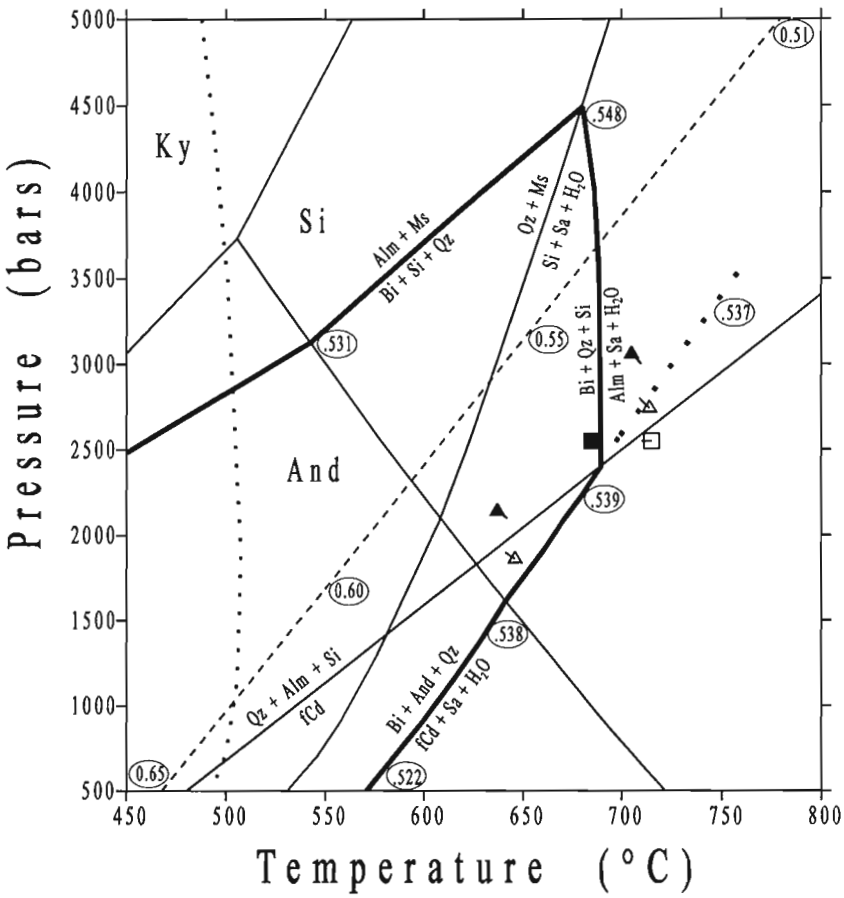

Figure 5.

P-T diagram showing breakdown of Fe-biotite + aluminosilicate + quartz. Dotted curve is position of equilibrium D computed for stoichiometric annite. Heavy solid curves (with dotted metastable extension for equilibrium A) are computed with thermodynamic data based on new experimental data of this study. Thin dashed curve is position of equilibrium A calculated with thermodynamic data of Holland and Powell (1990). Numbers beside curves are predicted Al contents (n_{Al} = $^{[4]}Al$-1 = $^{[6]}Al$) of stable biotite. Experimental data are for equilibrium D (squares; this study) and equilibrium A (triangles; Holdaway and Lee, 1977), with solid and open symbols denoting growth of low- and high-T assemblages, respectively.

Table 3. Experiments on equilibrium D.

#	Duration (days)	T(°C)	P(kbar)	Stable Assemblage[1]	% Reaction Observed
1	20	691±4.0	2.45±0.05	Bi+Si+Qz	70
3	24	709±4.0	2.34±0.09	Alm + Sa	30
4	23	728±5.0	2.48±0.07	Alm + Sa	70
2	21	748±4.0	2.43±0.07	Alm + Sa	90

DISCUSSION

Although a number of petrogenetic grids have been proposed involving biotite, most do not make explicit allowance for the incorporation of excess Al in biotite (e.g. Spear and Cheney, 1990; Pattison and Tracy, 1991). Exceptions are the grids derived by Powell and Holland (1990) and Xu et al. (1994), which use estimated thermodynamic properties for Sdr based on the assumption of zero enthalpy change for the internal equilibrium: Sdr + Phl = East + Ann. The present experimental data on equilibrium C allow direct determination of thermodynamic properties of Sdr which can be more confidently applied to petrological calculations. Because of the limited range of biotite Al contents produced in these experiments (Table 2), however, Fe-Al mixing properties can not be determined from the results on equilibrium C alone. Combination of these data with those for equilibrium D is required to provide constraints on Fe-Al mixing as discussed below.

For thermodynamic calculations we assume that Al orders onto the M1 site (Circone et al., 1991), Al-Si mixing occurs on 4 equivalent tetrahedral sites, and that all excess Al in the experimental biotites is related to Tschermak's substitution. With Sdr properties defined by the data for equilibrium C, the experimental bracket for equilibrium D is approximately 20°C higher than computed with the assumption of ideal Fe-Al mixing on the M1 site. A maximum value of W_{FeAl} = -14.3 kJ/mol is required to provide the required additional stabilization of the biotite solid solution. This value is not unreasonable considering the negative excess volume of mixing on this join (Hewitt and Wones, 1975), and compared to Fe-Al interactions obtained in studies on other silicates (Mader and Berman, 1992; Berman and Aranovich, in press).

The derived thermodynamic properties can be used to compute the equilibrium Al content and its effect on Fe-biotite stability as a function of P-T and bulk composition. Figure 5 shows some results for the upper temperature stability of the assemblage Fe-biotite + sillimanite + quartz, calculated with the program THERIAK (de Capitani and Brown, 1987). Excess Al in biotite increases very slowly as P and T increase along the breakdown curves to fCd + Sa at low P and to Alm + Sa at pressures above about 2.4 kbar (solid heavy curves in Fig. 5). Compared to the computed position for equilibrium A with pure annite (dotted curve in Fig. 5), excess Al solubility in biotite stabilizes the biotite assemblage by approximately 200°C!

The results presented above can be compared with two previous studies. First, our computed curve for equilibrium A is in excellent accord with Holdaway and Lee's (1977) bracket at 710°C (Fig. 5), and only slightly outside their 650°C bracket. This overall agreement suggests that their biotite, in spite of being synthesized with the wrong Al content, approached the equilibrium Al content during their experimental runs, and that hercynite impurities present in their starting materials did not significantly affect their interpretation of run direction. Second, experiments by Hoffer (1976) using natural Fe-Mg Cd and Bi separated from the same rock, and assumed to be in exchange equilibrium, occur about 0.5 kbar lower than predicted by calculations based on our data (Berman and Aranovich, in prep.). This correspondence is encouraging since additional Fe^{3+} in Hoffer's QFM-buffered biotite should have expanded the biotite stability field. Third, the (metastable) position of equilibrium A computed with thermodynamic data of Holland and Powell (1990; thin dashed curve in Fig. 5) lies approximately 100°C lower than our curve based on the new experimental results. Nevertheless, the magnitude of their predicted Al contents of Fe-biotite are in overall accord with the experiments reported in this paper, although their calculations show a strong decrease in Al with increasing temperature that is not supported by our results (Fig. 5). The main reason for the difference in the position of equilibrium A is the relative instability of their annite endmember, which is based on Fe-Mg exchange experiments between Bi, Gt, and Opx, as well as constraints from natural biotite-chlorite parageneses. It is the relative instability of biotite with respect to almandine that leads to exclusion of Bi + And + Qz as a stable paragenesis in their KFMASH grids (Powell and Holland, 1990; Xu et al., 1994), a point discussed further in Part 1.

In addition to their direct impact on computed petrogenetic grids, the present results have important implications for the application of Fe-Mg exchange thermometers involving biotite. Starting with the work of Indares and Martingole (1985), many workers (Sengupta et al., 1990; McMullin et al., 1991; Patino-Douce et al., 1993) have attempted to use natural partitioning data to calibrate the effect of octahedral Al on Fe-Mg partitioning, with widely divergent results. Analysis of Fe-Mg partitioning constrains only the difference between Al interactions with Fe and Mg, commonly expressed as the difference between Margules parameters, $W_{FeAl} - W_{MgAl}$. As discussed above, analysis of the experimental data presented in this study constrains $W_{FeAl} < -14.3$ kJ/mol. Circone and Navrotsky (1992) derived $W_{MgAl} = 22.8 \pm 18.7$ kJ/mol from their calorimetric measurements (assuming symmetric mixing). As this value implies a solvus between Phl-East that is not observed in single phase syntheses (Robert, 1976), we consider it more likely that W_{MgAl} is near the low end of their uncertainty range, consistent with linear volumes across the Phl-East join (Hewitt and Wones, 1975). Assuming $W_{MgAl} = 0$, the present experimental results provide a minimum estimate of $W_{FeAl} - W_{MgAl} = -14.3$ kJ/mol, which translates to approximately 80°C lower Gt-Bi temperatures for common pelitic compositions. Larger temperature corrections apply to other geothermometers which have smaller enthalpy changes than Gt-Bi. Excess Al has a much more profound effect, for example, on Fe-Mg exchange between Cd and Bi, and successful calibration and application of this thermometer must account for this effect.

CONCLUSIONS

The experimental data presented in this study tightly bracket the Al content of Fe-biotite in assemblages with sillimanite+sanidine+quartz+H_2O. The results show negligible temperature dependence of Al solubility, and are in good accord with observations on natural biotites if the effects of Ti and Fe^{3+} are considered. Reversals obtained on equilibrium D allow unambiguous definition of the stability of Fe-Bi+Si+Qz with respect to high-T, anhydrous assemblages. These data lend some support to the earlier work of Holdaway and Lee (1977), and are at odds with petrogenetic grids proposed by Spear and Cheney (1989) and Powell and Holland (1990). Preliminary analysis of the combined set of experiments indicates stabilization of Al-saturated Fe-biotite by approximately 200°C over stoichiometric annite. The derived negative excess enthalpy of mixing on the Ann-Sdr join provides the first experimental determination of Fe-Al interactions in biotite, which in combination with estimated Mg-Al biotite energetics, dictates a significant correction to Fe-Mg exchange thermometers.

To refine the effect of Al on Fe-Mg partitioning, exchange experiments involving Fe-Mg-Al biotites are in progress. An additional bracket on equilibrium D is also in progress to provide tighter constraints on the slope of biotite – almandine net transfer reactions.

ACKNOWLEDGMENTS

In addition to acknowledgements given in Part 1, we thank M. St-Onge and K.L. Currie for their helpful reviews.

REFERENCES

Bailey, S.W.
1984: Crystal chemistry of the true micas; in Micas, Reviews in Mineralogy, P.H. Ribbe (ed); Mineralogical Society of America, p. 13-60.

Berman, R.G., Aranovich, L.Y., Genkin, M., and Mader, U.K.
1995: Phase equilibrium constraints on the stability of biotite. Part 1: Mg-Al biotite in the system K_2O-MgO-Al_2O_3-SiO_2-H_2O-CO_2; in Current Research 1995-E; Geological Survey of Canada, this volume.

Berman, R.G. and Aranovich, L.Y.
in press: Optimized standard state and mixing properties of minerals: I. Model calibration for olivine, orthopyroxene, cordierite, garnet, and ilmenite in the system FeO-MgO-CaO-Al_2O_3-SiO_2-TiO_2; Contributions to Mineralogy and Petrology, accepted for publication, March 1995.

Cheney, J.T. and Guidotti, C.V.
1975: Interrelationship between Mg/Fe ratio and octahedral Al content in biotite; The American Mineralogist, v. 60, p. 849-853.

Chou, I.-M. and Cygan, G.L.
1990: Quantitative redox control and measurement in hydrothermal experiments; in Fluid-mineral interactions: a tribute to H.P. Eugster, R.J. Spencer and I.-M. Chou (ed.); The Geochemical Society, Special Publication no. 2, p. 3-15.

Circone, S. and Navrotsky, A.
1992: Substitution of Al-6,Al-4 in Phlogopite: High temperature solution calorimetry, heat capacities, and thermodynamic properties of the phlogopite-eastonite join; The American Mineralogist, v. 77, p. 1191-1205.

Circone, S., Navrotsky, A., Kirkpatrick, R.J., and Graham, C.M.
1991: Substitution of Al-6,Al-4 in Phlogopite - Mica Characterization, Unit-Cell Variation, Al-27 and Si-29 MAS-NMR Spectroscopy, and Al-Si Distribution in the Tetrahedral Sheet; The American Mineralogist, v. 76, p. 1485-1501.

Cygan, G.L., Chou, I.-M., and Sherman, D.M.
in press: The annite decomposition reaction using hydrogen sensor techniques; The American Mineralogist.

de Capitani, C. and Brown, T.H.
1987: The computation of chemical equilibrium in complex systems containing non-ideal solutions; Geochimica et Cosmochimica Acta, v. 51, p. 2639-2652.

Eugster, H.P. and Skippen, G.B.
1967: Igneous and metamorphic reactions involving gas equilibria; in Researches in Geochemistry, P.H. Abelson (ed.); John Wiley and Sons, p. 377-396.

Eugster, H.P. and Wones, D.R.
1962: Stability relations of the ferruginous biotite, annite; Journal of Petrology, v. 3, p. 82-125.

Guidotti, C.V.
1984: Micas in metamorphic rocks; in Micas, Reviews in Mineralogy, P.H. Ribbe (ed.); Mineralogical Society of America, p. 357-468.

Guidotti, C.V. and Dyar, M.D.
1991: Ferric iron in metamorphic biotite and its petrologic and crystallochemical implications; The American Mineralogist, v. 76, p. 161-175.

Harte, B. and Hudson, N.F.C.
1979: Pelite facies series and the tempeartures and pressures of Dalradian metamorphism in E. Scotland; in The Caledonides of the British Isles - reviewed, A.L. Harris, C.H. Holland and B.E. Leake (ed.); Geological Society of London Special Publication, p. 323-336.

Hewitt, D.A. and Wones, D.R.
1975: Physical properties of some synthetic Fe-Mg-Al trioctahedral biotites; The American Mineralogist, v. 60, p. 854-862.
1984: Experimental phase relations of the micas; in Micas, Reviews in Mineralogy, P.H. Ribbe (ed.); Mineralogical Society of America, p. 201-256.

Hoffer, E.
1976: The reaction sillimanite + biotite + quartz = cordierite + k-feldspar + H_2O and partial melting in the system K_2O-FeO-MgO-Al_2O_3-SiO_2-H_2O; Contributions to Mineralogy and Petrology, v. 55, p. 127-130.

Holdaway, M.J. and Lee, S.M.
1977: Fe-Mg cordierite stability in high-grade pelitic rocks based on Experimental, theoretical, and natural observations; Contributions to Mineralogy and Petrology, v. 63, p. 175-198.

Holland, T.J.B. and Powell, R.
1990: An internally consistent thermodynamic dataset with uncertainties and correlations: the system K_2O-Na_2O-CaO-MgO-MnO-FeO-Fe_2O_3-Al_2O_3-TiO_2-SiO_2-C-H_2-O_2; Journal of Metamorphic Geology, v. 8, p. 89-124.

Indares, A. and Martingole, J.
1985: Biotite-garnet geothermometry in the granulite facies: the influence of Ti and Al in biotite; The American Mineralogist, v. 70, p. 272-278.

Mader, U.K. and Berman, R.G.
1992: Amphibole thermobarometry: a thermodynamic approach; in Current Research, Part E; Geological Survey of Canada Paper 92-1E, p. 393-400.

McMullin, D.W.A., Berman, R.G., and Greenwood, H.J.
1991: Calibration of the SGAM Thermobarometer for Pelitic Rocks Using Data from Phase-Equilibrium Experiments and Natural Assemblages; Canadian Mineralogist, v. 29, p. 889-908.

Partin, E.
1984: Ferric/ferrous determinations in synthetic biotite; M.Sc. thesis, Virginia Polytechnic Institute, Blacksburg, Virginia.

Patino Douce, A.E., Johnston, A.D., and Rice, J.M.
1993: Octahedral excess mixing properties in biotite: a working model with applications to geobarometry and geothermometry; The American Mineralogist, v. 78, p. 113-131.

Pattison, D.R.M. and Tracy, R.J.
1991: Phase equilibria and thermobarometry of metapelites; in Contact Metamorphism, Reviews in Mineralogy, P.H. Ribbe (ed.); Mineralogical Society of America, p. 105-206.

Powell, R. and Holland, T.
1990: Calculated mineral equilibria in the pelite system, KFMASH (K_2O-FeO-MgO-Al_2O_3-SiO_2-H_2O); The American Mineralogist, v. 75, p. 367-380.

Rebbert, C.R.
1986: Biotite oxidation: an experimental and thermodynamic approach, M.Sc. thesis, Virginia Polytechnic Institute, Blacksburg, Virginia.

Robert, J.L.
1976: Phlogopite solid solutions in the system K_2O-MgO-Al_2O-SiO_2-H_2O; Chemical Geology, v. 17, p. 195-212.

Rutherford, M.J.
1973: The phase relations of aluminous iron biotites in the system $AlSi_3O_8$-$KAlSiO_4$-Al_2O_3-Fe-O-H; Journal of Petrology, v. 14, p. 159-180.

Schairer, J.F. and Bowen, N.L.
1955: The system K_2O-Al_2O_3-SiO_2; American Journal of Science, v. 253, p. 681-746.

Sengupta, P., Dasgupta, S., Bhattacharya, P.K., and Mukherjee, M.
1990: An orthopyroxene-biotite geothermometer and its application in crustal granulites and mantle-derived rocks; Journal of Metamorphic Geology, v. 8, p. 191-197.

Spear, F.S. and Cheney, J.T.
1989: A petrogenetic grid for pelitic schists in the system SiO_2-Al_2O_3-FeO-MgO-K_2O-H_2O; Contributions to Mineralogy and Petrology, v. 101, p. 149-164.

Xu, G., Will, T.M., and Powell, R.
1994: A calculated petrogenetic grid for the system K_2O-FeO-MgO-Al_2O_3-SiO_2-H_2O, with particular reference to contact-metamorphosed pelites; Journal of Metamorphic Geology, v. 12, p. 99-119.

Geological Survey of Canada Project 880014

Solubility of Al_2O_3 in orthopyroxene equilibrated with almandine in the system FeO-Al_2O_3-SiO_2

L.Ya Aranovich[1] and R.G. Berman
Continental Geoscience Division

Aranovich, L.Ya and Berman, R.G., 1995: Solubility of Al_2O_3 in othopyroxene equilibrated with almandine in the system FeO-Al_2O_3-SiO_2; in Current Research 1995-E; Geological Survey of Canada, p. 271-278.

Abstract: Preliminary reversed phase equilibrium data have been collected which constrain the solubility of Al_2O_3 in ferrosilite (Fs) in equilibrium with almandine garnet (Alm). The new data indicate significantly lower Al_2O_3 solubility in orthopyroxene (Opx) in the Fe-bearing system compared to the Mg-system. Orthopyroxene-garnet thermometry in crustal rocks based on the equilibrium: Fs + Al_2O_3 = Alm studied here is considerably more robust than previous calibrations based on the equivalent equilibrium in the Mg system. Results for several granulite terrannes show that Al-Opx temperatures based on the new experimental data generally yield higher temperatures than results based on Fe-Mg exchange thermometry, consistent with suggestions of previous workers. The differences in apparent closure temperatures between these equilibria (40-80°C) do not, however, appear to be as extreme as those based on previous experimental data.

Résumé : Les données préliminaires sur l'équilibre de phase inversé renseignent sur la solubilité de Al_2O_3 dans la ferrosilite (Fs) en équilibre avec l'almandin (Alm). Les nouvelles données indiquent une solubilité de Al_2O_3 significativement plus basse dans l'orthopyroxène du système à Fe que dans le système à Mg. La thermométrie de l'orthopyroxène-grenat dans les roches de la croûte basée sur l'équilibre Fs + Al_2O_3 = Alm à l'étude dans le cas présent est considérablement plus robuste que les étalonnages précédents basés sur l'équilibre équivalent dans le système à Mg. Les résultats obtenus pour plusieurs terranes de granulites révèlent que les températures de Al-Opx basées sur les nouvelles données expérimentales donnent généralement des températures plus élevées que les résultats basés sur la thermométrie de l'échange Fe-Mg, ce qui corrobore les propositions faites antérieurement par les chercheurs. Les différences dans les températures de fermeture apparentes entres ces équilibres (40-80°C) ne semblent pas, cependant, être aussi extrêmes que celles fondées sur des données d'expériences antérieures.

[1] Institute of Experimental Mineralogy, Chernogolovka, Russia

INTRODUCTION

The Al_2O_3 content in orthopyroxene coexisting with garnet in a variety of rock types has long been recognized as a sensitive indicator of the pressure (P)-temperature (T) conditions at which rocks equilibrated. Initial experimental investigations focussed on the simplest chemical system, MgO-Al_2O_3-SiO_2 (MAS), in order that P-T estimates could be derived for ultramafic, upper mantle xenoliths (e.g. Boyd, 1973). More recent interest in Opx-Gt thermobarometry stems from attempts to understand lower crustal processes by defining metamorphic conditions for granulite facies rocks. Of fundamental importance to these endeavors are inferences that the Al_2O_3 content of Opx in equilibrium with Gt (here referred to as "Al-Opx" thermobarometry) may be considerably more resistant to post-peak temperature re-equilibration than Fe-Mg exchange thermometers (Aranovich and Podlesskii, 1989; Fitzsimons and Harley, 1994; Pattison and Bégin, 1994; Bégin and Pattison, 1994). The interpretation that the Al-Opx thermometer may be better able to "remember" near-peak P-T conditions is based on observed compositional maps of Opx (Pattison and Bégin, 1994), but particularly on comparative Al-Opx versus Fe-Mg thermometry, the results of which are extremely sensitive to thermometer calibration.

The amount of Al_2O_3 entering orthopyroxene in the MAS system was experimentally calibrated as a function of pressure and temperature by Perkins et al. (1981), Gasparik and Newton (1984), and Aranovich and Kosyakova (1984) for garnet-, spinel-, and cordierite-bearing assemblages, respectively. Most recent studies have attempted to calibrate the P, T, and compositional dependence of Al_2O_3 in Opx in the system FeO-MgO-Al_2O_3-SiO_2 (FMAS) which more closely represents orthopyroxene occurrences in crustal rocks (e.g. Kawasaki and Matsui, 1983; Harley, 1984; Aranovich and Kosyakova, 1984, 1987; Lee and Ganguly, 1988; Eckert and Bohlen, 1992). All of these studies demonstrated the large effect of Fe on Al_2O_3 solubility in Opx: in garnet-bearing assemblages Al_2O_3 decreases with increasing bulk Fe/Mg ratio, while in cordierite-bearing assemblages Al_2O_3 increases with increasing Fe/Mg. Unfortunately, there is no consensus among these studies in quantifying this effect: the data of Harley (1984) seem to indicate a very sharp decrease in Al-solubility while those of Aranovich and Kosyakova (1984, 1987) a rather smooth one; the other studies fall in between these extremes.

A major drawback of the FMAS studies mentioned above is that, with the exception of 3 experimental brackets of Lee and Ganguly (1988), equilibrium was not demonstrated by reversals of the Al_2O_3 content of Opx approached from under- and oversaturation. Lack of reversed phase equilibrium data makes modelling of the thermodynamic properties of Al-bearing Opx highly uncertain, and prevents robust calibration of thermobarometers involving aluminous Opx. We became aware of this uncertainty in the course of a thermodynamic analysis of high-temperature minerals in the system FMAST (Berman and Aranovich, in press), and found that this uncertainty severely affects the conclusions regarding the possibility of recovering "near-peak temperatures" of granulite-facies metamorphism with Al-Opx and Fe-Mg exchange thermometry.

To help resolve these uncertainties in the primary experimental data as well as the ambiguities in applications, reversed experimental data that constrain thermodynamic properties of Al-Opx in Fe-rich systems are sorely needed. In this report we present preliminary data for the equilibrium:

$$Fe_3Al_2Si_3O_{12} = 3\ FeSiO_3 + Al_2O_3 \qquad (1)$$

in which the orthopyroxene solid solution is expressed using the components, ferrosilite (Fs) and orthocorundum (Ok = Al_2O_3). From an experimental standpoint, the advantage of employing this equilibrium is that it involves only one binary solid solution phase (Opx) whose equilibrium composition can be approached from opposite directions at fixed P-T conditions.

EXPERIMENTAL METHODS

Starting materials

Starting almandine garnet was prepared following the procedure suggested by Bohlen et al. (1983). First, almandine glass was obtained by melting 0.5 g of a stoichiometric mix of Fe_2O_3, Al_2O_3, and SiO_2 (all oxides as reagent grade chemicals) in a graphite crucible at 1-atmosphere and 1300°C for about 20 minutes. The glass had a homogeneous dark green colour and was practically void of metallic Fe inclusions. Its chemical composition determined by microprobe analysis exactly corresponded to almandine stoichiometry. Almandine was crystallized from the finely ground glass using a graphite container in a piston-cylinder apparatus at 20 kbar and 1200°C for approximately 24 hours. No phases other than

Table 1. Chemical analyses (wt.% and cations) of synthetic minerals.

Phase	Alm	Fs	Al-Fs (avg.)	Al-Fs 1	Al-Fs 2	Al-Fs 3
# of analyses	8	6	20	1	1	1
$FeO^{\$}$	43.05	45.76	51.86	50.59	54.08	51.31
Al_2O_3	20.38		5.08	5.24	2.99	5.91
SiO_2	36	54.61	42.84	42.75	44.3	42.24
Total	99.43	100.37	99.78	98.58	101.37	99.46
Si	2.99	1	0.93	0.94	0.95	0.92
Al	1.99		0.13	0.13	0.08	0.15
Fe	3.01	1	0.94	0.93	0.97	0.93
Oxygen	12	3	3	3	3	3

$^{\$}$ All Fe as FeO

Analyses in last 3 columns show range of Al-Fs analyses

almandine were identified in the synthesis products. Almandine had a greenish colour with very little brown-red tint, suggesting almost no Fe^{3+}. Unit cell parameters are in very good agreement with that determined by Bohlen et al. (1983). Electron microprobe analysis of the synthetic garnet (Table 1) also showed excellent agreement with theoretical almandine stoichiometry, thus implying no significant ferric iron.

End-member ferrosilite was crystallized from a mechanical mix of Fe-oxalate with silica in sealed Au capsules in a piston-cylinder device at 900°C and 15 kbar for 24 hours. Approximately 5 wt.% excess SiO_2 was added to the ferrosilite mix to saturate the fluid phase that was formed on decomposition of Fe-oxalate with respect to silica. The synthesis products were relatively coarse grained ferrosilite with subordinate amounts of quartz and graphite. No other phases were determined by optical, XRD, and SEM analysis. Presence of graphite precipitated from the C-O-H fluid phase during the syntheses indicates rather low oxygen fugacity conditions (about 1 log unit below those on the QFM buffer). Both unit cell parameters and chemical composition of the synthetic ferrosilite (Table 1) suggest that little to no Fe^{3+} is present.

Orthopyroxene containing 5 wt.% Al_2O_3 (Al-Fs) was synthesized in a two-step procedure similar to that suggested by Gasparik (1987) for making Al-rich Opx on the enstatite-Mg-Tschermak join. First, a mechanical mix of Fe-oxalate, silica, and γ-Al_2O_3 was melted in a sealed Au capsule at 1050°C and 15 kbar in piston-cylinder apparatus for 30 minutes. Then the temperature was decreased to 950°C , and the sample held at this lower temperature for another 3 hours. The products of the syntheses consisted of orthopyroxene, with minor quartz and graphite, and traces of fayalite as inclusions in the central parts of large Opx grains (Fig. 1a). No individual fayalite grains were identified by optical, XRD, SEM, or microprobe analysis. The aluminous Opx crystallized metastably (see discussion below regarding stable assemblage at these conditions) as large elongate grains with subordinate short-prismatic grains. The crystals had a dark-green colour and strong pleochroism, similar to that of pure ferrosilite. Its chemical composition ranged from 3.6-6.0 wt.% Al_2O_3 (Table 1: Al-Fs #1-3) clustering at the nominal 5 wt.% (Table 1). Unit cell parameters show a systematic decrease from those of Fs, indicating that Al_2O_3 in Fe-orthopyroxene has a similar, but somewhat greater effect on Opx volume compared to the MAS system.

Two starting mixes were used for the reversal runs: one consisted of equal amounts of Alm and Fs (mix "a" in Table 2), and another of equal amounts of Alm and Al-Fs (mix "b" in Table 2). In a few runs we employed the starting mix used for the Al-Fs synthesis (mix "c" in Table 2), in order to compare the results of these "synthesis" runs to other studies that employ non-crystalline starting materials (Kawasaki and Matsui, 1983; Harley, 1984).

In the reversal experiments, 3 to 4 mg of starting mix was loaded in 1/2-inch Au capsules along with 0.5-1.0 mg of hydrated oxalic acid and about 0.2 mg graphite powder. Capsules were then sealed by arc welding and placed in the high-pressure assembly described below.

Apparatus and run procedure

All experiments were carried out in a conventional piston-cylinder apparatus with 19.01 mm diameter furnace assemblies and pistons. The assembly and technique for bringing P-T parameters of the runs up to the required values exactly corresponded to those described in detail by R.C. Newton in Johannes et al. (1971) and Johannes (1973). Temperature was measured with W-Re thermocouples with no correction for the effect of pressure on emf. No pressure correction was applied to the NaCl assemblies in accord with the findings of many workers (e.g. Johannes et al., 1971). P-T fluctuations during the runs did not exceed 0.1 kbar and 1°C, respectively.

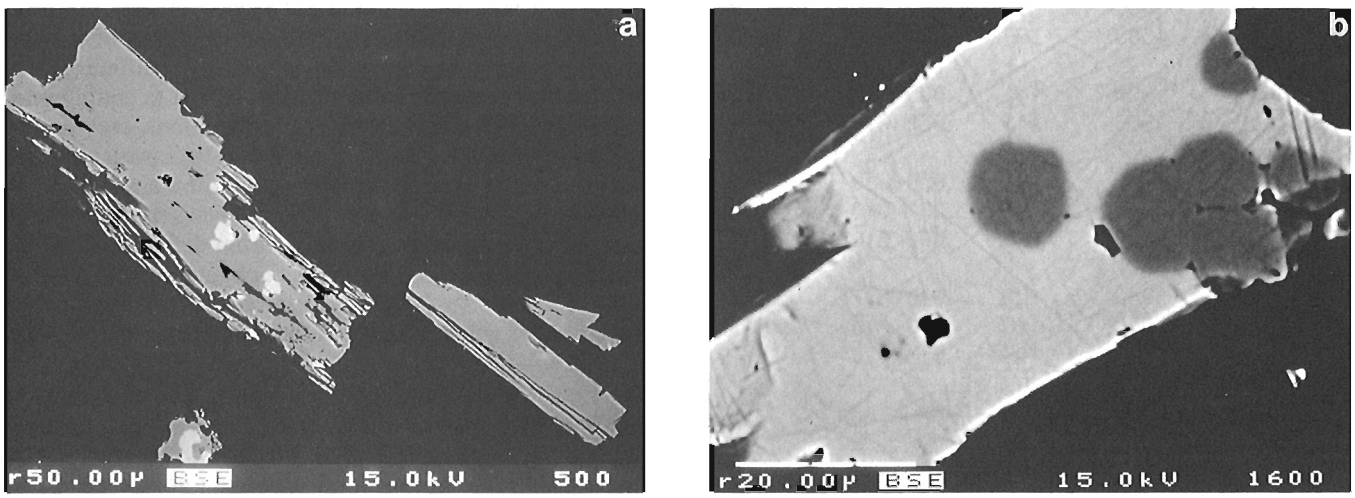

Figure 1. *Backscattered electron images of synthesis and reversal run products: (**a**) synthetic Opx with 5 wt% Al_2O_3; bright spots are fayalite nuclei; (**b**) almandine (dark spots)-Opx (bright matrix) intergrowth in run 2b.*

Overall uncertainties associated with temperature gradient along the graphite heater and pressure calibration of the NaCl assembly are no greater than ± 5°C and 0.4 kbar, respectively.

Two capsules, one containing mix a and the other mix b, were placed horizontally inside graphite cylinders and run simultaneously to eliminate possible differences in P-T conditions for each reversal experiment. Run duration varied from 2 days at 1000°C to 6 days at 850°C.

RUN PRODUCTS

All run products were analyzed optically, by SEM, and by electron microprobe. X-ray diffraction was not used to analyze products of the reversal runs in order to avoid grinding of the samples that could obscure any possible within-grain inhomogeneity of run products. Optical examination was found quite sufficient for identifying final phases in the runs, primarily due to the fairly distinct optical properties of the phases. The results of optical studies were always supported by back-scattered electron images and microprobe analysis.

Analyses were made using the University of Chicago Cameca SX-50 automated electron microprobe. Operating conditions were 15 kV accelerating potential, 25 nA current as measured by the Faraday cup, and a focused electron beam. X-ray intensities were obtained using wavelength dispersive spectrometers with backgrounds obtained by offsetting spectrometers on either side of the peak. Standards were natural anorthite for Al and natural Fe-rich olivine for Fe and Si. Matrix corrections were those supplied by the manufacturer (PAP correction procedure). Estimated uncertainties of the analyses do not exceed 2% of the amount present.

Table 2. Experimental data for equilibrium (1).

#.	P (kbar)	T°C	Time (hours)	Final X_{ok} Range	Eqm X_{Ok} [2]
1a	15	950	70	.007-.015	0.015
1b	15	950	70	.067-.016	0.016
1c	15	950	94	.009-.018	
2a	15	1000	69	.012-.019	0.019
2b	15	1000	69	.062-.020	0.020
3a	15	900	141	.005-.012	0.012
3b	15	900	141	.068-.014	0.014
4a	15	850	169	.000-.010	0.010
4b	15	850	169	.081-.010	0.010
4c	15	850	188	.008-.016	
5a	12	950	120	.010-.017	0.017
5b	12	950	120	.070-.019	0.019
5c	12	950	144	.014-.020	
6a	10	900	167	Alm+Fa+Qz	
6b	10	900	167	Alm+Fa+Qz	

All runs contain Alm + Al-Opx, except for 6a and 6b; Runs 5a-5c also contain Fa
[1] X_{Ok} = Al cations / 2
[2] Estimated equilibrium value based on most advanced Opx compositions

Special care was taken in selecting spots for microprobe analysis. Due to the same Fe:Si ratio in garnet and orthopyroxene any possible overlap of the analyzed Gt and Opx grains would have produced "artificial" Opx compositions with high Al_2O_3 content. To avoid this problem, back-scattered electron imaging was used to select all analysis spots. Opx grains were not analyzed closer than 3 μm to the rims, to avoid "edge effects" (Ganguly et al., 1988).

Individual analyses were accepted if elemental oxide totals were 100 ± 2% and stoichiometries did not deviate by more than 1.5% in any cation site from ideal almandine or orthopyroxene mineral formulae. With these criteria applied, no appreciable ferric iron in either garnet or orthopyroxene was indicated in the microprobe analyses. Very good agreement between calculated octahedral and tetrahedral Al atoms in Opx provided an additional indication of the high quality of the accepted analyses.

EXPERIMENTAL RESULTS

A major difficulty in interpreting the results of experiments on solid-solution bearing equilibria in systems containing Al_2O_3 arises from compositional inhomogeneity of run products (e.g. Perkins et al., 1981; Aranovich and Kosyakova, 1984; Aranovich and Pattison, 1995). We also encountered this problem in our study. Opx from any single experimental charge varies in composition both within individual grains and from grain to grain. The intergranular compositional heterogeneity was found to be more pronounced than zoning within crystals, indicating that the major mechanism of equilibration was dissolution-precipitation via a fluid phase rather than solid state diffusion (e.g. Pattison, 1994).

About 20-30 grains of Opx were analyzed in each run. A group (not less than 4 individual points) of spot analyses, either of separate homogeneous grains or of rims of a single zoned grain, representing compositions most different from the starting ones were assumed to be closest to equilibrium. These compositions, along with run conditions, are given in Table 2. With the exception of run # 4a at the lowest temperature, we did not observe pure Fs in runs with starting mix "a", whereas most runs using mix "b" contained some Opx grains with Al contents indistinguishable from that of Al-Fs. This contrast indicates that forward reaction rate is faster than the backward reaction (1). Such "asymmetry" in the rates of forward and backward reactions seems to be a typical feature of solid solution reactions (e.g. Aranovich, 1976; Aranovich and Pattison, 1995). One implication is that midpoints of compositional brackets for these reactions may not represent the most probable equilibrium position (as is assumed in least-squares methods of fitting phase equilibrium data).

Unlike the results obtained on similar reactions in MAS (e.g. Perkins et al., 1981; Aranovich and Kosyakova, 1984), our data do not show any overlapping of the most advanced

compositions of Opx in the coupled runs. This is most likely explained by faster reaction rates for both half-reactions in the FAS compared to MAS system. In addition, microprobe analysis of FAS run products was facilitated by the greater difference in atomic numbers between Al and Fe compared to Mg and Al.

Also presented in Table 2 are the results of a few "synthesis"-type experiments in which the same mechanical mix as for the Al-Opx synthesis was used as a starting material. With sufficient duration, these runs produced low-Al Opx and almandine, suggesting that syntheses of Al-Fs involved metastable growth of higher Al Opx (~5% Al_2O_3) during much shorter run times. The compositional range of the resulting Opx (Table 2) was generally not as large as that in the runs using the crystalline starting mixes, and in all cases the range spanned that of the equilibrium value determined with the crystalline materials. Thus, although the results produced by the synthesis runs are consistent with those produced with crystalline starting materials, the knowledge of the direction of compositional approach to equilibrium with the latter materials yields a more precise estimate of equilibrium compositions.

Our data indicate very limited solubility of Al_2O_3 (<0.02 X_{Ok}) in Fe-Opx, which is significantly lower than that in Mg-Opx (~0.06 X_{Ok}) under the same P-T conditions. This result is consistent with the much larger stability field of almandine relative to pyrope and the much smaller stability field of ferrosilite relative to enstatite. Unfortunately, we have been able to collect data on equilibrium (1) over a rather restricted range of P-T conditions. At higher temperature we observed melting of Alm in presence of H_2O-CO_2 fluid. At lower pressure, Al-free Opx decomposes to Fa+Qz (Bohlen et al., 1980; Bohlen and Boettcher, 1981). In the FAS system, the lower pressure limit of Opx stability is defined by the univariant reaction (Fig. 2):

$$2[(x)FeSiO_3 + (1\text{-}x)Al_2O_3] = (4x\text{-}3)Fe_2SiO_4 + 2(1\text{-}x)Fe_3Al_2Si_3O_{12} + (4x\text{-}3)SiO_2$$

In runs at 950°C and 12 kbar (# 5a, 5b in Table 2) we did observe fayalite in run products. Although the above equilibrium has not been reversed, we believe that these conditions are very close to the univariant equilibrium for the following reasons. First, both half-reversal runs produced very similar final Opx compositions (X_{Ok} = .017-.019) which implies that Opx was stable. Second, the calculated position of this equilibrium, using thermodynamic properties that do not incorporate constraints on its location, is within 200 bars of these nominal P-T coordinates (Fig. 2). Further experiments are planned to extend the present data set to higher pressure.

DISCUSSION

The phase equilibrium data presented above provide important constraints on the position and slope of isopleths of Opx Al_2O_3 content in the FAS system. Figure 2 shows isopleths computed with thermodynamic data based on the data presented in this study in addition to a large body of other experimental data constraining FMAS minerals. Derivation of the thermodynamic data (available on request from the second author) incorporates uncertainties in P, T, and composition, and is discussed in detail elsewhere (Berman and Aranovich, in press). Of primary importance is the conclusion based on the new experiments that Al_2O_3 solubility in FAS Opx is considerably lower than the value based on the lone other reversal (at 46 kbar and 1300°C) by Kawasaki and Matsui (1983). Constraints provided by the volume of Al-Fs determined in this study do not allow these high pressure data to be accommodated within the uncertainties of the present data set. Also important is the conclusion (Berman and Aranovich, in press) that the present experimental data are completely compatible with the only other reversed Al_2O_3 solubilities, in MAS (Perkins et al., 1981) and in FMAS (Lee and Ganguly, 1988), and merge more easily with the combined FMAS data set than the Kawasaki and Matsui bracket. Taken together, these results suggest that quantitative calculations applied to natural FMAS Opx can now be more reliably performed.

The FAS equilibrium (1) investigated in this study is linearly related to an equivalent MAS equilibrium

$$Py = En + Ok \qquad (2)$$

which intersects the Fe-Mg exchange equilibrium between Opx and Gt

$$Py + 3\,Fs = Alm + 3\,En \qquad (3)$$

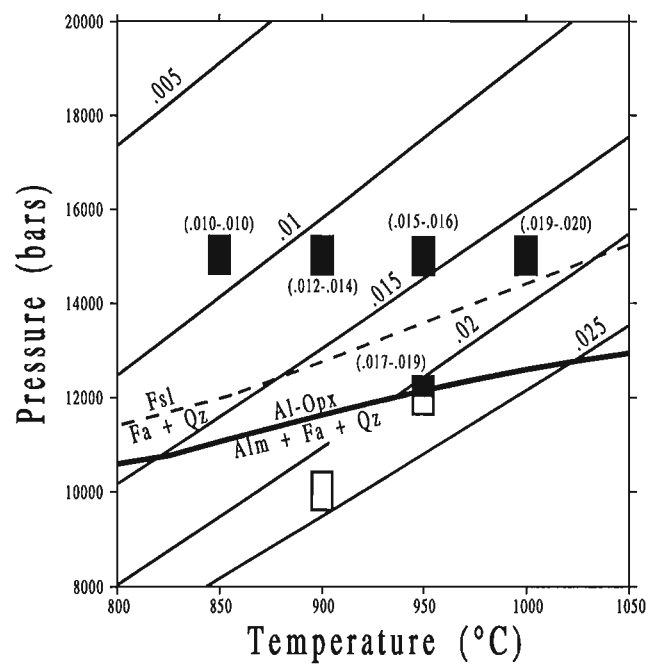

Figure 2. Experimental results constraining the equilibrium: 3 Fs + Ok = Alm (1). Size of boxes shows experimental P-T uncertainties, with nominal X_{Ok} values in parentheses. Experiments produced the assemblages: Opx + Gt (solid), Opx + Gt + Fa (half-filled box), and Gt + Fa + Qz (open box). Isopleths of X_{Ok} (lighter curves), and univariant phase boundaries (heavy curves) calculated as described in text.

at an invariant point (Fig. 3). Compared to the MAS equilibrium (2), the FAS equilibrium (1) has a considerably larger enthalpy and entropy of reaction, which makes it a much more robust thermobarometer. The MAS equilibrium has a more shallow slope than the FAS equilibrium (Fig. 3), a difference that dictates that it will always produce poorer agreement with the exchange equilibrium (3) than equilibrium (1), except if pressure estimates yield the invariant point. Under optimal circumstances, intersection of equilibrium (1) and (3) define P and T uniquely, but the acute angle of intersection of these equilibria is not conducive to reliable P-T determinations. A better approach is to use a net transfer equilibrium involving garnet and plagioclase as a barometer, and retrieve T estimates from comparison of the positions of equilibria (1) and (3).

Applications

Recent applications, utilizing the MAS equilibrium and Harley's experimental data as a basis of calculations (Bégin and Pattison, 1994), have concluded that Al-Opx yields significantly higher P-T results than the Fe-Mg exchange equilibrium. These results appear consistent with compositional maps of Opx that show greater zonation in Fe-Mg ratio than Al_2O_3 contents (Pattison and Bégin, 1994), and that have been attributed to diffusional reequilibration at lower than peak temperatures. Following a correction procedure suggested by Fitzsimons and Harley (1994) based on pressure differences recorded by equilibrium (2) and the Gt-Opx-Plag-Qz barometer, Bégin and Pattison (1994) estimated the amount of Fe-Mg re-equilibration from the difference in temperatures computed with equilibrium (2) and (3). "Peak" temperatures are then recomputed from Opx and Gt compositions adjusted for this late Fe-Mg exchange. With this technique, Bégin and Pattison (1994) computed P-T conditions for paragneisses from the Minto Block, northern Quebec between 5.7-10.9 kbar and 760-1035°C (circles in Fig. 3), up to 300°C higher than unadjusted Fe-Mg exchange temperatures. Their results show a regional difference in P-T conditions with generally higher pressures in the west part of the region, and near-isobaric P-T paths.

Figure 3 shows preliminary results of thermobarometric calculations utilizing the thermodynamic data based on the experiments reported in this paper. For the same Minto Block mineral core compositions used by Bégin and Pattison (1994), we calculate (triangles in Fig. 3) considerably lower temperatures (625-850°C) with equilibrium (1). For the two highest T rocks, equilibrium (1) yields higher temperatures than equilibrium (3), but the differences are less than 40°C. The lowest T rock shows lower Al-Opx than Fe-Mg exchange temperatures. Our results therefore suggest that the less pronounced compositional zoning profiles for Al_2O_3 compared to Fe-Mg in Opx observed by Pattison and Bégin (1994) correspond to small differences (up to 40°C) in closure of the two thermometers. The lower temperatures computed here also lead to calculated pressures that are 2.5-3.0 kbars lower (<6.7 kbar), and which do not show any systematic regional

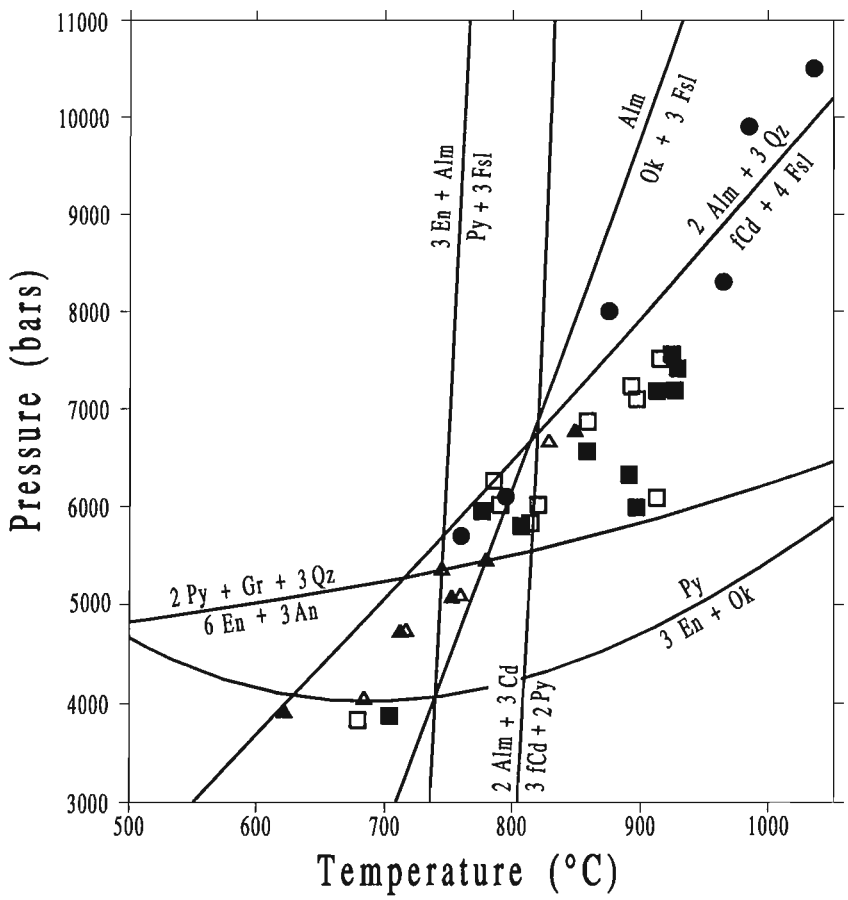

Figure 3.

Computed P-T results for Opx-Gt samples from the Minto block (Bégin and Pattison, 1994) and Ashuanipi complex (Percival, 1991). Curves shown for Minto sample B74B. Note geometry of invariant point which dictates that the MAS equilibrium (2) always yields more discordant temperatures than the FAS equilibrium (1), compared to the Fe-Mg exchange thermometer (equilibrium 3). P-T results for Minto samples (triangles) and Ashuanipi samples (squares) are based on intersection of the Opx-Gt-Plag-Qz barometer with the FAS equilibrium (1; solid symbols) or with the Fe-Mg exchange equilibrium (3, open symbols). Circles show P-T results of Bégin and Pattison (1994) for Minto block samples.

variation. These results are in excellent agreement with Al-hornblende pressures reported by Percival et al. (1992). It should be noted, however, that our calculations apply only to six samples for which representative data were published by Bégin and Pattison (1994), and only one (P88) is from the high-P region computed by them.

P-T results for diatexites and paragneisses of the Ashuanipi Complex, northern Quebec (Percival, 1991) are also shown in Figure 3. For this group of samples, Al-Opx temperatures are generally higher than Fe-Mg temperatures, with two samples showing differences up to approximately 80°C. Overall, the entire group of Ashuanipi samples yields higher temperatures than the Minto Block samples, with all but one sample in the 790-900°C range. The difference with the Minto Block rocks is not easily related to calibration problems because both groups of samples have very similar chemical compositions. Taken as a whole, the combined results support previous suggestions (Aranovich and Podlesskii, 1989; Fitzsimons and Harley, 1994; Bégin and Pattison, 1994) that Al_2O_3 solubility in Opx is less susceptible to post-thermal peak reequilibration. Al-Opx calculations based on the more robust FAS equilibrium (1) indicate that the maximum difference in closure temperature of Al-Opx versus Fe-Mg exchange is likely in the order of 40-80°C. Smaller differences recorded by many of the samples shown in Figure 3 are probably related to textural differences, such as grain size and proximity of Opx-Gt grains.

Both the Minto block and Ashuanipi Complex are dominated by unmetamorphosed granodioritic rocks (Percival et al., 1992) with subsidiary amounts of metasedimentary supracrustal rocks. Bégin and Pattison (1994) presented petrogenetic grid arguments that minimum temperatures in the Minto block were at least 800°C to form Gt-Opx-Plag-Qz-melt assemblages, and they also reported spinel + Qz inclusions in cordierite that may indicate even higher temperatures. If these observations are extrapolated to a regional scale, they suggest that the two terranes may have formed under very similar P-T conditions, and that the dominant contrast between them is in their post-"peak" P-T history. Available U-Pb data for zircon and monazite (Percival et al., 1992) point to a more protracted cooling history, including localized amphibolite retrogression, for the Ashuanipi complex compared to that of the Minto block. This contrast between the records preserved by the isotopic and thermobarometric systems seems most compatible with post-thermal peak re-equilibration being strongly affected by local variations in the availability of fluids.

ACKNOWLEDGMENTS

LYA's work on this project was supported by the NSF grant EAR-9310264 (to R.C. Newton). Bob Newton's very helpful advice regarding experiments are greatly appreciated. We also thank Ian Steele for his generous help with the microprobe analyses and Joe Pluth for assistance with XRD measurements.

REFERENCES

Aranovich, L.Y.
1976: Phase correspondence in the system epidote-garnet according to experimental data; in Contributions to physico-chemical petrology, Nauka Press, Moscow, p. 14-33 (in Russian).

Aranovich, L.Y. and Kosyakova, N.A.
1984: Experimental study of the equilibrium: cordierite+orthopyroxene+quartz in the system $FeO-MgO-Al_2O_3-SiO_2$; Doklady Akademii Nauk SSR, v. 274, p. 399-401 (in Russian).
1987: The cordierite = orthopyroxene + quartz equilibrium: laboratory data on and thermodinamics of ternary Fe-Mg-Al orthopyroxene solid solutions; Geochemistry International, v. 24, no. 3, p. 111-131.

Aranovich, L.Y. and Pattison, D.R.M.
1995: Reassessment of the garnet-clinopyroxene Fe-Mg exchange thermometer: I. Reanalysis of the Pattison and Newton (1989) run products; Contributions to Mineralogy and Petrology, v. 119, p. 20-31.

Aranovich, L.Y. and Podlesskii, K.K.
1989: Geothermobarometry of high-grade metapelites: simultaneously operating reactions; in Evolution of Metamorphic Belts, R.A. Cliff, B.W.D. Yardley and J.S. Daly (ed.); Blackwell Scientific Publications, Oxford, p. 45-62.

Bégin, N.J. and Pattison, D.R.M.
1994: Metamorphic evolution of granulites in the Minto block, northen Quebec: extraction of peak P-T conditions taking account of late Fe-Mg exchange; Journal of Metamorphic Geology, v. 12, p. 411-428.

Berman, R.G. and Aranovich, L.Y.
in press: Optimized standard state and mixing properties of minerals: I. Model calibration for olivine, orthopyroxene, cordierite, garnet, and ilmenite in the system $FeO-MgO-CaO-Al_2O_3-SiO_2-TiO_2$; Contributions to Mineralogy and Petrology, (accepted for publication, March 1995).

Bohlen, S.R. and Boettcher, A.L.
1981: Experimental investigations and geological applications of orthopyroxene geobarometry; The American Mineralogist, v. 66, p. 951-964.

Bohlen, S.R., Essene, E.J., and Boettcher, A.L.
1980: Reinvestigation and application of olivine-orthopyroxene-quartz barometry; Earth and Planetary Science Letters, v. 47, p. 1-10.

Bohlen, S.R., Wall, V.J., and Boettcher, A.L.
1983: Experimental investigations and geological applications of equilibria in the system $FeO-TiO_2-Al_2O_3-SiO_2-H_2O$; The American Mineralogist, v. 68, p. 1049-1058.

Boyd, F.R.
1973: A pyroxene geotherm; Geochimica et Cosmochimica Acta, v. 37, p. 2533-2546.

Eckert, J.O. and Bohlen, S.R.
1992: Reversed experimental determinations of the $Mg-Fe^{2+}$ exchange equilibrium in Fe-rich garnet-orthopyroxene pairs; Transactions of the American Geophysical Union, v. 73, p. 608.

Fitzsimon, I.C.W. and Harley, S.L.
1994: Disequilibrium during retrograde cation exchange and recovery of peak metamorphic temperatures: a study of granulites from Antarctica; Journal of Petrology, v. 35, p. 543-576.

Ganguly, J., Bhattacharya, R.N., and Chakraborty, S.
1988: Convolution effect in the determination of composition profiles and diffusion coefficients by microprobe step scans, American-Mineralogist, v. 73, p. 901-909.

Gasparik, T.
1987: Orthopyroxene thermobarometry in simple and complex systems; Contributions to Mineralogy and Petrology, v. 96, p. 357-370.

Gasparik, T. and Newton, R.C.
1984: The reversed alumina contents of orthopyroxene in equilibrium with spinel and forsterite in the system $MgO-Al_2O_3-SiO_2$; Contributions to Mineralogy and Petrology, v. 85, p. 186-196.

Harley, S.L.
1984: The solubility of alumina in orthopyroxene coexisting with garnet in $FeO-MgO-Al_2O_3-SiO_2$ and $CaO-FeO-MgO-Al_2O_3-SiO_2$; Journal of Petrology, v. 25, p. 665-696.

Johannes, W.
1973: Eine vereinfachte piston-zylinder-apparatur hoher genauigkeit; Neues Jahrbuch fuer Mineralogie. Monatshefte, v. 7/8, p. 337-351.

Johannes, W., Bell, M., Mao, H.K., Boettcher, A.L., Chipman, D.W., Hays, J.F., Newton, R.C., and Seifert, F.
1971: An interlaboratory comparison of piston-cylinder pressure calibration using the albite-breakdown reaction; Contributions to Mineralogy and Petrology, v. 32, p. 24-38.

Kawasaki, T. and Matsui, Y.
1983: Thermodynamic analyses of equilibria involving olivine, orthopyroxene and garnet; Geochimica et Cosmochimica Acta, v. 47, p. 1661-1679.

Lee, H.Y. and Ganguly, J.
1988: Equilibrium compositions of coexisting garnet and orthopyroxene: Experimental determinations in the system $FeO-MgO-Al_2O_3-SiO_2$, and applications; Journal of Petrology, v. 29, p. 93-113.

Pattison, D.R.M.
1994: Are reversed Fe-Mg exchange and solid solution experiments really reversed?; The American Mineralogist, v. 79, p. 938-950.

Pattison, D.R.M. and Bégin, N.J.
1994: Compositional maps of metamorphic orthopyroxene and garnet: Evidence for a hierarchy of closure temperatures and implications for geothermometry of granulites; Journal of Metamorphic Geology, v. 12, p. 387-410.

Percival, J.A.
1991: Granulite-facies metamorphism and crustal magmatism in the Ashuanipi complex, Quebec Labrador, Canada; Journal of Petrology, v. 32, p. 1261-1297.

Percival, J.A., Mortensen, J.K., Stern, R.A. and Card, K.D.
1992: Giant granulite terrains of northeastern Superior Province: the Ashuanipi complex and Minto block; Canadian Journal of Earth Sciences, v. 29, p. 2287-2308.

Perkins, D., Holland, T.J.B., and Newton, R.C.
1981: The Al_2O_3 contents of enstatite in equilibrium with garnet in the system $MgO-Al_2O_3-SiO_2$ at 15-40 kbar and 900-1600C; Contributions to Mineralogy and Petrology, v. 78, p. 99-109.

Geological Survey of Canada Project 880014

The petrological variations of the Ordovician felsic volcanic rocks of the Tetagouche Group, New Brunswick[1]

Neil Rogers
Continental Geoscience Division

Rogers, N., 1995: The petrological variations of the Ordovician felsic volcanic rocks of the Tetagouche Group, New Brunswick; in Current Research 1995-E; Geological Survey of Canada, p. 279-286.

Abstract: The Acadians Range Complex in northern New Brunswick contains extensively deformed felsic volcanic rocks of the Middle Ordovician Tetagouche Group. The felsic volcanic rocks contain a cryptic stratigraphy that has been obscured by deformation and low grade metamorphism. Using detailed petrology and geochemistry the felsic volcanic rocks have been subdivided into three formations and two intrusive lithodemes.

The Caribou Mine Formation consists of three distinct feldspar phyric members and is readily distinguished from the rest of the complex by its phenocryst population. The approximately contemporary Nepisiguit Falls Formation consists of a series of mostly pyroclastic quartz-feldspar porphyries. The Flat Landing Brook Formation is dominated by nearly aphyric ignimbrites and rhyolite flows. A region of coarse co-ignimbritic breccias is interpreted to represent a caldera. The two lithodemes are quartz-feldspar porphyries that are identified by their phenocryst populations and their chemical compositions.

Résumé : Le Complexe d'Acadians Range dans le nord du Nouveau-Brunswick contient des roches volcaniques felsiques très déformées du Groupe de Tetagouche de l'Ordovicien moyen. Les roches volcaniques felsiques contiennent une stratigraphie cryptique qui a été masquée par la déformation et un faible métamorphisme. En utilisant une pétrologie et une géochimie détaillées, on a subdivisé les roches volcaniques felsiques en trois formations et deux lithodèmes intrusifs.

La Formation de Caribou Mine est composé de trois membres distincts à phénocristaux de feldspath qui se distinguent facilement du reste du complexe par ses phénocristaux. La Formation de Nepisiguit Falls à peu près contemporaine est constituée d'une série de porphyres quartzofeldspathiques surtout pyroclastiques. La Formation de Flat Landing Brook est surtout composée d'ignimbrites quasi aphyriques et de coulées de rhyolite. Une région de brèches co-ignimbritiques grossières est interprétée comme une caldeira. Les deux lithodèmes sont des porphyres quartzofeldspathiques que l'on identifie par leurs populations de phénocristaux et leur composition chimique.

[1] Contribution to the 1994-1999 Bathurst Mining Camp, Canada-New Brunswick Exploration Science and Technology (Extech) Initiative

INTRODUCTION

The Ordovician felsic volcanic rocks of the Tetagouche Group, collectively the Acadians Range Complex, are a sequence of generally highly deformed extrusive and shallow level intrusive rocks (Rogers, 1994). Previously the Acadians Range Complex rocks were subdivided into the Nepisiguit Falls and Flat Landing Brook formations (van Staal and Fyffe, 1991). However, Rogers (1994) has shown that the Acadians Range Complex needs to be further subdivided with the incorporation of another formation and two lithodemic units – the Caribou Mine Formation and Devils Elbow Brook and Wildcat porphyries, respectively (Fig. 1). The aim of this paper is to describe the petrographic and physical features which enable the recognition of the various units of the Acadians Range Complex.

This subdivision of the Acadians Range Complex rocks became apparent following a combined study of the physical features, paleogeography, and geochemistry. The chemistry provided a "window" through the pervasive deformation, enabling the recognition of distinct petrographic features for all the units. As many elements are mobile under the low-grade metamorphic conditions present within the region, analysis was largely based on the relatively immobile high-field-strength (HFSE) group of elements (Fig. 2, 3). Identification of the individual rock units were primarily carried out on a Zr/TiO_2-Y/TiO_2 discrimination diagram (Rogers, 1994). This diagram also illustrates the possible evolutionary trends based on assimilation-fractional crystallization models.

GEOLOGICAL SETTING

The Tetagouche Group consists mainly of bimodal mafic-felsic volcanic rocks interbedded with subordinate sedimentary rocks, which have been imbricated into several, generally northwardly younging, major thrust sheets (van Staal et al., 1991). It lies disconformably upon the clastic sediments of the Miramichi Group (van Staal and Fyffe, 1991). In addition to the formations containing Acadians Range Complex felsic volcanic rocks, four other formations have been defined (van Staal and Fyffe, 1991; van Staal et al., 1992). These are (i) the Patrick Brook Formation, which consists of dark grey sandstones, characterized by abundant volcanic quartz phenoclasts, interlayered with black slates; (ii) the Vallée Lourdes Formation, comprising greenish-grey siltstones interbedded with calcareous sandstones and minor polymictic conglomerates; (iii) the Canoe Landing Lake Formation, which consists of two basaltic suites (the Canoe Landing Lake suite and the structurally overlying Nine Mile Brook suite); (iv) the Boucher Brook Formation, which consists of thinly bedded, dark grey to black, feldspathic wacke/slate rhythmites grading upward into a black slate. Deformation was polyphase and complex (van Staal and Williams, 1984). The S1 foliation, which is related to thrusting, is penetrative and generally parallel to bedding, whilst the F4 and F5 structures are responsible for most of the large scale regional distributions of rocks. Associated with the D1 deformation is low-grade regional metamorphism, dated at 447 ± 6 Ma (van Staal et al., 1990).

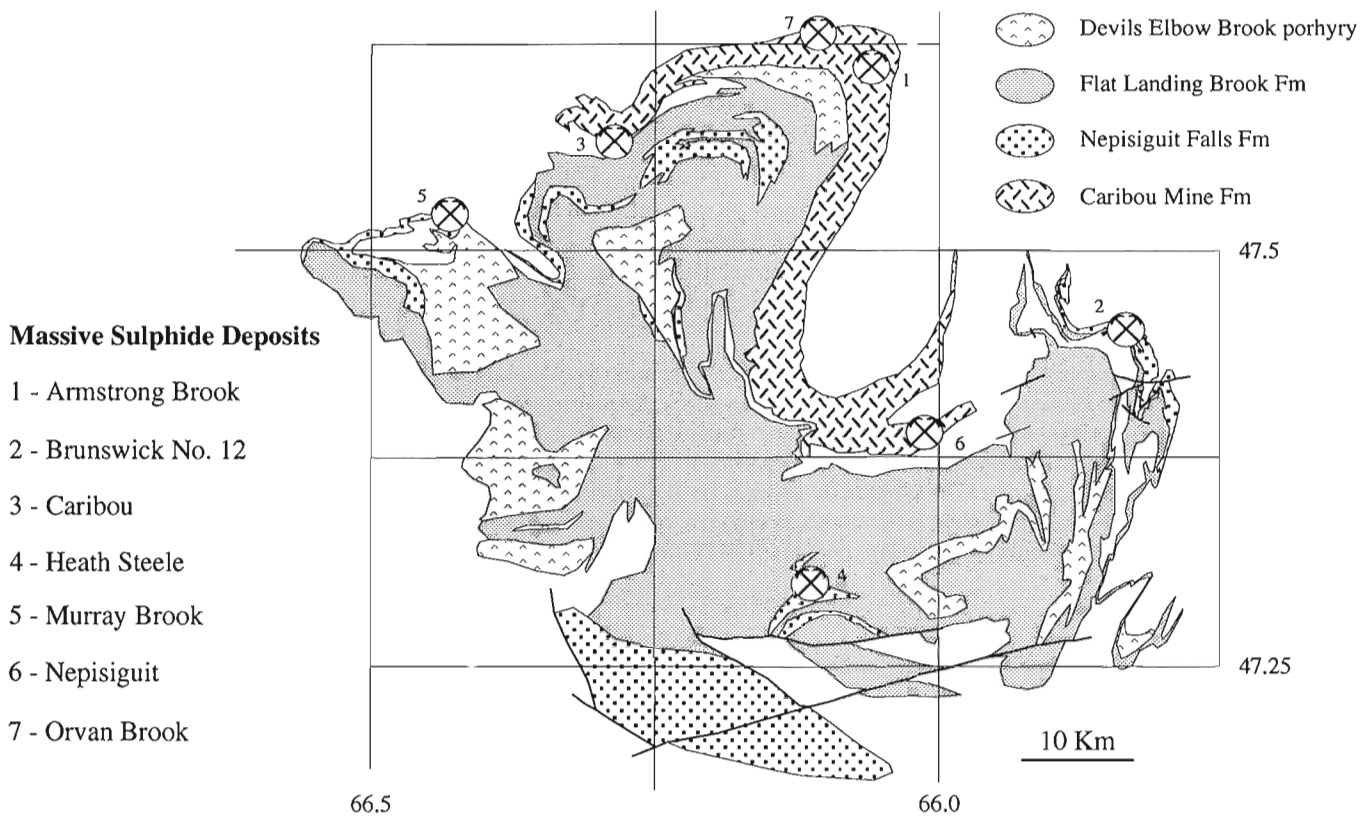

Figure 1. Geological map of the Acadians Range Complex.

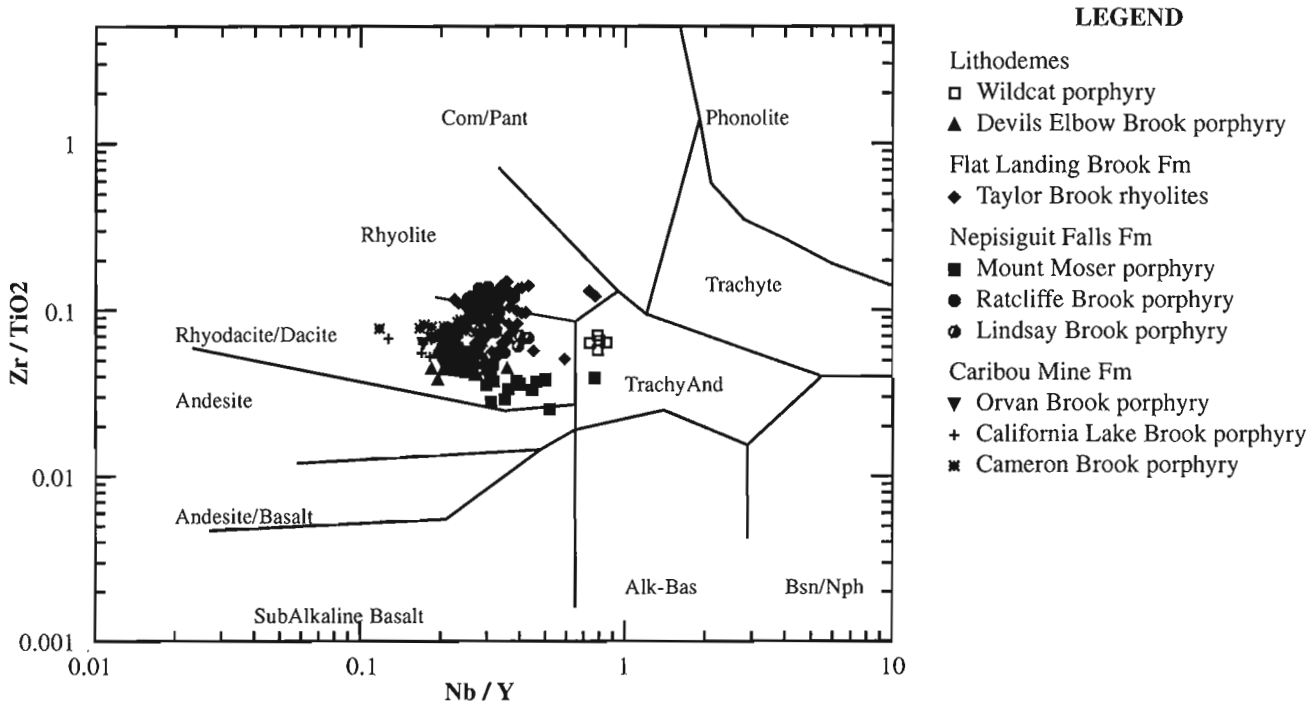

Figure 2. HFSE rock discrimination for the Acadians Range Complex (after Winchester and Floyd, 1977).

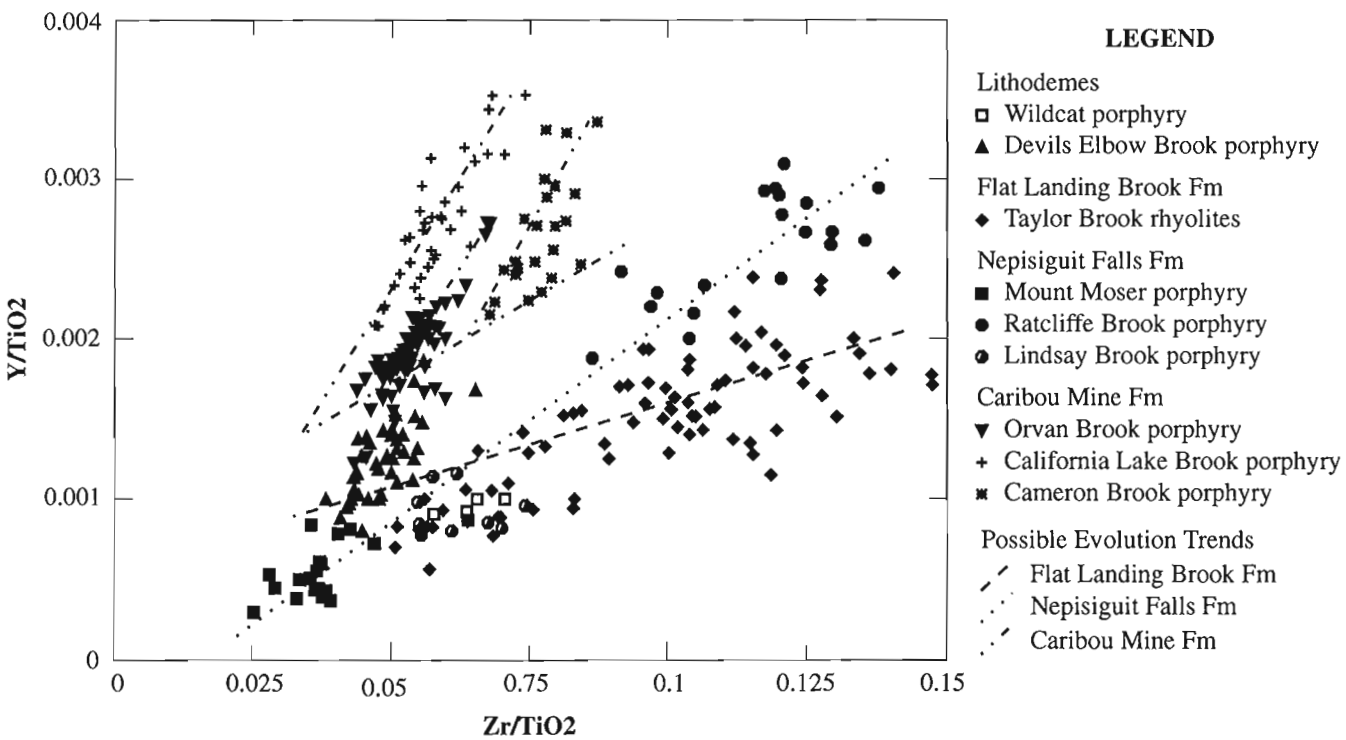

Figure 3. HFSE discrimination of the Acadians Range Complex, with the possible evolution trends of each formation.

ACADIANS RANGE COMPLEX

The complex contains almost all of the felsic volcanic rocks of the Tetagouche Group (some unrelated comendites occur in the Boucher Brook Formation (van Staal et al., 1991)). It is divided into the Caribou Mine, Nepisiguit Falls, and Flat Landing Brook formations and the lithodemic Devils Elbow Brook and Wildcat porphyries (Fig. 1, 4). The Wildcat porphyry has an alkalic chemical signature (Fig. 2), which implies that it might be unrelated to the surrounding felsic volcanic rocks.

CARIBOU MINE FORMATION

The Caribou Mine Formation consists of three feldspar phyric members – the Cameron Brook, California Lake Brook and Orvan Brook porphyries. They range in composition from dacites to rhyodacites and appear to be related by assimilation-fractional crystallization processes. These rocks were previously assigned to the Flat Landing Brook Formation (van Staal and Fyffe, 1991).

The Caribou Mine members are distinguished from the rest of the Acadians Range Complex by their typically moderate to high concentration of relatively large feldspar phenocrysts, combined with an absence of quartz phenocrysts. Chemically they are characterized by higher Cl, Ga, Rb and Y, and lower NaO_2, Zn and Zr compositions than the other felsic volcanic rocks and are readily distinguished on a Zr/TiO_2-Y/TiO_2 discrimination diagram. The three felsic volcanic members are separated primarily on the basis of their chemistry, although some recognizable petrographic variations have been identified.

The Caribou Mine Formation is completely bounded by ductile thrusts, which means that a complete section is not preserved. Furthermore, until all the members have been radiometrically dated, it will not be possible to determine the internal stratigraphy. In the structural hanging-wall of the Caribou Mine, the Cameron Brook porphyry is overlain respectively by the California Lake Brook and then the Orvan Brook porphyries. Whether this sequence represents a right way-up stratigraphy or not is unclear at present. In addition, the relative distributions of the members across the formation as a whole could relate to the partially overlapping extrusion of coeval magmas, rather than any particular "layer-cake" type stratigraphy. The formation is restricted in its distribution to a relatively narrow zone along the northern margin of the Acadians Range Complex, largely stretching between the Nepisiguit A and Caribou massive sulphide deposits. Other massive sulphide deposits that are contained within this formation include the Armstrong Brook and Orvan Brook deposits.

Cameron Brook porphyry

Field relations, such as the association with sediments and lack of autobrecciated margins, imply that the Cameron Brook porphyry consists primarily of shallow level sheets and cryptodomes. It is a bimodal feldspar porphyry, with the phenocrysts pseudomorphed by metamorphic microcline

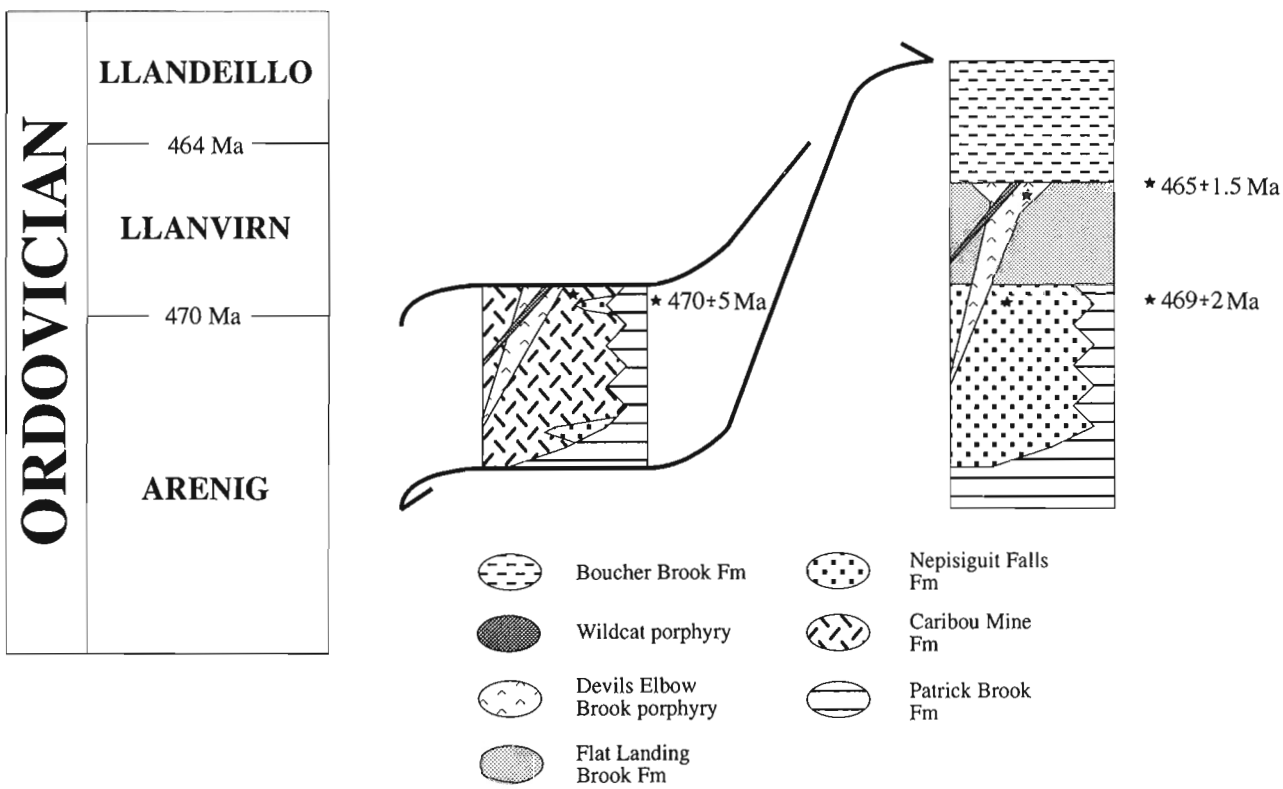

Figure 4. Stratigraphy of the Acadians Range Complex.

(originally sanidine). The microscopic cherty appearance and lack of pyroclastic indicators (such as lithic fragments) indicate an effusive origin.

The feldspar phenocrysts have a maximum size of 10 by 5 mm, with a modal size of 5 by 3 mm. In hand specimen they are pink or white; the colour is probably due to the local oxidation effects induced by metamorphic/metasomatic alteration. The concentration of phenocrysts ranges between 5% and 30% by volume, with the variable degree of shear being a major control on the amount of phenocrysts preserved. Moderate amounts of shearing preferentially removes groundmass materials and hence tends to increase the proportion of phenocrysts, whereas more intense shearing causes the destruction and/or recrystallization of the phenocrysts into mortared augen and so reduces the phenocryst proportion. In regions of relatively low strain the feldspar phenocrysts are typically euhedral to slightly subhedral in form with sharp edges. They appear to have originally consisted of sodium-rich sanidine, with simple twinning, which during metamorphic replacement has caused the typical blotchy extinction and occasionally patch perthite to develop. The generally anhedral feldspar microphenocrysts range from 0.1 to 0.6 mm in size and constitute up to 10% of the total rock by volume.

The groundmass is a lower greenschist assemblage of feldspar, quartz, chlorite, sericite, muscovite, and epidote. Preserved primary features include lithosae, recrystallized quartz-feldspar-chlorite-filled amygdales and perlitic fractures. The main distinguishing features are the high concentration of well formed blotchy potassium feldspars, crowded microphenocryst assemblage and presence of lithosae.

California Lake Brook porphyry

The California Lake Brook porphyry is a light to dark green bimodal feldspar porphyry, which at least partially overlies the Cameron Brook porphyry. The feldspar phenocrysts have a maximum size of 8 by 5 mm and a modal size of 3 by 2 mm and are generally white or occasionally pink. The concentration of phenocrysts ranges from 15% to 40% of the total rock volume, with the modal concentration being circa 25% by volume. They are generally subhedral in form, with a typical slight rounding to the corners when compared to the Cameron Brook porphyry. The blotchy extinction, which is typical of the Cameron Brook porphyry, is quite rare, whilst the development of patch perthite and chessboard albite is fairly common in the California Lake Brook porphyry, as are granophyric textures.

The anhedral microphenocrysts range in size up to 0.5 mm and comprise between 1% and 10% of the total rock by volume. Overall the main distinguishing petrographic features for the California Lake Brook porphyry are (i) its high concentration of relatively large potassium feldspars; (ii) well formed, but slightly rounded edges to the phenocrysts; (iii) common formation of patch perthite, chessboard albite and myrmekite; (iv) and generally the lowest concentration of microphenocrysts within the Caribou Mine Formation.

Orvan Brook porphyry

The Orvan Brook porphyry is very limited in distribution, although this may be as a result of thrust excision. Currently the sole radiometric date for the California Mine Formation is a U-Pb zircon age of 470 ± 5 Ma (van Staal and Sullivan, 1992) for the Orvan Brook porphyry; this is of little use, as the error covers all of the Acadians Range Complex volcanism. Although further age constraint comes from the local interfingering of Nepisiguit Falls Formation volcanic rocks (Fig. 4).

The Orvan Brook porphyry is a light to dark green bimodal feldspar porphyry, with subhedral phenocrysts that range of between 2 and 6 mm long. They are pink or white and account for 3 to 20% of the total rock by volume depending on the state of strain. The feldspars crystallized as sanidine and were later altered by metamorphism/metasomatism predominantly to microcline. The formation of alteration textures such as patch perthite and chessboard albite is less common than in the other members of this formation, although blotchy extinction is frequently developed. The anhedral microphenocrysts range in size from 0.1 to 0.8 mm and constitute up to 15% of the total rock by volume. The most distinctive feature of the Orvan Brook porphyry is the presence of opaque pseudomorphs after biotite phenocrysts, that range in size from 0.2 to 1 mm and constitute between 0.5% and 3% of the total rock by volume.

In summary the distinguishing features of the Orvan Brook porphyry are the slightly smaller phenocrysts than the other members of the California Mine Formation, in association with larger microphenocrysts. Also, the feldspar phenocryst typically exhibit blotchy extinction and only occasionally patch perthite. However, the main distinguishing feature is the high concentration of opaque pseudomorphs after biotite.

NEPISIGUIT FALLS FORMATION

Three quartz-feldspar phyric members that range from dacite to rhyolite occur in the Nepisiguit Falls Formation – Lindsay Brook, Ratcliffe Brook and Mount Moser porphyries. They are readily distinguished from the approximately contemporary California Mine Formation (Fig. 4) by the presence of quartz, as well as feldspar phenocrysts. Chemically the Nepisiguit Falls Formation is characterized by a lower mean Zr content than the other quartz-feldspar porphyries in the Acadians Range Complex, while the three felsic volcanic members distinguished from each other on a Zr/TiO_2-Y/TiO_2 discrimination diagram (Fig. 3). Contained within the Nepisiguit Falls Formation are a number of the massive sulphide deposits present in the Acadians Range Complex (e.g. Brunswick No. 12).

Lindsay Brook porphyry

The Lindsay Brook porphyry has a limited distribution and occurs nearly at the base of the Nepisiguit Falls Formation. The exact age relations of the felsic volcanic rocks of the

Nepisiguit Falls Formation have not been confirmed, as this member has not yet been radiometrically dated and no complete section through the formation is known.

The Lindsay Brook porphyry is a light brown to grey quartz-feldspar porphyry. The phenocrysts are dominantly subhedral alkali feldspars, with fewer and smaller quartz crystals. The occasional preservation of quartz-filled amygdales, along with the evidence for an explosive origin (e.g. lithic fragments) and the close association of volcanogenic sandstones, points towards formation as a partly-welded pyroclastic flow in a shallow marine environment.

The quartz phenocrysts account for circa 25% of the total phenocryst population, which relates to 7% of the whole rock by volume. They have a modal diameter of approximately 1 mm, but range up to 3 mm. The feldspar phenocrysts have a modal size is 2 by 1.5 mm and account for circa 20% of the total rock volume. They are typically subhedral with slightly rounded edges and are frequently glomeroporphyritic. The compositional ratio of the feldspar phenocrysts is approximately 3:1 for albite in respect to potassium feldspar. Irregularly shaped quartz and feldspar microphenocrysts, less than 0.2 mm long, are scattered throughout the groundmass of the unit and appear to have resulted from crystal shattering due to thermal shock during explosive eruption. The groundmass is recrystallized tuff, consisting of quartz, feldspar, sericite, and chlorite, with small amounts of muscovite and epidote; it is unclear if it was initially a welded tuff.

Chemically the Lindsay Brook porphyry has the highest mean concentrations of Na_2O and Zr in the Nepisiguit Falls Formation. The Zr/TiO_2-Y/TiO_2 plot is unable to distinguish this member independently from the Taylor Brook rhyolites or Wildcat porphyry, both of which partially occupy the same field (Fig. 3). However, by combining the petrographic data, confusion with the apparently aphyric Taylor Brook rhyolites is very unlikely and the Nb/Y ratio readily distinguishes it from the Wildcat porphyry (Fig. 2). The distinctive petrographic features of this member are (i) its high proportion of albite phenocrysts; (ii) volcaniclastic nature; and (iii) common glomerophyritic feldspars.

Ratcliffe Brook porphyry

The Ratcliffe Brook porphyry appears to overlie the Lindsay Brook porphyry, when the latter is present. The only radiometric date for the Ratcliffe Brook porphyry is 465 ± 5 Ma (van Staal and Sullivan, 1992). This error effectively covers the entire time-scan of the Acadians Range Complex (470 to 465 Ma); hence it cannot define the stratigraphic position of the Ratcliffe Brook porphyry. The intimate association with sediments with this member indicated a submarine environment of formation.

The Ratcliffe Brook porphyry is a light brown to grey quartz-feldspar porphyry, containing approximately equal quantities of quartz and feldspar phenocrysts. The quartz phenocrysts are approximately equant, with a modal diameter between 0.6 and 2 mm, and account for 5 to 20% of the total rock by volume. In hand specimen they generally have a dark smoky and slightly resinous appearance. In thin section they are shown to be typically rounded and embayed. The alkali feldspar phenocrysts are slightly larger, typically subhedral and consist more of albite than microcline. The groundmass is predominantly feldspar, chlorite and sericite with quartz and minor amounts of epidote and muscovite. Occasionally remnants of cuspate and angular glass shards are preserved, as well as amygdales and spherulites where the phenocryst population is low. The spherulites are generally in the region of 0.5 mm in size, sometimes forming as a mantle around a phenocryst. It is not clear if these formed in an effusive flow or a pyroclastic flow where heat retention has occurred.

The ratio of phenocrysts and rounded nature of the quartz are the main petrographic features that distinguishes this member from the rest of the Nepisiguit Falls Formation, whilst the dark smoky and rather resinous appearance of the quartz phenocrysts distinguishes it from the remaining porphyries in the complex.

Mount Moser porphyry

The Mount Moser porphyry appears to be the youngest felsic volcanic member of the Nepisiguit Falls Formation, as it largely if not completely overlies the Ratcliffe Brook porphyry. The Mount Moser porphyry exhibits a variety of modes of formation, from pyroclastic eruption to shallow level intrusive units. A U-Pb zircon age determination yielded a date of 469 ± 2 Ma (van Staal and Sullivan, 1992). Thus if the stratigraphic interpretations are correct, all the members of the Nepisiguit Falls Formation are 467 Ma or older.

The Mount Moser porphyry is a brown to dark grey quartz-feldspar porphyry, containing more quartz than feldspar phenocrysts. The size range for quartz phenocrysts is between 0.5 and 6 mm, with a modal range of 1 to 2 mm; they are generally equant in their shape and subhedral to anhedral in form. Their edges are typically slightly rounded and very commonly embayed. The feldspar phenocrysts are predominantly subhedral albites, ranging between 3 and 2 mm; they account for approximately 40% of the total phenocryst population and between 10% and 25% of the total rock composition by volume. Locally, for example, near the Brunswick No. 6 massive sulphide deposit, the feldspar phenocrysts are pseudomorphed by hydrothermal alteration associated with the sulphide mineralization to quartz, albite, sericite, and chlorite aggregates; consequently this rock superficially appears to be a quartz porphyry. The groundmass is predominantly feldspar, chlorite, sericite, and quartz, with minor muscovite and epidote, which gives it a distinctive "dirty-looking" appearance.

The Mount Moser porphyry is distinguished from the rest of the Nepisiguit Falls Formation by having more and larger phenocrysts and by its "dirty" chloritic groundmass.

FLAT LANDING BROOK FORMATION

The Flat Landing Brook Formation is dominated by the felsic volcanic products of a single explosive centre, that ranges in composition from dacites to rhyolites and has

been separated on a basis of macroscopic petrology into the Taylor Brook rhyolites and Grants Lake pyroclastics. The Flat Landing Brook Formation occupies the central portion of the Acadians Range Complex and is its most voluminous part.

Taylor Brook rhyolites

The Taylor Brook rhyolites represent the predominantly fine grained units of the Flat Landing Brook Formation and as such consist of a series of sparsely feldspar-phyric ignimbrites, co-ignimbritic tuffs, and rhyolitic flows and dykes. The only U-Pb zircon age determination currently available gives a date of 466 ± 5 Ma (Sullivan and van Staal, 1990). This age is consistent with the field data which shows that the Flat Landing Brook Formation conformably overlies the Nepisiguit Falls Formation in the Brunswick Mines area.

The range of volcanic types in the Taylor Brook rhyolites means that they are very variable in petrology. However, they generally have an aphyric appearance in the field (even though they are almost invariably sparsely feldspar-phyric), which easily identifies them from the felsic volcanic rocks of the other formations in the Acadians Range Complex. In addition to phenocrysts, some of the less deformed samples have preserved xenoliths, fiamme, flow banding, amygdales, and/or spherulites. Evidence for the environment of formation is only circumstantial, but the distribution of contemporary sedimentary rocks points towards the central portion of this formation having been subaerial, whereas the outer margins were submarine. This suggests that the Flat Landing Brook Formation may represent part of the edifice of a volcanic island.

The feldspar phenocrysts are generally equant and relatively small, only rarely exceeding 1 mm in diameter. They consist mostly of albite, although locally up to 40% are potassium feldspar, and account for between 0.5 and 5% of the total rock composition by volume. The groundmass is predominantly feldspar and chlorite, with quartz, epidote, calcite and sericite as minor phases. Locally a number of different volcanic textures are preserved, although even in these examples evidence for the nature of the eruptive environment is frequently masked, by the extremely poor quality of the outcrops. The most rarely seen of these textures is flow banding. Radiate textures (spherulites and variolites) are far more commonly seen, although they are very localized in their distribution and probably represent devitrification. Hydration contemporary with emplacement causes the development of perlite where water percolating through cracks, probably caused by thermal stresses, has altered the surrounding glass. Amygdales are the most commonly preserved volcanic texture, the great majority being quartz filled, while a few are filled by chlorite. Amygdales, perlite and spherulites occur in the ignimbrites, extrusive rhyolite flows, and rhyolite dykes. Consequently their presence does not indicate the unit's mode of formation.

The combined effects of compaction, welding, and regional metamorphism have made the nature of the fragments in the ignimbrites hard to identify. Therefore shards, fiamme, and xenoliths are only occasionally seen in the fine grained units which dominate this member. The xenoliths are typically less than 5 by 2 mm in size and primarily consist of penecontemporaneous felsic volcanic fragments, but also include basalt and shale; the presence of these foreign materials may have a significant effect on the integrity of the whole rock chemistry. Occasionally double grading between lithic and pumice clasts is preserved, indicating an ignimbritic origin. Locally co-ignimbritic breccias with clasts in the order of 2 cm are preserved. These are mostly small, isolated deposits related to a facies change in an ignimbrite flow and are classified as Harrts Lake-type pyroclastics.

The Taylor Brook rhyolites seem to consist largely of ignimbrites with minor rhyolite flows. The relative proportion of rhyolite flows increasing towards the east of the formation. The rhyolites and ignimbrites are frequently hard to distinguish from each other due to the effects of alteration, tectonism and poor exposure. However their apparently aphyric nature makes them relatively easy to distinguish from the rest of the Acadians Range Complex.

Grants Lake pyroclastics

The Grants Lake pyroclastics occupy a discrete region approximately central to the Acadians Range Complex, that is interpreted to represent the caldera for the Flat Landing Brook Formation. The only parts of this formation that do not seem to be related to the caldera are the scattered dykes and small effusive flows of the Taylor Brook rhyolites. The effusive flows have mainly been preserved towards the outer margins of the formation and hence probably formed parasitic to the main volcanic edifice. The Grants Lake pyroclastics are dominated by very coarse pyroclastics (including co-ignimbritic breccias and lahars), which contain blocks of penecontemporaneous rhyolite up to 1 m^3.

DEVILS ELBOW BROOK PORPHYRY

The Devils Elbow Brook porphyry is an intrusive quartz-feldspar phyric dacite, which is widely distributed throughout the Acadians Range Complex. Prior to this study these rocks were designated as a porphyritic unit of the Flat Landing Brook Formation, but as they do not appear to be related to this formation, they have been designated as a lithodeme. An intrusive nature is implied by its distribution, which consists of several large homogeneous units which seem to cut across other units of the Acadians Range Complex. A U-Pb zircon age of 465 ± 1.5 Ma has been obtained for the porphyry (van Staal and Sullivan, 1992). Consequently the Flat Landing Brook Formation is older than 465 ± 1.5 Ma (as the Devils Elbow Brook porphyry intrudes it) and younger than 469 ± 2 Ma (as it overlies the Nepisiguit Falls Formation).

The Devils Elbow Brook porphyry is primarily distinguished petrologically from the other quartz-feldspar porphyries in the Acadians Range Complex by its quartz phenocrysts, which account for approximately 35% of the total phenocryst population. These are relatively large, 2 mm diameter, clear, glassy and embayed, but the most distinctive feature is the commonly rather jagged margins. The feldspar phenocrysts, which account for 65% of the total phenocryst population, are either white or pink and consist of slightly more potassium feldspar (microcline) than albite. Together they make up circa

20% of the whole rock by volume. The albite phenocrysts are typically 2 by 1 mm in size with a subhedral to anhedral form. The microclines have better form, show simple twinning and are larger (between 3 and 6 mm long). Metasomatic/metamorphic alteration has caused the common formation of patch perthites and chessboard albites, as well as causing blotchy extinction in the microclines. The groundmass is predominantly microcline, sericite, quartz, and muscovite with minor chlorite and epidote. The grain size of the groundmass is marginally larger than the average for the other units in the region, as an original microcrystalline groundmass developed in contrast to the cherty (cryptocrystalline) ones developed in extrusive flows.

In summary the Devils Elbow Brook porphyry is petrographically distinguished from the rest of the Acadians Range Complex macroscopically by its large, clear, glassy quartz crystals and by its light grey granular groundmass. Microscopically the jagged margins to the quartz and presence of blotchy potassium feldspar, patch perthite, and chessboard albite are the most distinctive features.

WILDCAT PORPHYRY

The Wildcat porphyry is a quartz-feldspar porphyry, that is limited to a single, highly deformed horizon. The phenocrysts, which only rarely escape intact from the pervasive shear, are scattered, making up 5% of the whole rock by volume and contain more quartz than feldspar. It is classified as a lithodeme as it is intrusive and highly deformed, with intrusive and/or tectonic contacts with the other rock units. A cross-cutting relationship with the Devils Elbow Brook porphyry indicates that the Wildcat porphyry is younger than the previously described units. However, the Wildcat porphyry has an unusual alkalic Nb/Y signature (Fig. 2), that indicates that it may be substantially younger and not part of the Acadians Range Complex volcanism.

The quartz phenocrysts are equant, with an average diameter of 0.8 mm and constitute 3% of the total rock by volume. The equant, subhedral feldspar phenocrysts consist of approximately twice as much albite as microcline and have a diameter between 0.4 and 2 mm. The most distinctive petrographic feature of this rock unit is the unusually high concentration of apatite phenocrysts (although this is still less than 0.2% of the whole rock by volume). They are equant and euhedral to subhedral in form and typically less than 0.25 mm in diameter. The groundmass is recrystallized feldspar, quartz, chlorite, muscovite, and epidote.

CONTINUING RESEARCH

Although the Acadians Range Complex has been divided, as outlined above, into a number of units which can readily be identified macroscopically to at least their formation in all but the most highly deformed ultramylonites, many aspects still remain unresolved. Foremost amongst these is the relationship between the felsic volcanic rocks and massive sulphide deposits. Rogers (1994) has proposed a spatial link between the top of the Caribou Mine Formation and Nepisiguit Falls Formation; it is hoped that the on-going mapping of the complex will confirm these relationships.

In addition to field mapping, the addition of rare earth data and improved accuracy from ICP-MS analysis of HFSE should help to further constrain the chemostratigraphic discrimination of the units within the Acadians Range Complex.

ACKNOWLEDGMENTS

I am grateful to John Winchester and all the staff in the Department of Geology at the University of Keele, England for their interesting discussions and valuable advice which has helped in the defining of my ideas. Many thanks are extended to the department's technicians, especially Margaret Akin and David Emley, who have enabled this project to go ahead. Cees van Staal is thanked for his many constructive comments that helped improve the paper. I acknowledge the support of a NSERC Visiting Fellowship held at the Geological Survey of Canada. This is part of the EXTECH II research project.

REFERENCES

Rogers, N.
1994: The geology and geochemistry of the felsic volcanic rocks of the Acadians Range Complex, Tetagouche Group, New Brunswick; Ph.D. thesis, Keele University, U.K., 420 p.

Sullivan, R.W. and van Staal, C.R.
1990: Age of a metarhyolite from the Tetagouche Group, Bathurst, New Brunswick, from U-Pb isochron analyses of zircons enriched in common Pb; in Radiogenic Age and Isotopic Studies: Report 3; Geological Survey of Canada, Paper 89-2, p. 109-117.

van Staal, C.R. and Fyffe, L.R.
1991: Dunnage and Gander Zones, New Brunswick: Canadian Appalachian Region; New Brunswick Department of Natural Resources and Energy, Mineral Resources Branch, Geoscience Report 91-2, 39 p.

van Staal, C.R. and Sullivan, R.W.
1992: Significance of U- Pb zircon dating of silicic volcanic rocks associated with the Brunswick-type massive sulphide deposits of the Tetagouche Group; in Program with Abstracts, Joint Annual Meeting, May 1992, Wolfville, Nova Scotia; Geological Association of Canada/Mineralogical Association of Canada, v. 17, p. A112.

van Staal, C. R. and Williams, P.F.
1984: Structure, origin and concentration of the Brunswick No. 12 and No. 6 ore bodies; Economic Geology, v. 79, p. 1669-1692.

van Staal, C.R., Ravenhurst, C.E., Winchester, J.A., Roddick, J.C., and Langton, J.P.
1990: Evidence for a post-Taconic blueschist suture in northern New Brunswick, Canada; Canadian Journal of Earth Sciences, v. 15, p. 207-209.

van Staal, C.R., Fyffe, L.R., Langton, J.P., and McCutcheon, S.R.
1992: The Ordovician Tetagouche Group, Bathurst Camp, northern New Brunswick, Canada: history, tectonic history and distribution of massive-sulphide deposits; Exploration and Mining Geology, v. 1, p. 93-103.

van Staal, C.R., Winchester, J.A., and Bédard, J.H.
1991: Geochemical variations in Middle Ordovician volcanic rocks of the northern Miramichi Highlands and their tectonic significance; Canadian Journal of Earth Sciences, v. 28, p. 1031-1049.

Winchester, J. A. and Floyd, P. A.
1977: Geochemical discrimination of different magma series and their differentiation products using immobile elements; Chemical Geology, v. 20, p. 325-343.

Geological Survey of Canada Project 940001-1A

Automated microprobe analysis of compositional zoning and heterogeneity in thin section: a facility for making high-resolution compositional maps at the Geological Survey of Canada

R.J. Scammell, R.G. Berman, G.J. Pringle[1], and J.A.R. Stirling[1]
Continental Geoscience Division

Scammell, R.J., Berman, R.G., Pringle, G.J., and Stirling, J.A.R., 1995: Automated microprobe analysis of compositional zoning and heterogeneity in thin section: a facility for making high-resolution compositional maps at the Geological Survey of Canada; in Current Research 1995-E; Geological Survey of Canada, p. 287-292.

Abstract: The need to better evaluate compositional zonation and heterogeneity within and among minerals, at thin-section scales, has lead to the development of an analytical technique which uses a CAMECA-SX50 electron microprobe. The instrument is configured for automated stage movements over a user-defined grid, to provide short-duration (1-2 s) point analyses of four elements. Spatial co-ordinates and respective element concentrations are recorded in ASCII format, which is imported into visualization software that allows evaluation of the spatial distribution of concentrations. Compared with quantitative microprobe analysis, advantages of the technique include: (i) it is more time-effective, (ii) it can facilitate rapid assessment of a whole thin section, (iii) it is flexible in that different user-defined grids can be used to assess different problems, (iv) it provides as much, and possibly more information, and (v) it can be used to identify areas for quantitative microprobe analysis.

Résumé : La nécessité de mieux évaluer la zonation selon la composition et l'hétérogénéité dans les minéraux et entre les minéraux, à l'échelle des lames minces, s'est traduite par l'élaboration d'une technique d'analyse recourant à une microsonde électronique CAMECA-SX50. L'instrument est configuré pour des déplacements automatisés des stades au-dessus d'une grille définie par l'utilisateur afin de permettre des analyses ponctuelles de courte durée (1-2 s) de quatre éléments. Les coordonnées spatiales et les concentrations des éléments respectifs sont enregistrées dans le format ASCII que l'on peut visualiser de façon à évaluer la répartition spatiale des concentrations. Comparativement à l'analyse quantitative par microsonde, cette technique offre les avantages suivants : i) elle dure moins longtemps, ii) elle peut accélérer l'évaluation de toute une plaque mince, iii) elle est souple du fait qu'on peut utiliser les différentes grilles définies par l'utilisateur pour évaluer des problèmes différents, iv) elle fournit autant et peut-être plus d'informations et v) on peut l'utiliser pour déterminer les domaines d'analyse quantitative par microsonde.

[1] Mineral Resources Division

INTRODUCTION

Since the advent of electron microprobe analysis in the 1960s, much attention has been given to the quantitative study of chemical zoning in both igneous and metamorphic minerals, and it is now widely appreciated that chemical zoning preserves an important record of a variety of geological processes (e.g. Tracy, 1982; Nixon and Pearce, 1987). Many studies that have documented the complexity of zoning in metamorphic minerals (e.g. Tracy et al., 1976; Thompson et al., 1977; Yardley, 1977; Spear et al., 1990; Spear, 1993; Robinson, 1991; Scammell, 1993), have relied on constructing contour maps from individually selected spot analyses, a procedure that is time-intensive and does not ensure complete coverage of the mineral. In order to address these shortcomings, a number of petrology laboratories are now equipped with integrated hardware and software for producing high-resolution compositional maps of selected areas of a thin section, or an entire thin section. In the present communication, we present an in-house (GSC-Ottawa) method for preparing high-resolution compositional maps with a minimum of operator time and effort. Before describing the method, we briefly review some applications that underscore the importance of obtaining a complete assessment of chemical zoning, and any other compositional heterogeneity, with particular reference to metamorphic samples.

COMPOSITIONAL ZONING AND HETEROGENEITY IN METAMORPHIC ROCKS

Zoned minerals are important indicators of the crystal growth process and reaction history of metamorphic rocks. For example, Thompson et al. (1977) reconstructed the entire prograde reaction sequence with the help of compositional maps showing inclusions and Ca-Fe-Mg-Mn contours of a ~1 cm diameter, growth-zoned garnet from the Gassetts schist, Vermont. Their maps clearly show radially asymmetric zoning that could lead to erroneous interpretations from a single, rim to rim compositional transect through the centre of the grain. Grover et al. (1992) constructed element composition maps that outline a relict euhedral, high-Mn core surrounded by a low-Mn rim in a garnet interpreted to have formed in two different stages of growth. Continued interest in zoning stems from the introduction of techniques of reconstructing pressure-temperature histories and related tectonic processes from zoned garnets (Spear and Selverstone, 1983; St-Onge, 1987).

Careful assessment of zoning and other types of compositional heterogeneity is also required for thermobarometric calculations which rely on the assumption of chemical equilibrium (e.g. Essene, 1982; Newton, 1983; Berman, 1991). Therefore, the extent to which mineral compositions have changed through the process of diffusional reequilibration is one of the most critical effects to quantify in high-grade rocks, and this has been demonstrated in several studies which have been successful at establishing the relationship of diffusion zoning to detailed petrographic features (Tracy et al., 1976; Yardley, 1977; Grover et al., 1992; Pattison and Begin, 1994, Scammell, in prep.). Also of considerable importance for thermobarometry is establishing the amount of chemical heterogeneity in plagioclase. Due to kinetic factors, plagioclase tends not to form zoned crystals, but instead to nucleate discrete grains of different composition (e.g. Spear, 1993). Recognition of different plagioclase compositions, both as porphyroblast inclusions or as discrete matrix grains, is critical to successful determination of P-T conditions and P-T paths (Spear and Florence, 1992; Ravindi Kumar and Chacko, 1994).

Thus, for both P-T-t and standard P-T analysis it is imperative to assess the compositional variations within crystals, across crystal interfaces, and both within and between domains of a thin section. Complex zoning that is not radially symmetric and that depends on intergrain boundaries (inclusion-host, porphyroblast-matrix, etc.) is difficult to recognize using classical microprobe spot analyses. In addition, minute inclusions or matrix grains of key metamorphic minerals can be easily missed in petrographic analysis. In this contribution we document the availability of a recently implemented procedure at the GSC – Ottawa laboratories to produce high-resolution compositional maps. Perhaps the best feature of the method is that most of the work (i.e. data collection) is automated. We strongly recommend use of this method as the first step in routine thermobarometric analysis.

NEW TECHNIQUE

High-resolution digital composition maps are produced on microbeam instruments by acquiring X-ray counts from a large number of grid points on the sample. It is essential to keep the point sampling time to a minimum. The most time efficient systems accentuate beam rastering and minimize stage movement. Also when dealing with multi-element maps, energy-dispersive spectrometers are intrinsically more efficient than wavelength-dispersive spectrometers.

The available beam control and energy-dispersive software in the microprobe laboratory is obsolete. The computer is just adequate for general analytical work but lacks the processing speed and capacity necessary for efficient mapping. At the present time the available software configuration in the scanning electron microscope laboratory (SEM) only allows for automated coverage of approximately 1 cm^2.

The pressing need for high resolution X-ray maps caused us to develop a procedure using the CAMECA-SX50 electron microprobe. The procedure is a combination of existing SX50 features. Some efficiency was sacrificed in favour of lower development time and expense.

In the procedure, movement is by stage automation only, determinations are practically limited to a selection of four elements during each session and the turn-around is approximately 7 seconds per point for a 1 second counting time. A typical (thin-section scale) run analyzing four elements at 32 000 points requires 62 hours (1 weekend) of instrument time. The inclusion of more than four elements in a run would involve spectrometer movement consuming prohibitive amounts of time.

Stage movement is controlled by a file of grid co-ordinates that is generated when the operator selects the corners of the grid and the sampling interval. The grid may cover up to an entire polished thin section. The grid is rectangular with square grid elements given in micrometres. Trials of the system used grid sizes in the 50 to 150 μm range.

Spatial resolution in the maps is a function of beam size, sample grain size, and grid-element size. The smallest beam size possible in the instrument is less than 5 μm, which is small relative to grain size in most samples, and leads to grid element size as the major control on spatial resolution.

Compositions are reported as weight per cent (wt.%) of the analyzed element. Analyses are semi-quantitative at best, however for compositions greater than 2 wt.% the relative precision should approach what is expected in normal quantitative analysis. The mapping of trace compositions below 2 wt.% is a special problem where background interferences may be significant. As a matter of routine the technique has been established with a 2% wt.% detection limit, and a relative compositional resolution of 2% of the amount present. The 2% detection limit is a conservative estimate which is dependent on spectral interferences.

The data generated are written in an ASCII file that can be read by most spreadsheet or contouring software packages, and includes the point co-ordinates so that they may be revisited manually for more careful attention. For this study we have used the scientific visualization software called "Transform" which is marketed by SPYGLASS®, and operates under MICROSOFT™ WINDOWS or MACINTOSH. It very conveniently reads the microprobe output file and makes various types of compositional maps and three-dimensional images that can be output in a variety of graphic-file formats.

EXAMPLES

To document the capabilities of the above procedure we present several figures produced with the hardware-software combination described above. Figure 1 shows a thin section from high-grade pelitic schists in the northern Monashee Mountains of British Columbia (for details see Scammell, 1993). Figures 2 and 3 show compositional maps for the whole thin section, and the ~1 cm diameter garnet in the thin section. Figures 2 and 3 are based on 32 743 and 19 092 spot analyses, respectively, which were obtained during automated runs lasting up to two days (one weekend).

Once familiar with the capabilities of the software, the composition maps displayed in Figures 2 and 3 took approximately 10 minutes to generate from the output file containing the microprobe data. Each square (pixel) in these images represents one grid-element of information which has associated with it a discrete value for the concentration of the respective element, based on a single spot analysis which is smaller than the grid element. In these images the lowest to highest values are represented by a black to white "colour"

Figure 1. *Plane-light, microscopic view of a high-grade, migmatitic, K-feldspar-sillimanite-garnet-biotite schist. See Figure 2 for scale. Sample R155-2a. See Scammell (1993) for a detailed petrographic description. White areas are leucosomes composed mostly of quartz and plagioclase. Middle-grey areas are intergrowths of sillimanite and biotite. Black grains are biotite. The large, equant, middle-grey grain close to the center of the thin section is garnet which has an inclusion rich-core mantled by a thin (~1 mm thick) clear rim.*

scheme. Note, to better illustrate grid-elements outside of the selected range for each map, values which are higher are shown as black, and values which are lower are shown as white. This serves to accentuate grid element values which are outside of the range, and could be interpreted as part of a compositional zoning trend if higher values were white and lower values were black, for the selected "colour" scheme. For example, with respect to the garnet in Figures 2 and 3, this assignment of outlier tones emphasizes the distribution of grid elements which represent inclusions, and also emphasizes the margins of the garnet relative to matrix grid element analyses. It is particularly noteworthy that most software offers the choice of true colour schemes which greatly enhance data analysis, relative to the black and white images shown here. Also most software offers a variety of methods to statistically treat the data (e.g. linear interpolation, kernel smoothing, kriging).

Figure 2 illustrates several key observations: (i) the sub-horizontal leucosomes contain considerable amounts of untwinned plagioclase of variable composition, (ii) plagioclase of variable composition is present in the pressure shadows around the garnet, and (iii) the garnet is strongly zoned in Ca.

Figure 3 illustrates the zoning of all analyzed elements in the garnet. From the central region to the rim of the garnet, Fe shows a strong increase, while Ca and Mn show distinct decreases in abundances. Mg is particular interesting as it shows a distinct increase from the core region to the region near the inner part of the thin clear rim, then a subtle decrease towards the outer part of the clear rim. Figure 3 also illustrates that while zonation of the four elements is roughly concentric, the extreme values in the core region also roughly coincide, but are not at the geometric centre of the grain. Clearly conventional core-rim thermobarometry would lead to erroneous core P-T estimates with this garnet.

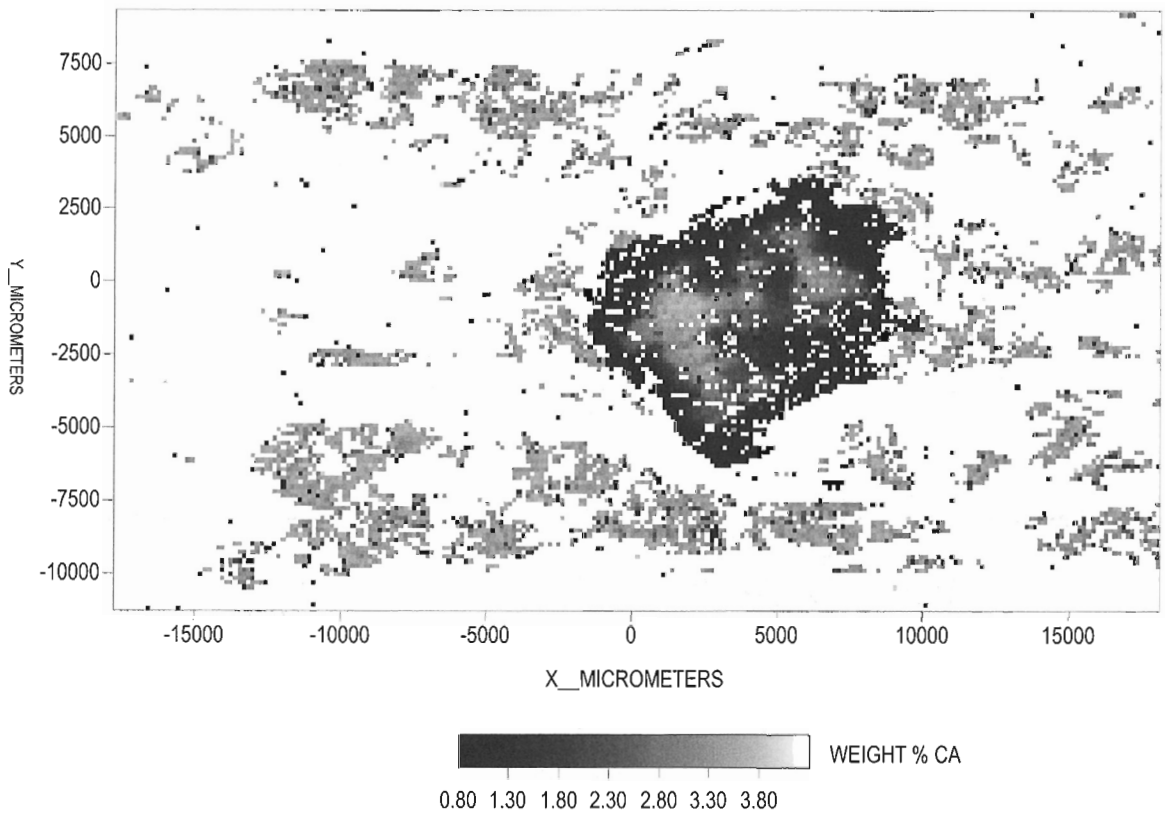

Figure 2. *Compositional map of Ca in the thin section of sample R155-2a shown in Figure 1. See text for discussion. The map was constructed from 32 743 point-analyses of wt.% Mn, Mg, Ca, and Fe. Each point analysis represents a 150 X 150 μm grid element with a concentration value based on a single spot analysis with diameter of the electron beam, (~5 μm in this example). X ranges from 18000 to 17700 μm, and Y ranges from 9225 to -11175 μm. Analytical conditions were as follows: 15 kV acceleration voltage; 5 μm beam; 100 nA sample current; 1 s count times; Mn, MgO, wollastonite and magnetite standards; and uncorrected for background or matrix interferences.*

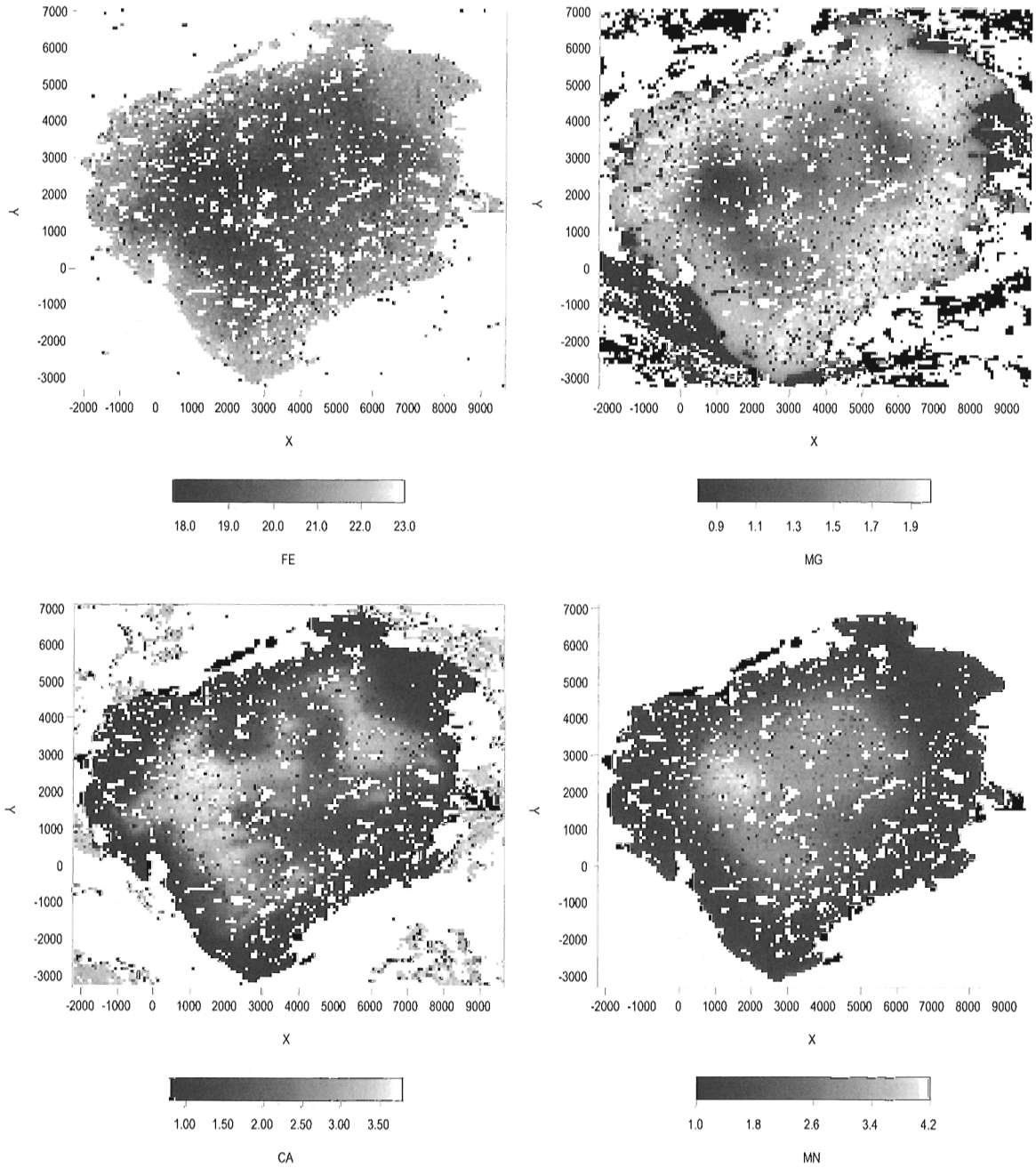

Figure 3. *Compositional maps of Fe, Mg, Ca and Mn in the garnet from sample R155-2a See text for discussion. The map was constructed from 19 092 point-analyses of wt.% Mn, Mg, Ca, and Fe. Each point analysis represents an 80 X 80 μm grid element with a concentration value based on a single spot analysis with diameter of the electron beam, (~5 μm in this example). X ranges from -2178 to 9582 μm, and Y ranges from 7034 to -3206 μm. Analytical conditions were as follows: 15 kV acceleration voltage; 5 μm beam; 100 nA sample current; 2 s count times; Mn, MgO, wollastonite, and magnetite standards; and uncorrected for background or matrix interferences.*

In addition, with respect to the garnet, Figure 3 illustrates essentially the same information as derived through several weeks of work which involved detailed, quantitative point analyses (646 analyses), spreadsheet manipulation, and contouring using less sophisticated software (Scammell, 1993). It should also be noted that the microprobe technique we have used has detected variations in compositions <2 wt.% in Mg and Mn.

Scammell (1993) has evaluated microtextures and mineral compositional zonation in this sample. In summary, he interpreted the inclusion-rich core to have grown during prograde (heating-decompression) metamorphism, and to have experienced some compositional homogenization during the thermal peak of metamorphism. The clear rim grew during the thermal peak of metamorphism, and was resorbed in the upper-right and lower-left quadrants during a retrograde, strain-enhanced reaction. Recognition of the compositional zoning in this sample, and its interpretation, has allowed the derivation of P-T estimates in a texturally complex sample with minerals which have a large amount of chemical heterogeneity and zonation (Scammell, 1993).

SUMMARY

We have presented an analytical technique to evaluate compositional zonation within minerals, and compositional heterogeneity among minerals, at thin-section scales. The technique uses a CAMECA-SX50 electron microprobe configured for automated stage movements over a user-defined grid, to provide short-duration (1-2 s) point analyses of Fe, Mg, Ca, and Mn which and are subsequently assessed using visualization software. The technique has been tested through comparison with samples that are well known through rigorous quantitative microprobe analysis, and subsequent contouring evaluation. These tests have proven that the technique is more time-effective, and can provide as much, and possibly more information at a reconnaissance level with respect to compositional zonation and heterogeneity, than the traditional quantitative microprobe analyses. The technique is most useful as a tool to identify target areas for quantitative microprobe analysis, and can be tailored to specific needs. For example, if one was primarily interested in establishing if a particular mineral has been overlooked during microscopic evaluation, a relatively coarse grid (e.g. 200 mm spacing) could be employed. Alternatively, if assessment of zoning around inclusions was being evaluated, a relatively fine grid (e.g. 5 μm spacing) could be employed. We believe the technique is a useful tool that can be utilized to assess compositional zoning and heterogeneity in thin sections.

ACKNOWLEDGMENT

We thank Kip Hodges for critically reading the manuscript.

REFERENCES

Berman, R.G.
1991: Thermobarometry using multiequilibrium calculations: a new technique with petrological applications; Canadian Mineralogist, v. 29, p. 833-856.

Essene, E.J.
1982: Geologic thermometry and barometry; Reviews of Mineralogy, v. 10, p. 153-206.

Grover, T.W., Rice, J.M., and Carey, J.W.
1992: Petrology of aluminous schist in the Boehls Butte region of northern Idaho: phase equilibria and P-T evolution; American Journal of Science, v. 292, p. 474-507.

Newton, R.C.
1983: Geobarometry of high-grade metamorphic rocks; American Journal of Science, v. 283-a, p. 1-28.

Nixon, G.T. and Pearce, T.H.
1987: Laser-interferometry study of oscillatory zoning in plagioclase: the record of magma mixing and phenocryst recycling in calc-alkaline magma chambers, Iztaccihuatl Volcano, Mexico; American Mineralogist, v. 72, p. 1144-1162.

Pattison, D.R.M. and Begin, N.J.
1994: Compositional maps of metamorphic orthopyroxene and garnet: Evidence for a hierarchy of closure temperatures and implications for geothermometry of granulites; Journal of Geology, v. 12, p. 387-410.

Ravandi Kumar, G.R. and Chacko, T.
1994: Geothermometry of mafic granulites and metapelites from the Palghat Gap, southern India: petrological evidence for isothermal uplift and rapid cooling; Journal of Metamorphic Geology, v. 12, p. 479-492.

Robinson, P.
1991: The eye of the petrographer, the mind of the petrologist; American Mineralogist, v. 76, p. 1781-1810.

St-Onge, M.R.
1987: Zoned poikiloblastic garnets: P-T paths and syn-metamorphic uplift through 30 km of structural depth, Wopmay Orogen, Canada; Journal of Petrology, v. 28, p. 1-21.

Scammell, R.J.
1993: Mid-Cretaceous to Tertiary thermotectonic history of former mid-crustal rocks, southern Omineca belt, Canadian Cordillera; unpublished Ph.D. Thesis, Queen's University, Canada, 576 p.

Spear, F. S.
1993: Metamorphic phase equilibria and pressure-temperature-time paths; Mineralogical Society of America, Washington, D.C.; 799 p.

Spear, F.S. and Florence, F.P.
1992: Thermobarometry in granulites – pitfalls and new approaches; Precambrian Research, v. 55, p. 209-241.

Spear, F.S. and Selverstone, J.
1983: Quantitative P-T paths from zoned minerals: theory and tectonic applications; Contributions to Mineralogy and Petrology, v. 83, p. 348-357.

Spear, F.S., Hickmott, D.D., and Selverstone, J.
1990: Metamorphic consequences of thrust emplacement, Fall Mountain, New Hampshire; Geological Society of America Bulletin, v. 102, p. 1344-1360.

Thompson, A.B., Tracy, R., Lyttle, J.P., and Thompson, J.B. Jr.
1977: Prograde reaction histories deduced from compositional zonation and mineral inclusions in garnet from the Gassetts schist, Vermont; American Journal of Science, v. 277, p. 1152-1167.

Tracy, R.J.
1982: Compositional zoning and inclusions in metamorphic minerals; Reviews in Mineralogy, v. 10, p. 355-397.

Tracy, R., Robinson, J.P., and Thompson, A.B.
1976: Garnet composition and zoning in the determination of temperature and pressure metamorphism, central Massachusetts; American Mineralogist, v. 61, p. 762-775.

Yardley, B.W.D.
1977: An empirical study of diffusion in garnet; American Mineralogist, v. 62, p. 793-800.

Geological Survey of Canada Project 880014

Petrography of coarse clastic facies, Fisset Brook Formation and Horton Group (Upper Devonian-Lower Carboniferous), Lake Ainslie and Margaree map areas, Cape Breton Island, Nova Scotia[1,2]

Frances J. Hein[3] and Alexandra M. Arnott[4]
GSC Atlantic, Dartmouth

Hein, J.F. and Arnott, A.M., 1995: Petrography of coarse clastic facies, Fisset Brook Formation and Horton Group (Upper Devonian- Lower Carboniferous), Lake Ainslie and Margaree map areas, Cape Breton Island, Nova Scotia; in Current Research 1995-E; Geological Survey of Canada, p. 293-300.

Abstract: In central and western Cape Breton Island, Nova Scotia, the Fisset Brook Formation and the Horton Group comprise the initial syn-rift volcanic and nonmarine clastic deposits of the Magdalen Basin. Distinction of the various coarse clastic successions is difficult in areas of geological complexity, such as near fault zones or pre-Carboniferous highlands. Petrographically, the following distinctions are made: Fisset Brook – quartzofeldspathic subarkose to arkosic arenite, with white-buff "leached"oarse clasts; Craignish quartz-rich facies – quartz arenite and subarkose; Craignish green polymict facies – more feldspathic, subarkose and arkosic arenite, with green-white altered matrix; Craignish red polymict facies – more quartz-rich, subarkose and arkosic arenite, with red-altered hematitic matrix, and red-stained quartz-grains; Judique – tan and brown subarkose and sublitharenite, with black shale intraclasts; Strathlorne – grey, less feldspathic subarkose/sublitharenite or arkose; Ainslie – grey with red, compositionally varied arenite, ranging from quartz arenite, to arkose and lithic arenite.

Résumé : Dans le centre et l'ouest de l'île du Cap-Breton (Nouvelle-Écosse), la Formation de Fisset Brook et le Groupe de Horton comprennent les volcanites initiales contemporaines du rifting et les dépôts clastiques continentaux du bassin de la Madeleine. Il est difficile de faire la distinction entre les diverses successions de roches clastiques grossières dans les régions de géologie complexe, comme les zones de failles voisines ou les hautes terres précarbonifères. Sur le plan pétrographique, les distinctions suivantes sont établies : Fisset Brook – subarkose quartzofeldspathique à arénite arkosique, renfermant des clastes grossiers blanc-chamois «décolorés»; faciès riche en quartz de Craignish – quartzarénite et subarkose; faciès polygénique vert de Craignish – subarkose et arénite arkosique plus feldspathiques, avec matrice altérée vert-blanc; faciès polygénique rouge de Craignish – subarkose et arénite arkosique plus riches en quartz, avec matrice hématitique altérée rouge et grains de quartz tachés de rouge; Judique – subarkose et sublitharénite ocre et brun avec des intraclastes de shale noir; Strathlorne – subarkose/sublitharénite ou arkose grise moins feldspathique; Ainslie – arénite de composition variée grise avec du rouge, variant de quartzarénite à arkose et arénite lithique.

[1] Contribution to Canada-Nova Scotia Cooperation Agreement on Mineral Development (1992-1995), a subsidiary agreement under the Canada-Nova Scotia Economic and Regional Development Agreement.
[2] Contribution to Magdalen Basin NATMAP Project
[3] Department of Geology and Geophysics, University of Calgary, Calgary, Alberta T2N 1N4
[4] Department of Earth Sciences, Dalhousie University, Halifax, Nova Scotia, B3H 3J5

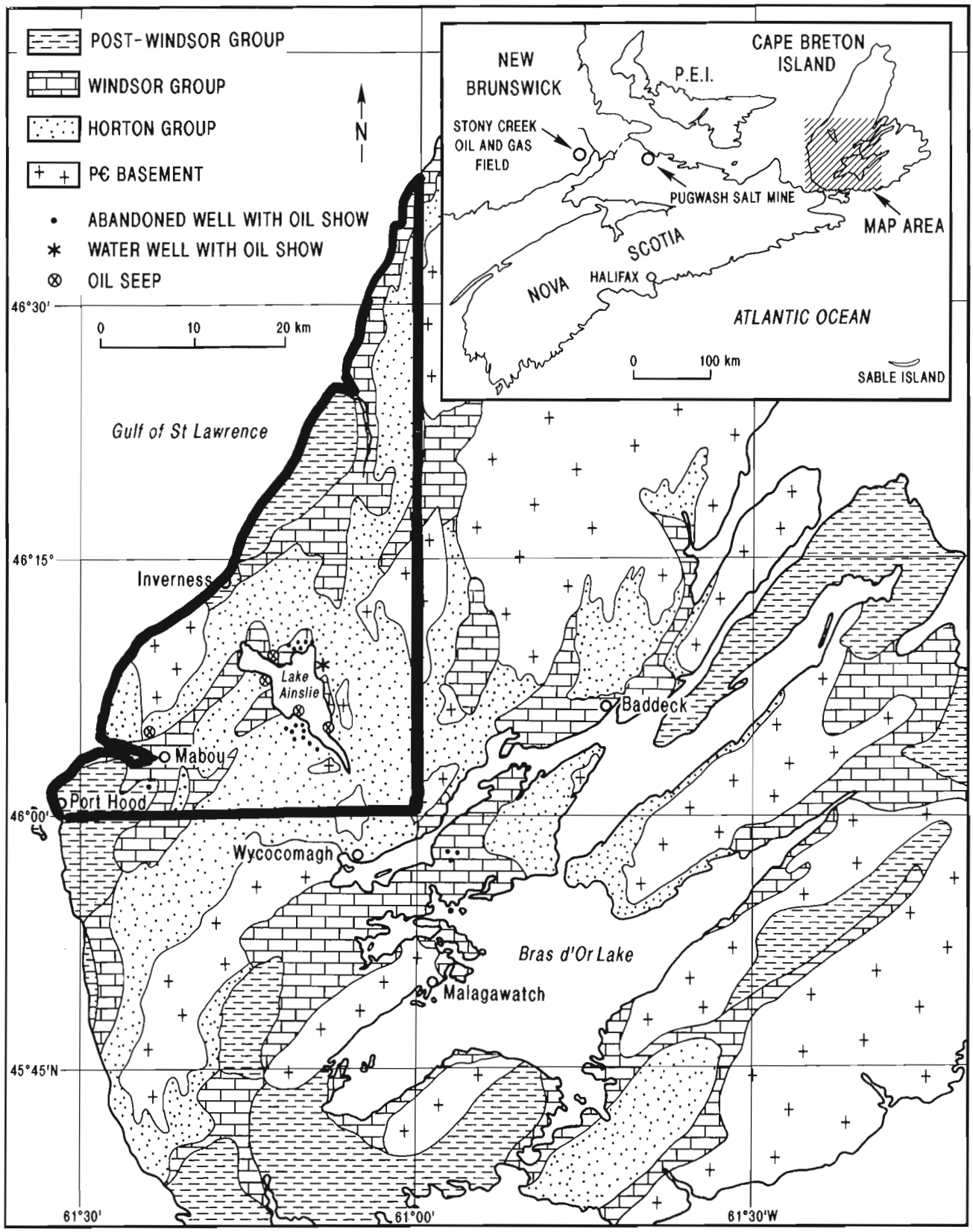

Figure 1. Simplified geologic map of western Cape Breton Island, showing the distribution of Devonian and older basement, Horton, Windsor and post-Windsor groups (from Fowler et al., 1993).

INTRODUCTION

This report summarizes the results of a petrographic study of coarse clastic sediments, following two field seasons investigating the stratigraphy and sedimentology of coarse clastic facies within the Upper Devonian-Lower Carboniferous successions of the Lake Ainslie (11K/3) and Margaree (11K/6) map areas, Cape Breton Island, Nova Scotia. A review of stratigraphic nomenclature, previous work, and objectives of the project are given in Hein (1994).

In central and western Cape Breton Island, the Fisset Brook Formation and the Horton Group comprise the initial post-Acadian volcanic and nonmarine clastic deposits that underlie the marine deposits of the Windsor Group. Previous work has established a three-fold subdivision of finer grained Horton facies (Murray, 1960; Hamblin, 1989; Hamblin and Rust, 1989) that characterize the centre of the Lake Ainslie map area (NTS 11K/3) (Fig. 1, 2). Subsequent mapping of the Lake Ainslie and Margaree map areas shows that this tripartite subdivision of the Horton Group must be modified to account for complex facies changes in areas proximal to pre-Carboniferous highlands (Fig. 3) (Hein, 1994; Giles et al., maps in prep.). At some localities, where there are structural complications and/or stratigraphic omissions, it is difficult to separate some of the coarse clastic units from one another. For this reason a detailed petrographic analysis was done on selected coarse clastic units belonging to the Fisset Brook Formation and the Craignish, Strathlorne, and Ainslie formations of the Horton Group, to aid in the distinction of these units.

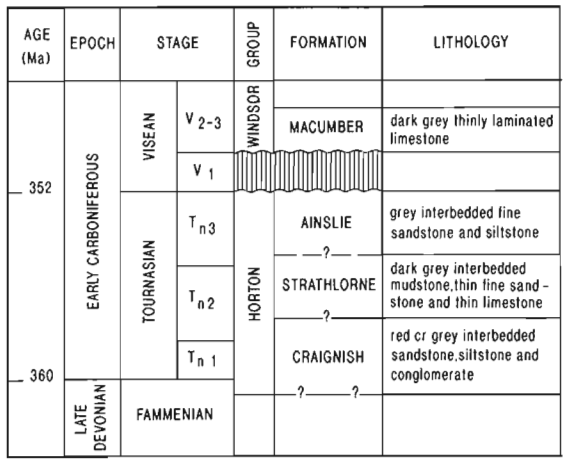

Figure 2. Stratigraphy of the finer-grained clastic successions of the Horton Group on Cape Breton Island (from Hamblin, 1989 and Hamblin and Rust, 1989).

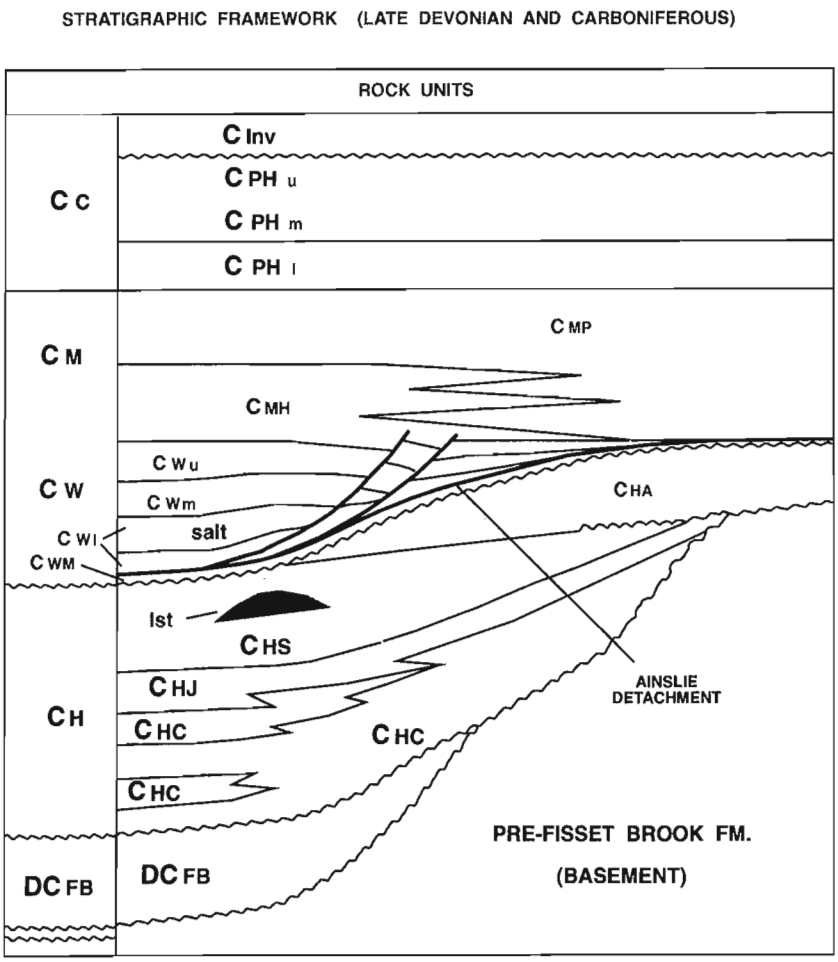

Figure 3.

Revised stratigraphic framework for Carboniferous rock units of western Cape Breton Island. Age designations:
DC – Devono-Carboniferous
EC – Early Carboniferous
C – Carboniferous
LC – Lower Carboniferous Group and formation designations
FB – Fisset Brook Formation
H – Horton Group
W – Windsor Group
M – Macumber Formation
Wl – lower Windsor Group
Wm – middle Windsor Group
Wu – upper Windsor Group
M – Mabou Group
Mg – grey Mabou
Mr – red Mabou
C – Cumberland Group
PHl – lower Port Hood Formation
PHm – middle Port Hood Formation
PHu – upper Port Hood Formation
Inv – Inverness Formation
Unconformities shown by wavy lines; interfingered relationships shown by jagged lines; major fault splays along the Ainslie Detachment shown by bold, smooth arching lines. (from Giles et al., map in prep.).

METHODS

Thirty sandstone and conglomerate samples from the Fisset Brook Formation and 113 sandstone and conglomerate samples from the Horton Group were analyzed. Samples were cut in the field and were impregnated with a blue-stained epoxy resin prior to thin sectioning. For the sandstones, estimates of framework grain mineralogy, per cent matrix and void-space were made by point-counting a minimum of 294 grains per thin section. For the conglomerates, samples were slabbed and examined under the binocular microscope with areal percentages used to estimate the grain components. Several of the conglomerates were analyzed by both thin- and slab-section, and for these samples it was found that thin-section analysis tends to underestimate the percentage of feldspar and rock-fragments, while overestimating the percentage of quartz. This reflects a grain-component variation between the matrix and coarse clasts within the conglomerates. Because the present study emphasizes the coarse-clast composition, most of the conglomerates were analyzed by slab-section. Normalized percentages were calculated for each thin slab-section to represent the percentage of quartz, feldspar, and rock fragment components of the grains.

The major detrital grain components identified include: monocrystalline quartz, polycrystalline quartz, K-feldspar, plagioclase, metamorphic and igneous rock fragments, carbonate and shale intraclasts, micas (mainly muscovite, less commonly biotite), opaques and other accessories. Detailed results of the petrographic work are given in Hein (in prep.) and summarized in Figures 4 and 5. Sandstones and conglomerates were classified according to Dott's (1964) scheme (Fig. 6) in which composition is described on a ternary graph by the three main framework components: quartz (Q), feldspar (F) and lithic or rock fragments (Rk) (Fig. 4, 5, 6).

PETROGRAPHIC SUMMARY

Fisset Brook Formation. Latest Devonian to earliest Carboniferous. In the field comprises basalt, with minor rhyolite, and interbedded sandstone and conglomerate, less commonly, siltstone and fine grained sandstone. The top of the formation is marked by a tuff. The siltstone and fine grained sandstone interbeds are commonly red with green reduction spots, less commonly grey. Rock fragments are predominantly volcanic and shale clasts.

Petrographically, the coarse clastics belonging to the Fisset Brook Formation are mainly composed of "white conglomerate/pebbly sandstone." The colour is white to buff, and individual clasts seem to have etched edges, giving the clasts a "bleached" appearance. Compositionally the sediments are classified as quartzofeldspathic subarkose to arkosic arenite, less commonly lithic arenite (Fig. 4, 6).

Craignish Formation. Latest Devonian to Early Carboniferous. In the field includes three facies assemblages: 1) quartz-rich facies (CHC(q)), 2) a green-white, polymict facies

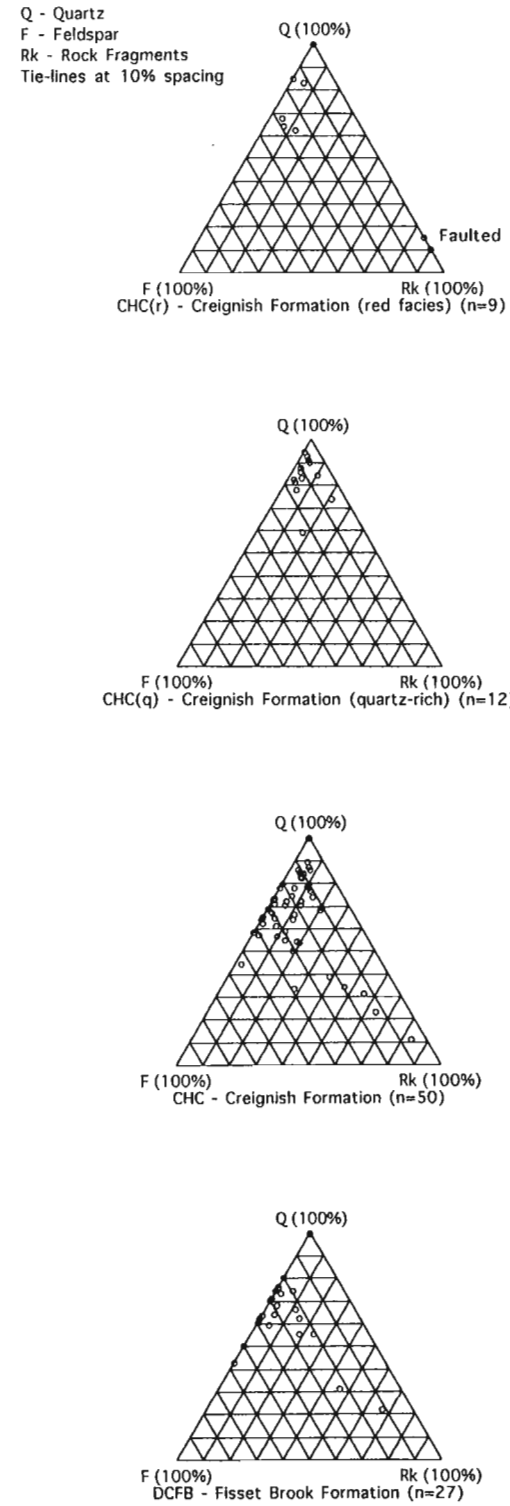

Figure 4. *Ternary plot of the composition of the coarse fraction of sandstones and pebbly sandstones/conglomerates of the Devono-Carboniferous Fisset Brook Formation (DCFB); and the Carboniferous Craignish Formation, including the green-white polymict facies (CHC), the quartz-rich facies (CHC(q)), and the red polymict facies (CHC(r)) from the Lake Ainslie and Margaree map areas, western Cape Breton Island; n indicates the number of analyses.*

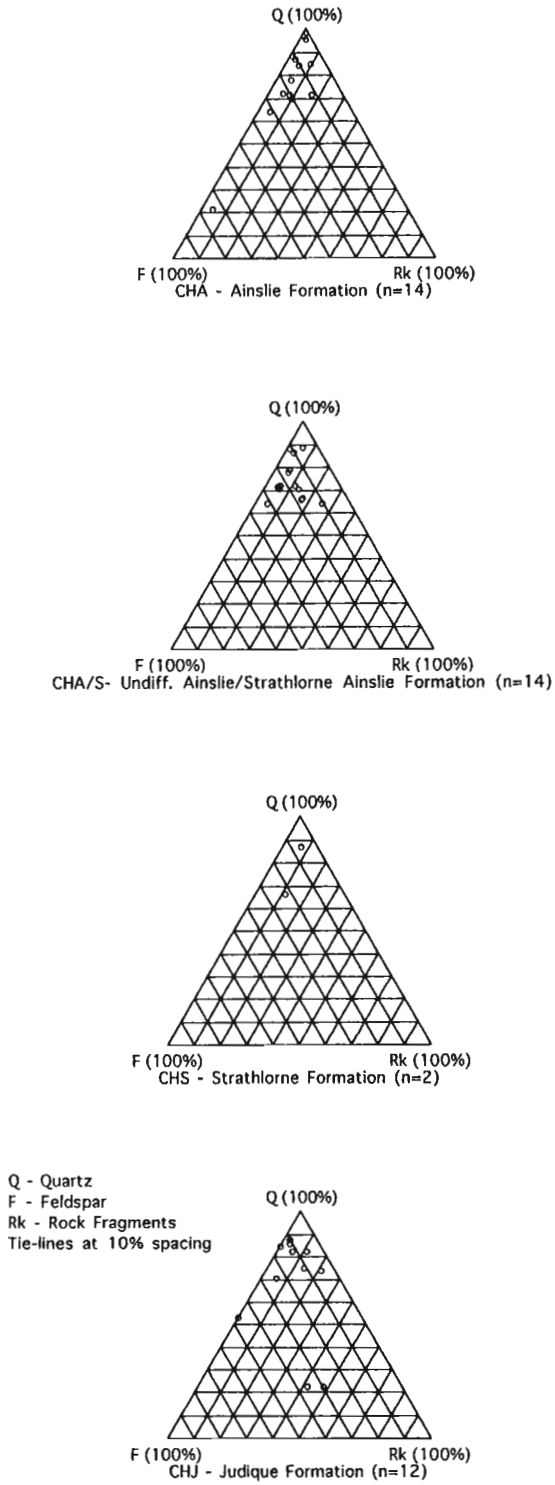

Figure 5. *Ternary plot of the composition of the coarse fraction of sandstones and pebbly sandstones/conglomerates of the Carboniferous Judique Formation (CHJ), the Strathlorne Formation (CHS), the Ainslie Formation (CHA), and the undifferentiated Strathlorne and Ainslie formations (CHS/A) from the Lake Ainslie and Margaree map areas, western Cape Breton Island; n indicates the number of analyses.*

(CHC), or 3) a red polymict facies (CHC(r), that mainly occurs in the Margaree map area, and the south-central and southeastern part of the Lake Ainslie map sheet.

Quartz-rich facies (CHC(q)): comprises sandstone, pebbly sandstone and conglomerate, pale grey or white; conglomerates typically contain dark grey to black shale clasts. This facies is areally restricted to southeastern part of the Lake Ainslie map area, and is more common to the north on the Margaree map area.

Petrographically, the coarse clastics belonging to the quartz-rich facies of the Craignish Formation are mainly composed of quartz (80-95%), with less common feldspar (5-10%), volcanic and igneous rock fragments (3-9%) (Fig. 5), carbonate rock fragments (5%), rare opaques (1%) and mica (0-5%). Sediments are poorly sorted, and quartz-rich, and are classified as quartz arenite and subarkose; less commonly as sublitharenite or lithic arenite (Fig. 4, 6).

Green-white polymict facies (CHC): more feldspathic than the quartz-rich facies (CHC(q)) and represents the bulk of the Craignish Formation. In the field this unit consists of conglomerate, pebbly sandstone ranging to conglomeratic, as well as sandstone, with minor shale and siltstone interbeds; grey and greenish-grey, locally altered red; poor to moderate sorting, abundant rock fragments, mainly volcanic and plutonic; locally cut by mafic dykes.

Petrographically, the coarse clastics belonging to the green-white polymict facies of the Craignish Formation have a green-altered matrix; and sediments have variable compositions, as follows: quartz (10-95%), feldspar (5-90%), volcanic, plutonic and metamorphic rock fragments (3-89%), carbonate rock fragments (5-10%), rare opaques (1-2%), and mica (1-10%). Sediments are better sorted, more micaceous, and more feldspathic than the interbedded quartz-rich facies; and the coarse-clast composition is much more varied. Sediments are classified as subarkose and arkosic arenite; less commonly as sublitharenite or lithic arenite (Fig. 4, 6).

Red polymict facies (CHC(r)): less feldspathic and more quartz-rich than the green-white polymict facies (CHC); in the field consists of a conglomerate, pebbly sandstone ranging to conglomeratic, and sandstone, with minor shale and siltstone interbeds; red; poor to moderate sorting, abundant rock fragments, mainly volcanic and plutonic.

Petrographically, the coarse clastics belonging to the red polymict facies of the Craignish Formation have a hematitic red-altered matrix and red-stained quartz grains. Clasts have variable compositions, as follows: quartz (60-95%), feldspar (0-38%), volcanic, plutonic and metamorphic rock fragments (0-89%), carbonate rock fragments (5-10%), rare opaques (1-2%), and mica (1-10%). Sediments are better sorted, more micaceous, and more feldspathic than the interbedded quartz-rich facies, and the coarse-clast composition is less varied than the green polymict facies. Hematitic red-staining is

characteristic of both the matrix and clasts. Sediments are classified mainly as subarkose and arkosic arenite, with rare quartz arenite or lithic arenite (Fig. 4, 6). Lithic arenites represent areas where the red polymict facies is faulted.

Judique Formation. Early Carboniferous. In the field is coarse- to fine-grained sandstone, locally pebbly to conglomeratic, white, tan, red-brown; at the base of channel fill successions, commonly has abundant black shale intraclast horizons. In some localities the Judique sediments are gradational with sediments of the underlying Craignish Formation. This facies is areally restricted to the north on the Margaree map area.

Petrographically, the coarse clastics belonging to the Judique Formation consist mainly of quartz (19-85%), with less common feldspar (6-30%), volcanic and igneous rock fragments (2-70%), carbonate rock fragments (0-10%), rare opaques (1-2%), and mica (0-10%). Sediments are moderately sorted and quartz rich. Compositionally, the sediments are classified as mainly subarkose and sublitharenite, with less common arkosic arenite and lithic arenite (Fig. 5, 6).

Strathlorne Formation. Early Carboniferous. In the field is mainly a siltstone, grey with minor red colouration, with thin oolitic and stromatolitic limestones; intercalated sandstones are grey, and may locally dominate the succession.

Petrographically, the sandstones belonging to the Strathlorne Formation consist mainly of quartz (75-85%), with less common feldspar (5-10%), volcanic and igneous rock fragments (2-9%), carbonate rock fragments (0-10%), rare opaques (1-2%), and mica (2-4%). Sediments are moderately to well sorted and quartz rich. Compositionally, the sediments are classified as mainly subarkose/sublitharenite or arkose (Fig. 5, 6).

Ainslie Formation: Early Carboniferous. In the field is mainly a sandstone, locally conglomeratic near highland areas, grey, with less common grey siltstone and shale, and tan carbonate-intraclast horizons.

Petrographically, the coarse sandstones belonging to the Ainslie Formation consist mainly of quartz (22-95%), with less common feldspar (5-80%), volcanic and igneous rock fragments (4-28%); and variable proportions of carbonate rock fragments

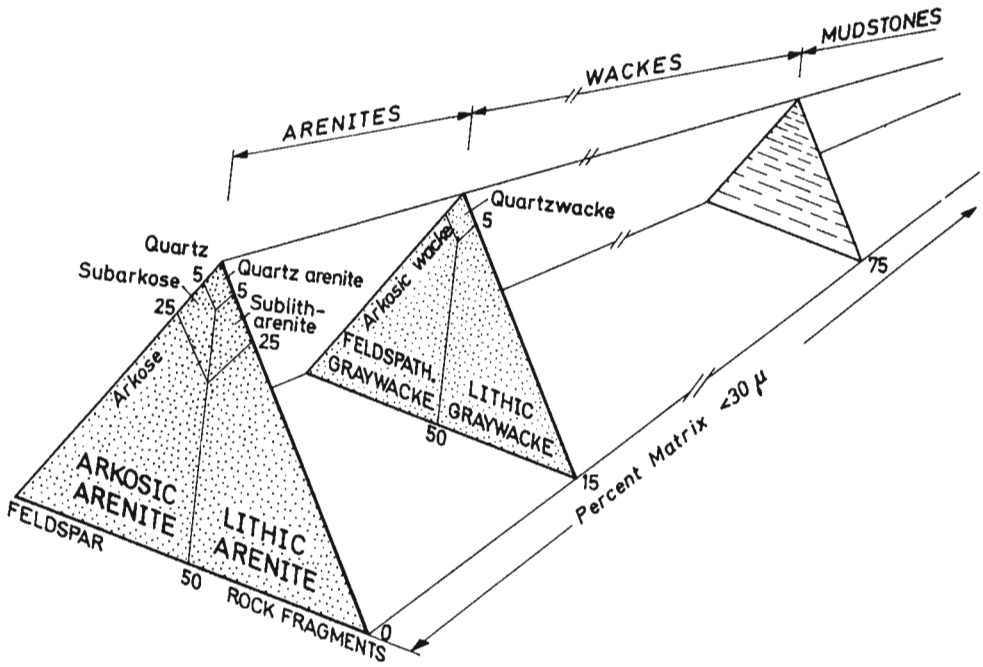

Figure 6. *Classification of terrigenous and marine sandstones (from Pettijohn et al., 1972, modified from Dott, 1964, Fig. 3).*

(5-45%) and mica (3-45%), rare opaques (1-2%). Sediments are poorly sorted or moderately to well sorted. Sediments are classified as quartz arenite, subarkose and arkosic arenite, sublitharenite and lithic arenite (Fig. 5, 6). Compositionally, this is a much more varied coarse-clastic composition, and may reflect more local controls on sedimentation.

DISTINCTION OF COARSE CLASTICS BELONGING TO THE FISSET BROOK FORMATION AND HORTON GROUP: A DISCUSSION

In Cape Breton, the Upper Devonian-Lower Carboniferous rocks unconformably overlie the crystalline basement. These rocks consist of the Fisset Brook Formation, a succession of interbedded sedimentary and volcanic rocks, overlain by the clastic sedimentary rocks of the Horton Group. The Fisset Brook Formation was originally defined by Kelley and MacKasey (1964) as a lower, chiefly sedimentary unit, a predominantly andesitic unit, and an upper mainly rhyolitic unit. Further studies of the Fisset Brook Formation show a bimodal volcanic suite of tholeiitic basalt and rhyolitic composition (Blanchard et al., 1984; Arnott, 1994) interbedded with sedimentary rocks of mainly quartzofeldspathic conglomerates and red micaceous sandstones (Arnott, 1994).

East of Lake Ainslie, basalt is mixed with siltstone in a perperitic structure where the basalt flowed over water-saturated sediments (Arnott, 1994). Generally, in the area east of Lake Ainslie and to the north, in the Chéticamp area, the Fisset Brook coarse clastic sediments are characterized by a white-buff coloured, quartzofeldspathic coarse sandstone to pebble conglomerate, interbedded with red and grey siltstones to very fine sandstones. In the Trout Brook drainage, on the east side of Lake Ainslie, these clastics of the Fisset Brook Formation are directly overlain by a white, well-rounded, quartz-pebble conglomerate, in turn, succeeded by an angular polymictic conglomerate with green- and white-altered matrix of the lower Craignish Formation (Hein, 1994). The lower Craignish "white conglomerate" was also observed by Arnott (1994) in the Gillanders Mountain area, east of Lake Ainslie; however, this facies is generally absent west of Lake Ainslie (Hamblin, 1989; Giles et al., map in prep.). The contact between the Fisset Brook and Craignish formations is poorly exposed in the Lake Ainslie area.

To the north, near Chéticamp, the Fisset Brook-Craignish contact is well-exposed, where sediments of the Craignish Formation immediately overlie deposits of the Fisset Brook Formation, with no sign of faulting or baking (cf. Arnott, 1994). As with the samples examined in the present study (Fig. 5, 6), there is a similar petrographic composition of the sandstones and pebbly sandstones between the Fisset Brook and lower Craignish formations (Fig. 7). Sediments of the Fisset Brook Formation appear, on average, to have slightly more quartz, and in one sample have significantly more rock fragments. In the field and in hand specimen, the Fisset Brook (DCFB) conglomerates and coarse sandstones are typically very white to buff coloured, with a bleached appearance. In contrast, the green-white polymict conglomerates and coarse sandstones (CHC) of the lower Craignish Formation lack the bleached aspect and the very white colouration; they have a more reddish colouration to the matrix, and are more feldspathic in coarse clast composition. The fine grained interbeds of the Fisset Brook Formation are red siltstone/fine grained sandstone with green reduction spots or grey siltstone. By contrast, the fine grained interbeds of the lower Craignish Formation are red siltstone/fine grained sandstone.

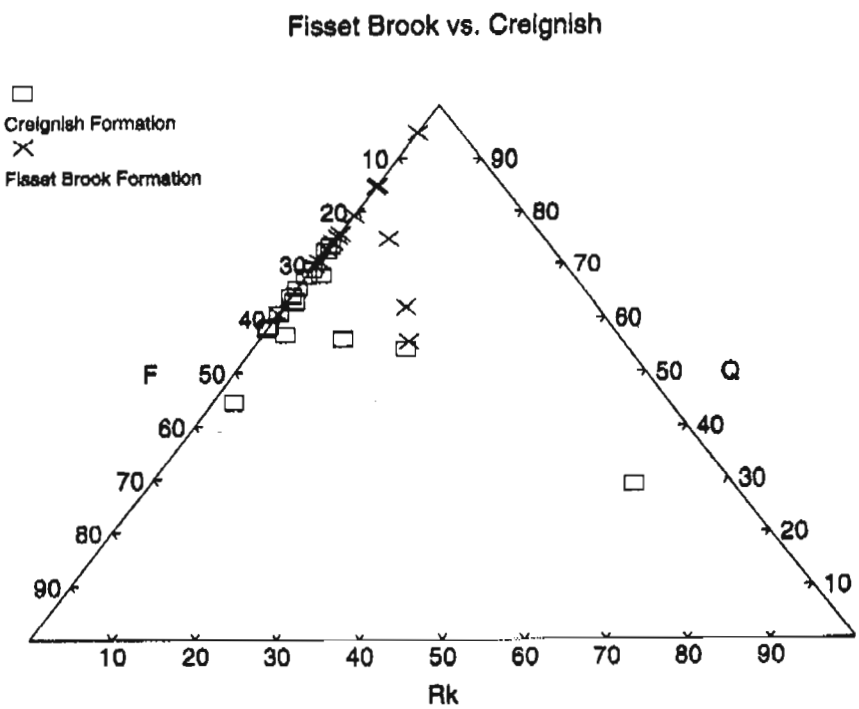

Figure 7.

Ternary plot of the composition of the coarse fraction of sandstones and pebbly sandstones/conglomerates of the Devonian-Carboniferous Fisset Brook Formation and the Lower Carboniferous Craignish Formation.

FUTURE WORK

Although there appear to be minor compositional differences between the coarse clastics of the Fisset Brook and Craignish formations, their distinction in the field is not always straightforward, particularly in areas of complex geology. The main difference is that the Craignish sediments are slightly more feldspathic, but this is not always identifiable in the field. The colour variations and occurrence of reduction spots are diagenetic effects and may not be reliable for field distinction of these units.

Preliminary petrographic analysis of the Horton Group clastics suggests that there may be an increase in maturity with age, from Judique to Strathlorne to Ainslie. The Craignish successions appear to have their own trend, again distinct from the Fisset Brook units. In a rough way, these trends may approximate evolution of the Horton Group succession, but this maturation trend must be tested with further analyses, showing proximal – distal trends within given stratigraphic horizons, as well as an evaluation of general background levels within the basin.

Ongoing stratigraphic work and mapping in the Chéticamp area to the north of the Margaree map area will help delineate the stratigraphic and sedimentological relationships between coarse clastic successions of the Fisset Brook Formation and lower Craignish Formation of the Horton Group; as well as documenting proximal-distal petrographic variation within different horizons of the horton Group successions.

ACKNOWLEDGMENTS

R. Brown (University of Calgary), T. Allen and B. Creaser (Dalhousie University) provided capable field assistance. P. Mindermann (University of Calgary) and D. Horton (Technical University of Nova Scotia) assisted in laboratory analyses. Principal funding and logistical support for the project was provided under Canada-Nova Scotia Cooperation Agreement on Mineral Development (1992-1995), a subsidiary agreement under the Canada-Nova Scotia Economic and Regional Development Agreement. Partial support for field, laboratory and computer costs was provided by an NSERC Individual Operating Grant to Hein (PIN 014445). P.S. Giles, J. Utting and A.P. Hamblin are thanked for their critical reviews of an earlier version of the manuscript.

REFERENCES

Arnott, A.M.
1994: Petrology and geochemistry of the Fisset Brook Formation in the Gillanders Mountain area, Cape Breton Island, Nova Scotia; B.Sc. [Honours] thesis, Acadia University, Wolfville, Nova Scotia, 117 p.

Blanchard, M-C., Jamieson, R.A., and More, E.B.
1984: Late Devonian-Early Carboniferous volcanism in western Cape Breton Island, Nova Scotia; Canadian Journal of Earth Sciences, v. 21, p. 762-774.

Dott, R.L., Jr.
1964: Wacke, graywacke and matrix – what approach to immature sandstone classification?; Journal of Sedimentary Petrology, v. 34, p. 625-632.

Fowler, M.G., Hamblin, A.P., MacDonald, D.J., and McMahon, P.G.
1993: Geological occurrence and geochemistry of some oil shows in Nova Scotia; Bulletin of Canadian Petroleum Geology, v. 41, p. 422-436.

Hamblin, A.P.
1989: Sedimentology, tectonic control and resource potential of the Upper Devonian-Lower Carboniferous Horton Group, Cape Breton Island, Nova Scotia; Ph.D. thesis, Ottawa-Carleton University, Ottawa, Ontario, 300 p.

Hamblin, A.P. and Rust, B.R.
1989: Tectono-sedimentary analysis of alternate-polarity half-graben basin-fill successions: Late Devonian-Early Carboniferous Horton Group, Cape Breton Island, Nova Scotia; Basin Research, v. 2, p. 239-255.

Hein, F.J.
1994: A preliminary report on the stratigraphy and petrography of coarse clastic facies, Horton Group (Upper Devonian-Lower Carboniferous), Lake Ainslie map area, Cape Breton Island, Nova Scotia; in Current Research 1994-E; Geological Survey of Canada, p. 211-218.

Kelley, D.G. and MacKasey, W.O.
1964: Basal Mississippian volcanic rocks in Cape Breton Island, Nova Scotia; Geological Survey of Canada, Paper 64-34, 10 p.

Murray, B.C.
1960: Stratigraphy of the Horton Group in parts of Nova Scotia; Nova Scotia Research Foundation, Halifax, Nova Scotia, 160 p.

Pettijohn, F.J., Potter, P.E., and Siever, R.
1972: Sand and Sandstone; Springer-Verlag, New York, 600 p.
1987: Sand and Sandstone; New York, Springer-Verlag, Second Edition, 553 p.

Geological Survey of Canada Project 920062

Canada and Article 76 of the Law of the Sea: defining the limits of Canadian resource jurisdiction beyond 200 nautical miles in the Arctic and Atlantic oceans

Ron Macnab
GSC Atlantic, Dartmouth

Macnab, R., 1995: Canada and Article 76 of the Law of the Sea: defining the limits of Canadian resource jurisdiction beyond 200 nautical miles in the Arctic and Atlantic oceans; in Current Research 1995-E; Geological Survey of Canada, p. 301-311.

Abstract: Article 76 of the Law of the Sea permits coastal nations with wide continental margins to extend their jurisdiction over certain mineral and biological resources beyond 200 nautical miles, and to assume increased environmental and conservation responsibilities.

Existing data bases would appear to substantiate Canadian jurisdiction over about 750 000 km^2 in the Atlantic, and 500 000 km^2 in the Arctic. A strategic program for acquiring new data could strengthen and maximize these claims, in which case the total area of jurisdiction beyond 200 nm under the Law of the Sea could potentially equal the three Prairie Provinces combined.

Current indications are that the zone defined by Article 76 in the Atlantic would hold significant potential for gas, oil, and gas hydrates; less is known about the fishery potential of sedentary species identified under Article 76. Information about most Arctic resources is inadequate for a reliable assessment of their potential, although the outlook for gas and oil appears generally favourable.

Résumé : L'article 76 du droit de la mer permet aux États côtiers présentant de larges marges continentales d'étendre leur juridiction à certaines ressources minérales et biologiques situées au-delà de la limite des 200 milles marins et d'accepter des responsabilités accrues en matière d'environnement et de conservation.

Les bases de données existantes sembleraient démontrer le bien-fondé des revendications du Canada quant à l'extension de sa juridiction à près de 750 000 km^2 dans l'Atlantique et 500 000 km^2 dans l'Arctique. Un programme stratégique d'acquisition de nouvelles données pourrait permettre d'étayer et de maximiser ces revendications; la superficie totale visée par l'extension de la juridiction en vertu du droit de la mer deviendrait alors équivalente à celle de l'ensemble des trois provinces des Prairies.

D'après les indications actuellement disponibles, la zone économique dans l'Atlantique définie en vertu de l'article 76 renfermerait d'importantes ressources potentielles en gaz, en pétrole et en hydrates de gaz; les ressources halieutiques sédentaires potentielles reconnues en vertu de l'article 76 sont moins bien connues. L'information disponible concernant les ressources potentielles dans l'Arctique est insuffisante et n'en permet pas une évaluation fiable, bien que les perspectives en ce qui a trait au gaz et au pétrole semblent généralement favorables.

AN INTRODUCTION TO ARTICLE 76 OF THE LAW OF THE SEA

General principles

Upon ratification by 60 nations, the 1982 UN Convention on the law of the Sea came into force on 14 November 1994. Developed during a decade of multilateral negotiations, the new law embodies substantial changes to the regulations governing the peaceful uses and exploitation of the world's oceans.

Article 76 of the Law of the Sea will have significant potential impact on Canada and other coastal nations with wide continental margins, because it provides these nations with a means of ensuring international recognition of national jurisdiction in new marine areas beyond the limits of present economic zones. With certain qualifications, these extended jurisdictions apply to non-living resources of the seabed and its subsoil, and to living resources that dwell upon the sea floor.

New limits to which a coastal state can claim jurisdiction must be established on the basis of information submitted by the state concerning the nature of the submerged prolongation of its land mass beyond 200 nautical miles. The nature of this information involves a series of criteria based on bathymetric and geological factors. A claim must be submitted to the UN Commission on the Limits of the Continental Shelf; this body will make a recommendation on the basis of which the coastal state shall establish 'final and binding' limits of its continental shelf.

The dozen or so wide-margin coastal states among the first 60 ratifying nations have until 14 November 2004 to define the new outer limits of their resource jurisdiction. Wide-margin coastal states that ratify the Convention after 14 November 1994 have ten years from the date of their respective ratifications to define their own outer limits.

The meaning of the juridical continental shelf

With Article 76, a new definition of continental shelf' entered the lexicon: the term now applies to the 'natural prolongation' of a coastal state's land territory. In this sense, it does not refer explicitly to the physiographic continental shelf; in fact, it encompasses all three physiographic components of the continental margin – shelf, slope, and rise.

Where the outer edge of this legal or juridical continental shelf is located depends on the width of the continental margin. If the margin is narrow (as off western Canada) the juridical shelf has a width of 200 nautical miles (about 365 km). If the margin is wide (as off eastern and northern Canada), the width of the juridical shelf depends on the topography of the sea floor and sub-bottom, and must be determined in accordance with the provisions of Article 76.

With its potential for creating confusion, this altered nomenclature seems to be an unfortunate amendment to the language. Nevertheless, the new meaning of 'continental shelf' is firmly embedded in the vocabulary of international law. Therefore in any context it is important to be explicit about the definition that applies.

The case for Canada

Article 76 provides Canada with a means of ensuring international recognition of national jurisdiction over significant territory beyond the edge of the physiographic continental shelf on the Atlantic and Arctic margins, but not on the Pacific margin, where the continental margin is narrow.

The Atlantic margin (Fig. 1) encompasses broad shelves such as the Scotian Margin and the Grand Banks of Newfoundland, as well as natural components of the continental margin such as Flemish Cap and Orphan Knoll. The Arctic margin (Fig. 2) includes the Alpha Ridge and part of the Lomonosov Ridge, two structures that extend well offshore.

GENERAL IMPLEMENTATION OF ARTICLE 76

Justification for extending the 200 nautical mile limit

Before proceeding to implement Article 76, a wide-margin state must identify seabed features to be enclosed within the new continental shelf, and justify them as components of the

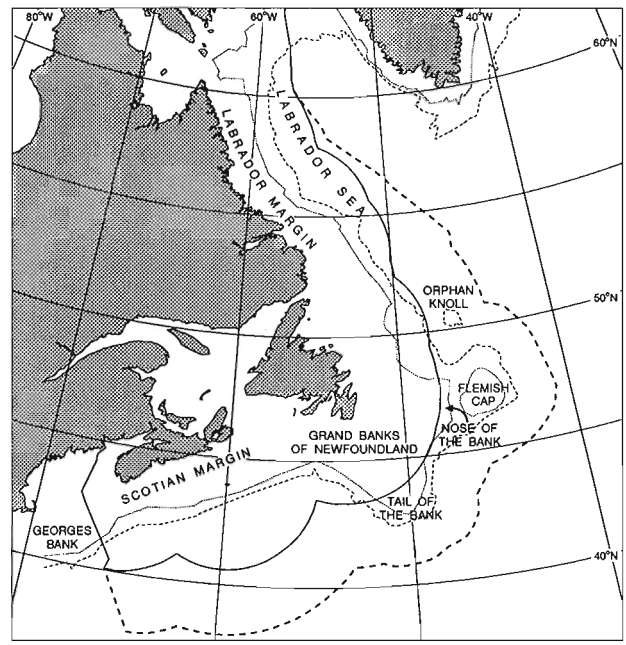

Figure 1. Canada's Atlantic margin. Solid line: Fishing Zone limits that circumscribe present jurisdiction over marine resources. Light dots and dashes: 500 and 2500 m depth contours, respectively. Heavy dashes: location of the bounding line, explained in the text.

'natural prolongation of its land territory'. Physiographic considerations are likely to be important in most cases, but Article 76 provides scope for developing geological arguments in particular situations where submarine elevations retain continental affinities even when separate from parent physiographic continental shelves.

After the identification of these features, there are three steps for defining the outer limit (Figure 3).

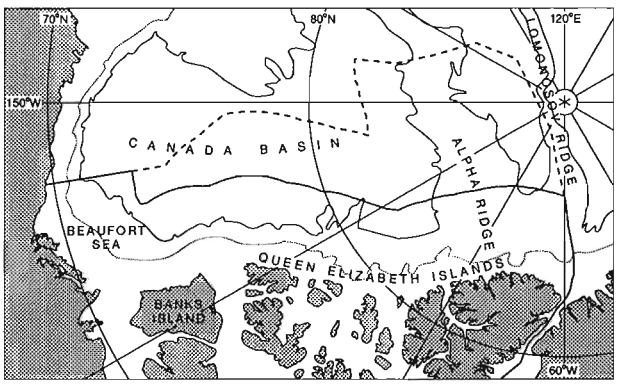

Figure 2. Canada's Arctic margin. Lines and symbols as for Figure 1.

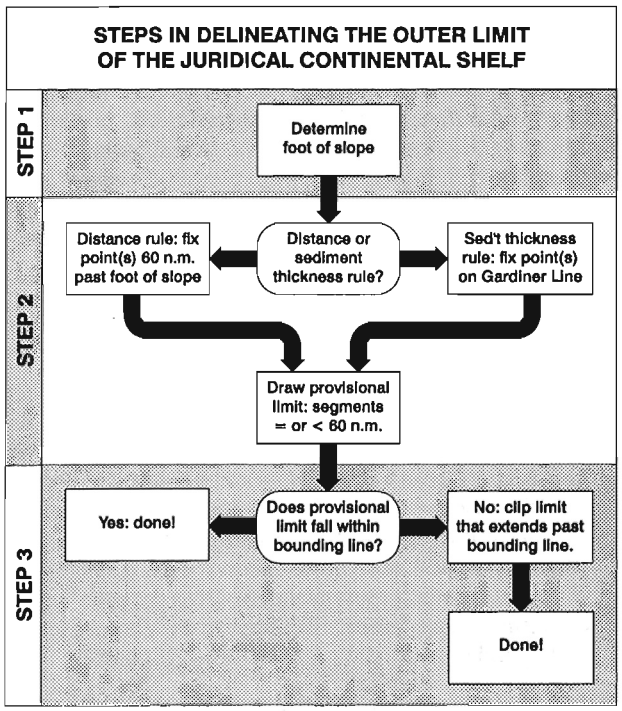

Figure 3. A simplified representation of the procedures specified in Article 76, for defining the outer limits of partial resource jurisdiction beyond the 200 nautical mile limit.

The foot of the slope

The first step requires the location of the 'foot of the continental slope', the line along the base of the slope where the gradient of the sea floor undergoes maximum change. This key feature provides a baseline for subsequent procedures; its delineation has a significant effect on the location of the final outer limit.

Distance and sediment thickness formulas

The second step involves the definition of a provisional outer limit by a series of straight lines that join fixed points no more than 60 nautical miles apart. The locations of these fixed points are determined according to their distance from the foot of the continental slope, evaluated by the distance formula or the sediment thickness formula (Fig. 4).

The distance formula involves a simple measurement of distance: 60 nautical miles to seaward from the foot of the slope. The sediment thickness formula is more complicated, and requires the measurement of sediment thickness: the fixed point is where sediment thickness equals one per cent of the distance back to the foot of the slope. The limit defined by a succession of such points is known colloquially as the Gardiner Line, after its principal architect (Gardiner, 1978).

The concept of the bounding line

Regardless of the formula chosen, the outer limit cannot extend beyond a maximum of 350 nautical miles from the state's territorial sea baselines, or 100 nautical miles beyond

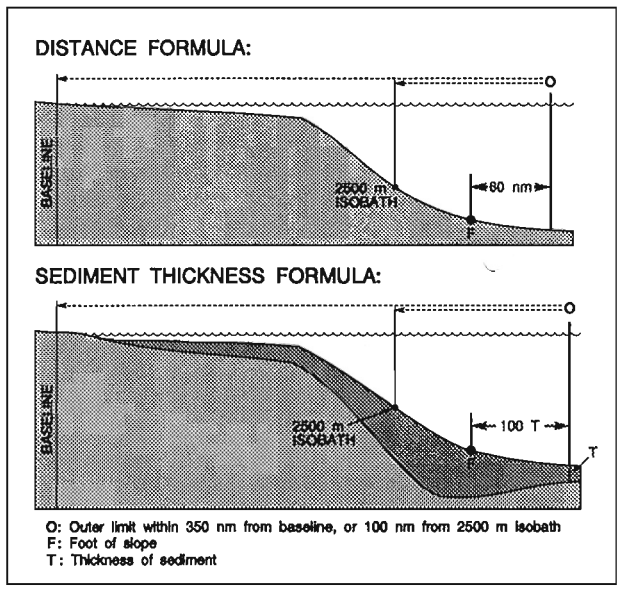

Figure 4. The distance and sediment thickness formulae specified by Article 76 for delineating the outer limit of the juridical continental shelf. It is left to the coastal state to decide whether the formulae should be applied singly or in combination.

the 2500 m isobath, unless the features being claimed are 'submarine elevations that are natural components of the continental margin, such as plateaux, rises, caps, banks, and spurs'. For the purposes of this discussion, it will be assumed also that the outer limit does not extend beyond boundaries with neighbour states. For technical convenience, these three limiting features can be amalgamated into a single *bounding line* beyond which the outer limit may not extend.

The heavy dashed lines in Figures 1 and 2 illustrate bounding lines off eastern and northern coasts, according to present information.

The outer limit of the continental shelf

The third step is to determine whether portions of the provisional outer limit (as determined by the distance and/or sediment thickness formulas) protrude beyond the bounding line, and to eliminate those that do. The resulting line is a composite of the provisional outer limit and the bounding line, and represents the new outer limit of the juridical continental shelf.

Information requirements and the effects of errors

As outlined above, the locations of five features must be known accurately for Article 76 purposes: (1) the 200 nautical mile limit measured from the territorial seas baseline; (2) the 350 nautical mile limit measured from the same baseline; (3) the foot of the continental slope; (4) the 2500 m isobath; and (5) the Gardiner Line.

The locations of the first and second features – the 200 and 350 nautical mile limits - are relatively straightforward to determine graphically from charts, or numerically by geodetic computation.

Delineating the third feature – the foot of the slope – requires the knowledge of water depths along a series of profiles perpendicular to the edge of the continental shelf, with analysis to identify the line of maximum change of seabed gradient along the base of the continental slope. This procedure doesn't require absolute accuracy in the measurement of depth, but the geographic coordinates of the depth values along each profile must be accurately known. The outcome of this analysis depends heavily on the quantity and distribution of profiles, and on interpretive criteria. Errors at this stage will propagate into applications of the distance and sediment thickness formulas.

The location of the fourth feature – the 2500 m isobath – is required as a baseline for constructing a limiting line 100 nautical miles to seaward, which defines part of the bounding line. This requires the measurement of water depths at the highest accuracy, which is presently considered to be plus or minus 1% of the water depth. At a depth of 2500 m over sea floor with a 2 degree slope, this error leads to a potential uncertainty of plus or minus 715 m in the inferred location of the 2500 m isobath, and in the corresponding segment of the bounding line. This may translate into uncertainty over the size of the area encompassed by the new outer limit.

The location of the fifth feature – the Gardiner Line – requires the measurement of sediment thickness by the seismic technique. The velocity of sound in sediment is not well known, with inaccuracies in reflection measurements typically approaching 10%. This can have a significant impact on the location of the Gardiner Line: if 1 km of sediment thickness is measured 100 km from the foot of the slope, a 10% thickness error translates into a 10 km distance uncertainty. There are other ambiguities in the interpretation of the seismic profile, such as encountered in distinguishing between sediment and underlying crystalline basement, or in determining the location of the 1% sediment thickness line over rugged acoustic basement.

RATIONALE FOR AND BASIS OF CANADIAN JURISDICTION

The Atlantic margin

Canada's Atlantic margin is characterized by a wide, shallow continental shelf (Fig. 1). Physiographic and geological considerations provide strong grounds for asserting that the Grand Banks and Flemish Cap are 'submerged prolongations' of the country's land mass. The case for Orphan Knoll and its associated basin is less clearcut, however both features are believed to be underlain by continental crust. In any case, the area to be claimed under Article 76 cannot extend beyond the bounding line shown in Figure 1.

Article 76 interests in the Atlantic region are primarily resource driven. For the most part, shelf areas on this margin are within relatively easy commercial access: the region's fishery potential has dwindled in recent years, but there is a promise of substantial hydrocarbon resources. In the past, Canada has unilaterally claimed ownership of some of these resources through the issuance of exploration permits to the petroleum industry. Article 76 offers a procedure for formalizing this resource jurisdiction through the mechanism of international recognition.

The Arctic margin

In contrast, Canada's Arctic margin has a fairly narrow continental shelf, but it features two relatively deep ridge structures oriented perpendicular to the coast and extending well into the Arctic Ocean (Fig. 2). Current geological evidence supports the case for considering the Alpha Ridge and part of the Lomonosov Ridge as 'submerged prolongations' of the Canadian landmass: the former shows geological affinity with Canada's northernmost island, whereas the latter appears to be continental in nature. The area to be claimed cannot extend beyond the bounding line shown in Figure 2.

Resource access is severely hampered on this margin by water depth, by permanent ice cover, and by unfavourable climatic and operating conditions. The region features major offshore sedimentary basins with good long-term hydrocarbon potential, but their commercial development will likely have to wait for advances in exploitation technology, not to

mention global economic changes. For short and medium terms therefore, Article 76 interests in this region are not primarily resource driven.

Article 76 interests may however be driven by environmental concerns in the Arctic; with only one deep-water channel linking it to the world ocean, the Arctic Ocean is essentially an enclosed sea that has become a repository of long-lasting toxic wastes. Monitoring and mitigating the effects of these materials will probably require a coordinated international approach, which may persuade Arctic coastal nations to establish a regime for protecting and managing their common offshore - a regime based upon clear definitions of each country's zone of interest and responsibility.

KNOWN AND POTENTIAL RESOURCES IN THE AREAS AFFECTED

Hydrocarbons of the Atlantic margin

Oil and natural gas occur in sedimentary basins, and studies confirm the existence of vast basins throughout the entire Atlantic margin from Georges Bank to the northern Labrador Sea (Procter et al, 1984; Bell and Campbell, 1990). Known and potential hydrocarbon resources in these regions offer the primary economic justification for seeking international recognition of Canadian jurisdiction over an extended continental shelf.

Gas hydrates of the Atlantic and Arctic margins

Gas hydrates are a particular form of hydrocarbons that occur globally beneath the world's oceans (Kvenvolden et al., 1993), and like oil and natural gas may be of considerable economic significance in the outer continental margin. Studies on the Atlantic margin of the United States indicate that the methane in gas hydrates is a possible major energy resource. Comparable studies have not been carried out on the Canadian margins, but current knowledge plus an extrapolation of US studies suggest that the Atlantic seabed in Canada's prospective zone of extended jurisdiction could contain nearly 200 000 trillion cubic feet of gas. Similarly, the seabed in the Arctic could contain up to 150 000 trillion cubic feet.

Minerals

Off Canada as off most coastal nations, contemporary marine mining operations are generally confined to the continental shelf, relatively close to shore and thus not likely to be affected by the provisions of Article 76. Beyond the edge of the continental shelf, manganese nodules, crusts, and coatings represent the mineral resource that has so far drawn the most attention (Hale, 1990). Off Canada's coasts, there is unlikely to be a significant quantity of this resource within the zone of jurisdiction potentially claimable under Article 76.

Fisheries of the Atlantic margin

Article 77 of the Law of the Sea defines these exploitable resources as 'living organisms belonging to sedentary species, that is to say, organisms which, at the harvestable stage, either are immobile on or under the seabed or are unable to move except in constant physical contact with the seabed or subsoil'. In addition, Articles 118, 145, and 192 describe the responsibilities of coastal states with respect to fisheries and environmental management in the areas beyond 200 nautical miles.

Limited information is available on the harvestable bottom-dwelling species of the slope, rise, and deeper areas of the continental margin. A comprehensive research program would be needed to assess fully the region's potential. Also important to consider are a wide variety of species that lack direct commercial potential, but which are significant to the environment and seabed habitats, and as food web resources.

USE OF EXISTING DATA BASES FOR JURIDICAL SHELF DELINEATION

The Atlantic margin

Bathymetry (Fig. 5)

Much information exists on the Atlantic margin, acquired mostly by agencies of the Canadian Government since the early 1960s. The quality and distribution of these observations are very uneven: many were collected prior to the 1982 UN Convention, with no particular attention being paid to sea bed features relevant to Article 76.

The data base is probably adequate for foot of slope determination off the Scotian and north Labrador Margins, but not off the Grand Banks, Flemish Cap, Orphan Knoll, and the south Labrador Margin. Determining the 2500 m isobath may be problematic in all areas, because measurements were made with old technology featuring poor to non-existent velocity control, using wide beam echo sounders that ensonified wide swaths on the sea floor and which were therefore constrained to derive average depths within their large footprints. This database probably needs to be upgraded in selected areas through the collection of new data with the aid of modern technology.

Sediment thickness (Fig. 6)

Compared to assembled observations over the shallow parts of the margin, seismic measurements are not plentiful in deeper waters. The data have been acquired by a variety of academic, government, and commercial organizations, from Canada and elsewhere. Measurements represent a mix of single- and multi-channel reflection seismic observations, with refraction profiles in certain areas.

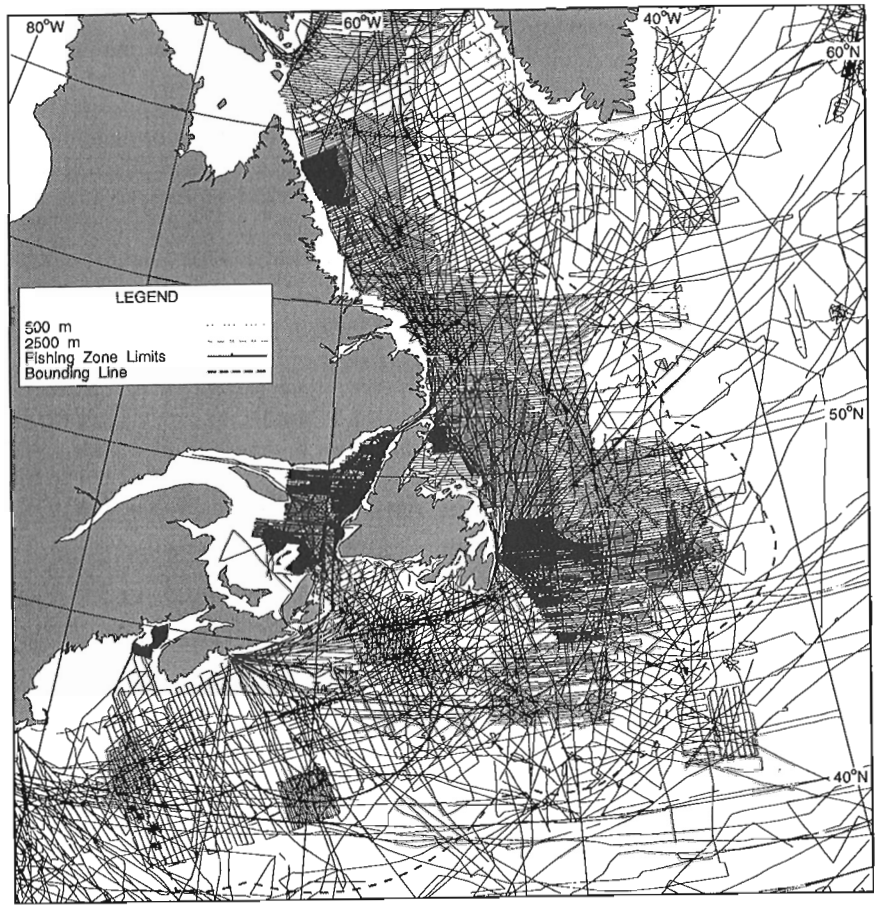

Figure 5. Locations where depth of water has been measured during surveys and scientific expeditions by vessels of the Canadian Government and other agencies, from the early 1960s to the present. Off Nova Scotia and Labrador, this database is probably adequate for determining the foot of the continental slope, less so for locating the 2500 m isobath. In the deep water areas adjacent to the Grand Banks and Flemish Cap, the database defines them less accurately.

Many of the single-channel profiles don't show acoustic basement, and thus are unsuitable for Article 76 purposes. Quality and distribution of the remaining data are very uneven: nowhere are there enough profiles to determine the location of the Gardiner Line at the required 60 nautical mile spacing. This data base needs upgrading in most areas beyond 200 nautical miles through the systematic acquisition of new reflection and refraction data.

The Arctic margin

Bathymetry (Fig. 7)

Most observations consist of spot soundings taken through the ice by helicopter-transported surveyors of the Canadian Hydrographic Service. Measurements were made for the most part with portable echo sounders that featured low power and wide beams; consisting of average depths from their large ensonified footprints, these observations are isolated from other soundings, and so provide only a limited indication of sea bed morphology.

The quality and distribution of these observations is uneven: the data may be adequate for locating the foot of slope and the 2500 metre isobath in the Beaufort Sea and off Banks Island, but not elsewhere. The database needs upgrading in the deeper waters off the Queen Elizabeth Islands and over the Alpha and Lomonosov ridges.

Sediment thickness (Fig. 8)

Available observations are scarce, consisting for the most part of seismic refraction profiles over Alpha and Lomonosov Ridges. Currently-available data are insufficient for determination of the Gardiner Line.

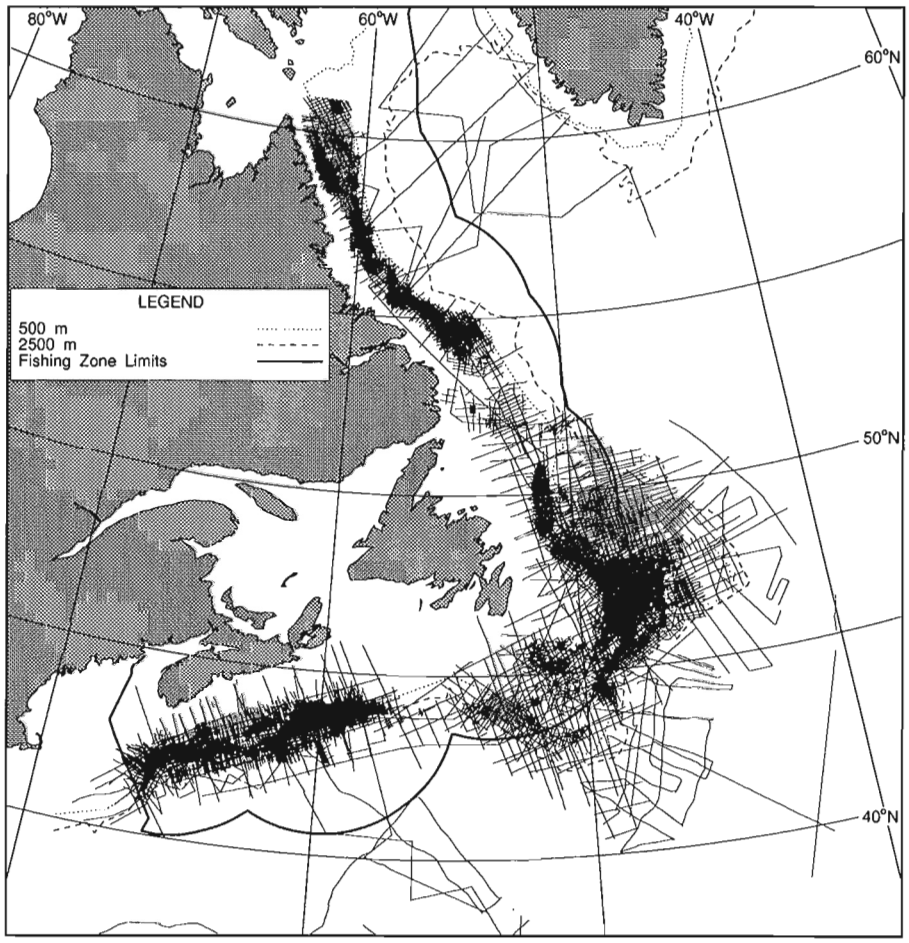

Figure 6. Locations where seismic reflection data have been collected during multichannel surveys by vessels operating for the most part on behalf of the gas and oil industry; most data were collected during the 1970s and early 1980s. Portions of this data base may be suitable for determining the thickness of sediment and the location of the Gardiner Line in the deep water areas adjacent to the Grand Banks and Flemish Cap. Off Nova Scotia and Labrador, the data are less precise in establishing the Gardiner Line.

PROVISIONAL OUTER LIMITS DEVELOPED WITH EXISTING DATABASES

The outer limits described in the paragraphs that follow have been developed from preliminary determinations of: the foot of the continental slope and a limiting line 100 nautical miles seaward of the 2500 m isobath in the Atlantic and Arctic; and the Gardiner Line in the Atlantic. These features have been defined on the basis of existing databases that are known to be incomplete. A thorough analysis of better quality information is necessary before the outer limits can be drawn in their definitive form.

Outer limits based on the distance formula

These are developed in Figures 9 and 10 for the Atlantic and Arctic, respectively. In the first stage (part A of both figures) a provisional outer limit is constructed by projecting the foot of the slope seaward for a distance of 60 nautical miles; in the second stage (part B of both figures) a definitive outer limit is produced by combining segments of the provisional outer limit, the Fishing Zone limit, and the bounding line.

In the Atlantic margin, this encloses an area beyond 200 nm of about 590 000 km^2, consisting of: a minor extension south of Nova Scotia; an extension that is close to the maximum permissible around the Grand Banks, Flemish Cap and Orphan Knoll; and a moderate extension off Labrador. In the Arctic margin, the extension consists of an area covering the Alpha Ridge and part of the Lomonosov Ridge, encompassing approximately 470 000 km^2.

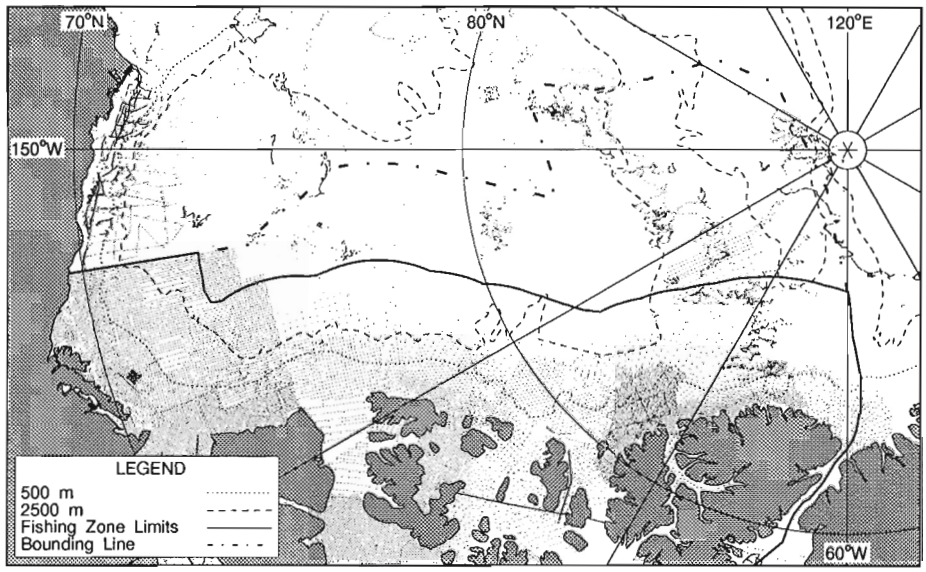

Figure 7. Locations where depth of water has been measured during surveys and scientific expeditions by Canadian Government and other agencies, from the 1960s to the present. Portions of this database are probably adequate for determining the foot of the continental slope and the 2500 m isobath in the Beaufort Sea and off Banks Island, but elsewhere the definition is less well controlled.

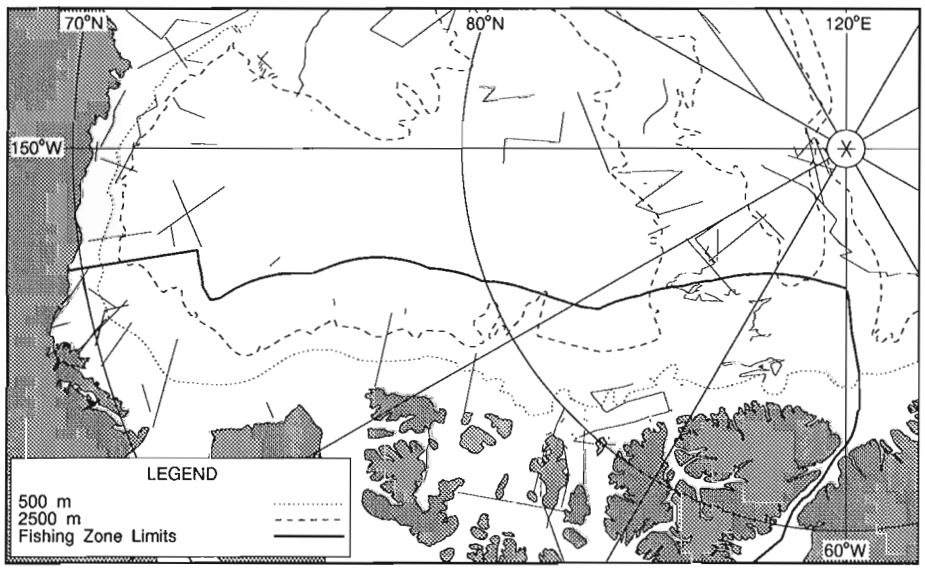

Figure 8. Locations of seismic refraction experiments performed by agencies of the Canadian Government, operating from camps established on the permanent polar pack ice. Observations include sediment thickness and velocity, but they are too sparse for determining the location of the Gardiner Line consistently throughout the region on a regional basis.

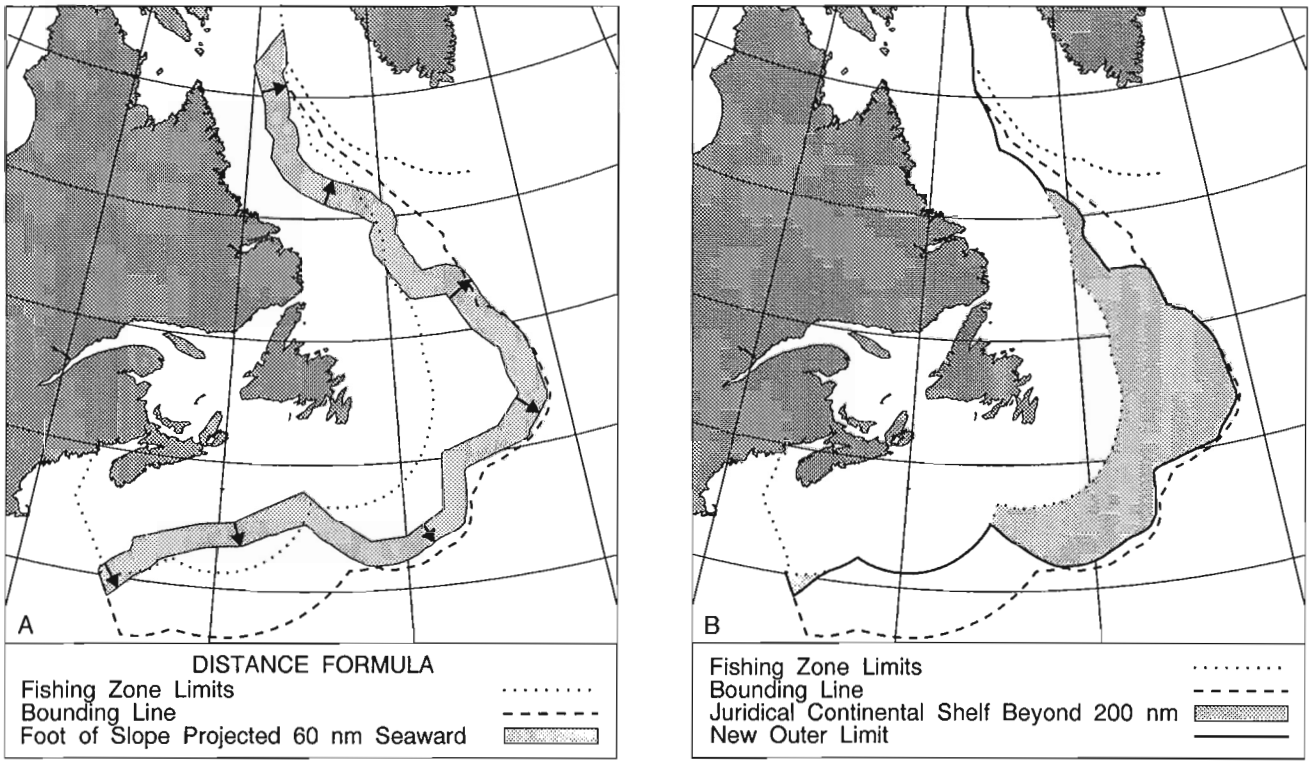

Figure 9. *The outer limit of the juridical continental shelf in the Atlantic, based on the application of the distance formula to existing information. In* ***A****, the foot of the continental slope is projected 60 nautical miles seaward to form a provisional outer limit. In* ***B****, this is combined with the 200 mile limit and the bounding line to form a new outer limit that extends the zone beyond the 200 nm limit by some 591 200 km*^{2}*.*

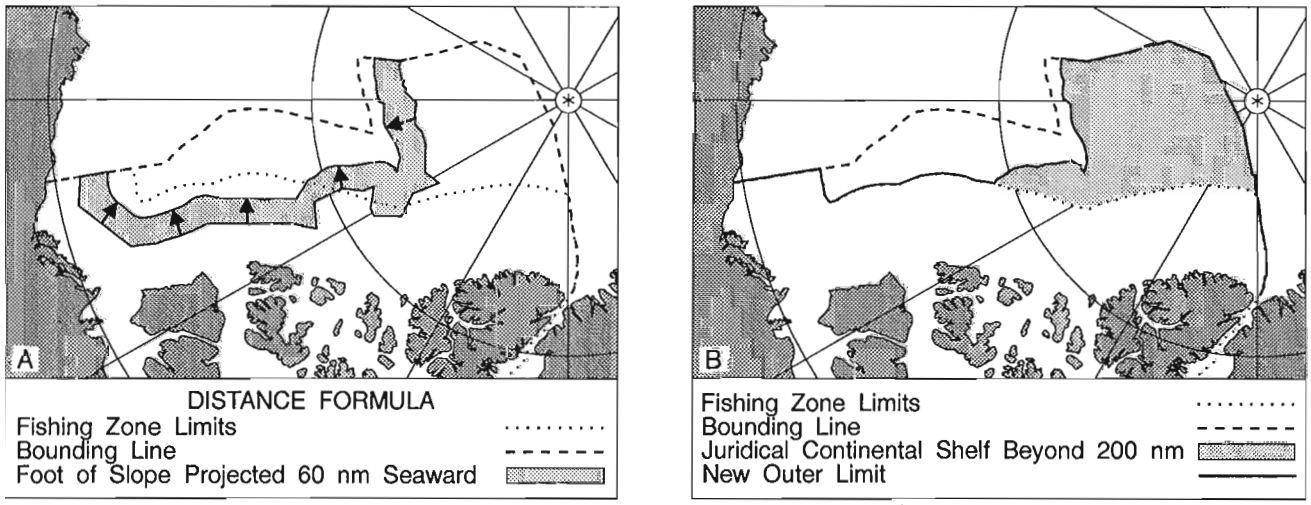

Figure 10. *The outer limit of the juridical continental shelf in the Arctic, based on the application of the distance formula to existing information. In* ***A****, the foot of the continental shelf is projected seaward by 60 nautical miles to form a provisional outer limit. In* ***B****, this is combined with the 200 mile limit and the bounding line to form a new outer limit that extends the zone beyond the 200 nm limit by some 470 000 km*^{2}*.*

Outer limit based on the sediment thickness formula

This is shown in Figure 11 for the Atlantic only (at present, the sediment thickness formula cannot be implemented in the Arctic for lack of seismic data). In the first stage (part A) a provisional outer limit is constructed by projecting the foot of the continental slope seaward to the Gardiner Line; in the second stage (part B) this is combined with segments of the provisional outer limit, the Fishing Zone limit, and the bounding line to create a definitive outer limit. This adds approximately 760 000 km^2 to the area defined by the distance formula: it consists of moderate extensions off Nova Scotia and Labrador, along with most of the zone within the bounding line around the Grand Banks, Flemish Cap, and Orphan Knoll.

Outer limits based on combined formulas

A wide margin state is permitted by Article 76 to combine the results of the distance and sediment thickness formulas in order to define its new outer limits to best advantage. At present, combined formulas are not possible in the Arctic, given the lack of sediment thickness information. In the Atlantic, the distance and sediment thickness formulas are almost equivalent everywhere except in the Scotian Basin, where the latter encompasses a significantly greater area. Off Labrador and the Grand Banks, the difference between formulas represents a total area of about 50 000 km^2. In the Scotian Basin, the sediment thickness formula represents an additional area, beyond that defined by the distance formula of about 110 000 km^2.

Outer limits developed with enhanced databases

Properly designed and executed, a program for acquiring new bathymetric and seismic data could provide the information required to substantiate jurisdiction over a larger area. This would support Canada's jurisdiction over resources beyond 200 nm over an estimated 1 750 000 km^2, an area roughly equivalent to Canada's three Prairie Provinces.

CONCLUSIONS

Benefits of Article 76 to Canada

Article 76 of the UN Convention on the Law of the Sea provides a legal framework whereby Canada may support its claim to jurisdiction over extended portions of its wide continental margins in the Atlantic and Arctic oceans. On the basis of existing information, about 750 000 km^2 in the Atlantic, and nearly 500 000 km^2 in the Arctic, could be added

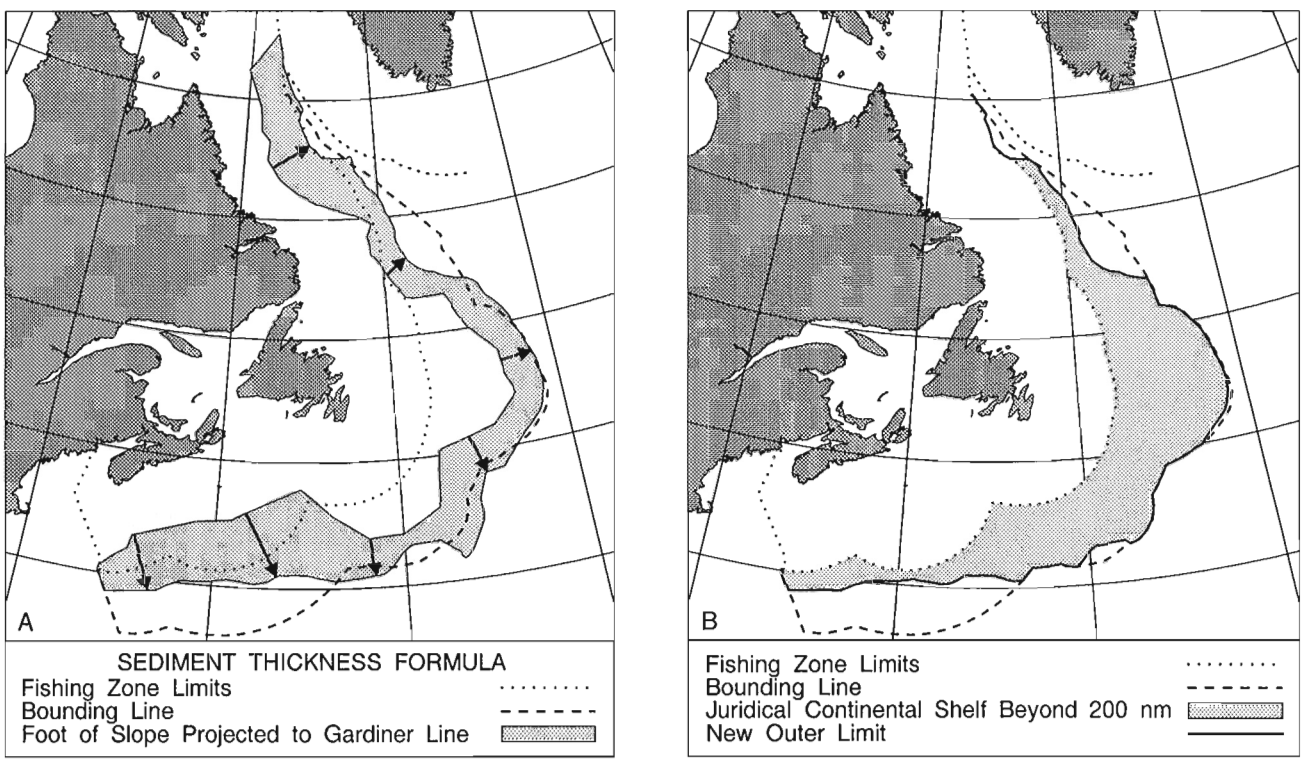

Figure 11. *The outer limit of the juridical continental shelf in the Atlantic, based on the application of the sediment thickness formula to existing information. In* ***A****, the foot of the continental slope is projected out to the Gardiner Line (where the thickness of sediment is equal to 1% of the distance to the foot of the slope) to form a provisional outer limit. In* ***B****, this is combined with the 200 mile limit and the bounding line to form a new outer limit that extends the zone beyond the 200 nm limit by some 761 000 km^2.*

to Canada's present economic zones. With judiciously acquired bathymetric and seismic information, these figures could be increased by an estimated 500 000 km^2.

A decision to proceed with the delineation of new limits of the juridical continental shelf would result in two primary and significant benefits: (1) international recognition of resource jurisdiction over substantial portions of the sea floor beyond 200 nautical miles; and (2) formal authority for dealing effectively with environmental issues in the high seas adjacent to the nation's zones of economic interest.

Unknowns

The locations of potential new limits are only provisionally known at this time, as they have been derived from preliminary assessments of incomplete data sets. Substantial work remains to be done: (1) in assembling and rationalizing all remaining information into a coherent database; (2) in analyzing the resulting body of information with the aim of defining a more objective delineation of the edge of the juridical continental shelf; and (3) in developing a program to acquire new information where needed to supplement the existing databases.

At present, we possess mixed knowledge of the resource potential of the extended shelf areas. Quantitative knowledge of the hydrocarbon potential is fairly good in the Atlantic margin on account of a long-standing program for assessing gas and oil resources in this region: there are clear indications that extending the juridical shelf edge to the limit permitted by Article 76 will prove to be beneficial in this respect. Except for the Beaufort Sea, our equivalent knowledge in the Arctic is poor to zero. The potential for gas hydrates is promising in both the Atlantic and the Arctic, but it is based on general formulas that have been derived from their inferred occurrence in other parts of the world.

Deep-sea mineral resources remain an unknown quantity in the extended shelf areas in the Atlantic and Arctic. The exploitable fishery is limited to bottom-dwelling species with a number of restrictions; this potential is only partially known in the Atlantic, less so in the Arctic.

ACKNOWLEDGMENTS

Most of the data sets used to conduct this review were extracted from the digital archives of the Geological Survey of Canada (Atlantic) by Gordon Oakey, Allen Stark, and Kate Dickie. Locations of bathymetric data in the Arctic were extracted from the digital archives of the Geological Survey of Canada (Ottawa) with the assistance of Walter Roest. Comments on resource potentials were based on information provided by John Wade, Alan Grant and Richard Haworth of the Geological Survey of Canada, and Terry Rowell of the Biological Studies Branch of Fisheries and Oceans Canada. Figures were prepared by David Vardy.

Some aspects of this report are based on the results of an unpublished investigation performed in the early 1980s by George Somers under the guidance of the late Michael Keen, who was then Director of the Atlantic Geoscience Centre.

REFERENCES

Bell, J.S. and Campbell, G.R.
1990: Petroleum resources, Chapter 12 in Geology of the Continental Margin of Eastern Canada, M.J. Keen and G.L. Williams (ed.); Geological Survey of Canada, Geology of Canada, no. 2, p. 677-720.

Gardiner, P.R.R.
1978: Reasons and methods for fixing the outer limit of the legal continental shelf beyond 200 nautical miles; Iranian Review of International Relations, no. 11-12, Spring 1978, p. 145-170.

Hale, P.B.
1990: Mineral resources, Chapter 13 in Geology of the Continental Margin of Eastern Canada, M.J. Keen and G.L. Williams (ed.); Geological Survey of Canada, Geology of Canada, no. 2, p. 721-741.

Kvenvolden, K.A., Ginsburg, G.D., and Soloviev, V.A.
1993: Worldwide distribution of subaquatic gas hydrates; GeoMarine Letters, v. 13, p. 32-40.

Procter, R.M., Taylor, G.C., and Wade, J.A.
1984: Oil and natural gas resources of Canada - 1983; Geological Survey of Canada, Paper 83-31, 59 p.

Geological Survey of Canada Project 303002

A preliminary report on the stratigraphy of Late Namurian to Stephanian fluviatile strata in southeastern New Brunswick[1]

Susan C. Johnson[2]
GSC Atlantic, Dartmouth

Johnson, S.C., 1995: A preliminary report on the stratigraphy of Late Namurian to Stephanian fluviatile strata in southeastern New Brunswick; in Current Research 1995-E; Geological Survey of Canada, p. 313-320.

Abstract: Late Namurian to Stephanian strata in southeastern New Brunswick have traditionally been assigned to the Enragé, Boss Point, Salisbury, Richibucto, and Tormentine formations, equivalent to parts of the recently redefined Cumberland and Pictou groups. Recent mapping, palynology studies, and revisions made in the type localities of the Cumberland and Pictou groups have necessitated the reassignment of some of these strata. Preliminary results indicate the Salisbury and Richibucto formations are not facies equivalent and need to be formally redefined. Spore assemblages in the Richibucto Formation are mid-Westphalian C to Stephanian whereas those in the Salisbury Formation are latest Westphalian B to Westphalian C. Based on similar lithostratigraphy, the Richibucto Formation is tentatively correlated with the Malagash Formation which forms the top of the Cumberland Group in the Cumberland subbasin. The overlying Tormentine Formation would therefore be equivalent to the lowermost Pictou Group in Nova Scotia.

Résumé : Les couches du Namurien tardif au Stéphanien dans la partie sud-est du Nouveau-Brunswick ont historiquement été intégrées aux formations d'Enragé, de Boss Point, de Salisbury, de Richibucto et de Tormentine équivalentes à des parties des groupes récemment redéfinis de Cumberland et de Pictou. Des révisions des localités types des groupes de Cumberland et de Pictou, des études palynologiques et des travaux de cartographie récemment effectués exigent une reclassification de certaines de ces couches. Les résultats préliminaires indiquent que les formations de Salisbury et de Richibucto ne sont pas des faciès équivalents et doivent être formellement redéfinies. Les assemblages de spores de la Formation de Richibucto datent du Westphalien C moyen au Stéphanien alors que ceux de la Formation de Salisbury datent du Westphalien B sommital au Westphalien C. D'après une lithostratigraphie similaire, la Formation de Richibucto est, de manière tentative, corrélée à la Formation de Malagash qui forme le sommet du Groupe de Cumberland dans le sous-bassin de Cumberland. La formation sus-jacente de Tormentine serait alors équivalente aux couches basales du Groupe de Pictou en Nouvelle-Écosse.

[1] Contribution to the Magdalen Basin NATMAP Project.
[2] New Brunswick Department of Natural Resources and Energy, Sussex, New Brunswick, E0E 1P0.

INTRODUCTION AND GEOLOGICAL SETTING

A 1:50000 scale mapping program, funded by the Magdalen Basin NATMAP Project, was initiated in the fall of 1994 to investigate the stratigraphy and resource potential of Carboniferous rocks in southeastern New Brunswick. The improved stratigraphic framework will be integrated with recent stratigraphic revisions in the Cumberland subbasin, immediately across the border in Nova Scotia. The first phase of this project involved stratigraphic, structural and palynological investigations in the Cape Tormentine (11 L/04), Port Elgin (21 I/01), and northern part of the Amherst (21 H/16) map areas. This work will continue on the Moncton (21 I/02), Hillsborough (21 H/15), and southern parts of the Amherst (21 H/16) map areas during the 1995 field season (Fig. 1).

Regionally, the study area is situated within the western part of the Maritimes Basin (Fig. 2) considered to be a successor basin initiated in Late Devonian time following the Acadian Orogeny (Roliff, 1962; Williams, 1974; McCutcheon and Robinson, 1987). The basin as a whole comprises several subbasins isolated by basement blocks or uplifts. Although the depositional history of each subbasin contains unique elements, the basin fill can be subdivided into five lithostratigraphic divisions (e.g. Ryan et al., 1991; St. Peter, 1993) ranging in age from Late Devonian to Permian. In ascending order they comprise the Horton, Windsor, Mabou (Hopewell), Cumberland, and Pictou groups.

This paper focuses on the stratigraphy of Late Namurian to Stephanian units covered during the first phase of mapping and on correlation of these units with established stratigraphic subdivisions elsewhere in the Maritimes Basin.

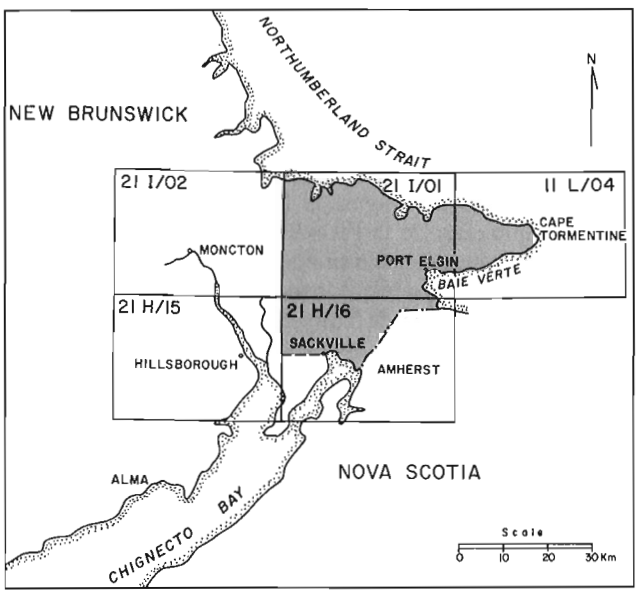

Figure 1. Location of 1:50 000 scale NTS map areas in study area. Mapping completed in shaded area.

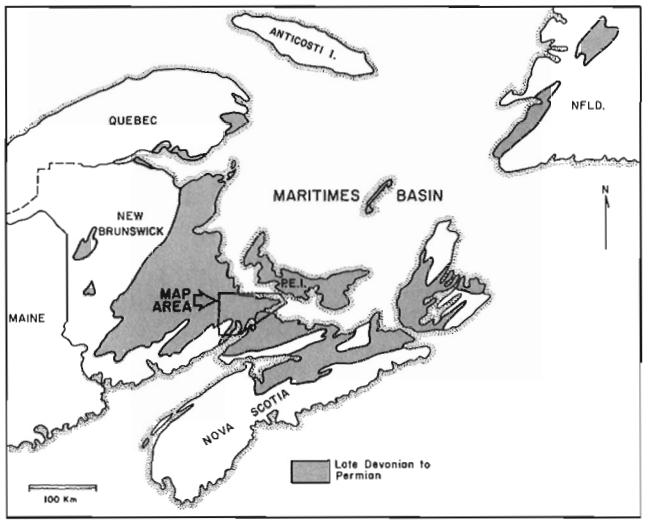

Figure 2. Regional location map of Maritimes Basin (after Ryan and Boehner, 1994).

PREVIOUS WORK AND NOMENCLATURE

Terminology applied to Upper Carboniferous strata in southern New Brunswick is in a state of confusion. The Pictou and Petitcodiac groups have been used interchangeably for all or parts of the stratigraphic record spanning Late Namurian to Stephanian time. The Lexicon of Canadian Stratigraphy (Williams et al., 1985) illustrates this problem, including rocks from the same geographic area in New Brunswick within both the Pictou and Petitcodiac Group definitions. Wright (1922) introduced the term Petitcodiac Series for rocks roughly equivalent to the Enragé, Boss Point, and Salisbury formations of later workers. Norman (1941) elevated the Petitcodiac to group status but excluded the Enragé Formation which formed the top of his newly defined Hopewell Group.

The first comprehensive study of Carboniferous rocks in New Brunswick was conducted by Gussow (1953). He introduced, in ascending order, the names Salisbury, Scoudouc, Richibucto and Tormentine formations for Upper Carboniferous rocks and assigned these formations to the Pictou Group. The underlying Boss Point Formation was included in the now abandoned Riversdale Group. Following Norman (1941), Gussow (1953) assigned the Enragé Formation to the Hopewell Group and considered it to be equivalent to the Claremont Formation, which at that time was assigned to the base of the Riversdale Group in Nova Scotia.

In the Moncton area, Carr (1968) abandoned the Scoudouc Formation, including it in his revised Salisbury and Richibucto formations. He assigned these rocks and the Boss Point Formation to the Petitcodiac Group (Fig. 3). Most subsequent workers have followed Gussow (1953), referring to Upper Carboniferous strata overlying the Boss Point Formation, as Pictou Group (van de Poll, 1970; McLeod and Ruitenberg, 1978; Ball et al., 1981; St. Peter, 1993).

STRUCTURE AND BASEMENT FEATURES

Although subsurface information is limited, it is known that Upper Carboniferous strata exposed at surface were also deposited on the Westmorland Uplift and within the Sackville subbasin in the northern and southern parts of the map area respectively. These features are bounded by steeply dipping, normal faults, most of which are concealed beneath a blanket of Upper Carboniferous rocks (Fig. 4).

The Westmorland Uplift (Gussow, 1953) is a roughly east-west trending basement ridge extending from the Hillsborough area to Cape Tormentine, a distance of over 95 km. Granite exposed at surface in a quarry near Calhoun, west of the map area, is part of this ridge. Deep boreholes indicate that the sedimentary cover progressively thickens towards the north and east. The oldest strata encountered in these boreholes were probably Enragé Formation (Late Namurian). It is not known if lower Carboniferous rocks were removed by erosion during exhumation of the granite or whether this area was topographically high at this time.

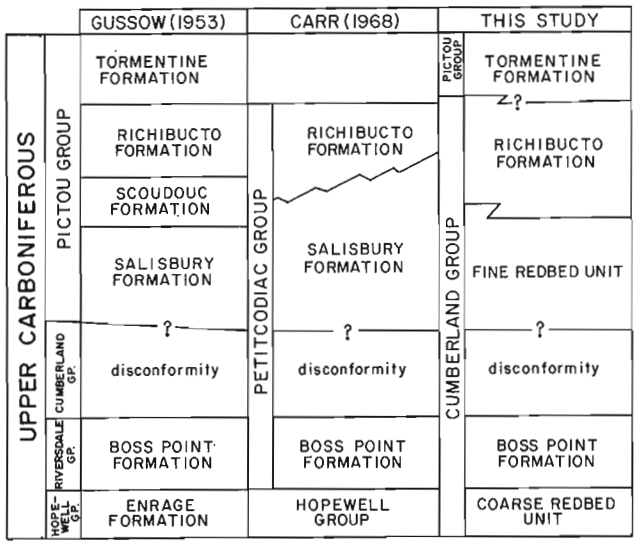

Figure 3. Nomenclature of Upper Carboniferous strata in southeastern New Brunswick.

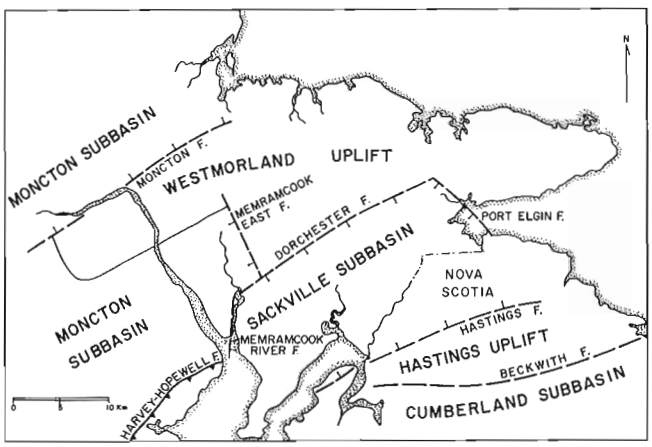

Figure 4. Generalized map of subbasins, uplifts and faults in southeastern New Brunswick and northwestern Nova Scotia (modified after St. Peter in Foley, 1989).

Upper Carboniferous rocks overlying this ridge are gently warped into a broad, shallowly east-plunging anticline referred to as the Westmorland Anticline. This structure, which exposes progressively younger beds to the east, is curvilinear east-west, generally conforming to the trend of the basement ridge. Based on this geometric configuration, Gussow (1953) suggested that this anticlinal structure was more influenced by basement topography than by tectonic processes.

The Sackville subbasin, defined by Martel (1987) using deep seismic reflection profiles and deep borehole data from two wells in the Dorchester area, contains a thick succession of continental clastic rocks and marine evaporites. The Horton, Windsor, and base of the Hopewell groups are not exposed at surface in the map area but are present at depth. Shell Dorchester No. 1, the deepest hole drilled in the basin, terminated in the Albert Formation (Horton Group). Horton Group strata are interpreted from seismic reflection data to thin toward the Sackville Arch, a local topographic high (Martel, 1987). As the Windsor Group is absent in this area, the arch apparently remained relatively high during Windsor time, and the Horton Group is disconformably overlain by the Hopewell Group. The Hopewell Group was succeeded by late basin-fill sediments that overstepped the bounding faults onto the Westmorland and Hastings uplifts. At surface, they are gently folded into the east-northeast-trending, doubly plunging Dorchester anticline and syncline.

STRATIGRAPHY

Descriptive terms have been used for units which may be redefined or renamed later in this project. Type sections for most units have never been formally established although informal nomenclature is firmly entrenched in the literature. No attempt has been made at this stage to erect formal type sections although it is a long-term goal of the project. Lithostratigraphy of the map units is based on preliminary field investigation and petrography and applies to the map area only, unless otherwise indicated.

Coarse Redbed unit

The oldest rocks encountered at surface in the map area are dominantly coarse, red fluviatile rocks which conformably underlie the Boss Point Formation. Limited exposures of these rocks, all northwest of Sackville, occur on the headwaters of Breau Creek and in the vicinity of the old Dorchester Copper mine (Fig. 5). Redbeds in a similar stratigraphic position were encountered 890 m below surface in Imperial Port Elgin #1 borehole, 30 km northeast of Sackville, and 520 m below surface in Imperial Dorchester #1 borehole, 6 km south of the surface exposure.

The lower contact was penetrated in these boreholes indicating that the unit, in part, overlies fine grained redbeds of the Maringouin Formation but also directly overlaps basement. The upper contact is exposed in the adit of the old Dorchester Mine, where the redbeds form the footwall to the copper ore body at the redbed-greybed transition. The unit comprises alternating beds of reddish-brown to brick-red, polymictic, pebble to cobble conglomerate, arkose, pebbly arkose, siltstone, and mudrocks. The fine grained rocks very commonly contain green reduction spheroids.

Thickness estimates vary for this unit. The surface exposures form a southeast-younging sequence on the north limb of the Dorchester syncline. Based on surface distribution and dip in this area, the thickness is in the order of 200-300 m, but the section is truncated by the Dorchester Fault. An 800 m thickness was intersected in Imperial Dorchester #1 to the south. The unit thins considerably over the Westmorland Uplift, where only 30 m of strata were encountered in Imperial Port Elgin #1, directly overlying granitic basement.

The Coarse Redbed unit was designated undivided Hopewell Group by Norman (1941) and Gussow (1953), although the latter author alluded to the Enragé affinity of these beds by stating that the Maringouin and Shepody formations were missing in this area. The Hopewell Group, as defined in the type area, traditionally comprised a conformable sequence consisting of, in ascending order, the Maringouin, Shepody, and Enragé formations (Norman, 1941; Flaherty and Norman, 1941). Gussow (1953) redefined the base of the Enragé Formation as a regional unconformity. Subsequently, these coarse grained red strata and similar redbeds, which unconformably overlie older Carboniferous strata or basement in the southeastern Moncton subbasin, were assigned to the Enragé Formation (McLeod and Ruitenberg, 1978; St. Peter, 1992, 1993).

Recent work by van de Poll (1994) has demonstrated that the majority of what was originally defined as Enragé Formation is lithologically more akin to the overlying Boss Point Formation than to the underlying Hopewell Group. A new spore locality in the Shepody Formation underlying the Enragé Formation in the Chignecto Bay area indicates it is most likely Late Namurian age (G. Dolby, written communication, 1995). This adds strength to van de Poll's (1994) argument that the Shepody and Enragé formations are part of the Cumberland Group rather than the Hopewell Group which gradationally overlies Viséan rocks.

Conglomerates from the Coarse Redbed unit in the map area are unlike those found in the Enragé Formation in the type section, which are relatively mature, well-sorted, distal-type lithofacies (van de Poll, 1994). Although both the Enragé and Coarse Redbed unit conformably underlie the Boss Point Formation, and may be time equivalent, the latter are poorly sorted, immature and polymictic suggesting they have a proximal source. For these reasons it is suggested the use of the term Enragé be restricted to the unit described by van de Poll (1994). Similar immature, redbed conglomerate units in the same stratigraphic position occur 1) in the southeastern

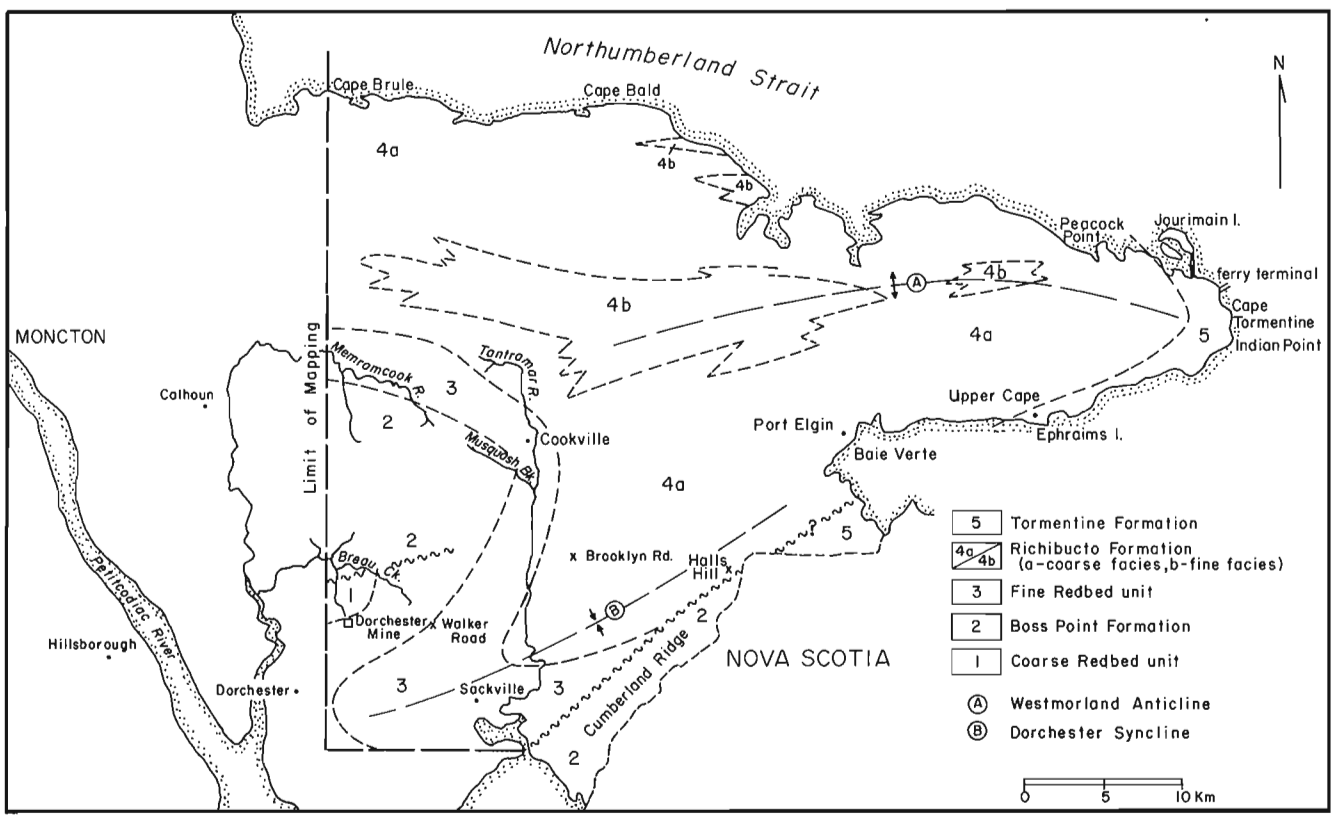

Figure 5. General geology of Upper Carboniferous rocks in southeastern New Brunswick.

Moncton subbasin (mapped as Enragé), 2) on the Central Platform margin (Shin Redbeds), and 3) Cumberland subbasin in Nova Scotia (Claremont Formation).

Boss Point Formation

Strata assigned to the Boss Point Formation conformably overlie the Coarse Redbed unit in the Dorchester area and are concordantly overlain by a unit of red siltstone and sandstone, quartz-rich sandstone, pebbly sandstone, conglomerate. The lower contact was described in the previous section. The upper contact is described below. The type section is at Boss Point, Cumberland County, Nova Scotia (Browne, 1991). The formation is present in the Sackville area, and occurs as a separate belt on the Cumberland Ridge adjacent to the Nova Scotia border. To the north, it is exposed on Musquash Brook and the Memramcook River in the Cookville area (Fig. 5).

The dominant lithofacies is fine-to medium-grained, trough crossbedded sandstone ranging in composition from quartz arenite to subarkose and sublitharenite. The sandstone is characterized by its yellow weathering and ubiquitous carbonized plant debris that is commonly associated with pyrite nodules and thin discontinuous coal seams. Pebbly sandstones containing quartz pebbles or grey mud clasts are common at the base of the sandstone beds. Thin units of dusky grey mudstone and siltstone are also associated with the sandstone units.

Thick (up to 30 m), massive and trough crossbedded conglomerate units predominate in the Breau Creek and Cumberland Ridge sections. The conglomerate is typically polymictic, but quartz dominated, and contains subordinate felsic volcanic and intrusive clasts and intraformational grey mud clasts. It is dominantly clast supported in the Breau Creek area and contains subrounded pebbles and cobbles up to 20 cm in diameter. Sandstone bodies within the conglomeratic sections are typically less than a metre thick and wedge shaped. Grey siltstone and mudstone form discontinuous lenses. On Cumberland Ridge, the conglomerate bodies are both matrix and clast supported and are interbedded with thick, trough crossbedded sandstone units which locally cut into the underlying conglomerate. Large spherical manganese concretions up to a metre in diameter occur in the sandstone bodies.

A distinctive, highly indurated, grey to pink quartz arenite, exposed as undulating polished outcrops in the bed of the Memramcook River, is commonly mottled grey and buff and contains fairly abundant disseminated pyrite. This unit may be similar to one described by Carr (1968) and Hamilton and Sutherland (1968), near the top of the Boss Point in the Moncton map area to the west. Although the Boss Point lithofacies are overwhelmingly grey, brownish-red, fine grained, thin bedded sandstone and pebbly sandstone are interbedded with grey Boss Point sandstones above the quartz arenite unit. The upper contact is not exposed and therefore, the exact position below the top of the formation is not known.

At several localities in the Sackville area superpositional relationships indicate that grey Boss Point sandstone is overlain by and interfingers with fine-to coarse-grained red, quartz-rich rocks and siltstone. This unit is also present in several boreholes in the map area and may be correlative with the above described unit on the Memramcook River. Newly exposed outcrop near the Walker Road overpass on the Trans Canada Highway passes through this contact. As it is not yet clear if these rocks are part of the Boss Point Formation they will be described in detail in the section titled Fine Redbed unit.

Thickness estimates for the Boss Point Formation range considerably throughout the map area. Over the Westmorland uplift the formation is thin (80 m) to absent but in the Sackville subbasin it thickens dramatically. A conservative estimate using sections constructed across the Cumberland Ridge indicates that 800 m of strata are present, but neither the base or top is exposed. A section from the lower contact at the Dorchester Mine indicates a thickness in the order of 850 m.

Palynomorphs recovered from the formation range from Late Namurian to Early Westphalian A (G. Dolby, written communication, 1995), ages similar to those determined for the type section (Browne, 1991).

Fine Redbed unit

These rocks lie concordantly above the Boss Point Formation with the lower contact placed at the highest thick section of grey trough crossbedded sandstone. The upper contact is not exposed. These strata lie in the same stratigraphic position as the Salisbury Formation and were mapped as such by Gussow (1953). The trace of this unit follows the Boss Point Formation contact along the nose and northern limb of the Dorchester syncline west of Sackville. It continues to the north where it outcrops on Musquash Brook and possibly on the Memramcook River (Fig. 5). In the subsurface, similar rocks were encountered in Shell Westmorland #1 and D'arcy Exploration Cape Bald #2.

The dominant lithofacies is brownish-red to brick-red, very fine grained, parallel-laminated sandstone, siltstone and mudrocks with subordinate medium grained, trough crossbedded sandstone. A bed of pinkish-maroon, medium- to coarse-grained quartz arenite and pebbly sandstone near the base is distinctive. Maroonish-red and buff mottled coloration is common as are manganese oxides, which occur as coatings on sand grains and spheroidal concretions. Grey, plant-rich sandstone similar to those of the Boss Point Formation occur at several stratigraphic positions throughout the unit.

The base of this unit is exposed adjacent to the Trans Canada highway near the Walker Road overpass. At this locality, the Boss Point section is overlain by red and minor grey mudrocks and siltstone, and parallel-laminated very fine grained sandstone. Above this is a horizon of mottled red sandstone with buff chalky alteration and incipient silicification. The overlying reddish, quartz-rich, small-pebble conglomerate contains intraformational clasts of the underlying mottled rocks. The conglomerate is overlain by reddish-brown, coarse grained quartz-rich sandstone containing lenses of quartz-pebble conglomerate and pebbly sandstone.

The exposed thickness at the Walker Road locality is 45 m but the top is not exposed. A section constructed from the base to the axis of the Dorchester syncline indicates the unit is in the order of 500 m thick.

The basal contact of this unit in the Sackville area has been placed at several stratigraphic positions (compare Gussow 1953; van de Poll, 1973; McLeod and Ruitenberg, 1978). This is probably due, in part, to poor exposure and the presence within the map unit of lithologies typical of both the Boss Point and Salisbury formations. McLeod and Ruitenberg (1978) recognized and mapped parts of this unit east of Dorchester (unit 6d) assigning them to the Boss Point Formation. Their lithostratigraphic subdivisions were not supported by Browne (1991). The current study has shown that the unit is mappable in this area and may be present to the west of the map area, south of Moncton. Gussow (1953) described a sequence in this area, which he placed near the base of the Salisbury Formation, of pinkish-grey sandstone, some almost pure quartz sandstone and grey to buff sandstone quite similar to those of the Boss Point which "interrupt the continuity of the thick red Salisbury section". The apparent interfingering nature of the contact would seem to indicate continuous deposition from the Boss Point to the overlying redbeds. This presents a problem as this contact has traditionally been thought to represent a major disconformity. Spore assemblages indicate a substantial time gap between Late Namurian-Early Westphalian A deposition of Boss Point strata and the overlying Salisbury Formation which has yielded spores no older than latest Westphalian B (St. Peter, 1993).

If the Westphalian B hiatus is not a function of inadequate sampling, the quartz-rich base of the Fine Redbed unit may reflect erosion of the quartz-rich Boss Point rocks. As critical exposures of these rocks occur outside of the area mapped to date, the Fine Redbed unit will not be assigned to the Salisbury Formation until further work is completed.

Richibucto Formation

The Richibucto Formation is composed mainly of grey, multistoried sandstone interstratified with red-mudrock dominated sequences. It is overlain by the Tormentine Formation and underlain by the Fine Redbed unit. The base and top are not exposed but there is no apparent discordance in bedding above or below the formation boundaries. The type section is located near the town of Richibucto, 65 km north of the map area. The Richibucto Formation is widely distributed in the area forming the majority of surface exposures on the Port Elgin and Cape Tormentine map sheets. It is well exposed in cliffs along Northumberland Strait from Cape Brulé to Peacock Point and in the Baie Verte-Port Elgin area. To the southwest the formation is exposed at Halls Hill and the Brooklyn Road, southeast of Sackville (Fig. 5).

The formation consists of grey and minor greyish-red and brownish-red, feldspathic litharenite, litharenite, lithic arkose and subarkose, calcareous mud-chip conglomerate, pebbly sandstone and minor grey, limestone pebble to cobble conglomerate. Fine grained facies include brick red to brownish-grey, mudrocks, siltstone and very fine grained sandstone. Large scale trough crossbedded, medium grained sandstone bodies form stacked units with total thicknesses of up to 75 m. Intraformational conglomerate containing red and minor grey mud chips commonly occur at the base of the channel sands. Coalified plant fragments and fossil logs are locally abundant in the sandstone units.

Very fine grained sandstone within the red mudrock-dominated units are characterized by ripple laminations shown as well developed rib and furrow structures. Minor discontinuous coal seams (<8 cm thick) are also associated with the fine grained facies. The fine to coarse ratio in the Richibucto Formation in the map area is approximately 0.5.

Thickness estimates for the Richibucto Formation based on surface exposure are extremely unreliable due to the low angle of dip and undulating nature of the beds. A minimum thickness for this unit is 170 m, intersected in a diamond-drill hole near Melrose, but neither the base or top were encountered.

The rocks assigned to the Richibucto Formation in the map area were divided into the Scoudouc and overlying Richibucto formations by Gussow (1953). Carr (1968) abandoned the Scoudouc Formation assigning the overwhelming majority of these rocks to the underlying Salisbury Formation. Based on their laterally equivalent position and overlapping spore assemblages he considered the Richibucto and Salisbury to be facies equivalent.

Based on field mapping and relogging of approximately 1000 m of drill core, it is evident the Scoudouc Formation as defined by Gussow (1953) is a dominantly red, fine grained facies of the Richibucto Formation. However, it is unlikely it is part of the Salisbury Formation. Re-examination of the spore localities, which Carr (1968) mapped as Salisbury Formation, indicates vastly different ages (G. Dolby, written communication, 1995). The Scoudouc River locality,

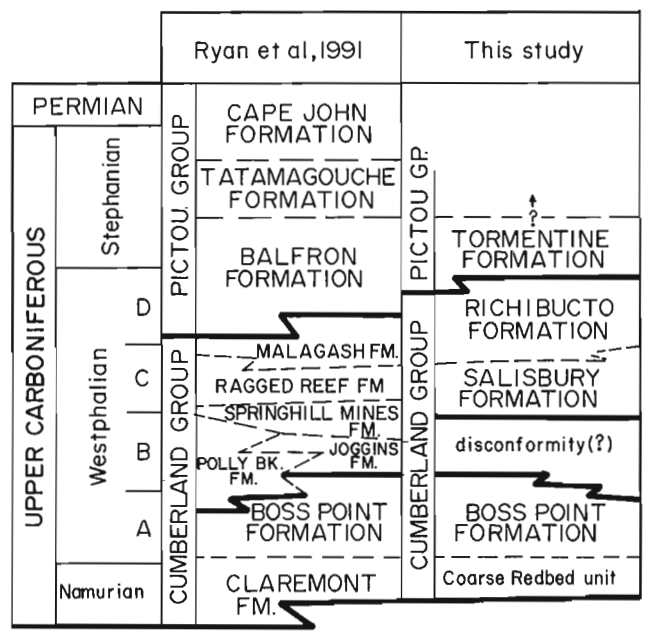

Figure 6. Lithostratigraphic correlation of units in the map area and Cumberland subbasin, Nova Scotia.

Gussow's type section for that formation, indicates an age no older than Westphalian D, similar to several sites in the Richibucto Formation which range from no older than mid Westphalian C to Stephanian. The other locality, mapped as Salisbury Formation by both Carr (1968) and Gussow (1953), has been reassigned an age no younger than Early Westphalian C, most likely latest Westphalian B, the same age as a coal seam near the Salisbury type section (St. Peter, 1993).

As previously stated, the contact relationship between the Richibucto and Salisbury formations is presently unknown but may be slightly diachronous as the Salisbury has yielded spores as young as mid to Early Westphalian C (G. Dolby, written communication, 1995). The Salisbury and Richibucto formations occupy the same stratigraphic position as the upper parts of the Ragged Reef Formation and overlying Malagash Formation in the Cumberland subbasin in Nova Scotia (Fig. 6).

Tormentine Formation

Brick red to brownish-red, sandstone, conglomerate, siltstone and mudrocks are the dominant lithotypes in the Tormentine Formation. The unit overlies the Richibucto Formation and contains the youngest strata exposed in the map area. The formation occurs as a narrow, 2.5 km wide belt exposed in cliffs and the intertidal zone along Northumberland Strait from Jourimain Island to the Cape Tormentine ferry terminal where it swings southwest along the shore of Baie Verte to Ephraims Island in the vicinity of Upper Cape (Fig. 5).

Strata of the Tormentine Formation are characterized by their bright brick-red colour but various shades of brownish-red to greyish-red are locally predominant. A typical section comprises repetitive fining upward sequences of red, very fine grained sandstone, siltstone, and mudrocks alternating with mainly fine- to medium-grained, trough crossbedded and planar crossbedded sandstone. Composition of the sandstones range from feldspathic litharenite to lithic arkose and subarkose. The mudrock dominated units, which attain thicknesses of 2 m, commonly contain green reduction spheroids and are locally ripple marked. Calcareous mud-chip conglomerates contain red, flattened and crescent-shaped mud clasts, and commonly have a calcareous matrix. They occur as lensoid bodies at the base of channels in the sandstone units and, therefore, are interpreted as channel lag deposits. The thickest conglomerate noted was 2 m.

Ball and pillow horizons up to 15 cm thick occur in the section on Ephraims Island and calcareous concretionary sand bodies are common throughout the formation. Spherical, tiered spheres and composite (dumb-bell shaped) forms are most common. Elongate, pool-shaped calcareous concretionary bodies associated with carbonate-replaced plant stems and fragments are common in some sand beds. These features were commonly found to have their long axis parallel to the local paleocurrent direction, suggesting a channel origin.

The maximum exposed thickness of the formation is approximately 160 m along the shore from Cape Tormentine to Indian Point. A section from the coast at Ephraims Island, inland through a Carboniferous Drilling Project borehole indicates that at least 250 m of Tormentine strata are present. The upper contact is not exposed.

The stratigraphic position of the Tormentine Formation indicates a Stephanian or younger age. Based on stratigraphic position, lithology, and geographic distribution, the Tormentine Formation may be equivalent to the Balfron Formation in adjacent Nova Scotia. The Balfron Formation forms the base of the Pictou Group in that area (Fig. 6).

Sediment dispersal trends

Only a preliminary assessment of sediment dispersal trends was possible during this phase of the study. A total of 69 paleocurrent measurements were made using large scale trough crossbedding, a Rank 5 current indicator of Miall (1974). All measurements were taken at coastal exposures where the most reliable data could be obtained. For this reason, no data for the Boss Point Formation were collected. Browne (1991) and Browne and Plint (1994) reported regional variations in the paleocurrent direction for Boss Point strata across the Harvey-Hopewell Fault. North of the fault paleoflow trends are directed north and northeast whereas south of the fault they are east and southeast. Paleocurrent data for the Richibucto and Tormentine formations are shown as a rose diagram (Fig. 7) using 30° class intervals. These data, albeit limited, suggest a flow direction from the southwest. A vector mean of 45° with a vector strength of 75% was calculated using the methods of Potter and Petitjohn (1977).

Van de Poll (1970) conducted an extensive study of the sediment dispersal trends in this area, which yielded vector means ranging from 22 to 72°.

CONCLUSIONS

The preliminary results of this study suggest that Upper Namurian to Stephanian strata in southeastern New Brunswick are in need of revision. The following lithostratigraphic changes have been informally proposed:

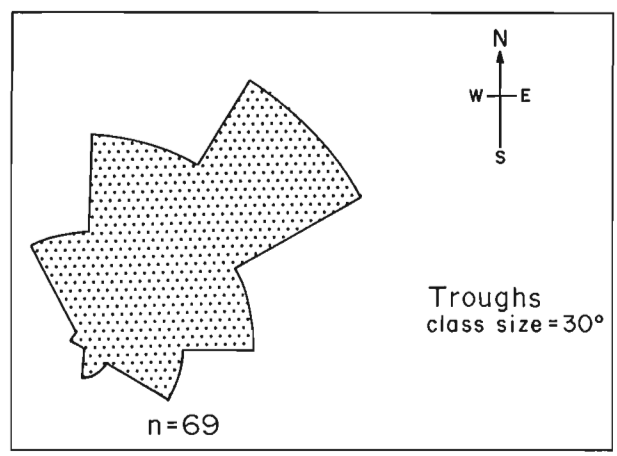

Figure 7. Rose diagram for paleocurrent measurements in the study area.

1. A unit of coarse redbeds conformably underlying the Boss Point Formation may not be equivalent to the Enragé Formation in its type section in the Chignecto Bay area.
2. The Salisbury Formation is not a facies equivalent of the Richibucto Formation but underlies it, probably conformably.
3. The abandoned Scoudouc Formation is the facies equivalent of the Richibucto Formation.
4. The Salisbury and Richibucto formations may be correlative with the upper part of the Ragged Reef and overlying Malagash formations which form the top of the revised Cumberland Group in the Cumberland subbasin in Nova Scotia.
5. The Tormentine Formation is most probably equivalent to the Balfron Formation at the base of the revised Pictou Group in Nova Scotia.

ACKNOWLEDGMENTS

Funding for this study was provided by Natural Resources Canada through the Magdalen Basin NATMAP Project. The author acknowledges the enthusiastic field assistance of Derek Brown, Alan Lines, Jason Ross, and Kay Muir. I am indebted to Malcolm McLeod for valuable discussions and independent mapping during the early stages of the project. The author benefitted from discussions with Clint St. Peter and Peter Giles. Constructive comments by Malcolm McLeod and Peter Giles greatly improved this manuscript. Thanks are also extended to Graham Dolby for the palynological support.

REFERENCES

Ball, F.D., Sullivan, R.M., and Peach, A.R.
1981: Carboniferous Drilling Project; New Brunswick Department of Natural Resources, Mineral Development Branch, Report of Investigations 18, 109 p.

Browne, G.H.
1991: The sedimentology of the Boss Point Formation, New Brunswick and Nova Scotia; Ph.D. thesis, University of Western Ontario, London, Ontario.

Browne, G.H. and Plint, A.G.
1994: Alternating braidplain and lacustrine deposition in a strike-slip setting: the Pennsylvanian Boss Point Formation of the Cumberland Basin, Maritime Canada; Journal of Sedimentary Research, v. B64, no. 1, p. 40-59.

Carr, P.A.
1968: Stratigraphy and spore assemblages, Moncton map-area, New Brunswick; Geological Survey of Canada, Paper 67-29, 47 p.

Flaherty, G.F. and Norman, G.W.H.
1941: Albert, Albert County, New Brunswick; Geological Survey of Canada, Map 648A (with marginal notes), scale 1:63 360.

Foley, S.L.
1989: Geology of the Stoney Creek Oil and Gas Field, and its implications regarding the tectonic evolution of the eastern Moncton Subbasin; New Brunswick Department of Natural Resources and Energy, Mineral Resources Branch, Geoscience Report 89-1.

Gussow, W.C.
1953: Carboniferous stratigraphy and structural geology of New Brunswick, Canada; American Association of Petroleum Geologists Bulletin, v. 37, no. 7, p. 1713-1816.

Hamilton, J.B. and Sutherland, J.K.
1968: Silica in New Brunswick. New Brunswick Department of Natural Resources, Mineral Resources Branch, Report of Investigation 2, 43 p.

Martel, A.T.
1987: Seismic stratigraphy and hydrocarbon potential of the strike-slip Sackville subbasin, New Brunswick; in Sedimentary Basins and Basin-forming Mechanisms, C. Beaumont and A.J. Tankard (ed.); Canadian Society of Petroleum Geologists, Memoir 12, p. 319-334.

McLeod, M.J. and Ruitenberg, A.A.
1978: Geology and mineral deposits of the Dorchester area, map area W-22, W-23 (21 H/15E, 21 H/16W); New Brunswick Department of Natural Resources, Mineral Resources branch, Map Report 78-4, 27 p.

McCutcheon, S.R. and Robinson, P.T.
1987: Geological constraints on the genesis of the Maritimes Basin, Atlantic Canada; in Sedimentary Basins and Basin-forming Mechanisms, C. Beaumont and A.J. Tankard (ed.); Canadian Society of Petroleum Geology, Memoir 12, p. 287-297.

Miall, A.D.
1974: Paleocurrent analysis of alluvial sediments: a discussion of directional variance and vector magnitude; Journal of Sedimentary Petrology, v. 4, p. 1174-1185.

Norman, G.W.H.
1941: Hillsborough, Albert and Westmorland Counties, New Brunswick; Geological Survey of Canada, Map 647A (with marginal notes), scale 1:63 360.

Potter, P.E. and Pettijohn, F.J.
1977: Paleocurrents and Basin Analysis, Second Edition; Springer-Verlag, Berlin, 424 p.

Roliff, W.A.
1962: The Maritime Carboniferous basin of eastern Canada. Geological Association of Canada, Proceedings, v. 14, p. 21-41.

Ryan, R.J. and Boehner, R.C.
1994: Geology of the Cumberland Basin, Cumberland, Colchester and Pictou Counties, Nova Scotia; Nova Scotia Department of Natural Resources and Energy, Memoir 10, 222 p.

Ryan, R.J., Boehner, R.C., and Calder, J.H.
1991: Lithostratigraphic revisions of the upper Carboniferous to lower Permian strata in the Cumberland Basin, Nova Scotia and the regional implications for the Maritimes Basin in Atlantic Canada; Bulletin of Canadian Petroleum Geology, v. 39, p. 289-314.

St. Peter, C.
1992: Lithologic facies, seismic facies and strike-slip setting of the Lower Carboniferous alluvial/fluvial/lacustrine Albert Formation of New Brunswick; New Brunswick Department of Natural Resources and Energy, Mineral Resources, Geoscience Report 92-2, 145 p.
1993: Maritimes Basin evolution: key geologic and seismic evidence from the Moncton subbasin of New Brunswick; Atlantic Geology, v. 29, p. 233-270.

van de Poll, H.W.
1970: Stratigraphic and sedimentological aspects of Pennsylvanian strata in southern New Brunswick; Ph.D. thesis, University of Wales, U.K, 140 p.
1973: Geology Cumberland basin area; New Brunswick Department of Natural Resources and Energy, map plate 73-2, scale 1:50 000.
1994: Carboniferous provenance and lithostratigraphy of the Chignecto Bay region, New Brunswick: a preliminary assessment; in Current Research 1993, compiled and edited by S.A.A. Merlini; New Brunswick Department of Natural Resources and Energy, Minerals and Energy Division, Miscellaneous Report 12, p. 188-201.

Williams, E.P.
1974: Geology and petroleum possibilities in and around Gulf of St. Lawrence; American Association of Petroleum Geologists Bulletin, v. 58, no. 6, p. 1137-1155.

Williams, G.L., Fyffe, L.R., Wardle, R.J., Colman-Sadd, S.P., and Boehner, R.C.
1985: Lexicon of Canadian Stratigraphy, Volume VI – Atlantic Region; Canadian Society of Petroleum Geologists, 572 p.

Wright, W.J.
1922: Geology of the Moncton map area; Geological Survey of Canada, Memoir 129, 69 p.

Geological Survey of Canada Project 920062

The pseudo-geological log: using geophysical logs as an aid to geological logging in volcanogenic massive sulphides

P.G. Killeen, C.J. Mwenifumbo, and B.E. Elliott
Mineral Resources Division

Killeen, P.G., Mwenifumbo, C.J., and Elliott, B.E., 1995: The pseudo-geological log: using geophysical logs as an aid to geological logging in volcanogenic massive sulphides; in Current Research 1995-E; Geological Survey of Canada, p. 321-330.

Abstract: Geophysical borehole logs, which measure the physical properties of the rocks surrounding the hole, can be used as an aid to geological core logging, because they are continuous with no missing sections, and because they show changes that are not detectable with the naked eye. Three examples of the application of borehole geophysical logs to the problem of core logging in areas of volcanogenic massive sulphide deposits, are discussed. The Mudhole prospect in Newfoundland is a simple case of the obvious relation between geophysical logs and geological logs. In the Buttle Lake area of British Columbia, the experience gained from the Mudhole prospect was used to derive a pseudo-geological log based on the gamma-ray log. The pseudo-geological log was improved further in the Kam-kotia mine area in Ontario by using three geophysical parameters. In all three cases, the geological interpretation from the geophysical logs was subjective. An objective, computer-based method of deriving the pseudo-geological log, as a tool for the geologist, is being investigated.

Résumé : Les diagraphies de sondage géophysiques qui mesurent les propriétés physiques des roches autour du trou peuvent servir à compléter les données fournies par les carottes (diagraphie géologique) étant donné qu'elles sont continues sans section manquante et qu'elles montrent des changements non décelables à l'oeil nu. L'application des diagraphies géophysiques pour résoudre les problèmes de carottage dans les zones renfermant des gisements de sulfures massifs volcanogènes est traitée à l'aide de trois exemples. Le prospect Mudhole à Terre-Neuve est un cas simple de la relation évidente qui existe entre les diagraphies géophysiques et les carottages. Dans la région de lac Buttle en Colombie-Britannique, l'expérience acquise au prospect Mudhole a servi à dériver une diagraphie pseudo-géologique basée sur la diagraphie par rayons gamma. La diagraphie pseudo-géologique a pu être améliorée dans la région de la mine Kam-kotia en Ontario en utilisant trois paramètres géophysiques. Dans les trois cas, l'interprétation géologique établie à partir de diagraphies géophysiques s'est révélée subjective. La mise au point d'une méthode informatisée objective pour établir une diagraphie pseudo-géologique comme outil géologique est à l'étude.

INTRODUCTION

For more than ten years, the Borehole Geophysics section of the Geological Survey of Canada (GSC) has conducted multiparameter geophysical logging in boreholes associated with volcanogenic massive sulphide deposits, at locations from Newfoundland to British Columbia (Killeen and Mwenifumbo, 1988; Killeen, 1991). Excellent correlation of geophysical logs with geological logs has been observed, as well as cases indicating incorrect depth assignments of some geological units or features, due to core loss or other errors.

Geological logging of the drill core in greenstone belts can be difficult because different volcanic and volcaniclastic rocks are often visually similar. Geophysical logging tools measure physical and chemical properties that are not visible and therefore complement observations made in geological logs. The geophysical data provide a more complete and reassuring geological interpretation of the lithology intersected by the drillholes.

Three examples will be discussed here: the Mudhole base metal prospect near Buchans, Newfoundland; the Buttle Lake (Myra Falls) area on Vancouver Island, British Columbia; and the Kam-kotia mine area near Timmins, Ontario. The examples demonstrate the benefits of using geophysical logs as an aid to core logging, and point out the possibilities for development of a semi-automated interactive 'pre-picking' of the geology by computer, based on the geophysical logs. Before discussing the examples, some background on the relation between geology and geophysical parameters measured will be reviewed.

RELATIONSHIP BETWEEN GEOPHYSICAL LOGS AND GEOLOGY

In general, different rock types have different physical and chemical properties. An understanding of the physical rock properties to which each of the geophysical parameters respond is critical to interpreting correctly the relation between the logging data and the geology. Some of the geophysical logs respond to specific physical properties while others respond to a variety of physical properties (Killeen et al., 1994; Mwenifumbo et al., 1993a, b; Pflug et al., 1994). The following is a brief discussion of the response characteristics of each of the geophysical logs recorded in the areas mentioned in this paper.

1. Magnetic susceptibility

The magnetic susceptibility (MS) of a volume of rock is a function of the amount of ferromagnetic minerals – magnetite and pyrrhotite – contained within the rock. Magnetic susceptibility measurements can provide a rapid estimate of the magnetic minerals in the rock. These measurements are interpreted to reflect lithological changes, degree of homogeneity and the presence of alteration zones. Basic flows and diabase dykes containing higher concentrations of magnetic minerals are easily detected with magnetic susceptibility measurements. During hydrothermal alteration, magnetic minerals such as magnetite in the host rock tend to be altered to weakly magnetic minerals (e.g. hematite) or to non-magnetic minerals. Therefore, within a given lithological unit, anomalously low magnetic susceptibilities will generally indicate altered zones.

2. Induced polarization

In time domain induced polarization (IP) measurements a current is passed through the earth in a series of off-on pulses and the rate of decay of the voltage is measured during the current off-time. The measured voltage is related to the electrical polarizability of the rock and is called chargeability. A high chargeability response is an indication of the presence of metallic sulphides and oxides or cation-rich clays such as illite and montmorillonite (Mwenifumbo, 1989). One of the major alteration processes within a number of base metal and gold mining camps is pyritization and this is a target for most IP logging.

3. Resistivity

The electrical resistivity of rocks depends on several factors. Conductive minerals such as base metal sulphides, oxides, and graphite in the rock have a strong influence on the resistivity. Most rocks are usually poor conductors and their resistivities are governed primarily by their porosity and salinity of the pore fluids and to a lesser extent by the intrinsic minerals that constitute the rock. Some alteration processes such as silicification and carbonatization tend to reduce the rock porosity and hence increase the formation resistivities. Thus in rocks where no significant amounts of conductive minerals occur, the most important factors affecting the resistivities are fracturing, porosity, the degree of saturation of pore spaces, and the nature of the electrolytes in the pore fluids. Since resistivities depend on a number of factors, geological interpretation from resistivity measurements is fairly difficult without complementary information from other geophysical measurements or geological logs. Massive sulphide deposits however, often consist of conductive ore zones and therefore delineation of the ore horizons by electrical resistivity logging is usually straightforward.

4. Self potential

Large self potentials observed within and around sulphides are mainly caused by electrochemical reactions (oxidation-reduction reactions). Electrofiltration processes may also be responsible for generating some relatively small amplitude anomalies where there is groundwater flow in the presence of ionic concentration gradients. Low resistivity anomalies correlating with SP anomalies are, therefore, good indications of the presence of conductive base metal sulphides. At Buttle Lake, SP anomalies generally indicate the presence of base metal sulphides including pyrite.

5. Temperature

Although a number of variables affect the temperature-depth profile in a borehole, temperature measurements have been successfully used to map lithology where significant thermal

conductivity contrasts exist. They can also be used to detect and map fracture zones, and to delineate massive sulphide mineralization.

Large concentrations of metallic sulphides and oxides perturb the local isothermal regime since metallic minerals have high thermal conductivities. The perturbation of the local geothermal gradient, however, would be observed only in a thermally quiet environment. In areas where there are numerous fracture zones with ground water movements, thermal anomalies due to ground water flow are much larger than those that would be caused by changes in the thermal conductivity (e.g. the presence of metallic minerals).

6. Natural gamma-ray spectrometry

The gamma ray probe measures the natural gamma radiation emitted by potassium-40 (K), and uranium (U) and thorium (Th) series nuclides in the rocks. Four logs are produced: the Total Count (TC), K, U and Th logs. The main minerals contributing to an increase in potassium-40 are the K-feldspars and micas. Uranium and thorium are usually contained in minerals such as allanite, apatite, monazite, sphene, and zircon. Differences in the percentages of these minerals in various rocks make it possible to identify and characterize different units by their levels of radioactivity.

At the Buttle Lake area, for example, the different volcanic units have different amounts of potassium minerals (potassium-40 being the principal source of the natural gamma radiation). Feldspar porphyry sills with higher concentrations of K-feldspar minerals should be easily identified as anomalously high radioactivity zones on the gamma ray logs. Often during hydrothermal alteration processes associated with mineralization, the radioactive elements potassium, uranium, and thorium may be preferentially concentrated in certain lithological units. Alteration in the Buttle Lake area is mainly characterized by the development of sericite (a potassium mineral), epidote, and chlorite. Sericite enriched zones are excellent targets for gamma ray logging.

7. Spectral gamma-gamma (density and heavy element indicator)

The spectral gamma-gamma probe measures the density of the rock around the borehole and provides information on the effective atomic number (Zeq) of the rock. The spectral gamma-gamma ratio (SGGR) is the measured quantity that is related to the presence of heavy elements.

In most mining environments, minerals forming the country rock consist mainly of low-atomic number (Z) elements (e.g. silicates and carbonates with the major elemental constituents being Al, Fe, Mg, Ca, K, Na, C and O) while the base metal sulphide ores consist of high Z elements (e.g. Pb, Cu, Zn, Fe sulphides and/or oxides). The high Z elements within the ore raise the Z_{eq} of the rocks as well as their density. Thus on SGGR and density logs, base metal ore zones are evident as zones of anomalously high values. Since the SGGR correlates so well with the ore grade, a simple regression can be used to establish a predictor of ore grade based on the SGGR log.

The density response is not only affected by variations in the whole rock chemistry of the formation but also by secondary physical properties that include porosity and water content. Porosity can be estimated from the density log by simple empirical linear transformations. Decreases in densities generally indicate increases in porosities.

THE MUDHOLE BASE METAL PROSPECT, NEWFOUNDLAND

This example is a 'text-book' case of the correlation between geology and geophysical logs in volcanic rocks.

Natural gamma ray logging was carried out in two holes at the Mudhole prospect near Buchans, Newfoundland. The gamma ray logs recorded with the GSC R&D logging system in hole MH2572 were published by Mwenifumbo and Killeen (1987). The 280 m hole was logged at 3 m/min using a 25 x 76 mm BGO detector and a 4 second sample time. The holes intersected volcanic, volcaniclastic, and sedimentary rocks which included andesite, rhyolite, dacite, diabase intrusions, tuff, agglomerate, arkose, siltstone, and greywacke. These rock units were easily characterized by their natural gamma ray activity. The Total Count gamma ray logs showed rhyolite and trachyte as producing the highest gamma ray count rate while the diabase intrusions were characterized by their extremely low gamma ray activity. A frequency distribution plot (histogram) of the Total Count gamma log was clearly multi-modal, with five peaks which could be related to diabase, andesite, amygdaloidal andesite, rhyolite, and trachyte, in increasing order of gamma ray count.

That study indicated that the total count gamma ray logs could be applied in the Buchans area with a high degree of confidence for the identification of the different volcanic rock types. Because contacts between major volcanic units were well defined on the gamma ray logs, the thicknesses of individual units could also be easily determined. Mwenifumbo and Killeen (1987) concluded: "Gamma ray logs, in conjunction with the geological logs can be used to provide a more complete and reassuring geological interpretation of the lithology intersected in diamond-drill holes".

The use of gamma ray spectral logs in the area might provide additional information on the relative concentrations of the naturally occurring radioelements, U, Th, and K, permitting further subdivision of the geological units not possible on the basis of the total count logs alone.

In most cases it is not as simple to relate the geology directly to a single geophysical parameter. Usually two or more physical rock property measurements are necessary to yield a unique signature for any given rock unit.

THE BUTTLE LAKE AREA, BRITISH COLUMBIA

Borehole geophysical measurements were made in several boreholes in the Buttle Lake area on Vancouver Island, British Columbia. The geophysical logging objectives were to

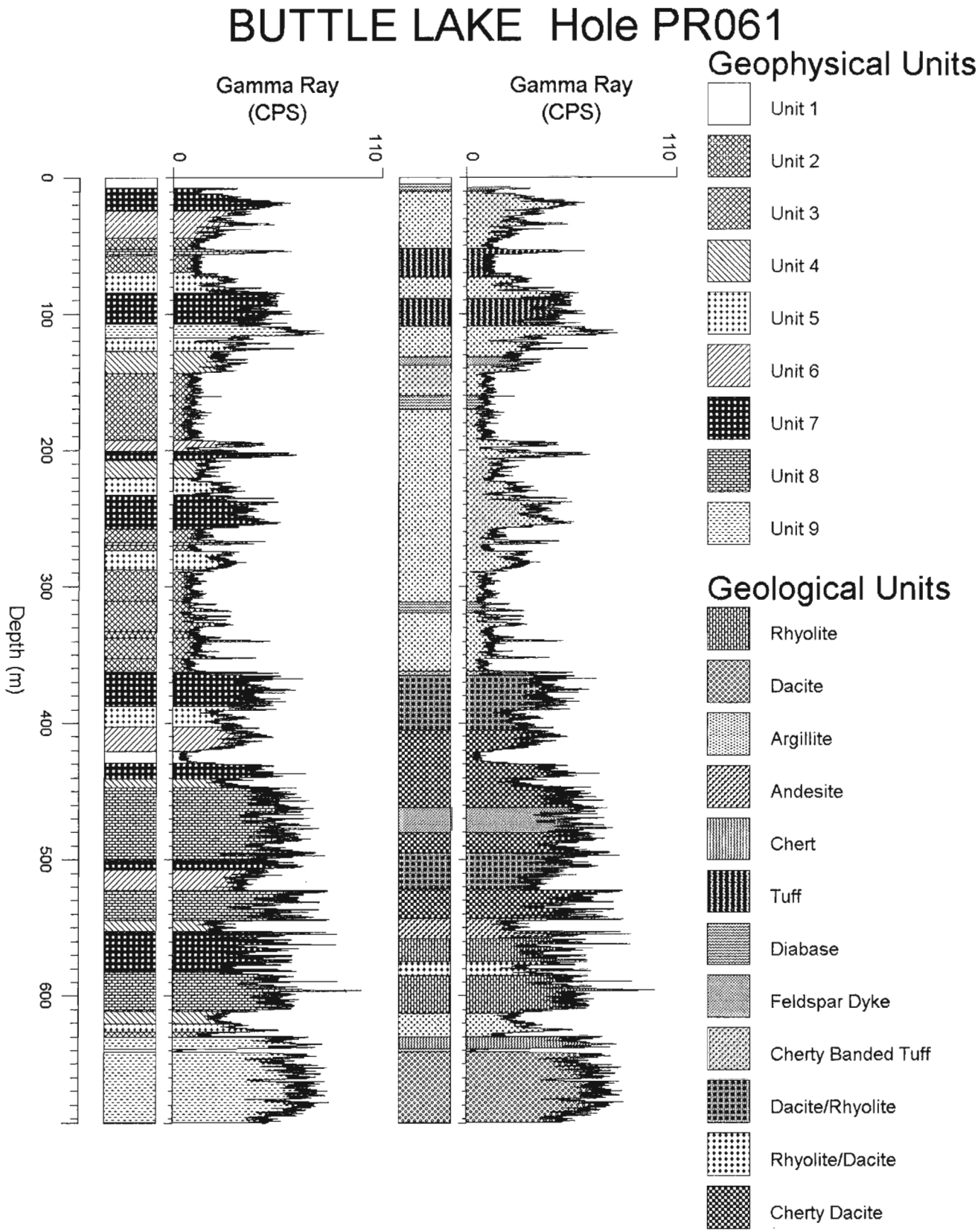

Figure 1. *Gamma-ray log from Buttle Lake hole PR061 plotted twice for comparison of pseudo-geological log (left) and core log (right).*

determine the geophysical signature of the deposit and host rocks, and to establish an in situ physical rock property database that would facilitate the development of geophysical methods for discovering new ore bodies (Killeen et al., 1989). The holes were drilled in 1979 at the Myra Falls mining operations by Wesmin Resources in one of several polymetallic (Cu-Zn-Pb) volcanogenic massive sulphide orebodies comprising pyrite, chalcopyrite, and sphalerite with minor galena. The mineralization is hosted by felsic volcanic rocks that are intruded by quartz-feldspar porphyritic bodies. The volcanic stratigraphy and structure of the deposit are fairly complex.

Geophysical logs were acquired with the GSC R&D logging system in 1987, as part of a multi-year, multi-deposit project, using five different probes. Variables measured included: three electrical logs (IP, Self Potential and Resistivity), Magnetic Susceptibility, Natural Gamma ray Spectrometry (Total Count, K, U, Th), Spectral Gamma Gamma (density and SGGR), Temperature and Temperature Gradient. The results of the multiparameter logging are presented in a GSC Open File Report covering work at several deposits in British Columbia (B.E. Elliott et al., in prep.).

In general, the geophysical logs provided information regarding the lithology, alteration, sulphide distribution, and fracturing. Of the logs recorded, several gave distinct signatures in different volcanic rocks whereas other logs were able to accurately delineate sulphide mineralization. Only the gamma ray logs digitally recorded in one 700 m hole (PR061) with a 25 x 76 mm sodium iodide detector, at 3 m/min, will be discussed here because they best reflected the geology.

Development of the 'pseudo-geological' log

The most significant indicators of geological variations were the nuclear logs; the natural gamma and the SGG/density logs. These respond to the geochemical changes in the rock; the natural gamma ray responding to lithology due to variations in the concentrations of potassium, uranium, and thorium. The density log is often a good indicator of changes in lithology, however, the density response to alteration and the degree of fracturing sometimes obscures the lithological variations.

Using the experience with the observations at the Mudhole prospect as a guide, an attempt was made to produce a 'pseudo-geological' log from the Buttle Lake geophysical logs. As a first step it was decided to use the gamma ray log as a means of defining different 'geophysical units' which had different count rates or degree of variability (homogeneity). The result is shown in Figure 1, where for comparison purposes, the gamma ray log from hole PR061 is plotted twice, with cross-hatched fill under the log trace representing the 'real' and the 'pseudo' geological logs. On the left is the log composed of 9 different 'geophysical units', and on the right is the traditional geological core log composed of 12 different geological units. The similarities are obvious but there are a number of significant differences. It is apparent that the geophysical log has more boundaries or contacts (44 zones in total) than the core log (27 zones), even though the gamma log indicated there were only nine different units and the core log had twelve different units. This shows that geological features such as sericite alteration for example, can change a physical property (such as the natural gamma radiation), but not represent a change in rock type. Therefore a pseudo-geological log based on a single geophysical log will be inadequate for determining the geological log, although it will be of some help to the geologist doing core logging, in directing his attention to changes in the core, some of which may be subtle and difficult to discern with the naked eye. For example, at depth 190 to 290 m, the pseudo-log is divided into variable thin zones of geophysical units 6, 7, 4, 5, 7, and 3, from top to bottom, whereas the core log describes the entire depth range as 'cherty banded tuff'. However, the detailed core log contains an entire page of notes regarding changes in the core observed in this section, such as 'minor carbonate stringers; variations in the percentage of chert; laminations; siliceous zones; minor mafic clasts; weakly sheared zones; colour changes, and other variations'. Some of these changes are likely distinguishable on the geophysical logs because they represent changes in physical properties which are measureable. However, 'these changes do not a different rock type make'.

Similarily, the 'cherty dacite' from 400 to 460 m was divided into five different geophysical units. It is fair to say that more bed boundaries are in agreement than in disagreement between the core and pseudo logs. However the geophysicist is perhaps overly optimistic in selecting geological contacts solely on the basis of gamma ray logs. The next example from the Kam-kotia mine area in Ontario is an attempt to improve the pseudo-geological log by using the 'best' three logs selected from a multiparameter suite of logs recorded with the GSC R&D logging system.

THE KAM-KOTIA MINE AREA, ONTARIO

In November 1993 a suite of more than ten logs was recorded in a 600 m deep hole, immediately after it was drilled, in the Kam-kotia mine area, west of Timmins. Strictly on the basis of variations in physical properties, a pseudo-geological log was produced, before the geologist had logged the core from the hole. Based on the use of multiple logs, the results were much more accurate than for the previous examples, with about 90% of the geological units being 'picked' correctly by the pseudo-log. It was determined that the geophysical parameters that most closely reflected the changes in the geology were the gamma ray, density and magnetic susceptibility logs.

Figure 2 shows the three logs plotted with the area under the log-trace filled with the different geophysical unit symbols. The three logs illustrate how one parameter may change within a single unit, while the others are relatively constant. For example in unit 1 between 130 and 220 m the gamma ray log and density log are fairly homogeneous, but the MS log shows large variations indicating this unit has 'magnetic' sections (increased magnetite content). Based on what was learned in the two previous examples, new geophysical units were not defined on the basis of variations in the MS alone. It was also tempting to subdivide the log between 400 and 500 m into more and thinner geophysical units based on the observed changes in the logs. The derivation of the pseudo-geological log was subjective, but the experience gained would be invaluable in formulating an algorithm for objective production of the pseudo-log by a computer.

Figure 3 shows the geological log which was produced from observation of the core. The rocks consist of massive flows, felsic volcanics, tuffs and diabase sills, with varying degrees of alteration. The zone between 130 and 220 m mentioned above is identified as 'massive flow/intrusive', and the MS log variations were not the result of an identity change. Between 400 and 500 m, the geologist did assign an additional unit (chloritic intermediate tuff), not defined as a geophysical unit. A good method of comparing the core and pseudo-logs is to display them in the same form as was done for the Buttle Lake logs in Figure 1.

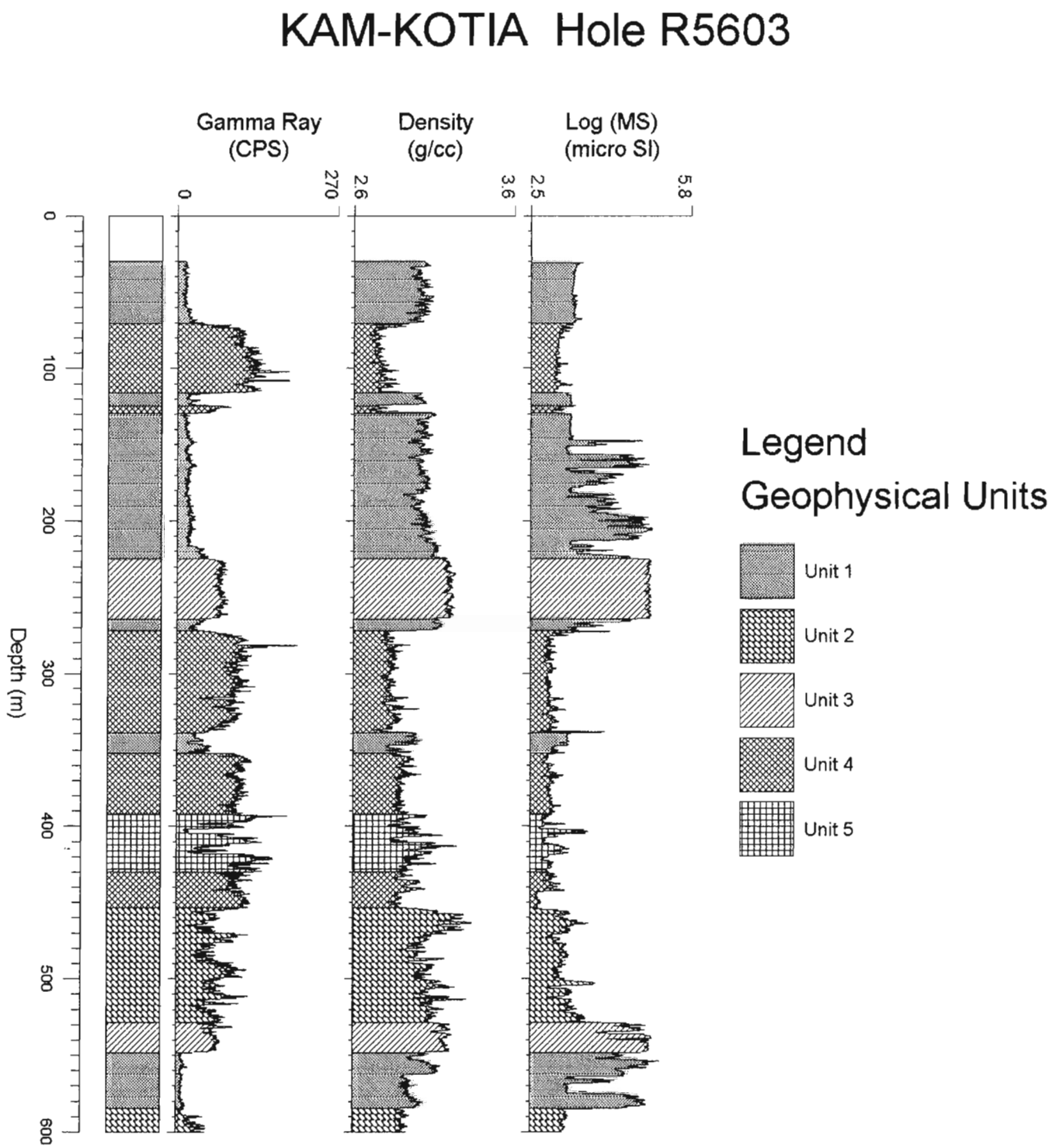

Figure 2. Gamma-ray, density and magnetic susceptibility (MS) logs for Kam-kotia hole R5603 showing the pseudo-geological log as cross-hatched fill.

The gamma-ray logs from the Kam-kotia hole R5603 are plotted twice in Figure 4, with the geophysical unit log (pseudo-geological log) on the left, and the geological log (core-log) on the right. Most of the geophysical contacts agree with the geological contacts. Some geological units relate to specific geophysical units such as:

unit 1 = massive flow/intrusive;
unit 2 = intermediate mafic tuffite and chloritic intermediate tuff;
unit 3 = diabase;
unit 4 = felsic volcanic, felsic intrusive volcanic, and felsic quartz eye tuff;
unit 5 = chloritic/sericitic felsic tuff.

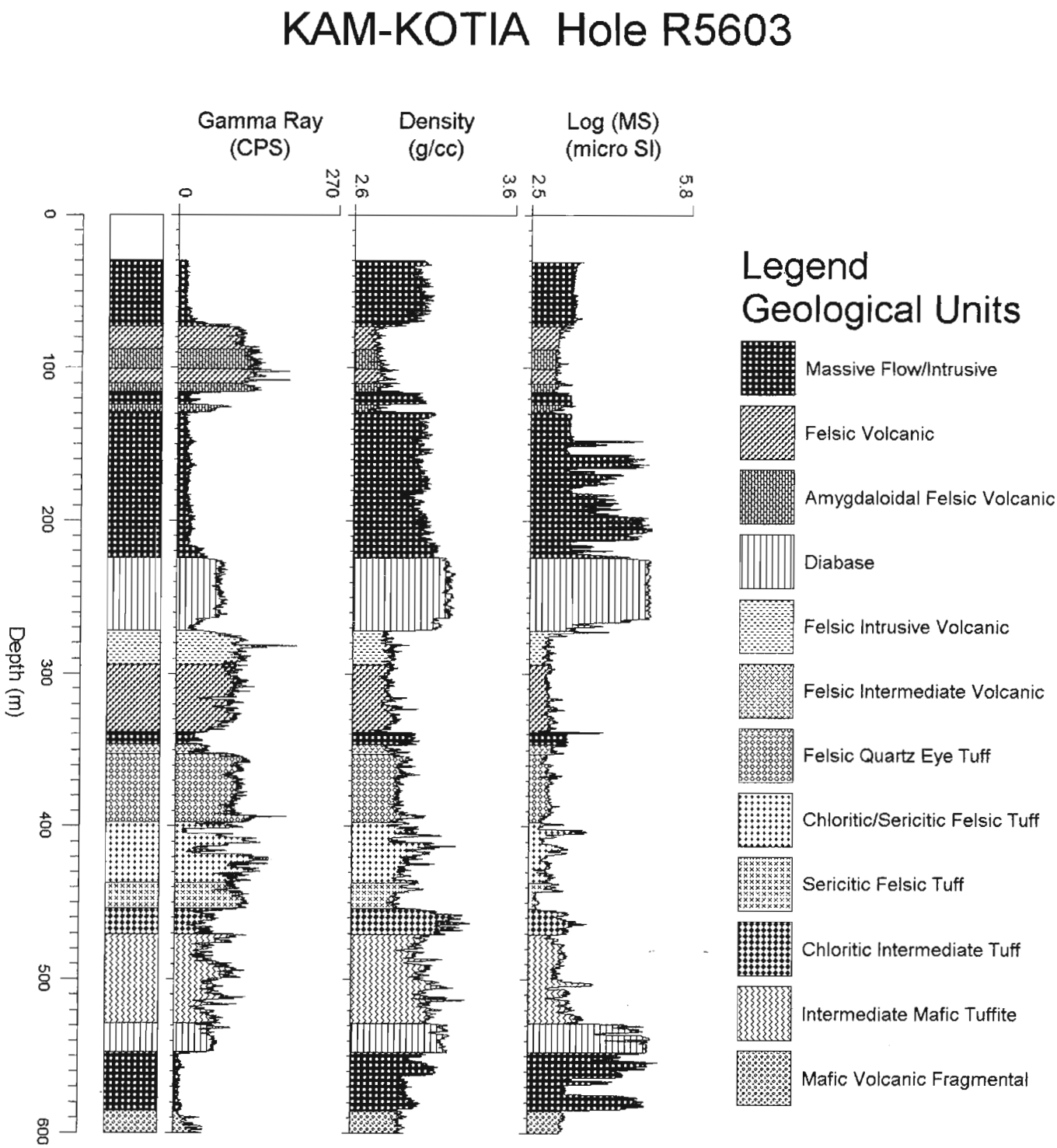

Figure 3. *Gamma-ray, density and magnetic susceptibility (MS) logs for Kam-kotia hole R5603 showing the core log as cross-hatched fill.*

It is clear that both geological contacts and geological units bear a distinct relationship to the geophysical logs in the Kam-kotia example shown in Figures 2, 3 and 4.

CONCLUSIONS

The experience in determining the relation between geology and geophysics via in situ logging of physical rock property measurements leads to the conclusion that considerable time could be saved and accuracy in depth positioning of geological contacts could be improved through the aid of geophysical logs. In a given area, such as local exploration in the vicinity of a mine, it may be possible to rely on pseudo-geological logs for rapid information during a drilling program. This would permit the explorationist to use the knowledge to direct the drill during the program. It is entirely feasible to develop computer software to produce the pseudo-geological log objectively, in real-time in the field. Its accuracy would be dependant on the number of parameters it had to work with, as well as previous 'training' from other holes in the area.

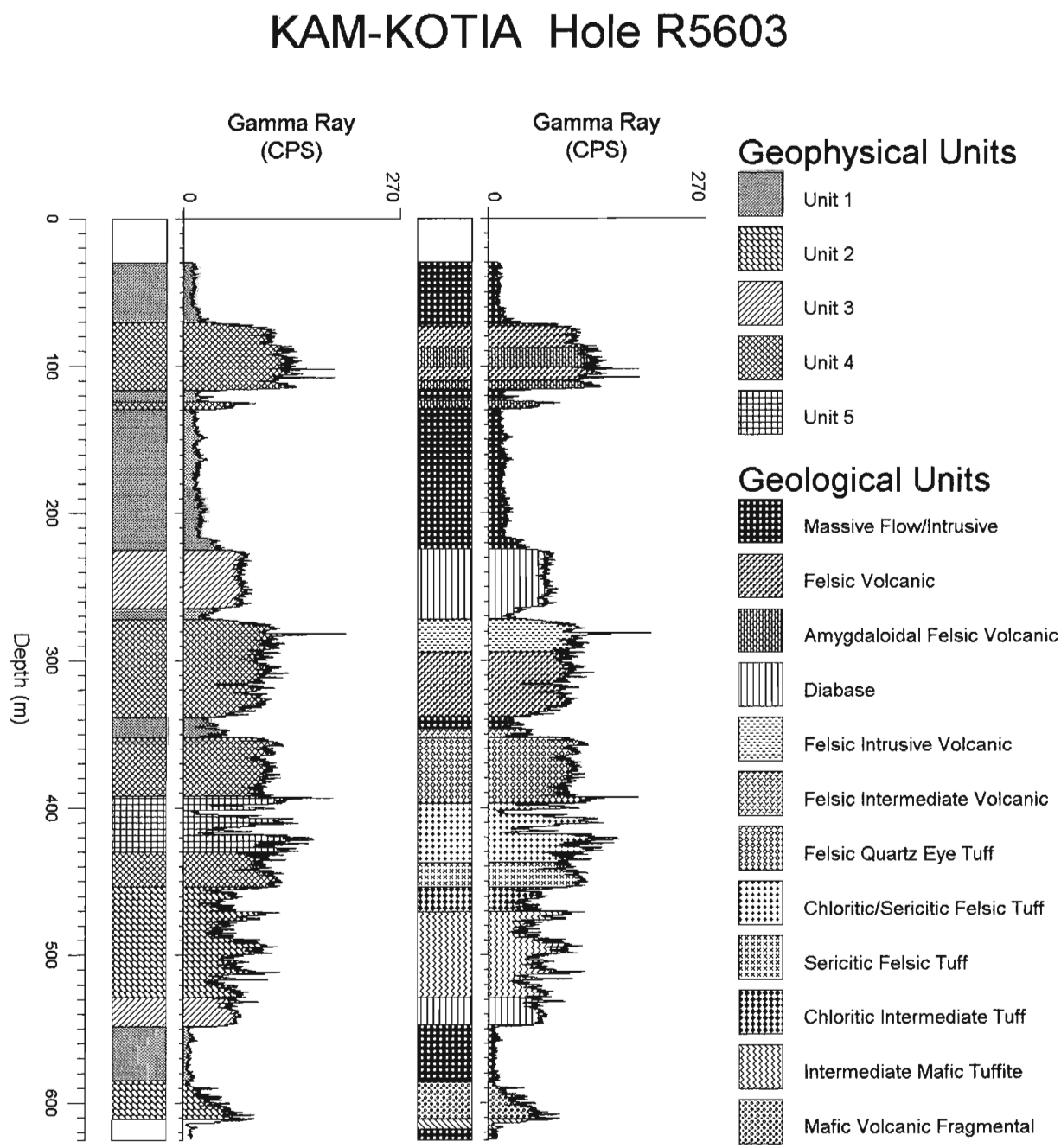

Figure 4. *Gamma-ray log from Kam-kotia hole R5603 plotted twice for comparison of pseudo-geological log (left) and core log (right).*

The GSC has commenced work towards development of such an 'artificial intelligence' system.

ACKNOWLEDGMENTS

We wish to thank Bill Hyatt and Andrew Wray for their contribution to the data acquisition and processing. We also thank Cliff Pearson of Wesmin Resources, Ray Band and John Pattison of Falconbridge, and ASARCO Inc. and Abitibi-Price Inc. for their collaborative support of this work, as well as permission to publish the results.

REFERENCES

Killeen, P.G.
1991: Borehole geophysics: taking geophysics into the third dimension; GEOS, v. 20, no. 2, p. 1-10.

Killeen, P.G. and Mwenifumbo, C.J.
1988: Interpretation of new generation geophysical logs in Canadian mineral exploration; in 2nd International Symposium on Borehole Geophysics for Minerals, Geotechnical and Groundwater Applications, Oct. 6-8, 1987, Golden, Colorado, p. 167-178.

Killeen, P.G., Elliott, B.E., and Mwenifumbo, C.J.
1989: Borehole geophysics applied to massive sulphide deposits in the Cordillera: a report on the 'B.C. Mineral Logging Group' Study, Preliminary Report, May, 2, 1989, submitted to the B.C. Mineral logging Group, 44 p.

Killeen, P.G., Mwenifumbo, C.J., Pflug, K.A., and Elliott, B.E.
1994: Borehole geophysical signatures and test sites at major deposits in Ontario: New developments in 1993; in Summary Report, 1993-1994, Northern Ontario Development Agreement, (ed.) N. Wood, R. Shannon, L. Owsiacki, and M. Walters, co-published by Natural Resources Canada, and the Ontario Ministry of Northern Development and Mines, p. 122-125.

Mwenifumbo, C.J.
1989: Optimization of logging parameters in continuous, time-domain induced polarization measurements; in Proceedings of the third International Symposium on Borehole Geophysics for Mineral, Geotechnical, and Groundwater Applications, Oct. 2-5, 1989, Las Vegas, Nevada, v. 1, p. 201-232.

Mwenifumbo, C.J. and Killeen, P.G.
1987: Natural gamma ray logging in volcanic rocks: the Mudhole and Clementine base metal prospects; in Buchans Geology, Newfoundland: 1982-1984, ed. R.V. Kirkham, Geological Survey of Canada, Paper 86-24, p. 263-272, Report 16.

Mwenifumbo, C.J., Killeen, P.G., and Bernius, G.R.
1993a: Ore deposit signatures by borehole geophysics; in Summary Report, 1992-1993, Northern Ontario Development Agreement, (ed.) N. Wood, R. Shannon, L. Owsiacki and M. Walters, co-published by Energy, Mines and Resources Canada and Ontario Ministry of Northern Development and Mines, p. 123-125.

Mwenifumbo, C.J., Killeen, P.G., Elliott, B.E., and Pflug, K.A.
1993b: The borehole geophysical signature of the McConnell Nickel Deposit, Sudbury area; in Proceedings of the 5th International Symposium of the Minerals and Geotechnical Logging Society, Tulsa, 24-28 October 1993.

Pflug, K.A., Killeen, P.G., and Mwenifumbo, C.J.
1994: Acoustic velocity logging at the McConnell nickel deposit, Sudbury area, Ontario: preliminary in situ measurements; in Current Research 1994-C; Geological Survey of Canada, p. 279-286.

Geological Survey of Canada Project 880030

APPENDIX 1

GEOPHYSICAL LOGGING PROCEDURES

The following brief notes provide information on some of the relevant logging procedures related to depth determination accuracy, sampling density, and other correlation considerations.

The depths are measured with an accuracy of 1 mm by the optical depth encoder located on the wellhead pulley assembly. All logs were obtained continuously at a speed of 3 to 6 m/minute while sampling at a depth interval of 5 to 20 cm (based on a 1 or 2 second sample time interval). Data were acquired while logging both downwards (downrun) and upwards (uprun) providing redundancy of data for most of the parameters recorded.

Correlation problems: matching the logs to the geology

There are sometimes problems in making correlations between the geophysical responses and the geological information. The greatest difficulty arises with discrepancies in depths between the two data sets. Errors exist in core data depths due to possible missing or lost core during drilling. Depth errors can also exist in geophysical logs that are mainly due to slippage and/or cable stretching. These errors must be corrected for all the logging data. The zero depth reference for the logging data is at the top of the casing which may not be the zero reference level for the geological log. (All depths on the geophysical logs are lengths along the drillholes and not true vertical depths, which is also true for the core log.) Another problem arises from the fact that geological contacts are not always well defined. They are quite often gradational and hence are somewhat subjective. The interpreted geological contacts may not coincide with the changes in the bulk physical or chemical properties of the formation.

AUTHOR INDEX

NOTE TO CONTRIBUTORS

Submissions to the Discussion section of Current Research are welcome from both the staff of the Geological Survey of Canada and from the public. Discussions are limited to 6 double-spaced typewritten pages (about 1500 words) and are subject to review by the Chief Scientific Editor. Discussions are restricted to the scientific content of Geological Survey reports. General discussions concerning sector or government policy will not be accepted. All manuscripts must be computer word-processed on an IBM compatible system and must be submitted with a diskette using WordPerfect. Illustrations will be accepted only if, in the opinion of the editor, they are considered essential. In any case no redrafting will be undertaken and reproducible copy must accompany the original submissions. Discussion is limited to recent reports (not more than 2 years old) and may be in either English or French. Every effort is made to include both Discussion and Reply in the same issue. Current Research is published in January and July. Submissions should be sent to the Chief Scientific Editor, Geological Survey of Canada, 601 Booth Street, Ottawa, Canada, K1A 0E8.

AVIS AUX AUTEURS D'ARTICLES

Nous encourageons tant le personnel de la Commission géologique que le grand public à nous faire parvenir des articles destinés à la section discussion de la publication Recherches en cours. Le texte doit comprendre au plus six pages dactylographiées à double interligne (environ 1500 mots), texte qui peut faire l'objet d'un réexamen par le rédacteur scientifique en chef. Les discussions doivent se limiter au contenu scientifique des rapports de la Commission géologique. Les discussions générales sur le Secteur ou les politiques gouvernementales ne seront pas acceptées. Le texte doit être soumis à un traitement de texte informatisé par un système IBM compatible et enregistré sur disquette WordPerfect. Les illustrations ne seront acceptées que dans la mesure où, selon l'opinion du rédacteur, elles seront considérées comme essentielles. Aucune retouche ne sera faite au texte et dans tous les cas, une copie qui puisse être reproduite doit accompagner le texte original. Les discussions en français ou en anglais doivent se limiter aux rapports récents (au plus de 2 ans). On s'efforcera de faire coïncider les articles destinés aux rubriques discussions et réponses dans le même numéro. La publication Recherches en cours paraît en janvier et en juillet. Les articles doivent être envoyés au rédacteur en chef scientifique, Commission géologique du Canada, 601, rue Booth, Ottawa, Canada, K1A 0E8.

The Geological Survey of Canada publishes reports on current field work and laboratory studies twice a year in January and July. The four volumes published in January 1995 (Current Research 1995-A to D) are listed below and can be purchased separately. This volume, Current Research 1995-E, was released in July 1995.

La Commission géologique du Canada publie les résultats de travaux en cours sur le terrain et en laboratoire deux fois par année, soit en janvier et en juillet. Les quatre volumes publiés en janvier 1995 (Recherches en cours 1995-A à D), énumérés ci-dessous, sont vendus séparément. Le présent volume, Recherches en cours 1995-E, a été diffusé en juillet 1995.

1995-A
Cordillera and Pacific Margin
Cordillère et marge du Pacifique

1995-B
Interior Plains and Arctic Canada
Plaines intérieures et région arctique du Canada

1995-C
Canadian Shield
Bouclier canadien

1995-D
Eastern Canada and National and General Programs
Est du Canada et programmes nationaux et généraux

1995-E
(this volume)
(ce volume)